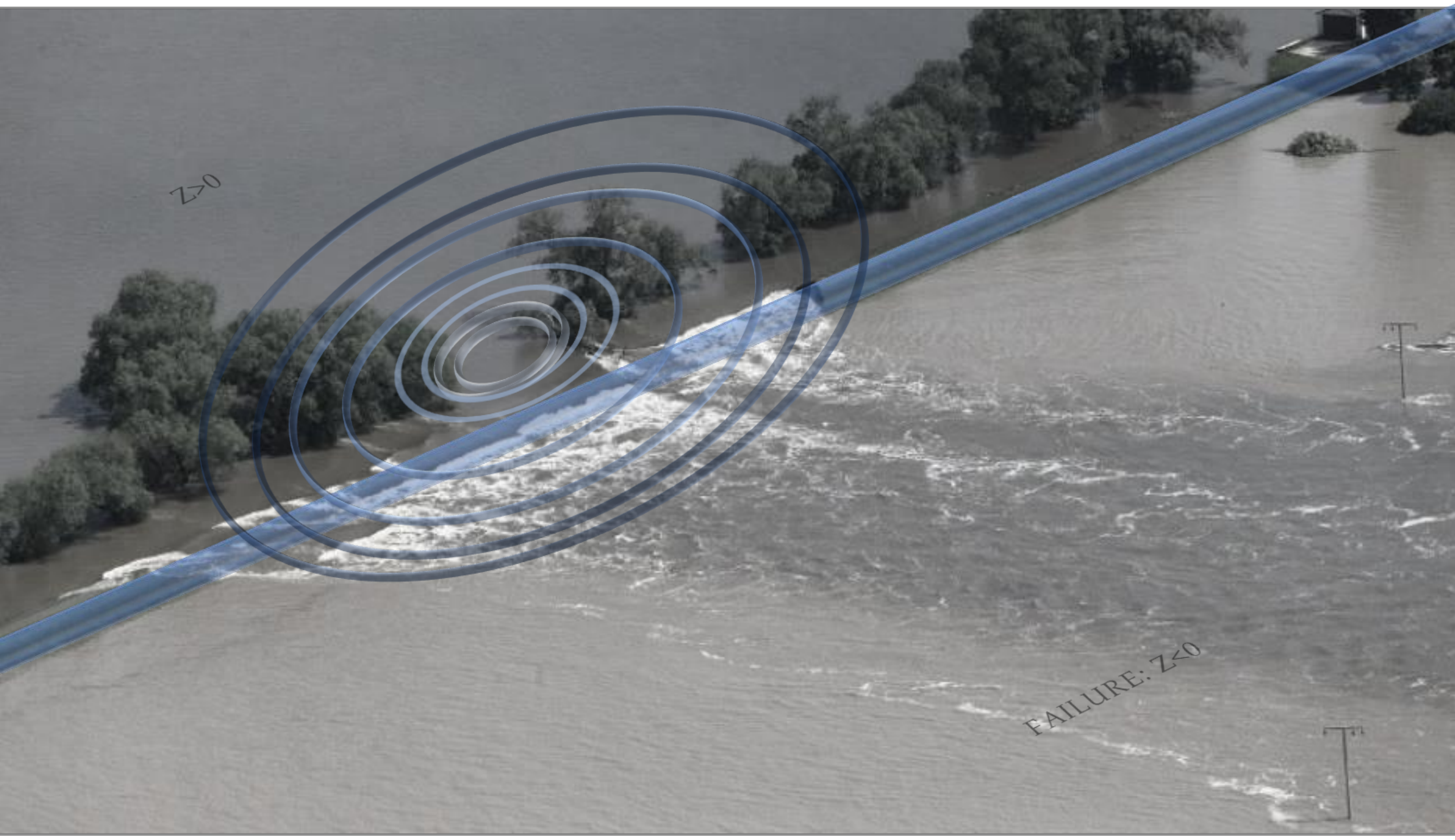

AN ANALYSIS OF THE INFLUENCE OF THE FLOOD DURATION ON SLOPE STABILITY

Master Thesis

Pauline van Leeuwen- 4277929

August 2019

Cover photo: Elbe river dike breach of 2013. https://www.augsburger-allgemeine.de/panorama/Massiver-Deichbruch-an-der-Elbe-in-Sachsen-Anhalt-id25580711.html

AN ANALYSIS OF THE INFLUENCE OF THE FLOOD DURATION ON SLOPE STABILITY

WHAT IS THE INFLUENCE OF THE FLOOD DURATION ON SLOPE STABILITY AND IN WHAT DEGREE AFFECTS THE FLOOD DURATION THE DESIGN?

By

P. van Leeuwen

in partial fulfilment of the requirements for the degree of

Master of Science
in Hydraulic Engineering

at the Delft University of Technology,
to be defended publicly on Wednesday Augustus 14, 2019 at 15:30 AM.

Supervisor:	Ir. J.C. Pol	
Thesis committee:	Prof. dr. ir. M. Kok,	TU Delft, HKV Consultants
	Ir. J.C. Pol,	TU Delft, HKV Consultants
	Dr. ir. W. Kanning,	TU Delft, Deltares
	Dr. Ir. A.P. van den Eijnden	TU Delft

An electronic version of this thesis is available at http://repository.tudelft.nl/.

PREFACE

Over the last nine months I had the pleasure to research the effects of time dependency in dike stability. Using multiple models to estimate the variables and probabilities, things were never straightforward. Even the smallest errors could result in rework and running all models again. With little research done towards the influence of time in dike stability, it sometimes felt like taking one step forward and three steps backwards. In the end the pieces fell in their places with as result the report you now have in front of you. During the time working on this research I had the opportunity to talk with a lot of experts to share experiences and knowledge on the topic. After months of hard work, I got to understand the complexities of time influencing all various aspects of dike stability.

During the time working on my research, many people offered great help in this research. A special thanks to GeoStudio for letting me use their software, without it, this thesis would not have been possible. Further I would like to thank Mick Montfoort and Jan Tigchelaar for sparring with me about my research and providing me with helpful suggestions to move forward. Also, a big thanks to my other colleagues at HKV for helping me getting through the days and the nice stories we shared during lunchtime.

A special thanks to my committee who helped me understand the problem and guiding me through the thesis. Even though I sometimes lost hope, you always got me back with your positivity, Matthijs Kok. Wim Kanning for providing direction and critical comments during the progress meetings. Bram van den Eijnden, thank you for time, feedback and the willingness to always provide a critical look on the thesis progress. Joost Pol, you have been a great help in the development of this thesis. It was great fun in helping you also with the piping experiment and seeing the effects of piping.

Finally, I would like to thank my boyfriend, Jeroen for letting me transform the house in a data centre (the six computers running the models on the kitchen table were really necessary) and for the endless support and good care while working on this thesis. Finally, I would like to thank my family for taking care of me during stressful moments and understanding moments I could not join activities to finish this research.

Pauline van Leeuwen,

Delft, August 2019

ABSTRACT

In most current dike assessments only the stationary water levels are investigated in the assessment of the stability of the inner slope, while there are differences for all kind of dikes between the stationary and transient pore water pressures and therefore in the stability. This results in a conservative probability of failure, while determinisation of a probability of failure should not be conservative but should be as realistic as possible. When time dependency is included in a calculation, an average flood duration is used, while the flood duration is highly variable.

The following research question is defined to address the problem:

"What is the influence of the flood duration on slope stability and in what degree affects the flood duration the design?"

The degree of influence of time dependency on the pore water pressures and slope stability depends on dike characteristics, flood wave characteristics and the delay in failure. The basis for answering the research question is the software SEEP/W to model the time dependent pore water pressures and the software SLOPE/W to calculate the safety factor for the stability of the inner slope. In the research theoretical dike are used and there is focused on the flood waves in the Rhine and Meuse. A correlation analysis is performed to get insight in the contribution of different flood wave shape variables to the safety factor. And a probabilistic analysis is performed using transient and stationary water levels to know the differences in probability of failure between taking the shape of a flood wave into account or not. In both probabilistic analyses is varied in the permeability and the strength of the material; the shape of the flood waves is varied in the transient analysis. In this way the contribution of the flood to the probability of failure can be quantified.

Dike characteristics

The differences in pore water pressure are especially large for dikes that consist of an impermeable material such as clay. When only the subsoil consists of clay, larger differences are expected than when only the dike body consist of clay. However, large differences in pore water pressures do not necessary lead to large differences in the safety factor. The largest differences in safety factor are obtained when uplifting of the hinterland takes place during the stationary state and/ or during the passage of a flood wave. A transient calculation is therefore most useful for dikes with an aquifer and a thin (thinner than 5 m) weak (low POP values) hinterland.

Flood wave characteristics

The differences in safety factor during a permanent water level and the passage of a flood wave are large when no stationary conditions are reached during the passage of a flood wave. This is the case for high and short flood waves. Both in the Rhine and Meuse, the amount of short waves (< 7days) is high, which increases the influence of a time dependent calculation. Also, the importance of a time dependent calculation increases when the response to the increased pore water pressures is delayed caused by the permeability of the material. The influence of the height of a flood wave on the stability increases when the soil is permeable.

Delay in failure

Time dependency causes failure of the embankment to not occur simultaneously with the maximum wave height. The flood wave is decisive for the dike failure, but the permeability and the strength of the dike determines the moment of failure.

Influence on design

Taking time dependency into account leads to higher safety factors and lower probabilities of failure with exception for dikes that consist completely out of sand. For these types of dikes, the probability of failure and safety factors are the same order of magnitude. This could affect the design, because the dikes are safer when time dependency is considered. The strength of the material is the largest contributor to the distribution of safety factors and therefore to the probability of failure (60-95%). Whereas the contribution of the permeability to the probability of failure is small (2-12%), the variation in the height and duration of a flood wave contribute for 2-20% to the probability of failure. In a permeable dike this contribution is mainly determined by the height of a flood wave, while in an impermeable dike the duration of a flood wave is of importance.

Considering the influence of time in stability probabilities of failure, this research proved that probabilities of failure taking the duration into account differ significantly from stationary calculations. It is therefore useful to take time dependency into account when determining the correct safety factor for impermeable dikes, but it is not useful in determining the correct safety factor for permeable dikes, because a stationary calculation is sufficient. In clay dikes it is useful to take the variation in height and duration into account, while for a sand dike it is sufficient to only consider the variation in height of a flood wave.

When the variation of the duration of a flood wave is not considered, it is recommended to use a representative duration of a flood wave; that results in the same total probability of failure as when the variation of the duration is included. At Lobith the duration of the representative flood wave varies from 13 - 16 days. At Borgharen the representative duration varies between the 10 – 11 days for different dike types.

TABLE OF CONTENTS

PREFACE IV
ABSTRACT V
TABLE OF CONTENTS VII
LIST OF FIGURES X
LIST OF TABLES XIII
LIST OF SYMBOLS XIV

1. INTRODUCTION 1
1.1. Problem definition 1
1.2. Relevance of the problem 2
1.2.1. Elbe river 2
1.2.2. New Orleans 4
1.2.3. Cases from the Netherlands 4
1.2.4. Conclusion 5
1.3. Objective and research question 5
1.4. Methodology and report structure 6
1.5. Definition of key concepts 7

2. LITERATURE STUDY 9
2.1. Failure mechanisms 9
2.1.1. Slope instability 10
2.2. Dike types 15
2.2.1. Lake dike 15
2.2.2. Coastal dike 16
2.2.3. River dike 16
2.2.4. Canal dike 16
2.2.5. Overview 16
2.3. Probabilistic methods 17
2.3.1. Probability of failure 18
2.3.2. Fragility curve 18
2.3.3. Overview 19
2.4. Dike assessment 19
2.4.1. Method WBI 20
2.4.2. External hydraulic processes 21
2.4.3. Internal hydraulic processes 22
2.4.4. Shear strength models 27

3. INFLUENCE OF TIME DEPENDENCY ON PORE PRESSURES AND SAFETY FACTORS 30
3.1. Goal 30
3.2. Method 31

3.2.1. *Location* 31
3.2.2. *Dike cross-section* 31
3.2.3. *Hydraulic boundary condition* 32
3.2.4. *Pore pressure field model* 34
3.2.5. *Slope stability model* 36
3.2.6. *Pore pressure field* 37
3.2.7. *Sensitivity assessment* 38
3.2.8. *Block-waves* 39
3.3. RESULTS 40
3.3.1. *Pore-water pressure field* 40
3.3.2. *Sensitivity assessment* 47
3.3.3. *Block-waves analysis* 52
3.4. CONCLUSION 54

4. CORRELATION ANALYSIS BETWEEN FLOOD WAVE VARIABLES AND DIKE STABILITY 56

4.1. GOAL 56
4.2. METHOD 56
4.2.1. *Dike cross-section* 56
4.2.2. *Hydraulic boundary condition* 56
4.2.3. *Pore pressure field model* 57
4.2.4. *Slope stability model* 57
4.2.5. *Correlation analysis* 58
4.2.6. *Probability density function* 60
4.2.7. *Response surface plot* 61
4.3. RESULTS 61
4.3.1. *Correlation analysis* 61
4.3.2. *Partial correlation analysis* 64
4.3.3. *Safety factor fit* 65
4.3.4. *Probability density functions* 66
4.4. CONCLUSION 66

5. PROBABILISTIC ANALYSIS USING TRANSIENT AND STATIONARY PRESSURES 67

5.1. GOAL 67
5.2. METHOD 68
5.2.1. *Dike cross-section* 68
5.2.2. *Hydraulic boundary condition* 68
5.2.3. *Pore pressure field model* 69
5.2.4. *Slope stability model* 70
5.2.5. *Probabilistic analysis* 70
5.3. RESULTS 74
5.3.1. *Safety factor* 74
5.3.2. *Safety factor to probability of failure* 75
5.3.3. *Total probability of failure* 76
5.3.4. *Sensitivity data* 77
5.3.5. *Delay in failure* 80
5.3.6. *Accuracy model* 81

5.4. Conclusion 82

6. REPRESENTATIVE FLOOD WAVE 84

6.1. Goal 84
6.2. Method 84
6.3. Results 85
6.4. Conclusion 86

7. DISCUSSION 87

7.1. Initial pore water pressures 87
7.2. GRADE dataset combined with SOBEK 88
7.3. Application of the probabilistic approach 88
7.4. Generalization results 90

8. CONCLUSIONS AND RECOMMENDATIONS 92

8.1. Recommendations 94

9. REFERENCES 95

APPENDICES 100

APPENDIX A. FAILURE MECHANISMS 101

APPENDIX B. RELIABILITY METHODS 105

APPENDIX C. EQUATIONS INTERNAL HYDRAULIC PROCESSES 108

APPENDIX D. GEOSTUDIO 112

APPENDIX E. METHOD WBI FOR SLOPE STABILITY 117

APPENDIX F. WATERSTANDSVERLOPENTOOL 120

APPENDIX G. INPUT SEEP/W 122

APPENDIX H. INPUT SLOPE/W 129

APPENDIX I. RESULTS PORE PRESSURE FIELD 134

APPENDIX J. RESULTS SENSITIVITY ASSESSMENT 148

APPENDIX K. UNIVARIATE PROBABILITY DISTRIBUTIONS 155

APPENDIX L. RESULTS CORRELATION ANALYSIS, SAFETY FACTOR 157

APPENDIX M. RESULTS CORRELATION ANALYSIS, VARIABLES 164

APPENDIX N. RESULTS PARTIAL CORRELATION ANALYSIS 189

APPENDIX O. RESULTS SAFETY FACTOR FITS 202

APPENDIX P. PROBABILITY DENSITY FUNCTIONS 218

APPENDIX Q. RESULTS PROBABILISTIC ANALYSIS 221

LIST OF FIGURES

Figure 1.1: Comparison of saturation state during permanent state of a flooding situation and transient state 1
Figure 1.2: Illustration of standard hydrograph method [Rijkswaterstaat, 2012] 2
Figure 1.3: Schematization storm surge [Van Velzen *et al, 2007*] 2
Figure 1.4: June 8th, 2013 at 8:36 am, initial crack 3
Figure 1.5: June 8th, 2013 at 10:38, vertical crack on the landside 3
Figure 1.6: June 8th, 2013 at 8:55 pm, continuous failure 3
Figure 1.7: June 12th, 2013 at 4.00 pm, east breach edge 3
Figure 1.8: I-wall after a gap is formed between the sheet 4
Figure 1.9: Sliding of the dike at Streefkerk [Van Ooijen, 1984] 4
Figure 1.10: Objective of the research 5
Figure 1.11: General outline of the research framework 7
Figure 2.1: Schematic overview of the most relevant failure mechanisms of flood defences [Jonkman *et al*, 2018]... 9
Figure 2.2: Slope stability inner slope [Zwanenburg *et al*, 2013] 10
Figure 2.3: Slope stability outer slope [Zwanenburg *et al*, 2013] 10
Figure 2.4: General approach limit equilibrium method [Cirkel, 1985] 13
Figure 2.5: Uplift induced dike failure 13
Figure 2.6: Van's slip surface model [Sharp *et al*, 2013] 13
Figure 2.7: Overview water systems in the Netherlands 15
Figure 2.8: Probability of failure [Jonkman *et al*, 2016] 19
Figure 2.9: Fragility curves [Pol, 2014] 19
Figure 2.10: Illustration determination failure per dike section adapted from 20
Figure 2.11: Dependence pore water response and other processes 24
Figure 2.12: Response of the phreatic surface to 25
Figure 2.13: Intrusion of pore water pressure [Van der Meer *et al*, 2004] 26
Figure 2.14: Lag in the pore water response [Van der Meer *et al*, 2004] 26
Figure 2.15: Shallow slip for purely frictional (c=0) case [Geo-Slope International, 2012] 27
Figure 2.16: Deep slip surface for homogeneous undrained case [Geo-Slope International, 2012] 27
Figure 2.17: Buoyancy of the hinterland [Van der Meer *et al*, 2004] 29
Figure 3.1: Outline to answer sub-question 1 and 2 30
Figure 3.2: Locations and rivers [Wojciechowska, 2015] 31
Figure 3.3: Typical levee cross-sections in the Netherlands 32
Figure 3.4: Example dimensions dike used in sensitivity assessmentr 32
Figure 3.5: Permanent water levels and flood waves with respect to bottom river 33
Figure 3.6: Example of the used block-waves 33
Figure 3.7: Accuracy mesh grid 35
Figure 3.8: Mesh pattern and boundary conditions used in finite element method 36
Figure 3.9: WBI Failure definition 37
Figure 3.10: Used entry and exit range in the models shown in red including number of increments 37
Figure 3.11: Locations for the pore water pressure plots 38
Figure 3.12: Phreatic surface in time 39
Figure 3.13: Factor of safety vs Time 39
Figure 3.14: Example results research question 2, sensitivity assessment 39
Figure 3.15: Example results sub-question 2: block-wave analysis 40
Figure 3.16: Pore water pressure during passage of a flood wave in the Rhine for different dike types 41
Figure 3.17: Pore water pressure over the total length of the dike body for different timesteps (cross section B)... 42
Figure 3.18: Inflow through the slope in the dike body during the passage of a flood wave. cross section C 43
Figure 3.19: Inflow from the aquifer into the dike body during the passage of a flood wave, cross section D 44
Figure 3.20: Phreatic surface for different subsoil layer materials 46
Figure 3.21: Results at the Rhine for cases with different dike core materials 48
Figure 3.22: Phreatic surface with and without core 48
Figure 3.23: Results at the Rhine for cases with and without foreshore 49
Figure 3.24: Results at the Rhine for cases with and without ditch 49
Figure 3.25: RSFD uplifting scenarios for the Rhine (left) 49

Figure 3.26: Results at the Rhine for cases with different hinterland materials ... 50
Figure 3.27: Results at the Rhine for cases with different sublayer materials ... 51
Figure 3.28: Results at the Rhine for cases with different sublayer thicknesses ... 51
Figure 3.29: Results at the Rhine for cases with different POP values ... 52
Figure 3.30: Result block-waves analysis for dike type 1 ... 53
Figure 3.31: Result block-waves analysis for dike type 2 ... 53
Figure 3.32: Result block-waves analysis for dike type 3 ... 53
Figure 3.33: Result block-waves analysis for dike type 4 ... 54
Figure 4.1: Outline to answer sub-question 3 ... 56
Figure 4.2: 1557 Selected flood waves at Lobith ... 57
Figure 4.3: 1485 Selected flood waves at Borgharen ... 57
Figure 4.4: Initial state before the passage of a flood wave ... 57
Figure 4.5: Illustration of the shape variables for two different flood waves ... 59
Figure 4.6: Example scatterplot for different dike types ... 60
Figure 4.7: Example partial scatterplot ... 60
Figure 4.8: Correlation plots between DL and the safety factor for different dike types at Lobith ... 62
Figure 4.9: Contour plot of the governing safety factor followed from the block-wave analysis ... 62
Figure 4.10: Duration (DL) and height ($hmax$) of waves in the Rhine and the Meuse ... 63
Figure 4.11: Partial scatterplot between DL the safety factor given A0 ... 64
Figure 4.12: Safety factor fit at Lobith for dike type 1 ... 65
Figure 4.13: Generalized Pareto, Lobith, b= 5.5, loc= 32.4 and scale= 0.62 ... 66
Figure 4.14: Weibull minimum, Lobith, c= 1.8 loc= 7.4 and scale= 8.3 ... 66
Figure 4.15: Student's t, Borgharen, t=7.59, loc= 33.04 and scale= 0.19 ... 66
Figure 4.16: Student's t, Borgharen, t= 4.8e+7, loc=8.63 and scale= 2.99 ... 66
Figure 5.1: Outline to answer sub-question 4 and 5 ... 67
Figure 5.2: New levee cross-sections with used mean values ... 68
Figure 5.3: 25 Selected flood waves at Lobith and Borgharen ... 69
Figure 5.4: Phreatic surface calculated with SEEP/W and calculated using the method of WBI (2017) ... 70
Figure 5.5: Extra- and interpolated probability of failure ... 72
Figure 5.6: Example of total probability of failure calculation ... 72
Figure 5.7: Example sensitivity data ... 73
Figure 5.8: Probability of failure versus average safety factor to predict the probability of failure ... 74
Figure 5.9: Safety factors for stationary water levels and during the passage of a flood wave ... 75
Figure 5.10: Probability density function for a clayey dyke on sand subsoil for a flood wave from the Meuse ... 77
Figure 5.11: Reflex response for dike type 1 for flood waves from the Rhine ... 77
Figure 5.12: Time after the peak of the flood wave where the safety factor is smallest ... 80
Figure 5.13: Time of failure (FoS<1) ... 80
Figure 5.14: Time of failure including probability of occurrence P(FoS<1) × pf(hmax)/50 × pf (D50) ... 80
Figure 5.15: Accuracy check for dike type 1 at Lobith ... 81
Figure 6.1: Probability density function without including probability of occurrence of the duration ... 84
Figure 6.2: All 1557 flood waves at Lobith with different percentile flood waves ... 84
Figure 6.3: Representative flood wave at Lobith ... 86
Figure 6.4: Representative flood wave at Borgharen ... 86
Figure A.1: Micro instability process [Hart, 2018] ... 102
Figure A.2: Pipe development clayey levee on sand soil [[Hart, 2018] ... 103
Figure A.3: Pipe development levee on clay/peat layer [Hart, 2018] ... 104
Figure B.1: Probability density functions showing the variations in load (red) and resistance (green) ... 107
Figure C.1: Flow over layer separations [Van der Meer *et al*, 2004] ... 111
Figure D.1: Volumetric water content (storage) function [Geo-Slope International Ltd., 2012] ... 113
Figure D.2: Typical storage functions for 3 soil types [Geo-Slope International Ltd., 2012] ... 113
Figure D.3: Sample functions in GeoStudio ... 114
Figure D.4: Half-sine interslice force function [Geo-Slope International Ltd., 2012] ... 115
Figure D.5: A factor of safety versus lambda plot [Geo-Slope International Ltd., 2012] ... 115
Figure D.6: Slip surface without considering the crack angle [Geo-Slope] ... 116
Figure D.7: The force of the normal at the base of the first slice points away from the slice ... 116
Figure D.8: Slip surface with considering the crack angle [Geo-Slope] ... 116
Figure F.1: Design hydrograph of the water level Rotterdam, Rhine and Meuse ... 121

Figure G.1: Red point indicates point for which the pressure is compared ... 124
Figure G.2: Accuracy mesh grid ... 124
Figure G.3: Accuracy right boundary ... 125
Figure G.4: Accuracy right boundary in time ... 126
Figure G.5: Accuracy left boundary ... 127
Figure G.6: Accuracy left boundary in time ... 128
Figure H.1: Entry and exit range ... 131
Figure H.2: Accuracy entry range ... 131
Figure H.3: Accuracy exit range ... 132
Figure H.4: Accuracy radius ... 133
Figure I.1: RPD In time for different dike types for different flood waves ... 147

LIST OF TABLES

Table 2.1: Overview influence hydraulic loads on failure mechanisms ... 10
Table 2.2: Overview different static slope stability methods ... 14
Table 2.3: Overview different models to analyse slope stability ... 14
Table 2.4: Overview dike types and their characteristics adapted from [Van der Meer *et al*, 2004] ... 17
Table 2.5: Comparison different reliability methods ... 19
Table 2.6: Indicated characteristic duration boundaries ... 21
Table 2.7: Phreatic surface different cases [Van der Meer, 2004 & Kanning, 2016] ... 23
Table 2.8: Overview different software packages for groundwater flow calculations ... 24
Table 3.1: Variable variables in the sensitivity assessment ... 32
Table 3.2: Delay in response during the passage of a flood wave in days ... 45
Table 3.3: RPD for different dike types for different water level hydrographs ... 45
Table 4.1: Analysed flood waves shape variables ... 59
Table 4.2: Spearman correlation between variables and the safety factor ... 61
Table 4.3: Partial correlation between the FoS, DL and the shape variables ... 64
Table 4.4: RMSE fit based on hmax and D50 & Hmax and RA0 ... 65
Table 4.5: Extrapolated height and duration for which the safety factor is 1 ... 65
Table 5.1: Selected flood waves in the Rhine at Lobith ... 69
Table 5.2: Selected flood waves in the Meuse at Borgharen ... 69
Table 5.3: Stochastic variables with distribution type ... 71
Table 5.4: Safety factor and probability of failure of two events from the Rhine ... 75
Table 5.5: Probability of failure including probability of occurrence ... 77
Table 5.6: Relative Contribution of a variable to the spread of the safety factor in a transient calculation [%] ... 79
Table 5.7: Relative Contribution of a variable to the spread of the safety factor in a stationary calculation ... 79
Table 5.8: Relative Contribution of a variable to the spread of the safety factor ... 79
Table 5.9: total probability of failure calculated with 25 and 1500 flood waves ... 82
Table 6.1: Duration that results in the same total probability of failure ... 85
Table D.1: Overview differences choices WBI and GeoStudio looking at uplifting ... 116
Table E.1: Model factors in Ring test [WBI, 2016] ... 118
Table E.2: Material factors in Ring test [WBI, 2016] ... 118
Table F.1: Input Waterstandsverlopentool ... 121
Table G.1: Accuracy mesh grid, error ... 125
Table G.2: Accuracy right boundary, error ... 126
Table G.3: Accuracy right boundary in time, error ... 126
Table G.4: Accuracy left boundary, error ... 127
Table G.5: Accuracy left boundary in time, error ... 128
Table H.1: Accuracy entry range, error ... 131
Table H.2: Accuracy exit range, error ... 132
Table H.3: Accuracy radius, error ... 133
Table M.1: Spearman correlation between local shape variables at Lobith ... 165
Table M.2: Spearman correlation between local shape variables at Borgharen ... 165
Table N.1: Partial correlation between the shape variables and the safety factor given DL ... 190
Table N.2: Partial correlation between the shape variables and the safety factor given AL ... 193
Table N.3: Partial correlation between the shape variables and the safety factor given $RA0$ ... 197
Table N.4: Partial correlation between the shape variables and the safety factor given $hmax$ ... 199
Table O.1: Coefficients safety factor fit based on hmax and D50 ... 203
Table O.2: RMSE fit based on hmax and D50 & Hmax & RA0 and DL and AL and RA0 ... 203
Table O.3: Coefficients safety factor fit based on hmax and RA0 ... 207
Table O.4: RMSE fit based on hmax and D50 & Hmax & RA0 and DL and AL and RA0 ... 207
Table O.5: RMSE fit based on hmax and D50 & Hmax & RA0 and DL and AL and RA0 ... 212
Table O.6: RMSE fit based on hmax and D50 & Hmax & RA0 and DL and AL and RA0 ... 213
Table O.7: RMSE fit based on hmax and D50 & Hmax & RA0 and DL and AL and RA0 ... 216

LIST OF SYMBOLS

Romans Symbols	Explanation	Unit
A_0	The area above the level $h = 0$ (total area)	[L²]
$A_{50\%}$	The storm area above the level h= $0.5h_{max}$	[L²]
$A_{85\%}$	The storm area above the level $h = 0.5\ h_{max}$	[L²]
a_l	Mechanism sensitive factor of the dike trajectory length	[-]
A_L	The area above the level h= $L\ m$	[L²]
b_l	Representative length for the analysis in a cross-section	[m]
C	Hydraulic resistance	[day]
c'	Cohesion	[kN/m²]
c_v	Consolidation coefficient	[m²/s]
d	Depth of sand with respect to the polder water level	[m]
D	Thickness aquifer	[m]
D_d	Drainage distance	[m]
$D_{50\%}$	The duration that the water level is higher than the level $h = 0.5h_{max}$	[T]
$D_{50,i}$	Range of the duration between $\min(D_{50})$ and $\max(D_{50})$ with 100 steps	[T]
$D_{85\%}$	The duration that the water level is higher than the level $h = 0.85h_{max}$	[T]
D_L	The duration the water level is higher than a chosen level L, $h = L$	[T]
E	The interslice normal force	[N]
f_{D50}	Fitted probability density function of the duration	[-]
f_{hmax}	Fitted probability density function of the maximum water level	[-]
f_R	Distribution function for resistance	[-]
f_{RS}	Joint probability density function	[-]
f_s	Distribution function for load	[-]
F	Total probability of failure	[-]
$FoS_{Stationary}$	Safety factor in the stationary state	[-]
$FoS_{Transient}$	Lowest safety factor in the transient state	[-]
FoS_{design}	Factor of safety for dike stability	[-]
$f(x)$	A function for the interslice force	[N]
g	Gravitational acceleration	[m²/s]
h	Head related to the base of the aquifer	[m]
h_{max}	Maximum water level	[L]
$h_{max,i}$	Range of the maximum height between $\min(h_{\max})$ and $\max(h_{max})$ with 100 steps	[m]
k	Darcy's coefficient of permeability or hydraulic conductivity	[m/s]
K_0	Matching point at saturation	[cm/day]
$K(S_e)$	Hydraulic conductivity function	[m²/day]
L	Empirical pore-connectivity variable	[-]
$L_{traject}$	Length of the dike trajectory, as stated in the Dutch water	[m]
m	Stress increase exponent	[-]
M_a	Driving moment	[N m]
M_r	Resisting moment	[N m]
m_v	Ground compressibility	[m²/N]
n	Effective phreatic porosity	[-]
n_d	Measure of the pore-size distribution	[-]
N	Nett rain infiltration	[m/s]
N_{dsn}	Length-effect factor	[-]
$n_{50\%}$	Duration above a certain threshold, $h = 0.5h_{max}$, divided by the total duration	[-]
$n_{85\%}$	Duration above a certain threshold, $h = 0.85h_{max}$, divided by the total duration	[-]
n_l	Duration above a certain threshold, $h = L$, divided by the total duration	[-]
$P_{dsn,norm}$	Norm / target probability of failure	[1/year]

$P_{f,dsn}$	Probability of failure per cross-section	[1/year]
$P_{f,i}$	Probability of failure per cross-section per scenario	[1/year]
$P_{norm,dsn}$	Required probability of failure per cross-section	[1/year]
P_{norm}	Safety standard of the dike	[1/year]
$P(S_i)$	Probability of the scenario	[1/year]
$p_{Stationairy}$	Pressure during stationary state	[N/m²]
$p_{Transient}$	Pressure during transient state	[N/m²]
q	Specific discharge	[m/s]
Q	Composite forces	[N]
RA_0	A_0 divided by the product of the total duration and maximum water level	[-]
$RA_{50\%}$	$A_{50\%}$ divided by the product of $D_{50\%}$ and h_{max} relative to level $h = 0.5h_{max}$	[-]
$RA_{85\%}$	$V_{85\%}$ divided by the product of $D_{85\%}$ and h_{max} relative to level $h = 0.85h_{max}$	[-]
RA_L	A_L divided by the product of D_L and h_{max} relative to level $h = L\ m$	[-]
R_k	Characteristic value for the resistance	
S_e	Effective saturation	[-]
S_k	Characteristic value for the load	
s_u	The undrained shear strength	[kN/m²]
t_{99}	Hydrodynamic period	[s]
t	Time	[s]
T	Transmissivity	[m²/day]
u	Internal pore pressure	[kN/m²]
X	The interslice shear force	[N]
z	Altitude of considered point related to reference plan	[m]

Greek Symbols	**Explanation**	**Unit**
α	Related to the inverse of the air entry suction	[1/cm]
α_i	Sensitivity factor of a variable	
β	Reliability index	[-]
β_c	Water compressibility	[m²/N]
$\beta_{norm,dsn}$	Required reliability index	[-]
γ	Partial factor	[-]
γ_d	Model factor	[-]
γ_s	Volumetric weight of the soil	[kN/m³]
γ_n	Damage factor, β_T – dependent	[-]
γ_w	Water volumetric weight	[kN/m³]
λ	Leakage factor	[m]
λ_{dec}	The percentage (in decimal form) of the function used	[-]
$\theta(\psi)$	Water retention curve	[-]
θ_r	Residual water content	[-]
θ_s	Saturated water content	[-]
μ_z	Mean of the limit state equation	
ρ	Volumetric mass	[kN/m³]
ρ_s	Spearman correlation coefficient	[-]
σ	Normal stress	[N m⁻²]
σ'	Effective stress	[kN/m²]
σ_i	Standard deviation of a variable	
$\sigma'_{v,i}$	In situ effective vertical stress	[kN/m²]
σ'_{vs}	Effective stress at the layer separation	[kN/m²]
σ'_{vy}	Vertical yield stress	[kN/m²]
σ_z	Standard deviation of the limit state equation	
τ	Shear stress	[N m⁻²]
φ	Head	[m]
φ'	Effective friction angle	[°]
ϕ_n	Cumulative normal distribution	[-]

ϕ	Internal friction angle	[°]
ϕ_g	Boundary potential	[m]
ϕ_p	Polder water level	[m]
ψ	Suction pressure	[cm]
ω	Contribution of a failure mechanism to the total failure	[-]
ϖ_{factor}	Factor that indicates the differences between the safety factor in the transient and stationary state	[-]
Φ	Crack angle	[°]

Abbreviations	**Explanation**	**Unit**
CDF	Cumulative density function	
FEM	Finite Element Method	[-]
LEM	Limit equilibrium method	[-]
NTS	Not to scale	[-]
OCR	Overconsolidation ratio	[kN/m²]
PDF	Probability density function	
POP	Pre-overburden pressure	[kN/m²]
R	Resistance	
RPD	Relative pressure difference	[-]
RSFD	Relative safety factor difference	[-]
S	Load	
SRM	Strength reduction method	[-]
STD	Standard deviation	
Z	Limit state	

1. INTRODUCTION

1.1. Problem definition

All levees are subjected to internal flows caused by permanent or transient external hydraulic conditions. Several failure mechanisms of dikes are driven by these internal flows, because it determines the pore pressure field. How the pore water responses, depends on geotechnical variables, but also on the flood duration. In most current stability analyses and designs the flood duration is either neglected (stationary assumed) or an average flood duration is used, where the last is often used for analysing revetments.

Slope stability calculations are performed with a permanent water level, since working with a permanent water level is easier and often safer to analyse the levee with [Sharp *et al*, 2013]. It is a conservative choice because sometimes higher seepage pressures, volumes, velocities and gradient are found [Sharp *et al*, 2013]. In Figure 1.1 the differences are shown between a permanent state and a transient state.

a) Permanent flow

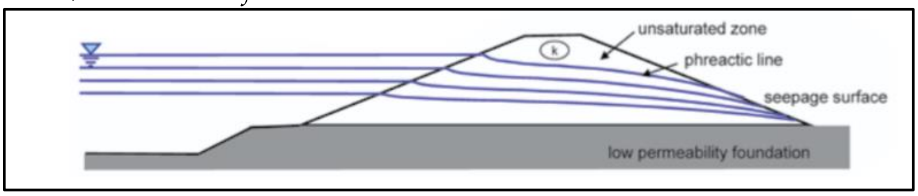

b) Transient flow

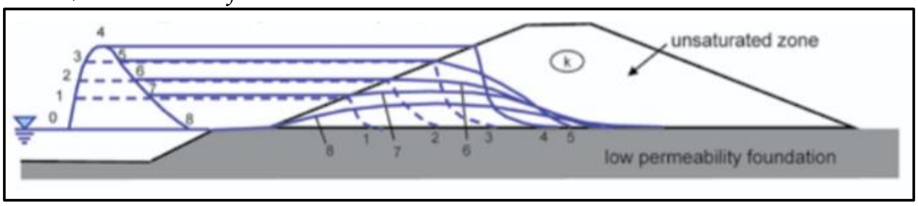

FIGURE 1.1: COMPARISON OF SATURATION STATE DURING PERMANENT STATE OF A FLOODING SITUATION (A) AND TRANSIENT STATE (B) [SHARP *ET AL*, 2013]

It is less suitable to determine the risk of failure of a levee based on models that neglect the duration of the flood duration. However, determinisation of a probability of failure should not be conservative but should be as realistic as possible [Moellmann *et al*, 2011]. In the international levee handbook (2013) is stated that it is relevant to take the duration of flood (the hydrograph of the flood level) into account. A transient analysis provides a more realistic and less conservative representation of the pore pressures, because it takes the response of the pore pressures of the flood wave into account. However, such calculations are more complex and time-consuming than steady-state analyses [Sharp *et al*, 2013].

When a transient analysis is performed, a shape of a flood wave is used with an average duration. Storm surge at sea is modelled with a trapezium shape with a duration of 33.2 hours. Figure 1.2 and Figure 1.3 illustrates the used flood waves and storm surge in transient calculations.

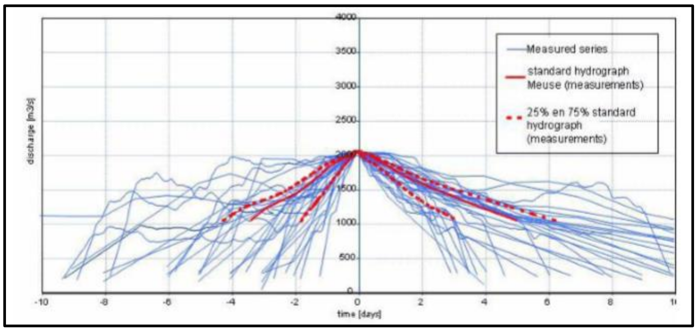

FIGURE 1.2: ILLUSTRATION OF STANDARD HYDROGRAPH METHOD [RIJKSWATERSTAAT, 2012]

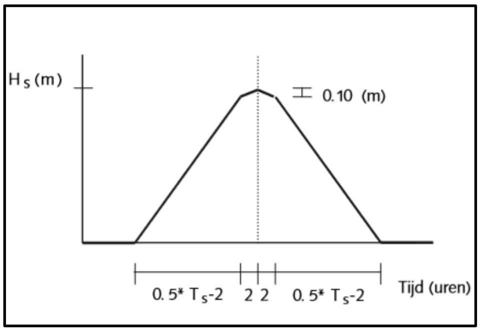

FIGURE 1.3: SCHEMATIZATION STORM SURGE [VAN VELZEN *ET AL, 2007*]

When a duration is used, an average duration is used, but the flood duration is highly variable and ranges from hours along coastal levees to weeks for levees along the rivers. Especially rivers located downstream are enforced with a long flood duration. Additionally, effects of flood duration are non-linear: two floods with a duration of 5 days are not as dangerous as one flood with a duration of 10 days. Also, the storm surge is not constant in duration and shape. Ideally, the duration is assessed probabilistically in a stability calculation, to include the large variation in duration and the non-linear effect.

A probabilistic approach is a good technique for considering all uncertainties towards hydrological, hydraulic and geotechnical variables [Moellmann *et al,* 2011]. The disadvantage a probabilistic approach is that the magnitude and frequency of loadings must be determined; variables, their statistical distribution and analytical models must be selected and the magnitude and extent of physical changes must be assessed. To apply the probabilistic approach in a correct maar, the underlying mechanisms must be understood and determined appropriately. Using a probabilistic transient analysis, it is expected that this will lead to higher loads than in current deterministic approaches, because the flood duration is not averaged [Pol, 2018]. Sharp *et al* (2013) suggests using a back-analysis to compare the computational predictions with levees for which monitoring data is. A sensitivity assessment can also be useful to verify the performance of levees under high water.

1.2. Relevance of the problem

In most current slope stability analyses the flood duration is neglected and therefore time dependent processes in the levee are neglected. But time dependent processes play an important role in the shear failure of dikes. To illustrate this, different cases are compared; failure and non-failure dikes along the Elbe river during a flood in June 2013, failure of different flood protections in New Orleans caused by hurricane Katrina and shear failure cases in the Netherlands.

1.2.1. Elbe river

In May and June 2013, heavy rainfalls lead to high water levels and extreme discharges in the Elbe river. At several location the water rose with 4.6 meter between March 15th and June 8th. During the passage of the flood wave; a variety of dikes breached or were damaged. Looking at a dike near Breitenhagen, the damage started on June 8th with the appearance of a crack next to the road on the edge of the land side slope. The crack grew for two hours, after which the inner slope slid away within a minute. After two hours the inner slope slid horizontally and within four hours the breakdown reached the waterside slope. After 10 hours the water retaining function was lost and the hinterland was flooded, see Figure 1.4 till Figure 1.7. [Gesellschaft für Grundbau und Umwelttechnik mbH, 2013]

The dike did not fail immediately when the peak water level was reached at June 8th. The steady state phreatic line was not reached, due to the shape of the flood wave and the permeability of the dike and layer material. There was a delay in the increase of the phreatic water level in the dike of maximum three days. From this can be concluded, that the flood wave was decisive for the breaching, the increase of the phreatic line and the pore water pressure determined the moment of failure. [Gesellschaft für Grundbau und Umwelttechnik mbH, 2013]

During the same flood, sliding only occurred for one other dike in Hohengöhren [Herzlichst, 2013]. The increase of the phreatic line and the pore water pressures were not large enough to cause the dike to fail. Where the dike failed at Breitenhagen, the duration of the flood at Hohengöhren too short to cause a dike breach.

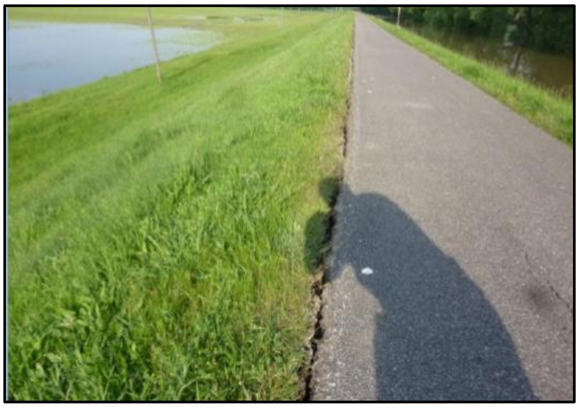

FIGURE 1.4: JUNE 8TH, 2013 AT 8:36 AM, INITIAL CRACK [GESELLSCHAFT FÜR GRUNDBAU UND UMWELTTECHNIK MBH, 2013]

FIGURE 1.5: JUNE 8TH, 2013 AT 10:38, VERTICAL CRACK ON THE LANDSIDE [GESELLSCHAFT FÜR GRUNDBAU UND UMWELTTECHNIK MBH, 2013]

FIGURE 1.6: JUNE 8TH, 2013 AT 8:55 PM, CONTINUOUS FAILURE [GESELLSCHAFT FÜR GRUNDBAU UND UMWELTTECHNIK MBH, 2013]

FIGURE 1.7: JUNE 12TH, 2013 AT 4.00 PM, EAST BREACH EDGE [GESELLSCHAFT FÜR GRUNDBAU UND UMWELTTECHNIK MBH, 2013]

1.2.2. New Orleans

During Hurricane Katrina in 2005, over fifty breaches were counted in New Orleans. Most of the failures were dikes that contained an I-wall in the middle. The increasing water level caused by the Hurricane, caused the amount of turbulence and erosion to increase in front of the I-wall. A gap arose causing the wall to deflect and after the water filled the gap the walls destabilized when finally, the inner slope failed [Sharp *et al*, 2013]. The duration of the flood has in this example influence on the development of the gap in front of the I-wall and on the development of the pore water pressure, which caused sliding of the inner slope, see Figure 1.8 [Duncan *et al,* 2014].

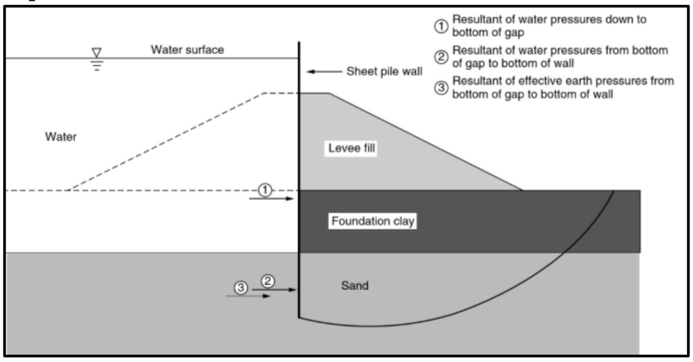

FIGURE 1.8: I-WALL AFTER A GAP IS FORMED BETWEEN THE SHEET PILE AND THE LEVEE DIKE [DUNCAN *ET AL,* 2014]

1.2.3. Cases from the Netherlands

In the Netherlands there are different dikes that failed in a similar way as shown in the example above. For example, in 1984, the Lekdijk near Streefkerk, when the hinterland still consisted of sand and on top of the hinterland a weak clayey layer was present. During high water, the pore water pressures in the aquifer increased and lifted the weak layers. A crack was formed and sliding occurred, see Figure 1.9 [van den Dikkenberg, 2009]. The largest deformation at Streefkerk occurred within a day, where the next day the deformation velocity decreased. Another example is in Bergambacht when a sliding test was performed. This showed, that the largest deformation occurred within an hour and in another test at the IJkdijk sliding even occurred within a few minutes [WBI, 2016]. For all three cases, sliding occurred of the inner slope caused by uplifting of the weak layers, but the failure time is completely different. From these cases can be concluded that the dike stabilities are dependent of time. In these cases, the flood duration played an important role in the development of the pore water pressures under the weak soil layers.

FIGURE 1.9: SLIDING OF THE DIKE AT STREEFKERK [VAN OOIJEN, 1984]

1.2.4. Conclusion

The duration of the flood wave plays an important role in slope failures. First, the flood duration influences the development of the pore water pressures (phreatic surface and the hydraulic head). The phreatic line in the dike and the hydraulic head in the aquifer under the dike increase during the passage of a flood wave and therefore determines the moment of failure (but the height and the duration of the flood wave are decisive). Besides, the duration also affects mechanisms like erosion. When the duration of the flood wave is short or the permeability of the dike material is low, the effect on the failure mechanism is smaller. The longer the duration, the larger the damage.

1.3. Objective and research question

The following research question is defined to address the problem:

"What is the influence of the flood duration on slope stability and in what degree affects the flood duration the design?"

The research question is addressed by six sub-questions:

1. What is the influence of time dependency on the pore water pressures?
2. What is the influence of time dependency on slope stability?
3. Which Rhine and Meuse flood wave shape variables affect the stability of the inner slope?
4. What is the effect on the probability of failure of slope stability by taking time dependency into account and wat are the main variables determining this effect?
5. What are the differences in slope stability using the simplified pore water pressures of WBI and the transient pore water pressures?
6. What is a representative flood wave in a deterministic stability calculation?

The objective of the research is to investigate the variation in the duration and height of a flood wave, the effect of it on the response of the pore water pressures and the effect of the pore water pressures on the stability of the inner slope (see Figure 1.10). These three processes are combined in deterministic and probabilistic calculations to investigate how it affects the design of a dike. Finally, an advice is given about which variables are dominant in the determination of time dependent behaviour and to which degree it effects the design compared to stationary calculations. The research is focused on stability of the inner slope. The distribution of flood waves are investigated in the Rhine and the Meuse.

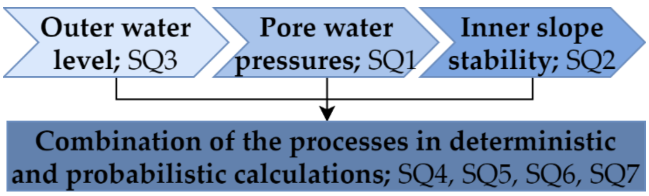

FIGURE 1.10: OBJECTIVE OF THE RESEARCH

1.4. Methodology and report structure

The objective of this thesis is addressed by performing a model study to develop a calculation method in which time dependent process are considered in the assessment of the stability of the inner slope. The software SEEP/W is used to model time dependent pore water pressures and the software SLOPE/W is used to calculate the stability safety factor of the inner slope. The research uses a theoretical dike and focuses on the flood waves in the Rhine and Meuse. The general outline of the research framework is shown in Figure 1.11. A detailed description of the method is given in the first paragraphs of Chapter 3, 4 and 5. In which sub-question 1 till 5 are answered.

The first Chapter provides a brief introduction to the relevance of time dependent processes in the assessment of slope stability, followed by the problem statement along with objectives and research questions. In Chapter 2, the theoretical background about the failure mechanisms slope stability, dike assessment and the software GeoStudio are provided.

In Chapter 3, the pore pressure field is modelled for a transient and stationary state to know the difference in the pressure field when the flood duration is taken into consideration. Secondly, influence of time dependency on slope stability is investigated by performing a sensitivity assessment, from which is concluded which dike variables are sensitive for a transient calculation. Chapter 3 is used to answer sub-question 1 and 2 and is needed for the next sub-questions.

The influence of different flood wave shape variables on the stability of the inner slope is investigated in Chapter 4 and is used to answer sub-question 3. From this can be concluded which duration and height shape variables of a flood wave can be used to predict the safety factor of the inner slope. This is investigated by performing a correlation analysis between the shape variables of the flood waves from the Rhine and the Meuse and the safety factors of different theoretical dikes.

In Chapter 5, a probabilistic analysis is performed using stationary and transient water levels. In both analyses, the permeability and strength of the material are uncertain. In the transient analysis, the shape of the flood waves is uncertain as well. The probability of failure by considering the probability of occurrence of an event is determined, the influence of the uncertainties is quantified and the main variables that have the greatest effect on the probability of failure are determined. Doing this, the effect of considering time dependency on the probability of failure of slope stability is investigated. Resulting safety factors for inner slope are also compared to the case when the pore water pressures are calculated using the method described by WBI (2017). In Chapter 5, sub-question 4 and 5 are answered.

In Chapter 6 an advice is given about the use of a representative flood wave in a deterministic calculation and with this advice sub-question 6 is answered.

In Chapter 7 a discussion is given about the obtained results, followed by a conclusion by answering the research question in Chapter 8.

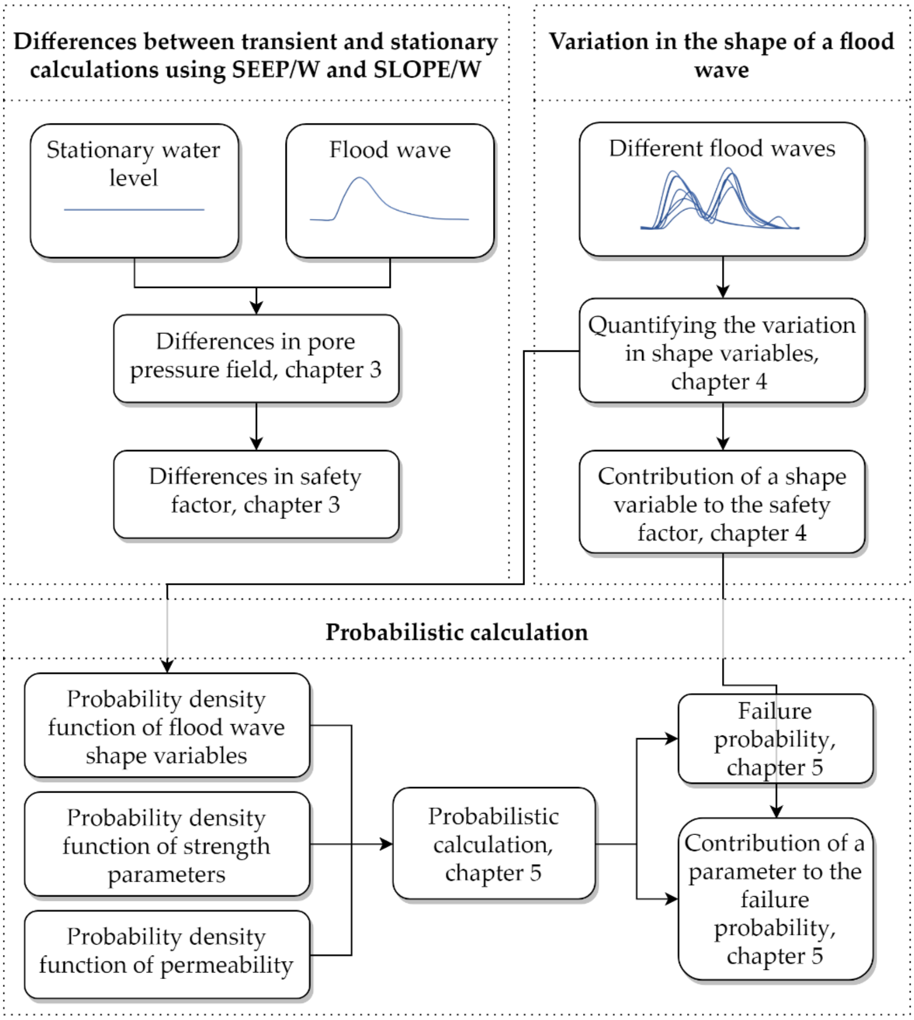

FIGURE 1.11: GENERAL OUTLINE OF THE RESEARCH FRAMEWORK

1.5. Definition of key concepts

When the duration of the water level is neglected (infinite adopted), the water level is constant and does not vary, we speak of a **stationary/permanent water level.** The mean statistical properties do not vary in time. The **design water level** in the Netherlands is a permanent water level for which the probability of exceedance is chosen in such a way that the safety standard satisfies the specified conditions.

A **hydrograph** shows discharge or water level in time. A **flood wave** shows the discharge or water level in time for a **flood,** which is a hydrologic event that is used to evaluate risk with. A **design flood** or **design hydrograph** is used in the consideration of defined design criteria. The peak discharge has a predefined return period or probability of exceedance, and the shape is determined by averaging all hydrographs in a dataset. When in this thesis is spoken about a hydrograph or flood wave, a variation in the water level over time is meant.

The **flood duration** is the duration of the elevated water level and discharge above some threshold. When in this thesis is spoken about duration, the duration of the elevated water level above a threshold is meant.

Steady state pore water pressures are reached during the occurrence of a permanent water level. The pore water pressures are in equilibrium. This equilibrium is not reached during the passage of a flood wave, when the soil is partially saturated. The pore water pressures are now depending on time; it refers to a temporary condition. There is spoken about pore water pressures that shows **time dependent/ transient** behaviour.

The **water table** is the surface where the water pressure head is equal to the atmospheric pressure. In an unconfined aquifer it is the same as the **piezometric surface** or **phreatic surface.** This provides an indication of the direction of groundwater flow and it determines the hydraulic gradients.

Slope stability is the process where the ground slides over a deep slip surface. The cause of this phenomenon is the loss of equilibrium in the groundmass due to an increase of the water pressure in the soil, increase of the driving moment or a decrease of the opposing moment

The **representative pressure difference (*RPD*)** is a variable introduced in this thesis to compare the steady state pore water pressures during a permanent water level with the pore water pressure caused by the passage of a flood wave. It is the permanent pore water pressure divided by the transient pore water pressures. The larger this variable, the larger the differences between the permanent and transient state.

A similar variable, the **representative safety factor differences (*$RSFD$*)** is introduced. This variable is used to compare the governing safety factor for stability of the inner slope during the passage of a flood wave with the safety factor associated with a permanent water level. The $RSFD$ is the governing safety factor during the passage of a flood wave divided by the safety factor associated with the parament water level. The larger this factor the larger the differences between the stationary and transient states.

2. LITERATURE STUDY

This research focusses on the effect of the variation of the flood wave on the pore water pressures and the effect of the pore water pressures on the stability of the inner slope. In this section is looked at how different failures of mechanisms are impacted by variations of flood waves with the focus on the mechanism slope stability of the inner slope. Follow up with considering different dike types on systems characteristics and loads, to know which dike types are expected to be important in the consideration of time dependent processes. Furthermore, a dike assessment is performed to get an insight in all processes involved. After this assessment more attention is paid to the deterministic and probabilistic calculations, because all processes are combined in this type of calculations. At the end of each section an overview is given, which is used later on the research.

2.1. Failure mechanisms

A dike should guarantee a barrier between the water and the protected area. Any water that surpasses the dike during high water should not be too big since it can cause failure of the dike. In Figure 2.1 the relevant failure mechanisms of primary flood defences are shown. In *Appendix A. Failure mechanisms*, a short description of the failure mechanisms is given, a dike fails when it loses its water retention function. When some parts of a dike collapse (e.g. sliding of the inner slope), it does not necessarily lose its water retention function and therefore it does not always lead to a dike failure.

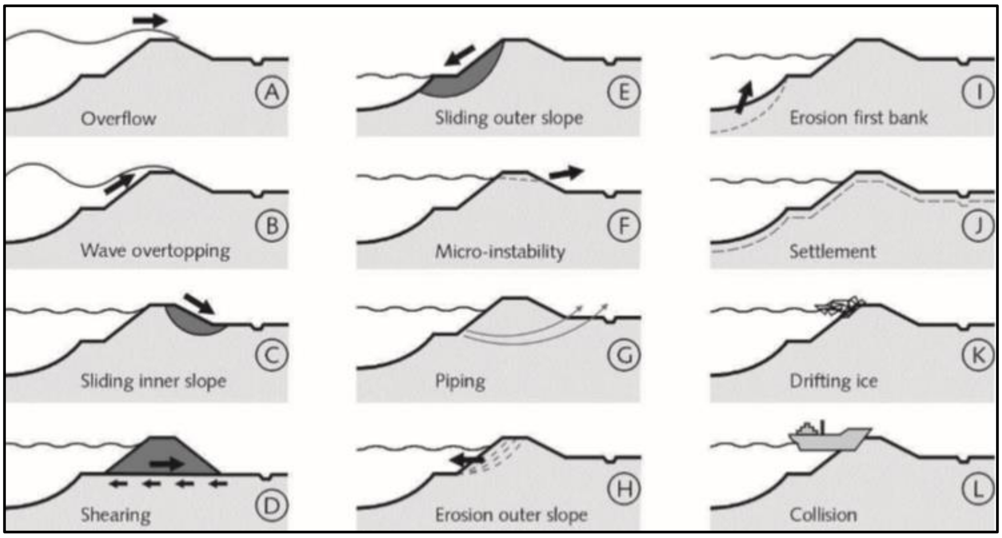

FIGURE 2.1: SCHEMATIC OVERVIEW OF THE MOST RELEVANT FAILURE MECHANISMS OF FLOOD DEFENCES [JONKMAN *ET AL*, 2018]

In Table 2.1 an overview is given on the influence of the different hydraulic loads on the failure mechanisms. Therefore, it can be concluded that internal erosion, slope stability, micro stability and settlement failure mechanisms are dependent on internal hydraulic processes (pore water pressure and flows), high water levels and the duration of the different water levels. This research will focus on the mechanism slope stability of the inner slope. Slope stability of the inner slope is important when the pore water pressure is high in both the cover layer and the dike body itself.

The chart below displays the important soil structure characteristics for the inner slope stability mechanisms [Förster *et al*, 2017].

- Pore water pressure in dike body, aquifer and cover layer of the hinterland
- Weak soil layers hinterland
- Clay/ sand dike on permeable/ impermeable soil

TABLE 2.1: OVERVIEW INFLUENCE HYDRAULIC LOADS ON FAILURE MECHANISMS

Failure mechanism	High water level	Low water level (after high water level)	Internal hydraulic processes	Waves	Duration of different water levels	Precipitation
Overflow	+	-	-	+/-	-	-
Overtopping	+	-	-	+	-	-
Slope instability:						
- Inner slope	+	-	+	-	+	+
- Outer slope	+/-	+	+	-	+/-	+
Micro instability	+	+	+/-	-	+	+
Shearing	+		-	-	-	-
Piping	+	-	+	-	+	+
Settlement	+/-	-	+/-	-	+/-	+/-
	Legend: + Important +/- Of influence - Not relevant					

2.1.1. Slope instability

A phenomenological description of slope failure is given below. Following up this description are the detailed calculation methods. At last there will be an overview with the available software.

2.1.1.1. Phenomenological description

Slope stability is the process where the ground slides over a deep slip surface. The cause of this phenomenon is the loss of equilibrium in the groundmass due to an increase of the water pressure in the soil (high outer water level or heavy rainfall), increase of the driving moment (e.g. load on the levee, traffic) or a decrease of the opposing moment (construction of a ditch at the toe) [Hart, 2018]. This report concerns only the increase of the water pressures. Precipitation is not considered, because the chance of simultaneous occurrence of high water and extreme precipitation is small. Failure of the slopes can occur within a few hours to a few days. The process goes fast within the first hours, after which the sliding velocity decreases [Hart, 2018]. After sliding a new equilibrium is found; after which a second slide can occur. But the occurrence of a second slide does not occur necessary.

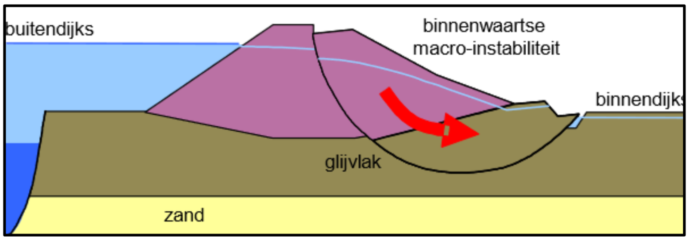

FIGURE 2.2: SLOPE STABILITY INNER SLOPE [ZWANENBURG *ET AL*, 2013]

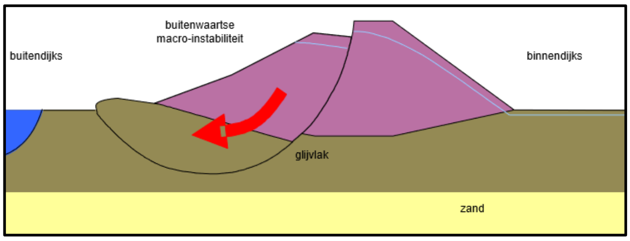

FIGURE 2.3: SLOPE STABILITY OUTER SLOPE [ZWANENBURG *ET AL*, 2013]

Inner slope

The phreatic level in the levee and the head in the soil under the levee will increase during high water as a result of infiltration of water in the outer slope or in the aquifers under the levee. This increases the pore water pressure which causes a reduction of the effective stress and so a reduction of the shear strength of the soil. The problem relating slope instability is mainly the reduction of the shear strength and not the increase of the load due to the water [Hart 2018]. Cracks will appear and indicate the place of the slip surface. On the landside of the crack the levee will slide. This process continues till a new equilibrium is found. The levee fails when it loses the water-retaining function. This usually implies the initiation or development of a breach due which water can pass the levee. The levee breach growth starts when the outer water level is equal to the crest height. Usually the initial slip surface will not lead to failure, but the follow-up mechanisms will. Some examples of follow-up mechanisms are: overflow, micro instability or a second slip surfaces arise. [Hart, 2018]

A special case of slope instability is when the soil under the levee consist of a permeable aquifer which is connected to a river on the landside with on top a weak impermeable layer, the head in the aquifer now depends on the water level in the river. When the water level is high, the water pressure in the aquifer will increase due which the impermeable weak layer will lift. This case takes place especially in the western part of the Netherlands and is called 'uplifting'. After uplifting a crack will form at the place of the slip surface and the same follow-up mechanisms can take place [Hart, 2018]. The duration of uplifting is dependent on the flood duration[Vierlingh, 1989].

Outer slope

The slope stability of the outer slope partly corresponds with the mechanism of the inner slope. So, first the water level pressure increases due to rainfall or infiltration in the dike when the outer water level is high. When the water level is high and water infiltrates, the water causes a force against the outer slope (and so an opposing moment), therefore, this is not the governing load condition looking at the stability of the outer slope compared to governing load condition of the inner slope. The load is governing when the water level decreases rapidly, the phreatic level cannot follow the outer water level. Looking at a rainfall event, the load is governing when the dike saturates but the outer water level remains low. The water pressure is high which results in a low shear strength.

Cracks could appear in the crest or in the outer slope which indicates the place of the slipping surface as explained for the inner slope, the ground will settle very slow until the point where the slope will slip, and a new equilibrium is found. Also, for the outer slope follow-up mechanisms like slope erosion or a second slip surface can occur through which the levee can fail. The breach growth will start when the crest level is at the same height as outside the levee. [Hart, 2018]

2.1.1.2. Calculation methods

First, the most used static slope stability calculations methods are explained. Second, an overview is given of the methods and last the different software that can be used for slope stability calculations are compared with each other.

Static slope stability methods

Currently the most used static slope stability methods are limit equilibrium methods and stress-deformation methods. The advantage of the limit equilibrium method is that complex soil profiles, seepage and a variety of loading conditions can be handled. The differences in the methods are caused by the procedure (explicitly, iteratively or explicitly solved), the satisfied equilibrium condition (vertical, horizontal and/or global moment), the shape of the slip surface (planer, circular, etc.) and the different assumptions made. .

All methods calculate the equilibrium of forces on different slip surfaces. The driving moment is calculated by using equation 2.1 and is caused by external forces along the slip surface, for example the self-weight, traffic loads and external pore water pressure. These forces result in a driving moment around the centre, see Figure 2.4. The resisting moment can be calculated using equation 2.2 and are caused by the internal forces like the shear stress, effective stress and the pore water pressure. The factor of safety is determined in terms of moment equilibrium, equation 2.3. By doing this for several slip surfaces, the critical slip surface with the lowest factor of safety is found [Cirkel, 1985].

$$M_a = aQ \tag{2.1}$$

$$M_r = \sum(\tau \Delta s r) = \int_{-\theta_2}^{+\theta_1} \tau r^2 d\theta \tag{2.2}$$

$$FoS = \frac{M_r}{M_a} \tag{2.3}$$

In which:

M_a	=	Driving moment [Nm]
M_r	=	Resisting moment [Nm]
Q	=	Composite forces [N]
σ	=	Normal stress [N/m^2]
τ	=	Shear stress [N/m^2]

In the daily consulting practice the following methods are used [Zwanenburg *et al*, 2013]:

- Bishop method: This method makes use of circular slip surfaces; the normal force is assumed to be in the center of the base of each slice and the shear interslice stress is neglected. The maximum resisting moment is calculated by dividing the soil into slices and by calculating each slice to the maximum shear stress. Besides the moment equilibrium, also vertical equilibrium is checked. It is a simple method and has a relatively short calculation time. The disadvantage of this method is that in case of uplift, the zone in which the shear stresses are reduced is hardly included in this analysis [Sharp *et al*, 2013].
- Spencer method: The method of spencer does not only make use of circular slip surfaces but of all shapes of slip surfaces. This is useful when sliding against a circular slip surface is not governing, which for example could be the case when a layer with limited thickness and low strength is present. This method considers, next to moment equilibrium, also horizontal and vertical equilibrium [Zwanenburg *et al*, 2013]. The disadvantage of this method is the longer calculation time due to all shape of slip surfaces which are considered and the fact that there is not much experience with the model.

- Liftvan's method: For many dikes, especially in the lower part of the Netherlands, uplift is the dominant failure mechanism because high design water levels are applied [Sharp *et al*, 2013]. Failure occurs along a relatively deep sliding plane, see Figure 2.5. This zone is hardly included in circular analysis, like Bishop's. The Liftvan's method therefore uses one segment and two arcs of a circle as slip surface as indicated in Figure 2.6. The soil is divided into slices and the slices are modelled such that the horizontal forces are transferred properly from the active to the passive side. This is an advantage compared to Bishop, because it considers besides momentum and vertical equilibrium also horizontal equilibrium.

- Finite element method (FEM): In this method a stress-deformation analysis is included. And the method can model irregular geometries, complex soil behaviour, complex boundary conditions and a variety of construction phases. The advantage of this method is that it predicts the slope deformation, the location of the most critical stress zone and it considers the effect of slope failure on other structures [Sharp *et al*, 2013]. The disadvantage compared to a limit equilibrium method is the calculation time. Inaccuracies are strongly determined by the stress-strain model of the soil and the difficulty to measure soil variables properly [Duncan, 1996].

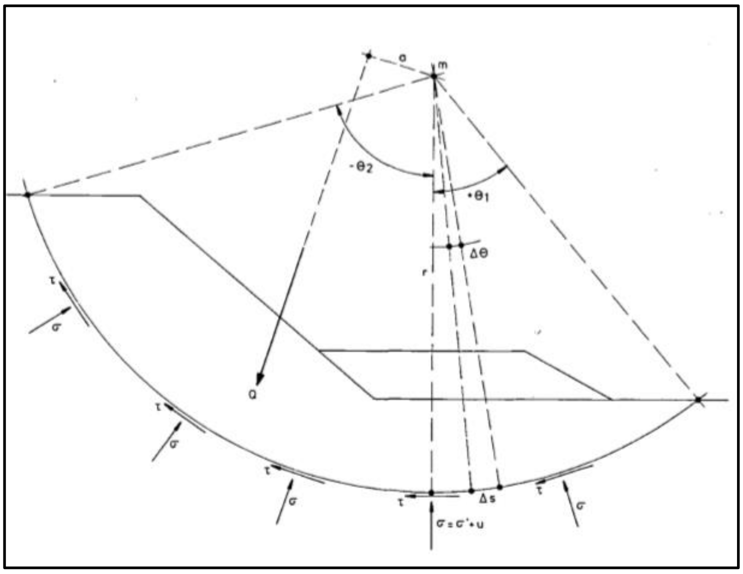

FIGURE 2.4: GENERAL APPROACH LIMIT EQUILIBRIUM METHOD [CIRKEL, 1985]

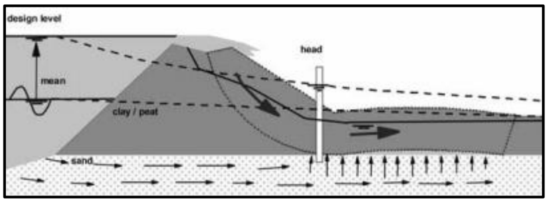

FIGURE 2.5: UPLIFT INDUCED DIKE FAILURE [SHARP *ET AL*, 2013]

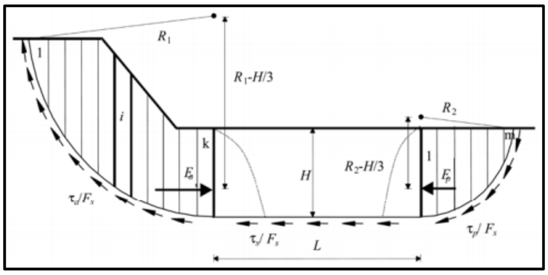

FIGURE 2.6: VAN'S SLIP SURFACE MODEL [SHARP *ET AL*, 2013]

Overview

In Table 2.2 an overview is given for the static slope stability methods explained above. A mechanism which takes the uplifting mechanism into account is preferred; in this instance Spencer, Upliftvan and a FEM method can be used. Another advantage of these methods compared to Bishop is that they calculate the horizontal equilibrium next to the vertical and momentum equilibrium. The FEM method is a relatively difficult method which requires a lot of calculation time. This can be used for water retaining structures with a complex geometry and soil layer. For more simple geometries Spencer or Upliftvan are preferred. In WBI (2017) Upliftvan is commonly used, because there is more experience with this model. Spencer calculates any slip surface shape. Therefore, in this thesis the Spencer method is used to calculate the slope stability.

TABLE 2.2: OVERVIEW DIFFERENT STATIC SLOPE STABILITY METHODS

	Experience	Uplifting	Calculation time	Equilibrium conditions satisfied			Shape slip surface
				V	*H*	*M*	
Bishop	+	-	+	+	-	+	Circular
Spencer	-	+	+/-	+	+	+	Any
Upliftvan	+	+	+/-	+	+	+	One segment and two arcs of circle
FEM	+/-	+	-	+	+	+	Any

There is many software available that can be used to analyse slope stability, an overview is given in Table 2.3. Strength reduction methods (SRM) is preferred, because in limit equilibrium methods (LEM) limitations are included. Despite the limitation, LEM leads still to accurate results, but this must be validated. A finite element method is also very accurate, but the calculation time is longer. Further, in this research a transient calculation must be performed. This is possible with Slope/W and Plaxis. For Plaxis it is more difficult because it must be coupled to PlaxFlow. With other software a transient analysis can be performed, but this must be calculated by hand or a coupling with other software must be made, which is more difficult. Also, a probabilistic calculation must be used in the research.

The probabilistic toolkit of Deltares can be used in combination with the software. But in PLAXIS, D-geo and Slope/W the probabilistic calculations are already included. The probabilistic toolkit of PLAXIS is still under development and is therefore not preferred. Taking this into account, it is decided to use SLOPE/W. This program includes SEEP/W which calculates the pore pressure field and performs a transient calculation. The model is user friendly and a probabilistic calculation is included. There are some inaccuracies caused using a limit equilibrium method to find the slip surface. But this inaccuracy is accepted when the results are checked.

TABLE 2.3: OVERVIEW DIFFERENT MODELS TO ANALYSE SLOPE STABILITY

	PLAXIS	D-Geo Stability	Slope/W	Slide	Geo5	FlacSlope
Batch calculation	+	+	+/-	+	-	-
Calculation pore pressure field	+	+/-	+	+	-	+
Finite element method	+	-	+	-	+	+
Free available	-	-	+/-	-	+	-
HKV license	-	+	-	-	-	-
Limit equilibrium method	-	+	+	+	+	+
Probabilistic calculation	+	+	+	-	-	-
Python Console	+	-	-	-	-	-
Sensitivity assessment	+	+	+	-	-	-
Soil deformation	+	-	+/-	-	+	+
Strength reduction method	+	-	-	-	-	+
Transient analysis	+/-	-	+	-	-	-
TU license	+	+	+/-	-	-	-
User Friendly	-	+	+	+	-	+

2.2. Dike types

Five different dike types can be distinguished based on hydraulic conditions: lake dikes, coastal dikes, upstream river dikes, downstream river dikes and canal dikes within a dike ring system [Jonkman *et al,* 2018]. In Figure 2.7 the different areas are shown, in which the downstream river area can be divided into a sea area, transition area and a river area. The upstream part is not influenced by the tide of the North Sea, while this in the downstream part is the case. The stability of all dikes is governed by an increase of the water pressure in the soil (high outer water level or heavy rainfall). Of each dike the governing failure mechanism, system characteristics and calculation methods are described in the sections below.

2.2.1. Lake dike

Lake dikes are dikes along greater waters (other than rivers) such as around the Zuider Sea, IJsselmeer polders, Grevelingen, etc [van der Kleij, 1999]. They generally consist of a sand core with a clay top layer, in which the bottom layer consist of soft soil is replaced by sand with a greater bearing capacity [Jonkman *et al,* 2018]. The governing load is caused by a combination of a high-water level in the lake and a strong wind. The water level fluctuation is small compared to sea dikes, because there is no tide. The focus in designing a lake dike lies on the stability of the inner slopes under high water loading. High water levels and waves on lakes are generally caused by wind set-up, sometimes in combination with flow from rivers. The high-water level fluctuations have a long duration compared to the variation caused by the wind. Next to stability of the inner slope also micro stability, slope stability and piping are import mechanism for considering a lake dike.

FIGURE 2.7: OVERVIEW WATER SYSTEMS IN THE NETHERLANDS [RIJKSWATERSTAAT, 2017]

2.2.2. Coastal dike

Sea dikes are primary flood defences that retains saltwater [van der Kleij, 1999]. In general, coastal dikes are sand dikes with some parts protected with a clay layer against currents and waves. Along the coast the governing hydraulic loads are caused by the tide and storms, leading to a storm surge and waves [Jonkman *et al*, 2018]. The high-water level has a short duration due to the tide, due to which the water in the dike has a transient behaviour. Most of the time, a low phreatic water surface is present, through which the pore water pressure has little influence on dike stability [Van der Meer *et al*, 2004]. Attention is paid to protections of the outer slope. The dominant failure mechanisms are wave overtopping, erosion and micro stability.

2.2.3. River dike

A river dike is a primary flood defence along the rivers. River dikes are clay dikes on top of a soft subsoil [Jonkman *et al,* 2018]. In the upstream part of a river the hydraulic loads are affected by the river discharge, while in the downstream part both the discharge and the tide affect the water level. The high-water level is the governing mechanism in the design process [Van der Meer *et al*, 2004]. In downstream river dikes the groundwater flow is non-stationary, while in the upstream part this is not the case due to the long duration of the high-water level. The focus lays on the stability of the inner slope, but in the upstream part as well as stability of the inner slope, uplift, heave, outer slope stability and piping are also governing mechanisms. Downstream, piping is less governing because the subsoil consists out of clay.

2.2.4. Canal dike

Canal dikes within a dike ring system are secondary water systems and are used to drain excess water from the polder to the 'boezem'. The water level in the polder is lower than the water level on the water side. Canal dikes are made of light-weight materials such as peat or clay. The water level within a dike ring system can be regulated with pumping stations and therefore has a relatively constant load. The head difference over the dike is an important mechanism for considering the pore water pressure [Van der Meer *et al*, 2004]. Especially when the water level on one side is high and the piezometric head far on the landside is low. The water level can be considered stationary because it can be regulated. The governing failure mechanism is horizontal sliding, because the freeboard is relatively small which can result in a critical effective stress at the base [Jonkman *et al,* 2018]. Slope stability is also an important failure mechanism and in periods of drought the pore water in the dike reduces, causing the weight to decrease further. This can become critical and must be considered in the design.

2.2.5. Overview

An overview of all dike types with the corresponding loads and failure mechanism is given in Table 2.4. To investigate the influence of the flood duration on dike stability a transient analysis must be performed. Canal dikes are less relevant because a stationary method is enough, the water level can be assumed to be constant in time.

From section 2.1, it is concluded that inner slope stability is an important mechanism when considering non-stationary water levels. The downstream river area has more water level variation in time compared to upstream river dikes and coastal dikes, because this is affected by both the tide and the river discharge. This also ensures it is the most complex system to analyse. Next to this, inner slope stability is important for clay dikes with a weak or thin cover layer on top of the hinterland. On top of that, the response of a clay dike to the water level is slower compared to a sand dike, through which the effect of a transient analysis is expected to be higher.

TABLE 2.4: OVERVIEW DIKE TYPES AND THEIR CHARACTERISTICS ADAPTED FROM [VAN DER MEER *ET AL*, 2004]

System characteristics			**Failure mechanisms**					**Loads**						**Method**
Dike type	Hydraulic boundary conditions	Dike and subsoil characteristics	Uplift / Heave	Micro stability	Slope stability	Piping	Importance water level on failure	Water level-River discharge	Water level – tide	Water level – wind	Wave - wind	Storm oscillation/ seiches- wind	Precipitation	Non-stationary
Lake dike	- Short duration of high water (wind) - Long duration of the lake water level	Sand dike on sand	+/-	+	+	+	+	+	-	+	+	+/-	+	+
Coastal dike	- Short tidal duration	Sand dike on clay layer	-	+	-	+/-	+/-	-	+	+	+	+	+/-	+
Downstream river dike	- Long flood duration - Short tidal duration	Clay dike on thick weak layers	+	+/-	+	+/-	+	+	+	+	+	+	+	+
Upstream river dike	- Long flood duration	Clay dike on thin clay layer	+	-	+	+	+	+	-	-	+/-	-	+	+
Canal dike	- Constant low polder water level - Constant high landside water level	Clay/ peat dike on weak layers	+/-	+/-	+	-	+	-	-	-	-	-	+	-
Legend: + Important +/- Of influence - Not relevant														

2.3. Probabilistic methods

As stated in the problem definition, dikes are currently assessed with conservative pore water pressures; which are less suitable to indicate the risk of failure of the levee. The probability of failure should not be conservative, but as realistic as possible. A probabilistic approach is a good technique for considering all uncertainties towards hydrological, hydraulic and geotechnical variables. To ensure this is conducted in the correct manner the mechanisms have to be understood and determined appropriately. In this section the probability of failure in general, fragility curves and differences in reliability methods are discussed. *Appendix B. Reliability methods*, gives a recap of the different reliability methods.

2.3.1. Probability of failure

A structure fails when the resistance is larger than the load. However, both the resistance and the load show spatial and time variations, because not one value is found. The probability of failure can be calculated as the probability that the load is larger than the resistance. This can also be formulated by means of the limit state, which is the difference between the load and the resistance. Failure occurs when Z<0 or when S>R. Another way to describe the failure is using the reliability index which is directly related to the probability of failure. All three ways are denoted in equation 2.5. [Jonkman *et al,* 2016].

$$Z = R - S \qquad 2.4$$
$$P_f = P[S > R] = P[Z < 0] = \Phi_{\mathrm{n}}(-\beta) \qquad 2.5$$

In which:

Z	=	Limit state
R	=	Resistance
S	=	Load
P_f	=	Probability of failure
Φ_{n}	=	Cumulative normal distribution
β	=	Reliability index

The limit state function depends on material properties, loads, geometrical properties and model uncertainties. For all variables the statistical distribution must be considered. When a variable can be considered constant in space and time, a deterministic value can be used. The Z=0 line in the (R, S)-plane represents the boundary between failure and non-failure. If the load and resistance are independent the joint probability density function represents a function of the distribution functions for resistance and load, as described in equation 2.6. In Figure 2.8, the joint probability density function is drawn using lines of equal probabilities. The probability of failure is equal to the volume of the joint probability density function in the unsafe domain which can be calculated using equation 2.7.

$$f_{RS}(r, s) = f_R(r)f_s(s) \qquad 2.6$$
$$P_f = \iint_{Z<0} f_R(r)f_s(s)drds \qquad 2.7$$

In which:

f_{RS}	=	Joint probability density function
f_R	=	Distribution function for resistance
f_s	=	Distribution function for load

2.3.2. Fragility curve

Fragility curves express the probability of failure as a function of the load and are therefore often used for performing a probabilistic calculation. For example, the probability of failure can be plot against the water level, so a water level prediction can be transformed into information on the reliability of a dike [van der Meer *et al*, 2009]. This makes it a useful tool for assessing a dike, the curve is also relatively easy to produce, another advantage is that different failure mechanism can be easily compared with each other. An example of fragility curves for different failure mechanisms is given in Figure 2.9. The probability of failure is plotted against the water level at Lobith.

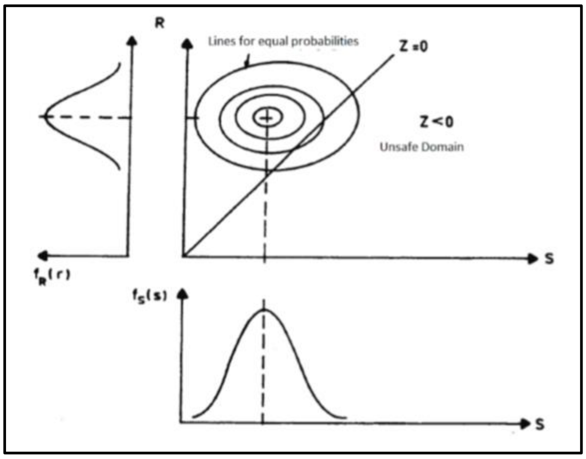

FIGURE 2.8: PROBABILITY OF FAILURE [JONKMAN *ET AL*, 2016]

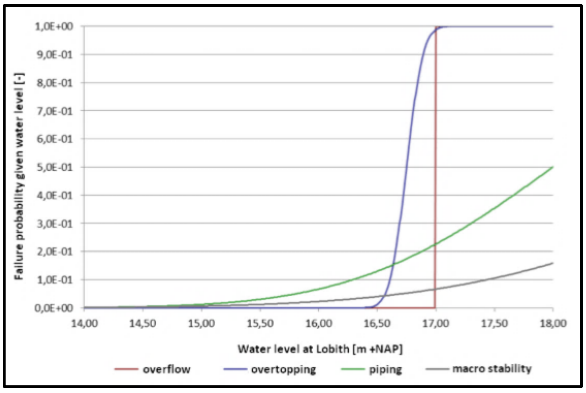

FIGURE 2.9: FRAGILITY CURVES [POL, 2014]

2.3.3. Overview

In Table 2.5 an overview is given for a deterministic, semi-probabilistic and a probabilistic calculation. Therefore, it can be concluded that although a probabilistic calculation has a long duration, the results are more realistic, and the uncertainty is characterized. Therefore, a probabilistic calculation is used in this research.

As probabilistic calculation a FORM calculation or Monte Carlo calculation can be used. A FORM calculation is less time-consuming and results in sensitivity factors (which describes the relative contribution of a variable to the uncertainty). The disadvantage of this method is that the linearization of the limit state function leads to a small error, therefore it is more optimal to use the Monte Carlo calculation.

TABLE 2.5: COMPARISON DIFFERENT RELIABILITY METHODS

	Deterministic	**Semi-probabilistic**	**Probabilistic**
Input	Nominal values	Design values	Statistical variables and distribution
Safety factor	Used	Used	Not used
Calculation duration	Very fast	Fast	Slow
Different runs of the fitting method	Generate the same results	Generate the same results	Results vary significantly
Accuracy	Very sensitive to noise	Sensitive to noise	More robust in the presence of noise
Characterization uncertainty	Not characterized	Not characterized	Characterized using the PDF
Output	Conservative results	Conservative results	More realistic results

2.4. Dike assessment

In this section, the dike assessment according WBI is explained, because dikes are being investigated in this way in the Netherlands. After that, processes in which time dependency play a role are discussed. Time dependency is important for assessing the outer water level, ground water flow and slope stability; because a change in the outer water level affects the ground water flow which again affects the stability of the inner slope.

2.4.1. Method WBI

The current method for accessing a dike is described in by the WBI [Rijkswaterstaat, 2017]. Before 2017 the probability of failure of a dike ring was defined as the exceedance probability of the design water level. In 2017, it was decided to define the probability of failure as the maximum probability of failure allowed when taking all failure mechanisms into account. By doing this, the amount of safety is better understood. Further, the probability of failure is defined for a dike trajectory instead of for a whole dike ring. A dike trajectory are parts of a dike which in case of failure results in the same consequences.

To get insight into the contribution of a failure mechanism towards the total failure, a simple safety check based on general characteristics and safe dimensions is first conducted. It is checked after a failure mechanism when the residual profile is enough to withstand the water retaining function. If this is the case, the probability of failure is negligible and a detailed analysis for that specific failure mechanism is not required. If the probability of failure is relevant, the dike must be assessed semi-probabilistically (by considering safety factors) for that failure mechanism.

Then, a detailed analysis is performed per dike section. First, the maximum allowed probability of failure (safety standard) for the complete dike trajectory is split into the different failure mechanisms, this is based on failure mechanism budget defined by WBI [Knoeff, 2016]. The standard failure mechanism budget can be used as start value and is shown in Figure 2.10. Every dike trajectory is divided again into different dike sections by considering the length-effect. As Vrouwenvelder (2006) mentions, the length effect is: 'The increase of the probability of failure with the length of a structure due to partial correlations and/or independence between different cross sections and/ or elements.' Taking this into account the probability of failure per dike section can be calculated using formula 2.8. The maximum allowed failure per dike trajectory is equal to $\omega \times P_{target}$. Using a length-effect factor results in a conservative probability of failure.

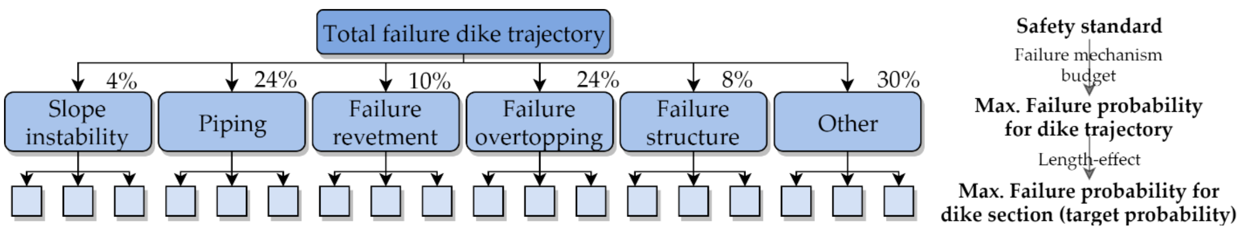

FIGURE 2.10: ILLUSTRATION DETERMINATION FAILURE PER DIKE SECTION ADAPTED FROM [KNOEFF, 2016 & RIJKSWATERSTAAT, 2017]

$$P_{dsn,norm} = \frac{\omega P_{norm}}{N_{dsn}} \qquad 2.8$$

In which:

$P_{dsn,norm}$	=	Norm / target probability of failure [1/year]
ω	=	Contribution of a failure mechanism to the total failure [-]
P_{norm}	=	Safety standard of the dike [1/year]
N_{dsn}	=	Length-effect factor [-]

The target probability of failure must be compared to the probability of failure of a cross section for a certain failure mechanism and is classified in assessment categories (I till VII). In these assessment categories, I stands for 'satisfies well', VI stands for 'does not satisfy well' and VII stands for 'no judgement yet' [Rijkswaterstaat, 2016]. The probability of failure of a cross section for a certain failure mechanism can be calculated probabilistically or semi-probabilistically.

WBI (2016) divides the different failure mechanisms into several groups. For example, the height, strength and erosion must be calculated probabilistically, while they use for piping and slope stability a semi-probabilistically calculation. In the semi-probabilistic calculation design values are used, which result in a factor of safety. With the use of the partial factor, the probability of failure can be calculated. The partial factor is calculated using the calibration formula, which always leads to a conservative value [Rijkswaterstaat, 2016]. The calibration formula for slope stability is further explained in
Appendix E. Method WBI for slope stability. If the probability of failure is too high a probabilistically analysis must be performed, the failure mechanism budget and the length-effect must not be considered or the dike must be reinforced [Montfoort, 2018].

2.4.2. External hydraulic processes

The water level at the outer side of a dike is caused by different processes such as river discharges and the sea water level. Each process has its own characteristic time duration as shown in Table 2.6. In the upstream part of a river, the local water level is most dependent on the river discharge, with the closer the sea the more the influence on the sea. Rijkswaterstaat (2017) calculates some dike stability mechanisms (slope stability, piping, etc.) with a design water level and other mechanisms (e.g. revetment calculations) with a design flood wave (in deterministic or semi-probabilistic calculations). This upcoming section will look at these processes in more detail, as well as explain GRADE datasets are explained, because they can be used to simulate river floods at the Rhine and Meuse.

TABLE 2.6: INDICATED CHARACTERISTIC DURATION BOUNDARIES

External hydraulic process	Indicated characteristic time duration
Discharge hydrograph	Days- weeks
Sea water level (tide and surge)	Hours- days
Seiches	Minutes– half hours
Sea waves	8- 15 seconds
Local waves	2- 7 seconds

2.4.2.1. Design water level

The design water level in the downstream river area is determined by the Rhine discharge, Meuse discharge, wind (velocity and direction), sea water level and the operation of the storm surge barriers. The sea water level and the wind are strongly correlated. The design water level in the Netherlands is a permanent water level for which the probability of exceedance is chosen in such a way that the safety standard satisfies the specified condition [Van Velzen *et al, 2007*]. In a probabilistic calculation, a probability density function of the top water level is used.

2.4.2.2. Design hydrograph

To determine the design hydrograph WBI (2017) uses GRADE (Generator of Rainfall And Discharge Extremes) project. GRADE was developed by Rijkswaterstaat and KNMI to generate precipitation and temperature series with a weather generator in such a way that statistical properties are not changed. A rainfall- runoff model is made, which calculates discharge series with a length of 50000 years. Using GRADE improves the determination of a design hydrograph.

Hydrographs from the GRADE dataset are selected when the peak discharge is above a certain threshold (Peaks, over Threshold- POT). Double- peaked flood hydrographs are merged into one hydrograph with the same peak discharge and duration as the two hydrographs together. After that, the shape of the design hydrograph is determined with the scaling method which results in a standard hydrograph shape. This method is explained in detail in 'Ontwerpbelastingen voor het rivierengebied'- appendix C2. Next, the mean duration is calculated for the selected hydrographs resulting in a standard design shape. It is noteworthy that, this method assumes that a standard hydrograph with a certain peak discharge results in a maximum water level with the same probability of occurrence as the peak discharge.

2.4.2.3. Sea water level

The sea water level fluctuations are determined by the astronomic tide and storm surge. The shape of the astronomic tide is determined by the mean sea water level and the shape of the tide. The shape varies per location along the coast. The shape of storm surge depends on the height of the storm surge, the storm duration and the phase shift between the peak of the storm surge and the peak of the tide. Storm surge is strongly dependent on the wind direction and velocity. The higher these values the higher the storm surge [Van Velzen *et al, 2007*]. A storm is often simulated with a trapezium shape with a duration of 33.2 hour [Van Velzen *et al, 2007*].

2.4.2.4. Precipitation

Precipitation is an important process for analysing a dike for slope stability; especially when the outer water level is low, and the dike is partly saturated by the rain. To account for rainfall the phreatic line is increased. In the downstream river area, extreme rainfall is accounted for by increasing the phreatic water level by 1 meter [Van Velzen *et al, 2007*]. In TAW (2005) a value of 0.50 m is recommended [Van der Meer *et al*, 2004]. In this thesis, precipitation is not considered. In WBI (2017) a conservative phreatic line is chosen (see section 2.4.3) in a way that no precipitation correction is required.

2.4.3. Internal hydraulic processes

All levees are subjected to internal flows caused by permanent or transient external hydraulic conditions. Several failure mechanisms of dikes are driven by these internal flows, as they determine the pore pressure field. Pore water response depends on geotechnical variables and flood duration. There are three possible causes that cause pore water pressure: ground water flow, soil pressure and soil deformation. The ground water flow is subdivided in three aspects: phreatic surface, the head in the intermediate layer and the head in the aquifer [Van der Meer *et al*, 2004]. Both stationary flows and transient flows; involved processes and calculation methods are discussed in this section.

2.4.3.1. Calculation methods

Flow analysis are based on hydraulic laws developed for saturated soils (a combination of Darcy's law and the continuity equation, see *Appendix C. Equations internal hydraulic processes*). However, when a flood occurs the levee body and foundation are not saturated, causing these laws to not fully be applicable anymore. Unsaturated flow can be considered by combining Darcy's law with the continuity equation, which results in a differential equation. This equation describes groundwater flow as a function of the head and the pore water pressure. These differential equations are included in complex numerical models to consider unsaturated soil flow [Sharp *et al*, 2013].

Waternet creator

In stability calculation according WBI (2017), a simplification is used in the calculation of the pore water pressures. The advantages of this simplification is, that it easily obtains insight into the ground water flow and the input is limited. The disadvantage of the model is that the dike geometry is simplified. The method can therefore only by used for simple cases. In analytical models 2-dimensional flow in a homogenous situation is assumed; this causes a smaller accuracy because the heterogeneity is not considered. The pore water pressure is dependent of the dike material. The following cases are distinguished [Van der Meer *et al*, 2004]. For each case the phreatic line is determined in Table 2.7.

- Case 1A: Clay dike on compressible subsoil [Kanning & Krogt, 2016]
- Case 1B: Clay dike on sand subsoil [Kanning & Krogt, 2016]
- Case 2A: Sand dike on compressible subsoil [Van der Meer *et al*, 2004],
- Case 2B: Sand dike on sand subsoil [Van der Meer *et al*, 2004].

TABLE 2.7: PHREATIC SURFACE DIFFERENT CASES [VAN DER MEER, 2004 & KANNING, 2016]

Case 1A and 1B	*Case 2A*	*Case 2B*
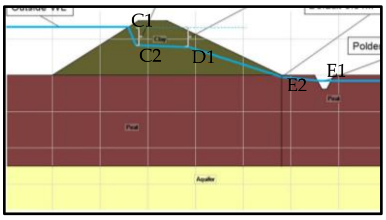	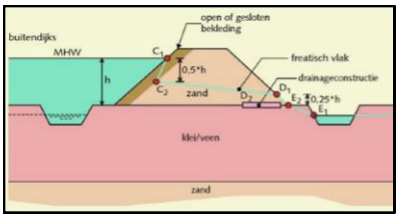	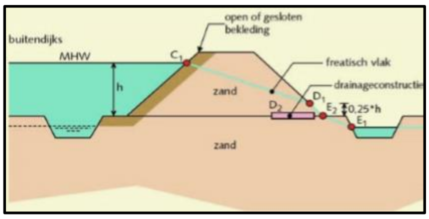
$C_1 = h$ $C_2 = C_1 - 1$ $D_1 = C_1 - 1.5$ Location E: ○ E_1 = Polder water level, if ditch if present ○ E_2 = Boundary inner slope and ground level, if no ditch is present	$C_1 = h$ Add point C_2 if impermeable cover layer: $C_2 = C_1 - 0.5h$ Location D: ○ $D_1 = 0.25h$ ○ $D_2 = 0$ when drain is present Location E: ○ E_1 = Polder water level, if ditch if present ○ E_2 = Boundary inner slope and ground level, if no ditch is present	$C_1 = h$ Location D: ○ $D_1 = 0.25h$ ○ $D_2 = 0$ when drain is present Location E: ○ E_1 = Polder water level, if ditch if present ○ E_2 = Boundary inner slope and ground level, if no ditch is present

Numerical method

Different numerical methods exist, that are generally more rigorous and include rapid computations. The disadvantage is that many variables are required, while it is unclear how large the influence of each variables exactly is.

It is recommended to validate the result by simple calculation to get insight into the order of magnitude [Sharp *et al*, 2013]. Finite element methods are often preferred for solving these problems because of the flexibility of this technique in capturing complex geometries [Brinkgreve *et al*, 2003]. Some models and their characteristics are shown in Table 2.8. Because of these characteristics it decided to use SEEP/W. SEEP/W is a Finite Element Method (FEM) which divides the dike into several smaller elements. The balance equation is then solved for all the smaller elements, which results in a solution for the entire dike. This program is user friendly and transient and probabilistic calculation can be performed. SEEP/W can easily be linked to SLOPE/W, to perform a stability calculation. In *Appendix D. GeoStudio,* more information about the used software is given.

TABLE 2.8: OVERVIEW DIFFERENT SOFTWARE PACKAGES FOR GROUNDWATER FLOW CALCULATIONS

	WATEX	MSEEP	SEEP/W	PLAXIS	SEEP2D	MODFLOW	MicroFEM
Based on FEM	-	+	+	+	+	+	+
Stability calculation	-	-	-	+	-	-	-
Transient calculation	+	+	+	+	-	+	+
3D	-	+	-	-	+	+	+
Both saturated and unsaturated flow	+	-	+	+	-	-	-
User friendly	+	+	+	-	+	-	-
Probabilistic calculation	-	-	+	-	-	-	-

2.4.3.2. Transient processes

If the external water level is variable in time, the ground water flow and the pore water pressure are non-stationary, which causes the slope stability of the inner slope to be time dependent. The pore water response depends on different processes, see Figure 2.11. All these processes are explained in this section. In *Appendix C. Equations internal hydraulic processes*, corresponding equations are given. In a transient slope stability analysis, uncertainties derive from the hydrograph of the water level, the response of the pore water pressures and the response of the inner slope to it.

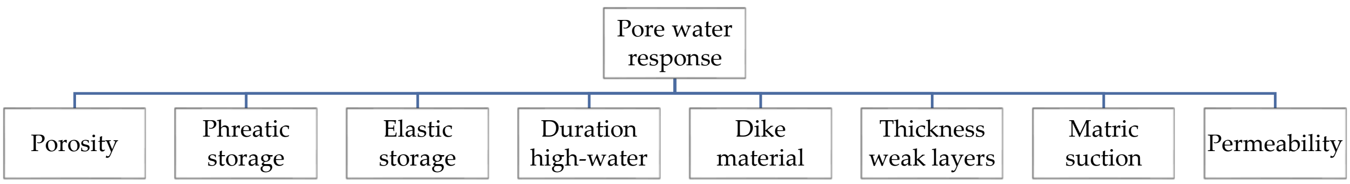

FIGURE 2.11: DEPENDENCE PORE WATER RESPONSE AND OTHER PROCESSES

Storage

Water can be stored above the water table (phreatic storage). In the weak layers the storage depends on deformation of the pores due to consolidation. In sand layers it depends on the compaction of the soil. [Van der Meer *et al*, 2004]. Phreatic storage ensures ground water flow is delayed and reduced. It is a time dependent process when it is caused by a variable water level; especially since the porosity determines the amount of phreatic storage.

Water can also be stored under the water table (elastic storage). Elastic storage is the storage caused due to a change in the effective stress. This effect can be considered in the consolidation process with the consolidation coefficient. Phreatic storage is larger than elastic storage.

The consolidation time for a sand aquifer is a maximum of an hour, while a clay layers can take a month. When comparing the consolidation time with the flood duration, it can happen that the groundwater flow in the aquifer is stationary while in the clay layer the flow is still non-stationary. Both layers are communicating with each other, causing a non-stationary effect in the sand aquifers [Van der Meer *et al*, 2004]. Hence, these non-stationaries are not caused by the storage capacity of the soil but due to the storage capacity of the surrounding layers.

Pore water pressures in dike body

Matric suction

To account for transient effect, the matric suction in the unsaturated zone above the phreatic line needs to be considered [Moellmann *et al*, 2011]. The behaviour can be described using the equations according to van Genuchten (1980) and according to van Genuchten and Mualem.

Horizontal intrusion length

The length which is affected by the increase of the water level is called the intrusion length, the longer the duration of a high-water event, the further the effect will reach within the dike and subsoil. After the intrusion length the phreatic line will follow the phreatic line of the previous water level, see Figure 2.12 [Van der Meer *et al*, 2004]. The intrusion length (L) depends on geohydrological variables and the duration of the high-water. The length increases with the root of the time, see equation 2.9. The length of intrusion is important for the inner slope stability because if the pore pressure increases, the effective stress and shear strength of the soil decreases and an instability of the inner slope can occur. The response of the phreatic surface of a dike on permeable soil is an order of magnitude lower [Van der Meer *et al*, 2004].

$$L: \sqrt{t} \tag{2.9}$$

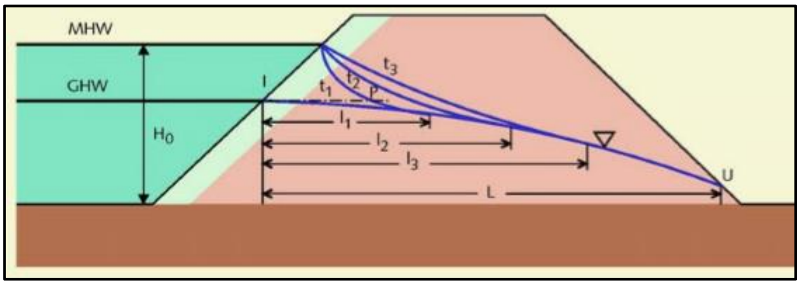

FIGURE 2.12: RESPONSE OF THE PHREATIC SURFACE TO THE OUTER WATER LEVEL [VAN DER MEER *ET AL*, 2004]

Capillary rise

Capillary rise is the zone above the phreatic surface where ground water is present. This causes a negative pore water pressure and an under pressure while the effective pressure also increases. Frans Barends (2004) recommended to not take capillary rise into account in the assessment of dike stability.

Pore water pressures in subsoil

Vertical intrusion length

The vertical intrusion length is the distance from the bottom of the impermeable cover layer over which the pore water pressure changes caused by the changing pore water pressures in the aquifer, see Figure 2.13. The pore water pressures in the aquifer are influenced by the outer water level. For example, in the downstream river area the water head in the aquifer follows the tide. [Barends, 2005]

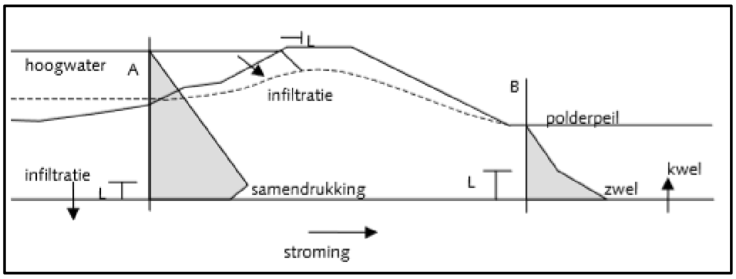

FIGURE 2.13: INTRUSION OF PORE WATER PRESSURE [VAN DER MEER *ET AL*, 2004]

Leakage length

The groundwater flow under the levee depends on the permeability capacity of the layers. This permeability capacity depends on the permeability of the aquifers and the hydraulic resistance of the weak layers. These processes together are called the leakage length. The leakage length can be modelled time dependent, in that way seepage, uplifting and infiltration can be modelled correctly when the flood duration is limited [Barends, 1982]. Because of the storage capacity of the soil, the pore water pressure cannot fully develop.

Flow over layer separations

Depending on the permeability ratio, a change in flow direction occurs at a layer separation for different soils [Van der Meer *et al*, 2004].

Lag in pore water response

During high-water, there is some lag between the pore water response and the outer water level, see Figure 2.14 [Barends, 1986]. The delay is caused by the storage capacity of the soil.

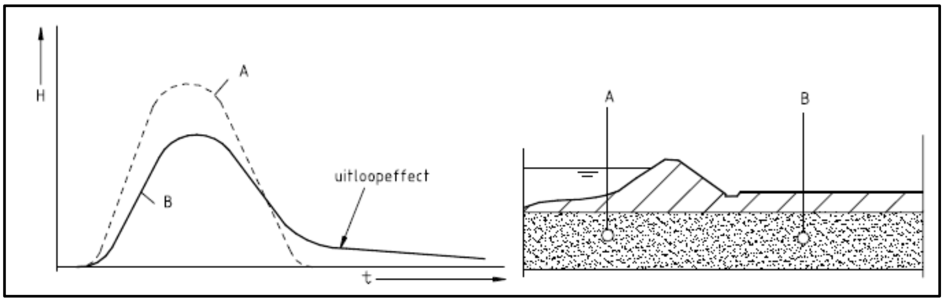

FIGURE 2.14: LAG IN THE PORE WATER RESPONSE [VAN DER MEER *ET AL*, 2004]

2.4.4. Shear strength models

The soil can be modelled using different shear strength models [Zwanenburg *et al*, 2013]:

- A drained analysis with effective shear strength variables
- An undrained analysis with effective shear strength variables
- An undrained analysis with undrained shear strength variables

A drained analysis is used to investigate the long-time behaviour of dikes or when the soil is very permeable. This type of analyses is not reliable when it comes to semi or impermeable layers as sliding occurs fast compared to the consolidation time. As a result, pore water pressures arise along the sliding plane, which influence the effective stress which again influences the slope stability. In case of semi- or impermeable layers it is recommended to use an undrained analysis. If the time of sliding or the hydraulic change is shorter than a hydrodynamic period (equation 2.10), sliding is considered to be fast [Zwanenburg *et al*, 2013]. In section 1.2, different cases were described which varies in the failure velocity. These differences are caused by drained or undrained behaviour of the soil.

$$t_{99} = 4\frac{D_d^2}{c_v} \tag{2.10}$$

In which:

c_v	=	Consolidation coefficient [m²/s]
t_{99}	=	Hydrodynamic period [s]
D_d	=	Drainage distance [m]

The position of the critical slip surface is strongly dependent on the choice of the shear strength model. When the cohesion of the soil is zero, the critical slip surface is parallel and next to the slope surface, Figure 2.15. When an undrained analysis is applied, the opposite occurs as the critical slip surface is very deep, see Figure 2.16.

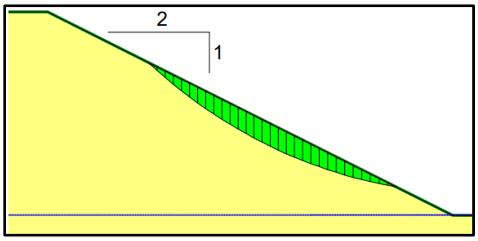

FIGURE 2.15: SHALLOW SLIP FOR PURELY FRICTIONAL (C=0) CASE [GEO-SLOPE INTERNATIONAL, 2012]

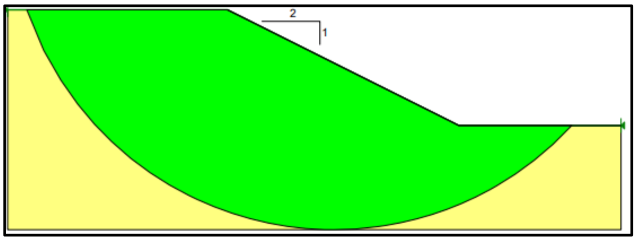

FIGURE 2.16: DEEP SLIP SURFACE FOR HOMOGENEOUS UNDRAINED CASE [GEO-SLOPE INTERNATIONAL, 2012]

2.4.4.1. Drained analysis

A drained analysis is based on the effective cohesion and the effective internal friction angle. The shear capacity can be calculated using the Mohr-Coulomb model, see equation 2.11. In a drained stability analysis, the effective shear stress is determined using the effective stress normal to the sliding plane. In semi- or impermeable layers pore water pressures arise along the sliding plane. This pressure results in a decrease in the effective stress and the shear strength. When these pressures are ignored, the stability is overestimated when the short-term behavior is investigated. [Zwanenburg *et al*, 2013]

$$\tau = c' + \sigma' \tan(\varphi') \qquad 2.11$$

In which:

c'	=	Cohesion [kN/m²]
φ'	=	Effective friction angle [°]
σ'	=	Effective stress [kN/m²]
τ	=	Ultimate shear stress [kN/m²]

2.4.4.2. Undrained analysis with effective shear stress variables

An undrained analysis with effective shear stress variables takes excess pore pressure into account. The excess pore pressure is difficult to determine because it is dependent on the stiffness of the soil, permeability of the soil, load change and the velocity of the load change. Because of these difficulties the analysis is robust and therefore not safe. Therefore, an undrained analysis with undrained shear stress variables is preferred. [Zwanenburg *et al*, 2013]

2.4.4.3. Undrained analysis with undrained shear stress variables

When excess pore water pressures are difficult to estimate, it is better to use an undrained analysis with undrained shear stress variables. As example, a SHANSEP model can be used, see equation 2.15 till 2.17 [Rijkswaterstaat, 2016]. The SHANSEP model was developed at MIT by Ladd and Foott (1974) and Ladd (1991). This model makes use of yield stress, which depends on the stress history of the soil.

The soil is under consolidated when the yield stress is lower than the actual stress; it is still consolidating under a previous applied load (OCR < 1). The soil is consolidated when the OCR is bigger or equal to 1. The soil is undrained and can be subdivided into four classes with the use of this OCR value [WBI, 2017].

* **Normal consolidated** soil with OCR = 1 and POP= 0 kN/m². The soil never experienced a yield stress that was greater than the actual vertical stress. The soil is lightly compressed causing the pore volume to be relatively large and therefore large excess pore water pressure are generated. The undrained shear stress is about half of the drained shear stress.

* **Slightly over consolidated** soil with OCR = 1 – 2 and POP > 0 kN/m². The soil is slightly compressed, causing the pore volumes to be smaller compared to normal consolidated soil, which again leads to smaller excess pore water pressures. The yield stress is larger than the actual effective stress.

* **Over consolidated soil** with OCR = 2 - 3. The yield stress is high compared to the actual stress; the soil is highly compressed. The pore volume is therefore relatively small, which generates smaller excess pore water pressures.

* **Over consolidated soil** with OCR > 3. The yield stress is very high compared to the actual stress and the soils shows dilatant behaviour. The undrained effective stress is larger than the drained effective stress.

$$s_u = \sigma'_{v,i} \times S \times OCR^m \quad 2.12$$

$$OCR = \frac{\sigma'_{vy}}{\sigma'_{v,i}} \quad 2.13$$

$$\sigma'_{vy} = \sigma'_{v,i} + POP \quad 2.14$$

In which:

s_u	=	The undrained shear strength [kN/m²]
$\sigma'_{v,i}$	=	In situ effective vertical stress [kN/m²]
σ'_{vy}	=	Vertical yield stress [kN/m²]
OCR	=	Overconsolidation ratio [-]
POP	=	Pre-overburden pressure [kN/m²]
m	=	Stress increase exponent [-]

2.4.4.4. Uplifting of the hinterland

A special case of slope instability is when the soil under the levee consist of a permeable aquifer connected to the river and a weak impermeable layer located on the landside on top of the aquifer. In this situation, the head in the aquifer depends on the water level in the river. Uplifting or a formation of a crack will arise when the pore water pressure in the aquifer equals the weight of the weak impermeable layers. The effective stress then becomes equal to zero.

$$\phi_g = \frac{\sigma'_{vs}}{\gamma_w} + \phi_p = \frac{\sum \gamma_{si} d_i}{\gamma_w} + \phi_p - d_z \quad 2.15$$

In which:

ϕ_g	=	Boundary potential [m]
σ'_{vs}	=	Effective stress at the layer separation [kN/m²]
γ_w	=	Water volumetric weight [kN/m³]
ϕ_p	=	Polder water level [m]
γ_s	=	Volumetric weight of the soil
d	=	Depth of sand with respect to the polder water level [m]

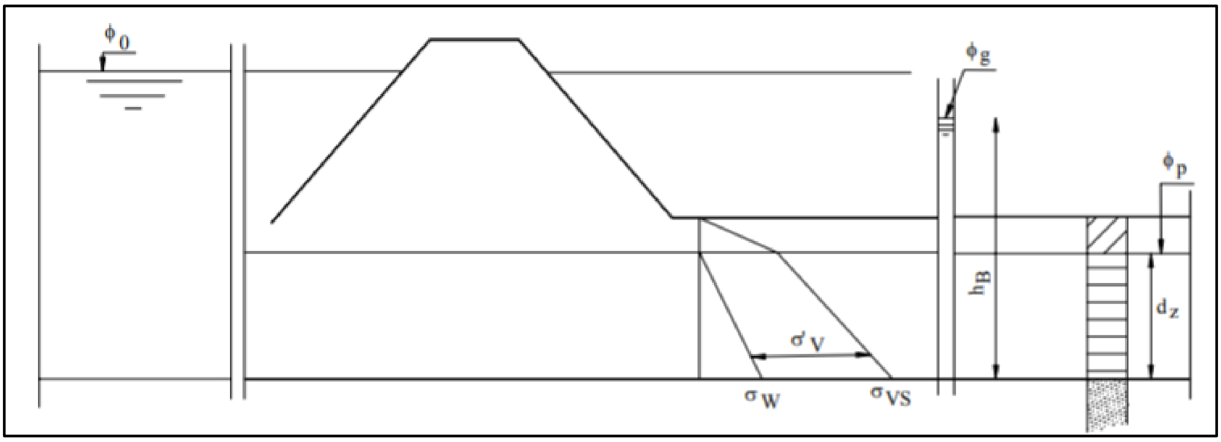

FIGURE 2.17: BUOYANCY OF THE HINTERLAND [VAN DER MEER *ET AL*, 2004]

3. INFLUENCE OF TIME DEPENDENCY ON PORE PRESSURES AND SAFETY FACTORS

3.1. Goal

This Chapter investigates the influence of time dependency on the pore pressure field and the safety factor of stability of the inner slope. The first part of this Chapter is related to sub-question 1 and the second part to sub-question 2. The goal of sub-question 1 is to know which dike characteristics and flood wave characteristics (height and duration of the flood wave) causes the largest differences in the pore pressure field between the stationary and transient state. To answer this question; a stationary pore pressure field caused by a constant water level is compared with a transient pore pressure field during the passage of a flood wave.

Differences in pore water pressure causes a difference in slope stability. Therefore, the influence of time dependency on stability of the inner slope is investigated in sub-question 2. A sensitivity assessment is performed to know which dike geometry characteristics cause the differences in safety factor during a constant water level and during the passage of a flood wave to be large. In the sensitivity assessment there is varied in presence of a foreshore, ditch, thickness of a cover layer and some material characteristics. Also, a block-wave analysis is performed, in which the safety factor for slope stability is calculated for different rectangular waves, that varies in height and duration. This way, it is known which flood wave characteristics are important for a transient calculation. Figure 3.1 shows the general outline to answer sub-question 1 and 2. The first row indicates the outline of sub-question 1 and the second and third row indicate the outline of sub-question 2. Finally, is investigated if large differences in pore pressure field also cause large differences in safety factor by comparing the results of the analyses.

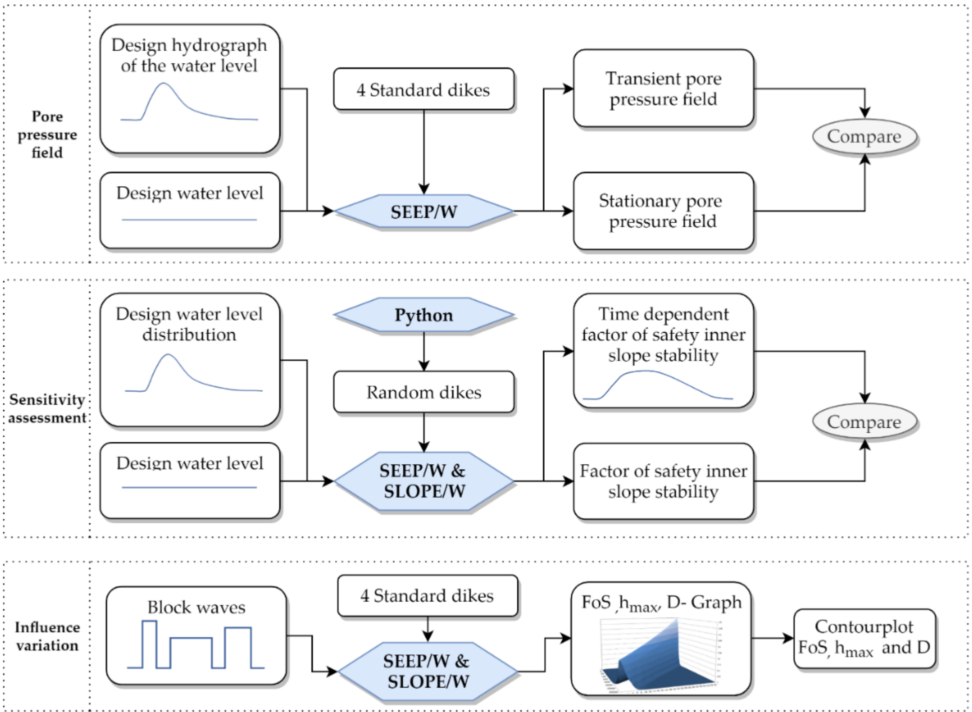

FIGURE 3.1: OUTLINE TO ANSWER SUB-QUESTION 1 AND 2

3.2. Method

3.2.1. Location

The flood waves used to model the pore pressure field and to perform the sensitivity assessment, are obtained from the Rhine at Lobith, from the Meuse at Borgharen and from the Sea at Rotterdam. The locations and the rivers are shown in Figure 3.2. The block-wave analysis does not use flood waves of a specific location.

FIGURE 3.2: LOCATIONS AND RIVERS [WOJCIECHOWSKA, 2015]

3.2.2. Dike cross-section

Figure 3.3 shows the four dike types that are used to investigate the pore pressure field. Also, the block-wave analysis uses these dike types. The geometry is fixed, but the material of the dike body and the subsoil have been varied. Dike type 2 is a typical coastal dike and the other three cross-sections are typical river dikes in the Netherlands. The crest is located at 34.5 meter with respect to the bottom of the model, the foreshore 29.5 meters, the hinterland 29.5 meters, the river bottom 25.5 meters and the polder water level is 29 meters. The crest width of the dike is 4 meters and the slope is set to 1:3.

In the sensitivity assessment clay dikes and dikes with a sand core on top of a thin/weak cover layer are investigated. In the assessment, the geometry of the dike is still fixed, the presence of sand core, thickness of the cover layer, presence of a foreshore, material of the hinterland, the presence of a ditch, the material of the aquifer and the POP value of the clayey material have been varied; see Table 3.1 and Figure 3.4.

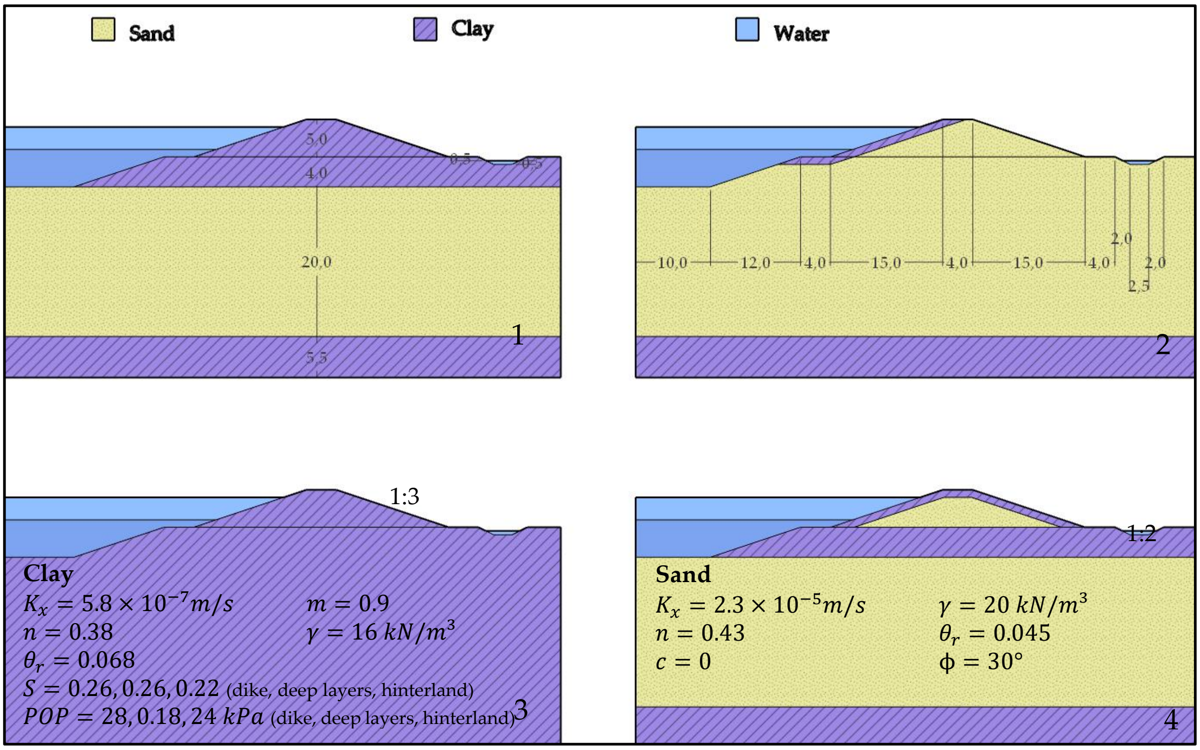

FIGURE 3.3: TYPICAL LEVEE CROSS-SECTIONS IN THE NETHERLANDS

TABLE 3.1: VARIABLE VARIABLES IN THE SENSITIVITY ASSESSMENT

Dike core	Ditch	Presence foreshore	Thickness cover layer	Material hinterland	Material aquifer	POP value clayey material
Sand/ clay	Present/ absent	Present/ absent	3/ 4/ 5/ 6 m	Sand/ clay	Sand/ clay	0/ 30/ 80/ 130 kPa

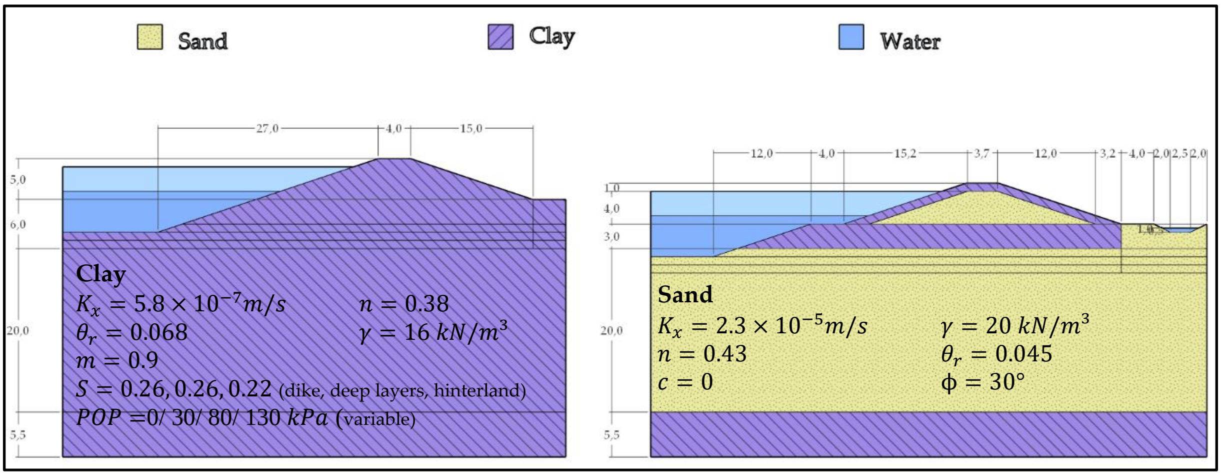

FIGURE 3.4: EXAMPLE DIMENSIONS DIKE USED IN SENSITIVITY ASSESSMENT; LEFT= CLAYEY CORE, NO DITCH, NO FORESHORE, COVER LAYER THICKNESS OF 6 METERS, CLAYEY HINTERLAND MATERIAL, CLAYEY AQUIFER; RIGHT = SAND CORE, DITCH, FORESHORE, COVER LAYER THICKNESS OF 3 METERS, SAND HINTERLAND MATERIAL, SAND AQUIFER

3.2.3. Hydraulic boundary condition

Two permanent water levels are investigated; one water level is located 1 meter below the crest (33.5 meters with respect to the bottom of the model), the other 1 meter above the foreshore (30.5 meters). Also, different flood waves are investigated.

The shapes of the waves are obtained from the Waterstandsverlopen Tool developed by WBI (2017). This tool calculates the water level hydrograph at a selected location. The shapes are obtained for the three locations discussed above; Lobith, Borgharen and Rotterdam. The peak of the flood wave corresponds with the chosen permanent level. For more information about this tool is referred to Thonus (2006), which based his calculation on RWS-RIZA.

The water levels and flood waves are shown in Figure 3.5. The flood wave at Lobith is multiplied with a factor $\frac{5}{6}$ to prevent the water level to be lower than the bottom of the river. Note that also combinations are investigated that are not realistic, for example a sand on sand dike with a flood wave from the Rhine. These hydraulic boundary conditions are used in the pore pressure field research and the sensitivity assessment.

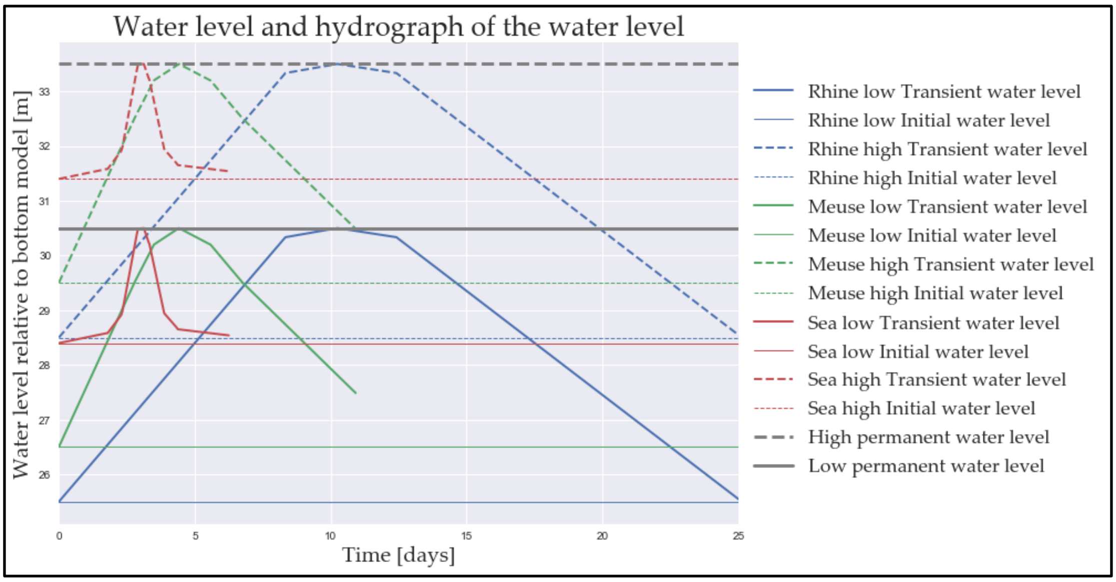

FIGURE 3.5: PERMANENT WATER LEVELS AND FLOOD WAVES WITH RESPECT TO BOTTOM RIVER

In the block-wave analysis the hydraulic boundary consists of different block-waves. Block-waves are rectangular waves with a certain height and duration. The height is varied between 30 till 33.5 meter with 7 steps with respect to the bottom of the model. The duration of the flood waves vary from 0.5 hour till 28 days with 25 steps. So, in total 175 block-waves are investigated. An example of different block-waves is shown in Figure 3.6.

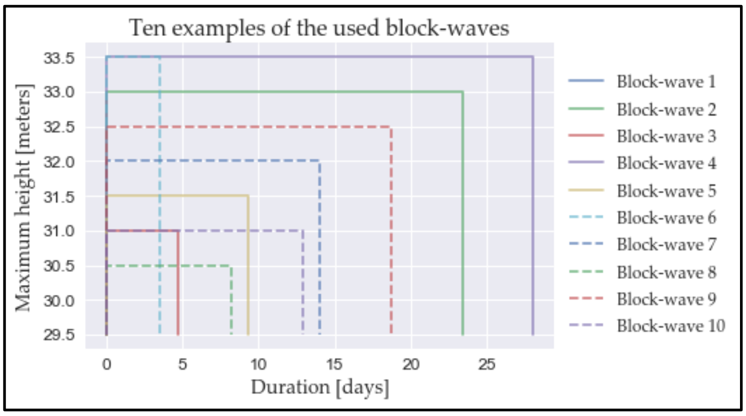

FIGURE 3.6: EXAMPLE OF THE USED BLOCK-WAVES

3.2.4. Pore pressure field model

In section 2.4.3.1 an overview is made of the different available software to model the stationary and transient pore water pressures. From this is concluded that SEEP/W in combination with SLOPE/W is most appropriate. SEEP/W is a FEM-program, which calculates the pore water pressures subjected to changing hydraulic conditions. More information about the used software is given in *Appendix D. GeoStudio.* The input of SEEP/W is given in *Appendix G. Input SEEP/W.* It is assumed that all soil layers are homogeneous.

3.2.4.1. Initial state

The outer water level before a flood wave passes; is equal to the first value of the output of the 'Waterstandsverlopentool', see Figure 3.5. This is a rough assumption; when a real case is chosen more attention must be paid to the initial outer water level. In the block-wave analysis the initial water level is 29.5 meter (at the height of the foreshore) before a block-wave passes.

3.2.4.2. Saturated and unsaturated flow

In SEEP/W, both saturated and unsaturated flow is incorporated. The saturated soil follows Darcy's law while unsaturated flow takes processes like phreatic storage, elastic storage and matric suction into account. In WBI (2017) matric suction is not considered; because this led to conservative outcomes. But results showed that the factor of safety increases with an increase in matric suction [Fourie, 2016]. Therefore, in this thesis matric suction is considered, because the pore pressure field should be modelled as realistic as possible to calculate a realistic probability of failure [Moellmann *et al*, 2011].

In this thesis, flow in the layers under the bottom of the river is assumed to be saturated, because the soil is always beneath the water table. The flow through the dike, foreshore and hinterland is partly saturated and partly unsaturated. In the unsaturated flow conditions, the hydraulic conductivity and volumetric water content functions are estimated with the use of built-in functions. The method defined by Van Genuchten (1980) is used to estimate the hydraulic conductivity. In the Van Genuchten equation, the hydraulic conductivity is a function of the matric suction.

3.2.4.3. Finite element method

Mesh pattern

To calculate the movement and pore-water pressure distribution within the materials, a finite element method is used which subdivides the model into nodes. As finite mesh pattern is chosen for quads and triangles. A global element size must be chosen, which determines the accuracy of the model. The smaller the mesh grid, the more accurate the results will be but the larger the calculation time of the model. To know the influence of the choice; the pressure in the dike for the four dike types is compared for varying element sizes, the results are shown in Figure 3.7. A linear line is fitted and the intercept indicates the value when an infinity small grid size is chosen, this value is used to estimate the order of the error with. Therefore, it is chosen to use a global element size of 0.5 meter. This method is explained in more detail in *Appendix G. Input SEEP/W.*

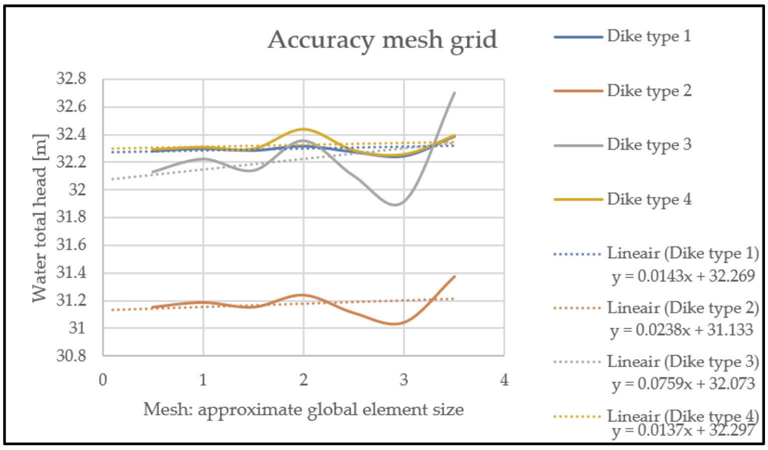

FIGURE 3.7: ACCURACY MESH GRID

Boundary conditions

Three boundary conditions are used in the model, which are indicated in Figure 3.8. The red colour indicates the outer water level and is specified by defining the total water head. In the stationary state, this value is constant; in the transient state a step data point function is used. At the left side of the model no boundary conditions are defined, which is the same as a no flow boundary. It is assumed that half of the water in a river flows to the left and the other half to the right, in the middle the water flows downward.

The river width upstream in the Rhine is around the 80 meters, upstream in the Meuse the width is around the 100 meters. While downstream near Rotterdam the width varies between the 265 and 465 meters. Therefore, the influence of the river width is investigated in a similar way as the mesh pattern, the results are presented in *Appendix G. Input SEEP/W.* From this is decided to use a width of 90 meters in the model (so the left boundary is presented at a distance of 45 meters).

In green the seepage boundary is indicated, which is defined as a water rate equal to 0 m^3/s. And with the light blue colour, the polder water level is indicated; which is constant for each case. The total water head is set to 29 meters.

At the right side of the model the same boundary is used, to indicate that it does not affect the flow pattern anymore. Ideally this boundary is present at an infinite distance, but that caused an infinitely large calculation time. Normally the right distance is set to a distance equal to 5 times the leakage length (997 meters). The leakage length can be calculated using equation C.10, from which follows a length of 199 meters. The influence of the distance on the right boundary is investigated in *Appendix G. Input SEEP/W*. From this is concluded that using a distance of 390 meters (2x the leakage length) is sufficient.

After defining the boundary conditions, the elevation of water level at each node is calculated. In the transient calculation a duration of 1.5 times the duration of flood wave is investigated, with 20 steps.

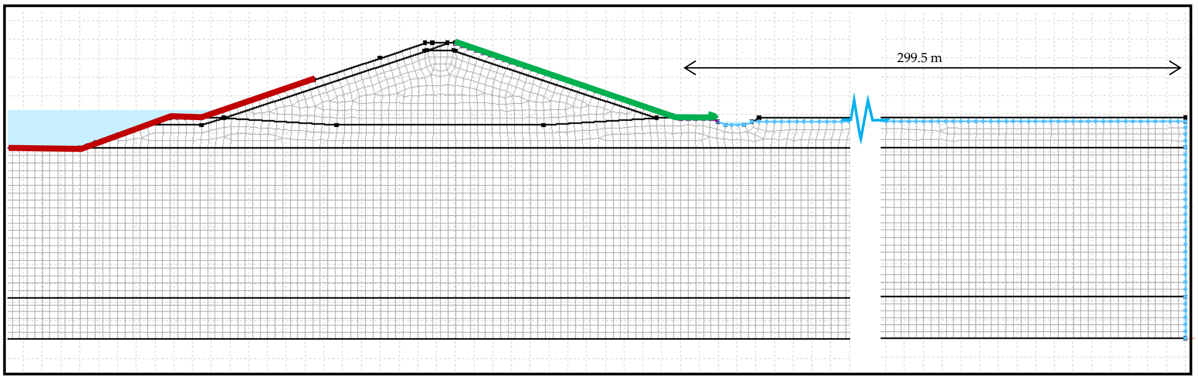

FIGURE 3.8: MESH PATTERN AND BOUNDARY CONDITIONS USED IN FINITE ELEMENT METHOD

3.2.5. Slope stability model

To calculate the inner slope safety factor, SLOPE/W is used. More information about SLOPE/W is given *Appendix D. GeoStudio.* The input of the software is shown in *Appendix H. Input SLOPE/W*. The slope stability calculation uses the pore pressure field calculated with SEEP/W. In this section choices about the material model, entry and exit range are explained.

3.2.5.1. Material model

The sand soils are modelled with the Mohr coulomb model. The SHANSEP material model is used for modelling the undrained shear strength in the clay layers. More information about these models is given in section 2.4.4. In the SHANSEP material model, the shear strength is a function of the effective overburden at the base of a slice which again is computed from the weight of the slice and the pore-water pressure acting at the base of that slice. When using the SHANSEP material model, a value for $\frac{\tau}{\sigma}$ needs to be specified. When the soil is normally consolidated this value is constant; but the soil is assumed to be overconsolidated, due to which the OCR value is dependent on the effective stress. Therefore, a function is incorporated with the use of Python, that replaces the shear stress with the undrained shear stress (see equation 3.1). The function uses the yield stress under daily conditions based on an average pore pressure field and calculates with these values the undrained shear stress. This method is also used by WBI (2017). The only variable in equation 4.1 is the effective stress, because S, m and POP depend on the material used.

POP-values do not only depend on the preloading of the soil but also on material characteristics, pressures and the amount of creep. For example, pressure changes caused by dehydration of shallow layers cause the POP-value of these layers to be higher than the POP-value of the deep layers [J. Tigchelaar, personal communication, July 8, 2019]. In 'Technisch rapport waterspanningen bij dijken' is stated that the POP-value for clay dike material is equal to 28 kPa, for the hinterland 18 kPa and for the deep layers 24 kPa. In the sensitivity assessment the POP-value is varied to understand the effect of this choice on a time dependent calculation. The values for m and S are given in *Appendix H. Input SLOPE/W.*

$$\frac{\tau}{\sigma} = \frac{S_u}{\sigma'_{v,i}} = S \times (OCR)^m = S \times \left(\frac{\sigma'_{v,i} + POP}{\sigma'_{v,i}}\right)^m \qquad 3.1$$

In some calculations at the crest of a dike, the normal force at the base of the first slice will point away from the slice, this indicates a tension force in the soil, which is not realistic. Therefore, a crack tension angle is introduced. When tension occurs, the slip surface is replaced by a crack. The crack angle is set to a value of 135 ($\Phi = 180 - \left(45 + \frac{0}{2}\right)$), because the internal friction angle in undrained soils is equal to zero. Further, the minimum slip surface thickness is 1 meter. Every slip surface with a smaller thickness is considered a micro instability of the slope, which is not considered in this thesis.

3.2.5.2. *Entry and exit range*

The slip surface method that is used is Spencer, the choice for this model is explained in section 2.1.1.2. The slip surfaces are calculated between an entry and exit range. According WBI (2017) only the slip surfaces that enter from the waterside to halfway the inner slope are relevant, see Figure 3.9. The number of increments over the range are chosen in such a way that it does not affect the safety factor too much. The choice is explained in more detail in *Appendix H. Input SLOPE/W*. Based on the effect on the safety factor it is decided to use 55 increments in the entry range, 10 increments in the exit range and 4 radius increments; see Figure 3.10.

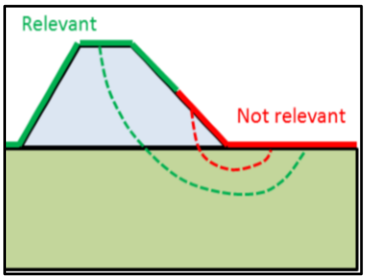

FIGURE 3.9: WBI FAILURE DEFINITION [MONTFOORT, 2018]

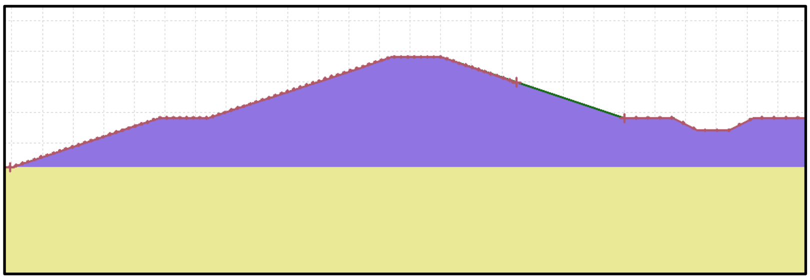

FIGURE 3.10: USED ENTRY AND EXIT RANGE IN THE MODELS SHOWN IN RED INCLUDING NUMBER OF INCREMENTS

3.2.6. Pore pressure field

To investigate the influence of time dependency on the pore pressure field, two parts of groundwater flow are distinguished: the pressure in the subsoils and the pressure in the dike body. The locations which are investigated are shown in Figure 3.11. Point A_1, point A_2 and cross section B are used to investigate the pressures in the subsoil, while cross section C and D are used to investigate the pore water pressures in the dike body. The pore pressure in the dike body are caused by inflow through the slope and inflow through the subsoil. Cross section C is used to investigate the inflow through the slope and cross section D is used to investigate the inflow through the subsoil.

The pressures of points A_1 and A_2 are plotted in time; the pressures of cross section B and C are plotted along the x-axis for different times steps and the pressures of cross section D, are plotted along the y-axis for different time steps.

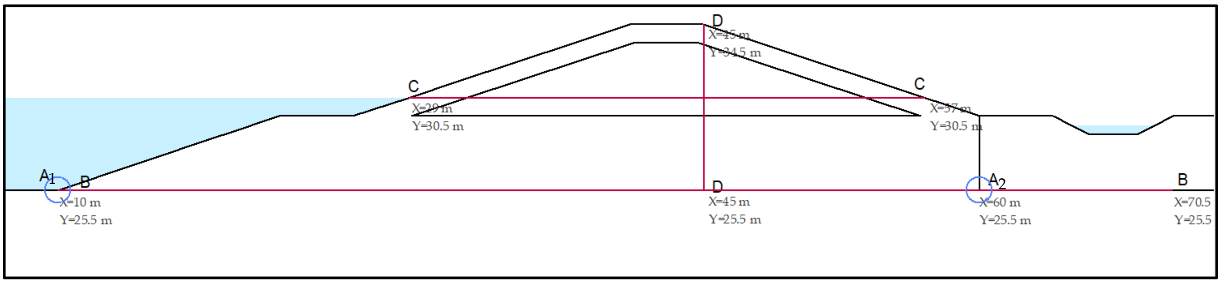

FIGURE 3.11: LOCATIONS FOR THE PORE WATER PRESSURE PLOTS

The pore pressure field caused by the permanent water level is compared with the pore pressure field during the passage of a flood wave with the use of equation 3.2, in which the relative pressure difference (RPD) is calculated. The pore pressure during the passage of a flood wave are dived by the pore pressure caused by a constant water level. RPD is calculated at the inner toe of the dike (point A_2) and under the crest of the dike at a height of 25.5 meter (point D).

$$RPD = \frac{p_{Stationary}}{p_{Transient}} \qquad 3.2$$

The lowest value in time of RPD indicates the most governing hydraulic state, because the pore pressures are highest in time. This moment in time is compared with the time of occurrence of the maximum outer water level.

3.2.7. Sensitivity assessment

A python model is developed that combines the variables provided in Table 3.1 (512 combinations in total). The python model is coupled with SEEP/W and SLOPE/W and calculates the factor of safety for inner slope stability (this is to our knowledge, not done before). For each combination a safety factor is calculated for the stationary water level and the flood waves at Rotterdam, Borgharen and Lobith. For the flood waves, different pore water pressures are found in time. For each time step, the factor of safety of the critical slip surface is selected and plotted against the time (see Figure 3.12 and Figure 3.13). So, the dominant slip surface can change in time. The factor of safety is calculated for a duration of 1.5 times the total duration of the flood wave with 20 timesteps. The results are compared with the use of a representative safety factor difference (RSFD) in which the governing factor of safety of the transient case (the lowest factor of safety in time) is divided by the factor of safety of the stationary case (see equation 3.3). A value of one indicates that stationary condition is reached during the passage of a flood wave, while value larger than one indicates that there are differences between the transient and stationary states. The larger this value, the larger these differences.

$$RSFD = \frac{\min(FoS_{Transient})}{FoS_{Stationary}} \qquad 3.3$$

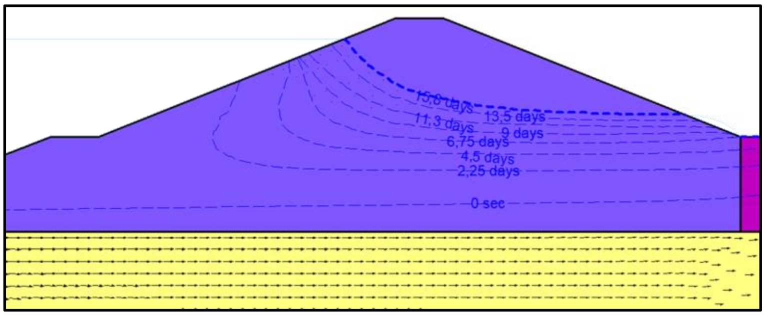

FIGURE 3.12: PHREATIC SURFACE IN TIME

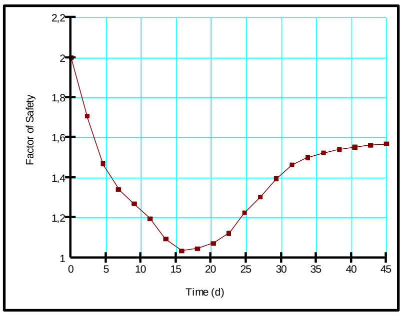

FIGURE 3.13: FACTOR OF SAFETY VS TIME

The results of the sensitivity assessment are presented as shown in Figure 3.14. The value of RSFD is calculated for all combinations. The cases with a specific characteristic are plotted against the same cases without that characteristic. For example, the results of dikes with a foreshore are plotted against the results of dikes without a foreshore. The same is done for the time after the maximum water level that is needed to reach the governing hydraulic state. In this way can be seen which variable are sensitive for a transient calculation, because when the results deflect to an axis, that variable is sensitive for a transient calculation.

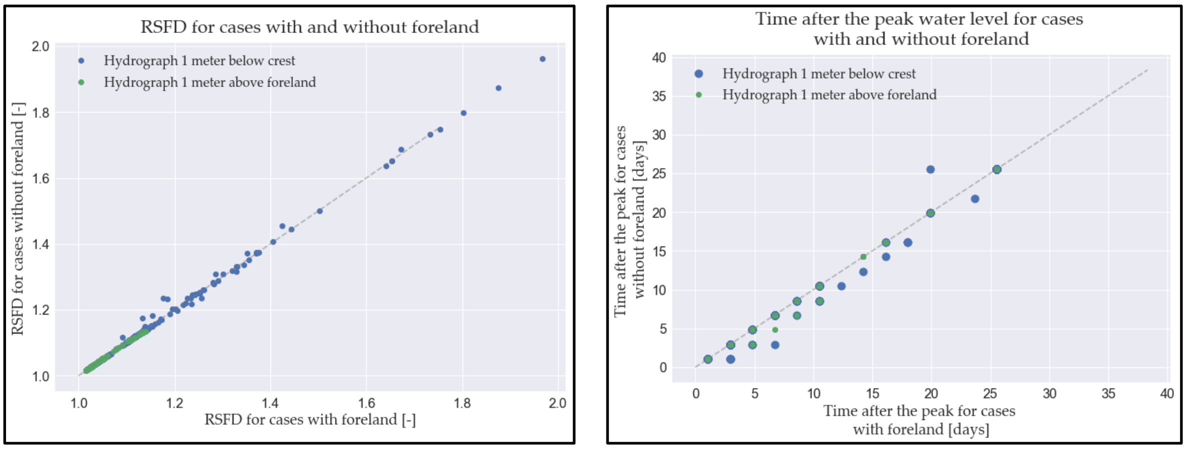

FIGURE 3.14: EXAMPLE RESULTS RESEARCH QUESTION 2, SENSITIVITY ASSESSMENT

3.2.8. Block-waves

The influence of variability in the height and duration of the flood wave on the safety factor is investigated with the use of block-waves (rectangular waves with a certain height and duration). This way, only the influence of these variables on the safety factor is investigated and the influence of other variables (for example the curvature of waves) is ignored. The waves with a short duration indicate the conditions at sea, while the waves with a longer duration indicates the conditions in the river. The duration has a maximum of 28 days, because this is a typical maximum duration for flood waves in the Rhine. Stationary conditions do not necessarily have to be achieved in the simulated duration. For each height and duration, the factor of safety for inner slope stability is calculated for the four dike types shown in Figure 3.3. The value of $RSFD$ is calculated and plotted in a 3D figure with the height and the duration on the x- and y-axis and the value of the RSFD on z-axis. The same results are presented in a contour plot. Next to the RSFD value, also the stationary and transient safety factors (lowest safety factor in time) are shown. In Figure 3.15 an example of the result is shown.

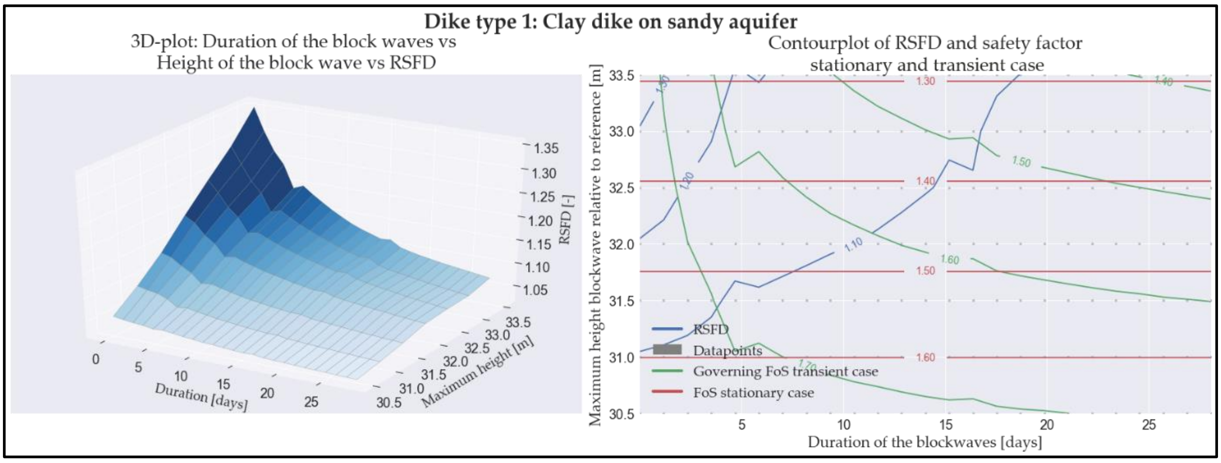

FIGURE 3.15: EXAMPLE RESULTS SUB-QUESTION 2: BLOCK-WAVE ANALYSIS

3.3. Results

The results of the pore-water pressure field, the sensitivity assessment and the block-wave analysis are discussed in this section. In this section the following terms are used: high-water wave (HW) and low-water wave (LW). The high-water wave represents the waves for which the top is presented 1 meter below the crest of the dike. Low-water waves are the waves for which the top is presented 1 meter above the foreshore. The results are presented in detail in *Appendix I. Results pore pressure field* and *Appendix J. Results sensitivity assessment.*

3.3.1. Pore-water pressure field

3.3.1.1. Pore-water pressure in subsoil

The subsoil of dike type 1, 2 and 4 consist of sand, while the subsoil material of dike type 3 consists of clay. In Figure 3.16 the pore water pressures at the inner and outer toe are plotted during the passage of a flood wave and during the stationary state. Looking at the pore pressure at the toe of the dike in the sand aquifer, a lag in the response can be noted, the peak is lower and the curve is wider. These differences are caused by the storage capacity of the soil. If the dike consists of permeable sand instead of clay (dike type 2) lower pressures are found in the aquifer, because the water can flow upwards and the storage capacity of sand is larger than that of clay. When an impermeable clay dike is present, the pressure in the aquifer built up because the upward flow is retained. Therefore, smaller differences are found for dike type 1 and 4 between the permanent and transient state. Looking at dike type 3, at the inner toe of the dike the pore water pressure remains unchanged. The permeability of the clay layer is smaller than the permeability of the sand layer due to which the increased pore pressure reaches less far in the dike.

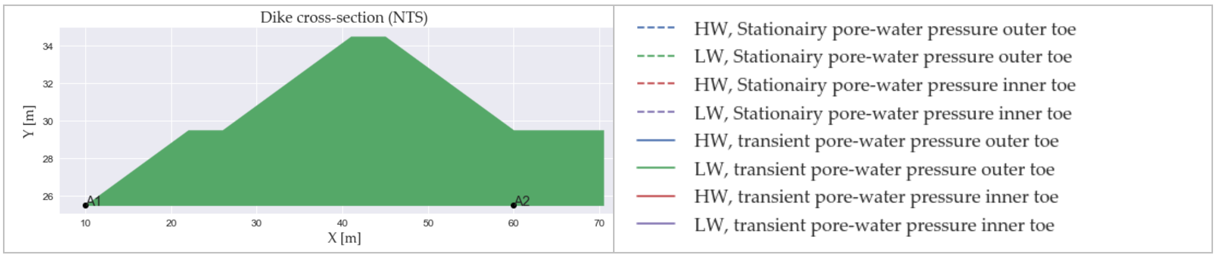

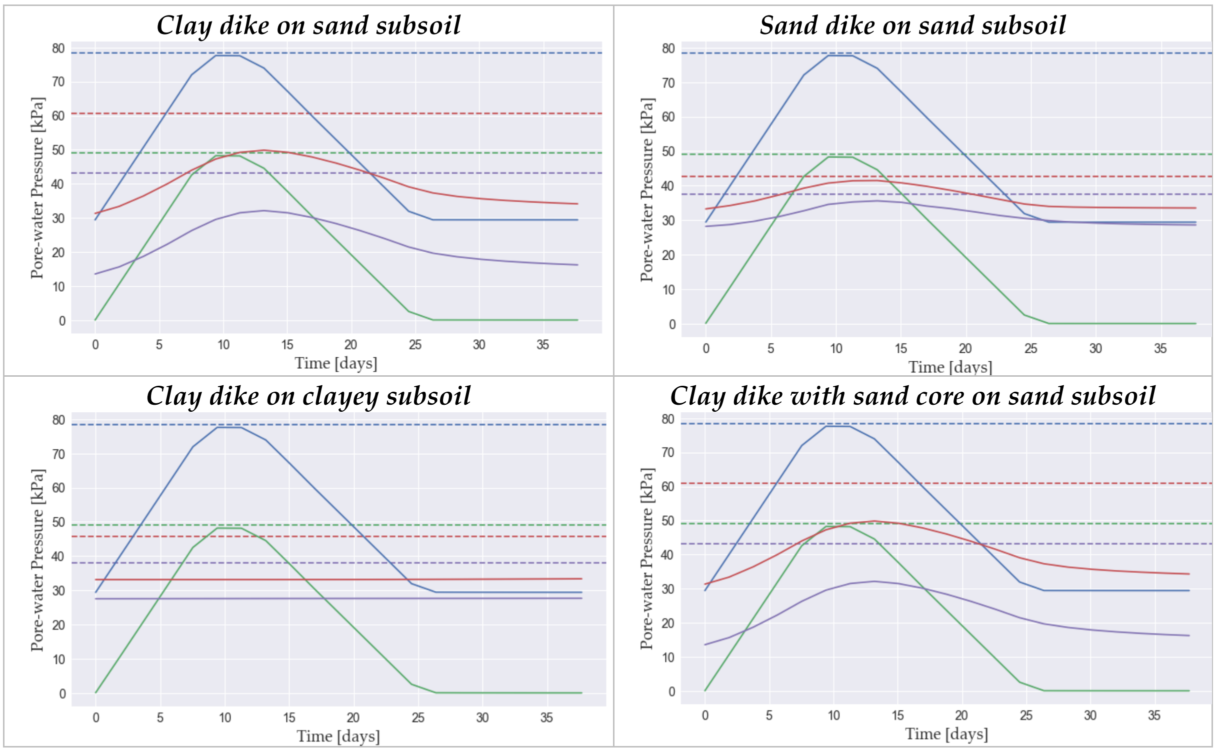

FIGURE 3.16: PORE WATER PRESSURE DURING PASSAGE OF A FLOOD WAVE IN THE RHINE FOR DIFFERENT DIKE TYPES AT THE TOE OF THE DIKE, POINT A

The effect of unchanged pressures in clay on clay dikes (dike type 3), can be illustrated with the use of the leakage length. In Figure 3.17, the pore-water pressures are plotted along the dike body for different time steps. The pore pressure at the outer toe increases with the outer water level and in case of sand subsoils, the effect reaches far in the subsoil. The leakage length for the clayey subsoil is an order smaller than that of sand (caused by the difference in permeability of the soil). This causes the increased pore pressure to reach less far in the dike. The differences between the permanent and transient state are therefore large, when a dike consist completely out of clay.

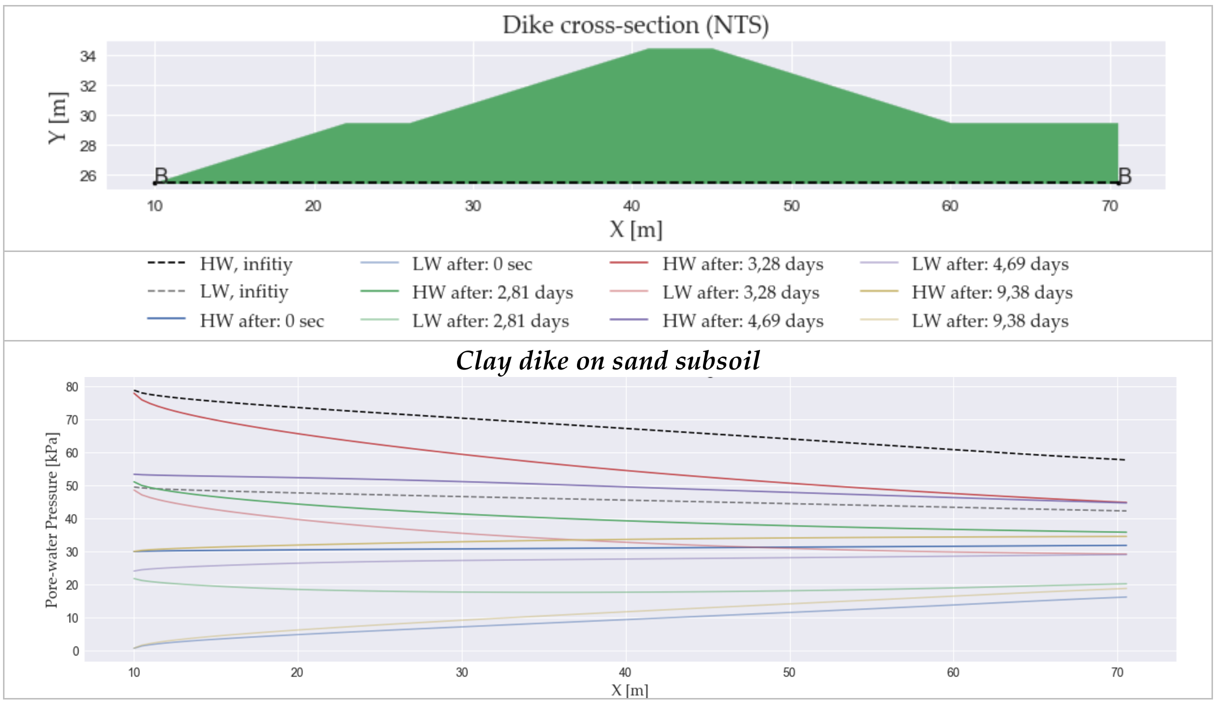

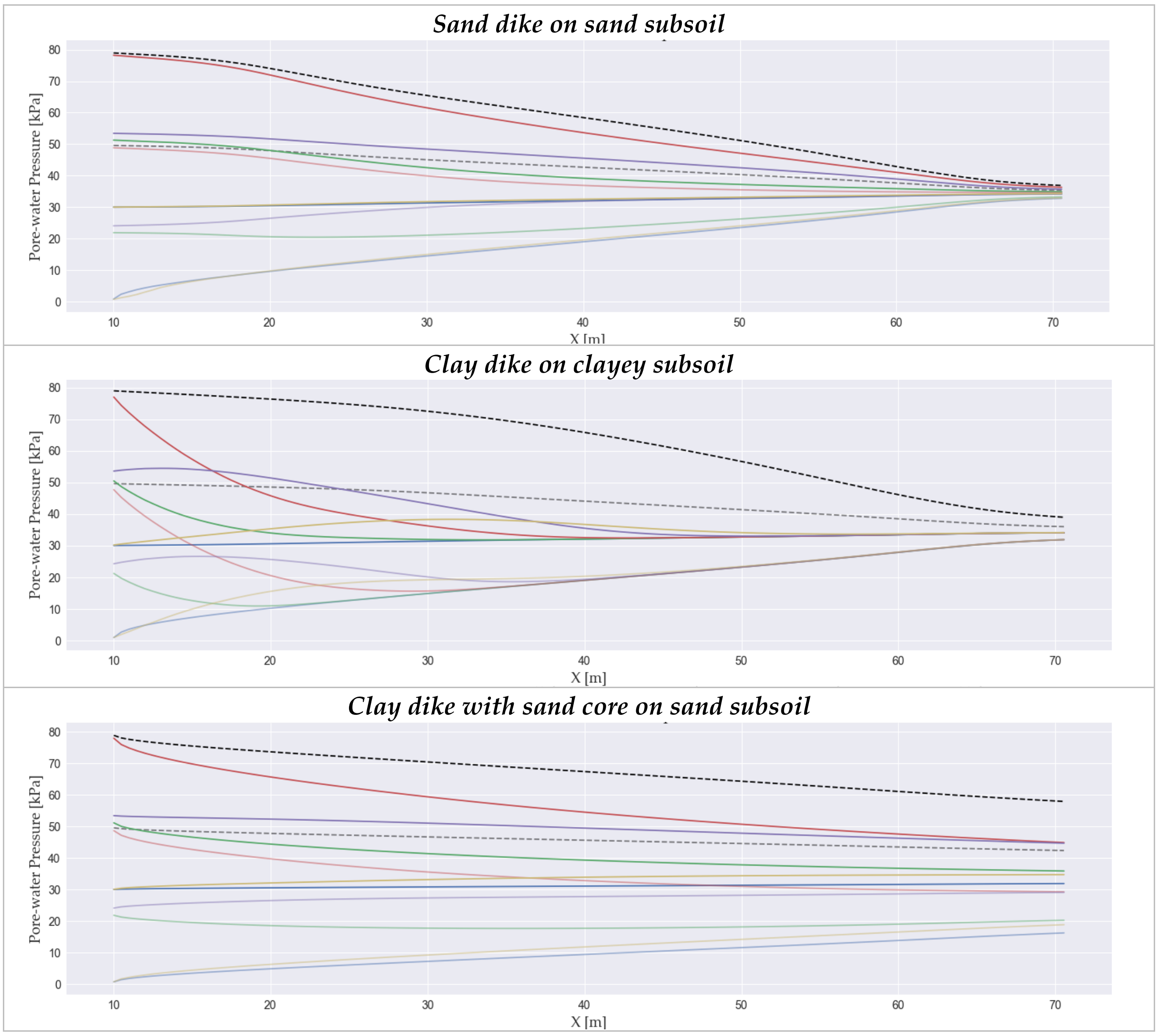

FIGURE 3.17: PORE WATER PRESSURE OVER THE TOTAL LENGTH OF THE DIKE BODY FOR DIFFERENT TIMESTEPS (CROSS SECTION B)

3.3.1.2. Pore-water pressure in dike body

The pore pressures in the dike body are caused by inflow through the slope and inflow from the aquifer. To investigate the inflow through the slope, the pore pressures 1 meter above the foreshore are plotted along the x-axis (Figure 3.18). To investigate the inflow from the aquifer the pore pressures under the crest of the dike are plotted along the y-axis (Figure 3.19).

For all cross-sections, the pore-water pressure at the outer slope follows the flood waves (see Figure 3.18); causing the differences between the transient and stationary state to be small. These differences increase the further the water reaches inside the dike body. The differences are smallest for the dike body consist of sand and largest for the dike bodies consist of clay, because the permeability of sand is higher than that of clay, causing the horizontal and vertical intrusion length to be larger. Also, lower pressures in the stationary state are found for sand dikes than clay dikes caused by the material characteristics (porosity and permeability), therefore the differences between the stationary and transient state are smaller. For the sand dike the inflow through the slope reaches till a distance of about X=50 m, while this distance is around the 45 meters for the clay dikes.

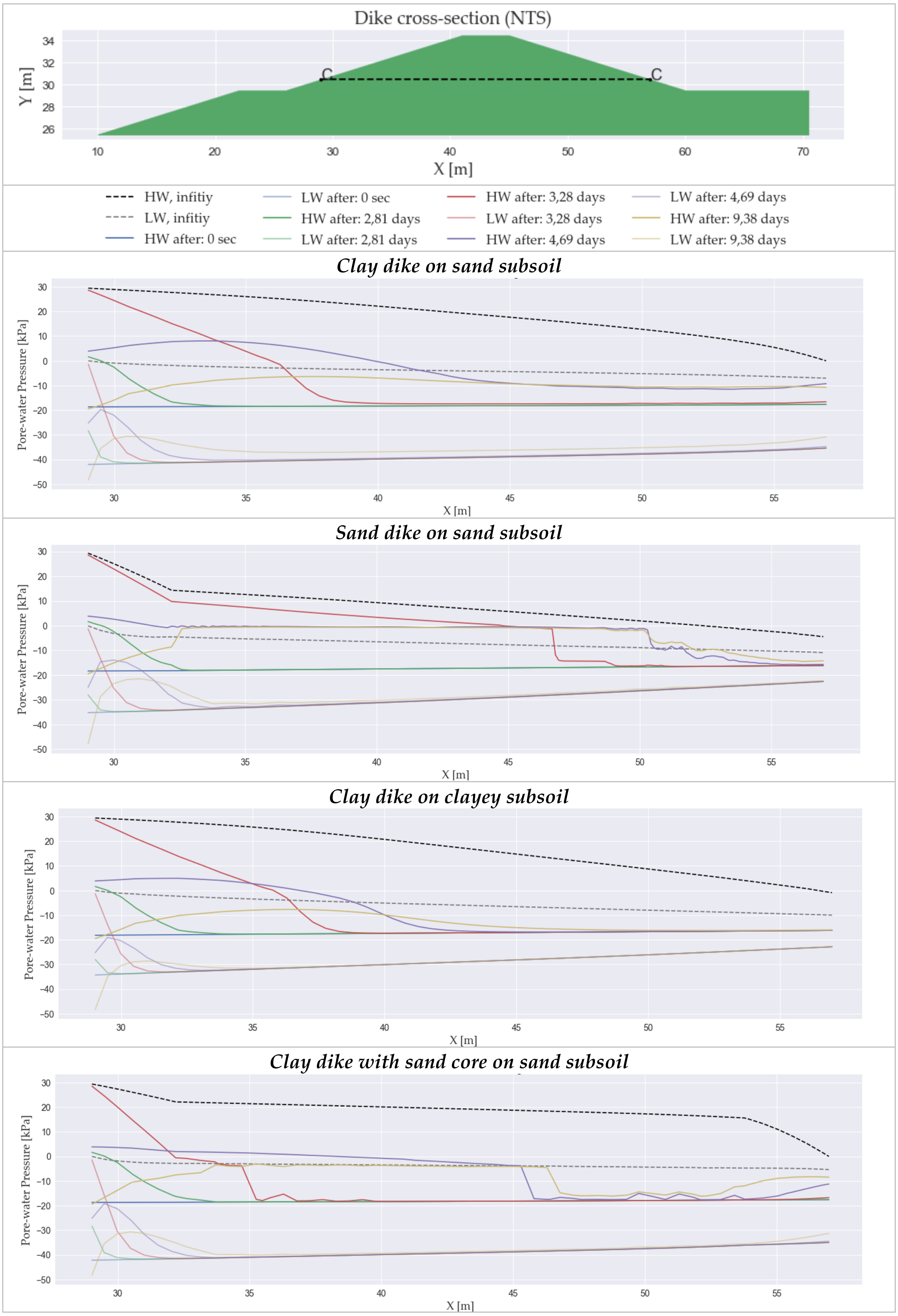

FIGURE 3.18: INFLOW THROUGH THE SLOPE IN THE DIKE BODY DURING THE PASSAGE OF A FLOOD WAVE. CROSS SECTION C

Looking at the inflow from the aquifer in the dike (Figure 3.19); there is hardly any inflow from subsoil into the dike when the subsoil consist of clay, because the increased pore water pressures reaches not that far in the clayey subsoil. When the subsoil consists out of sand, the pore pressure of both the clayey and sand dike bodies increases. The increase is largest when the dike body consist of sand.

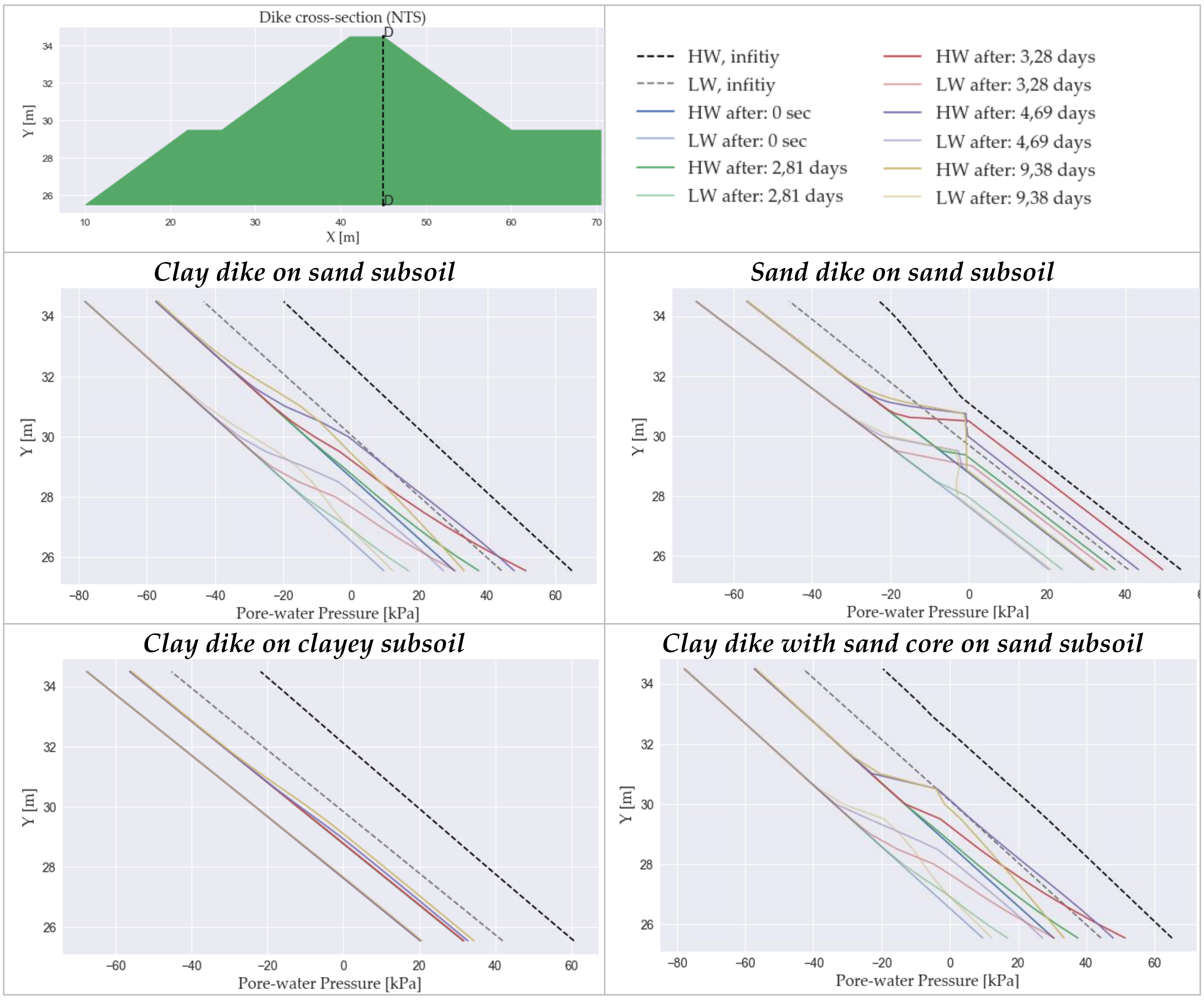

FIGURE 3.19: INFLOW FROM THE AQUIFER INTO THE DIKE BODY DURING THE PASSAGE OF A FLOOD WAVE, CROSS SECTION D

3.3.1.3. Delay in response

Governing hydraulic state is defined as the state where the highest pore water pressures are found and would therefore lead to the lowest safety factor, when looking at slope stability of the inner slope. The governing hydraulic state does not occur simultaneously with the maximum outer water level (see Figure 3.16). In Table 3.2, the delay in response is represented (the time of the governing hydraulic state after occurrence of the maximum flood wave height). Both dike type 1, 2 and 4; the time of the governing hydraulic state takes place shortly after the maximum water level is reached, while the governing hydraulic state of dike type 3 (the clay dike on clayey soil) takes much more time to reach. The governing hydraulic state is found in the last investigated time step (1.5 time the flood wave duration is investigated) for all flood waves in combination with the clay dike on clayey soil. So, the governing state could also occur later in time.

The results of the high-water curves and the low-water curves shows the same characteristics. Looking at the flood waves at the different location, the curves at Lobith shows the largest difference in time, followed by Borgharen and Rotterdam.

The differences are caused by the material of the subsoil. Both the subsoil material of dike type 1, 2 and 4 consist of permeable sand, while the material of dike type 3 consist of clay. The increased pressure in the aquifer (for dike type 1,2 and 4) causes next to inflow through the slope, also inflow form the aquifer into the dike bodies. Due to the two-sided flow, the governing hydraulic state is achieved earlier in time. While for the clay on clay dike, only the flow from the slope is governing, which causes the governing hydraulic state to be later in time.

TABLE 3.2: DELAY IN RESPONSE DURING THE PASSAGE OF A FLOOD WAVE IN DAYS

	Sea, Rotterdam		Meuse, Borgharen		Rhine, Lobith	
	LW	HW	LW	HW	LW	HW
Dike type 1	0.15	0.15	1.31 – 2.13	1.31 - 2.13	2.94	2.94
Dike type 2	0.15 – 0.62	0.15	1.31 - 2.13	1.31	2.94	1.06 - 2.94
Dike type 3	6.25	6.25	11.96	11.96	27.44	27.44
Dike type 4	0.15	0.15	1.31 – 2.13	1.31 - 2.13	2.94	2.94

3.3.1.4. Relative pressure differences

The RPD-values are shown in Table 3.3. The higher this value, the larger the differences are between the stationary and transient state. The differences are discussed per dike type, per flood wave and per initial state.

TABLE 3.3: RPD FOR DIFFERENT DIKE TYPES FOR DIFFERENT WATER LEVEL HYDROGRAPHS

	Sea, Rotterdam				Meuse, Borgharen				Rhine, Lobith			
	Crest		Toe		Crest		Toe		Crest		Toe	
	HW	LW	HW	LW	HW	LW	HW	LW	HW	LW	HW	LW
Dike type 1	1.17	1.27	1.18	1.28	1.22	1.37	1.24	1.39	1.19	1.32	1.21	1.33
Dike type 2	1.11	1.19	1.05	1.09	1.08	1.15	1.04	1.07	1.04	1.09	1.02	1.04
Dike type 3	1.28	1.34	1.13	1.16	1.62	1.76	1.29	1.31	1.74	2.02	1.36	1.37
Dike type 4	1.17	1.28	1.18	1.28	1.23	1.37	1.25	1.39	1.19	1.32	1.22	1.33

Differences per dike type

From Table 3.3 can be seen that there are differences between the stationary and transient state for all cases. The differences for dike type 2 (the sand on sand dike) are smallest, while the differences for dike type 3 (the clay on clay dike) are largest; however, there are some exceptions. From the sections before was concluded, that the inflow through the slope has effect until the crest, while inflow from a sand aquifer has influence over the whole bottom of the dike. The sand dike (type 2) has the highest hydraulic conductivity, causing the largest inflow from the aquifer, which again leads to the smallest differences between the states. The clay on clay dike (type 3) shows the largest differences because the hydraulic state on the inner side of the dike during the passage of a flood wave hardly adjust, due to the low hydraulic conductivity of the clayey material.

In some cases, dike type 1 and 4 (clay on sand dikes) show larger differences than dike type 3. This is for the low water curves from Rotterdam and the Meuse under the toe of the dike. The differences are caused by the shorter duration of the water level hydrographs of Rotterdam and Borgharen compared to the flood wave at Lobith. Due to the shorter duration, the increased pore water pressure does not reach till the inner toe op the dike; because the leakage length increases in time (see equation C.11) and is shorter than the width of the dike. So, the pore water pressure at the toe of the dike hardly adjusts to the outer water level, therefore the RPD is dependent of the initial state. For the low water curves, the outer water level of the initial state is lower than the polder water level. Looking at the location of the phreatic surface (Figure 3.20), a strong curvature near the ditch is found when the subsoil consists out of sand and the dike body out of clay. This is not the case when both the dike and the subsoil consist of clay, the phreatic surface increases gradually. This causes the value for the RPD to be high when the subsoil consists out of sand. Note that these results depend on the chosen initial water level.

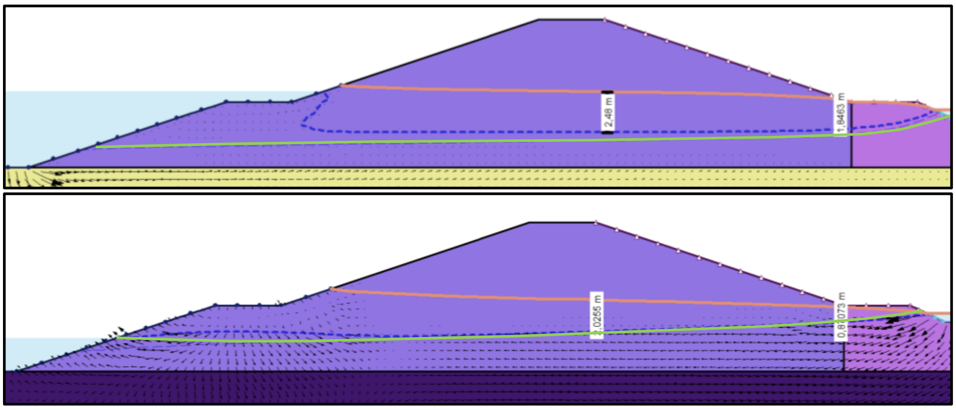

FIGURE 3.20: PHREATIC SURFACE FOR DIFFERENT SUBSOIL LAYER MATERIALS, GREEN = INITIAL PHREATIC SURFACE, ORANGE = STATIONARY PHREATIC SURFACE, BLUE= GOVERNING TRANSIENT PHREATIC SURFACE

Differences per flood wave

Looking at dike type 2 (the sand on sand dike), the largest differences are found for a flood wave from the sea. The duration is that short that the leakage length cannot fully develop and the increased pressure does not reach the inner toe of the dikes, as state above. Looking at dike type 3 (the clay on clay dike), the largest differences are found for a flood wave at Lobith, followed by Borgharen and Rotterdam. The height of the curves is largest at Lobith followed by Borgharen and Rotterdam. Because in the clayey soil the hydraulic state at the inner side of the dike hardly adjust during the passage of the water level hydrograph, the highest flood wave is governing and lead to the largest differences between the stationary and transient state.

Dike type 1 and 4 (clayey on sand dikes) show the largest differences during the passage of a flood wave from the Meuse. The largest differences are expected for high waves with a short duration, because the leakage length increases with the root of time. The waves at Lobith are highest and have the longest duration, followed by Borgharen and Rotterdam. At Lobith the value of RPD decreases due to the long duration, while at Rotterdam the value decreases due to the small height. Therefore, the flood wave from the Meuse shows the largest differences between the stationary and transient state.

Differences per initial state

When comparing the high-water curves with the low-water curves, the differences are larger for the low-water curves. For the high waves the inflow area over the slope is larger, more water can flow from the slope into the dike. So, the increased pore pressures reach further into the dike. The higher the pressures are in the dike during the passage of a flood wave the lower the value of RPD.

3.3.2. Sensitivity assessment

In the sensitivity assessment the effect of some dike characteristics on the safety factor is investigated. All results of the sensitivity assessment are presented in *Appendix J. Results sensitivity assessment*. The flood wave at Rotterdam shows the lowest values of $RSFD$, while the $RSFD$- values in the Rhine and the Meuse are of the same order of magnitude. A flood wave at Sea has the shortest duration, which cause the differences between the stationary and transient case to be large; but the height of the wave is low, which cause the differences to be lower. Only the results at Lobith are used to discuss the results with, because at all location the same characteristics are dominant and thus the same conclusion is obtained. Differences between the locations are obtained, when comparing the time of failure after the peak of the flood wave. Therefore, all locations are discussed when is looked at the governing safety factor in time.

A standard dike is used to show the effect of a certain characteristic on the value of $RSFD$. The standard dike has a clayey core, clayey hinterland, a sand aquifer, a ditch, a foreshore , a POP-value of 0 kPa and a thickness of the subsoil of 3 meter. For this specific dike type, a $RSFD$ of 1.41 is found. Which means that there are differences between the stationary safety factor and the lowest safety factor during the passage of a flood wave from the Rhine. After the results of the standard dike are discussed, all results are presented.

3.3.2.1. Dike core material

The $RSFD$ value of 1.65 is found for the standard dike[1] with a sand core, which means that the importance of a time dependent calculation increases when a sand core is present because larger differences are found between the safety factor. In Figure 3.21, all results are shown for cases that are varied in the core material. When a low flood wave passes the dike, the core material has no influence on the results. This can be declared, because the water does not pass the core.

For the high-flood wave, all $RSFD$ are higher when the core consists of sand (so not only for the standard dike with a sand core). In the stationary state, higher pressures are found in the dike with a sand core compared to the same dike with a clayey core. The flow changes direction at the layer separation, in such a way that higher pressures are found when the core consist of sand (section 2.4.3.2). In the transient state, there is hardly any difference in the hydraulic state between the two dike types (see Figure 3.22). The reason for this, is that the sand dike material is dry before the passage of a flood wave, while the clayey material consists some water due to the matric suction capacity.

[1] *Dike with clayey core, clayey hinterland, a sand aquifer, a ditch, a foreshore, a POP-value of 0 kPa and a thickness of the subsoil of 3 meter -->* $RSFD = 1.41$

The hydraulic conductivity of the sand core is therefore at some parts equal or even lower than the hydraulic conductivity of the clay core, because the hydraulic conductivity is dependent of the volumetric water content. So, during the stationary state higher pore pressures are obtained at the toe of the dike when the dike core consists out of sand, larger differences between the safety factors are found.

Also, can be seen that when the core consists out of sand it takes more time to reach the governing safety factor. But when the subsoil consists out of clay, it takes more time for the clayey core to reach the governing safety factor. The sand core is dry before the passage of the flood wave and it takes some time to fill with water. The flow from the subsoil has the largest contribution to this, therefore when the subsoil consists of clay, it took more time when the core consists of clay.

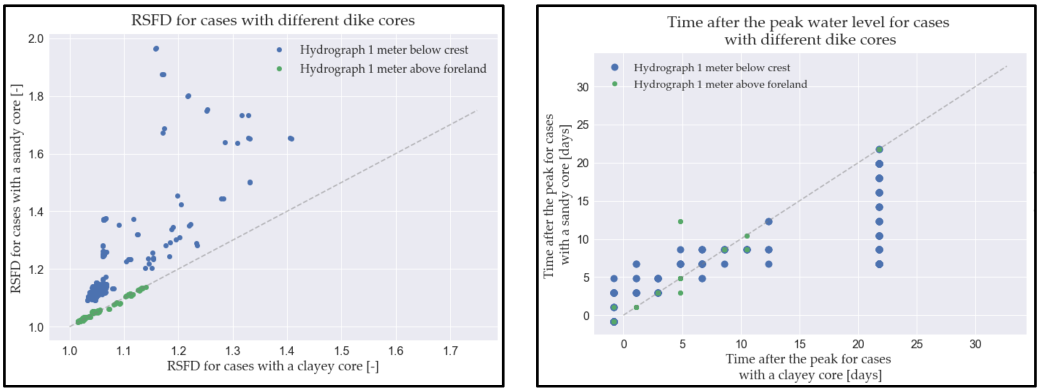

FIGURE 3.21: RESULTS AT THE RHINE FOR CASES WITH DIFFERENT DIKE CORE MATERIALS

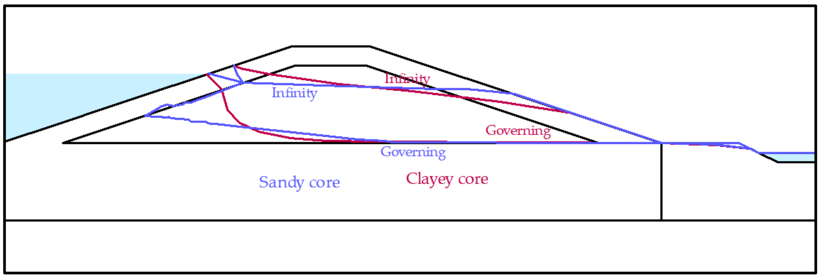

FIGURE 3.22: PHREATIC SURFACE WITH AND WITHOUT CORE DURING TRANSIENT(GOVERNING) AND STATIONARY(INFINITY) CASE

3.3.2.2. Presence or absence foreshore

A $RSFD$ value of 1.41 is found for the standard dike[1] without a foreshore. This mean that for this case the presence or absence of the foreshore has no influence on the importance of a time dependent calculation. When all results are compared (Figure 3.23), it can be noted that for all cases the value of $RSFD$ remains the same with or without foreshore. The presence of a foreshore has influence on horizontal intrusion length. But for both cases the water does not enter further than halfway the dike, therefore it has no influence on the safety factor of inner slope stability. Vertical intrusion via the aquifer is more of influence, but this effect is independent of the presence of the foreshore.

When a foreshore is absent the governing hydraulic state is reached earlier in time, because the flow path through the aquifer is shorter. In the results of the Rhine there are some exceptions on this rule for the cases where the subsoil consists out of clay.

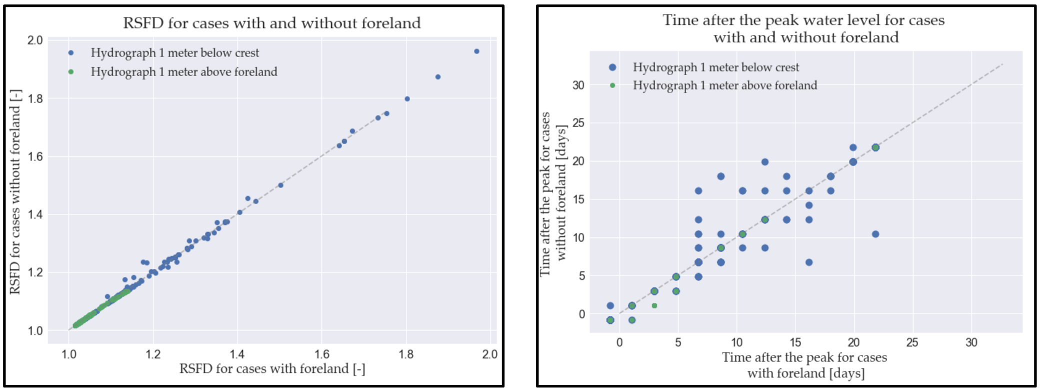

FIGURE 3.23: RESULTS AT THE RHINE FOR CASES WITH AND WITHOUT FORESHORE

3.3.2.3. *Presence or absence ditch*

The *RSFD* for the standard dike without ditch[1] is equal to 1.21. This implies that the presence of a ditch increases the difference in safety factor between the stationary and transient case. Looking at all results where is varied in the presence of a ditch (Figure 3.24), not all cases result in a higher *RSFD* value when a ditch is present. The results where *RSFD* is larger with a ditch, are the cases where with a ditch more uplifting of the hinterland occurs than without ditch. This concept is illustrated with an example: *RSFD* is larger with a ditch when uplifting of the hinterland occurs during the stationary and transient state, while without ditch only uplifting occurs during the stationary state. This is shown in Figure 3.25. When the same conditions occur, for example both with and without ditch the hinterland will not lift up, then larger values of *RSFD* are found in the absence of a ditch, because of the differences in the pore pressure field caused by the constant water level. Looking at the time after the peak of the flood wave, it can be seen that it takes much more time to reach the governing state when the hinterland does not lift up.

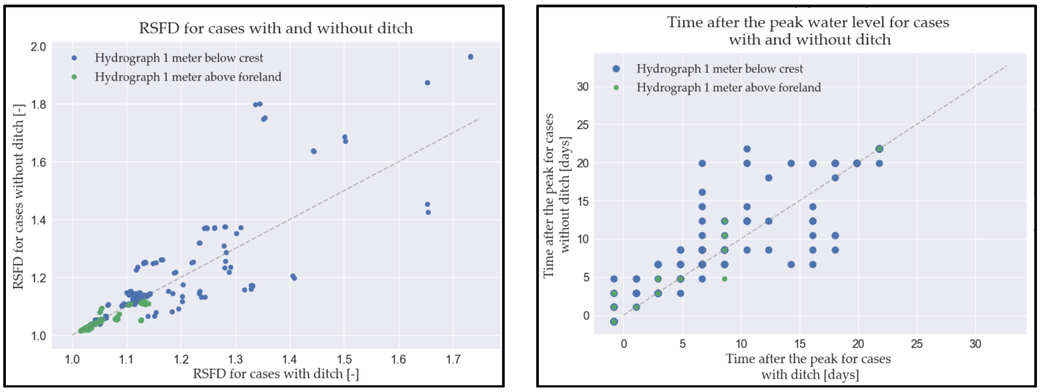

FIGURE 3.24: RESULTS AT THE RHINE FOR CASES WITH AND WITHOUT DITCH

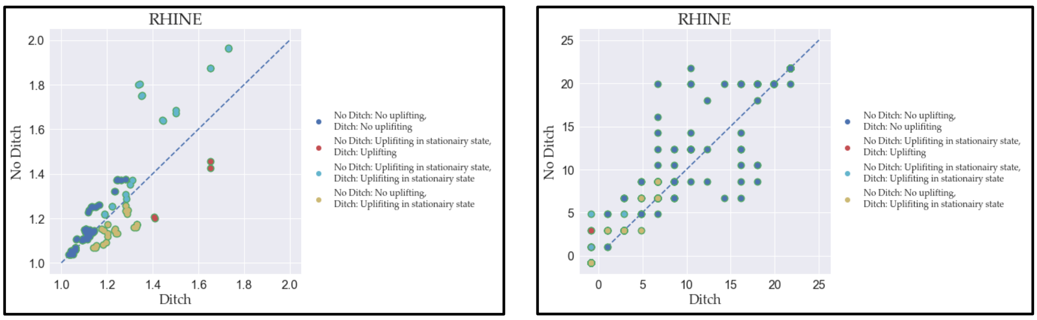

FIGURE 3.25: RSFD UPLIFTING SCENARIOS FOR THE RHINE (LEFT) AND TIME SCENARIOS (RIGHT)

3.3.2.4. *Hinterland material*

The $RSFD$ amounts 1.04 when the hinterland material of the standard dike[1] consist of sand. A low value of $RSFD$ implies that during the passage of a flood wave almost the same safety factor is reached as in the stationary state. The pore pressures in the dike body differ during the stationary and transient state, but this does not cause large differences in safety factor. While viewing the standard dike[1] results, uplifting occurs during the stationary state, resulting in very low safety factor (< 0.9). No uplifting of the hinterland occurs during the passage of a flood wave, through which a safety factor is found which is in the same order as when the hinterland consist of sand. In Figure 3.26 all results are shown where the material of the hinterland has been varied. The results divert strongly to the vertical axis, which implies that larger differences between the stationary safety factor and transient safety factor are found when the hinterland consist of clay. As state above, if the hinterland consist of sand uplifting does not take place, while it could take place when the hinterland consists out of clay and the subsoil out of sand. When uplifting occurs lower values of the safety factor are found during the stationary state than the transient state, because more parts of the hinterland lift up. Therefore, large values of $RSFD$ are found.

Looking at the time of the governing safety factor it can be seen that the hinterland material has influence on the time after the peak of the governing state. But no clear relation is found.

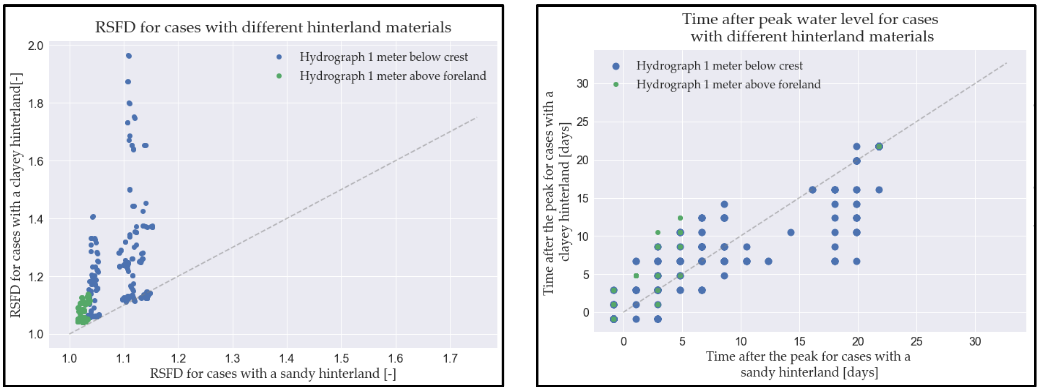

FIGURE 3.26: RESULTS AT THE RHINE FOR CASES WITH DIFFERENT HINTERLAND MATERIALS

3.3.2.5. *Sub-layer material*

When the sub-layer material of the standard dike[1] is changed in clay, a $RSFD$ of 1.06 is found. No large differences in safety factor are found between the stationary and transient state because uplifting of the hinterland cannot take place when a sand aquifer is absent. Considering all results (Figure 3.27) a strong deflection is found to the horizontal. When uplifting occurs, lower values of the safety factor are found during the stationary state than the transient state, because more parts of the hinterland lift up than during the passage of a flood wave. When the subsoil consists out of clay, the hydraulic conditions hardly changes during the passage of a flood wave. But this effect is small compared to the effect of uplifting of the hinterland.

Looking at the time that it takes to reach the governing safety factor, it takes much more time when a clayey layer is present under the dike. Note that at the Sea and in the Meuse the time is equal to the maximum investigated time, it could take more time.

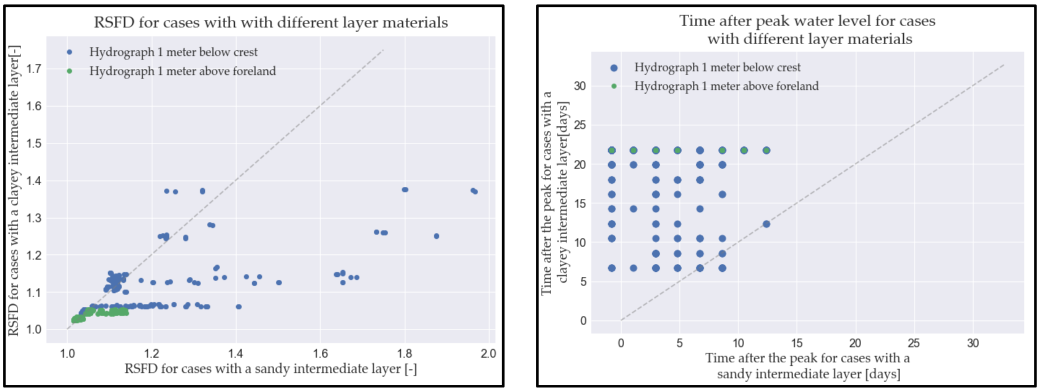

FIGURE 3.27: RESULTS AT THE RHINE FOR CASES WITH DIFFERENT SUBLAYER MATERIALS

3.3.2.6. Thicknesses of the cover layer

The $RSFD$-values are respectively 1.20, 1.14, 1.06 for the standard dike[1] that varies in the thickness of the sub-layer from 4 till 6 meters. This implies that an increasing sub-layer thickness decreases the differences in safety factor between the stationary and transient state. The thicker the hinterland the less often uplifting of the hinterland occurs. When uplifting occurs the differences between the stationary state are larger (see the section before).

Taking all results into account it can be noted that some $RSFD$-values are independent of the thickness. These are the cases where the subsoil consists completely out of clay and therefore the thickness of the cover layer has no effect. For the cases where the subsoil consists of sand a deflection to the horizontal axis is found (see Figure 3.28); which implies that the thicker the cover layer the smaller the value of $RSFD$ (there are some exceptions). All cases where the $RSFD$ of a thick layer is larger than the $RSFD$ of the cases with a cover layer thickness of 3 meter; are the cases where uplifting of the hinterland occurs during the stationary state but not during the passage of a flood wave. Under the same conditions, thicker layers show larger differences in safety factor.

At the Meuse and at Sea a strong curvature is found to the vertical axis when viewing the time after the peak of occurrence of the governing safety factor. When uplifting occurs, smaller values in time are found. At the Meuse and at Sea the initial water level is higher than the Rhine, causing uplifting of hinterland with a thickness of 3 meters to occur immediately after the peak of the high water. In the Rhine this takes more time.

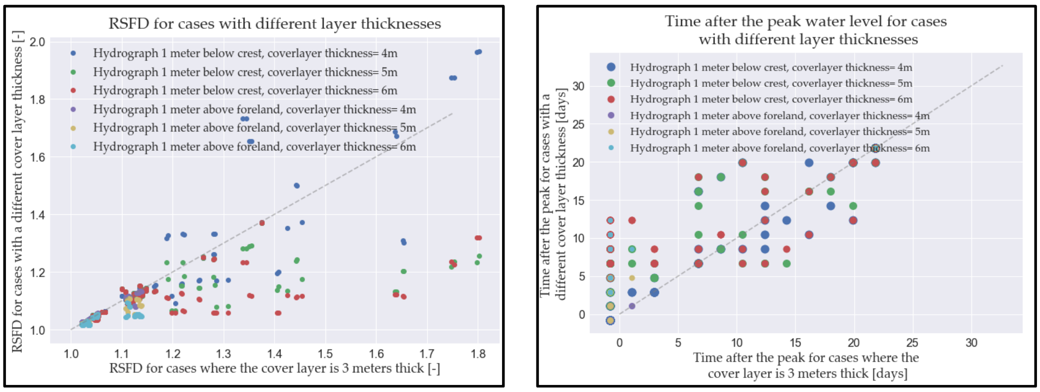

FIGURE 3.28: RESULTS AT THE RHINE FOR CASES WITH DIFFERENT SUBLAYER THICKNESSES

3.3.2.7. POP-value

An increasing POP-value from 0 (the POP-value of the standard dike[1)]) until respectively 30, 80 and 130 kPa results in a $RSFD$ of 1.28, 1.22 and 1.19. This implies that higher POP values result in lower $RSFD$. Looking at all results shown in Figure 3.29, indeed a deflection to the vertical can be seen. Which implies that higher values of POP leads to larger values of $RSFD$. There are some exceptions, these are the cases were both uplifting occurs during the stationary and transient state when the POP value is 50 kPa but only uplifting occurs during the stationary state when the POP value is higher. A stronger layer shows larger differences when the same conditions occurs. This confirms the findings from the section 3.3.2.6. So, when both uplifting occurs during the transient and stationary state with a POP value of 50 and 100, $RSFD$ is higher for the case with a POP value of 100 kPa.

Looking at the time of occurrence of the governing transient state, there are difference for different yield stresses and a positive trend can be seen.

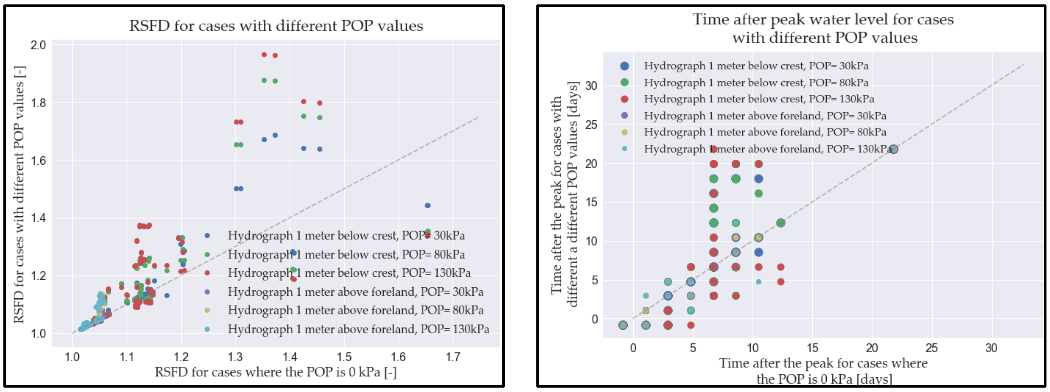

FIGURE 3.29: RESULTS AT THE RHINE FOR CASES WITH DIFFERENT POP VALUES

3.3.3. Block-waves analysis

The results of the block-waves are presented in Figure 3.30 till Figure 3.33. Dike types 1, 2 and 4 show the same curvature, but the $RFSD$ for dike type 4 is higher, followed by dike type 1 and 2. The differences for these dike types are largest when the duration is short and the height is high. For dike type 1, 2 and 4 a curvature is found in the 2D-plots of the governing safety factor in the transient state. This indicates that for these cases considering the duration in a probabilistic calculation is very useful. For dike 2, the curvature decreases when the duration increases; considering the variation of the duration in a probabilistic calculation is therefore less useful for a sand dike when the duration is longer than two weeks. Dike type 4 is independent of the duration of the block-waves. Therefore, is considering the duration in a probabilistic less useful for a dike consisting completely out of clay. Further it can be noted that for all dike type the safety factor during the stationary state increases linearly with the height of the block-waves.

Dike type 1, the clay on sand dike; has an intrusion length that slowly increases in time due to the low permeability of the clay. Therefore, it takes some time before the stationary state is reached. Therefore, the $RSFD$ is high when the block-wave is high and has a short duration.

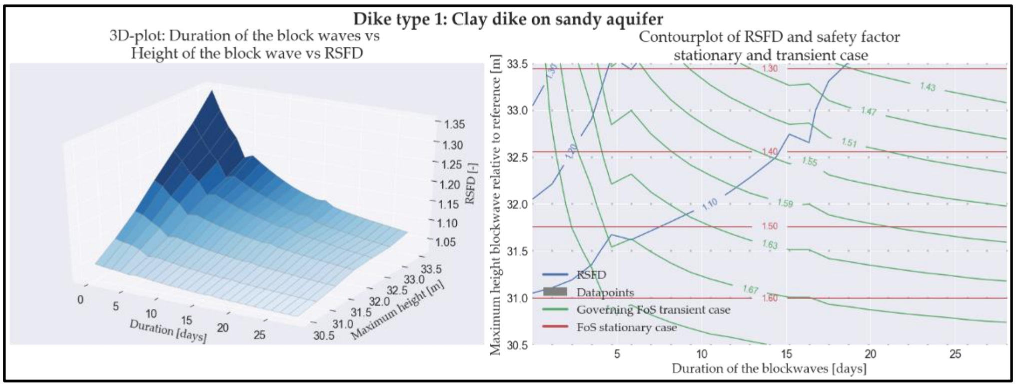

FIGURE 3.30: RESULT BLOCK-WAVES ANALYSIS FOR DIKE TYPE 1

Dike type 2, where the dike body consist of sand, is not very sensitive for a transient calculation. Sand has a high permeability, due to which the pore water pressure follows the outer water level fast. The delay is small and the intrusion length is high. Only when the duration of a block-wave is very short and the height is high; the pore pressures are not able to adjust to the outer water level and a difference is found between the states. No differences are obtained when the height of the block-wave is lower than 31.4 meters.

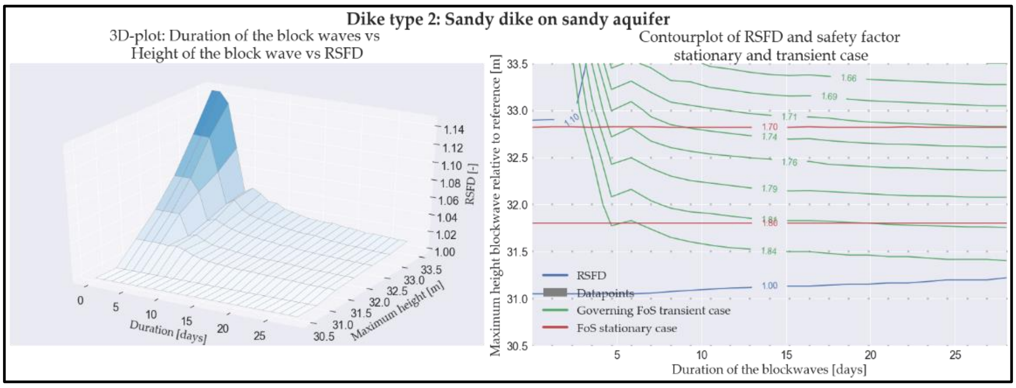

FIGURE 3.31: RESULT BLOCK-WAVES ANALYSIS FOR DIKE TYPE 2

Dike type 3, the clay on clay dike, is almost independent of the time for block-waves with a duration within 10 days. The safety factor of the transient case is constant, but still small values of $RSFD$ are obtained. During the stationary state, relatively low pore-water pressures are obtained at the inner toe of the dike. So, the differences in the pore water pressures at the inner toe are not that large. The differences in pore water pressure at the outer toe, on the other hand, are larger. But when viewing the stability of the inner toe, only the pressures at the inner side of the dike are important. Therefore, dike type 3, is not very sensitive for a transient calculation. Despite that in the simulated duration no stationary conditions are reached.

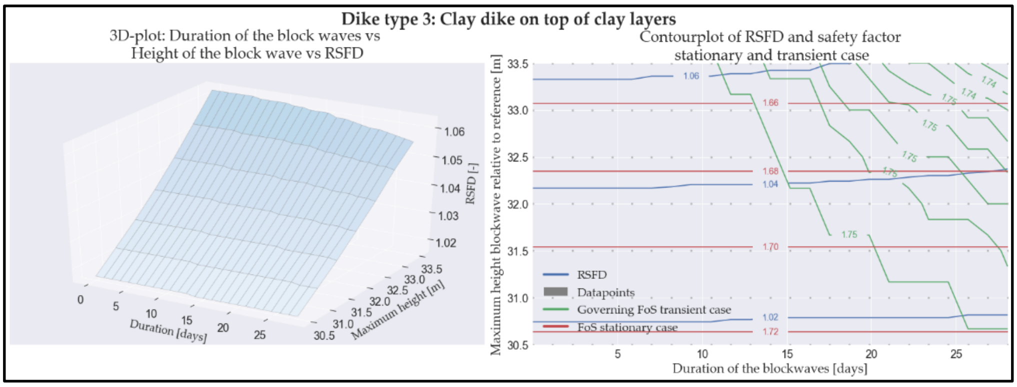

FIGURE 3.32: RESULT BLOCK-WAVES ANALYSIS FOR DIKE TYPE 3

The clay dike with a sand core on top of a sand subsoil is most sensitive for a transient calculation. *RSFD* shows the highest values, which indicates that the largest differences between the stationary and transient state are obtained for dike type 4. The clayey top layer of dike type 4 delayed the ability of the pore water pressures in the sand core to adjust to the outer water level. This caused the differences between the states to be high. The sand core causes in the stationary state large pore water pressures at the inner toe. For a completely clay dike these pore pressures are lower. Especially when the duration of the block-wave is small or the height is high, these pressures are not reached at the inner toe. Therefore, the largest differences are achieved for this dike type.

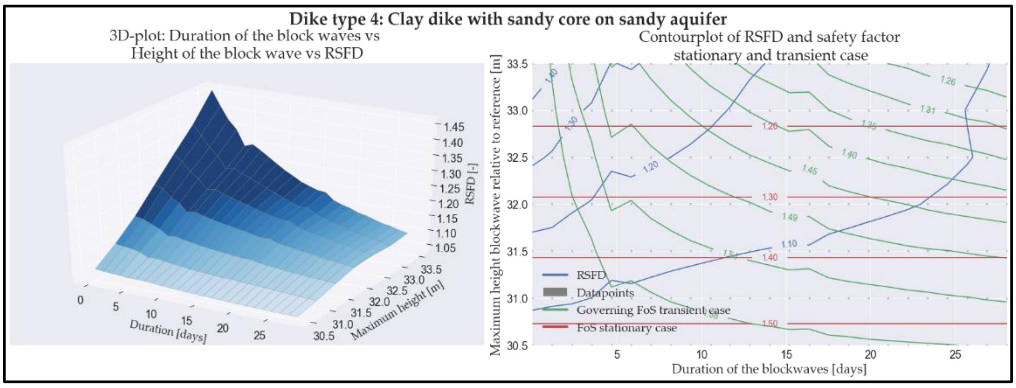

FIGURE 3.33: RESULT BLOCK-WAVES ANALYSIS FOR DIKE TYPE 4

3.4. Conclusion

What is the influence of time dependency on the pore water pressures?

- The influence of time dependency on the pore water pressures is mainly determined by the permeability of the dike body and subsoil.
- Large differences between the stationary and transient pore pressure field are obtained for cases where both the dike body and the subsoil consist of an impermeable material such as clay.
- High and short flood waves increase the differences in pore pressure field between the stationary and transient state.
- There is a lag in the response of the pore water pressures during the passage of a flood wave, especially the permeability of the subsoil affects the time of occurrence of the governing hydraulic state.

What is the influence of time dependency on slope stability?

- Large differences between the safety factor of slope stability of the inner slope during a constant water level and the passage of a flood wave are obtained when uplifting of the hinterland takes place during the stationary state and/ or during the passage of a flood wave.
- Large differences are obtained when an aquifer is present under the dike and a thin weak clay layer is present at the hinterland.
- Cases with a clayey subsoil, does not cause large differences in safety factor between the stationary and transient state.
- High and short flood waves increase the differences in safety factor when a permeable layer is present under the dike and the dike material consist of an impermeable material.

In most current dike assessments only the stationary water level is investigated when is looked at stability of the inner slope. But there are differences between the pore water pressures caused by a constant water level (stationary pore water pressures) and during the passage of a flood wave (transient pore water pressures). These differences cause a difference in stability of the inner slope. Higher safety factors are found when transient pore water pressures are used instead of stationary pore water pressures. The degree of influence of time dependency depends on dike characteristics, flood wave characteristics (height and duration) and the moment in time of the highest pore water pressures and lowest safety factor.

When an aquifer is present under a dike, smaller differences between the stationary and transient pore pressures are obtained, because next to inflow form the slope also water can flow in the dike body through the aquifer. The differences between the stationary and transient pore water pressures are especially large for dikes where both the subsoil and the dike body consist of an impermeable material such as clay, because both the intrusion length and the leakage length are small caused by the small permeability of the material. Large differences in pore water pressures cause a difference in safety factor (0-5%). But these differences are small compared with dikes where uplifting of the hinterland takes place during the stationary state and/ or during the passage of a flood wave (20-200%). Uplifting is of importance, when an aquifer is present under the dike and a thin (thinner than 5 meters) weak (low POP values) hinterland is present. The presence of a ditch can increase the difference in safety factor because the hinterland thickness is decreased at the place of the ditch, which increased the possibility of uplifting.

Also, a sand core increases the differences in safety factor compared to a clayey core (factor 1.2- 1.7). Because during the permanent water level, the pore pressure at the toe are larger for the sand core and the pore pressures are about the same during the passage of a flood wave. The presence or absence of a foreshore has hardly influence on the differences in safety factor.

Time dependency also causes the governing hydraulic state, which results in the lowest safety factor looking at slope stability, to not occur simultaneously with the maximum outer water level. There is a lag in the response of the pore water pressures during the passage of a flood wave, the time of the response is longer and the response is damped. The larger the permeability of the soil the smaller these effects. And the governing hydraulic state is achieved earlier in time when there is flow from the aquifer into the dike next to inflow through the slope. Also, the presence or absence of a foreshore influences the time of the occurrence of the lowest safety factor during the passage of a flood wave.

Considering the height and duration of a flood wave the differences in pore pressures between the two states are largest when the duration is short and the flood wave is high. When the duration is short, the leakage length in the aquifer cannot fully develop; causing these large differences. This is only the case when a permeable layer is present under the dike and the dike consist of an impermeable material. When the subsoil consists completely out of an impermeable material such as clay, the differences are almost independent on the duration of the flood wave. When the dike body consist of a permeable material such as sand, the pore water pressures easily adjust to the pressures of the flood wave. So, the safety factor comes close to the safety factor of the stationary state. Therefore, a sand dike is only of interest in a transient calculation for the really high and short flood waves.

4. CORRELATION ANALYSIS BETWEEN FLOOD WAVE VARIABLES AND DIKE STABILITY

4.1. Goal

A flood wave can be described in a simplified way by several variables, the shape variables. The influence of the different flood wave shape variables on the stability of the inner slope is investigated in sub-question 3. The goal of sub-question 3 is to know which duration and height shape variables affect the stability most. With this information, the shape variables can be used to calculate the probability of failure (see Chapter 5). To answer this question, a large number of floods from the GRADE dataset are simulated with SEEP/W and SLOPE/W to calculate the stability safety factor. Then, a correlation analysis is performed between the shape variables of the flood waves from the Rhine and the Meuse and the safety factors of different dike types. The safety factor is fitted using different shape variables, to check if there is indeed a relation between the safety factor and the shape variables. Probability density functions are used to describe the shape variables that affect the safety factor the most. These functions can be used in a probabilistic calculation. The detailed steps to reach these are given in Figure 4.1.

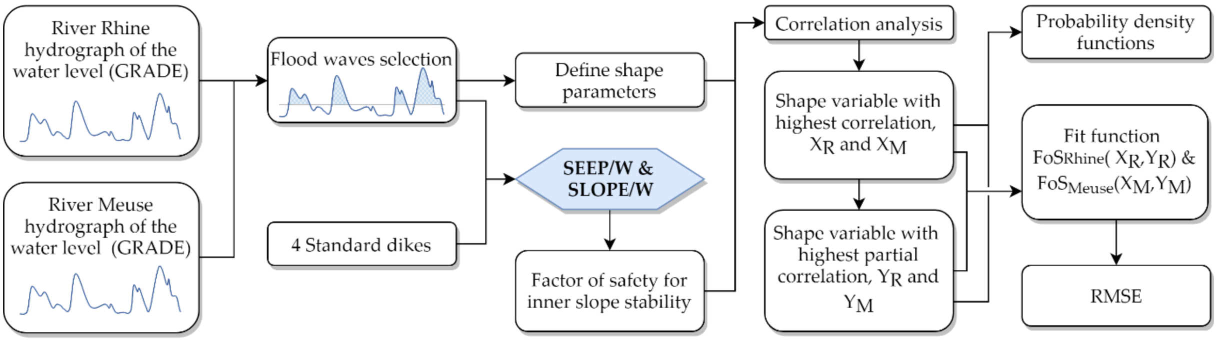

FIGURE 4.1: OUTLINE TO ANSWER SUB-QUESTION 3

4.2. Method

4.2.1. Dike cross-section

For this sub-question again the four dike types of sub-question 1 and the block-wave analysis are investigated, see Figure 3.10 of the Chapter before.

4.2.2. Hydraulic boundary condition

In this analysis GRADE discharge datasets (version of 2015) from the Rhine and the Meuse are used, which are simulated with the method described in section 2.4.2.2. The GRADE dataset has a length of 50000 years and contains daily discharges. The GRADE dataset is still being improved; datasets used in this thesis can differ from current datasets. In a previous research performed by Pol and Barneveld (2016), Rhine flood waves are selected from the GRADE dataset. In another research performed by Pol (2014) flood waves are selected in the Meuse. The flood waves with a peak discharge above respectively the 11000 m³/s and 2800 m³/s at Lobith and Borgharen are chosen. These flood waves are estimated to have a return period of 50 years or higher. In the research of Pol (2014) and Barneveld and Pol(2016); the discharge flood waves are transformed into hydrographs of the water levels at different location along that river with the use of SOBEK. At Lobith 1557 flood waves are investigated and at Borgharen 1486 flood waves. The flood waves are shown in Figure 4.2 and Figure 4.3. For more information about the selection and the SOBEK calculation is referred to the researches of Pol (2014) and Barneveld and Pol (2016).

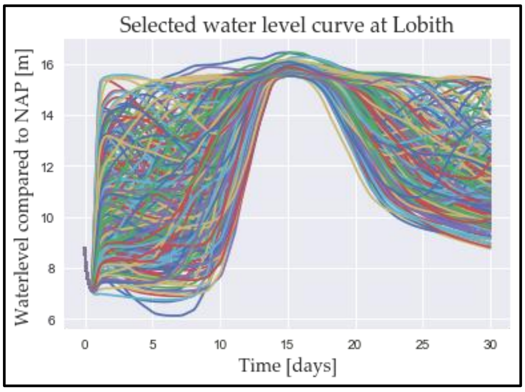

FIGURE 4.2: 1557 SELECTED FLOOD WAVES AT LOBITH

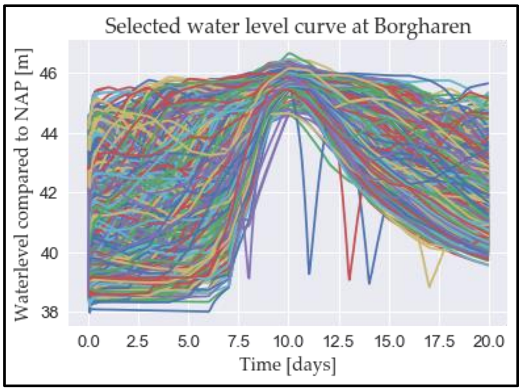

FIGURE 4.3: 1485 SELECTED FLOOD WAVES AT BORGHAREN

4.2.3. Pore pressure field model

The pore pressure field is modelled with the use of SEEP/W. For more details is referred to section 3.2.4 and an overview of the input of SEEP/W is given in *Appendix G. Input SEEP/W.* It is chosen that 75 waves can reach higher than 1 meter below the crest. This are in the Rhine the waves higher than 16 meters + NAP and for the Meuse are the waves higher than 46 meters + NAP. The initial state is the same for all waves and is set to the first value of the flood waves, which is constant 8.75 m + NAP for the waves from the Rhine and 38.71 m + NAP for the waves from the Meuse. The value is indicated in the Figure 4.4.

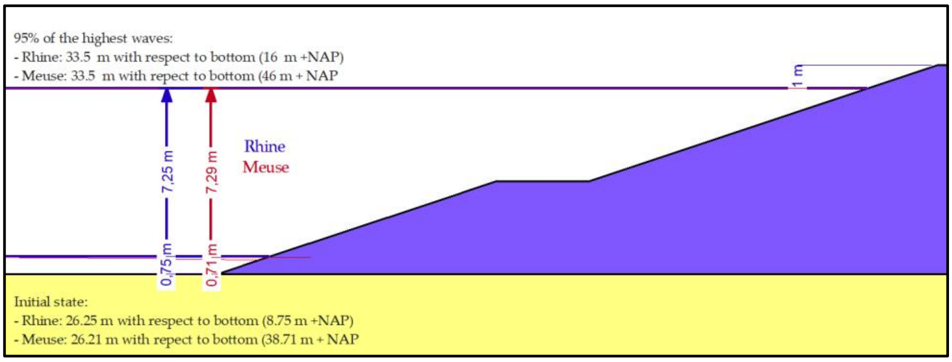

FIGURE 4.4: INITIAL STATE BEFORE THE PASSAGE OF A FLOOD WAVE

4.2.4. Slope stability model

The lowest safety factor for stability of the inner slope during the passage of the flood wave is calculated with the use of SLOPE/W. For more details is referred to section 3.2.5 and an overview of the input of SLOPE/W is given in *Appendix H. Input SLOPE/W.*

4.2.5. Correlation analysis

A correlation analysis is performed to find two variables that can be used to describe the lowest safety factor during the passage of a flood wave. The first variable that is used, is the shape variable that has the highest correlation with the safety factor. The second variable is the variable that has the highest partial correlation with the safety factor corrected for the effect of the first variables. These two variables are used to predict the lowest safety factors in time. Also, the probability density function of these variables is determined.

4.2.5.1. Shape variables

All flood waves are expressed in the variables given in Table 4.1. A similar method is used in a research of Pol (2014). All shape variables are shown in Figure 4.5 and are explained in this section. The maximum local water level is calculated with equation 4.1 and indicates the peak of the flood wave with respect to the bottom of the model.

$$h_{max} = \max(h) \tag{4.1}$$

The duration of the local water level is defined as the time that the water level is higher than a certain threshold. Secondary peaks are added to the duration. Four different thresholds are investigated and are calculated with formula 4.2 till 4.9. The level 'L' is set to a value with a return period of 10 years. This value is estimated with the use of HydraNL and is equal to 15.286 meters (32.786 with respect to the bottom of the model) at Lobith and equal to 44.048 meters (31.548 meters with respect to bottom of the model) at Borgharen.

$$L = h_{returnperiod=1/10\,year} \tag{4.2}$$
$$L_{85\%} = 0.85(h_{max} - h_{t=1\,day}) + h_{t=1\,day} \tag{4.3}$$
$$L_{50\%} = 0.50(h_{max} - h_{t=1\,day}) + h_{t=1\,day} \tag{4.4}$$
$$L_0 = h_{t=1\,day} \tag{4.5}$$

The area above a certain threshold and the flood wave is calculated with the trapezium rule. Hours are used as timesteps, see equation 4.6.

$$A_L \approx \sum_{i=1}^{t_{max}} \max\left(\frac{1}{2}(h_{i-1} + h_i - 2h_L)(t_i - t_{i-1}), 0\right) \tag{4.6}$$

The relative area is calculated with formula 4.7.

$$RA_L = \frac{A_L}{D_L(h_{max} - h_L)} \tag{4.7}$$

Also, a variable is introduced (n) to see how many peaks a flood wave has, see equation 4.8. This variable is calculated by dividing the duration at a certain threshold through the total time window of the peaks (see Figure 4.5). A value of one indicates that there is just one peak.

$$n_L = \frac{D_L}{T_L} \tag{4.8}$$

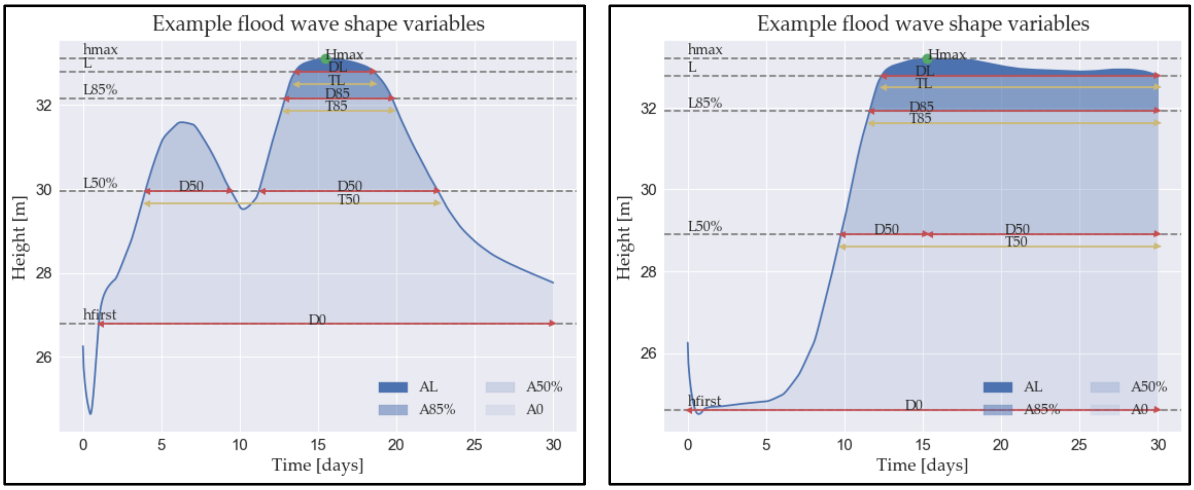

FIGURE 4.5: ILLUSTRATION OF THE SHAPE VARIABLES FOR TWO DIFFERENT FLOOD WAVES

TABLE 4.1: ANALYSED FLOOD WAVES SHAPE VARIABLES

Symbol	Definition	Unit
h_{max}	Maximum water level	L
D_0	The duration above the level after 24 hours (total duration)	T
D_L	The duration the water level is higher than a chosen level L, $h = L$	T
$D_{50\%}$	The duration that the water level is higher than the level $h = 0.5h_{max}$	T
$D_{85\%}$	The duration that the water level is higher than the level $h = 0.85h_{max}$	T
A_0	The area above the level after 24 hours (total area)	L^2
A_L	The area above the level h= $L\ m$	L^2
$A_{50\%}$	The storm area above the level h= $0.5h_{max}$	L^2
$A_{85\%}$	The storm area above the level $h = 0.5\ h_{max}$	L^2
RA_0	A_0 divided by the product of the total duration and maximum water level	-
RA_L	A_L divided by the product of D_L and h_{max} relative to level $h = L\ m$	-
$RA_{50\%}$	$A_{50\%}$ divided by the product of $D_{50\%}$ and h_{max} relative to level $h = 0.5h_{max}$	-
$RA_{85\%}$	$V_{85\%}$ divided by the product of $D_{85\%}$ and h_{max} relative to level $h = 0.85h_{max}$	-
n_l	Duration above a certain threshold, $h = L$, divided by the total duration	-
$n_{50\%}$	Duration above a certain threshold, $h = 0.5h_{max}$, divided by the total duration	-
$n_{85\%}$	Duration above a certain threshold, $h = 0.85h_{max}$, divided by the total duration	-

4.2.5.2. Selection first variable, X

The correlation coefficients between the shape variables and the lowest safety factor during a flood event are calculated with Spearman (4.9). In the Spearman equation are x_i and $\rho_{i,max}$ the rank of respectively X and FoS with n as the sample size. The advantages of this method are that non-linear relations are indicated and outliers can be dealt with. Scatterplots and rank scatterplots are made to get insight in the distributions of the correlation between the variables (see Figure 4.6). The shape variable with the highest correlation with the governing safety factor is chosen as first variable. The variables for the Rhine and Meuse can differ and it can also differ per dike type, but this is not preferred because that makes comparisons of the results more difficult.

$$\rho_s(X, FoS) = 1 - \frac{6\sum(x_i - FoS_i)^2}{n(n^2 - 1)} \qquad 4.9$$

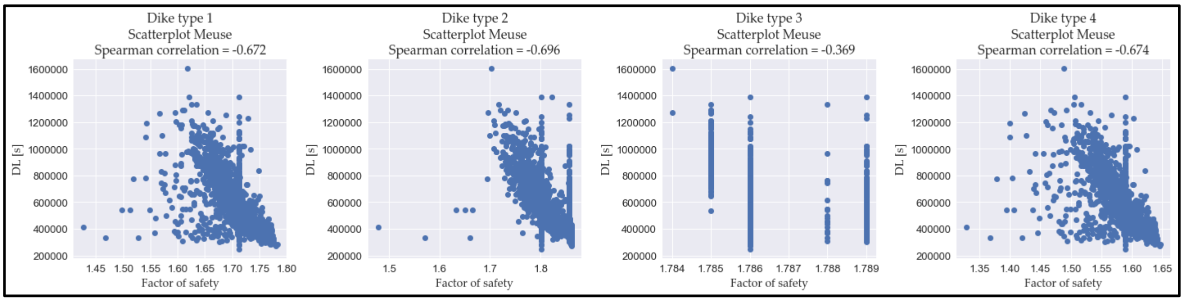

FIGURE 4.6: EXAMPLE SCATTERPLOT FOR DIFFERENT DIKE TYPES

4.2.5.3. *Selection second variable, Y*

The second variable is selected based on the partial correlation coefficient, see equation 4.10. This variable shows the correlation between the factor of safety for inner slope stability and the variable Y, given the condition X. The variable with the highest value is chosen as second variable. In this way it is considered that a second variable can improve the prediction of the safety factor. When two flood wave variables have the same partial correlation coefficient, the variable with the lowest correlation with the first variable is preferred; because independent variables are ideally used to calculate probabilities of failure. Probabilities of failure are calculated in the probabilistic analysis in Chapter 5. An example of the partial scatterplot is shown in Figure 4.7.

$$\rho(Y, FoS|X) = \frac{\rho_s(Y,FoS) - \rho_s(Y,X) \times \rho_s(FoS,X)}{\sqrt{1-\rho_s(Y,X)^2} \times \sqrt{1-\rho_s(FoS,X)^2}} \qquad 4.10$$

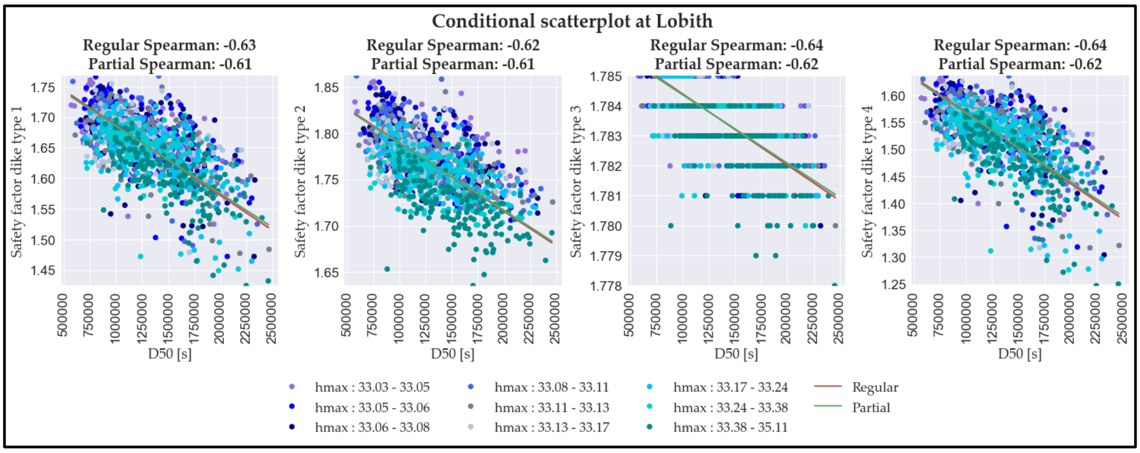

FIGURE 4.7: EXAMPLE PARTIAL SCATTERPLOT

4.2.6. Probability density function

The cumulative distribution functions (CDF) and probability density functions (PDF) of the two variables followed from the correlation analysis are estimated. A histogram is made (2 for the variables at Lobith and 2 at Borgharen) and different probability density function are fitted. In *Appendix K. univariate probability distributions*, the functions of the distributions are shown. The root mean square error is calculated for all distributions. The distribution where the frequency line results in the smallest error is chosen to be the PDF of that variable. In this way, the function describes the tail of the data accurate. The PDF is used later in this research to calculate the probability of failure.

4.2.7. Response surface plot

With the use of the variables that follows from the correlation analysis, a function that predicts the governing safety factor is fitted. This is done for the Rhine and the Meuse and for the four dike types, so in total 8 functions are fitted. Second degree polynomials are used to fit the safety factor with, see equation 4.11. This concept of estimating the optimal response is called response surface and was introduced by George and Wilson in 1951. The reliability of the fit is checked by calculating the RMSE. The function of the safety factor is only an approximation and is used to show that the safety can be described with the chosen variables. The function is also used to estimate the duration and the height of the flood waves that results in a safety factor of 1. The function is not used in the next Chapters of the research.

$$FoS(X,Y) = \rho_{00} + \rho_{10}X + \rho_{01}Y + \rho_{11}XY + \rho_{20}X^2 + \rho_{02}Y^2 \quad 4.11$$

4.3. Results

First the results of the correlation analysis and the partial correlation analysis are discussed. Secondly, the results of the statistical functions and the response surface are presented. When in this section is spoken about a value of a correlation coefficient, the absolute value of the correlation coefficient is meant.

4.3.1. Correlation analysis

The spearman correlation coefficients between the shape variables and the safety factors for the different dike types are shown in Table 4.2. The duration at a level 'L' (variable D_L) has the highest correlation with the safety factor for all dike types and for both locations, see Figure 4.8. Also, the area above the level 'L' (variable A_L) and the relative total area (variable RA_0) has a high correlation with the safety factor. Therefore, these three variables are investigated in the partial correlation analysis. The maximum peak height is an intuitive variable; therefore, this variable is also investigated in the partial correlation analysis. All results of the correlation analysis are presented in: *Appendix L. Results correlation analysis, safety factor.*

TABLE 4.2: SPEARMAN CORRELATION BETWEEN VARIABLES AND THE SAFETY FACTOR

	Average	**Dike type 1**		**Dike type 2**		**Dike type 3**		**Dike type 4**	
		Rhine	Meuse	Rhine	Meuse	Rhine	Meuse	Rhine	Meuse
h_{max}	-0.39	-0.43	-0.38	-0.56	-0.40	-0.41	-0.14	-0.43	-0.38
D_0	0.05	0.12	-0.01	0.08	-0.06	0.12	0.03	0.11	-0.01
D_L	0.70	-0.76	-0.67	-0.87	-0.70	-0.76	-0.37	-0.76	-0.67
D_{50}	-0.46	-0.63	-0.32	-0.62	-0.35	-0.64	-0.14	-0.64	-0.32
D_{85}	-0.50	-0.65	-0.38	-0.71	-0.44	-0.63	-0.16	-0.65	-0.38
A_0	-0.03	-0.08	0.04	-0.13	-0.01	-0.09	0.08	-0.09	0.04
A_L	-0.64	-0.65	-0.67	-0.78	-0.71	-0.65	-0.34	-0.65	-0.67
A_{50}	-0.15	-0.21	-0.09	-0.26	-0.14	-0.22	0.02	-0.22	-0.09
A_{85}	-0.10	-0.10	-0.10	-0.18	-0.16	-0.11	0.02	-0.10	-0.1
RA_0	-0.56	-0.73	-0.44	-0.71	-0.45	-0.73	-0.23	-0.74	-0.44
RA_L	0.25	0.53	-0.04	0.60	-0.09	0.52	-0.02	0.53	-0.04
RA_{50}	-0.16	-0.07	-0.28	-0.11	-0.30	-0.05	-0.1	-0.06	-0.28
RA_{85}	0.30	0.59	0.00	0.57	0.00	0.55	0.07	0.59	0.00
n_l	0.11	0.20	0.04	0.20	0.00	0.19	0.03	0.20	0.04
$n_{50\%}$	0.08	0.15	0.06	0.10	0.02	0.15	-0.02	0.15	0.06
$n_{85\%}$	0.15	0.26	0.06	0.20	0.05	0.22	0.04	0.27	0.06

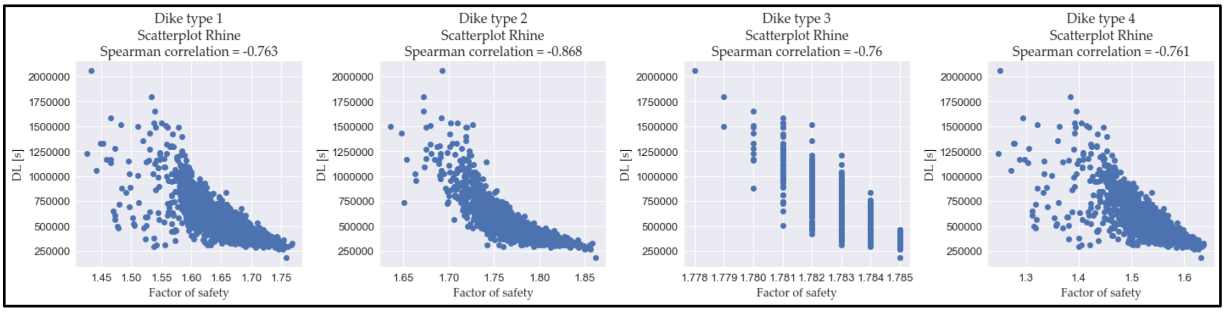

FIGURE 4.8: CORRELATION PLOTS BETWEEN DL AND THE SAFETY FACTOR FOR DIFFERENT DIKE TYPES AT LOBITH

The duration of a flood wave has a bigger impact on the safety factor than the height of a flood wave, because the correlation coefficients of the height are significantly lower than the correlation coefficients of the duration. The duration is of influence in a clay dike, because the response of the pore water pressures (5 days) is somewhat delayed through the low hydraulic conductivity of the clayey material (see Chapter 3). In the sand on sand dike the response is more instantaneously (within 3 days). Therefore, the correlation between the safety factor and the maximum height is somewhat higher for a sand on sand dike compared to the other dike types; but still the influence of the duration is higher than the height of the flood wave. To explain the correlation coefficients, the results of the governing safety factor followed from the block-wave analysis are combined with the height and duration shape variables of the correlation analysis (h_{max} and D_L), see Figure 4.9.

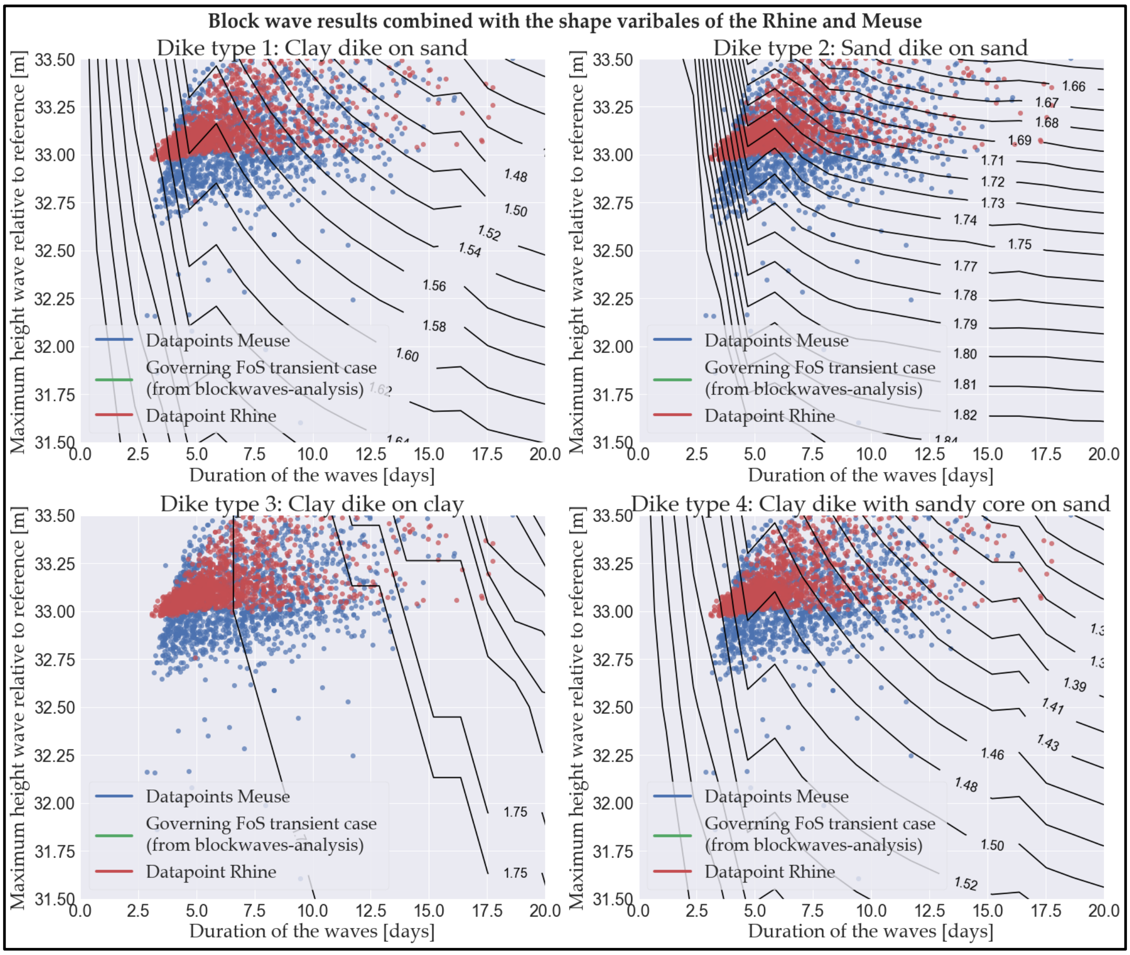

FIGURE 4.9: CONTOUR PLOT OF THE GOVERNING SAFETY FACTOR FOLLOWED FROM THE BLOCK-WAVE ANALYSIS COMBINED WITH THE h_{max} AND D_L OF THE RHINE AND THE MEUSE

The duration is of influence when the contour lines in Figure 4.9 deflect to the vertical axis and the maximum height is of influence when the lines deflect to the horizontal axis. For all dike types can be seen that the duration is of importance for the high waves and the height is of influence for the longer waves.

Looking at the sand on sand dike (dike type 2), flood waves with a duration shorter than 2 days do not affect the stability of the inner slope, because of the storage capacity of the soil delays the response. For these short waves, the safety is determined by the initial water level. The same holds for flood waves with a height less than 31.4 meters. Further can be seen in Figure 4.9, that the duration is hardly of influence after 8 days. So, the waves within a duration of 2-8 days are affected by the duration. 67% (based on D_L) of the investigated waves in the Meuse lies between this range, in the Rhine this percentage is 83%. The large amount of relatively short waves causes the high correlation with the duration. The correlation in the Rhine is also somewhat higher, since the amount of wave between this range is higher. The correlation with the maximum wave height is mainly determined by the waves with a longer duration (more than 14 days). From Figure 4.10 can be concluded that 2% of the waves at the Rhine have a duration longer than two weeks while in the Meuse this is 1% of the waves. The low number of long waves cause the low correlation with the maximum wave height. Because the number of waves with a long duration is higher in the Rhine, the correlation with the peak height is higher in the Rhine. Note that only the flood waves with a return period of at least 50 years are considered. The variation in the maximum water height is not that large. Therefore, it is less suitable to indicate the correlation with.

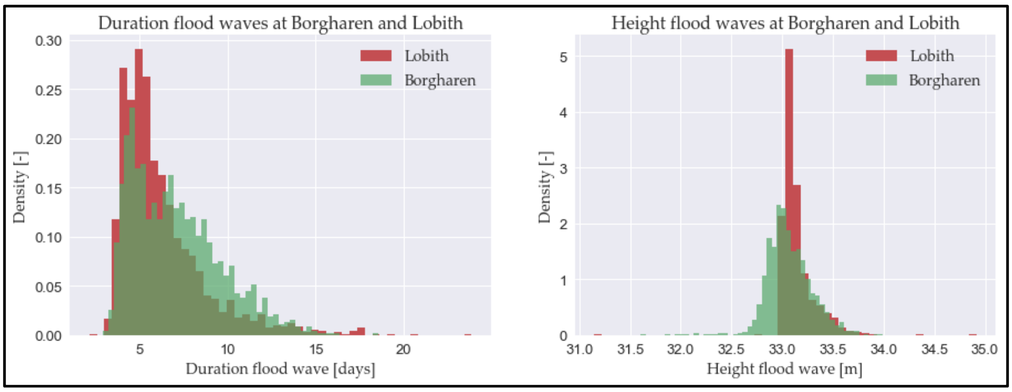

FIGURE 4.10: DURATION (D_L) AND HEIGHT (h_{max}) OF WAVES IN THE RHINE AND THE MEUSE

From the block-wave analysis of the clay on clay dike follows that the stability is almost independent of the flood duration and height, because the transient safety factor is 1.74-1.75 for all investigated heights and durations. Still a high correlation is obtained between the duration in the Rhine and the safety factor. A duration within the 6 days do not affect the safety factor of the inner slope. There is little flow through the subsoil in the dike body, causing a large delay in the response of the pore pressures. Within these days the safety factor is determined by the initial water level. It takes more time before the duration influences the safety factor compared to the other dike types; especially for the lower waves this takes more time. The amount of short waves causes the correlation with the Meuse flood waves to be lower than the Rhine flood waves. There are more short and low flood waves present in the Meuse (see Figure 4.10).

The clay on sand dikes (type 1 and 4), have similar correlation coefficients between the safety factor and the shape variables. Also, the correlation of the clay on sand dike is in the same order as the clay on clay dike. While it is expected that a height of a flood wave has more influence on the clay on sand dikes, because the aquifer is saturated and reacts fast (2-3 days) to the increased pore pressures of the flood wave. But also, for dike type 1 and 4 , the height of a flood is especially of influence for the longer waves. This amount of waves is limited and mainly short high waves are present (for which the duration in particular affects the safety factor). Therefore, the correlation is in the same order as the clay on clay dike.

Further, the variable that indicates the number of peaks of a flood wave (n), is not a good predictor of the safety factor, because the correlation coefficient with the safety factor is low.

4.3.2. Partial correlation analysis

From the partial analysis performed using the four variables D_L, A_L, RA_0 and h_{max} (*Appendix N. Results partial correlation analysis*), follows that the combination (h_{max}, D_{50}) and (RA_0, h_{max}) can be used to predict the safety factor. The results are shown in Table 4.3. Partial correlations of other variables are also high, but they also have a high correlation with the first variable. This is not preferred, because independent variables can be used in a probabilistic calculation. The correlation $\rho_{s,rhine}(h_{\max}, D_{50}) = 0.25$, $\rho_{s,Meuse}(h_{\max}, D_{50}) = 0.1$, $\rho_{s,Rhine}(h_{\max}, RA_0) = 0.25$ and $\rho_{s,Meuse}(h_{\max}, RA_0) = 0.21$. Because these correlations are relatively low, they are assumed to be independent. The two combinations are further investigated. Figure 4.11 shows the partial plot between the duration and the safety factor given the maximum height. All results of the partial correlation analysis are presented in *Appendix M. Results correlation analysis, variables*; and *Appendix N. Results partial correlation analysis.*

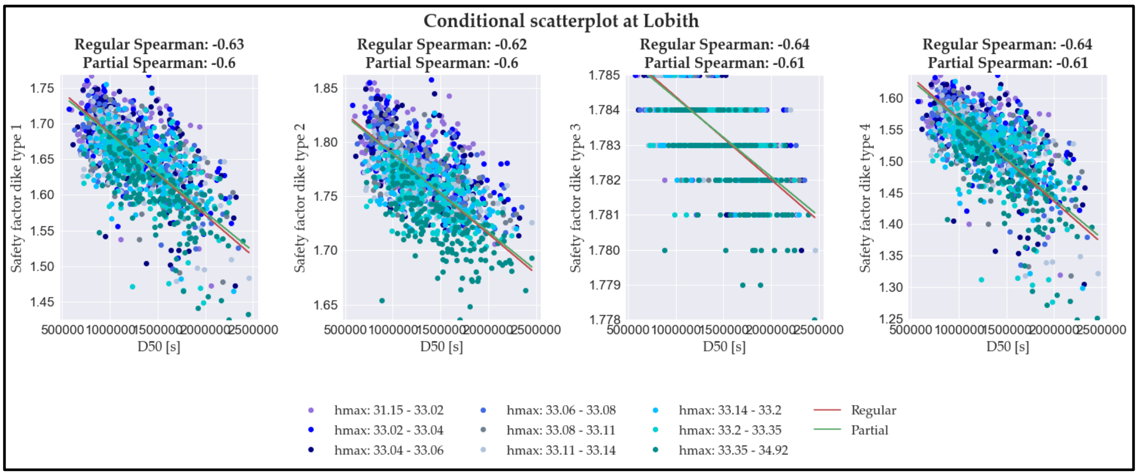

FIGURE 4.11: PARTIAL SCATTERPLOT BETWEEN DL THE SAFETY FACTOR GIVEN A0

TABLE 4.3: PARTIAL CORRELATION BETWEEN THE FOS, DL AND THE SHAPE VARIABLES

	Average	Dike type 1		Dike type 2		Dike type 3		Dike type 4	
		Rhine	Meuse	Rhine	Meuse	Rhine	Meuse	Rhine	Meuse
$\rho_s(RA_0, FoS)$	-0.56	-0.73	-0.44	-0.71	-0.45	-0.73	-0.23	-0.74	-0.44
$\rho_s(h_{max}, FoS\|RA_0)$	-0.34	-0.37	-0.33	-0.55	-0.35	-0.35	-0.09	-0.37	-0.33
$\rho_s(h_{max}, FoS)$	-0.39	-0.43	-0.38	-0.56	-0.40	-0.41	-0.14	-0.43	-0.38
$\rho_s(D_{50}, FoS\|h_{max})$	-0.43	-0.60	-0.28	-0.60	-0.31	-0.61	-0.12	-0.61	-0.28

4.3.3. Safety factor fit

A second-degree polynomial (other functions were also tested but did not provide a better prediction) can be used to describe the safety factor using the maximum height in combination with the duration or the relatively area. Also, a second-degree polynomial is fitted using one variable; just D_L, A_L or RA_0. The prediction is better for the events from the Rhine than for the Meuse, because the correlations for these events are higher.

Table 4.4 shows the RMSE of the different fits. The RMSE is lowest when only the duration at a level L is used to predict the safety factor with. The variation in the maximum height is small, because only the events are chosen with a return period of at least 50 years. The function does not hold anymore when waves with a lower return period are used. Therefore, a variable is preferred that includes the maximum wave height. The RMSE is lower for the fit based on the maximum height and the relatively total area, but the differences in RMSE are small. The combination of the maximum height and the duration is preferred, because these are intuitive variables. Therefore, it is decided to use these variables in the probabilistic calculation performed in Chapter 5. The RMSE is lower when the variation in safety factor is lower. This variation is small for the clay on clay dike, therefore low RMSE values are obtained. An example of the fit is shown in Figure 4.12. When the fit is extrapolated till the factor of safety is lower than 1, very high flood wave heights and duration are found. These events are rare, which indicates that the chosen theoretical dikes are too safe. This is caused by the relatively low permeability of the sand layers under the dike. All results of the fits through the safety factors based on the shape variables are presented in: *Appendix O. Results safety factor fits.*

TABLE 4.4: RMSE FIT BASED ON HMAX AND D50 & HMAX AND RA0

	Fit Hmax & D50		**Fit Hmax & RA0**		**Fit DL**		**Fit AL**		**Fit RA0**	
	Rhine	Meuse	Rhine	Meuse	Rhine	Meuse	Rhine	Meuse	Rhine	Meuse
Dike type 1	0.0356	0.0382	0.0317	0.037	0.0325	0.0344	0.0391	0.0345	0.0345	0.0385
Dike type 2	0.0207	0.0346	0.0181	0.0333	0.0162	0.0302	0.0199	0.0297	0.0233	0.0352
Dike type 3	0.0007	0.0011	0.0006	0.0011	0.0006	0.0011	0.0007	0.0011	0.0006	0.0011
Dike type 4	0.0388	0.0362	0.0346	0.035	0.036	0.0326	0.0433	0.0328	0.0375	0.0364
Average	**0.0257**		**0.0239**		**0.0230**		**0.0251**		**0.0259**	

TABLE 4.5: EXTRAPOLATED HEIGHT AND DURATION FOR WHICH THE SAFETY FACTOR IS 1

	Dike type 1		**Dike type 2**		**Dike type 3**		**Dike type 4**	
	Rhine	Meuse	Rhine	Meuse	Rhine	Meuse	Rhine	Meuse
h_{max}	36.5 m	35.5 m	37.4 m	35.7 m	61.2 m	62.7 days	35.5 m	35.3 m
D_{50}	37.6 days	27.9 days	35.2 days	25.2 days	188 days	216.7 days	31.0 days	27.9 days

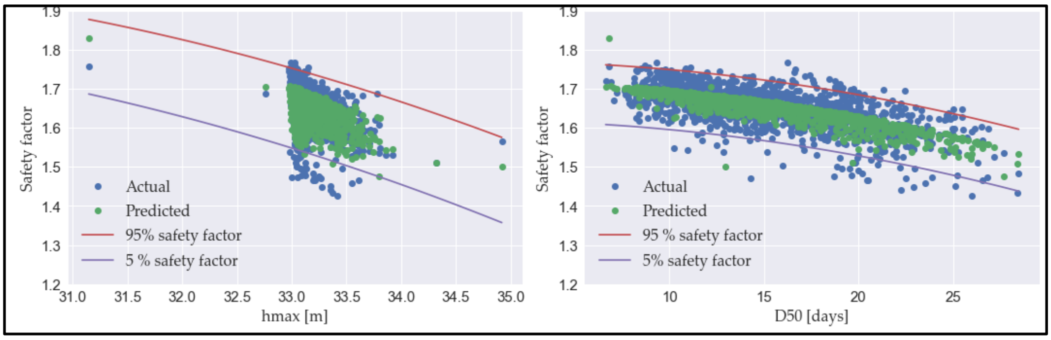

FIGURE 4.12: SAFETY FACTOR FIT AT LOBITH FOR DIKE TYPE 1

4.3.4. Probability density functions

A generalized Pareto function is used to describe the maximum water level at Lobith. At Borgharen a Student's t function is used. The duration halfway the flood wave (D_{50}) can be described using a Weibull minimum function at Lobith or a Student's t function at Borgharen. The fits are shown in Figure 4.13 till Figure 4.16. The probability density is chosen in such a way, that the RMSE of the frequency line is small. *Appendix P. Probability density functions* shows the frequency lines and the cumulative distribution functions. Note, only the events are included with a return period of at least 50 years.

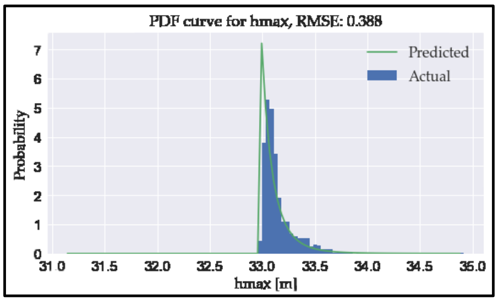

FIGURE 4.13: GENERALIZED PARETO, LOBITH, B= 5.5, LOC= 32.4 AND SCALE= 0.62

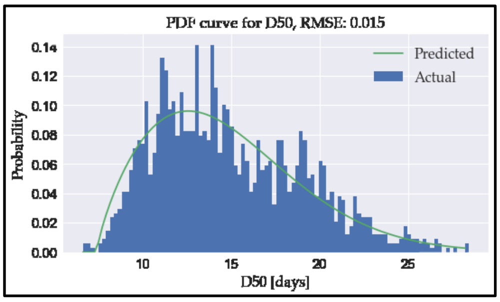

FIGURE 4.14: WEIBULL MINIMUM, LOBITH, C= 1.8 LOC= 7.4 AND SCALE= 8.3

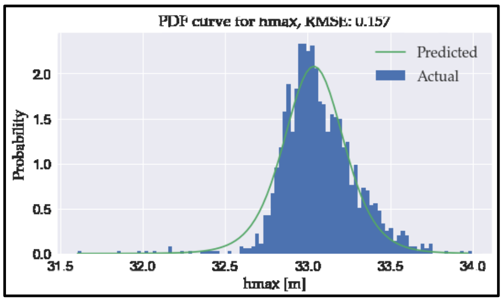

FIGURE 4.15: STUDENT'S T, BORGHAREN, T=7.59, LOC= 33.04 AND SCALE= 0.19

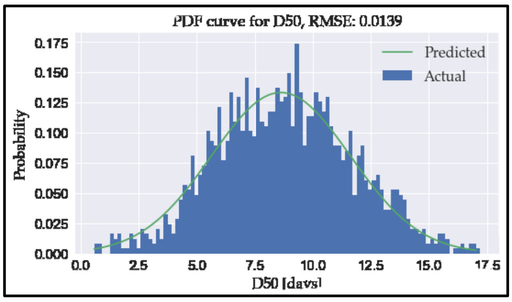

FIGURE 4.16: STUDENT'S T, BORGHAREN, T= 4.8E+7, LOC=8.63 AND SCALE= 2.99

4.4. Conclusion

Which Rhine and Meuse flood wave shape variables affect the stability of the inner slope?
The duration affects the stability most when the response to the increased pore water pressures is delayed caused by the hydraulic conductivity of the material. For example, a clay on clay dike is most affected by the duration of the flood event. The influence of the height of a flood wave on the stability increases when the soil is permeable, because the delay in response decreases. For example, a sand on sand dike reacts instantaneously to the flood wave, when the sand material is partly saturated. If the dike is dry before the passage of a flood wave, again the response is damped through the phreatic storage capacity of the material. Dikes with a low degree of saturation are therefore also more affected by the duration than the height of a flood wave. Also, the shape of the flood wave affects the influence of the height and duration of the flood wave on the stability of the inner slope. The influence of the duration increases for flood waves with a really short duration of the high water. The influence of the height increases for the longer waves. Both in the Rhine and Meuse, the amount of short waves (< 7days) is high (80-90%), which also increases the influence of the duration on the stability.

The safety factor can be approximated with a second-degree polynomial using the duration halfway a flood. Adding the maximum height of a flood improves the approximation.

5. PROBABILISTIC ANALYSIS USING TRANSIENT AND STATIONARY PRESSURES

5.1. Goal

In this Chapter the effect of time dependency on the probability of failure of slope stability is investigated. Three states are investigated; a transient pore pressure field, a stationary pore pressure field and a variant on the stationary pore pressure field. In the variant on the stationary pore pressure field the pore pressure field is calculated using the simplifications of WBI (2017). In the simplification, the permeability of the material is not considered directly. WBI (2017) makes a distinguish between sand or clay. The probability of failure of the transient calculation is compared with the probability of failure of the stationary calculation to answer sub-question 4. Finally, the transient calculation is compared with the variant of the stationary calculation to answer sub-question 5.

The goal of sub-question 4 is to understand the differences in safety factor between taking the shape of a flood wave into account or not and to study the effect of the uncertainties in the shape of the flood wave, the permeability and strength of the material. To answer this question a probabilistic analysis is performed using stationary and transient water levels. In both analyses the permeability and the strength of the material are varied; the shape of the flood waves is varied in the transient analysis. The total probability of failure by considering the probability of occurrence of an event is determined, the influence of the uncertainties on the probability of failure is quantified and the main variables that has the greatest effect on the probability of failure are determined.

The goal of sub-question 5 is to understand whether the simplification of WBI (2017) leads to an underestimation or overestimation of the probability of failure. Therefore, a probabilistic analysis is performed varying in the strength of the material using the pore water pressures according WBI (2017). The results of the probabilistic analysis are compared with the results of the transient probabilistic analysis, where also is varied in the flood wave variables and the permeability of the material. The detailed steps to answer sub-question 4 and 5 are provided in Figure 5.1

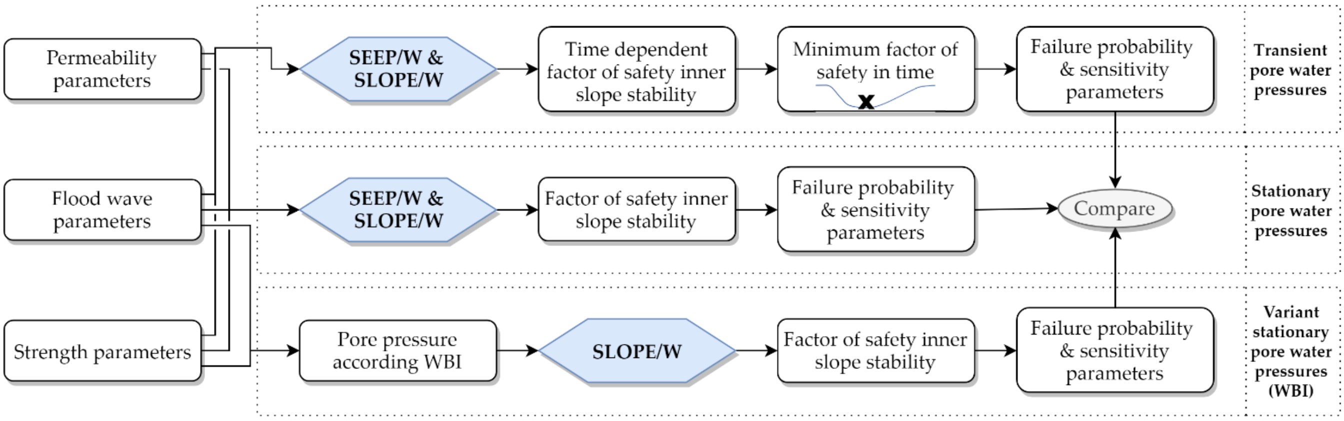

FIGURE 5.1: OUTLINE TO ANSWER SUB-QUESTION 4 AND 5

5.2. Method

5.2.1. Dike cross-section

From sub-question 3 follows that the four different dike types are too safe. Therefore, the four dikes types of sub-question 1 are adjusted to get lower safety factors. The slopes of the dikes are changed from 1:3 to 1:2.5, the permeability of the sand is increased from 2.3×10^{-5} to 2.3×10^{-4} m/s and of the clay from 5.8×10^{-7} to 1×10^{-6} m/s. The new dimensions are shown in Figure 5.2.

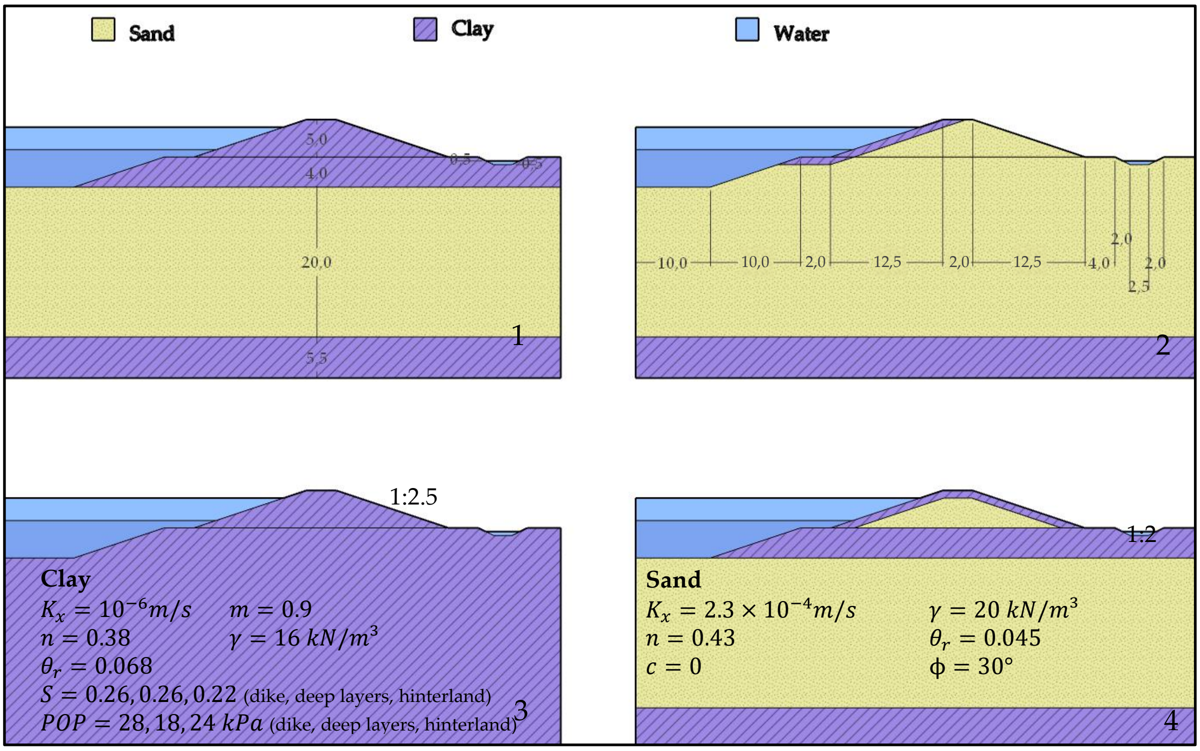

FIGURE 5.2: NEW LEVEE CROSS-SECTIONS WITH USED MEAN VALUES

5.2.2. Hydraulic boundary condition

The same GRADE discharge datasets are used as in Chapter 4 (see section 4.2.2). In previous research performed by Pol (2014) and Barneveld and Pol (2016), flood waves are transformed into hydrographs of the water level with the use of SOBEK. The shape of the flood waves is used for the Rhine at Lobith and in the Meuse at Borgharen. The flood waves with a return period of at least 50 year are expressed in the maximum height (h_{max}) and the duration halfway the height of the flood wave (D_{50}). From Chapter 4 follows that these flood wave variables can be used to describe the safety factor. The probability of failure is estimated as a function of the duration and height of the flood waves. To reduce the calculation time, 25 hydrographs are selected for the Meuse and 25 hydrographs are selected for the Rhine. The events are chosen in such a way that it represents the whole dataset. This is done by defining 5 equal probability classes for h_{max} between the minimum and maximum value and 5 equal probability classes for D_{50}. After that, the matrix is filled with events which satisfies both conditions (see Table 5.1 and Table 5.2). If more events fulfilled the conditions, one of them is chosen randomly. This result in 25 Rhine floods waves and 25 Meuse flood waves, see Figure 5.3.

TABLE 5.1: SELECTED FLOOD WAVES IN THE RHINE AT LOBITH

h_{max} class	D_{50} class				
	$8.38 - 13.17\ day$	$13.17 - 16.1\ day$	$16.1 - 20.08\ day$	$20.08 - 21.13\ day$	$21.13 - 25.08\ day$
$33.02 - 33.17\ m$	Event nr. 10318	Event nr. 10774	Event nr. 12393	Event nr. 15651	Event nr. 49032
$33.17 - 33.26\ m$	Event nr. 10037	Event nr. 10107	Event nr. 11834	Event nr. 11812	Event nr. 16976
$33.26 - 33.45\ m$	Event nr. 10077	Event nr. 10572	Event nr. 10639	Event nr. 12457	Event nr. 1519
$33.45 - 33.86\ m$	Event nr. 11136	Event nr. 11670	Event nr. 1147	Event nr. 11836	Event nr. 13046
$33.86 - 33.16\ m$	Event nr. 27484	Event nr. 16842	Event nr. 10940	Event nr. 11989	Event nr. 1711

TABLE 5.2: SELECTED FLOOD WAVES IN THE MEUSE AT BORGHAREN

H_{max} class	D_{50} class				
	$2.17 - 4.71\ day$	$4.71 - 8.48\ day$	$8.48 - 9.24\ day$	$9.24 - 11.79\ day$	$11.79 - 14.88\ day$
$32.25 - 32.91\ m$	Event nr. 86	Event nr. 2	Event nr. 8	Event nr. 32	Event nr. 39
$32.91 - 33.12\ m$	Event nr. 297	Event nr. 0	Event nr. 20	Event nr. 34	Event nr. 72
$33.12 - 33.35\ m$	Event nr. 16	Event nr. 30	Event nr. 10	Event nr. 101	Event nr. 427
$33.35 - 33.5\ m$	Event nr. 62	Event nr. 94	Event nr. 6	Event nr. 156	Event nr. 1359
$33.5 - 33.74\ m$	Event nr. 691	Event nr. 395	Event nr. 212	Event nr. 65	Event nr. 816

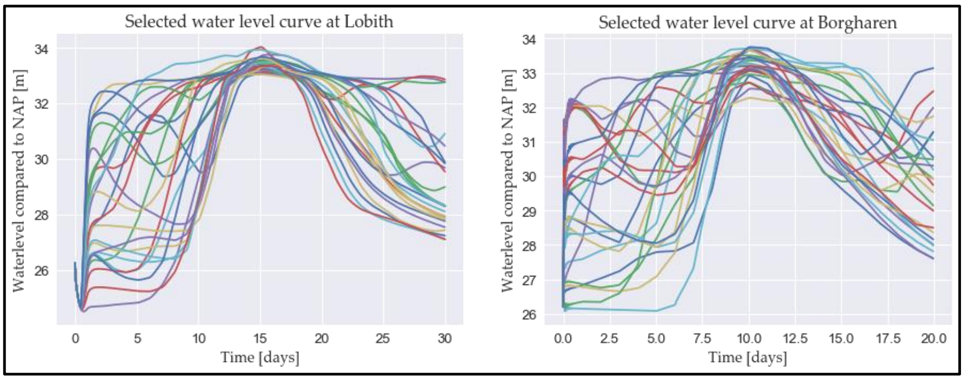

FIGURE 5.3: 25 SELECTED FLOOD WAVES AT LOBITH AND BORGHAREN

5.2.3. Pore pressure field model

Both the transient and stationary pore pressure fields are modelled with the use of SEEP/W. For more details is referred to section 3.2.4 and 4.2.3 and an overview of the input of SEEP/W is given in *Appendix G. Input SEEP/W.* These calculations depend on the permeability of the material.

The variant of the stationary pore pressure field is modelled using the simplification of WBI (2017), for which no software is needed. The procedure to calculate the pore pressures is summarized in section 2.4.3. For the detailed description of the procedure is referred to 'Veiligheidsbeoordeling WBI2017'. An example of the differences in pore water pressures is shown in Figure 5.4.

For the clay dike with a sand core the phreatic surface cannot be drawn correctly in SLOPE/W, therefore the phreatic surface is drawn as shown in the figure right below (red is the correct way). It is assumed that this difference will not cause large differences in the results, because only the stability of the inner slope is considered and at this side of the dike the pore water pressure hardly differs. The variant of the stationary pore pressure field is independent of the permeability of the material, WBI (2017) only makes a distinguish between sand and clay.

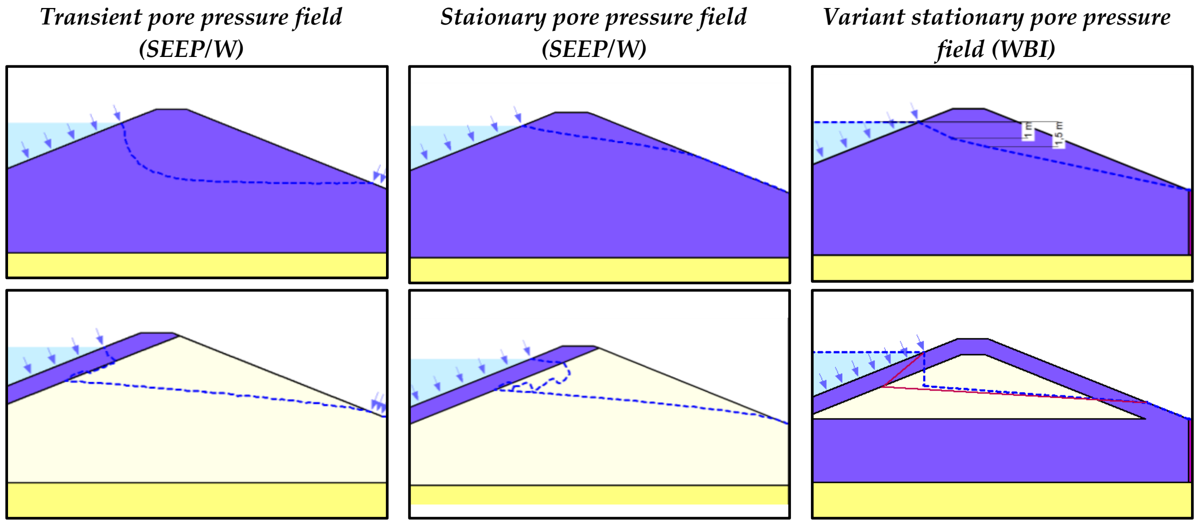

FIGURE 5.4: PHREATIC SURFACE CALCULATED WITH SEEP/W (FIRST AND SECOND LEFT) AND CALCULATED USING THE METHOD OF WBI (2017) (RIGHT)

5.2.4. Slope stability model

Both the stability of the dikes using the transient pore water pressures and the stationary pore water pressures (two variants) are calculated with the use of SLOPE/W. For the transient calculation, this results in a safety factor in time. The lowest value is chosen. The stationary calculations result in one safety factor. For more details is referred to section 3.2.5 and the input of SLOPE/W is given in *Appendix H. Input SLOPE/W.*

5.2.5. Probabilistic analysis

A probabilistic calculation is performed to assess the probability of failure per flood wave. In the transient calculation is varied in flood waves, permeability and strength of the material. In the stationary calculation also the flood waves, permeability and the strength are varied. Only the maximum height of each flood wave is used, because the duration has no impact on the failure probability in a stationary calculation. In the variant of the stationary calculation only the flood waves (the maximum height of the wave) and the strength of the material are varied.

The flood waves, pore water pressure and soil strength are assessed probabilistically with the Monte Carlo method. A python model is made that couples the variation of the different stochastic variables to the calculations executed in SEEP/W and SLOPE/W. To model spatial variation, ideally a variogram is used that depicts the spatial correlation. The spatial correlation is unknown, therefore not included in the model, so the soil is modelled homogeneous.

5.2.5.1. Stochastic variables

Based on a calibration study of Kanning *et al* (2016), the strength stochastic variables that affect the safety factor the most are chosen. For clayey material these are the normally consolidated undrained shear strength ratio (S), the strength increase exponent(m) and the pre overburden pressure (POP). For a sand embankment this is the internal friction angle. Not all variables are considered, because this increased the calculation time significantly. The distribution types and standard deviations of these stochastic variables are based on a research of Tigchelaar *et* *al* (2018) which based the chosen distribution types on a sample collection of HHNK [Tigchelaar, 2017]. Also, the permeability of the material is varied. The permeability of the material, the chosen distribution type and standard deviation are based on a research of Massop *et al* (2005), because in the research of Tigchelaar *et al* (2018) the permeability was not assessed probabilistically.

All stochastic variables and their distributions are given in Table 5.3. Only the 25 selected flood waves are used in the probabilistic calculation. For each flood wave the pore water pressures are calculated for 20 different permeabilities, so in total 500 internal hydraulic states are calculated. For each hydraulic state, 10 stability calculation are performed varying in the strength variables, which results in a total of 5000 calculations.

TABLE 5.3: STOCHASTIC VARIABLES WITH DISTRIBUTION TYPE

Stochastic	Symbol	Distribution type	Mean	Standard Deviation	Number
Maximum water level	h_{max}	25 flood waves	$Rhine$: 33.15 m $Meuse$: 33.07 m	$Rhine$: 0.17 m $Meuse$: 0.22 m	25
The duration that the water level is higher than the level $h = 0.5h_{max}$	D_{50}	25 flood waves	$Rhine$ 14.96 $days$ $Meuse$: 8.82 $days$	$Rhine$: 4.15 $days$ $Meuse$: 2.95 $days$	25
Hydraulic conductivity, clay	$k_{x,Clau}$	Lognormal	10^{-6} m/s	2.5×10^{-7} m/s	500
Hydraulic conductivity, sand	$k_{x,Sand}$	Lognormal	2.3×10^{-4} m/s	5.75×10^{-5} m/s	500
Normally consolidated undrained shear strength ratio, dike body	S_{dike}	Lognormal	0.26	0.03	5000
Normally consolidated undrained shear strength ration, hinterland	$S_{hinterland}$	Lognormal	0.22	0.03	5000
Internal friction angle	ϕ	Lognormal	30 °	3 °	5000
Strength increase exponent, dike body	m_{dike}	Lognormal	0.9	0.03	5000
Strength increase exponent, hinterland	$m_{hinterland}$	Lognormal	0.9	0.03	5000
Pre overburden pressure, dike body	$POP_{hinterla}$	Lognormal	18 kPa	8.1 kPa	5000
Pre overburden pressure, hinterland	POP_{dike}	Lognormal	28 kPa	12.6 kPa	5000

5.2.5.2. Probability of failure

The probability of failure must be estimated for each combination of the height and duration of a flood wave. Therefore, 25 flood waves are chosen in such a way that they represent the whole dataset (based on h_{max} and D_{50}). Per flood wave and for each dike type the probability of failure is calculated. The probability of failure is calculated by dividing the number of calculations where the safety factor is lower than 1 by the total calculations associated with that specific flood wave.

It is assumed that despite the changing dike geometry still the shape variables h_{max} and D_{50} can be used to describe the safety factor (for explanation see section 4.4) and therefore the probability of failure. The 25 flood waves are therefore expressed in these variables. To know the probability of failure for each combination of h_{max} and D_{50} the results are interpolated using linear interpolation and extrapolated using the nearest probability of failure, as shown in Figure 5.5. Actually, a 3D fragility curve is made.

5.2.5.3. Total probability of failure

The total probability of failure including the probability of occurrence is calculated by taking the integral of a 3-dimensional probability density function, see equation 5.1. The probability of failure corresponding with a value of h_{max} and D_{50} (obtained by interpolation and extrapolation, see section 5.2.5.2) is multiplied with the probability of occurrence of the h_{max} and D_{50} values. Fitted probability density functions are used for this multiplication (section 4.3.4). It is assumed that h_{max} and D_{50} are independent, since the correlation between the variables is low. Also, a multiplication with a factor 1/50 is required, because only flood waves are chosen with a return period of the peak discharge higher than 50 years. An example of the results is shown in Figure 5.6.

In the calculation of the probability of failure (section 5.2.5), each flood wave has an equal contribution to the probability of failure. The multiplication with the probability of occurrence of the events, cause that rare events have a smaller probability of failure than more common events and vice versa. Therefore, in the total probability of failure, the contribution of each flood wave is not equal.

$$F_{FoS<1|\underline{h_{max}}=h_{max},\underline{D_{50}}=D_{50}} = \frac{1}{50} f_{FoS<1|\underline{h_{max}}=h_{max},\underline{D_{50}}=D_{50}} \int_{-\infty}^{h_{max}} f_{\underline{h_{max}}}(h_{max}) dh_{max} \int_{-\infty}^{D_{50}} f_{\underline{D_{50}}}(D_{50}) \, dh_{50} \tag{5.1}$$

In which:

h_{max}	= Maximum flood wave height [L]
D_{50}	= Duration halfway the flood wave [T]
$F_{FoS<1\|\underline{h_{max}}=h_{max},\underline{D_{50}}=D_{50}}$	= Total probability of failure including occurrence of an event [1/year]
$f_{FoS<1\|\underline{h_{max}}=h_{max},\underline{D_{50}}=D_{50}}$	= Probability of failure given a height and duration of a flood [-]
$f_{\underline{h_{max}}}(h_{max})$	= Fitted probability density function of the peak water level [1/L]
$f_{\underline{D_{50}}}(D_{50})$	= Fitted probability density function of the duration [1/T]

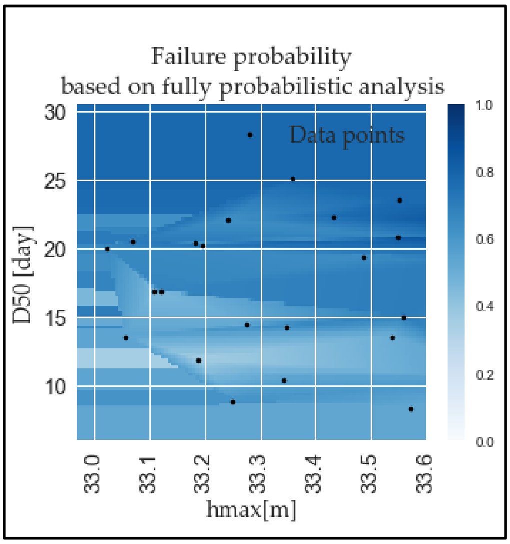

FIGURE 5.5: EXTRA- AND INTERPOLATED PROBABILITY OF FAILURE

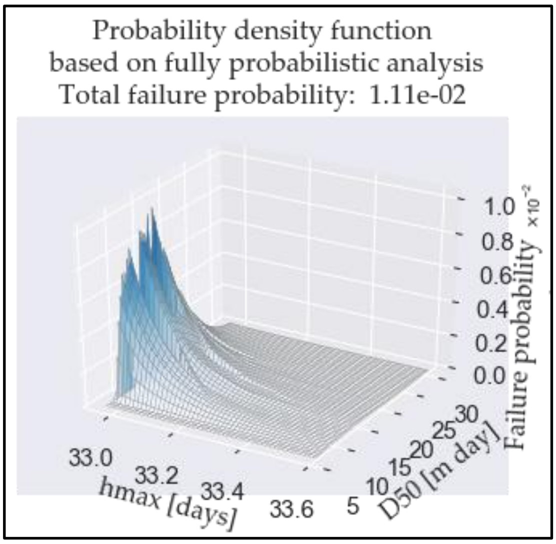

FIGURE 5.6: EXAMPLE OF TOTAL PROBABILITY OF FAILURE CALCULATION

5.2.5.4. Sensitivity stochastic variables

A sensitivity assessment is performed to understand the influence of each variable on the inner slope stability. A FORM calculation results in sensitivity coefficients, which are the percentage change of input divided by the percentage change of output. But in this thesis a Monte Carlo analysis is performed (the reason is explained in section 2.3.3), which does not result in these sensitivity coefficients. The sensitivity of each variable can still quantitively be determined with the use of a correlation or regression analysis between the input and output [Hamby, 1994]. It is chosen to determine the sensitivity using the Spearman coefficients. The drawback of this method is that different variables can be strongly correlated and cause the same correlation. But it still useful to determine the sensitivity in a general sense [Hoffman and Gardner, 1983]. An example of the output of the sensitivity analysis is shown in Figure 5.7. The higher the Spearman coefficients the more sensitive the safety factor is to any change in that input and vice versa.

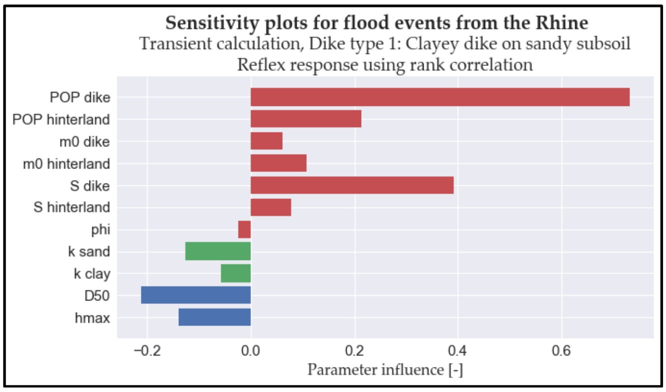

FIGURE 5.7: EXAMPLE SENSITIVITY DATA

In the stationary calculation the contribution of the duration is zero and in the variant on the stationary calculation also the contribution of the hydraulic conductivity is zero. The relative contribution of each variable is calculated by dividing the absolute value of a correlation coefficient through the sum of all absolute values of the correlation coefficients. The relative contribution indicates which specific variables have the largest contribution to the total probability of failure.

5.2.5.5. Accuracy choice 25 flood waves

The results of the correlation analysis (Chapter 4) are used to check the accuracy of the use of the 25 flood waves in the probabilistic calculation. In the correlation analysis is only varied in the shape of the flood wave. The strength and hydraulic conductivity have been chosen deterministically. The probability of failure of the 25 waves is plotted against the average safety factor and a linear line is fitted through the results, see Figure 5.8. In this way, the probability of failure for each of the 1500 waves is estimated. It is assumed that the changed geometry between the calculations of Chapter 4 and 5 would cause a difference in the mean of the results, but the spread in the results remains equal. To correct for this change in the mean, the predicted safety factors are reduced, in the way it equals the mean safety factor of the 25 flood waves. The total probability of failure is calculated for the 1500 waves. An identification of the accuracy is obtained by comparing the probability of failure associated with the 1500 waves with the probability of failure associated with the 25 waves.

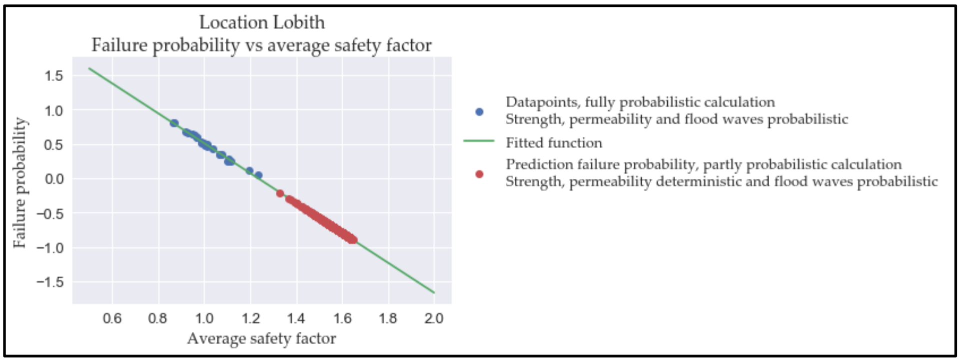

FIGURE 5.8: PROBABILITY OF FAILURE VERSUS AVERAGE SAFETY FACTOR TO PREDICT THE PROBABILITY OF FAILURE

5.3. Results

First, the results of the safety factors are discussed. Followed by the steps on the transformation from the distribution of safety factor to the probability of failure. Then, the differences between the stationary and transient total probability of failure are discussed followed by the results of the sensitivity assessment. Finally, the delay in failure is investigated. All results of the probabilistic calculation are presented in detail in *Appendix Q. Results probabilistic analysis.*

5.3.1. Safety factor

Figure 5.9 shows the safety factors for stationary water levels and during the passage of a flood wave for different dike types. Looking at the transient safety factors (shown in red) and the safety factor of the stationary calculation (shown in green). It can be noted that, larger safety factors are obtained when time dependency is considered with exception of dike type 2, the sand on sand dike. The higher permeability of the sand causes the internal pore pressures and therefore the safety factor to react instantaneously.

Looking at the variant of the stationary calculation (shown in blue), using the simplification in pore water pressures according WBI (2017), lower safety factors are obtained for both dike type 2 and 3. Assuming that the transient pore water pressures better approach the practice, this means that WBI (2017) overestimates the probability of failure for these type of dikes. Looking to the clay on sand dikes (type 1 and 4) lower safety factors are obtained in the transient calculation. Therefore, the method of WBI (2017) underestimates the probability of failure for the clay on sand dikes.

WBI does not take the permeability of the soil directly into account, the permeability is considered with the choice of the soil type (clay or sand). So, the results depend on the chosen permeability. When a calculation is repeated with another permeability of the soil, the WBI results remains the same while the transient results (and the stationary calculation with SEEP/W) differ. So, for the current values of the permeability, the results obtained with the WBI method leads to an underestimation of the probability of failure for clay on sand dikes.

The distribution of safety factors is of the same order of magnitude for all dike types and whether or not taking time dependency into account. Also, small differences in safety factors are seen comparing the results of the Rhine and the Meuse. This indicates that the flood wave variables have less influence on the safety factors than the strength of the material.

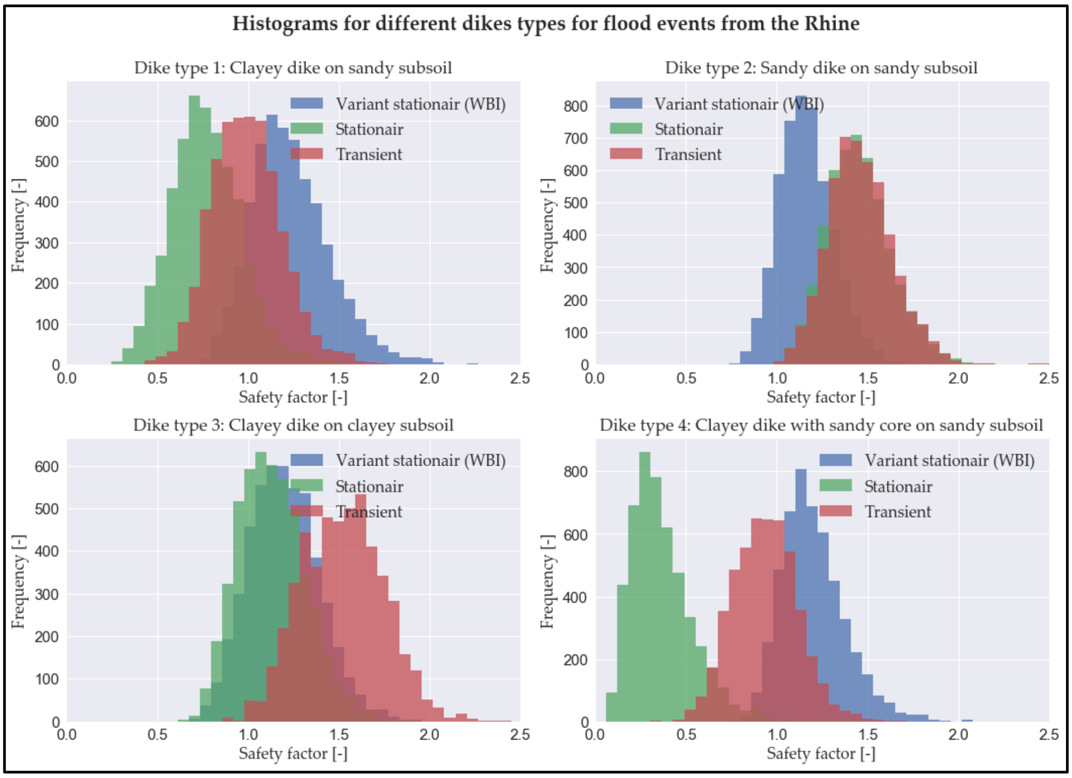

FIGURE 5.9: SAFETY FACTORS FOR STATIONARY WATER LEVELS AND DURING THE PASSAGE OF A FLOOD WAVE FOR DIFFERENT DIKE TYPES

5.3.2. Safety factor to probability of failure

The transformation from distribution of safety factor to probability of failure is shown in Table 5.4. For the two flood waves (one with a high peak and one with a low peak) the mean safety factor, the standard deviation and probability of failure are given for the different dike types and for the different calculation types. The results indicate that higher safety factors are obtained when the height of a flood wave is small, therefore the probability of failure decreases. Also, can be seen that for the transient and stationary calculation relatively low values of the safety factor are found for dike type 1 and 4, which results in a high probability of failure. On the contrary, the safety factor of dike type 2 and 3 are relatively high resulting in a low probability of failure. A higher safety factor will not always result in a lower probability of failure. When the standard deviation is large and the safety factor is high, still a high probability of failure can be found.

TABLE 5.4: SAFETY FACTOR AND PROBABILITY OF FAILURE OF TWO EVENTS FROM THE RHINE FOR TRANSIENT AND STATIONARY CALCULATIONS

		Transient				**Stationary (SEEP/W)**				**Variant Stationary (WBI)**			
	Dike type	1	2	3	4	1	2	3	4	1	2	3	4
High wave $h_{max} = 33.9\ m$ D_{50} =20.9 day	Safety factor (mean)	1.00	1.44	1.50	1.01	0.87	1.48	1.13	0.45	1.13	1.19	1.06	1.23
	Safety factor (std)	0.15	0.11	0.23	0.14	0.18	0.19	0.18	0.20	0.26	0.12	0.16	0.19
	Probability of failure	0.86	0.00	0.01	0.89	0.97	0.00	0.36	1.0	0.44	0.23	0.50	0.12

Low wave h_{max} = 33.0 D_{50} =20.0 day	Safety factor (mean)	1.27	1.55	1.54	1.03	1.12	1.53	1.21	0.52	1.13	1.21	1.09	1.28
	Safety factor (std)	0.17	0.19	0.42	0.19	0.16	0.15	0.11	0.08	0.13	0.22	0.27	0.17
	Probability of failure	0.56	0.00	0.00	0.66	0.85	0.00	0.21	0.99	0.36	0.02	0.43	0.10

5.3.3. Total probability of failure

The total probability of failure of the four dike types for both flood waves from the Meuse and Rhine is shown in Table 5.5. The probability of failure is equal to the integral of probability density function that depends on the value of h_{max} and D_{50}, an example of a function is shown in Figure 5.10. *Appendix Q. Results probabilistic analysis,* shows the probability density functions and the used 2D-fragility curves. From the plot can be seen that especially the events with a high probability of occurrence contributes to the probability of failure, despite the high probability of failure of the extreme events.

Lower total failure probabilities are obtained for the transient calculation compared to the stationary calculation with SEEP/W. For a clay on sand dike the difference in probability of failure are a factor of 1-2. For the clay on clay dike the differences in probability of failure are a factor 35-50. For the sand dike the smallest differences are obtained between the two states. The differences in probability of failure for the sand on sand dike are small, because the pore pressures react instantaneously, whereby almost a stationary condition is reached during the passage of a flood wave. The more clay is present, the more this response is delayed. Therefore, the clay on clay dike shows the largest differences.

Looking at the variant of the stationary calculation, the total probability of failure of dike type 2 and dike type 3 is higher than the transient total probability of failure, which indicates that the probability of failure is overestimated. Looking at dike type 1 and 4, the total probability of failure is higher using transient pore water pressure, which means that WBI underestimates the probability of failure. The probability of failure for dike type 1 are of the same order of magnitude. The total probability of failure using different calculation methods deviates maximum one order of magnitude; with exceptions of the sand on sand dike (type 2).

For the sand on sand dike very low total probabilities of failure are obtained, especially in the transient and stationary calculation using SEEP/W. The governing failure mechanism for a sand dike is micro stability, which is not investigated. So, considering only slope stability, a sand on sand dike is a safe dike, but taking other failure mechanism into account, this conclusion can differ. Looking at the other dike types, it can be concluded that that dike type 3, which consist completely out of clay is the safest dike, followed by dike type 1. Looking at slope stability the least safe dike is dike type 4, where the core consists of sand.

The total probabilities of failure for events from the Meuse are somewhat lower than the probability of failure for events from the Rhine. The reason for this finding, is the higher duration and height of the flood waves in the Rhine.

TABLE 5.5: PROBABILITY OF FAILURE INCLUDING PROBABILITY OF OCCURRENCE

	Dike type 1		Dike type 2		Dike type 3		Dike type 4	
	Rhine	Meuse	Rhine	Meuse	Rhine	Meuse	Rhine	Meuse
Transient	9.13e-03	5.70e-03	0.00	0.00	1.04e-04	9.87e-05	1.11e-02	7.02e-03
Stationary (SEEP/W)	1.71e-02	1.19e-02	3.91e-06	9.26e-07	4.92e-03	3.53e-03	1.96e-02	1.34e-02
Stationary (WBI)	2.29e-03	1.31e-03	1.82e-03	1.79e-03	3.05e-03	1.69e-03	1.72e-03	1.32e-03

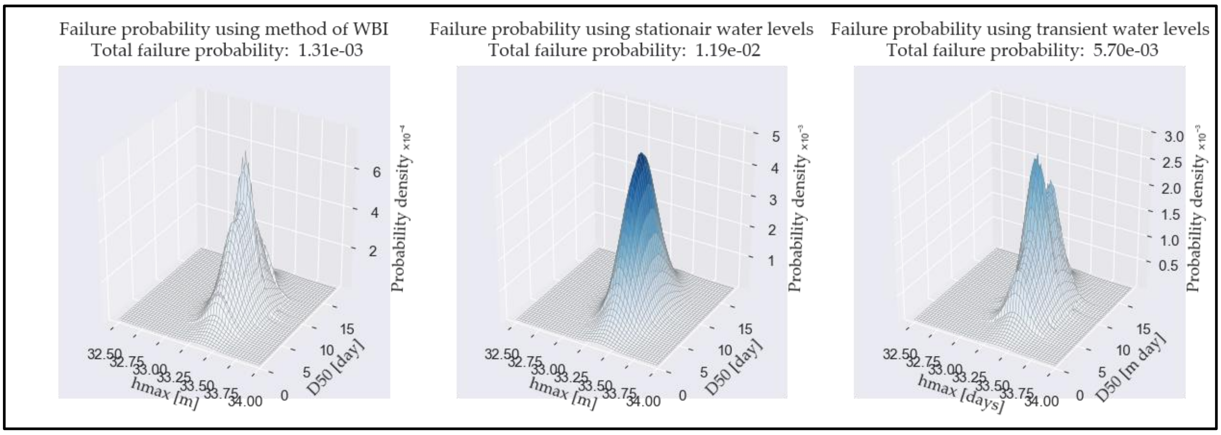

FIGURE 5.10: PROBABILITY DENSITY FUNCTION FOR A CLAYEY DYKE ON SAND SUBSOIL FOR A FLOOD WAVE FROM THE MEUSE

5.3.4. Sensitivity data

The duration and height of the flood waves and the permeability of the material are load variables, because they have a negative contribution to the probability of failure. A variable with a negative contribution increases the failure probability when the value of that variable increases. The strength variables have a positive contribution to the probability of failure. In some calculations the internal friction angle of the sand has a negative contribution to the probability of failure. This is shown in Figure 5.11.

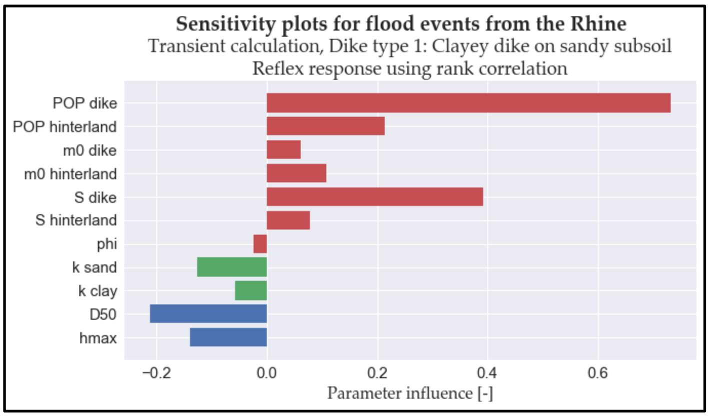

FIGURE 5.11: REFLEX RESPONSE FOR DIKE TYPE 1 FOR FLOOD WAVES FROM THE RHINE

Two parts determine the probability of failure; the calculation method (transient or stationary) determines the average safety factor, while the chosen probability density functions of the input variables determine the variation in the safety factor. The larger the variation in safety factor the larger the probability of failure, when the average factor of safety is higher than 1.

The variation in safety factor is represented by the Spearman correlation coefficient between the safety factor and the input. The higher the Spearman coefficients the more sensitive the safety factor is to any change in that input and vice versa. Table 5.6 till
Table 5.8 shows the relative contribution of the input to the distribution of the safety factor and therefore to the probability of failure.

For all dikes, the strength of the material is the largest contributor to the distribution of the safety factors and therefore to the probability of failure; followed by the shape of the flood waves and the permeability. The variation in the pre overburden pressure contributes the most to the distribution of the safety factors for clay dike bodies (dike type 1, 3 and 4). Especially the pre overburden pressure of the dike body has a large contribution to the distribution of safety factors of approximately 30-40%. Also, the normally consolidated undrained shear strength ratio of the dike body has a large contribution of approximately 10-30%. The biggest contribution for a sand dike is given by the variation in the internal friction angle, the contribution is approximately equal to 75-80%.

In the previous Chapter was concluded that the duration of a flood wave has more influence on the safety factor than the height of a flood wave. In the probabilistic calculation the geometry and the permeability of the dikes are adjusted. The permeability has been increased, causing the influence of the height to increase. In the transient calculation the height contributes for 10% to the distribution of the safety factors, while the contribution of the duration is 2-6%. For the clay dike types in combination with flood events from the Rhine, the duration is still more of influence on the distribution of the safety factors than the height of a flood wave. Looking at the events of the Meuse, the height has a larger contribution than the duration. The height of the flood waves is lower than the flood waves from the Rhine. This characteristic causes the large contribution of the height to the probability of failure; because variation in height is more of influence for the lower waves, this can be seen in the block-wave analysis.

When looking at the differences between the transient and stationary calculation, it can be noted that despite the fact that the duration in the stationary calculation does not contribute to the distribution of safety factors, the total contribution of the flood waves remains in the same order as in the transient calculation. In the stationary calculation the contribution of the flood waves is only caused by the peak wave height. In the stationary calculation the contribution of the strength is higher, while the contribution of the permeability is lower, because in the transient calculation the permeability determines the time of failure.

In the variant of the stationary calculation (WBI), the permeability of the material is not considered; and simplification are used to determine the pore pressure field. The variation in height of a flood wave hardly (1-6%) influences the distribution of safety factors for the clay dikes, because the pore pressure field at the inner toe remains almost the same. The distribution of safety factors is mainly determined by the strength variables. In the stability calculation of the sand on sand dike, the height contributes for 20-23% to the distribution of safety factors.

TABLE 5.6: RELATIVE CONTRIBUTION OF A VARIABLE TO THE SPREAD OF THE SAFETY FACTOR IN A TRANSIENT CALCULATION [%]

	Dike type 1		**Dike type 2**		**Dike type 3**		**Dike type 4**	
	Rhine	Meuse	Rhine	Meuse	Rhine	Meuse	Rhine	Meuse
h_{max}	6.5	14.2	10.8	11.8	1.0	1.7	6.4	17.4
D_{50}	9.8	9.3	2.8	6.1	6.0	0.4	11.8	11.6
$k_{x,Clau}$	2.7	3.8	1.9	1.7	4.2	3.8	3.6	5.0
$k_{x,Sand}$	5.9	5.9	0.9	1.2	0	0	5.4	6.5
ϕ	1.1	0.5	81.1	76.2	0	0	1.1	0.1
$S_{hinterland}$	3.7	3.2	0	0	6.1	6.5	1.4	1.4
S_{dike}	18.3	17.3	0.7	0.2	27.2	29.2	10.8	9.0
$m_{hinterland}$	5.0	4.2	0	0	2.7	2.7	2.6	2.2
m_{dike}	2.9	2.8	0.3	0.8	3.1	3.6	15.6	12.9
$POP_{hinterland}$	10.0	8.1	0	0	11.6	11.9	4.0	2.9
POP_{dike}	34.1	30.7	1.5	2.0	38.1	40.1	37.1	31.0
Flood wave	**16.3**	**23.5**	**13.6**	**17.9**	**7.0**	**2.1**	**18.2**	**29.0**
Permeability	**8.6**	**9.7**	**2.8**	**2.9**	**4.2**	**3.8**	**9.0**	**11.5**
Strength	**75.1**	**66.8**	**83.6**	**79.2**	**88.8**	**94.1**	**72.8**	**59.5**

TABLE 5.7: RELATIVE CONTRIBUTION OF A VARIABLE TO THE SPREAD OF THE SAFETY FACTOR IN A STATIONARY CALCULATION USING SEEP/W [%]

	Dike type 1		**Dike type 2**		**Dike type 3**		**Dike type 4**	
	Rhine	Meuse	Rhine	Meuse	Rhine	Meuse	Rhine	Meuse
h_{max}	16.4	19.9	8.9	12.7	6.2	9.1	19.8	28.2
$k_{x,Clau}$	3.2	2.3	1.9	1.7	0	0	0.4	0.2
$k_{x,Sand}$	5.9	5.0	0.8	1.3	0	0	4.3	4.5
ϕ	1.1	0.6	85.7	81.1	0	0	1.1	0.1
$S_{hinterland}$	3.6	3.5	0	0	6.4	6.3	1.5	1.6
S_{dike}	18.2	18.8	0.8	0.2	28.8	28.2	11.2	10.1
$m_{hinterland}$	5.0	4.6	0	0	2.8	2.6	2.7	2.5
m_{dike}	2.8	3.1	0.3	0.8	3.3	3.5	16.3	14.5
$POP_{hinterland}$	9.9	8.8	0	0	12.2	11.5	4.1	3.3
POP_{dike}	33.9	33.4	1.6	2.2	40.2	38.7	38.6	35.0
Flood wave	**16.4**	**19.9**	**8.9**	**12.7**	**6.2**	**9.1**	**19.8**	**28.2**
Permeability	**9.1**	**7.3**	**2.7**	**3.0**	**0**	**0**	**4.7**	**4.7**
Strength	**74.5**	**72.8**	**88.4**	**84.3**	**93.8**	**90.9**	**84.9**	**67.2**

TABLE 5.8: RELATIVE CONTRIBUTION OF A VARIABLE TO THE SPREAD OF THE SAFETY FACTOR IN A VARIANT OF THE STATIONARY CALCULATION USING SIMPLIFICATIONS OF WBI [%]

	Dike type 1		**Dike type 2**		**Dike type 3**		**Dike type 4**	
	Rhine	Meuse	Rhine	Meuse	Rhine	Meuse	Rhine	Meuse
h_{max}	2.7	3.8	23.7	30.9	1.8	2.7	4.3	6.2
ϕ	0.6	0.6	74.4	66.6	0	0	5.8	5.7
$S_{hinterland}$	5.6	5.7	0	0	5.6	5.6	8.2	8.1
S_{dike}	28.1	27.9	0	0.2	28.2	28.1	27.5	27.1
$m_{hinterland}$	2.4	2.3	0	0	2.5	2.3	2.7	2.5
m_{dike}	4.1	4.4	0.6	0.8	4.3	4.7	2.9	3.1
$POP_{hinterland}$	9.4	9.0	0	0	9.2	8.7	13.3	12.7
POP_{dike}	47.1	46.3	1.2	1.5	48.4	47.9	35.3	34.5
Flood wave	**2.7**	**3.8**	**23.7**	**30.9**	**1.8**	**2.7**	**4.3**	**6.2**
Strength	**97.3**	**96.2**	**76.3**	**69.1**	**98.2**	**97.3**	**95.7**	**93.8**

5.3.5. Delay in failure

The lowest safety factor during the passage of the flood wave is found after the peak of the flood wave (see Figure 5.12). The permeability of the material mainly determines the time of occurrence of the lowest safety factor. Dike type 1 and 4 (the clay on sand dikes) shows the same characteristics as each other. The time of the lowest safety factor is found in the first 5 days after the peak water level. Pore water pressures in the sand aquifer reacts fast to the increased pore water pressures of the flood wave and cause uplifting of the hinterland. Exceptions were found, where the permeability of the aquifer is low. The lowest safety factor for the sand on sand dike (dike type 2) occurs within a day after the peak of the flood wave. Dike type 3 (the clay on clay dike), do not reached stationary condition, because the response to the flood wave is delayed by the low permeability. Therefore, the safety factor is most found in the latest investigated timestep. Looking at the results of the Meuse (presented in *Appendix Q. Results probabilistic analysis),* the same results are obtained.

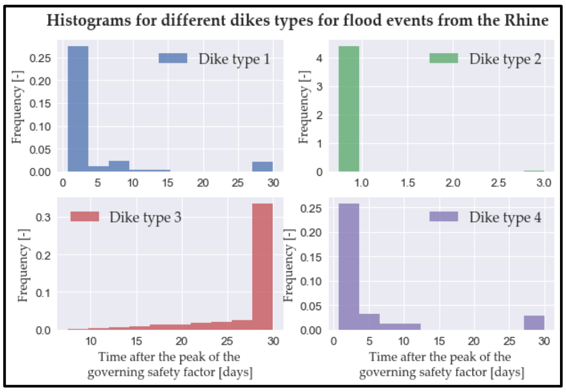

FIGURE 5.12: TIME AFTER THE PEAK OF THE FLOOD WAVE WHERE THE SAFETY FACTOR IS SMALLEST

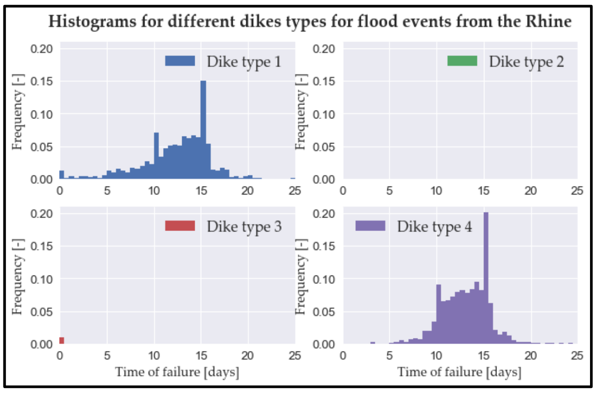

FIGURE 5.13: TIME OF FAILURE (FOS<1)

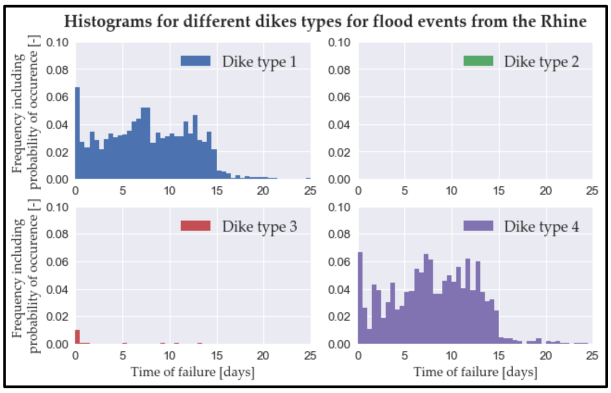

FIGURE 5.14: TIME OF FAILURE INCLUDING PROBABILITY OF OCCURRENCE P(FOS<1) × PF(HMAX)/50 × PF (D50)

Failure of a dike occurs when the safety factor is lower than 1. Figure 5.13 shows that the sand on sand dikes do not fail, and the clay on clay dikes hardly fail. The clay on sand dikes (type 1 and 4) usually fails before the peak water level is reached at t=15 days. The time of failure depends on flood wave characteristics, permeability characteristics and strength characteristics. High or long waves cause the failure to be earlier in time. When the probability of occurrence of the maximum wave height and duration is multiplied with the probability of failure in a specific time step, the results shown in Figure 5.14 are obtained.

In the first 10 days the probability is increased, while probability of occurrence of long or high wave is low. Therefore, this increase is not caused by the wave characteristics, but by the permeability and strength characteristics of the soil. When the clay material is weak, failure of an embankment occurs fast. For all 25 flood waves, dikes with a low strength are investigated, and therefore the probability is high in the first 10 days.

5.3.6. Accuracy model

Figure 5.15 gives an example of the probability density function and the probability of failure for the clay on sand dike at Lobith. The extrapolation and interpolation distance reduce with the use of the 1500 flood waves instead of the 25 flood waves. The reduced extrapolation and interpolation distances causes a smoother probability density function, which causes the estimation of the total probability of failure to be more accurate. Table 5.9 shows the total probability of failure for different dike types at Lobith and Borgharen. The differences in total probability of failure are 6-18 %. Despite, the use of 1500 waves lead to more accurate results; the differences are not that large. While using the 25 waves reduces the calculation time with a factor 60. The differences between the total probabilities of failure are larger for the dikes at Borgharen. At Borgharen the 25 flood waves are less uniformly distributed, causing the extrapolation distances to be larger; which again causes the error to be larger than at Lobith. So, to reduce the calculation time of a probabilistic calculation 25 flood waves can be used instead of the 1500 flood waves, but the waves have to be chosen uniformly distributed over the duration and height of the flood waves.

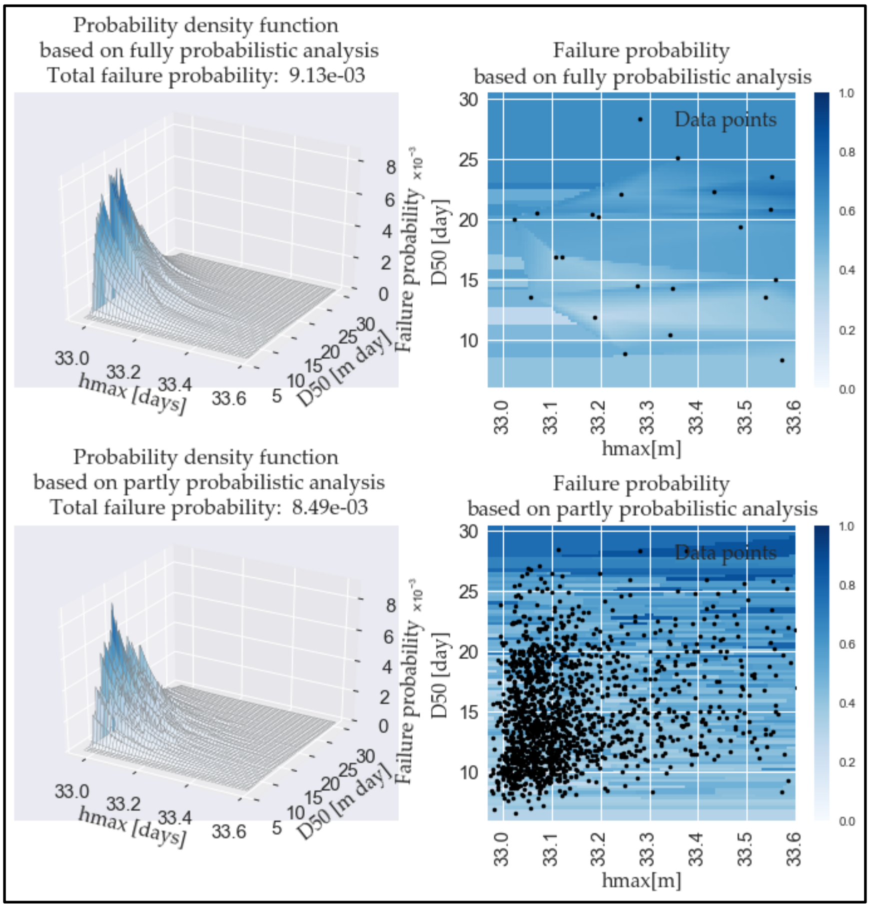

FIGURE 5.15: ACCURACY CHECK FOR DIKE TYPE 1 AT LOBITH

TABLE 5.9: TOTAL PROBABILITY OF FAILURE CALCULATED WITH 25 AND 1500 FLOOD WAVES

	Dike type 1		**Dike type 2**		**Dike type 3**		**Dike type 4**	
	Rhine	Meuse	Rhine	Meuse	Rhine	Meuse	Rhine	Meuse
Total probability of failure 25 flood waves	9.13e-3	5.70e-3	0	0	1.04e-4	9.87e-5	1.11e-2	7.02e-3
Total probability of failure 1500 flood waves	8.49e-3	5.16e-3	0	0	1.12e-3	1.17e-4	1.04e-2	6.39e-3
Differences	6.9 %	9.4 %	0 %	0 %	8.1 %	18.2 %	6.5 %	9.0 %

5.4. Conclusion

What is the effect on the probability of failure of slope stability by taking time dependency into account and wat are the main variables determining this effect?
Taking time dependency into account, higher safety factors (factor 1.5-2) are obtained; resulting in lower probabilities of failure. Except for a sand on sand dike, because the pore water pressures reacts instantaneously to the increased pressures during the passage of a flood wave; caused by the high permeability of the material. Therefore, the same order of safety factor is found.

Time dependency also causes failure of the embankment to not occur simultaneously with the maximum wave height. Failure of a clay on sand is most likely in the days before the maximum wave height. The time of failure is determined by the strength and permeability characteristics of the soil, which delays the response of the pore water pressures. For a sand on sand dike, this delay is minimal and the pore water pressures reacts within a day. For impermeable dikes located on a saturated aquifer, the maximum response to water level occurs within a week. For a completely impermeable dike, the delay in response is very large (more than 2 weeks).

For all dikes, the strength of the material is the largest contributor to the distribution of the safety factors and therefore to the probability of failure (approximately 60-95%). In a clay dike the contribution to the probability of failure is caused by the pre overburden pressure and the normally consolidated undrained shear strength ratio. In sand dikes the contribution to the failure probability is impacted by the value of the internal friction angle. The contribution of the strength decreases in a transient calculation, but the strength remains the largest contributor to the probability of failure.

In a transient calculation, flood wave variables contribute for 2-30% to distribution of safety factor. In permeable dikes this contribution is delivered by the height of the flood waves, while in impermeable dikes the contribution is delivered through the duration of a flood wave. The contribution of the permeability to the probability of failure is small, 2-12%.

Taking time dependency into account is useful for determining the correct safety factor but is less useful in determining the probability of failure; because the strength of the material has the largest contribution to the probability of failure. A sand on sand dike reacts instantaneously, therefore a stationary calculation is sufficient. The variation in the permeability in a probabilistic calculation can be neglected, because the contribution is 10-20 times lower than the strength of a dike.

What are the differences in slope stability using the simplified pore water pressures of WBI and the transient pore water pressures?

It is assumed that the transient pore water pressures are a better approximation of the practice. Therefore, using the pore water pressures according WBI (2017), the safety factors and the probability of failure are overestimated when a dike and subsoil consist completely out of sand or clay. But the probability of failure is underestimated when is looked at clay on sand dikes. Note that WBI does not take the permeability of the soil into account, so the results are dependent on the chosen permeability and this conclusion only holds for the investigated dike types.

The strength is the largest contributor to the safety factor for both calculation types. In a clay dike, the contribution is caused by the pre overburden pressure and the normally consolidated undrained shear strength ratio. In sand dikes the contribution is caused by the value of the internal friction angle.

6. REPRESENTATIVE FLOOD WAVE

6.1. Goal

In this chapter the use of a representative flood wave in a deterministic calculation is investigated. The goal is to give advice about which flood wave shape and duration can be used best in the Rhine and the Meuse. To find the representative flood wave, various flood waves are averaged and the duration that results in the same probability of failure as calculated in the probabilistic calculation is chosen.

6.2. Method

The duration of the representative flood wave is chosen in such a way that the total probability of failure including occurrence of the maximum height and the duration of a flood wave followed by the probabilistic calculation (equation 5.1) equals the total probability of failure where a fixed duration is chosen (equation 6.1). In equation 6.1 the probability of occurrence of the duration is not included but the cross-section associated with a duration that results in the same total probability of failure as the probabilistic calculation is chosen.

$$F_{FoS<1|\underline{h_{max}}=h_{max},\underline{D_{50}}=D_{50}} = \frac{1}{50} f_{FoS<1|\underline{h_{max}}=h_{max},\underline{D_{50}}=D_{50}} \int_{-\infty}^{h_{max}} f_{\underline{h_{max}}}(h_{max}) dh_{max} \qquad 6.1$$

In which:

h_{max}	= Maximum flood wave height [m]
D_{50}	= Duration halfway the flood wave [days]
$F_{FoS<1\|\underline{h_{max}}=h_{max},\underline{D_{50}}}$	= Total probability of failure including occurrence of the height [-]
$f_{FoS<1\|\underline{h_{max}}=h_{max},\underline{D_{50}}=D_{50}}$	= Probability of failure given a height and duration of a flood [-]
$f_{\underline{h_{max}}}(h_{max})$	= Fitted probability density function of the maximum water level [-]

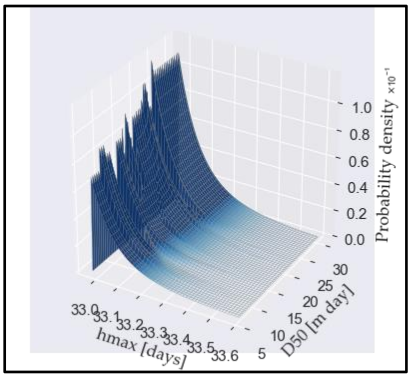

FIGURE 6.1: PROBABILITY DENSITY FUNCTION WITHOUT INCLUDING PROBABILITY OF OCCURRENCE OF THE DURATION

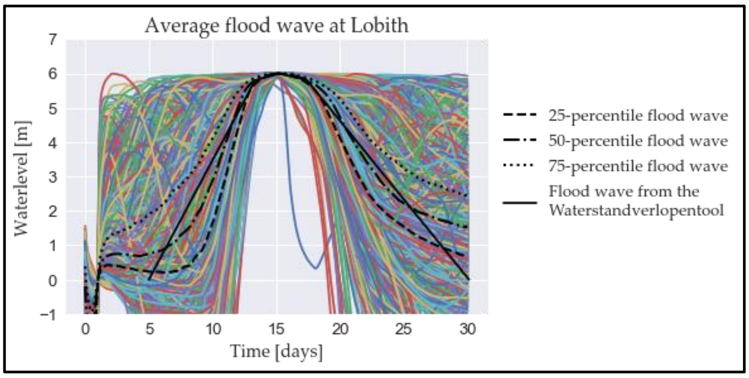

FIGURE 6.2: ALL 1557 FLOOD WAVES AT LOBITH WITH DIFFERENT PERCENTILE FLOOD WAVES AND THE FLOOD WAVE CALCULATED WITH THE WATERSTANDSVERLOPENTOOL

The 1557 flood waves at Lobith and the 1486 flood waves at Borgharen are used to find the representative shape of the flood wave. Section 4.2.2 describes how the GRADE dataset is transformed into hydrographs of the water level with the use of SOBEK. All flood waves are scaled by dividing the height with the differences between the maximum height and the height after one day. Next, the scaled waves are multiplied with the maximum height of the flood wave followed from the Waterstandsverlopentool. For each hour a percentile water level is chosen, which results in a percentile flood wave. The percentile flood wave that has the same duration as the duration explained in the paragraph above is chosen to be the representative flood wave. Figure 6.2 gives an example of different percentile flood waves. For each type of dike an advice is given about the use of a representative flood wave with exception of the sand dike on a sand soil, because according to the probabilistic analysis the probability of failure is zero.

6.3. Results

Table 6.1 shows the durations that results in the same total probability of failure as calculated in the probabilistic calculation. The duration for the clay dike on clayey soil (dike type 3) is higher than the duration found at dike type 1 and 4. This applies to both investigated locations. Shorter waves result in a lower probability of failure, because the intrusion length of the water is lower for this type of waves. This holds especially for dike type 3, because the permeability of the material is lower; therefore, higher durations are found. Figure 6.3 shows the representative flood wave for the three different dike types at Lobith. The percentiles are chosen in such a way that the flood wave has the same duration as found in Table 6.1. In Figure 6.4 the representative flood wave for Borgharen is shown. The flood waves at Borgharen have a longer duration than the flood wave used in the Waterstandsverlopentool, while the representative flood waves at Lobith are almost have the same duration.

TABLE 6.1: DURATION THAT RESULTS IN THE SAME TOTAL PROBABILITY OF FAILURE AS CALCULATED IN THE PROBABILISTIC CALCULATION

	Lobith			Borgharen		
Dike type	1	3	4	1	3	4
Duration [days]	13.42	16.38	13.92	10.36	10.91	10.36
Total probability of failure (probabilistic calculation, eq. 5.1)	9.13e-03	1.04e-04	1.11e-02	5.75e-03	1.24e-04	6.99e-03
Total probability of failure (eq. 6.1)	9.07e-03	1.06e-04	1.08e-02	5.76e-03	1.25e-04	6.97e-03

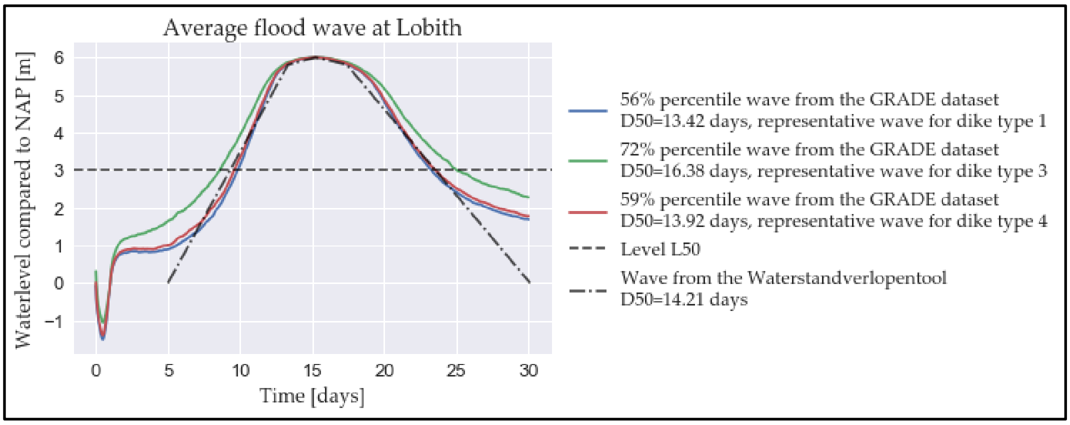

FIGURE 6.3: REPRESENTATIVE FLOOD WAVE AT LOBITH

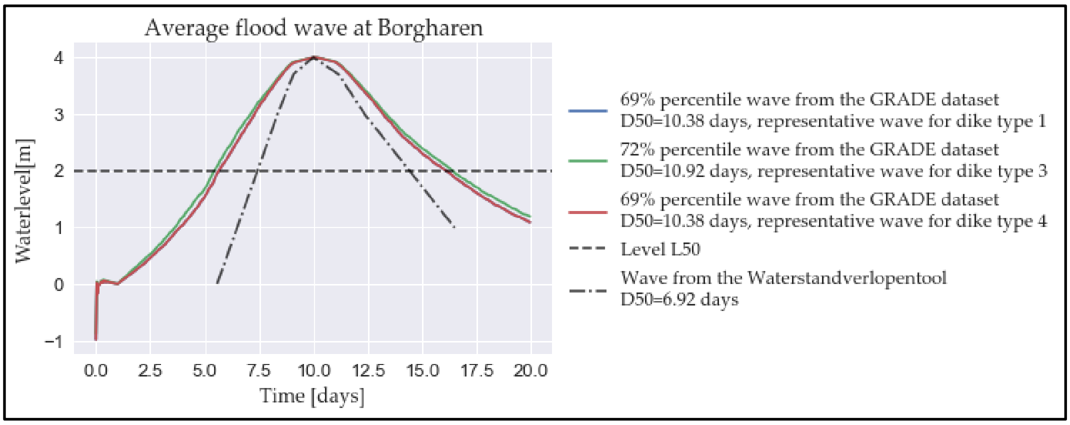

FIGURE 6.4: REPRESENTATIVE FLOOD WAVE AT BORGHAREN

6.4. Conclusion

What is a representative flood wave in a deterministic stability calculation?
Figure 6.3 shows the representative flood wave that can be used in a deterministic stability calculation at Lobith. The flood wave can be moved up or down to adjust the height of the flood wave, but the shape remains unchanged. The same holds for the representative flood wave at Borgharen, Figure 6.4 shows this representative wave. When both the dike body and the subsoil consist out of an impermeable material, it is advised to use a longer duration than when a permeable subsoil is present.

In some current calculations, average durations of flood waves are used in the deterministic calculations. At Lobith, this average wave deviates slightly from the representative flood waves. Using this average flood wave instead of the representative flood wave will lead to a slightly different total probability of failure. In contrast to the representative flood wave at Borgharen, which has a duration that is with a factor 1.5-1.6 higher than the average duration. Hereby, lower Probabilities of failure are found with the use of an average flood wave, which will underestimate the probability of failure. Concluding that, especially in the Meuse, it is advised to use the representative flood wave.

7. DISCUSSION

The main objective of this study was to investigate the variation in height and duration of a flood wave and the effect of it on the stability of the inner slope. This was done by performing a correlation analysis for different flood wave shape variables and a probabilistic analysis which varied in the shape of a flood wave, the permeability and strength of the material. The probabilistic analysis was used for both transient and stationary calculations of the pore water pressures. By comparing the results, it should become clear whether it is useful to perform a transient calculation in the assessment of slope stability.

7.1. Initial pore water pressures

In a transient calculation, the initial state before a flood wave passes must be chosen. In this study, the initial water level is set to the first value of the water level of a flood wave. This implies (especially since no rain is considered in the model), that a dike is dry before the passage of a flood wave. This choice makes it possible to compare the results without influence of the initial water level. Chances in safety factor can therefore only be caused by the variation in the shape of a flood wave. De Loor (2018) confirms that the same initial state must be used to adequately assess the effect of the different loads.

The pore water pressures in the dike, before the passage of a flood wave is determined by the residual water content and the matric suction capacity of the material. The matric suction capacity of sand is minimal, which causes the sand dike to be dry before a passage of a flood wave. The hydraulic conductivity depends on the degree of saturation, causing very low hydraulic conductivities in the sand material; therefore, the sand dikes react less instantaneously than expected. In the case of flood waves with a duration within 5 days, the correlation between the safety factor and the maximum height is affected. But the results still give an indication about the degree of influence, especially for the longer and lower waves.

For a clay dike, the response of the water pressures is delayed causing the first few days for the stability of the inner slope to be unchanged. The stability is determined by the choice of the initial water level and initial state (degree of saturation). To keep this initial state as close to practice, de Loor (2018) recommends applying several years of actual precipitation and evaporation in combination with an initial level based on measurements of an actual dike. From this can be concluded that a value that is too low of the initial state is chosen to represent the practice, because this is not included in the model. The results of the correlation analysis give still an indication of the influence of a variable. Increasing the initial state will decrease the time the safety factor is unaffected; this will again increase the influence of the height of a flood wave. In a permeable dike it is expected that the influence of the duration decreases and in an impermeable dike the influence of the duration is expected to increase.

The safety factor of a clay dike is expected to be too high. Stationary conditions are not reached; therefore, the initial state determines the safety factor. A higher initial state results in a lower safety factor. For sand on sand dikes also the safety factor is expected to be too high, because the degree is saturation is low, which causes a low hydraulic conductivity in the first days of a flood. Using a higher initial state, increases the response in the first days.

7.2. GRADE dataset combined with SOBEK

The GRADE dataset is used for the selecting hydrographs in the Rhine and the Meuse. The GRADE dataset has a length of 50000 year and prevents extrapolation of the results of measured data [Hegnauer *et al*, 2014]. The drawback of the use of GRADE is however that it uses daily time steps which could be too large to include the dynamical behavior in the Rhine and the Meuse. This would not affect the results of the correlation analysis, because the correlation analysis is performed on a certain height and duration. Changing a flood wave using a smaller time steps results in a changing the safety factor as well. This affected is assumed to be small, because from the correlation analysis follows that the number of peaks of a flood wave hardly influences the safety factor. If this influence is small, also the influence of temporal resolution is expected to be small.

The hydrographs of the water level calculated with SOBEK are not accurate within the first 24 hour. Very fast increases of the water level are obtained, which is not realistic. A wave that increases very fast in the first 24 hour is a wave, for which the initial water level was already high before the passage of the flood wave. In the correlation analysis, these 24 hours have been disregarded, but in the calculation with SEEP/W, the first 24 hours are included. This assumes that each wave has the same initial condition. As stated above, this is a good method to adequately assess the effect of the different loads; but it does not describe the practice. Further, in SOBEK flood waves with a maximum duration of 30 days are investigated, while some flood waves have a longer duration. The last part does not affect the results because the number of waves is less than 1% of the total amount of waves.

7.3. Application of the probabilistic approach

Probabilistic method

In this thesis a Monte Carlo calculation is used in combination with numerical integration over the loads. A Monte Carlo method provides a reasonably accurate estimate for the probability of failure; in contrast to a FORM method, linearization of the limit state function is not required. The drawback of a Monte Carlo method is the long calculation time. The calculation is especially long when the probability of failure is low and many variables are assessed probabilistically.

The advantage of numerical integration over the loads is that an error in the calculation of extreme events is reduced. When the probability of failure is low, ideally more calculations have to be done to obtain an accurate result. When numerical integration is used, this low failure probability is multiplied with the probability of occurrence of the event, this probability is low since the event is rare. The error in the calculation is therefore reduced compared to common events.

The use of the Monte Carlo method is not preferred for models with a large number of variables, because this would increase the calculation time significantly. When more variables are included, an Adaptive Response Surface (FORM-ARS) can be used. Moellmann *et al* (2011) uses this method in a research to embankment stability under transient seepage conditions.

This method reduces the calculation time in the determination of the probability of failure and is suitable if no limit state function is known. Moellmann *et al* (2011) has verified this method with the use of a Monte Carlo calculation.

Load distributions

The load distributions of the permeability and strength parameters of the soil are based on a sample collection of HHNK. The flood waves between a return period of 50 - 80,000 years were used in the research. For estimating the correct total failure probability, the lower limit of the range must be chosen based on the height below which it does not affect the stability of the slope. Tigchelaar *et al* (2018) uses in a research water levels with a return period between the 10 – 10,000 years. Tigchelaar *et al* (2018) investigated with the chosen return period a range of 3 meters in water level height, while in this research a range of 2 meter is investigated. The water level is Gumbel distributed; therefore, more variation is found in the water level for the lower return periods. Therefore, lower failure probabilities are obtained; which still can be used to illustrate how the method must be implemented.

The low variation in height, is not favorable to perform a correlation analysis with. The large variation in the duration of a flood wave can affect the correlation. The correlation of the duration is calculated correctly, but the correlation coefficient of the maximum height can be underestimated. A lower variation of variable results in a lower contribution to the probability of failure. The contribution of the flood wave to the probability of failure will therefore be larger in practice.

In this research rainfall is not included in the model; but easily can be implemented by adding a constant flow boundary to the model. The constant inflow rate can easily be varied in the Monte Carlo analysis, the investigate the effect of the variation on the failure probabilities.

Selection 25 flood waves

Applying numerical integration over the two load variables, requires a Monte Carlo calculation per combination of loads, because the failure probability per combination have to be known. This leads to a very long calculation time, which is not practical. 25 Flood waves based on the load parameters are chosen to reduce the calculation time. For each of the 25 flood waves a Monte Carlo calculation is executed. The probability of failure of each combination of loads is estimated by inter- and extrapolation of the results.

The 25 flood waves are chosen based on the height and the duration of a flood wave. It is assumed that these two parameters completely describes the shape of a flood wave. The variables have a high correlation with the safety factor, what supports this assumption. But it is recommended to estimate the error of the use of these 25 flood waves, by calculating the failure probability using all waves in the dataset. The assumption that two variables completely describes the flood waves, causes findings in the fragility curve such as a higher probability of failure for the same height when the duration of the flood is shorter.

The 25 flood waves are selected based on equal probability classes of the loads. The accuracy of this choice is checked in section 5.2.5.5. Because equal probability classes are used; rare events determine a large part of the probability of failure in the fragility curve. It is more accurate to select the events based on uniformly distributed classes. This causes the contribution of an event to the probability of failure to be equal. Also, it is preferred to reduce the extrapolated area, because this introduce the largest errors. To reduce the extrapolated area; it is recommended to choose 4 extreme events at the edges of the fragility curve.

Using all flood waves instead of the 25 flood waves reduces the extrapolation and interpolation distance, which causes a smoother probability density function, which causes the estimation of the total probability of failure to be more accurate. From section 5.2.5.5 can be concluded that this leads to a difference in the total probability of failure of 6-18 %. Despite, the use of 1500 waves leads to more accurate results; the differences are not that large. While using the 25 waves reduces the calculation time with a factor 60. Therefore, the use of 25 waves is a good method in determining the total probability of failure (if the 25 events are chosen correctly).

The use of 25 flood waves is not accurate in determining the representative flood wave, the probability density function is rough. The total probability of failure of a cross-section with a specific duration varies strongly over the different durations. The choice of the representative flood wave must therefore be based on multiple flood waves to increase the accuracy. So, the method illustrated in Chapter 6 can still be used, but the results are not accurate enough.

7.4. Generalization results

In this thesis generalized theoretical dikes are used. Obtained values are therefore useful to get an insight in the processes and it illustrates how the method can be implemented. It do not cover the full range of dike configuration in practice. There will always be special cases with its own behaviour.

The choice of the geometry and soil characteristics of the theoretical dike influences the degree of contribution of the duration and the maximum flood wave height to the safety factor. Which can be seen, because different correlations are obtained per flood wave characteristic per dike type. Therefore, specific results are obtained; but the conclusion is generalized. The findings should be confirmed with the use of a real case studies.

Especially, the comparisons of the results of the transient calculation with the variant of the stationary calculation using the simplified pore water pressure according WBI (2017) depends on the chosen permeability. The pore water pressures in the variant are independent of the permeability (WBI only make a distinguish between sand and clay). When, the permeability is changed in the transient calculation, the results will differ; while the results of the variant of the stationary calculation remains the same. Therefore, we cannot conclude, based on these results if WBI underestimates or overestimates these results. The only thing that can be concluded from the results is that a stationary calculation using the pore pressure according WBI (2017) could under or overestimate the results, but this depends on the chosen permeability.

7.5. Comparison results

The results of the sensitivity factors followed from the probabilistic calculation show a good agreement with the calibration STBI performed by Deltares (2016). Also, in this calibration study, the contribution of the permeability of the material to probability of failure is small, the largest contribution is delivered by the strength of the material. Both in this research and the calibration study of Deltares (2016); the contribution to the strength of a clay dike to the probability of failure is delivered by the pre overburden pressure and the normally consolidated undrained shear strength ratio. In sand dikes, the contribution is caused by the value of the internal friction angle.

From a research performed by Moellmann *et al* (2011) followed that the effective friction angle and the effective cohesion influences the failure probability; whereas the permeability has a negligible influence. This is in confirmation with the obtained findings of this thesis, where the strength characteristics of the soil influences most the probability of failure. It is a surprising result because the permeability of the soil should influence the internal pore water pressures in a transient calculation. But the same results are obtained from multiple studies (Moellmann *et al* (2009, 2011) and Deltares (2016)), even when the variation in permeability is increased; the permeability has a negligible effect on the probability of failure.

Further confirms Moellmann *et al* (2011) in his research the finding that the minimum safety factor does not occur simultaneously with the flood peak. There is a delay in the response which depends although Moellmann *et al* (2011) on the permeability and the initial degree of saturation.

Because multiple researches obtained the same results, it can be concluded that the software GeoStudio (package SEEP/W and SLOPE/W) can indeed be used to perform a transient analysis.

8. CONCLUSIONS AND RECOMMENDATIONS

The purpose of this thesis was to investigate the influence of the flood duration on the stability of the inner slope and in what degree it affects the design. The variation in the duration and height of the flood wave was investigated, the effect of it on the response of the pore water pressures and again the effect of the pore water pressures on the stability of the inner slope. An answer in this Chapter is provided to the following main question:

"What is the influence of the flood duration on slope stability and in what degree affects the flood duration the design?"

In most current dike assessments only the stationary water levels are investigated in the assessment of the stability of the inner slope, while there are differences for all kinds of dikes between the stationary and transient pore water pressures. The degree of influence of time dependency on the pore water pressures and slope stability depends on dike characteristics, flood wave characteristics and the delay in failure.

Dike characteristics

The differences in pore water pressure are especially large for dikes that consist of an impermeable material such as clay. When the subsoil consists of clay, larger differences are expected than when only the dike body consist of clay. Large differences in pore water pressures do not necessarily lead to large differences in the safety factor, for example a clay dike on top of clayey subsoil. The largest differences in safety factors are obtained when uplifting of the hinterland takes place during the stationary state and/ or during the passage of a flood wave. A transient calculation is therefore most useful for dikes with an aquifer and a thin (thinner than 5 m) weak (low POP values) hinterland. A permeable core of a dike increases the importance of a transient calculation.

Flood wave characteristics

The differences in safety factors during a permanent water level and the passage of a flood wave are large when no stationary conditions are reached during the passage of a flood wave. This is the case for high and short flood waves. Both in the Rhine and Meuse, the amount of short waves (< 7days) is high (80-90%), which increases the influence of a time dependent calculation.

Also, the importance of a time dependent calculation increases when the response to the increased pore water pressures is delayed caused by the hydraulic conductivity of the material. For example, a clay on clay dike is most affected by the duration of the flood event. The influence of the height of a flood wave on the stability increases when the soil is permeable, because the delay in response decreases. For example, a sand on sand dike reacts instantaneously to the flood wave, when the sand material is partly saturated. If the dike is dry before the passage of a flood wave, again the response is damped through the phreatic storage capacity of the material. Dikes with a low degree of saturation are therefore more affected by the duration than the height of a flood wave.

Delay in failure

Time dependency causes failure of the embankment to not occur simultaneously with the maximum wave height. The flood wave is decisive for the dike failure, but the permeability and the strength of the dike determines the moment of failure. Especially, the permeability of the subsoil determines the moment of failure. Failure for dikes on a permeable subsoil is most likely in the days before the maximum flood wave height. For impermeable dikes on an impermeable subsoil the delay in the response is large; causing the moment of failure to occur later in time.

Influence on design

Taking time dependency into account leads to higher safety factors and lower probabilities of failure with exception for dikes that consists completely out of sand. For these types of dikes, the probabilities of failure and safety factors are in the same order of magnitude. This could affect the design, because dikes need less reinforcement.

The strength of the material is the largest contributor to the distribution of the safety factors and therefore to the probability of failure (around the 60-95%). In a clay dike the large contribution in strength is caused by the pre overburden pressure and the normally consolidated undrained shear strength ratio. In sand dikes the contribution is caused by the value of the internal friction angle. Flood wave variables contribute for 2-30% to the distribution of safety factor. In permeable dikes this contribution is delivered by the height of the flood waves, while in impermeable dikes the contribution is delivered by the duration of a flood wave. The contribution of the permeability to the probability of failure is small, 2-12%. It is therefore useful to take time dependency into account in determining the correct safety factor for impermeable dikes. It is not useful in determining the correct safety factor for permeable dikes, because a stationary calculation is sufficient. A transient calculation inclusive the variation of flood waves is less useful; because the strength of the material has the largest contribution to the distribution of safety factors. Considering the variation in permeability in a transient calculation is not useful, because the contribution is 10-20 times lower than the strength of a dike.

When the variation of the duration of a flood wave is not considered, it is recommended to use a representative duration of a flood wave; that results in the same total failure probability as including the variation of the duration. For clay on sand dikes at Lobith the duration of the representative flood wave varies from 13 - 14 days. For completely impermeable dikes a duration of 16 days is recommended. At Borgharen the representative duration for clay on sand dikes is 10 days, while for a completely impermeable dike it is suggest using a duration of 11 days.

WBI (2017) uses a simplification in the calculation of the stationary pore water pressures in which the permeability is not considered directly. The probability of failure, using the pore water pressures according WBI (2017) is overestimated when a dike and subsoil consist completely out of sand or clay. But the probability of failure is underestimated when is looked at clay on sand dikes. Note that WBI does not take the permeability of the soil into account (they make a distinguish between sand and clay), so the results are dependent on the chosen permeability.

8.1. Recommendations

The following recommendations are based on the study findings and experiences while performing this study:

1. Validate the results with the use of a real cases for which pore water pressure measurement, soil characteristics and dike geometry are available. This confirms if obtained current practical findings approaches the practice.

2. To keep this initial level as close to practice, it is recommended to apply several years of actual precipitation and evaporation in combination with an initial level based on measurements of an actual dike.

3. Include a varying initial water level in the model. This could be done by using year time series instead of monthly time series. In this way inaccuracies in the first day of a flood way are left out of consideration and the initial state before a flood wave passes (and therefore the degree of saturation of the dike body) is better approached.

4. Further develop the method for coastal regions and the Rhine-Meuse Delta. These area deals with multiple time dependent loads (e.g. wind waves or the tide) that may affect the stability of the inner slope.

5. Include multiple failure mechanisms in the research to the influence of time dependency; like piping, overflow, micro stability and stability of the outer slope.

6. Couple the Dutch software D-GeoFlow and D-GeoStability to each other, to make it easier to perform a time-dependent calculation.

9. REFERENCES

Bakker, H., Breedeveld, J., Teunissen, H. (2011). Analyse Macrostabiliteit Dijken met de Eindige Elementen Methode. *RWS Waterdienst, Deltares.*

Barends, F. (1986). Uitloopeffect onder een dijk na hoogwater. *GeoDelft, Rapport CO-285690, 1986.*

Barneveld, H. & Van den berg, T. (2010). Effect herijking HBV op de golfvorm van de maas te Borgharen. *Lelystad: HKV Lijn in Water.*

Barneveld, H.& Pol, J. (2016). Invloed van afvoergolfvorm Rijn op waterstanden en overstromingskansen. *Case Retentiegebied Rijnstrangen. HKV Lijn in water, opdrachtgever: Rijkswaterstaat WVL.*

Bischiniotis, K. (2013). *Cost optimal river dike design using probabilistic methods* (Doctoral dissertation, MSc thesis, Delft University of Technology)

Brinkgreve, R., Al-Khoury, R., van Esch, J. (2003). *PLAXIS: PlaxFlow* (version 1). *905809569X.*

Carsel, R. F., & Parrish, R. S. (1988). Developing joint probability distributions of soil water retention characteristics. *Water resources research*, *24*(5), 755-769.

Cirkel, R. J. (1985). Leidraad voor het ontwerpen van rivierdijken: Deel 1: Bovenrivierengebied. *L1 isbn 901205169X*

Construction Industry Research, Information Association, Civiel Technisch Centrum Uitvoering Research en Regelgeving (Netherlands), & Centre d'études maritimes et fluviales (France). (2007). *The rock manual: the use of rock in hydraulic engineering* (Vol. 683). Ciria. CIRCIA, CUR, CETMEF.

Dikkenberg, van den B. (2009). Schuivende dijk in het gareel. *Published: 29/09/2009.*

Duncan, J. M. (1996). State of the art: limit equilibrium and finite-element analysis of slopes. *Journal of Geotechnical engineering*, *122*(7), 577-596

Duncan, J. M., Wright, S. G., & Brandon, T. L. (2014). *Soil strength and slope stability*. John Wiley & Sons.

Förster, U., de Visser, M., de Bruijn, H., Kruse, G., Hijma, M. & vanhögen-Peeters, L. (2017). *Schematiseringshandleiding Piping bij dijken.* WTI 2017. Deltares.

Fourie, A. B. (2016). Relying on suction to maintain slope stability.

GEO-SLOPE. (2012a). Seepage Modeling with SEEP/W. *An Engineering methodology, July 2012 Edition.*

GEO-SLOPE. (2012b). Stability Modeling with SLOPE/W. *An Engineering methodology, July 2012 Edition.*

GEO-SLOPE. (2017). Tension Cracks. Consulted on 24/02/2019. *Retrieved from geo-slope.com/geostudioresources/examples/9/0/SlopeW/Tension%20cracks.pdf*

Gesellschaft für Grundbau und Umwelttechnik mbH. (2013). Saaledeich bei Breitenhagen. *Osterwedding: GGU mbH, 2013. Bericht 3714/2013.*

Hamby, D. M. (1994). A review of techniques for variable sensitivity analysis of environmental models. Environmental monitoring and assessment, 32(2), 135-154.

Hart, R. (2018). Fenomenologische beschrijving, faalmechanismen WBI. *Deltares.*

Hegnauer, M., Beersma, J. J., Van den Boogaard, H. F. P., Buishand, T. A., & Passchier, R. H. (2014). Generator of Rainfall and Discharge Extremes (GRADE) for the Rhine and Meuse basins. *Final report of GRADE*, *2*, 1209424-004.

Herzlichst, B. (2013). Bericht über das Hochwasser im Juni 2013 in Sachsen-Anhalt, Entstehung, ablauf. *Management and statistische Eindordnung. LHW.*

Hoffman, F. O., & Gardner, R. H. (1983). Evaluation of uncertainties in environmental radiological assessment models. *Radiological assessments: a textbook on environmental dose assessment, 11, 1.*

Hoogwaterbescherming. *Ministerie van infrastructuur en milieu en het expertise netwerk veiligheid.*

Jansen, P.C. (2007). Beoordeling van de kwaliteit van hoogwatervariables berekend voor de Nederlandse Maas. *University of Twente, MSc thesis.*

Jongejan, R. van Bree, B. Knoef, H. de Visser & M. Blinde, J. (2016) Macrostabiliteit en verkeersbelasting. *Kennisplatform risico benadering. FACTSHEET.*

Jonkman, S., Jorissen, R., Schweckendiek, T., van den Bos, J. (2018). Flood defences (3rd edition). *Lecture notes CIE5314. Department of Hydraulic Engineering.*

Jonkman, S., Steenbergen, R., Morales-Nápoles, O. Vrouwenvelder & A., Vrijling, J. (2016). Probabilistic Design: Risk and Reliability Analysis in Civil Engineering (third version). *Lecture notes CIE4130. Department of Hydraulic Engineering, Delft University of Technology.*

Kanning, W. & van der Krogt, M.G. (2016). Memo: Pore water pressure uncertainties for slope stability. *Deltares. Ref. nummer, 1230090-034.*

Kanning, W., Huber, M., Krogt Mvd, S. T., & Teixeira, A. M. (2015). Derivation of the semi-probabilistic safety assessment rule for inner slope stability. *Deltares, Ref. nummer*, 1220080-003.

Kanning, W., Teixeira, A., van der Krogt, M., Rippi, K. (2016). Derivation of the semi-probabilistic safety assessment rule for inner slope stability. *Technical Report. Deltares project 1230086-009.*

Kleij, van der W. (1999). Guide on Sea and Lake Dikes. The Hague: Technical Advisory Comitte for Flood Defences, TAW.

Klopstra, D., & Duits, M. T. (1999). Methodiek voor vaststelling van de vorm van de maatgevende afvoergolf van de Maas bij Borgharen. *HKVConsultants in opdracht van WL| Delft Hydraulics en Rijkswaterstaat RIZA. Lelystad, maart.*

Knoeff, H. (2016). Kennisplatform risicobenadering. *Memo: Faalkansbegroting.*

Kok, M., Jongejan, R., Nieuwjaar, M., & Tanczos, I. (2016). Grondslagen voor hoogwaterbescherming. *ISBN/EAN: 978-90-8902-151-9*.

Kutzner, C. (1997). Earth and Rockfill dams. *Principles of Design and Construction.*

Loor, de, D. (2018). An Analysis of the Phreatic Surface of Primary Flood Defences. *Master Thesis*

Massop, H. T. L., van der Gaast, J. W. J., & Kiestra, E. (2005). De doorlatendheid van de bodem voor infiltratiedoeleinden; een gebiedsdekkende inventarisatie voor het Waterschap Peel en Maasvallei (No. 1212). *Alterra.*

Meer, J. van der. Ter Horst, W. & van Velzen, E. (2009). Calculation of fragility curves for flood defense assets. *Flood Risk Management: Research and Practice, 567-573.*

Moellmann, A., Vermeer, P. A., & Huber, M. (2011). A probabilistic finite element analysis of dike stability under transient seepage conditions. *Georisk*, *5*(2), 110-119.

Montfoort, M. (2018). Safety assessment method for macro-stability of dikes with high foreshores. *Master thesis: Delft University of Technology, Faculty of Civil Engineering and Geosciences.*

Ogink, H. J. M., & Barneveld, H. J. (2002). Quick scan maximale wateraanvoer Maas. *WL| Delft Hydraulics, Delft*

Oldhoff, R. (2013). Meetkwantiteit versus toetsingskwaliteit- onderzoek naar de invloed van informatiedichtheid op het toetsresultaat van de rekenregel van Sellmeijer voor de toetsing op piping. *Deventer: Afstudeerthesis, Universiteit Twente.*

Parmet, B. W. A. H., Van de Langemheen, W., Chbab, E. H., Kwadijk, J. C. J., Diermanse, F. L. M., & Klopstra, D. (2002). Analyse van de maatgevende afvoer van de Rijn te Lobith. *RIZA report*.

Pol, J. C. (2014). Hydrograph shape variability on the river Meuse, Evaluation of design hydrograph methods and probabilistic methods to estimate design water levels on the river Meuse. *Delft: Master Thesis.*

Rhine-Meuse-Scheldt delta (26 December 2018). https://en.wikipedia.org/wiki/Rhine%E2%80%93Meuse%E2%80%93Scheldt_delta. *Retrieved on 31-12-2018.*

Rijkswaterstaat (2012). GRADE, beoordeling/ advies ENW-rivieren. *Presentation at 20 September 2012.*

Rijkswaterstaat (2016). Regeling veiligheid primaire waterkeringen 2017, Bijlage III sterkte en veiligheid. Concept. *Ministerie van Infrastructuur en Milieu*.

Rijkswaterstaat (2017). Regeling veiligheid primaire waterkeringen 2017, Bijlage II voorschriften bepaling hydraulische belasting primaire waterkeringen. *Ministerie van Infrastructuur en Milieu.*

Rijkswaterstaat (2017). WBI2017 Code Calibration – Reliability based code calibration and semi-probabilistic assessment rules for the WBI2017. *RWS-information, Rijkswaterstaat Ministerie van Infrastructuur en Milieu.*

Rijkswaterstaat. (2016). WBI 2017: Schematiseringshandleiding Macrostabiliteit. Ministerie van Infrastructuur en Milieu.

Sharp, M., Wallis, M., Deniaud, F., Hersch-Burdick, R., Tourment, R., Matheu, E., & Sharp, P. (2013). The international levee handbook. CIRIA, London, 497-498.

TAW (1999). Technisch rapport zandmeevoerende wellen. *Technische Adviescommissie voor de Waterkeringen.*

Thonus, B. (2006). Waterstandsverlopen en snelle val indicatie. Fase 1: onderzoekmethode, invoer en gevoeligheid en Fase 2: uitvoeren van definitieve berekeningen voor benedenrivierengebied. *Lelystad: HKV Lijn in Water.*

Tigchelaar, J. (2017).170609_memo_grondvariables_macrostabiliteit *(werkwijze 13-5), Hollands Noorderkwartier, PR3489.10.*

Tigchelaar, J., Dupuits, G. & Zethof, M. (2018) Probabilistische beoordeling. Dijktraject 13-5 macrostabiliteit. *Eindrapport, HKV Lijn in water.*

Tijssen, A. (2010). Memo stormopzetduur bij Hoek van Holland – effecten op toetspeilen. *Deltares: 1202341-003-ZWS-0014.*

Turkstra, C. J., & Madsen, H. O. (1980). Load combinations in codified structural design. *Journal of the Structural Division*, *106*(12), 2527-2543.

USACE (1993). Engineering and design – hydrologic frequency analysis. *EM 1110-2-1415, US Army Corps of Engineers, Washington DC, USA.*

Van den Bos, W. (2006). Erosiebestendigheid van grasbekleding tijdens golfoverslag. *Afstudeeronderzoek.*

Van der Meer, J.W. (1993). Geometrical design of coastal structures. *Infram (www. Infram.nl), Marknesse*

Van der Meer, M. T., Niemeijer, J., Post, W. J., & Heemstra, J. (2004). Technisch rapport waterspanningen bij dijken Waterkeringen (TAW). *TR26-DWW-2004-057, isbn 90.269. 5565.3*.

Van Esch, J. (1994). *Tijdsafhankelijke stabiliteit van dijken*. Grondmechanica Delft.

Van Ooijen, D. (1984). DWW-waterkering rivierdijken schade door afschuiving. *ID333095.*

Van Velzen, E., Beyer, D., Berger, H., Geerse, C., & Schelfhout, H. (2007). *Technisch Rapport Ontwerpbelastingen voor het rivierengebied. TR28*

Verruijt, A. (2001). *Grondmechanica.* Technische Universiteit Delft, 2001.

Vierlingh, A. (1989). Leidraad voor het ontwerpen van rivierdijken, deel 0 benedenrivierengebied. *Technische adviescommissie voor de waterkering. Waltman, Delft.*

Vriend, De H., Kok, M., Pol, J. & Hegnauer, M. (2016). Heeft de Rijnafvoer bij Lobith een maximum? *Enw expertisenetwerk waterveiligheid.*

Vrouwenvelder, T. (2006, April). Spatial effects in reliability analysis of flood protection systems. *In Second IFED Forum, Lake Louise, Canada*

Wojciechowska, K. A. (2015). Advances in Operational Flood Risk Management in the Netherlands *Delft: Proefschrift, Technische Universiteit Delft.*

Zethof, M. (2017). Veiligheidsbeoordeling WBI2017 Balgzanddijk en Amsteldiepdijk. Hollands- Noorderkwartier: PR3489.10.

Zwanenburg, C., Van Duinen, A., & Rozing, A. (2013). Technisch rapport macrostabiliteit. *Deltares rapport 1204203-007-GEO-0003-gbh voor RWS-WD*.

APPENDICES

APPENDIX A. FAILURE MECHANISMS

Overflow

Overflow is when the still water level is higher than the crest level of the dike and therefore water will flow over the dike. Overflow can lead to direct flooding of the landside area and/or erosion of the inner slope. The last can finally lead to a dike breach. [Jonkman, 2018]

Overtopping

For overtopping, the still water level is under the crest level of the dike, when waves running up the slope the water can tops over. Wave overtopping can lead to erosion of the inner slope. [Jonkman, 2018]

Micro instability

Micro instability is caused by a high phreatic surface that reaches the inner slope of a levee. In case of a sand core with an impermeable cover on the inner slope, the increased pressure inside the levee causes the top layer to slide, the top layer to push off, a combination of both or the sand to wash away through the cracks in the top layer. If all material is permeable with a permeable top layer above water, the inner slope can slide or some sediment is washed out at the location where water flows horizontally from the exit point. When the top layer is under water washing out and sliding will occur for flow perpendicular to the slope. After the dike is affected at landside exit point, erosion processes and sliding processes will also occur above exit point. If the processes continue the inner slope or the crest are undermined and will slide till a new equilibrium is reached. If the crest becomes lower than the water side water level the breach process will start. Most of the time the dike already fails by other mechanisms, like piping or slope instability, see Figure A.1. [Hart, 2018]

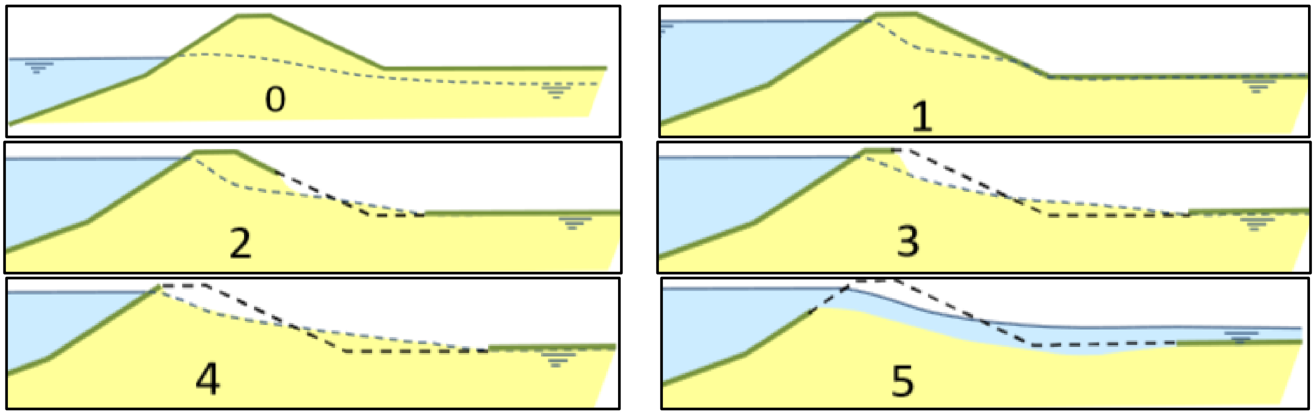

FIGURE A.1: MICRO INSTABILITY PROCESS [HART, 2018]

Shearing

Shearing is caused by a horizontal force of the water exerted on the outer slope. When the soil is relatively light (e.g. a peat dike) it can slide or shear along the base of the dike body. [Jonkman, 2018]

Piping

Piping is caused by a head difference between the outer and inner slope. It is the erosion of soil particles under the dike and is also called internal erosion. There are different forms of internal erosion:

- Erosion through cracks in cohesive material
- Backward erosion: soil particles are transported from the inner side and washed out. A pipe is formed under the dike in reverse direction of the flow from the outer to the inner side.
- Contact erosion: When a coarse layer is in contact with a fine layer. A strong flow can transport the fine material through the coarse material.
- Suffusion: The fine particles are washed out from the coarser particles. The soil skeleton of the coarse particle remains intact.

The first erosion type is in the Netherlands considered as a micro stability mechanism and the last two internal erosion types are not significant in the Netherlands because the soil in the Netherlands is relatively uniform and fine-grained. So, only the backward erosion will be further discussed in this section. [Hart, 2018]

There are two different situations distinguished for backward erosion. The first situation is when a clayey levee is located on top of a sand soil. There is no cohesive layer present on top of the sand layer at the inner side of the dike. The other situation is a levee which is located on a clay or peat layer. So, the levee is not directly located on top of the sand and between the ground level at the inner side and the sand layer a clay or peat layer is present. [Hart, 2018]

In the first case the sand layer is directly in contact with the outer water level. When the water level increases, a head difference occurs over the dike. When the hydraulic head difference at the exit point exceed a critical value, the granular material can be transported. Fine material is transported to the landside of the dike. When the outer water level further increased a pipe is formed. The pipe works like a drain and when it becomes longer the gradient in the sand layer becomes higher. If the flood duration is long enough a completely pipe will form under the dike. The seepage discharge and sand transport increase causing the levee to collapse by undermining, Figure A.2. [Hart, 2018]

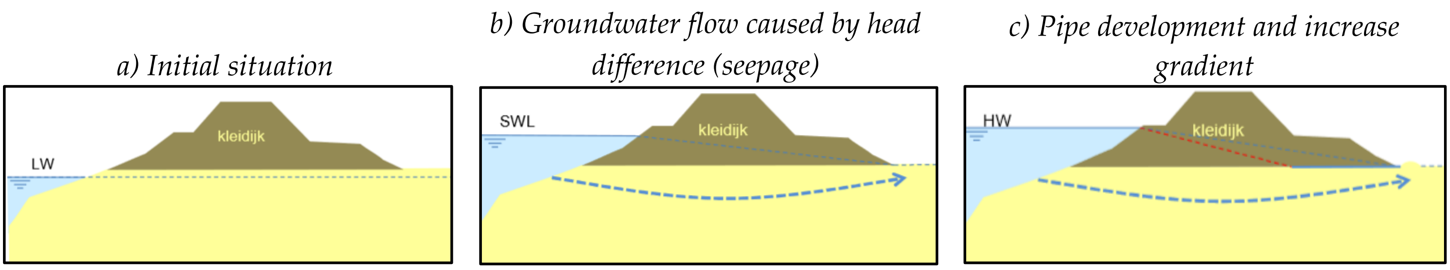

FIGURE A.2: PIPE DEVELOPMENT CLAYEY LEVEE ON SAND SOIL [[HART, 2018]

In the second case, more phases are distinguished. As in the case described above, first the water level increases. The pore water pressures in the sand layer also increase due to the hydraulic head difference over the dike. When the upward pressure on the landside exceeds the weight of the clay or peat layer, the layer is lifted and will crack. Water starts to flow upwards through the crack (seepage). If the gradient at the exit point exceeds a critical value, the granular material can start eroding (heave). Through the erosion a pipe is formed.

If erosion continues and the pipe further develops it can reach the water at the outer side of the levee. At this point, the seepage discharge and the granular material transport increases due to the loss of resistance. The structure can now collapse by undermining, Figure A.3. [Hart, 2018]

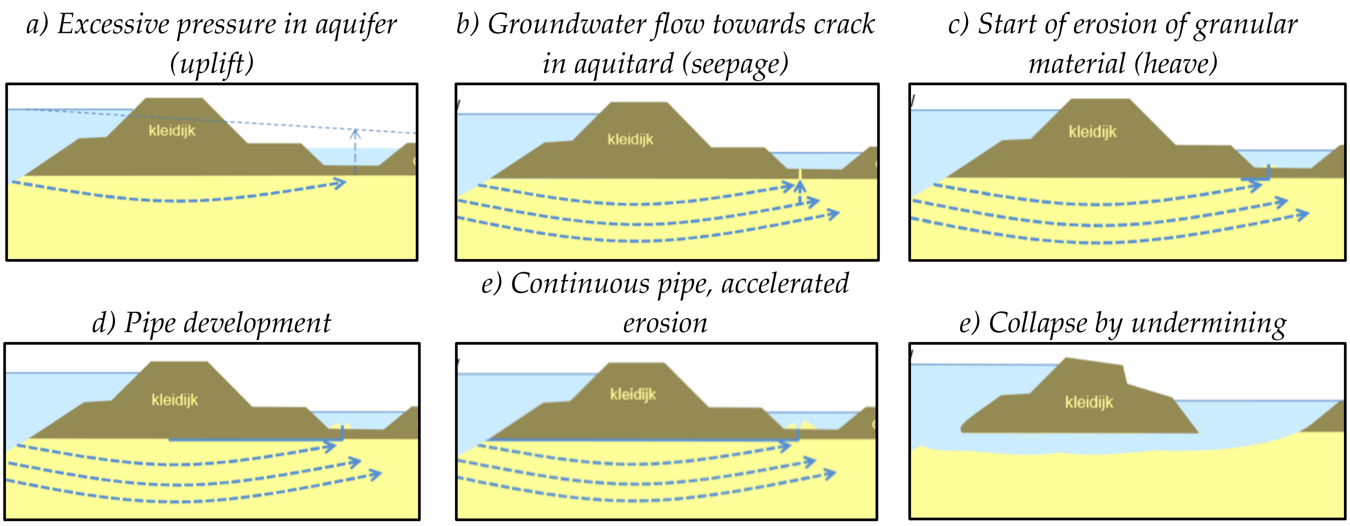

FIGURE A.3: PIPE DEVELOPMENT LEVEE ON CLAY/PEAT LAYER [HART, 2018]

If the flood duration is shorter than the duration needed to form a complete pipe, the dike will not collapse. In general, a river dike experiences a high-water level with less fluctuation and a longer duration (in order of two weeks). While downstream the water level is not only determined by the river discharge, but also by the water level from the sea. The tide is of influence. So, more fluctuations can be expected and the flood duration of a storm is relatively short (order of 1 day). [Hart, 2018]

Erosion

Next to internal erosion, erosion can also take place at the outer slope of a dike or at the foreshore. Erosion at the outer slope is caused by currents or waves. Dikes are protected against erosion with the use of a revetment. At a foreshore erosion is caused by currents and tidal currents. The slope becomes steeper till a flow slide occur. In a flow slide liquation, unstable breaching or both processes can take place. Liquefaction happens fast. In unstable breaching, sand from the slope will mix with the water after which a density current flows along the slope and causes further erosion. This process is a slow process. [Jonkman, 2018]

Settlement

After a dike construction the soil is submitted to instantaneous settlement occurring under undrained conditions, consolidation, creep and settlement due to irreversible lateral movement. During the entire lifetime a dike the crest level must be high enough. [Jonkman, 2018]

Others

Other processes like drifting ice, collision by vessels or failure of the revetment due to instability can cause dike failure.

APPENDIX B. RELIABILITY METHODS

There are different methods to calculate the probability of failure, which are generally divided into five levels. All described methods are based on lecture notes 'Probabilistic Design: Risk and Reliability Analysis in Civil Engineering' by Jonkman *et al (*2016).

Level IV methods

In this method next to the uncertainties also the consequences and risk are considered for the determination of the reliability. In this way a choice between different designs can made based on these aspects.

Level III methods

In this method the probability of failure is calculated exactly using analytical formulation, numerical integration or Monte Carlo simulation. The uncertainties are modelled by their joint distribution functions. Analytical formulation can only be used for a limited number of simple cases and numerical integration can be used when n is small. In the other cases Monte Carlo simulation must be used. In this simulation random samples are generated from a certain distribution. For each combination of samples, it is determined if a failure occurs. The percentage of samples in the failure domain is equal to the probability of failure. The advantage of Monte Carlo is that it is very flexible, empirical distributions can be handled. The disadvantage is that it takes much more time than analytical models and the solution depends on the number of drawn samples.

Level II methods

The joint probability density function is simplified and the limit state function is linearized in the design point, the point on the limit state function with the highest probability density. Finding the design point is an iterative process, which can be done by two methods. The first method transforms the base variables in a function of standard normally distributed values. A more frequently used method is FORM (First Order Reliability Method). The advantage of this method is that the base variables does not need to be transformed to a function of standard normally distributed variables. After linearization, the reliability index be calculated using equation B.1. The probability of failure is directly related to the reliability index. Sensitivity factors are calculated with equation B.2. Calculation of sensitivity factors is an advantage of this method compared to for example a Monte Carlo simulation, because it describes the relative contribution of a variable to the uncertainty. Another advantage is that a level II method is less time-consuming than a Monte Carlo simulation. The disadvantage of this method is that linearization of the limit state function leads to a small error. Another disadvantage of FORM is that it only can be used for an analytical limit state function consisting out of normally distributed values.

$$\beta = \frac{\mu_z}{\sigma_z} \qquad \text{B.1}$$

$$\alpha_i = \frac{\partial Z}{\partial X_i}\frac{\sigma_i}{\sigma_z} \qquad \text{B.2}$$

In which:

μ_z	=	Mean of the limit state equation
σ_z	=	Standard deviation of the limit state equation

σ_i	=	Standard deviation of a variable
α_i	=	Sensitivity factor of a variable.

Level I methods

Level I methods are semi-probabilistic calculation. Conservative values are chosen for the variables based on the probabilistic distribution, see equation B.3 and B.4. If an action is favourable the k-value is negative and the factor will be positive in case of a non-favourable action. Further, partial factors are used based on a level II calculation to transform the conservative values into design values. For load variables this is done by multiplying the conservative value with the partial factor and for strength variables the conservative value must divide by the partial factor. For a safe design equation B.5 must hold. The procedure is illustrated in Figure B.1.

$$R_k = \mu_R + k_R\sigma_R \qquad \text{B.3}$$

$$S_k = \mu_S + k_S\sigma_S \qquad \text{B.4}$$

$$\frac{R_k}{\gamma_R} > \gamma_s S_k \qquad \text{B.5}$$

In which:

R_k	=	Characteristic value for the resistance
S_k	=	Characteristic value for the load
k	=	Factor
γ	=	Partial factor

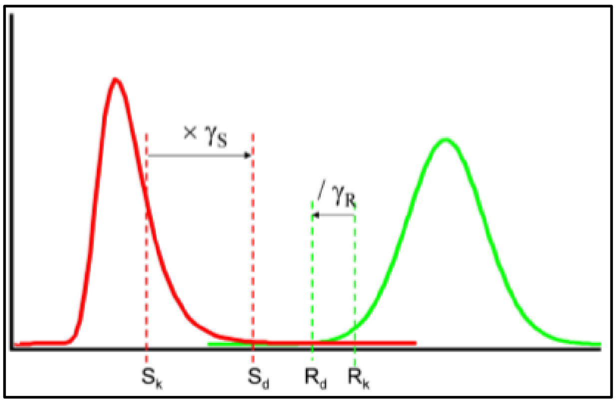

FIGURE B.1: PROBABILITY DENSITY FUNCTIONS SHOWING THE VARIATIONS IN LOAD (RED) AND RESISTANCE (GREEN) [JONKMAN *ET AL*, 2016]

Level 0 methods

Level 0 methods are deterministic calculations. It follows the same procedure as described for the level I method, but no characteristic values are used. The probabilistic distribution is not considered and a deterministic or nominal value is used in combination with a global safety factor.

APPENDIX C. EQUATIONS INTERNAL HYDRAULIC PROCESSES

Basic hydraulic laws

In all ground waterflow models and calculation are based on two main principle: Darcy's law and the continuity equation. The two main principles assume homogenous soil, incompressible liquid and isotropic permeability. Groundwater flow through saturated soil is described by Darcy's law, see the equations below.

$$q_x = -k\frac{\partial\varphi}{\partial x} \qquad \text{C.1}$$
$$q_y = -k\frac{\partial\varphi}{\partial y} \qquad \text{C.2}$$
$$q_z = -k\frac{\partial\varphi}{\partial z} \qquad \text{C.3}$$

In which:

q	=	Specific discharge [m/s]
k	=	Darcy's coefficient of permeability or hydraulic [m/s]
φ	=	$z + \frac{u}{\rho g}$ =Head [m]
z	=	Altitude of considered point related to reference plan [m]
u	=	Internal pore pressure [kN/m^2]
ρ	=	Volumetric mass [kN/m^3]
g	=	Gravitational acceleration [m^2/s]

For (quasi-)stationary flow the continuity equation can be derived from Darcy's law, see equation C.4. When the flow is not stationary; the continuity equation for phreatic storage is given by equation C.5 and for elastic storage by equation C.6 [Van der Meer *et al*, 2004]. Phreatic storage is the storage in the unsaturated soil and elastic storage is the storage in the soil skeleton [WBI, 2017].

$$\frac{\partial q_x}{\partial x} + \frac{\partial q_y}{\partial y} + \frac{\partial q_z}{\partial z} = 0 \qquad \text{C.4}$$
$$n\frac{\partial h}{\partial t} + \frac{\partial(hq_x)}{\partial x} + \frac{\partial(hq_y)}{\partial y} = N \qquad \text{C.5}$$
$$(m_v + n\beta_c)\frac{\partial u}{\partial t} = \frac{\partial q_x}{\partial x} + \frac{\partial q_y}{\partial y} + \frac{\partial q_z}{\partial z} \qquad \text{C.6}$$

In which:

h	=	Head related to the base of the aquifer [m]
N	=	Nett rain infiltration [m/s]
n	=	Effective phreatic porosity [-]
m_v	=	Ground compressibility [m^2/N]
β_c	=	Water compressibility [m^2/N]

Combining Darcy's law with the continuity equation, a differential equation is the result which describes groundwater flow as a function of the head and the pore water pressure. The differential equation can be solved analytical, numerical, geometrical and graphical which results in the location of the phreatic line [Van der Meer et al, 2004].

Water Retention Curve (WRC) and Hydraulic Conductivity Function (HCF)

The first equation describes the Water Retention Curve (WRC), which is the relationship between the volumetric water content and the matric suction, see equation C.7. The matric suction is defined as the pore air pressure minus the pore water pressure. The second equation describes the relation between relative permeability and matric suction and is called the Hydraulic Conductivity Function (HCF), see equation C.8.

$$\theta(\psi) = \theta_r + \frac{\theta_s + \theta_r}{\left[1 + (\alpha|\psi|)^n\right]^{1-\frac{1}{n_d}}} \qquad \text{C.7}$$

$$K(S_e) = K_0 S_e^L \left[1 - \left(1 - S_e^{\frac{1}{1-\frac{1}{n_d}}}\right)^{1-\frac{1}{n_d}}\right]^2 \qquad \text{C.8}$$

$$S_e(\psi) = \frac{\theta(\psi) - \theta_r}{\theta_s - \theta_r} \qquad \text{C.9}$$

In which:

K_0	=	Matching point at saturation [cm/day]
S_e	=	Effective saturation [-]
θ_r	=	Residual water content [-]
θ_s	=	Saturated water content [-]
$\lvert\psi\rvert$	=	Suction pressure [cm]
$K(S_e)$	=	Hydraulic conductivity function [m²/day]
L	=	Empirical pore-connectivity variable [-]
n_d	=	Measure of the pore-size distribution [-]
α	=	Related to the inverse of the air entry suction [1/cm]
$\theta(\psi)$	=	Water retention curve [-]

Leakage length

$$\lambda = \sqrt{TC} \qquad \text{C.10}$$

In which:

C	=	Hydraulic resistance [day]
D	=	Thickness aquifer [m]
$T = kD$	=	Transmissivity [m²/day]
k	=	Darcy's coefficient of permeability or hydraulic conductivity
λ	=	Leakage factor [m]

Time dependent leakage length

$$\lambda_t = \frac{\lambda}{\frac{1}{\sqrt{2\frac{t}{D^2/c_v}}} \coth \frac{1}{\sqrt{\frac{t}{D^2/c_v}}}} \qquad \text{C.11}$$

In which:

λ	=	Leakage length [m]
t	=	Time [s]
D	=	Thickness aquifer [m]
c_v	=	Consolidation coefficient [m²/s]

Change of flow direction

The change of flow direction is given in equation C.12 and the variables are shown in C.2

$$\frac{\tan \alpha_1}{\tan \alpha_2} = \frac{k_1}{k_2} \qquad \text{C.12}$$

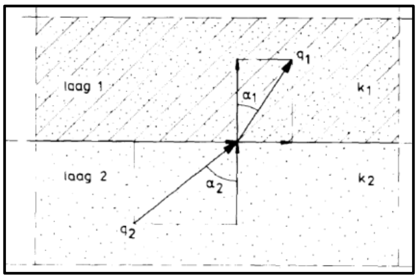

FIGURE C.1: FLOW OVER LAYER SEPARATIONS [VAN DER MEER *ET AL*, 2004]

APPENDIX D. GEOSTUDIO

In this section more details about the used Software are explained. For all details is referred to the website of GeoStudio: 'www.geoslope.com'. To model the groundwater flow SEEP/W is used, which models the flow using a finite element method. SEEP/W can model steady-state problems using Darcy's-law, also unsaturated transient analyses can be performed. SEEP/W can be coupled to SLOPE/W. SLOPE/W calculates the slope stability for different slip surfaces shapes, pore-water pressure conditions, soil properties and loading conditions. In this section some aspects used in the software are explained.

SEEP/W

All described aspects are adapted from the manual 'Seepage modelling with SEEP/W' by GEO-SLOPE International Ltd. (2012). SEEP/W assumes a constant total stress, so there is no loading or unloading of the soil mass; and it assumes that the pore-air pressure remains constant during a transient analysis and the geometry is fixed. All processes shown in Figure 2.11 are included in SEEP/W.

Material models and properties

Material models

There are different material models in SEEP/W: saturated/ unsaturated model, saturated only model and an interface model. The saturated/ unsaturated model makes use of a hydraulic conductivity function and a water content function. The saturated only model can be used when an area is always saturated, and make use of the hydraulic saturated conductivity, saturated water content and the coefficient of volume compressibility.

Soil water storage- water content function

When the soil is saturated, the pore spaces are filled with water. The water content of the soil is equal to the porosity. When the soil is unsaturated, the pores are also filled with air. The amount of water and air in the pores depend on the matric suction, which is the difference between the air pressure and water pressure. The volumetric water content function describes how the water content varies with changing soil pressures (Figure D.1).

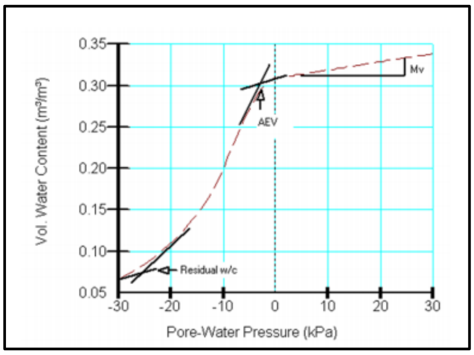

FIGURE D.1: VOLUMETRIC WATER CONTENT (STORAGE) FUNCTION [GEO-SLOPE INTERNATIONAL LTD., 2012]

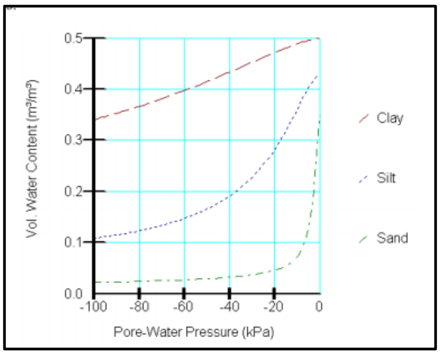

FIGURE D.2: TYPICAL STORAGE FUNCTIONS FOR 3 SOIL TYPES [GEO-SLOPE INTERNATIONAL LTD., 2012]

The function depends on the residual water content, the air-entry value and the coefficient of volume compressibility (m_v). The size of the soil particles and particle distribution influences these variables, see Figure D.2.

The coefficient of volume compressibility indicates the amount of water stored or released from the soil when the pore-water pressure changes. Water is assumed to be incompressible. Both phreatic storage and elastic storage are considered.

Storage function types

For a transient analysis the volumetric water content function is required. The function can be estimated in SEEP/W with methods. In this thesis the method with the sample functions is used. In this method typical water content function for different types of soils are used, see Figure D.3. Only the saturated water content and the residual water content must be specified.

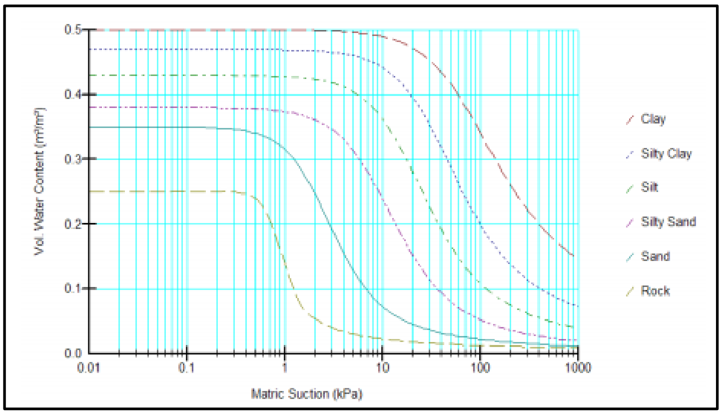

FIGURE D.3: SAMPLE FUNCTIONS IN GEOSTUDIO
[GEO-SLOPE INTERNATIONAL LTD., 2012]

Hydraulic conductivity

In saturated soils, the saturated hydraulic can be used. But when the is not fully saturated, ground water flow depends on the amount of water in the soil, which depends on the volumetric water content function. SEEP/W has different built-in function that estimates the hydraulic conductivity function based on the volumetric water content function and the saturated hydraulic conductivity. In this thesis the method defined by Van Genuchten (1980) is used. In the Van Genuchten equation, the hydraulic conductivity is a function of the matric suction.

SLOPE/W

All described aspects are adapted from the manual 'Stability Modelling with SLOPE/W' by GEO-SLOPE International Ltd. (2012).

Limit equilibrium fundamentals

The basics of the limit equilibrium methods are explained in section 2.1.1.2. The limit equilibrium methods are only based on summation of moment, vertical and horizontal forces. The method does not take displacements or strains into account. Therefore, local variation in the safety factor are not considered.

General limit equilibrium formulation

A general limit equilibrium formulation developed by Fredlund (1970) is based on two safety factors. One the safety factor expresses the moment equilibrium, while the other safety factor expresses the horizontal force equilibrium. The interslice shear forces in the limit equilibrium formulation are handled with equation D.1

$$X = E\,\lambda_{dec}\,f(x) \qquad \text{D.1}$$

In which:

E	=	The interslice normal force [N]
X	=	The interslice shear force [N]
$f(x)$	=	A function for the interslice force
λ_{dec}	=	The percentage (in decimal form) of the function used

Different function can be used in SLOPE/W to describe the interslice force, for example: half-sine, constant, clipped-sine, trapezoidal or fully specified functions. An example of the half-sine function is given in Figure D.4. The upper curve represents the actual specified function and the lower curve represents the used function. The ratio between these curves represents λ.

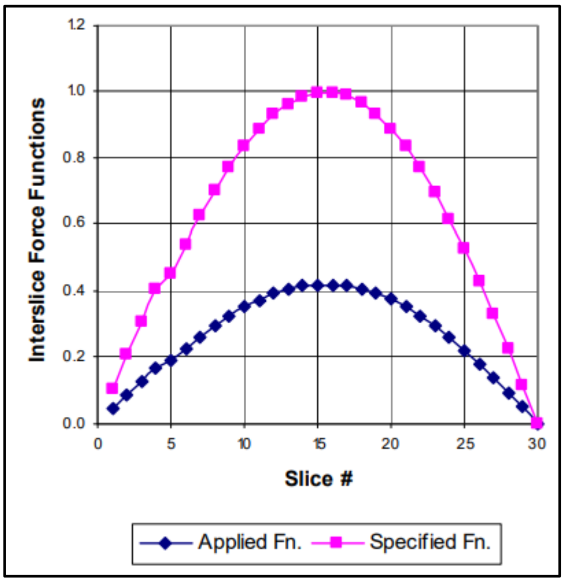

FIGURE D.4: HALF-SINE INTERSLICE FORCE FUNCTION [GEO-SLOPE INTERNATIONAL LTD., 2012]

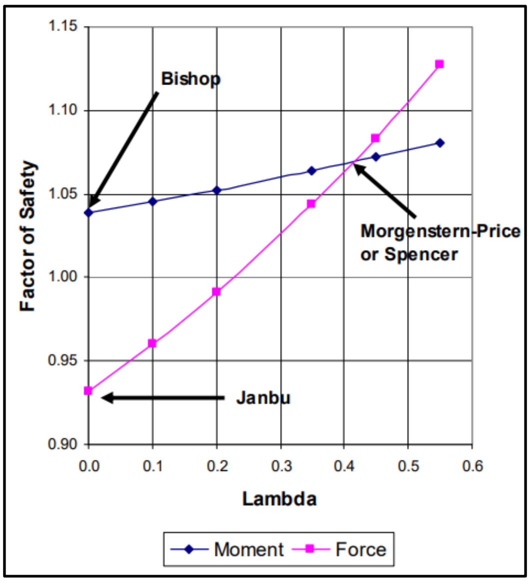

FIGURE D.5: A FACTOR OF SAFETY VERSUS LAMBDA PLOT [GEO-SLOPE INTERNATIONAL LTD., 2012]

The general limit equilibrium computes the safety factor for moment equilibrium and force equilibrium for a different range of lambda values. A plot like Figure D.5 is obtained. In this figure can be seen that Bishop indeed neglect interslice shear forces (because lambda is equal to 0) and the safety factor is only based on moment equilibrium. The Janbu's simplified method also ignores interslice forces and is based on force equilibrium. Morgenstern-Price and Spencer based the safety factor on both moment and force equilibrium. Spencer considered a constant function, which means that the ratio of shear to the normal is constant. Morgenstern-Price considered any general appropriate function, for example a half-sine or trapezoidal function.

Slip surface shapes

Different slip surface shapes are implemented in GeoStudio like: circular slip surfaces, planer slip surfaces, composite slip surfaces and block slip surfaces. The importance of the interslice force function is strongly related to the shape of the potential slip surface.

Tension cracks

In some calculations at the crest of a dike, the normal at the base of the first slice will point away from the slice, see Figure D.6 and Figure D.7. This phenomenon indicates the presence of tension in the soil. Which is, especially for non-cohesive soils, unrealistic. Therefore, tensions cracks are introduced. If the base of a slice exceeds a specific angle, the slip surface is removed from the analysis. The slice is ignored and replaced by a tension crack. The chosen tension crack angle is specified in equation D.2. It is the angle with the horizontal. By taking the crack angle into account, lower values of the factor of safety are found.

$$\Phi = 180 - \left(45 + \frac{\phi}{2}\right) \qquad \text{D.2}$$

In which:

ϕ	=	Internal friction angle [°]
Φ	=	Crack angle [°]

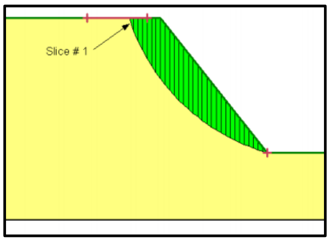

FIGURE D.6: SLIP SURFACE WITHOUT CONSIDERING THE CRACK ANGLE [GEO-SLOPE]

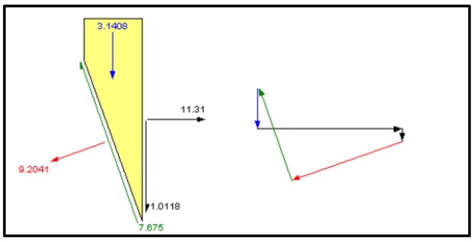

FIGURE D.7: THE RED FORCE OF THE NORMAL AT THE BASE OF THE FIRST SLICE POINTS AWAY FROM THE SLICE WHICH INDICATES TENSION [GEO-SLOPE]

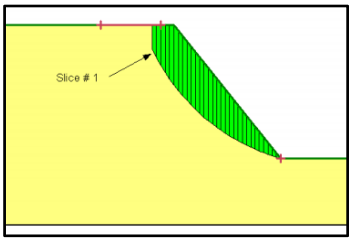

FIGURE D.8: SLIP SURFACE WITH CONSIDERING THE CRACK ANGLE [GEO-SLOPE]

Geometry

SLOPE/W uses a variable slice width, this is done to ensure that only one soil material exist at the bottom of a slice, to prevent surface break along the top of the slice and to prevent the phreatic surface to flow through the base of a slice

Uplifting of the hinterland

Uplifting occurs when equation D.3 satisfies. WBI (2017) made different conservative choices, looking at uplifting of the hinterland; while GeoStudio does not make these choices. An overview of the most important differences is shown in Table D.1.

$$Uplifting\ if\ \frac{\frac{\sigma'_{vs}}{\gamma_w} + \phi_p}{\phi_g} < \gamma \qquad \text{D.3}$$

TABLE D.1: OVERVIEW DIFFERENCES CHOICES WBI AND GEOSTUDIO LOOKING AT UPLIFTING

	WBI (2017)	**GeoStudio**
Hydraulic head in aquifer	Same as outer water level	Lower than outer water level, calculated using finite element method
Safety factor for uplifting (γ)	1.2	1.0
Effective stress reduction when uplifting occurs	Zero in the uplifting-zone which is defined as 2 times the thickness of the cover layer measured from the toe of the dike	Only zero at the places where uplifting occurs, so where equation 2.31 < 1.0

APPENDIX E. METHOD WBI FOR SLOPE STABILITY

For the detailed analysis of slope stability, a semi-probabilistic approach is used. Design values are used which are calculated using characteristic values in combination with partial safety factors (model factor, material factor and a damage factor). The uncertainty caused by the used model is covered by the model factor and are given in Table E.1. The material factor is calculated using a probabilistic study. Based on FORM sensitivity coefficients, it follows that the undrained shear strength has the highest influence and the other variables have little influence. Therefore, all material factors with exception of the undrained shear strength factor are equal to 1.0. For the undrained shear strength, a value between 1.0 and 1.3 can be used [WBI, 2016]. But still a factor of 1.0 is used. The first reason for this is that the safety format is easily kept and the second reason is that the uncertainty is already covered in the choice for the characteristic value. The material factors are shown in Table E.2.

TABLE E.1: MODEL FACTORS IN RING TEST [WBI, 2016]

Slip surface model	Model factor
Liftvan	1.06
Spencer- Van der Meij	1.07
Bishop	1.11

TABLE E.2: MATERIAL FACTORS IN RING TEST [WBI, 2016]

Variable	Material factor
Undrained shear strength ratio S [-]	1.0
Strength increase exponent m [-]	1.0
Boundary layer tension σ'_{vy} [kPa]	1.0
Undrained shear stress S_u [kPa]	1.0
Angle of internal friction φ [°]	1.0

The design values in the semi-probabilistic calculation are therefore the same as the characteristic values. This means that material factors do not have any influence, but in theory every variable should have a partial safety factor which depends on the target reliability. Therefore, the damage factor is introduced to cover all uncertainties and which is β_T – dependent [Kanning, 2016]. The safety requirements for slope stability are shown in equation E.1. However, the damage factor needs to be calibrated. This is done by investigating different cases probabilistically and semi-probabilistically. For all cases the β_T value is determined and is plotted against the damage factor. Finally, line is fit at the 20%-quantile of β_T and the empirical relation shown in equation E.1, E.2 and E.3 is found [WBI, 2016]. This calibration study is performed for the inner slope of normal dikes, but the relation is also used for the outer slope.

$$\frac{FoS_{design}}{\gamma_d \gamma_n} > 1 \qquad \text{E.1}$$

$$\gamma_n = 0.15\beta_{norm,dsn} + 0.41 \qquad \text{E.2}$$

$$\beta_{norm,dsn} = -\Phi^{-1}(P_{norm,dsn}) \qquad \text{E.3}$$

In which:

$P_{norm,dsn}$	=	Required probability of failure per cross-section [1/year]
$\beta_{norm,dsn}$	=	Required reliability index [-]
γ_d	=	Model factor [-]
γ_n	=	Damage factor, β_T – dependent [-]
FoS_{design}	=	Factor of safety for dike stability [-]

The probability of failure per cross-section per scenario can now be derived from this empirical relation and is given in equation E.4. The total probability of failure can be calculated with equation E.5. The probability of failure must be compared with the norm (equation 2.8) in which the length-effect for slope stability must be calculated with equation E.6. Because slope stability of the outer slope is an indirect process while inner slope instability is a direct mechanism, the norm of the outer slope must be multiplied with 10 [Rijkswaterstaat, 2016].

$$P_{f,i} = \Phi\left(-\frac{\left(\frac{FoS_i}{\gamma_d}\right) - 0.41}{0.15}\right) \quad \text{E.4}$$

$$P_{f,dsn} = \sum_{i=1}^{n} \left(P(S_i) P_{f,i}\right) \quad \text{E.5}$$

$$N_{dsn} = 1 + \frac{a_l L_{traject}}{b_l} \quad \text{E.6}$$

In which:

$L_{traject}$	=	Length of the dike trajectory, as stated in the Dutch water Act [m]
$P_{f,dsn}$	=	Probability of failure per cross-section [1/year]
$P_{f,i}$	=	Probability of failure per cross-section per scenario [1/year]
$P(S_i)$	=	Probability of the scenario [1/year]
a_l	=	Mechanism sensitive factor of the dike trajectory length [-]
b_l	=	Representative length for the analysis in a cross-section [m]

APPENDIX F. WATERSTANDSVERLOPENTOOL

Version 3.0.1 is used for the calculations of the design hydrograph of the water level.

TABLE F.1: INPUT WATERSTANDSVERLOPENTOOL

Location	Rotterdam	Rhine	Meuse
Location name	307841	100563	202434
Input database	Waterstandsverloop_Benedenrivieren-WBI2017	Waterstandverloop_Bovenrijn-WBI2017	Waterstandverloop_Bovenmaas-WBI2017
Calculation type	Design hydrograph of the water level	Design hydrograph of the water level	Design hydrograph of the water level
Maximum water level	5/ 8 m tov bottom river	5/ 8 m tov bottom river	5/ 8 m tov bottom river

ROTTERDAM 5 M TOV BOTTOM

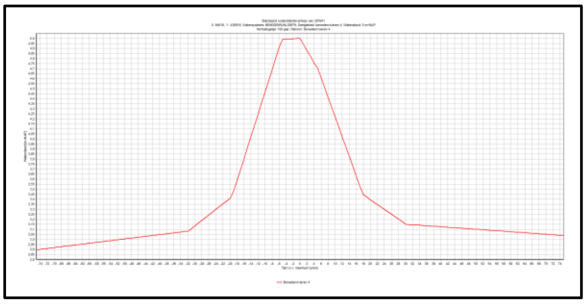

ROTTERDAM 8 M TOV BOTTOM

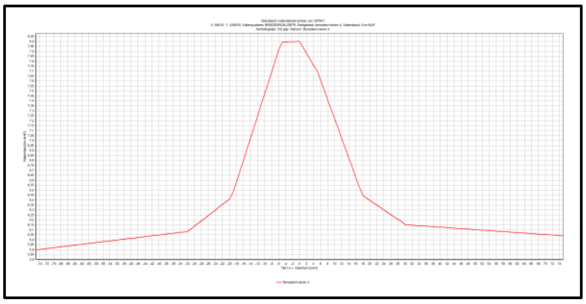

BORGHAREN 5 M TOV BOTTOM

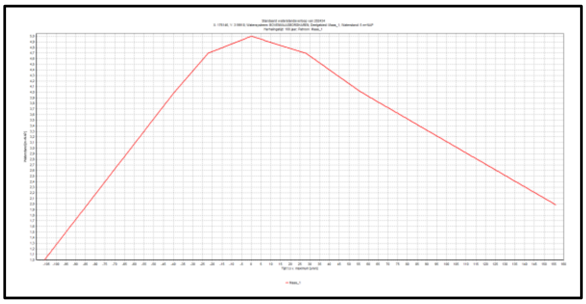

BORGHAREN 8 M TOV BOTTOM

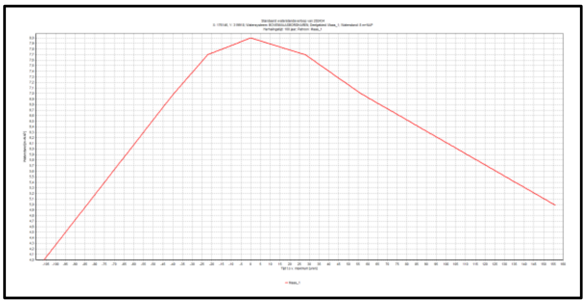

LOBITH 5 M TOV BOTTOM

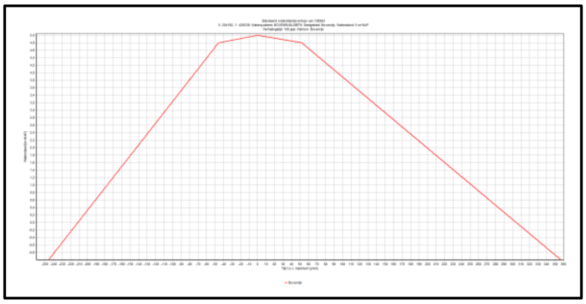

LOBITH 8 M TOV BOTTOM

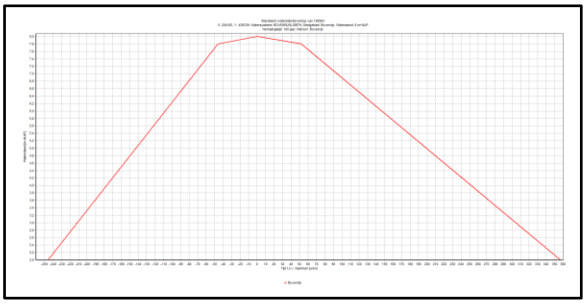

FIGURE F.1: DESIGN HYDROGRAPH OF THE WATER LEVEL ROTTERDAM, RHINE AND MEUSE

APPENDIX G. INPUT SEEP/W

The input of the program SEEP/W is summed up below. Some choices are further explained.

Time
Number of steps: 20
Steps Increase: Linearly
Duration: 1.5 x duration hydrograph of the water level

Boundary conditions
Drainage: Water Rate= 0 m^3/sec, potential seepage face review
Outer water level stationary: Water total head= constant value
Outer water level transient t=0: Water total head= constant value
Outer water level transient: Water total head= Step data point function
Polder water level: Water total head= constant value

Mesh
Approximate global element size: 0.5 m
Finite element mesh pattern: Quads & triangles

Water
Unit weight of water: 9.807 kN/m^3
Bulk modules of Pore-Fluid: 2.083.333,3 kPa

Deep Clay
Material model: Saturated only
Saturated X-Conductivity: 5.8e-07 m/sec [2] [4]
Sat. Vol water content: 0.38 [3]
Compressibility: 2e-3/kPa[4]
Ky'/Kx' Ratio: 0.333 [4]
Rotation: 0 degrees

Dike Clay
Material model: Saturated/ Unsaturated
Ky'/Kx' Ratio: 0.333 [4]
Rotation: 0 degrees
Compressibility: 2e-3 /kPa [3]
Estimation Method: Sample functions
Saturated WC: 0.38 [2]
Sample Material: Clay
Minimum suction: 0.01 kPa
Maximum suction: 30 kPa [5]
Estimation method: van Genuchten
Saturated Kx: 5.8e-07 m/sec [4]
Residual water content: 0,068 [2]

Hinterland clay
Material model: Saturated/ Unsaturated
Ky'/Kx' Ratio: 0.333 [4]
Rotation: 0 degrees
Compressibility: 2e-3 /kPa [3]
Estimation Method: Sample functions
Saturated WC: 0.38 [2]
Sample Material: Clay
Minimum suction: 0.01 kPa
Maximum suction: 30 kPa [3]
Estimation method: van Genuchten
Saturated Kx: 5.8 e-07 m/sec [4]
Residual water content: 0,068 [2]

Sand Layer
Material model: Saturated only
Saturated X-Conductivity: 2.3 e-05 m/sec [4]
Sat. Vol water content: 0.43 [2]
Compressibility: 1.5e-05 /kPa [3]
Ky'/Kx' Ratio: 0.667 [4]
Rotation: 0 degrees

Sand dike/ hinterland
Material model: Saturated/ Unsaturated
Ky'/Kx' Ratio: 0.667 [4]
Rotation: 0 degrees

[2] VERRUIJT, 2001
[3] CARSEL, 1988
[4] SMITH, 2013
[5] VAN DER MEER *ET AL*, 2004

Compressibility: 1.5e-05 /kPa [3]
Estimation Method: Sample functions
Saturated WC: 0.43 [2]
Sample Material: Sand
Minimum suction: 0.01 kPa
Maximum suction: 2.35 kPa[1]
Estimation method: van Genuchten
Saturated Kx: 2.3e-05 m/sec [4]
Residual water content: 0.045

Accuracy mesh grid

A global element size must be chosen, which determined the accuracy of the model. The smaller the mesh grid, the more accurate the results will be, but the larger the calculation time of the model. To know the influence of the choice; the pressure of the red point indicated in the figure below in the four dike types is compared for varying element sizes, the results are shown in Figure G.2. A linear line is fitted and the intercept indicates the value when an infinity small grid size is chosen. Which is used to estimate the order of the error, see Table G.1. Therefore, it is chosen to use a global element size of 0.5 meter.

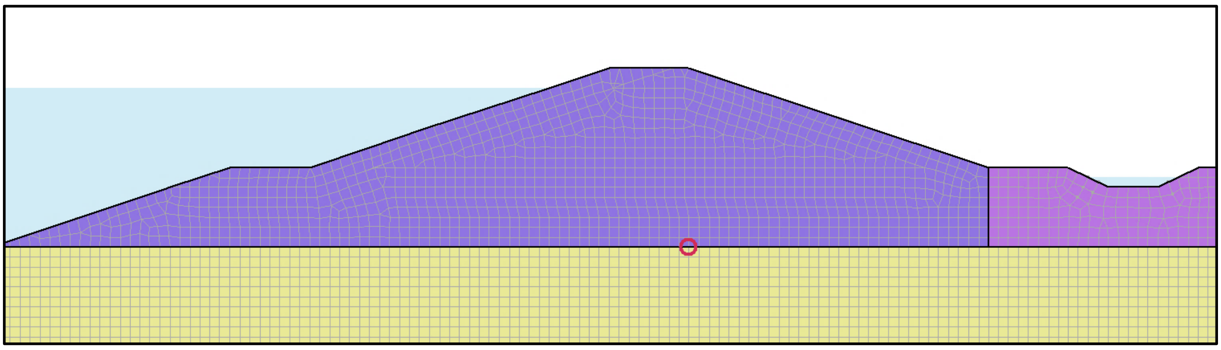

FIGURE G.1: RED POINT INDICATES POINT FOR WHICH THE PRESSURE IS COMPARED

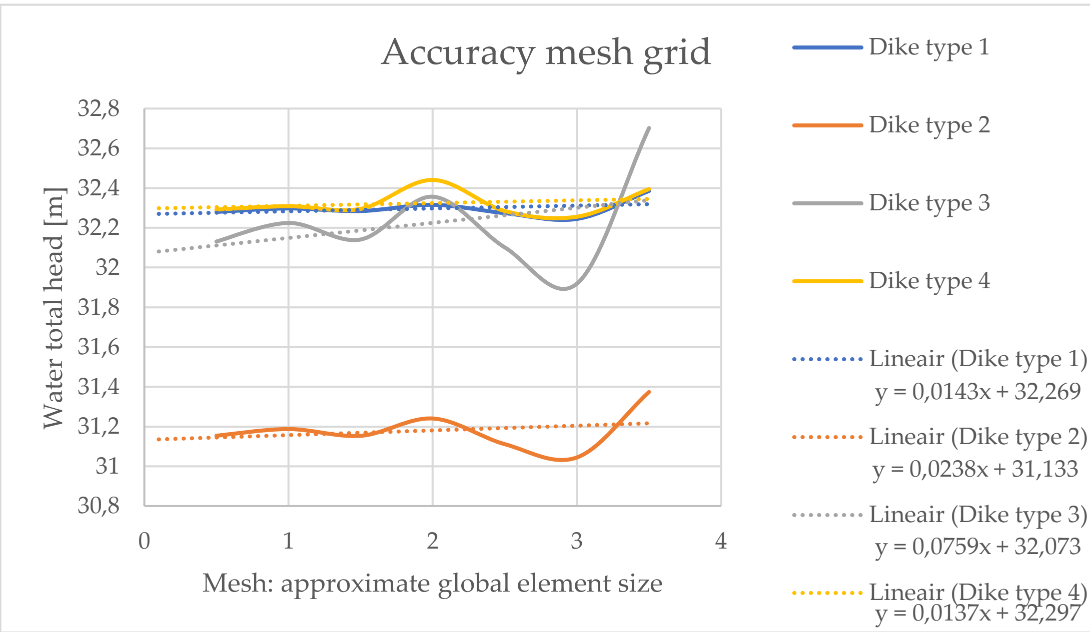

FIGURE G.2: ACCURACY MESH GRID

TABLE G.1: ACCURACY MESH GRID, ERROR

	Dike type			
Approximate global element size	1	2	3	4
3,5	0,4%	0,8%	2,0%	0,3%
3	0,1%	0,3%	0,5%	0,1%
2,5	0,0%	0,1%	0,1%	0,0%
2	0,1%	0,3%	0,9%	0,4%
1,5	0,0%	0,1%	0,2%	0,0%
1	0,1%	0,2%	0,5%	0,0%
0,5	0,0%	0,1%	0,2%	0,0%

Accuracy right boundary

At the right side of the model a boundary value needs to be specified, to indicate that there is no influence at the flow pattern anymore. Ideally this boundary is present at an infinite distance, but that caused an infinitely large calculation time. Normally the right distance is set to a distance equal to 5 times the leakage length (657 meters). To know the influence of this choice, first is looked at the stationary pressure of the point indicated in Figure G.1. The results are presented in Figure G.3. A polynomial is fitted through the result to estimate the intercept, which is used to estimate the accuracy with. From

Table G.2 is concluded that a distance of 195 m is sufficient. The influence is checked in time in the same way for the governing pressure in time and the time of the governing phreatic surface. The results are presented in Figure G.4 and Table 2.1. From this is concluded to use a distance of 390 meters (2x the leakage length).

$$\lambda = \sqrt{TC} = \sqrt{KDC} = \sqrt{2.3 \times 10^{-5} \times 20 \times 1000 \times 24 \times 3600} = 199\, m \qquad \text{G.1}$$

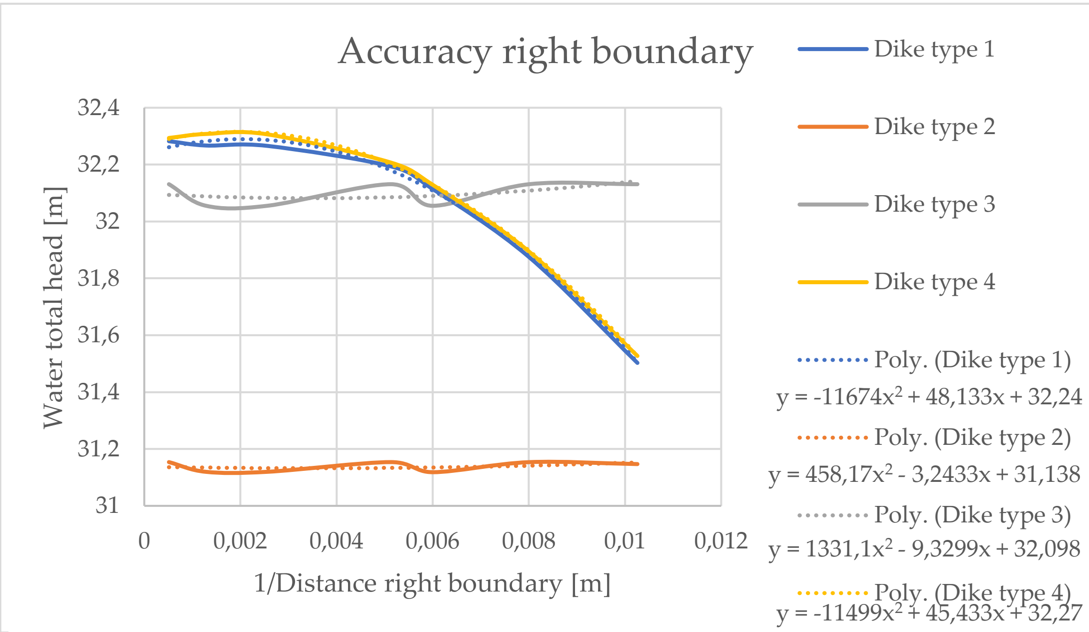

FIGURE G.3: ACCURACY RIGHT BOUNDARY

TABLE G.2: ACCURACY RIGHT BOUNDARY, ERROR

		Dike type			
λ	Leakage length [m]	1	2	3	4
0,5	97	2,3%	0,0%	0,1%	2,3%
0,6	125	1,1%	0,1%	0,1%	1,2%
0,9	170	0,4%	0,1%	0,1%	0,4%
1,0	195	0,1%	0,1%	0,1%	0,2%
2,0	390	0,1%	0,1%	0,1%	0,1%
3,9	780	0,1%	0,1%	0,1%	0,1%
9,8	1950	0,1%	0,1%	0,1%	0,1%

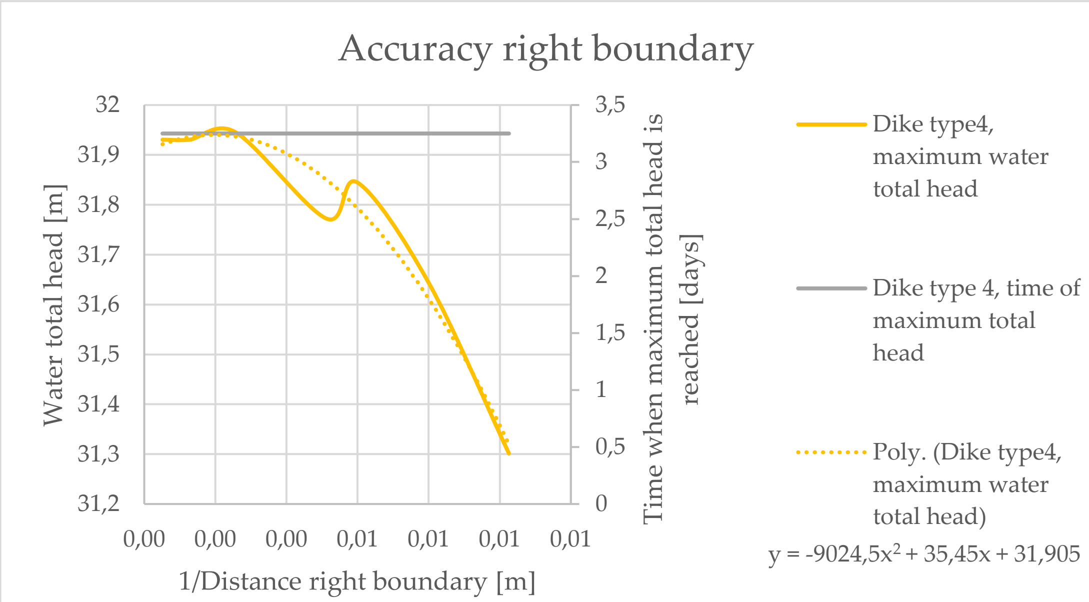

FIGURE G.4: ACCURACY RIGHT BOUNDARY IN TIME

TABLE G.3: ACCURACY RIGHT BOUNDARY IN TIME, ERROR

Lambda	Leakage length [m]	Time of maximum total water head	Maximum water total head
0,5	97	0%	1,9%
0,6	125	0%	0,8%
0,9	170	0%	0,2%
1,0	195	0%	0,4%
2,0	390	0%	0,1%
3,9	780	0%	0,1%
9,8	1950	0%	0,1%

Accuracy river width

The river width in upstream in the Rhine is around the 80 meters, upstream in de Meuse the width is around the 100 meters. While downstream near Rotterdam the width varied between the 265 and 465 meters. Therefore, the influence of the river width is investigated in a similar way as the right boundary. The results of the stationary case are presented in Figure G.5 and Table G.4, from which can be seen that the results do not vary a lot. This is also checked for the results in time, see Figure G.6 and Table G.5. From this is decided to use a width of 90 meters in the model (so the left boundary is presented at a distance of 45 meters).

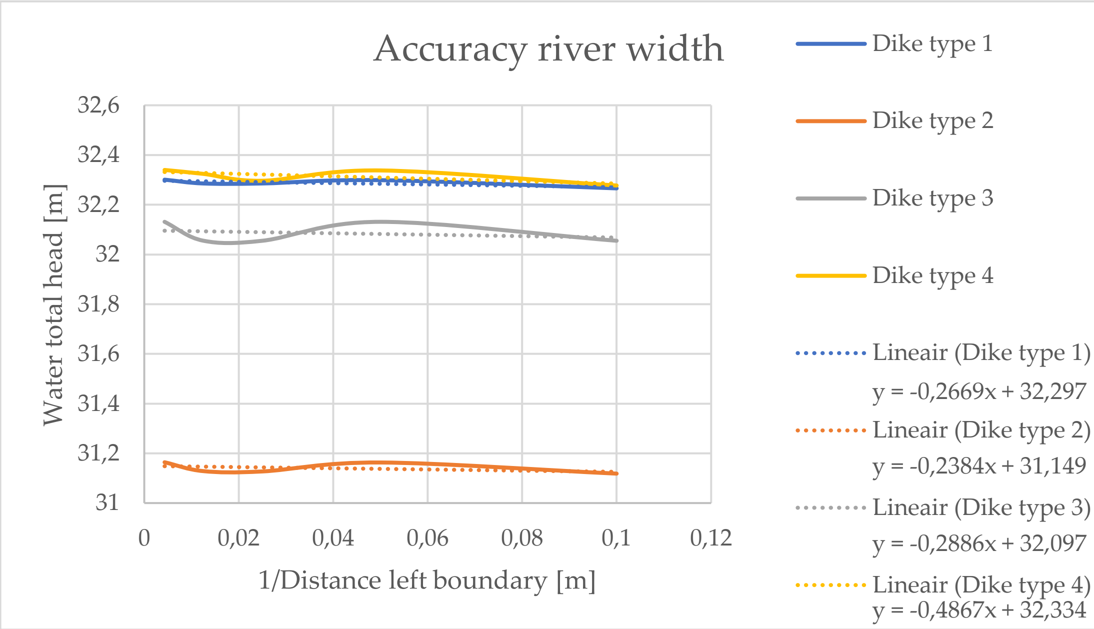

FIGURE G.5: ACCURACY LEFT BOUNDARY

TABLE G.4: ACCURACY LEFT BOUNDARY, ERROR

		Dike type			
half river width	1/ half river width	1	2	3	4
10	0,1	0,1%	0,1%	0,1%	0,2%
20	0,05	0,0%	0,0%	0,1%	0,0%
40	0,025	0,0%	0,1%	0,1%	0,1%
80	0,0125	0,0%	0,1%	0,1%	0,0%
232,5	0,004	0,0%	0,0%	0,1%	0,0%

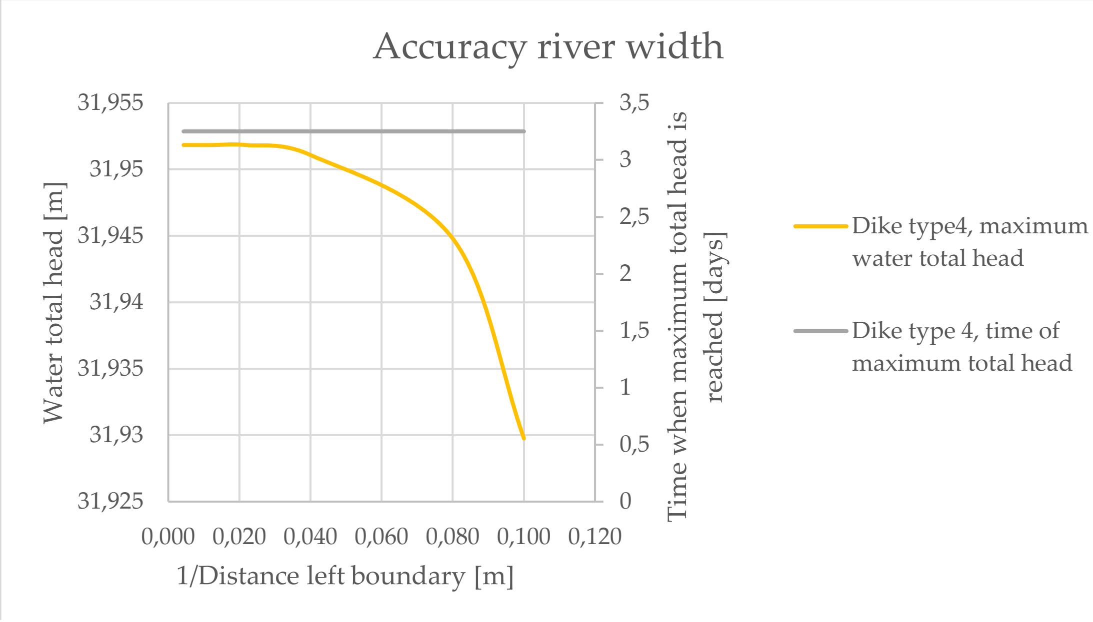

FIGURE G.6: ACCURACY LEFT BOUNDARY IN TIME

TABLE G.5: ACCURACY LEFT BOUNDARY IN TIME, ERROR

half river width [m]	1/ half river width	Time of maximum total water head	Maximum water total head
10,0	0,100	0%	0,07%
15,0	0,080	0%	0,02%
25,0	0,040	0%	0,00%
45,0	0,022	0%	0,00%
85,0	0,012	0%	0,00%
165,0	0,006	0%	0,00%
232,5	0,004	0%	0,00%

APPENDIX H. INPUT SLOPE/W

Settings
Analysis Type: Spencer
Direction of movement: Left to right
Slip Surface Option: Entry and exit
No. of critical slip surfaces to store: 1
Tension crack angle: 135 degrees

Clay- dike material
Material Model: SHANSEP
Unit Weight 16 kN/m³ [5]
Tau/Sigma=$\frac{S_u}{\sigma'_{v,i}} = S \times \left(\frac{\sigma'_{vy}}{\sigma'_{v,i}}\right)^m$
S= 0.26 [5]
m=0.9 [5]
POP =28 kPa [5]

Clay deep
Material Model: SHANSEP
Unit Weight 16 kN/m³ [2]
Tau/Sigma=$\frac{S_u}{\sigma'_{v,i}} = S \times \left(\frac{\sigma'_{vy}}{\sigma'_{v,i}}\right)^m$
S= 0.26 [5]
m=0.9 [5]
POP =24 kPa [5]

Hinterland material Clay
Material Model: SHANSEP
Unit Weight 16 kN/m³ [6]
Tau/Sigma=$\frac{S_u}{\sigma'_{v,i}} = S \times \left(\frac{\sigma'_{vy}}{\sigma'_{v,i}}\right)^m$
S= 0.22 [5]
m=0.9 [5]
POP =18 kPa [5]

Hinterland/dike material Sand
Material Model: Mohr-Coulomb
Unit Weight 20 kN/m³ [5]
Cohesion: 0 kPa
Phi=30 degrees [5]

Saturated Sand
Material Model: Mohr-Coulomb
Unit Weight 20 kN/m³ [5]
Cohesion: 0 kPa
Phi=30 degrees [5]

Time
Number of steps: 20
Steps Increase: Linearly
Duration: 1.5 x duration hydrograph of the water level

Slip Surface Entry and Exit Range:
Number of increments over entry range: 60
Number of increments over exit range: 20
Number of radius increments: 7

Accuracy number of increments entry range

The entry and exit range are shown in Figure H.1. The entry range is the is specified from the toe of the dike at the outer slope till halfway the inner slope. Ideally an infinite number of increments is used, but this caused the calculation time to be large. Therefore, the same method as described in the section above is used to find a correct number of increments. The only difference is that the safety factor for the inner slope is compared instead of the total water head. The results are presented in Figure H.2 and Table H.1, from which is decided to use 55 increment over the entry range.

[6] WBI, 2017

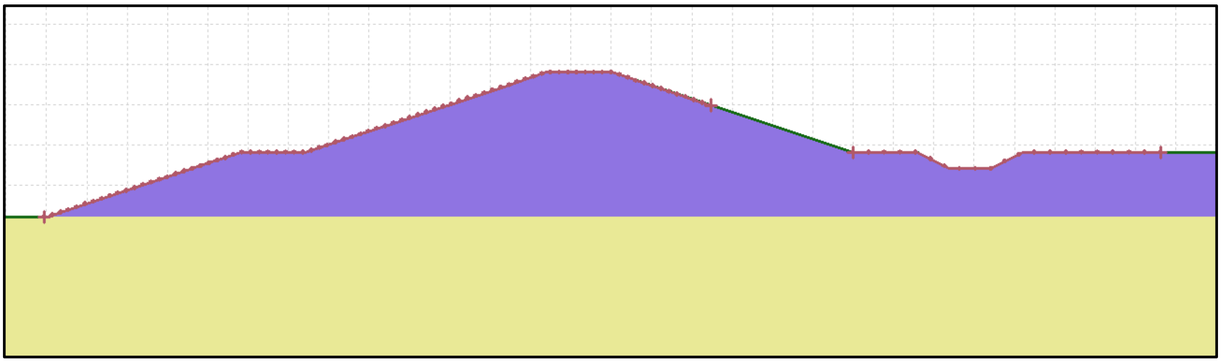

FIGURE H.1: ENTRY AND EXIT RANGE

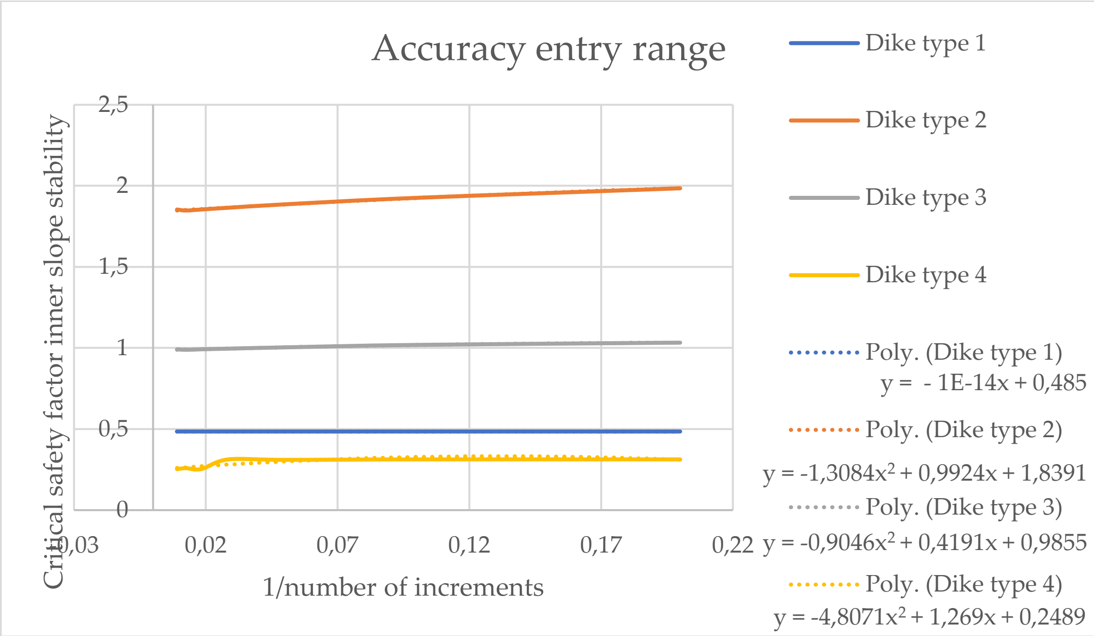

FIGURE H.2: ACCURACY ENTRY RANGE

TABLE H.1: ACCURACY ENTRY RANGE, ERROR

	Dike type			
Number of increments entry range	1	2	3	4
5	0,0%	7,9%	4,8%	25,8%
10	0,0%	4,7%	3,4%	25,8%
20	0,0%	2,6%	1,9%	24,5%
35	0,0%	1,4%	1,1%	25,8%
55	0,0%	0,8%	0,7%	1,6%
80	0,0%	0,5%	0,4%	4,1%
110	0,0%	0,8%	0,7%	1,6%

Accuracy number of increments exit range

The exit range is defined from the toe of the dike at the inner slope till four times the thickness of the cover layers right from the ditch. The same method as described for the entry range is used to define the number of increments for the exit range. The results are presented in Figure H.3 and Table H.2; therefore it is decided to use 10 increments in the exit range.

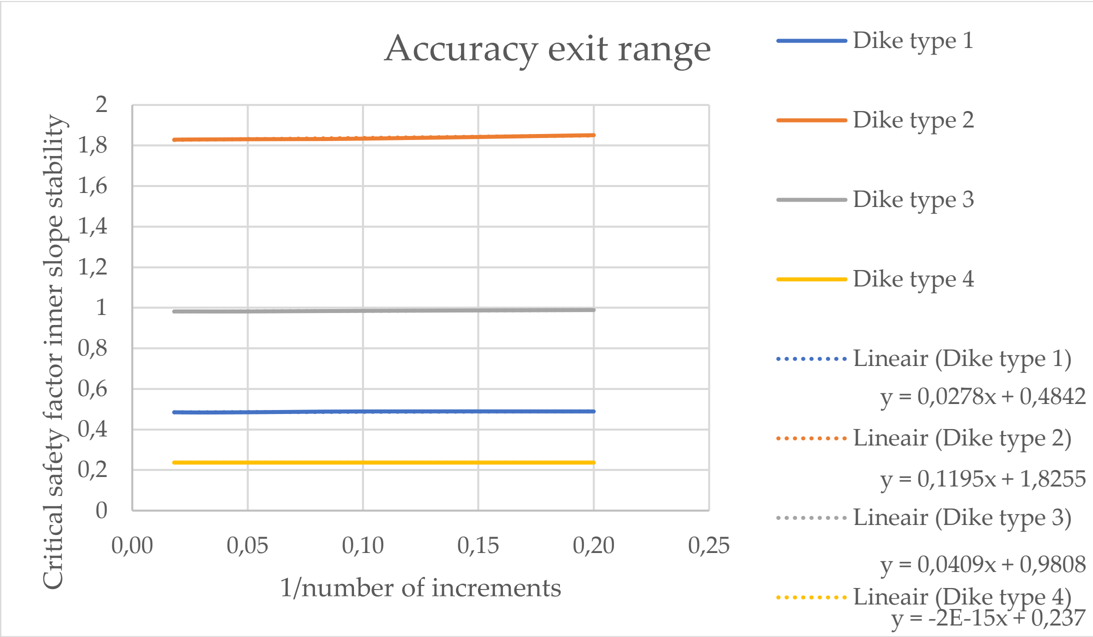

FIGURE H.3: ACCURACY EXIT RANGE

TABLE H.2: ACCURACY EXIT RANGE, ERROR

	Dike type			
Number of increments exit range	1	2	3	4
5	1,0%	1,4%	0,8%	0,0%
10	1,0%	0,5%	0,4%	0,0%
20	0,2%	0,3%	0,1%	0,0%
35	0,0%	0,2%	0,1%	0,0%
55	0,2%	0,2%	0,1%	0,0%

Accuracy number of increments radius

The method is repeated to determine the number of radius increments. The results are shown in Table H.3 and Figure H.4 from which is concluded to use 4 increments.

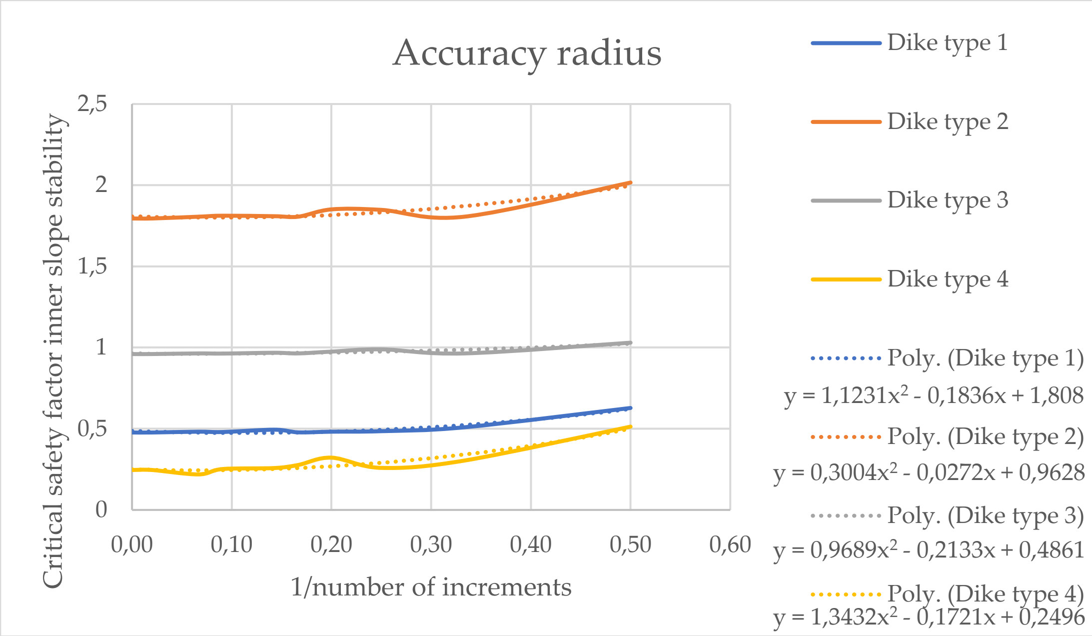

FIGURE H.4: ACCURACY RADIUS

TABLE H.3: ACCURACY RADIUS, ERROR

	Dike type			
Number of radius increments	1	2	3	4
2	27,3%	10,9%	6,7%	103,3%
3	3,2%	0,7%	0,1%	20,5%
4	1,7%	1,6%	2,5%	2,7%
5	2,3%	1,8%	1,0%	27,6%
6	3,1%	0,7%	0,1%	9,8%
7	0,2%	0,5%	0,3%	2,3%
11	2,7%	0,3%	0,2%	0,1%
15	2,3%	0,7%	0,1%	13,2%
55	3,3%	1,3%	0,5%	2,5%

APPENDIX I. RESULTS PORE PRESSURE FIELD

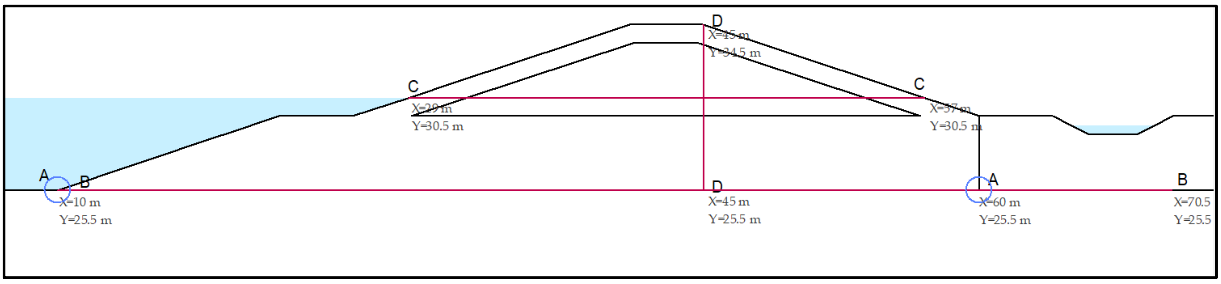

Location: Rhine, cross section: s1, description: clayey dike on sandy subsoil

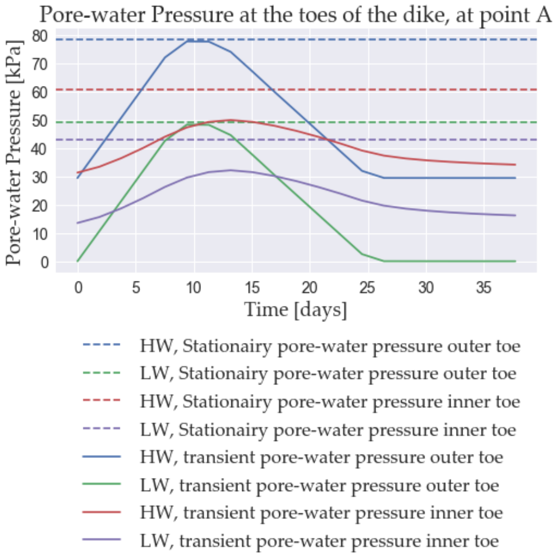

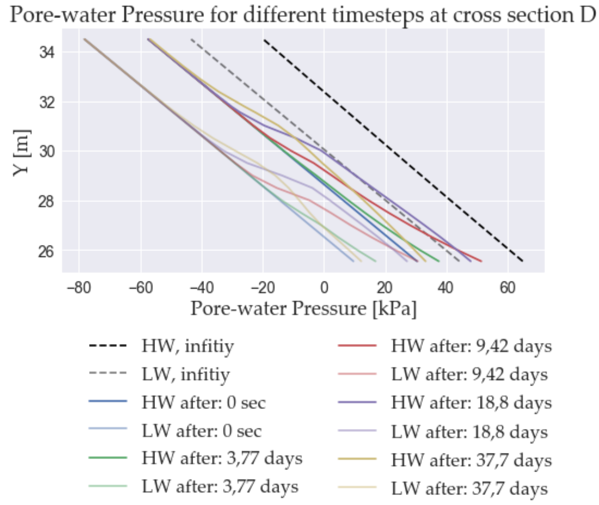

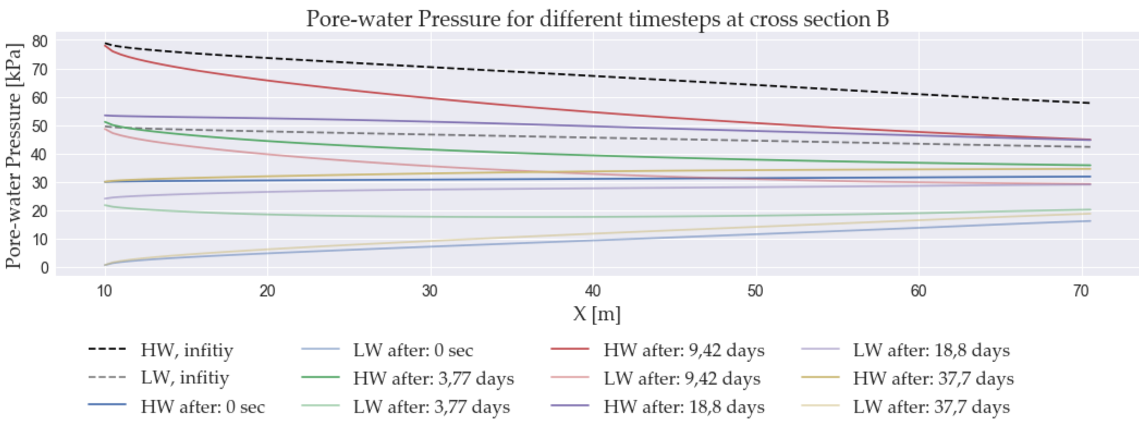

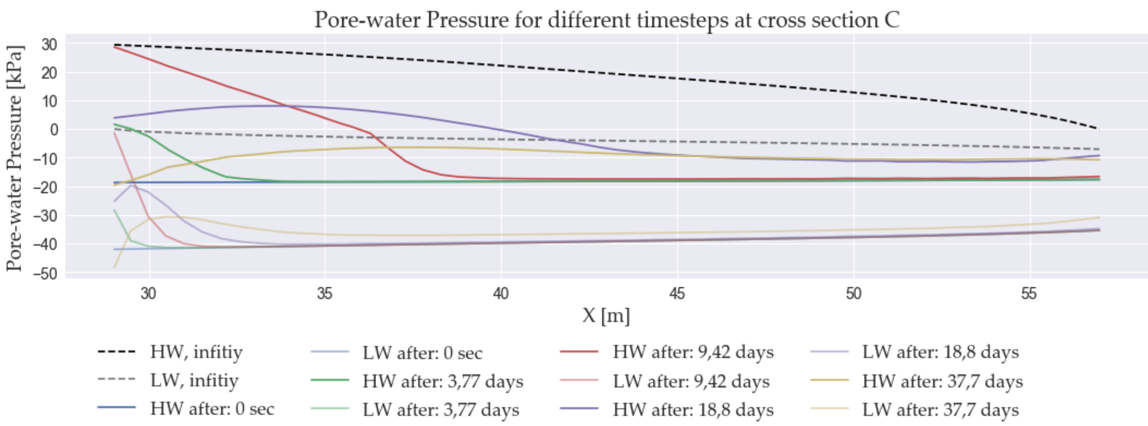

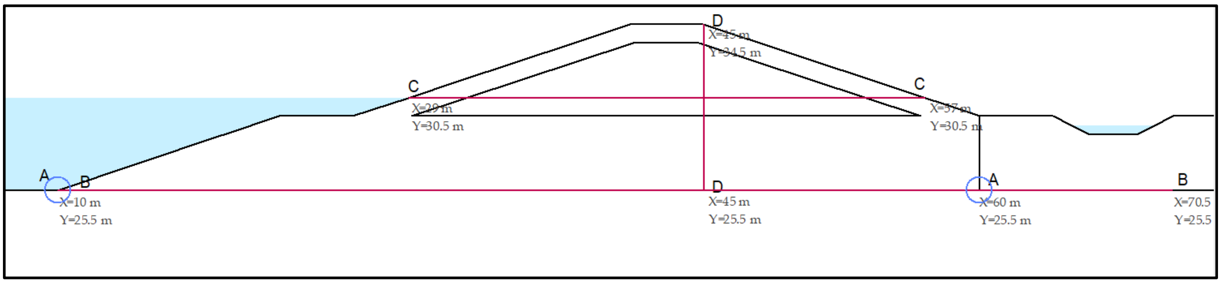

Location: Rhine, cross section: s2, description: sandy dike on sandy subsoil

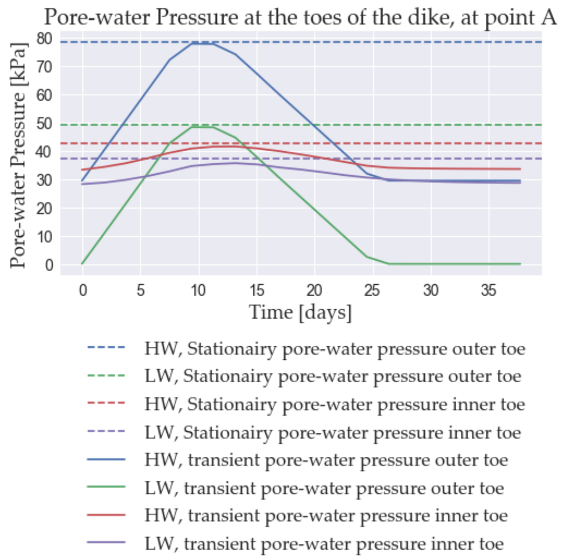

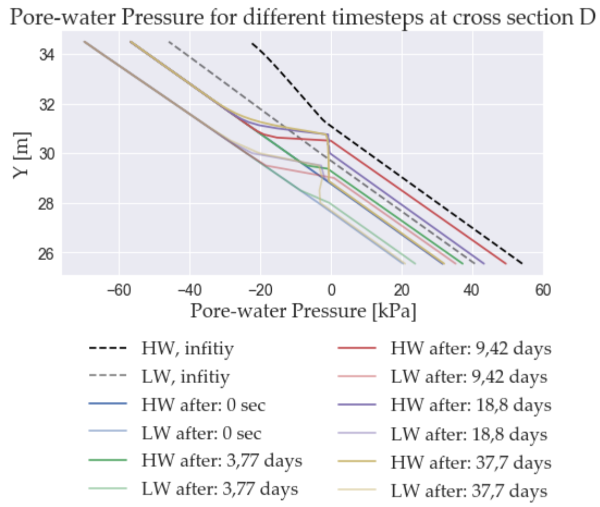

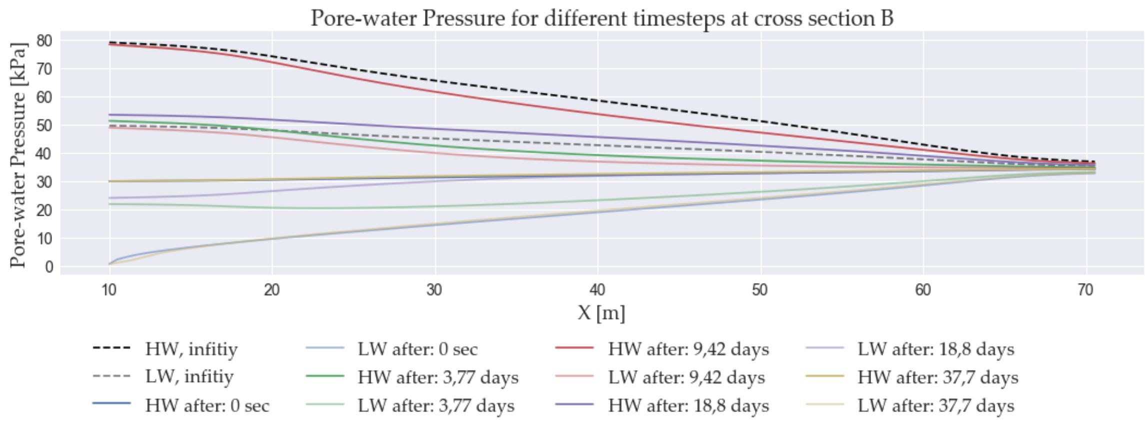

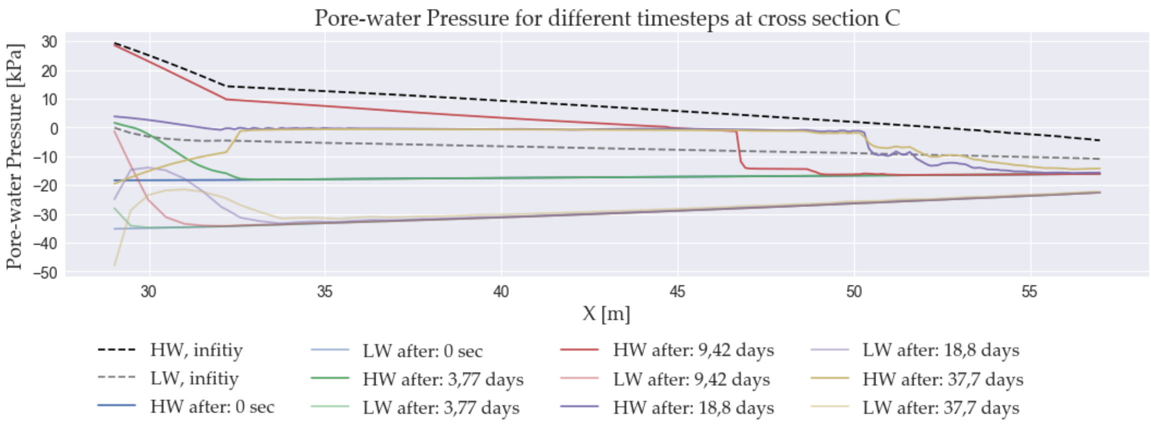

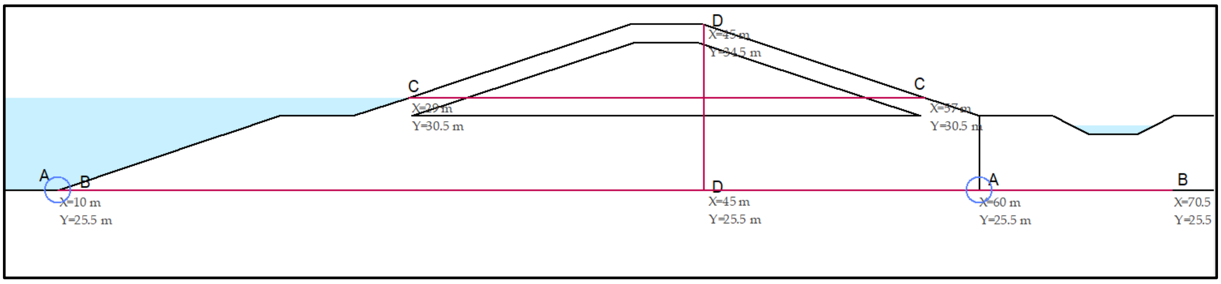

Location: Rhine, cross section: s3, description: clayey dike on clayey subsoil

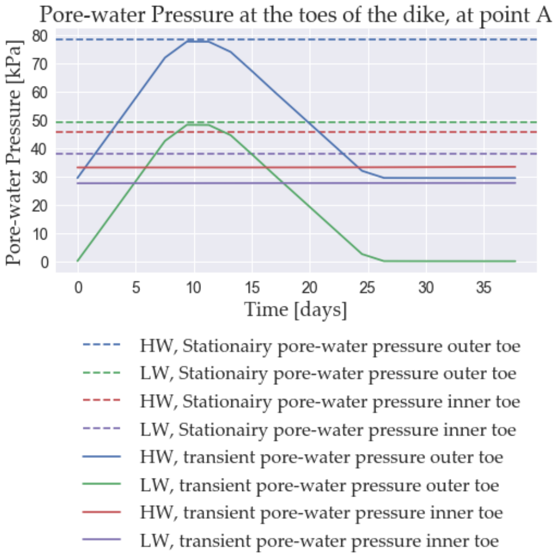

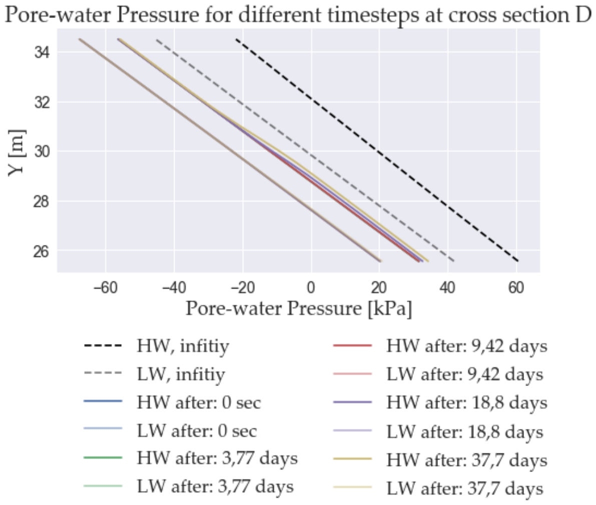

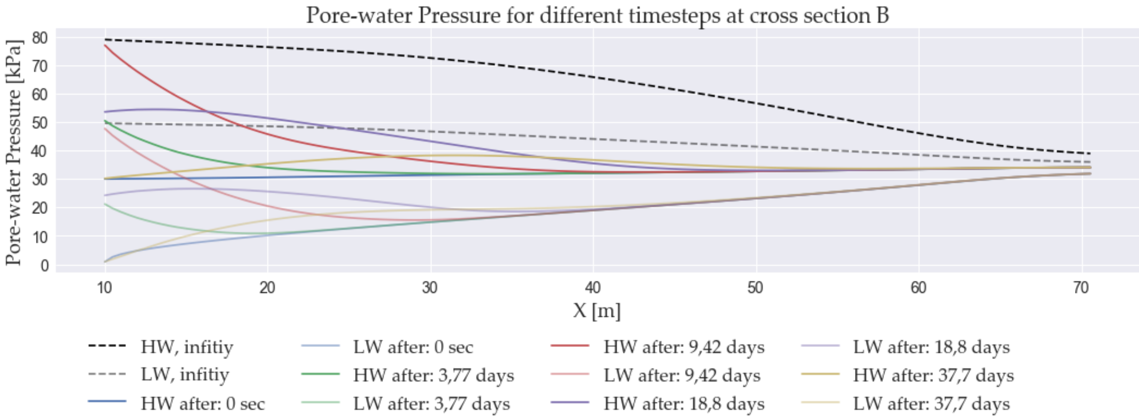

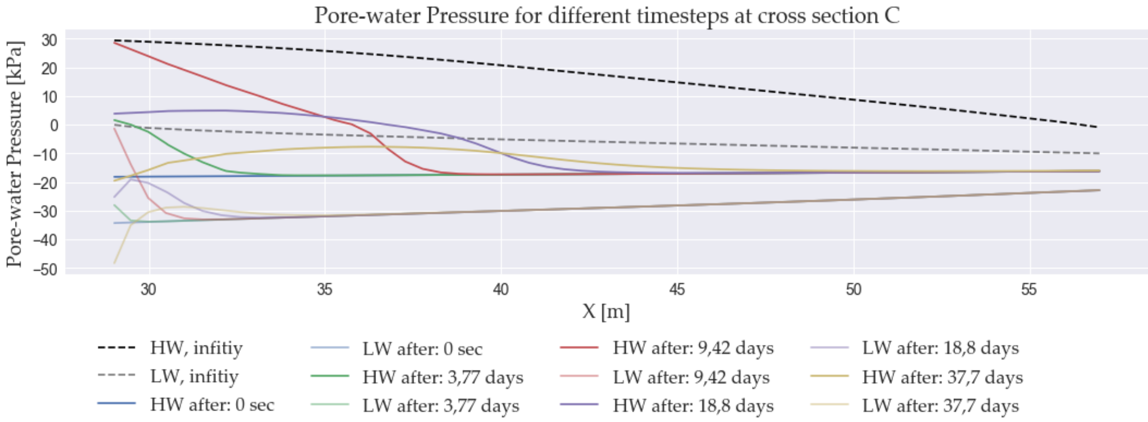

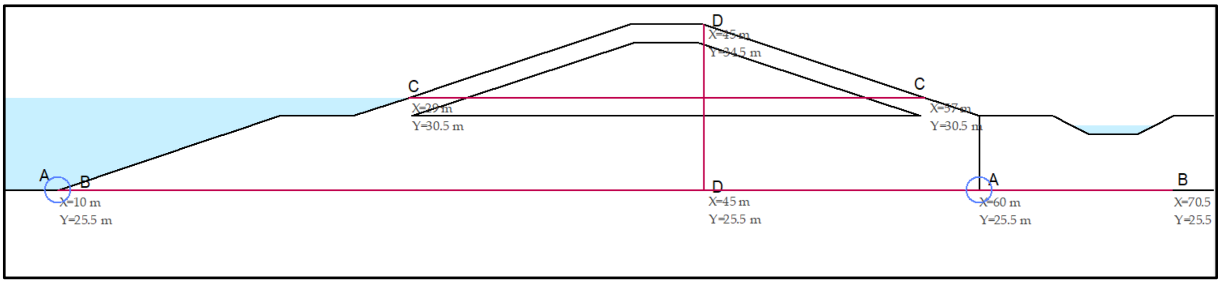

Location: Rhine, cross section: s4, description: clayey dike wity sandy core on sandy subsoil

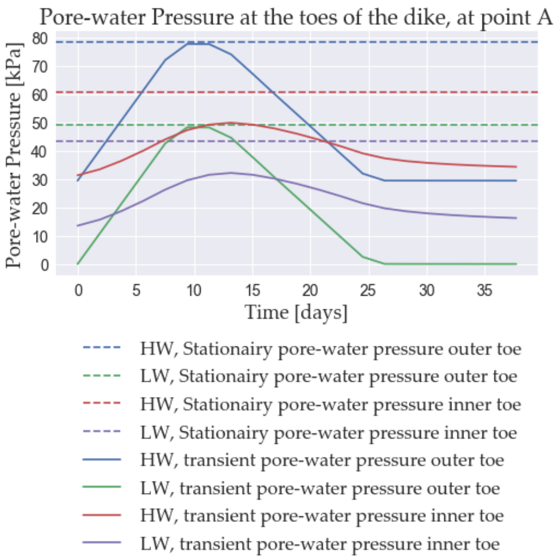

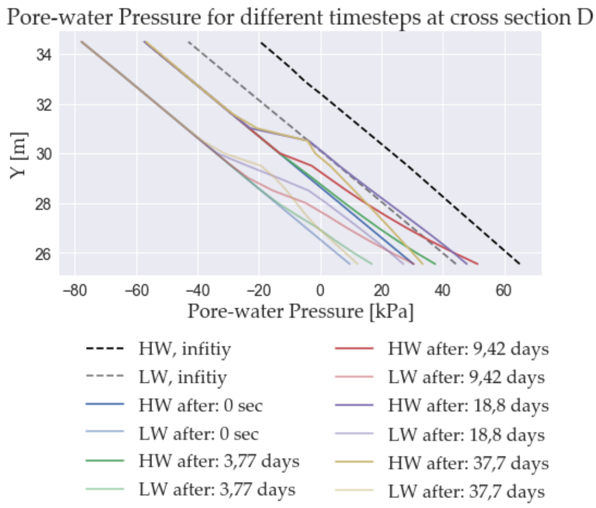

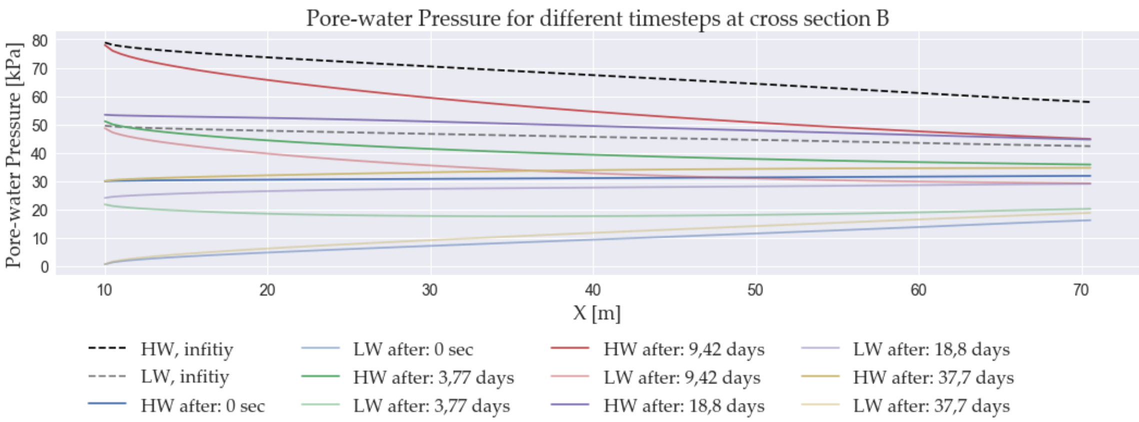

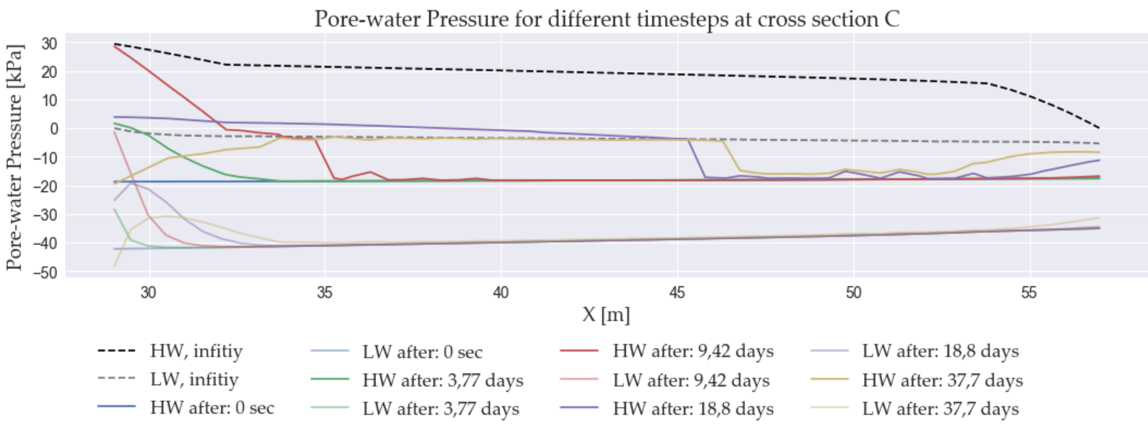

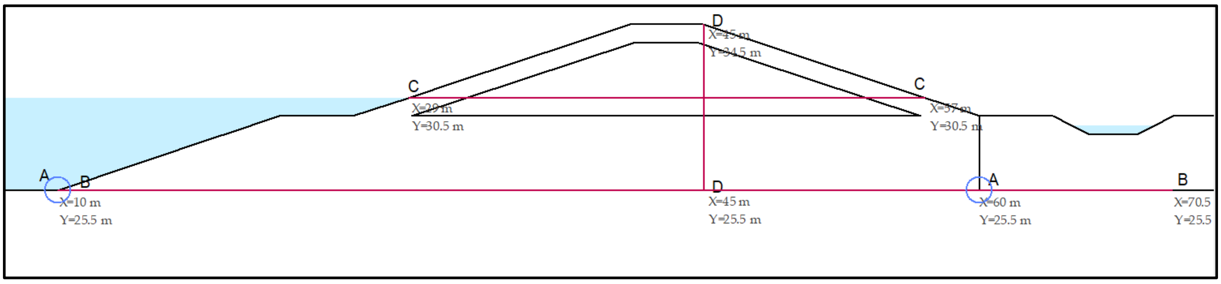

Location: Meuse, cross section: s1, description: clayey dike on sandy subsoil

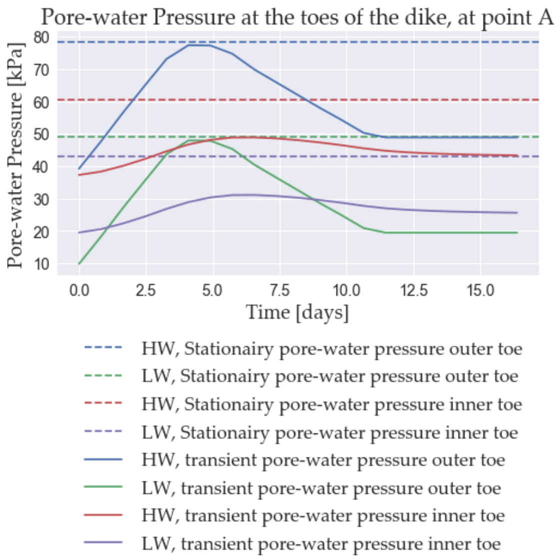

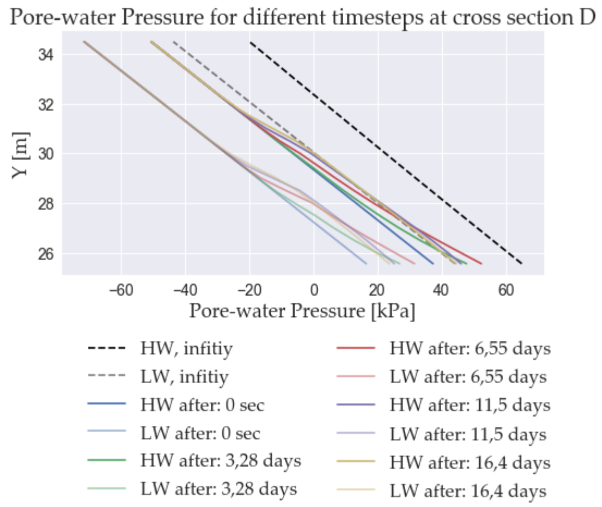

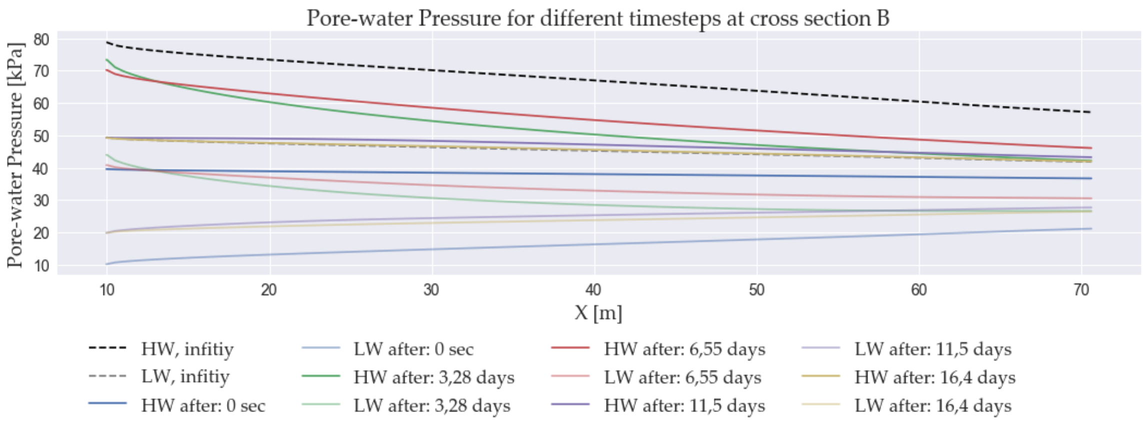

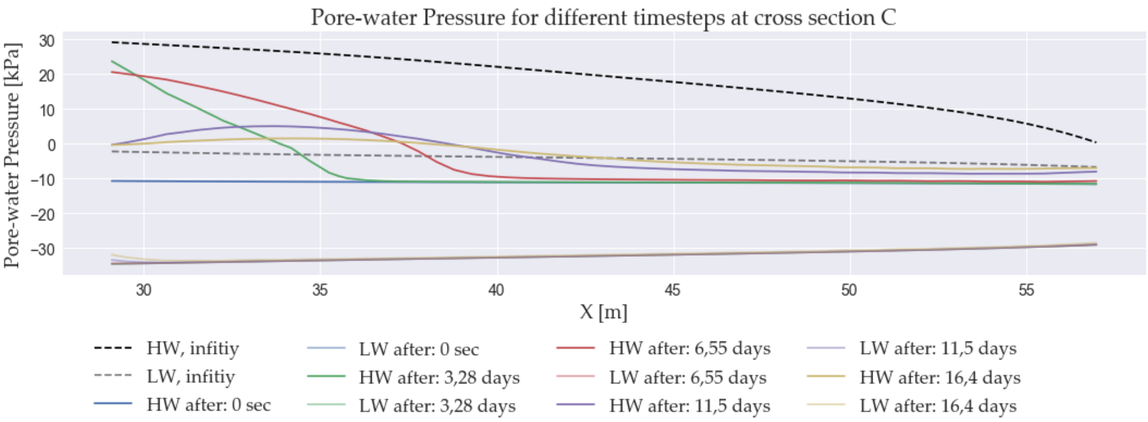

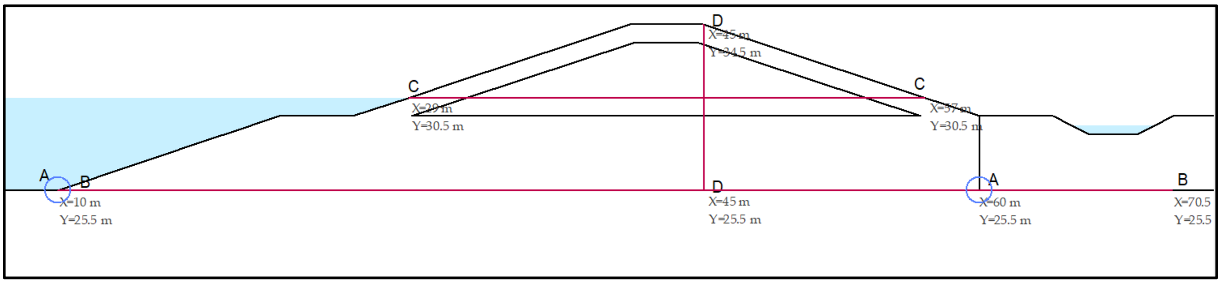

Location: Meuse, cross section: s2, description: sandy dike on sandy subsoil

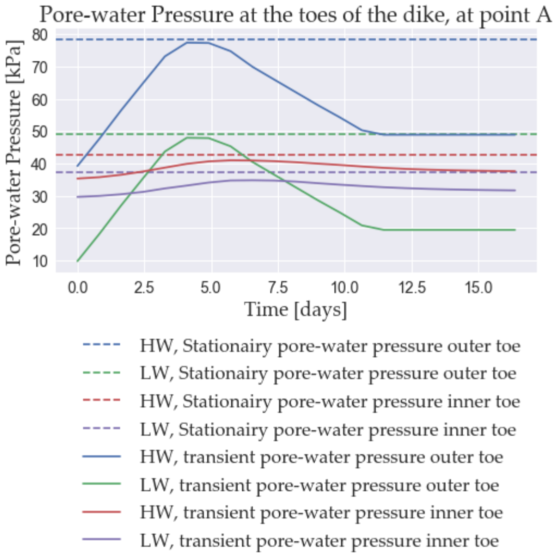

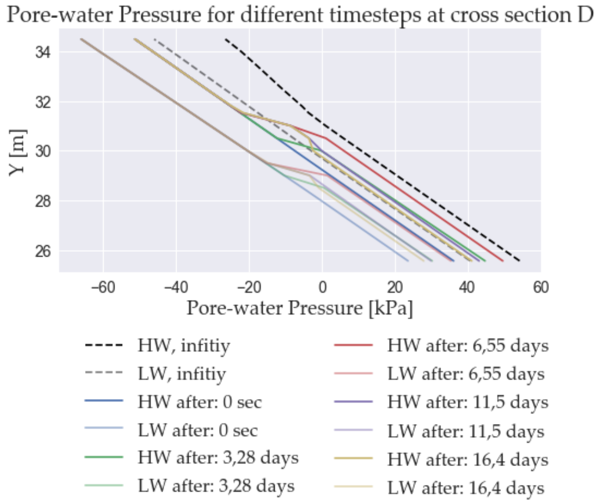

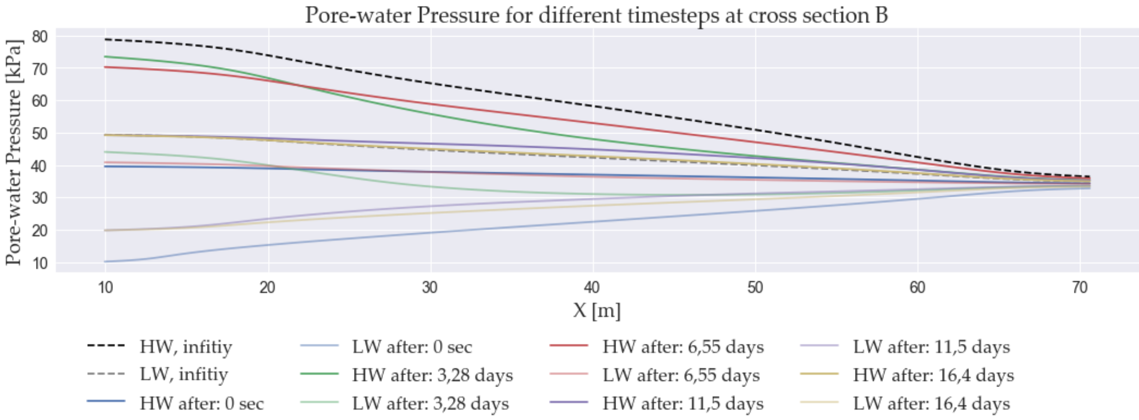

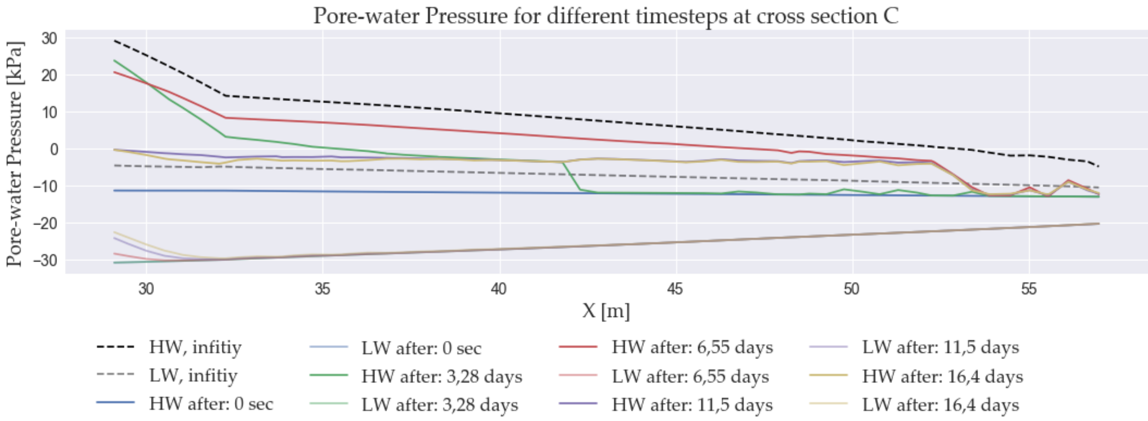

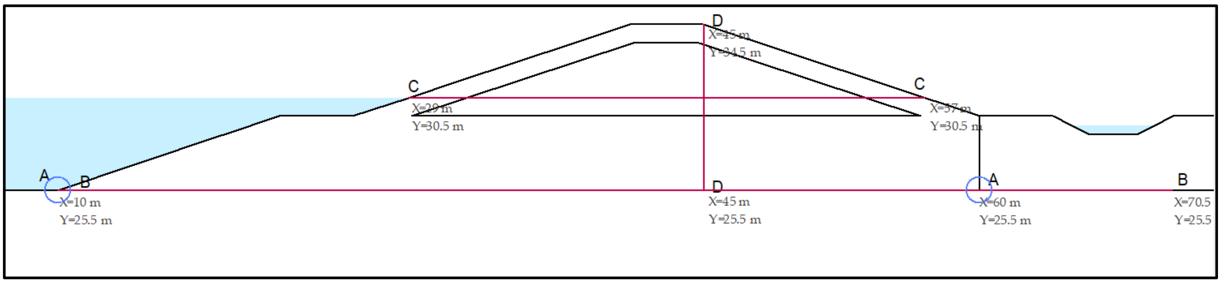

Location: Meuse, cross section: s3, description: clayey dike on clayey subsoil

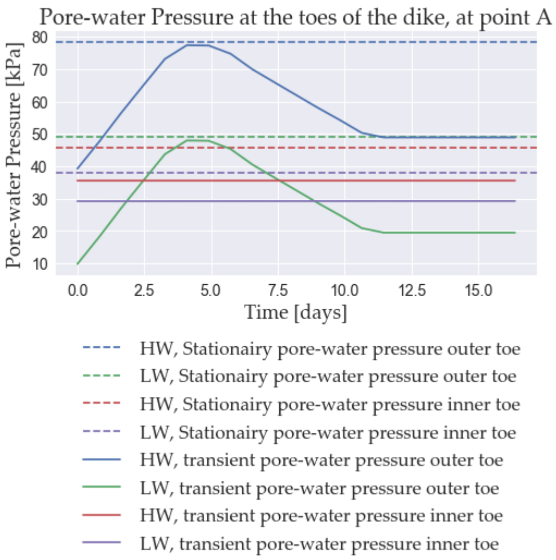

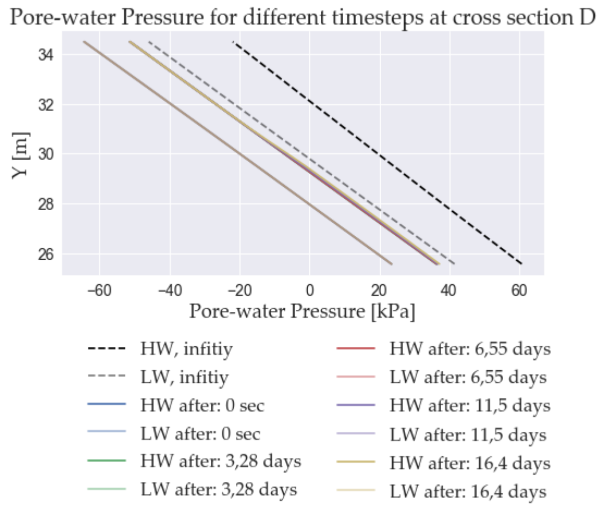

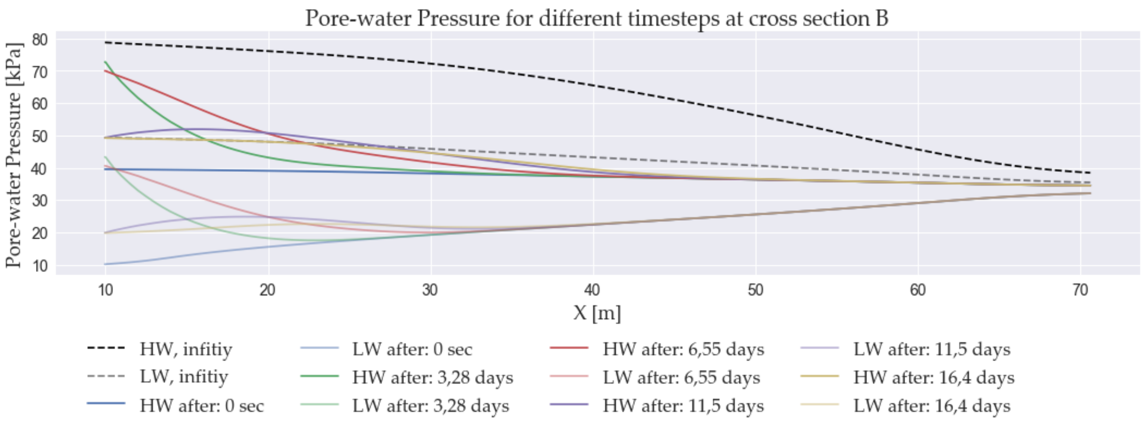

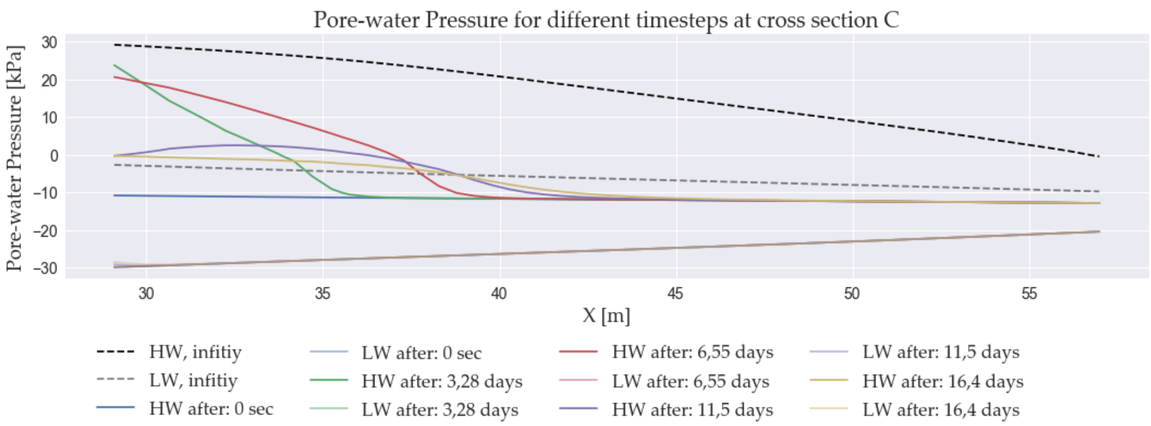

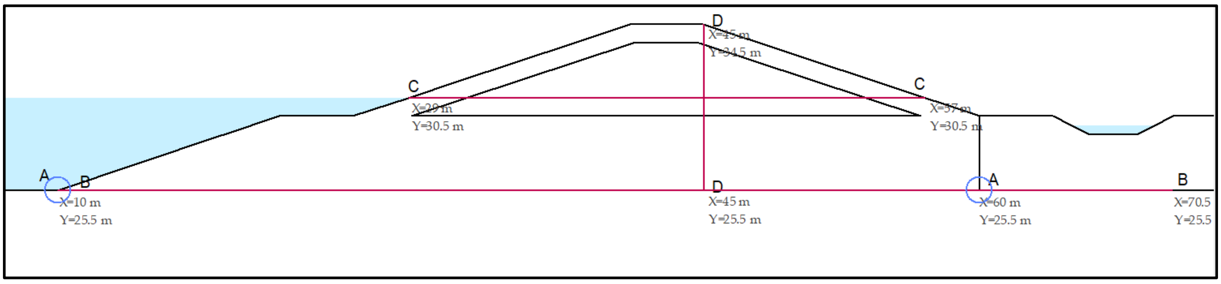

Location: Meuse, cross section: s4, description: clayey dike wity sandy core on sandy subsoil

Pore-water Pressure at the toes of the dike, at point A

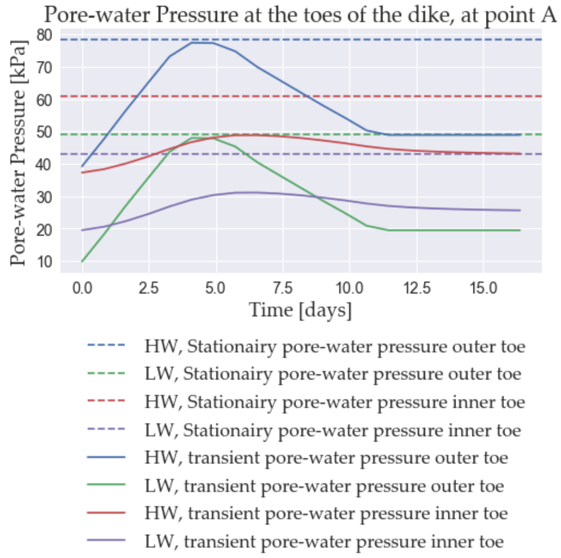

Pore-water Pressure for different timesteps at cross section D

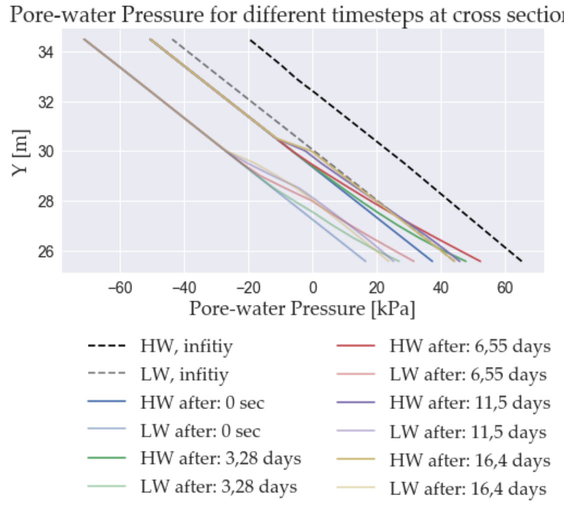

Pore-water Pressure for different timesteps at cross section B

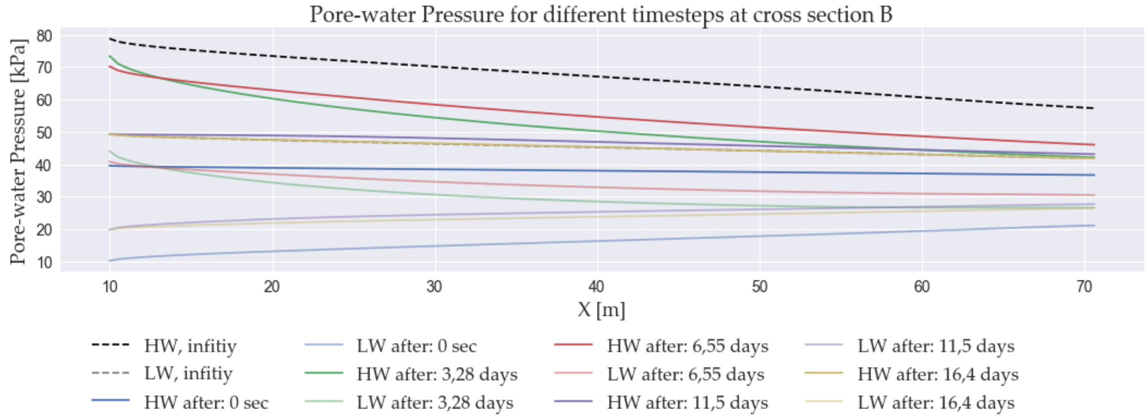

Pore-water Pressure for different timesteps at cross section C

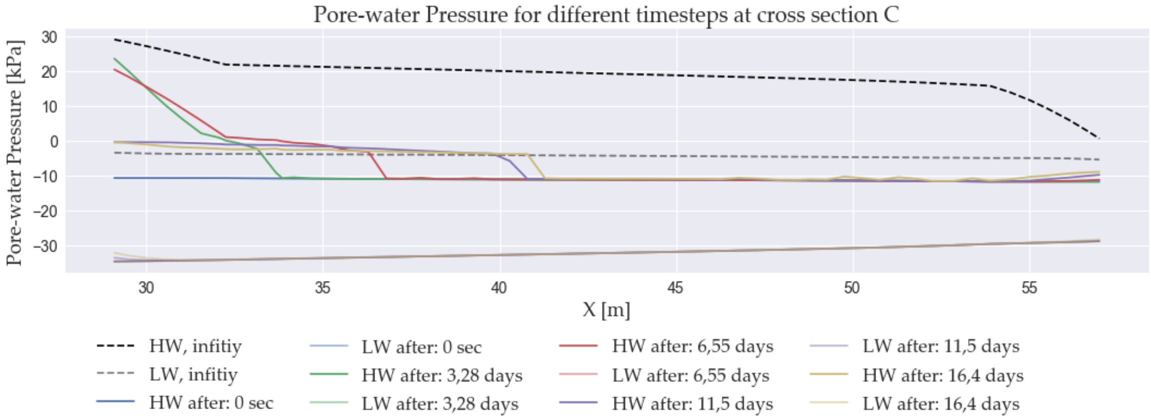

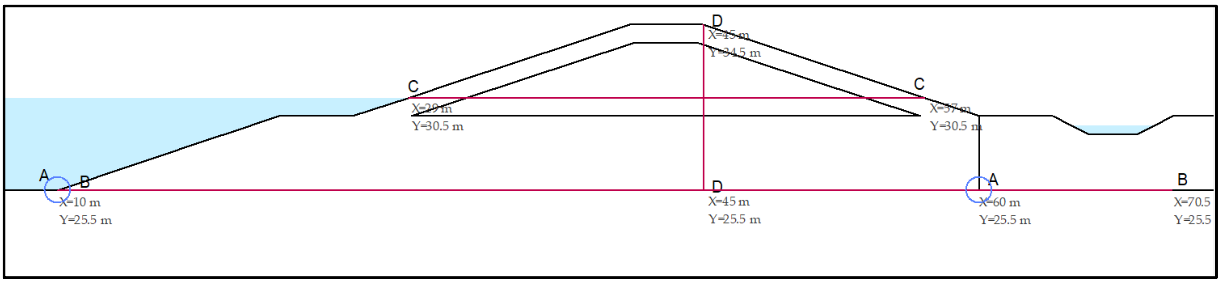

Location: Sea, cross section: s1, description: clayey dike on sandy subsoil

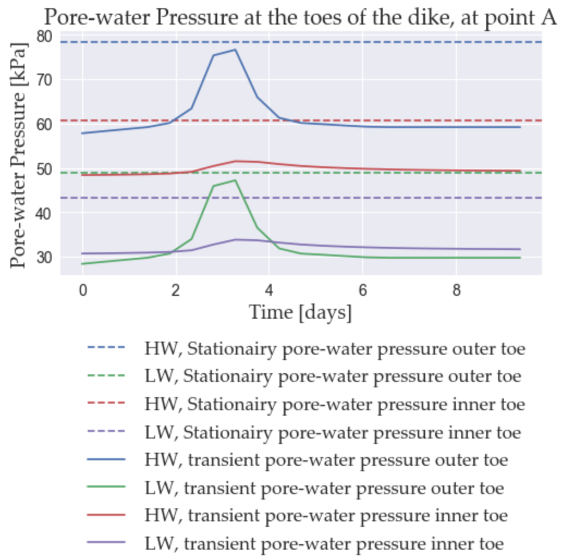

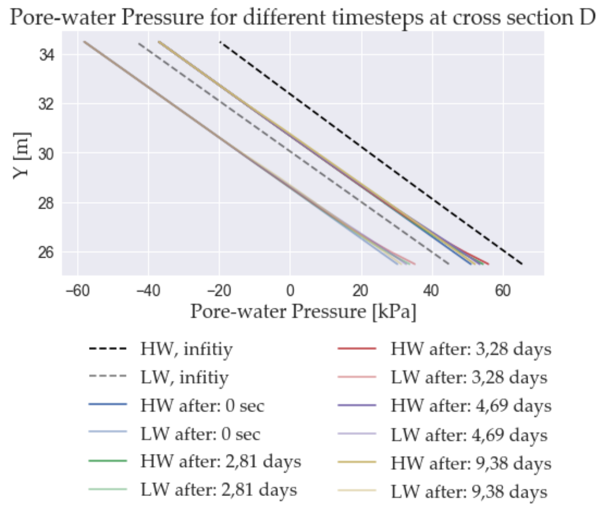

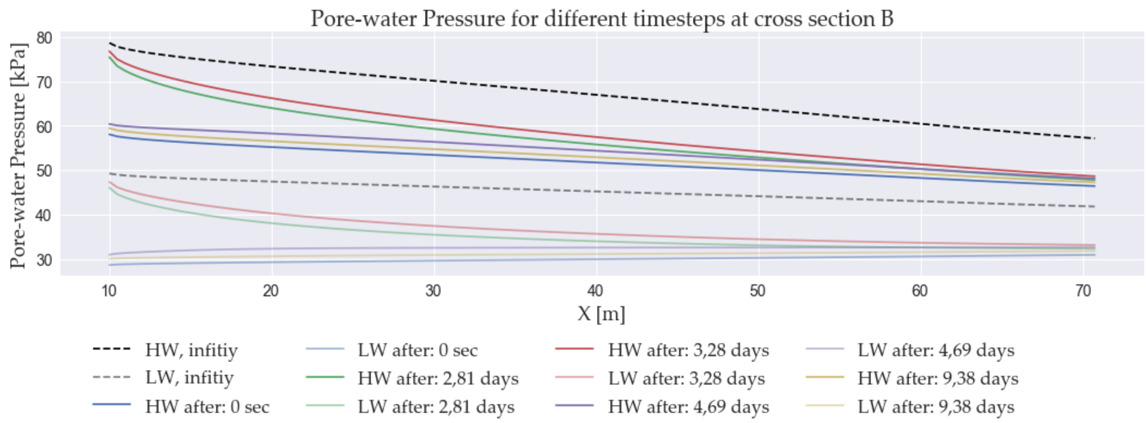

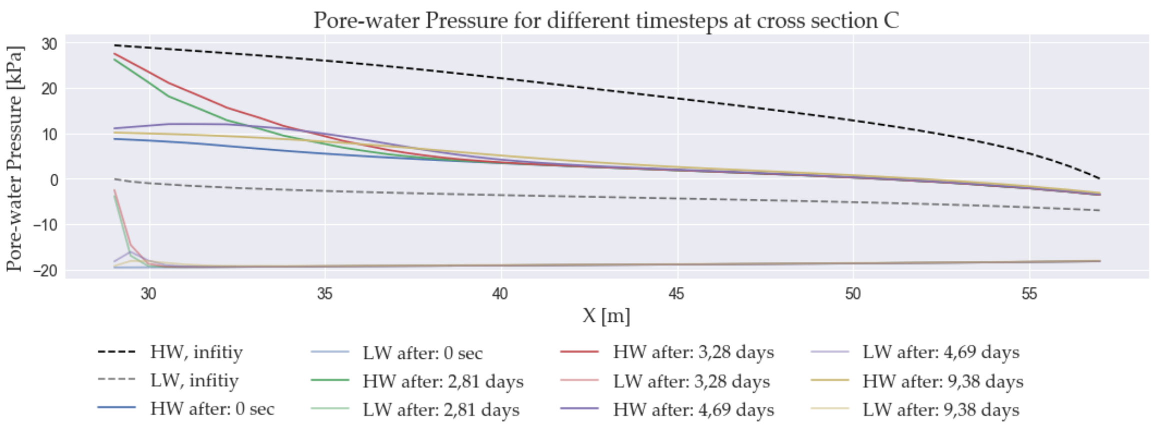

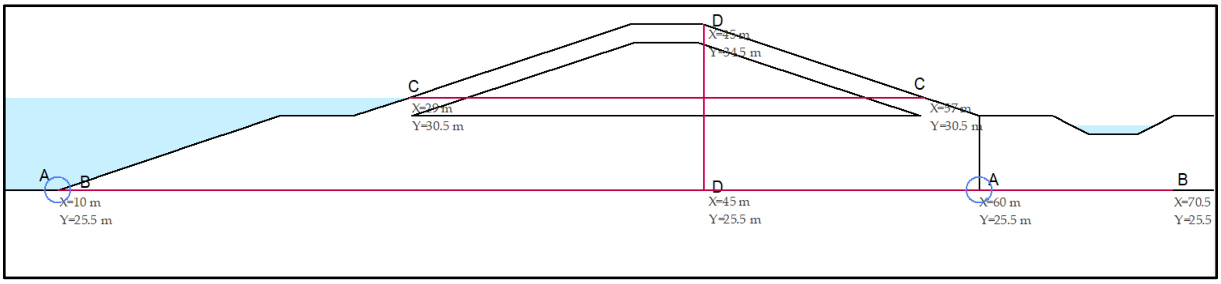

Location: Sea, cross section: s2, description: sandy dike on sandy subsoil

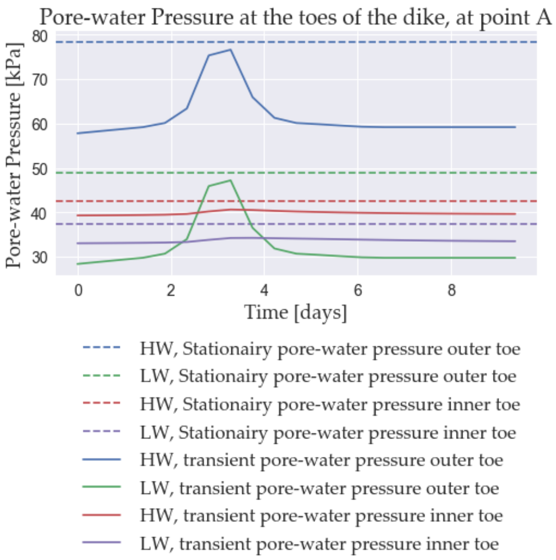

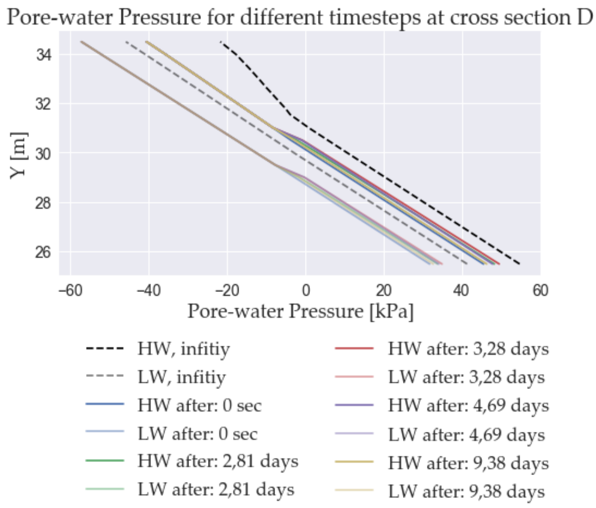

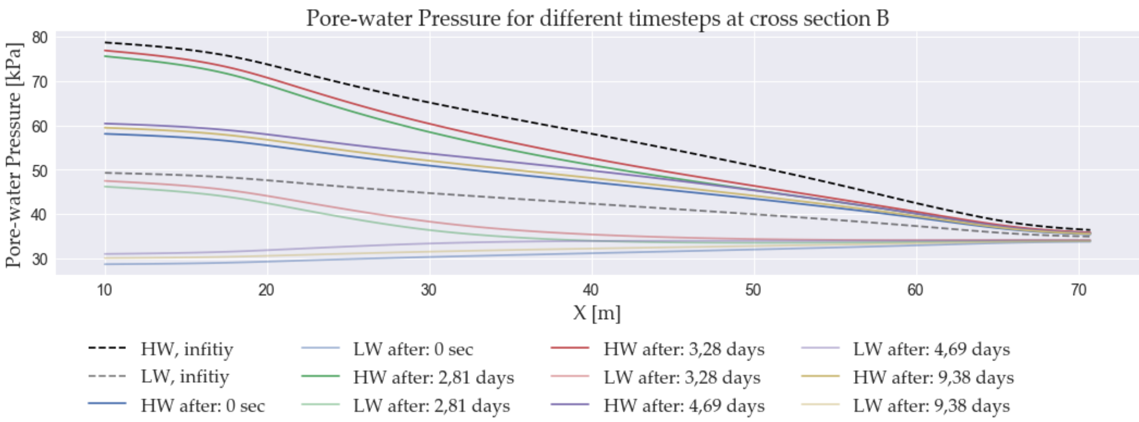

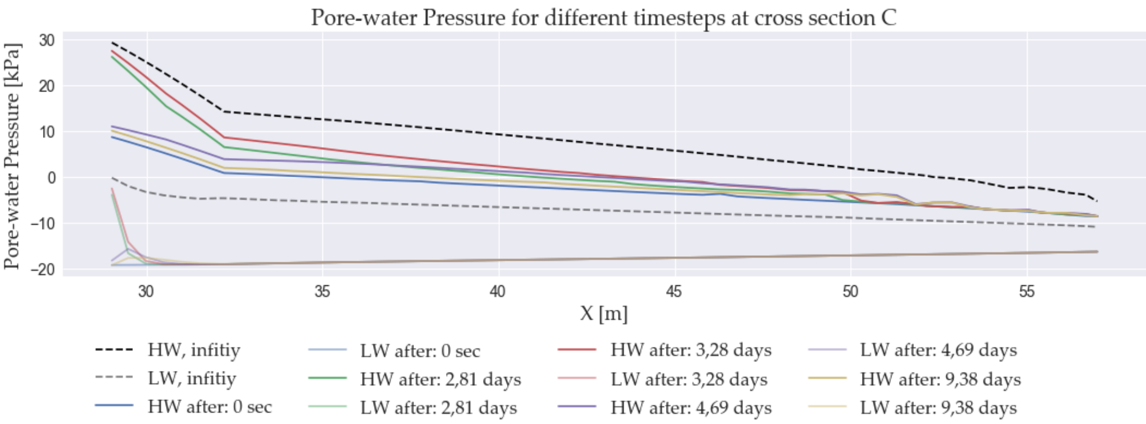

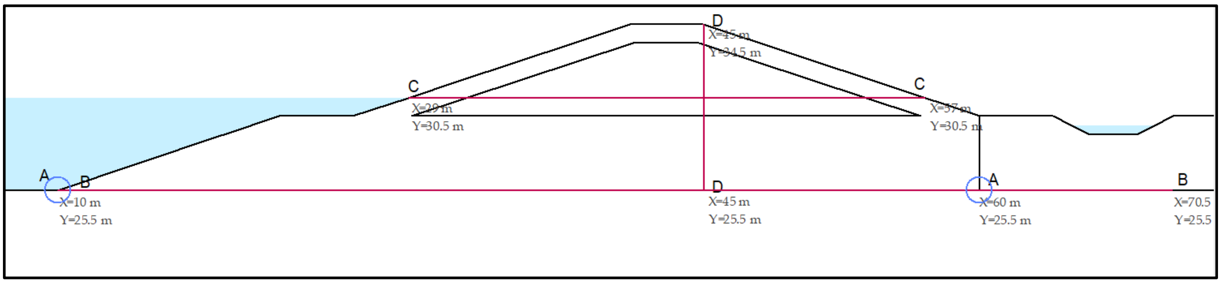

Location: Sea, cross section: s3, description: clayey dike on clayey subsoil

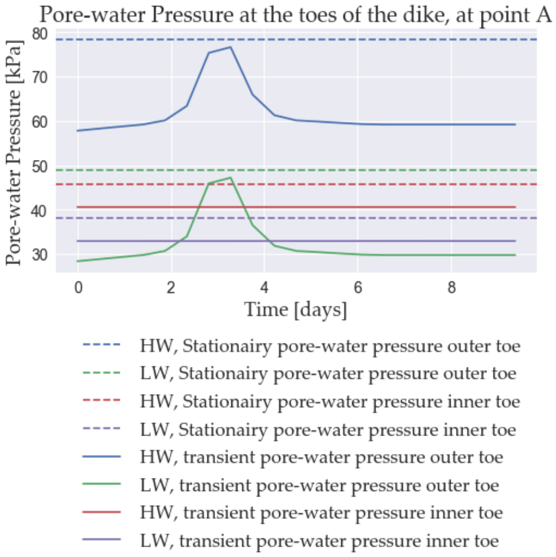

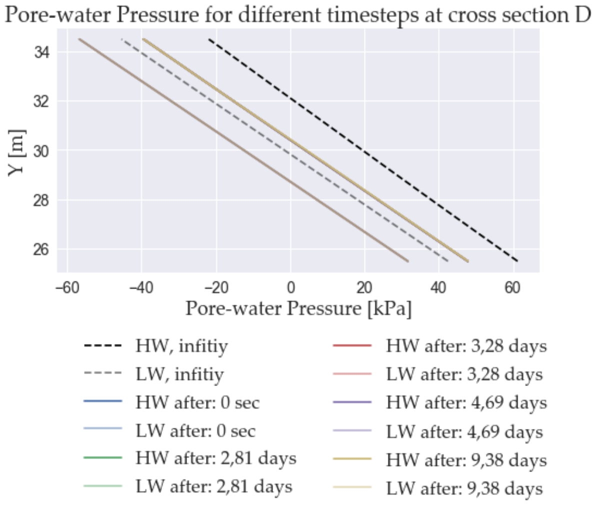

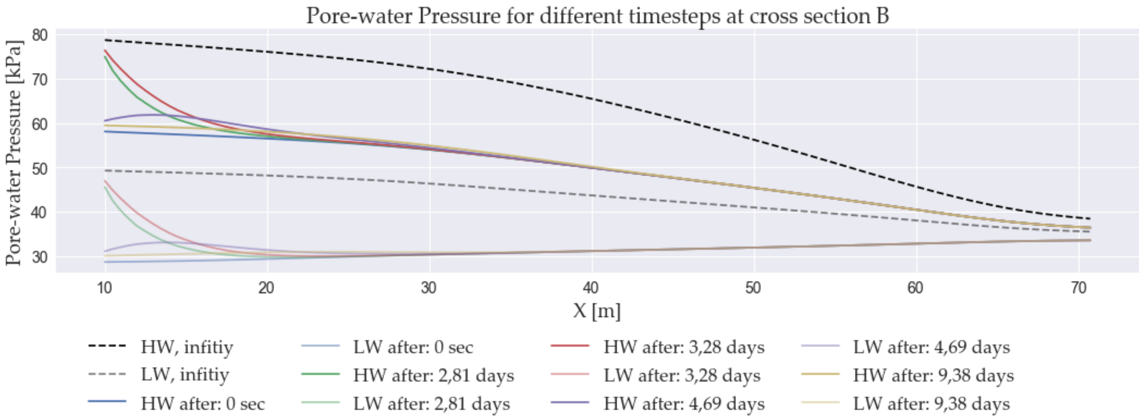

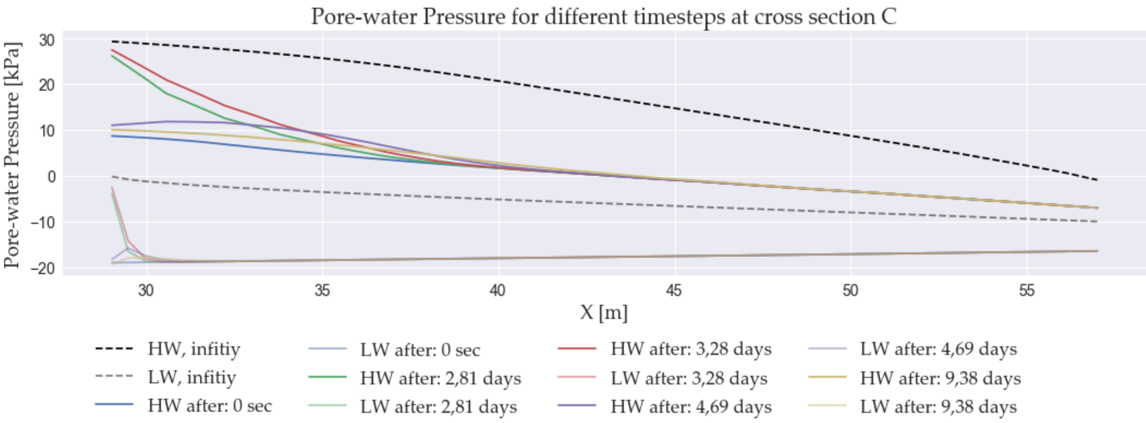

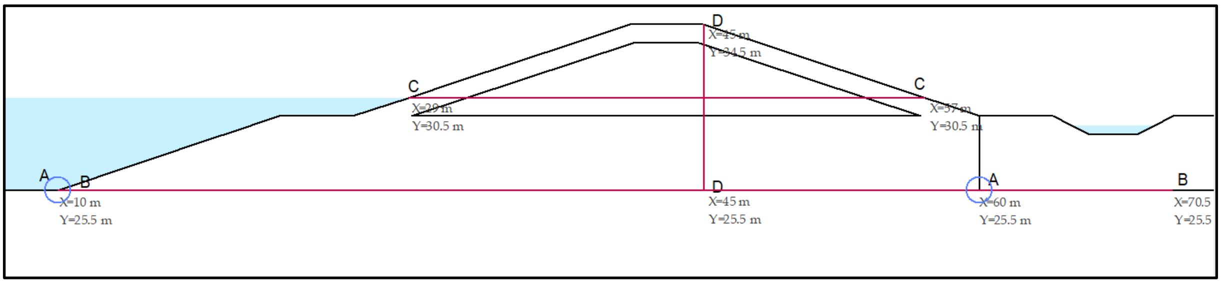

Location: Sea, cross section: s4, description: clayey dike wity sandy core on sandy subsoil

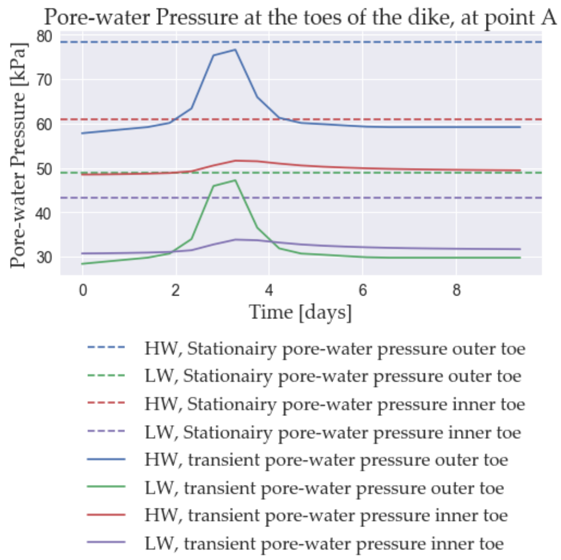

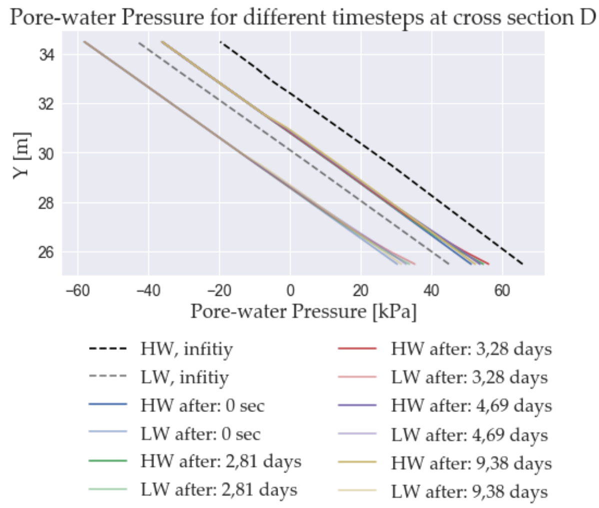

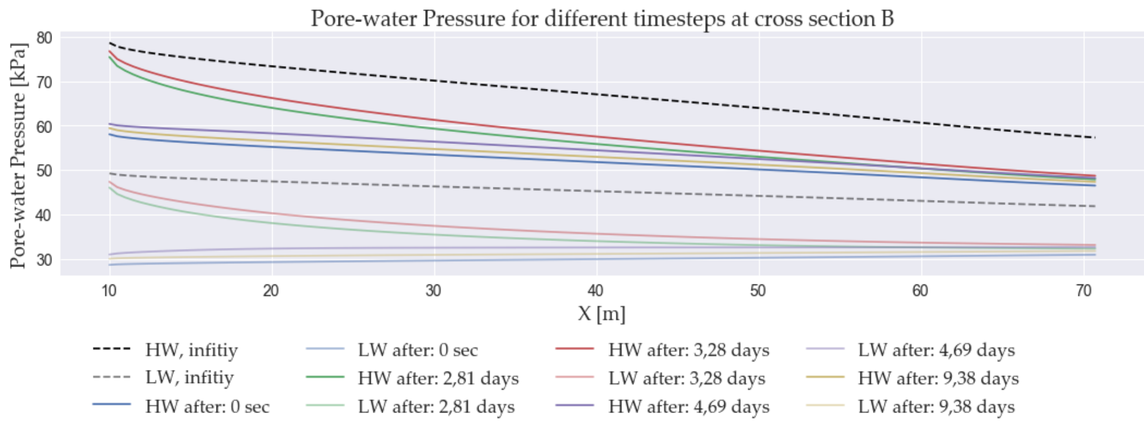

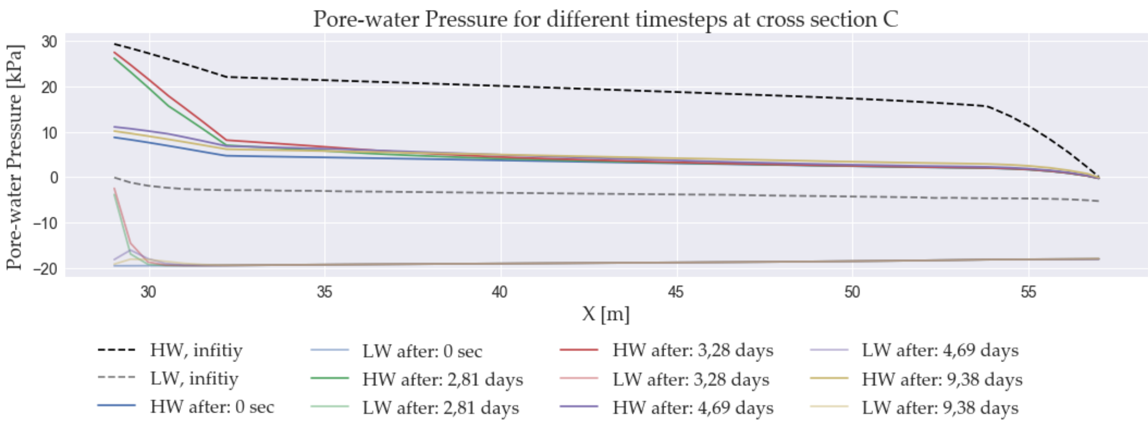

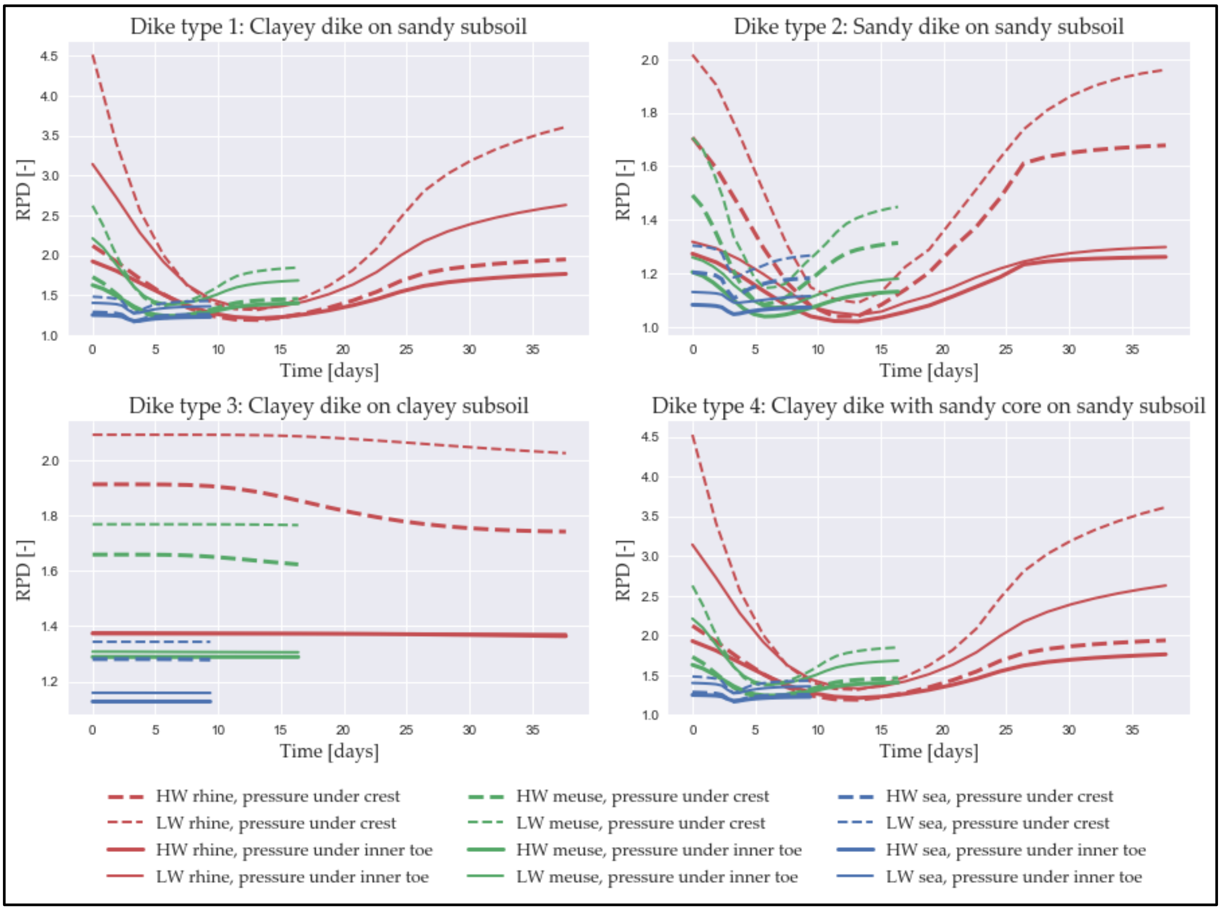

FIGURE I.1: *RPD* IN TIME FOR DIFFERENT DIKE TYPES FOR DIFFERENT FLOOD WAVES

APPENDIX J. RESULTS SENSITIVITY ASSESSMENT

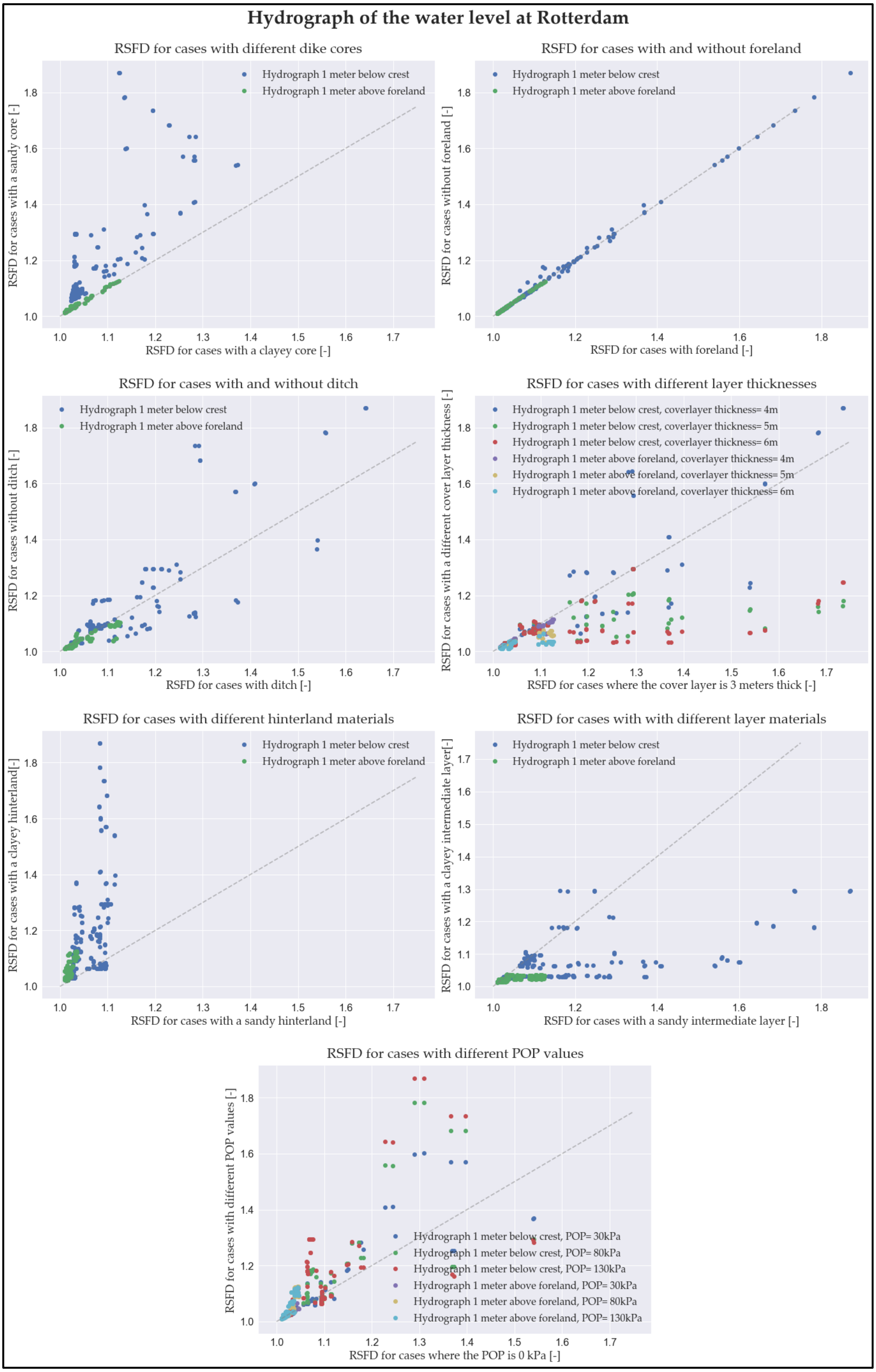
Hydrograph of the water level at Rotterdam
RSFD for cases with different dike cores
Hydrograph 1 meter below crest
Hydrograph 1 meter above foreland
RSFD for cases with a sandy core [-]
RSFD for cases with a clayey core [-]
RSFD for cases with and without foreland
RSFD for cases without foreland [-]
RSFD for cases with foreland [-]
RSFD for cases with and without ditch
RSFD for cases without ditch [-]
RSFD for cases with ditch [-]
RSFD for cases with different layer thicknesses
Hydrograph 1 meter below crest, coverlayer thickness= 4m
Hydrograph 1 meter below crest, coverlayer thickness= 5m
Hydrograph 1 meter below crest, coverlayer thickness= 6m
Hydrograph 1 meter above foreland, coverlayer thickness= 4m
Hydrograph 1 meter above foreland, coverlayer thickness= 5m
Hydrograph 1 meter above foreland, coverlayer thickness= 6m
RSFD for cases with a different cover layer thickness [-]
RSFD for cases where the cover layer is 3 meters thick [-]
RSFD for cases with different hinterland materials
RSFD for cases with a clayey hinterland[-]
RSFD for cases with a sandy hinterland [-]
RSFD for cases with with different layer materials
RSFD for cases with a clayey intermediate layer[-]
RSFD for cases with a sandy intermediate layer [-]
RSFD for cases with different POP values
Hydrograph 1 meter below crest, POP= 30kPa
Hydrograph 1 meter below crest, POP= 80kPa
Hydrograph 1 meter below crest, POP= 130kPa
Hydrograph 1 meter above foreland, POP= 30kPa
Hydrograph 1 meter above foreland, POP= 80kPa
Hydrograph 1 meter above foreland, POP= 130kPa
RSFD for cases with different POP values [-]
RSFD for cases where the POP is 0 kPa [-]

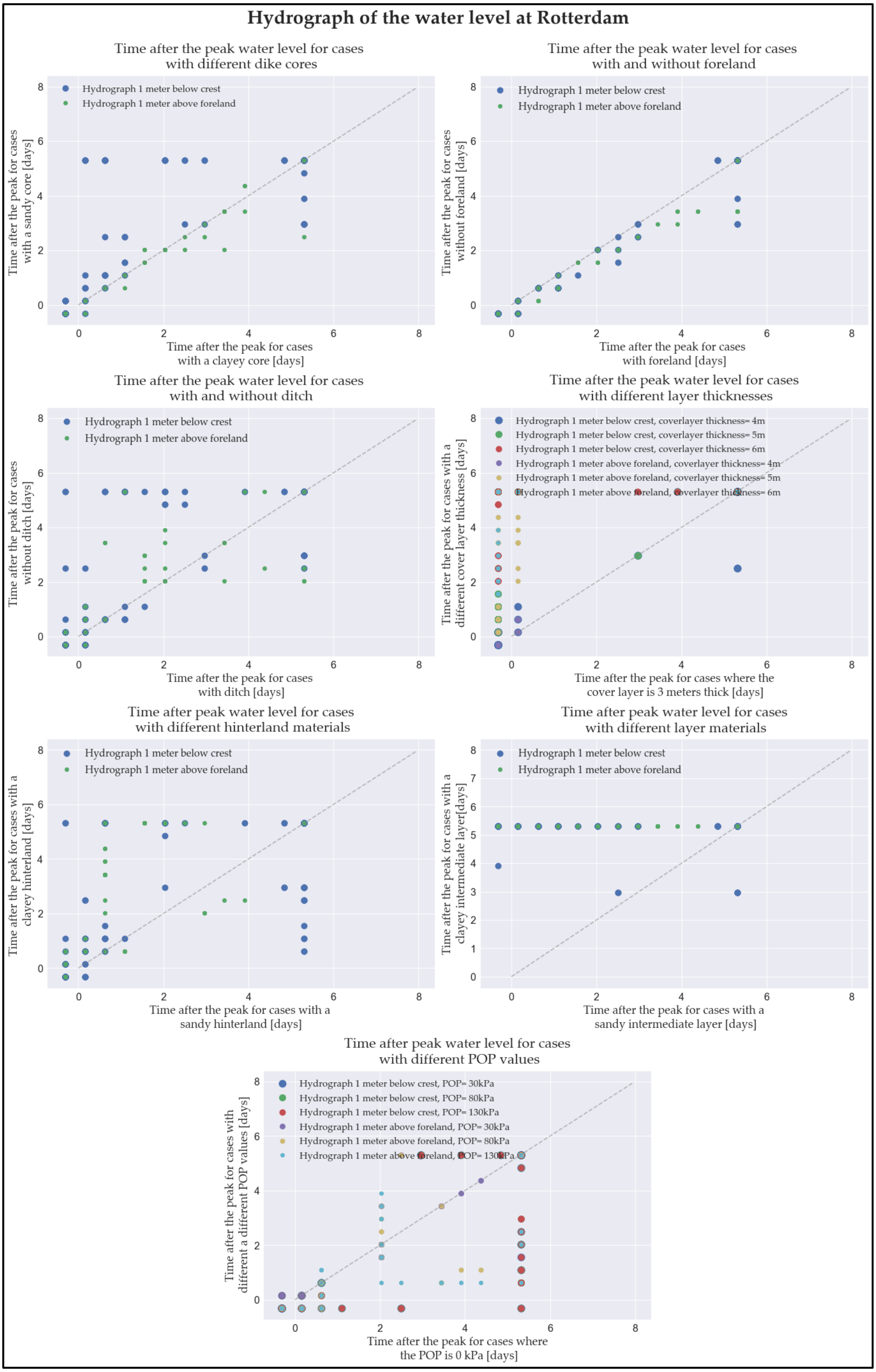
Hydrograph of the water level at Rotterdam
Time after the peak water level for cases with different dike cores
Hydrograph 1 meter below crest
Hydrograph 1 meter above foreland
Time after the peak for cases with a sandy core [days]
Time after the peak for cases with a clayey core [days]
Time after the peak water level for cases with and without foreland
Hydrograph 1 meter below crest
Hydrograph 1 meter above foreland
Time after the peak for cases without foreland [days]
Time after the peak for cases with foreland [days]
Time after the peak water level for cases with and without ditch
Hydrograph 1 meter below crest
Hydrograph 1 meter above foreland
Time after the peak for case without ditch [days]
Time after the peak for cases with ditch [days]
Time after the peak water level for cases with different layer thicknesses
Hydrograph 1 meter below crest, coverlayer thickness= 4m
Hydrograph 1 meter below crest, coverlayer thickness= 5m
Hydrograph 1 meter below crest, coverlayer thickness= 6m
Hydrograph 1 meter above foreland, coverlayer thickness= 4m
Hydrograph 1 meter above foreland, coverlayer thickness= 5m
Hydrograph 1 meter above foreland, coverlayer thickness= 6m
Time after the peak for cases with a different cover layer thickness [days]
Time after the peak for cases where the cover layer is 3 meters thick [days]
Time after peak water level for cases with different hinterland materials
Hydrograph 1 meter below crest
Hydrograph 1 meter above foreland
Time after the peak for cases with a clayey hinterland [days]
Time after the peak for cases with a sandy hinterland [days]
Time after peak water level for cases with different layer materials
Hydrograph 1 meter below crest
Hydrograph 1 meter above foreland
Time after the peak for cases with a clayey intermediate layer[days]
Time after the peak for cases with a sandy intermediate layer [days]
Time after peak water level for cases with different POP values
Hydrograph 1 meter below crest, POP= 30kPa
Hydrograph 1 meter below crest, POP= 80kPa
Hydrograph 1 meter below crest, POP= 130kPa
Hydrograph 1 meter above foreland, POP= 30kPa
Hydrograph 1 meter above foreland, POP= 80kPa
Hydrograph 1 meter above foreland, POP= 130kPa
Time after the peak for cases with different a different POP values [days]
Time after the peak for cases where the POP is 0 kPa [days]

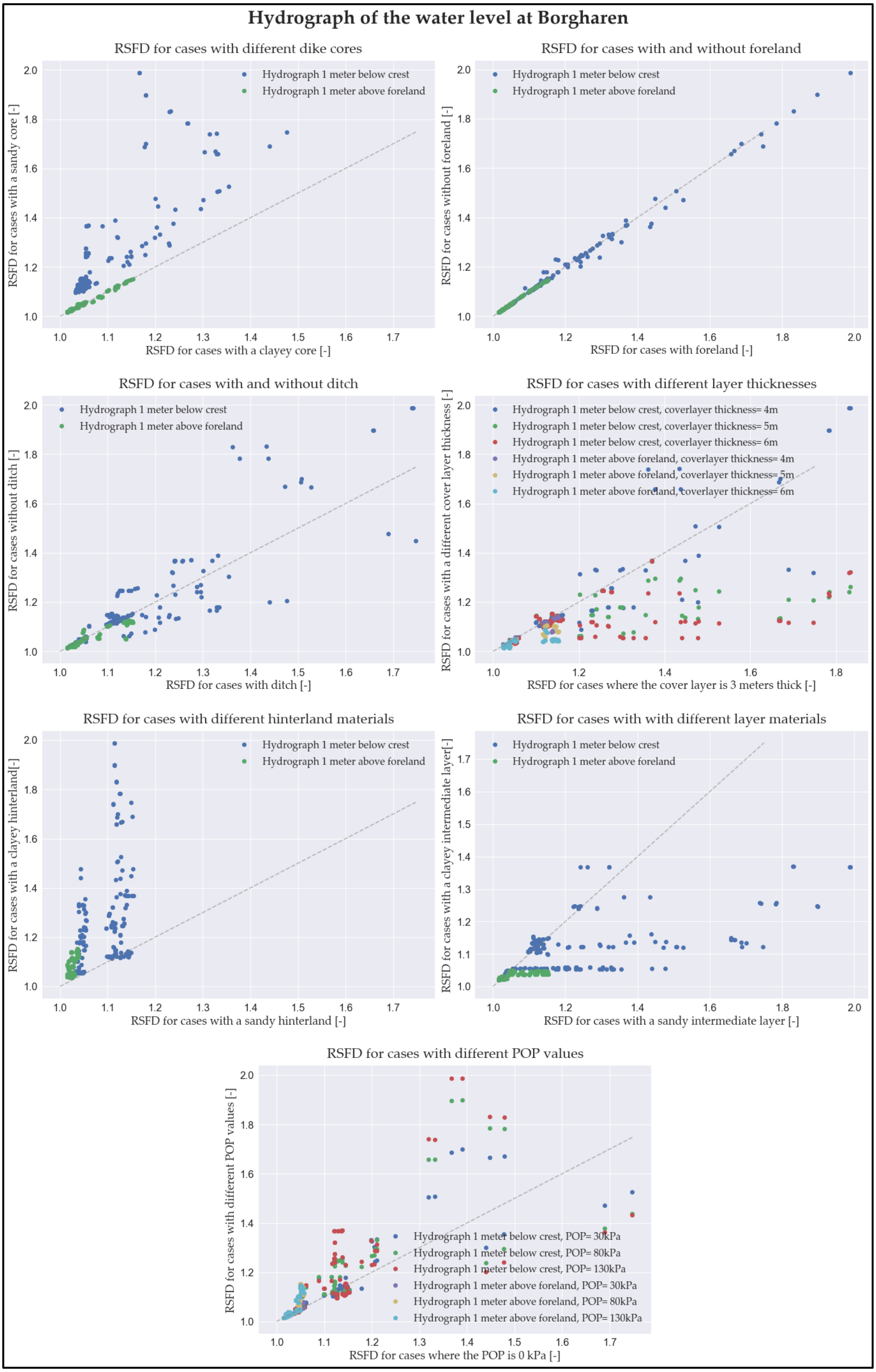
Hydrograph of the water level at Borgharen
RSFD for cases with different dike cores
RSFD for cases with a sandy core [-]
RSFD for cases with a clayey core [-]
Hydrograph 1 meter below crest
Hydrograph 1 meter above foreland
RSFD for cases with and without foreland
RSFD for cases without foreland [-]
RSFD for cases with foreland [-]
Hydrograph 1 meter below crest
Hydrograph 1 meter above foreland
RSFD for cases with and without ditch
RSFD for cases without ditch [-]
RSFD for cases with ditch [-]
Hydrograph 1 meter below crest
Hydrograph 1 meter above foreland
RSFD for cases with different layer thicknesses
RSFD for cases with a different cover layer thickness [-]
RSFD for cases where the cover layer is 3 meters thick [-]
Hydrograph 1 meter below crest, coverlayer thickness= 4m
Hydrograph 1 meter below crest, coverlayer thickness= 5m
Hydrograph 1 meter below crest, coverlayer thickness= 6m
Hydrograph 1 meter above foreland, coverlayer thickness= 4m
Hydrograph 1 meter above foreland, coverlayer thickness= 5m
Hydrograph 1 meter above foreland, coverlayer thickness= 6m
RSFD for cases with different hinterland materials
RSFD for cases with a clayey hinterland[-]
RSFD for cases with a sandy hinterland [-]
Hydrograph 1 meter below crest
Hydrograph 1 meter above foreland
RSFD for cases with with different layer materials
RSFD for cases with a clayey intermediate layer[-]
RSFD for cases with a sandy intermediate layer [-]
Hydrograph 1 meter below crest
Hydrograph 1 meter above foreland
RSFD for cases with different POP values
RSFD for cases with different POP values [-]
RSFD for cases where the POP is 0 kPa [-]
Hydrograph 1 meter below crest, POP= 30kPa
Hydrograph 1 meter below crest, POP= 80kPa
Hydrograph 1 meter below crest, POP= 130kPa
Hydrograph 1 meter above foreland, POP= 30kPa
Hydrograph 1 meter above foreland, POP= 80kPa
Hydrograph 1 meter above foreland, POP= 130kPa

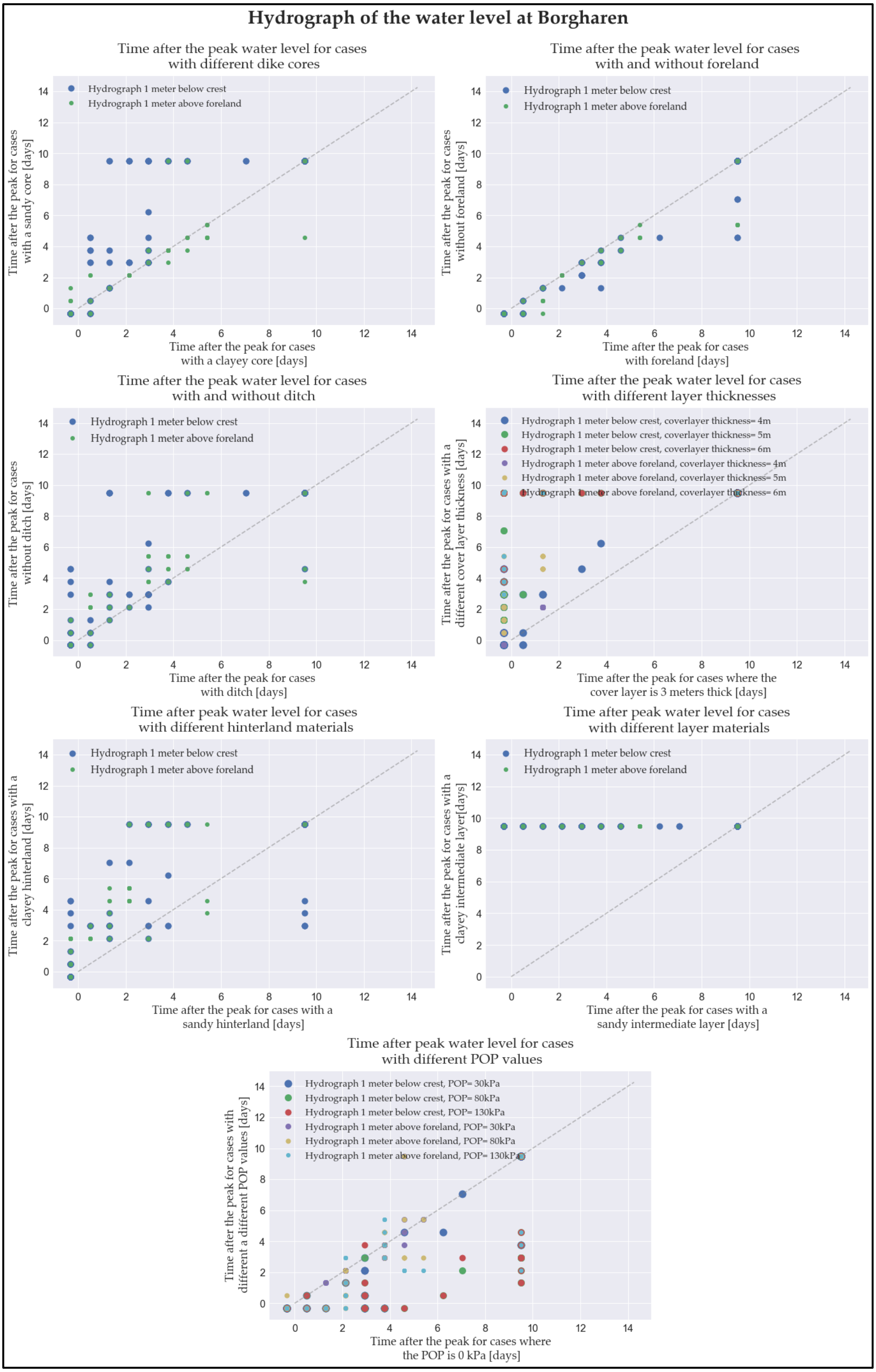
Hydrograph of the water level at Borgharen
Time after the peak water level for cases with different dike cores
Hydrograph 1 meter below crest
Hydrograph 1 meter above foreland
Time after the peak for cases with a sandy core [days]
Time after the peak for cases with a clayey core [days]
Time after the peak water level for cases with and without foreland
Time after the peak for cases without foreland [days]
Time after the peak for cases with foreland [days]
Time after the peak water level for cases with and without ditch
Time after the peak for case without ditch [days]
Time after the peak for cases with ditch [days]
Time after the peak water level for cases with different layer thicknesses
Hydrograph 1 meter below crest, coverlayer thickness= 4m
Hydrograph 1 meter below crest, coverlayer thickness= 5m
Hydrograph 1 meter below crest, coverlayer thickness= 6m
Hydrograph 1 meter above foreland, coverlayer thickness= 4m
Hydrograph 1 meter above foreland, coverlayer thickness= 5m
Hydrograph 1 meter above foreland, coverlayer thickness= 6m
Time after the peak for cases with a different cover layer thickness [days]
Time after the peak for cases where the cover layer is 3 meters thick [days]
Time after peak water level for cases with different hinterland materials
Time after the peak for cases with a clayey hinterland [days]
Time after the peak for cases with a sandy hinterland [days]
Time after peak water level for cases with different layer materials
Time after the peak for cases with a clayey intermediate layer[days]
Time after the peak for cases with a sandy intermediate layer [days]
Time after peak water level for cases with different POP values
Hydrograph 1 meter below crest, POP= 30kPa
Hydrograph 1 meter below crest, POP= 80kPa
Hydrograph 1 meter below crest, POP= 130kPa
Hydrograph 1 meter above foreland, POP= 30kPa
Hydrograph 1 meter above foreland, POP= 80kPa
Hydrograph 1 meter above foreland, POP= 130kPa
Time after the peak for cases with different a different POP values [days]
Time after the peak for cases where the POP is 0 kPa [days]

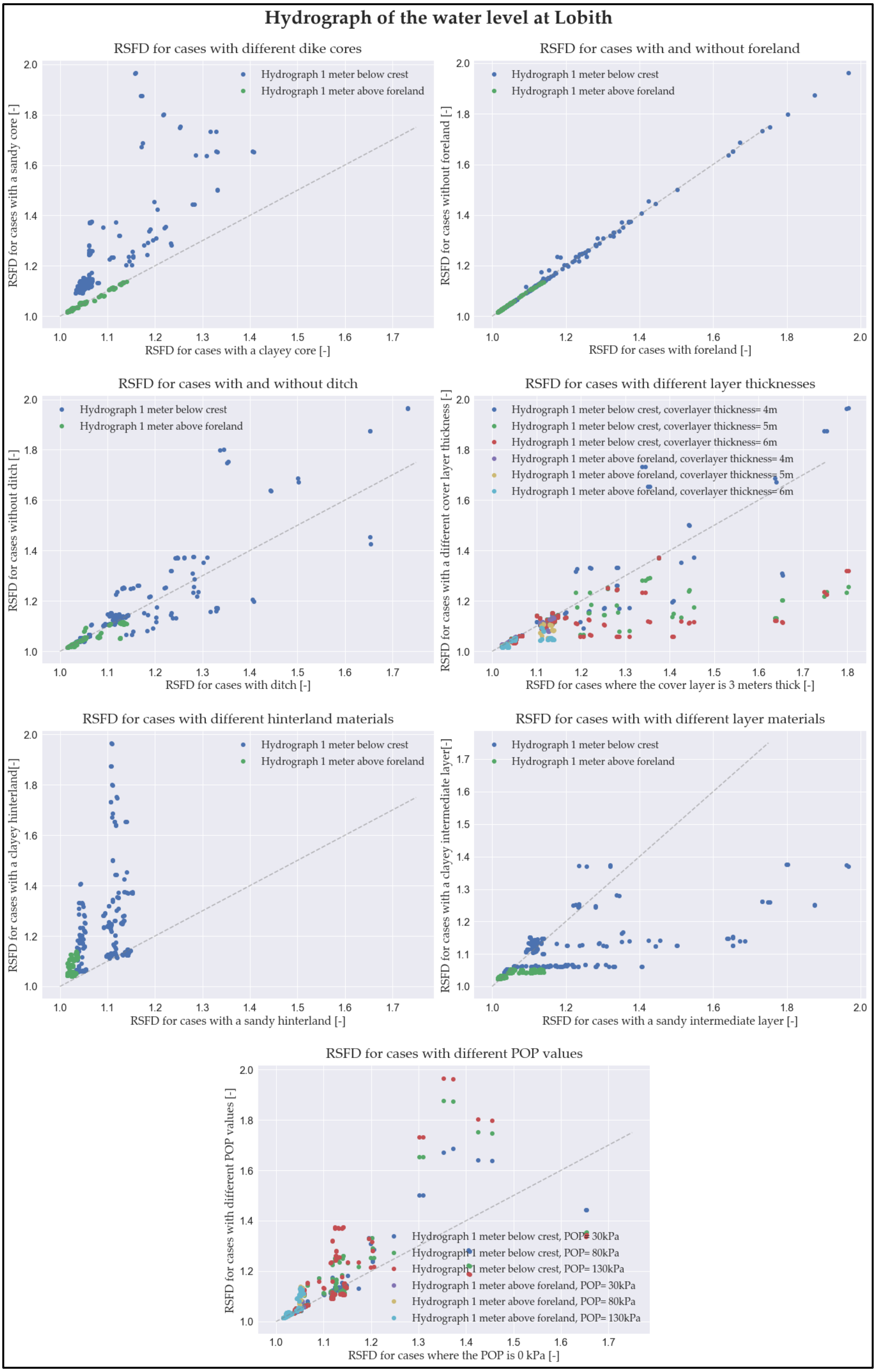
Hydrograph of the water level at Lobith
RSFD for cases with different dike cores
Hydrograph 1 meter below crest
Hydrograph 1 meter above foreland
RSFD for cases with a sandy core [-]
RSFD for cases with a clayey core [-]
RSFD for cases with and without foreland
Hydrograph 1 meter below crest
Hydrograph 1 meter above foreland
RSFD for cases without foreland [-]
RSFD for cases with foreland [-]
RSFD for cases with and without ditch
Hydrograph 1 meter below crest
Hydrograph 1 meter above foreland
RSFD for cases without ditch [-]
RSFD for cases with ditch [-]
RSFD for cases with different layer thicknesses
Hydrograph 1 meter below crest, coverlayer thickness= 4m
Hydrograph 1 meter below crest, coverlayer thickness= 5m
Hydrograph 1 meter below crest, coverlayer thickness= 6m
Hydrograph 1 meter above foreland, coverlayer thickness= 4m
Hydrograph 1 meter above foreland, coverlayer thickness= 5m
Hydrograph 1 meter above foreland, coverlayer thickness= 6m
RSFD for cases with a different cover layer thickness [-]
RSFD for cases where the cover layer is 3 meters thick [-]
RSFD for cases with different hinterland materials
Hydrograph 1 meter below crest
Hydrograph 1 meter above foreland
RSFD for cases with a clayey hinterland[-]
RSFD for cases with a sandy hinterland [-]
RSFD for cases with with different layer materials
Hydrograph 1 meter below crest
Hydrograph 1 meter above foreland
RSFD for cases with a clayey intermediate layer[-]
RSFD for cases with a sandy intermediate layer [-]
RSFD for cases with different POP values
Hydrograph 1 meter below crest, POP= 30kPa
Hydrograph 1 meter below crest, POP= 80kPa
Hydrograph 1 meter below crest, POP= 130kPa
Hydrograph 1 meter above foreland, POP= 30kPa
Hydrograph 1 meter above foreland, POP= 80kPa
Hydrograph 1 meter above foreland, POP= 130kPa
RSFD for cases with different POP values [-]
RSFD for cases where the POP is 0 kPa [-]

Hydrograph of the water level at Lobith

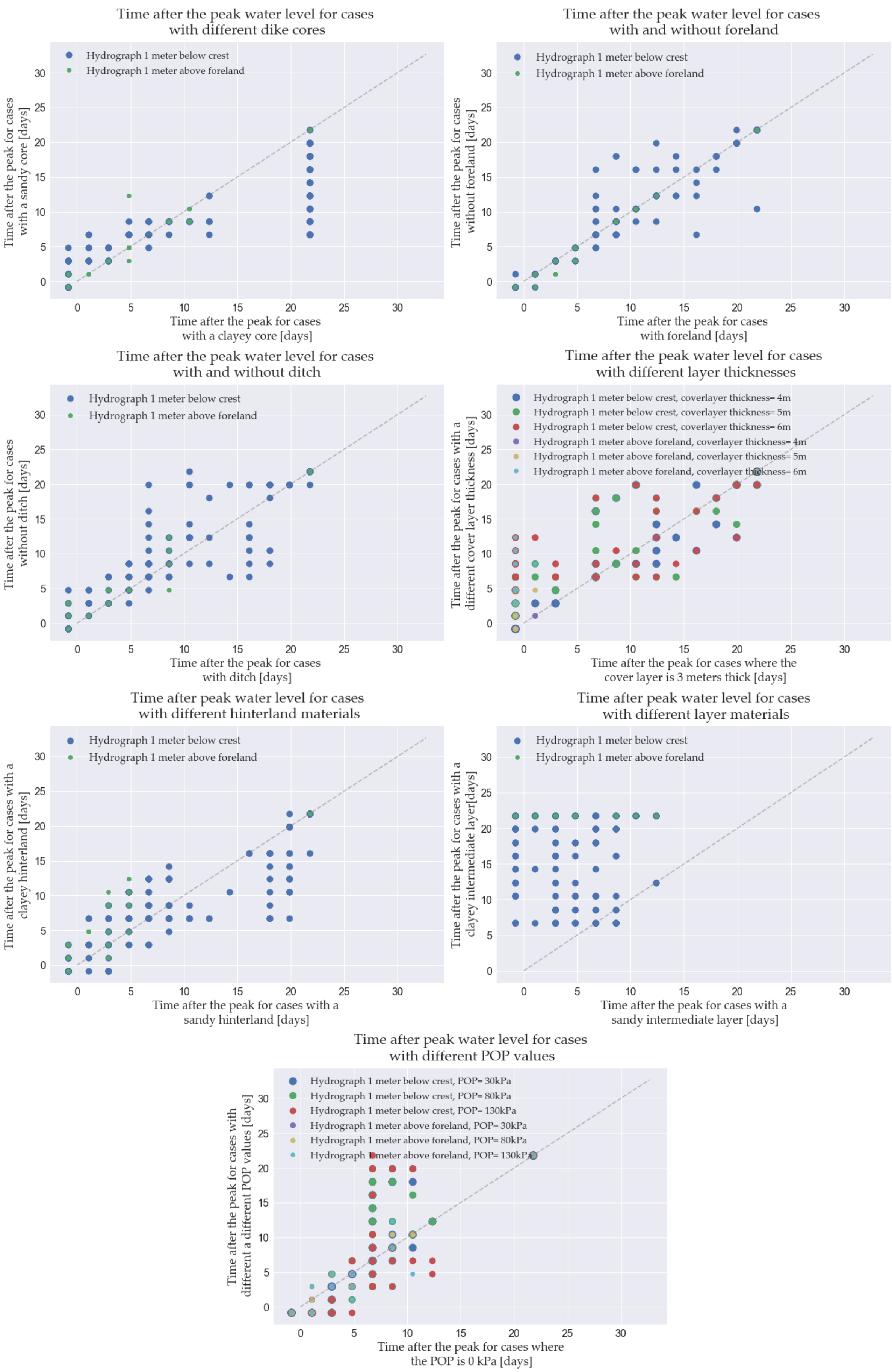

APPENDIX K. UNIVARIATE PROBABILITY DISTRIBUTIONS

The following Chapter is adopted from Pol (2014) - Hydrograph shape variability on the river Meuse

Generalized Extreme Value distribution (GEV):

$$F(x) = \exp\left(-\left(1 + k\,\frac{x-\mu}{\sigma}\right)^{-\frac{1}{k}}\right) \qquad k \neq 0$$

$$F(x) = \exp\left(-\exp\left(-\frac{x-\mu}{\sigma}\right)\right) \qquad k = 0$$

$$f(x) = \frac{1}{\sigma}\exp\left(-\left(1 + k\frac{x-\mu}{\sigma}\right)^{-\frac{1}{k}}\right)\left(1 + k\,\frac{x-\mu}{\sigma}\right)^{-1-\frac{1}{k}} \qquad k \neq 0$$

$$f(x) = \frac{1}{\sigma}\exp\left(-\left(\frac{x-\mu}{\sigma}\right) - \exp\left(-\left(\frac{x-\mu}{\sigma}\right)\right)\right) \qquad k = 0$$

k = shape, σ = scale, μ = location
If k = 0 this is a Gumbel distribution
If k < 0 this is a Weibull distribution
If k > 0 this is a Frechet distribution

Negative Weibull distribution:

$$F(x) = 1 - \exp\left(-\left(\frac{x}{a}\right)^{b}\right)$$

$$f(x) = \frac{b}{a}\left(\frac{x}{a}\right)^{b-1}\exp\left(-\left(\frac{x}{a}\right)^{b}\right)$$

a = scale, b = shape

Generalized Pareto Distribution (GPD):

$$F(x) = 1 - \left(1 + k\,\frac{x-\theta}{\sigma}\right)^{-\frac{1}{k}}$$

$$f(x) = \frac{1}{\sigma}\left(1 + k\,\frac{x-\theta}{\sigma}\right)^{-\frac{1}{k}-1}$$

k = shape, σ = scale, θ = threshold
If k = 0 and θ = 0, this is equivalent to exponential
If k > 0 and θ = σ/k, this is equivalent to Pareto

APPENDIX L. RESULTS CORRELATION ANALYSIS, SAFETY FACTOR

	Dike type 1		Dike type 2		Dike type 3		Dike type 4	
	Rhine	Meuse	Rhine	Meuse	Rhine	Meuse	Rhine	Meuse
h_{max}	-0,43	-0,38	-0,56	-0,4	-0,41	-0,14	-0,43	-0,38
D_0	0.12	-0.01	0.08	-0.06	0.12	0.03	0.11	-0.01
D_L	-0.76	-0.67	-0.87	-0.70	-0.76	-0.37	-0.76	-0.67
D_{50}	-0.63	-0.32	-0.62	-0.35	-0.64	-0.14	-0.64	-0.32
D_{85}	-0.65	-0.38	-0.71	-0.44	-0.63	-0.16	-0.65	-0.38
A_0	-0.08	0.04	-0.13	-0.01	-0.09	0.08	-0.09	0.04
A_L	-0.65	-0.67	-0.78	-0.71	-0.65	-0.34	-0.65	-0.67
A_{50}	-0.21	-0.09	-0.26	-0.14	-0.22	0.02	-0.22	-0.09
A_{85}	-0.10	-0.10	-0.18	-0.16	-0.11	0.02	-0.10	-0.1
RA_0	-0.73	-0.44	-0.71	-0.45	-0.73	-0.23	-0.74	-0.44
RA_L	0.53	-0.04	0.60	-0.09	0.52	-0.02	0.53	-0.04
RA_{50}	-0.07	-0.28	-0.11	-0.30	-0.05	-0.1	-0.06	-0.28
RA_{85}	0.59	0.00	0.57	0.00	0.55	0.07	0.59	0.00
n_l	0.20	0.04	0.20	0.00	0.19	0.03	0.20	0.04
$n_{50\%}$	0.15	0.06	0.10	0.02	0.15	-0.02	0.15	0.06
$n_{85\%}$	0.26	0.06	0.20	0.05	0.22	0.04	0.27	0.06

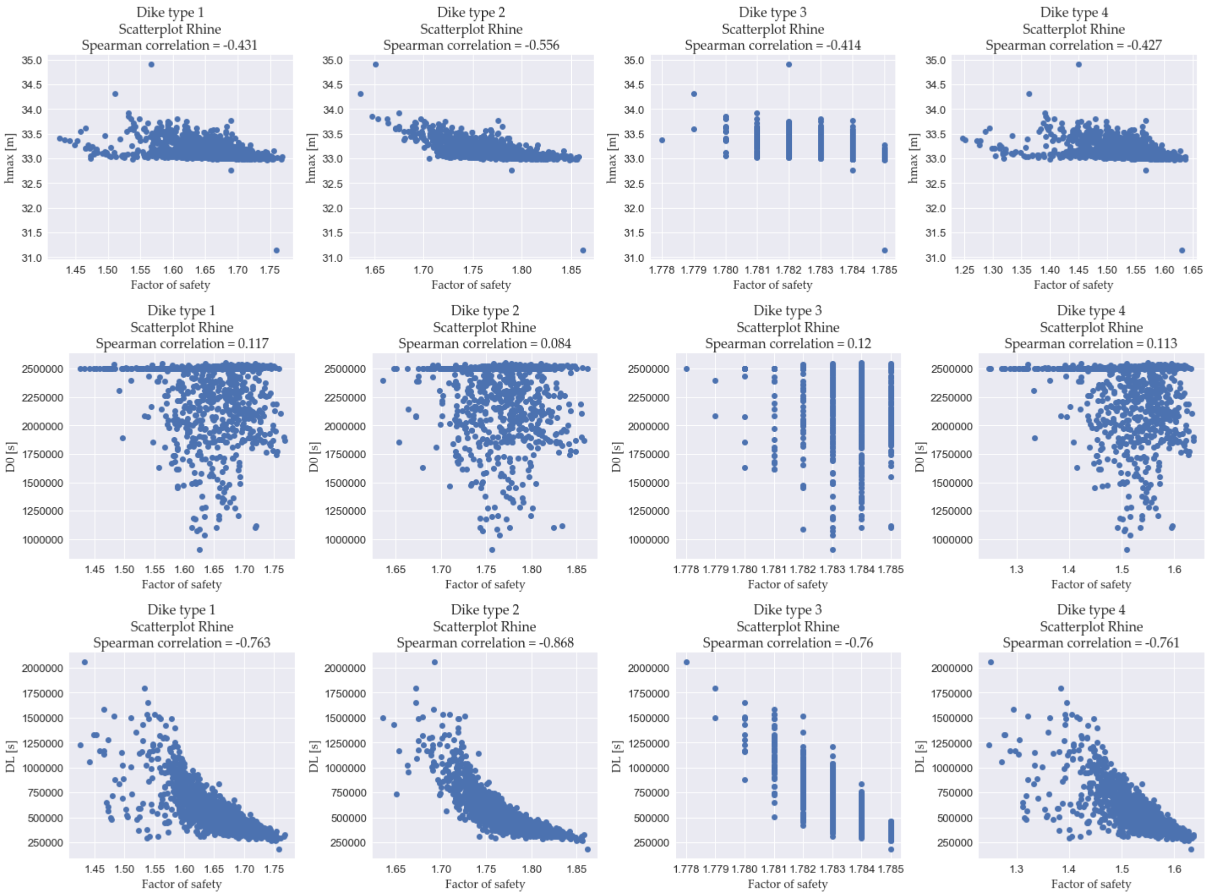

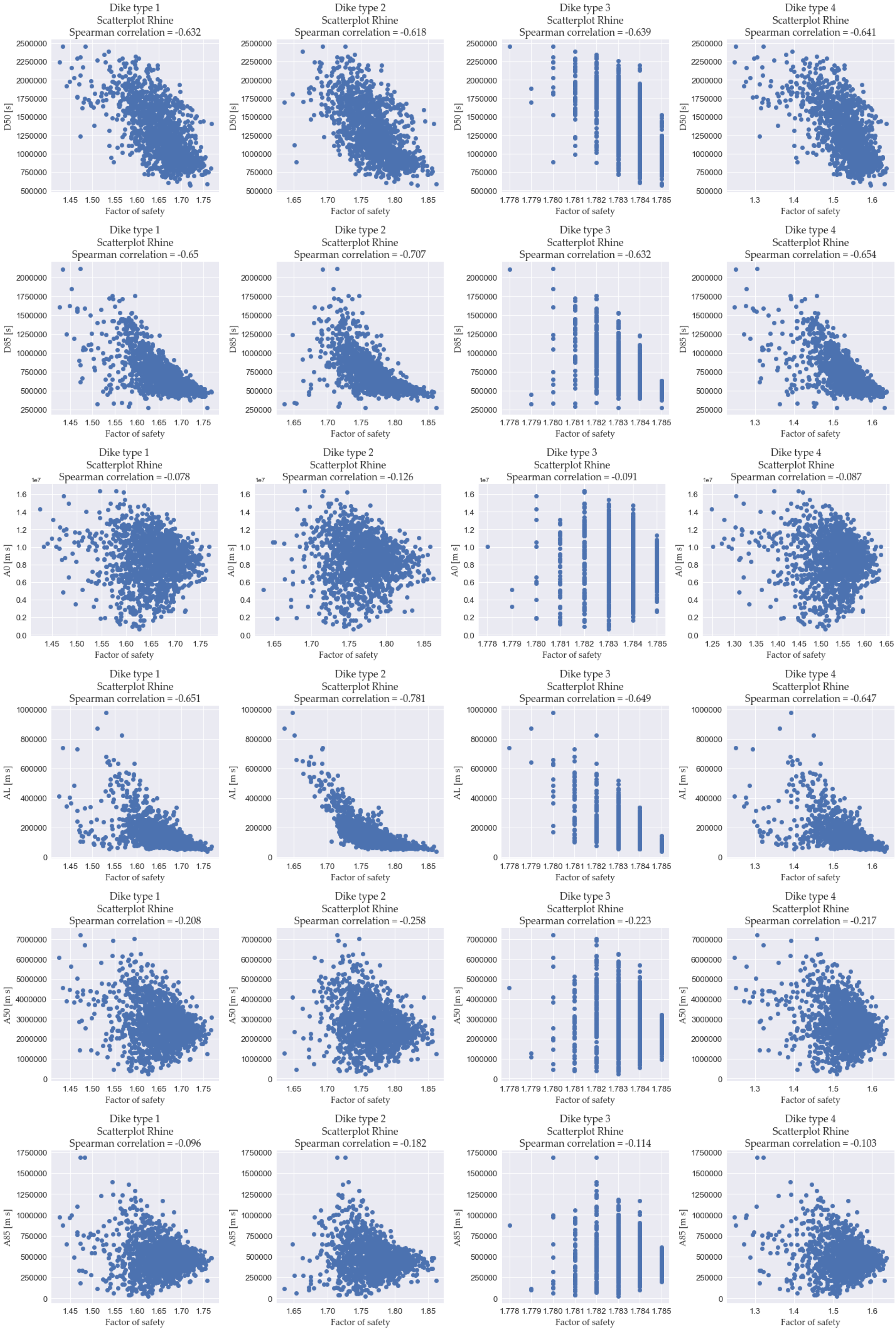
Dike type 1
Scatterplot Rhine
Spearman correlation = -0.632
Dike type 2
Scatterplot Rhine
Spearman correlation = -0.618
Dike type 3
Scatterplot Rhine
Spearman correlation = -0.639
Dike type 4
Scatterplot Rhine
Spearman correlation = -0.641
D50 [s]
Factor of safety
Dike type 1
Scatterplot Rhine
Spearman correlation = -0.65
Dike type 2
Scatterplot Rhine
Spearman correlation = -0.707
Dike type 3
Scatterplot Rhine
Spearman correlation = -0.632
Dike type 4
Scatterplot Rhine
Spearman correlation = -0.654
D85 [s]
Factor of safety
Dike type 1
Scatterplot Rhine
Spearman correlation = -0.078
Dike type 2
Scatterplot Rhine
Spearman correlation = -0.126
Dike type 3
Scatterplot Rhine
Spearman correlation = -0.091
Dike type 4
Scatterplot Rhine
Spearman correlation = -0.087
1e7
A0 [m s]
Factor of safety
Dike type 1
Scatterplot Rhine
Spearman correlation = -0.651
Dike type 2
Scatterplot Rhine
Spearman correlation = -0.781
Dike type 3
Scatterplot Rhine
Spearman correlation = -0.649
Dike type 4
Scatterplot Rhine
Spearman correlation = -0.647
AL [m s]
Factor of safety
Dike type 1
Scatterplot Rhine
Spearman correlation = -0.208
Dike type 2
Scatterplot Rhine
Spearman correlation = -0.258
Dike type 3
Scatterplot Rhine
Spearman correlation = -0.223
Dike type 4
Scatterplot Rhine
Spearman correlation = -0.217
A50 [m s]
Factor of safety
Dike type 1
Scatterplot Rhine
Spearman correlation = -0.096
Dike type 2
Scatterplot Rhine
Spearman correlation = -0.182
Dike type 3
Scatterplot Rhine
Spearman correlation = -0.114
Dike type 4
Scatterplot Rhine
Spearman correlation = -0.103
A85 [m s]
Factor of safety

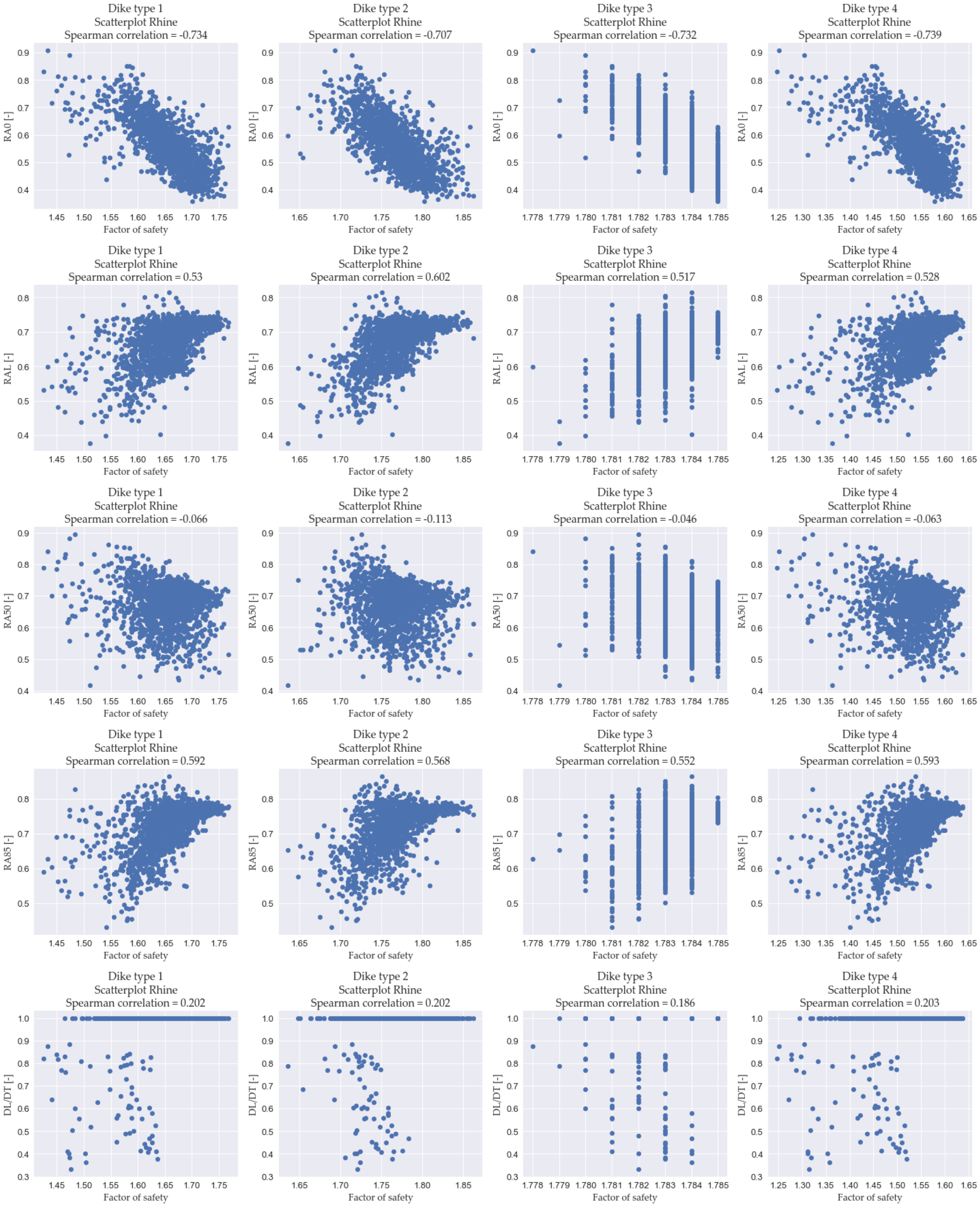
Dike type 1
Scatterplot Rhine
Spearman correlation = -0.734
Dike type 2
Scatterplot Rhine
Spearman correlation = -0.707
Dike type 3
Scatterplot Rhine
Spearman correlation = -0.732
Dike type 4
Scatterplot Rhine
Spearman correlation = -0.739
RA0 [-]
Factor of safety
Dike type 1
Scatterplot Rhine
Spearman correlation = 0.53
Dike type 2
Scatterplot Rhine
Spearman correlation = 0.602
Dike type 3
Scatterplot Rhine
Spearman correlation = 0.517
Dike type 4
Scatterplot Rhine
Spearman correlation = 0.528
RAL [-]
Factor of safety
Dike type 1
Scatterplot Rhine
Spearman correlation = -0.066
Dike type 2
Scatterplot Rhine
Spearman correlation = -0.113
Dike type 3
Scatterplot Rhine
Spearman correlation = -0.046
Dike type 4
Scatterplot Rhine
Spearman correlation = -0.063
RA50 [-]
Factor of safety
Dike type 1
Scatterplot Rhine
Spearman correlation = 0.592
Dike type 2
Scatterplot Rhine
Spearman correlation = 0.568
Dike type 3
Scatterplot Rhine
Spearman correlation = 0.552
Dike type 4
Scatterplot Rhine
Spearman correlation = 0.593
RA85 [-]
Factor of safety
Dike type 1
Scatterplot Rhine
Spearman correlation = 0.202
Dike type 2
Scatterplot Rhine
Spearman correlation = 0.202
Dike type 3
Scatterplot Rhine
Spearman correlation = 0.186
Dike type 4
Scatterplot Rhine
Spearman correlation = 0.203
DL/DT [-]
Factor of safety

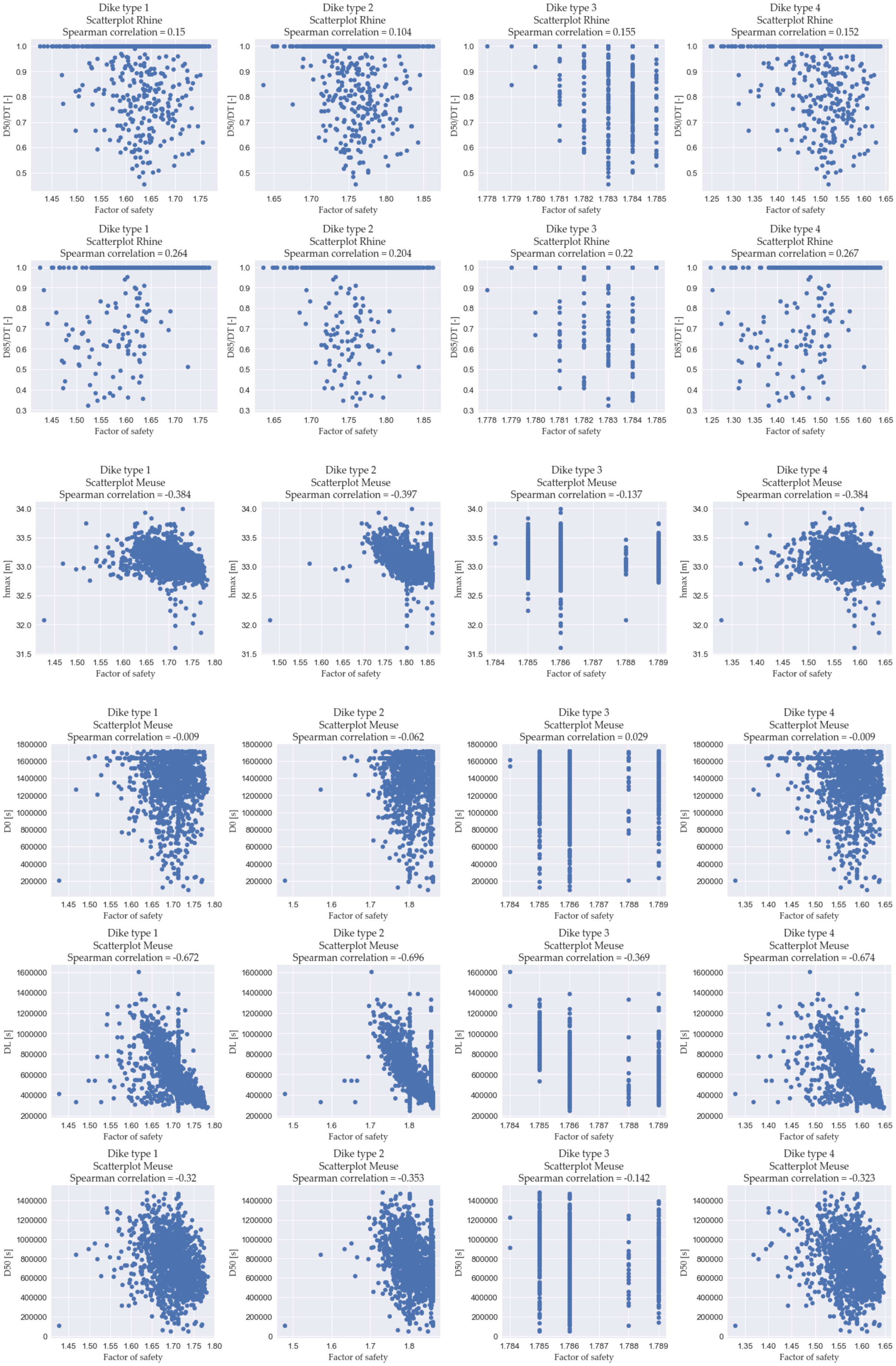
Dike type 1
Scatterplot Rhine
Spearman correlation = 0.15
Dike type 2
Scatterplot Rhine
Spearman correlation = 0.104
Dike type 3
Scatterplot Rhine
Spearman correlation = 0.155
Dike type 4
Scatterplot Rhine
Spearman correlation = 0.152
D50/DT [-]
Factor of safety
Dike type 1
Scatterplot Rhine
Spearman correlation = 0.264
Dike type 2
Scatterplot Rhine
Spearman correlation = 0.204
Dike type 3
Scatterplot Rhine
Spearman correlation = 0.22
Dike type 4
Scatterplot Rhine
Spearman correlation = 0.267
D85/DT [-]
Factor of safety
Dike type 1
Scatterplot Meuse
Spearman correlation = -0.384
Dike type 2
Scatterplot Meuse
Spearman correlation = -0.397
Dike type 3
Scatterplot Meuse
Spearman correlation = -0.137
Dike type 4
Scatterplot Meuse
Spearman correlation = -0.384
hmax [m]
Factor of safety
Dike type 1
Scatterplot Meuse
Spearman correlation = -0.009
Dike type 2
Scatterplot Meuse
Spearman correlation = -0.062
Dike type 3
Scatterplot Meuse
Spearman correlation = 0.029
Dike type 4
Scatterplot Meuse
Spearman correlation = -0.009
D0 [s]
Factor of safety
Dike type 1
Scatterplot Meuse
Spearman correlation = -0.672
Dike type 2
Scatterplot Meuse
Spearman correlation = -0.696
Dike type 3
Scatterplot Meuse
Spearman correlation = -0.369
Dike type 4
Scatterplot Meuse
Spearman correlation = -0.674
DL [s]
Factor of safety
Dike type 1
Scatterplot Meuse
Spearman correlation = -0.32
Dike type 2
Scatterplot Meuse
Spearman correlation = -0.353
Dike type 3
Scatterplot Meuse
Spearman correlation = -0.142
Dike type 4
Scatterplot Meuse
Spearman correlation = -0.323
D50 [s]
Factor of safety

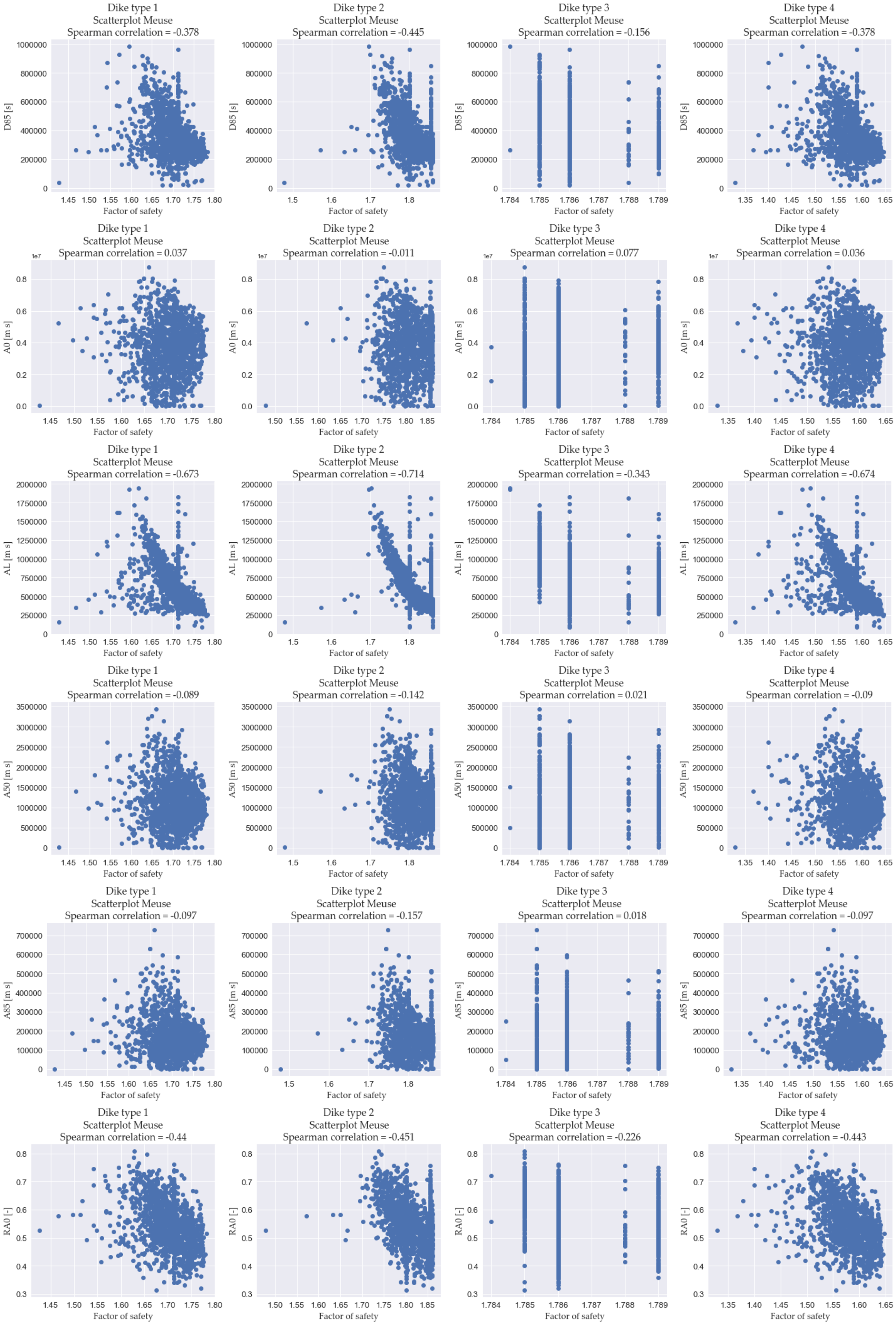
Dike type 1
Scatterplot Meuse
Spearman correlation = -0.378
D85 [s]
Factor of safety
Dike type 2
Scatterplot Meuse
Spearman correlation = -0.445
D85 [s]
Factor of safety
Dike type 3
Scatterplot Meuse
Spearman correlation = -0.156
D85 [s]
Factor of safety
Dike type 4
Scatterplot Meuse
Spearman correlation = -0.378
D85 [s]
Factor of safety
Dike type 1
Scatterplot Meuse
Spearman correlation = 0.037
A0 [m s]
Factor of safety
Dike type 2
Scatterplot Meuse
Spearman correlation = -0.011
A0 [m s]
Factor of safety
Dike type 3
Scatterplot Meuse
Spearman correlation = 0.077
A0 [m s]
Factor of safety
Dike type 4
Scatterplot Meuse
Spearman correlation = 0.036
A0 [m s]
Factor of safety
Dike type 1
Scatterplot Meuse
Spearman correlation = -0.673
AL [m s]
Factor of safety
Dike type 2
Scatterplot Meuse
Spearman correlation = -0.714
AL [m s]
Factor of safety
Dike type 3
Scatterplot Meuse
Spearman correlation = -0.343
AL [m s]
Factor of safety
Dike type 4
Scatterplot Meuse
Spearman correlation = -0.674
AL [m s]
Factor of safety
Dike type 1
Scatterplot Meuse
Spearman correlation = -0.089
A50 [m s]
Factor of safety
Dike type 2
Scatterplot Meuse
Spearman correlation = -0.142
A50 [m s]
Factor of safety
Dike type 3
Scatterplot Meuse
Spearman correlation = 0.021
A50 [m s]
Factor of safety
Dike type 4
Scatterplot Meuse
Spearman correlation = -0.09
A50 [m s]
Factor of safety
Dike type 1
Scatterplot Meuse
Spearman correlation = -0.097
A85 [m s]
Factor of safety
Dike type 2
Scatterplot Meuse
Spearman correlation = -0.157
A85 [m s]
Factor of safety
Dike type 3
Scatterplot Meuse
Spearman correlation = 0.018
A85 [m s]
Factor of safety
Dike type 4
Scatterplot Meuse
Spearman correlation = -0.097
A85 [m s]
Factor of safety
Dike type 1
Scatterplot Meuse
Spearman correlation = -0.44
RA0 [-]
Factor of safety
Dike type 2
Scatterplot Meuse
Spearman correlation = -0.451
RA0 [-]
Factor of safety
Dike type 3
Scatterplot Meuse
Spearman correlation = -0.226
RA0 [-]
Factor of safety
Dike type 4
Scatterplot Meuse
Spearman correlation = -0.443
RA0 [-]
Factor of safety

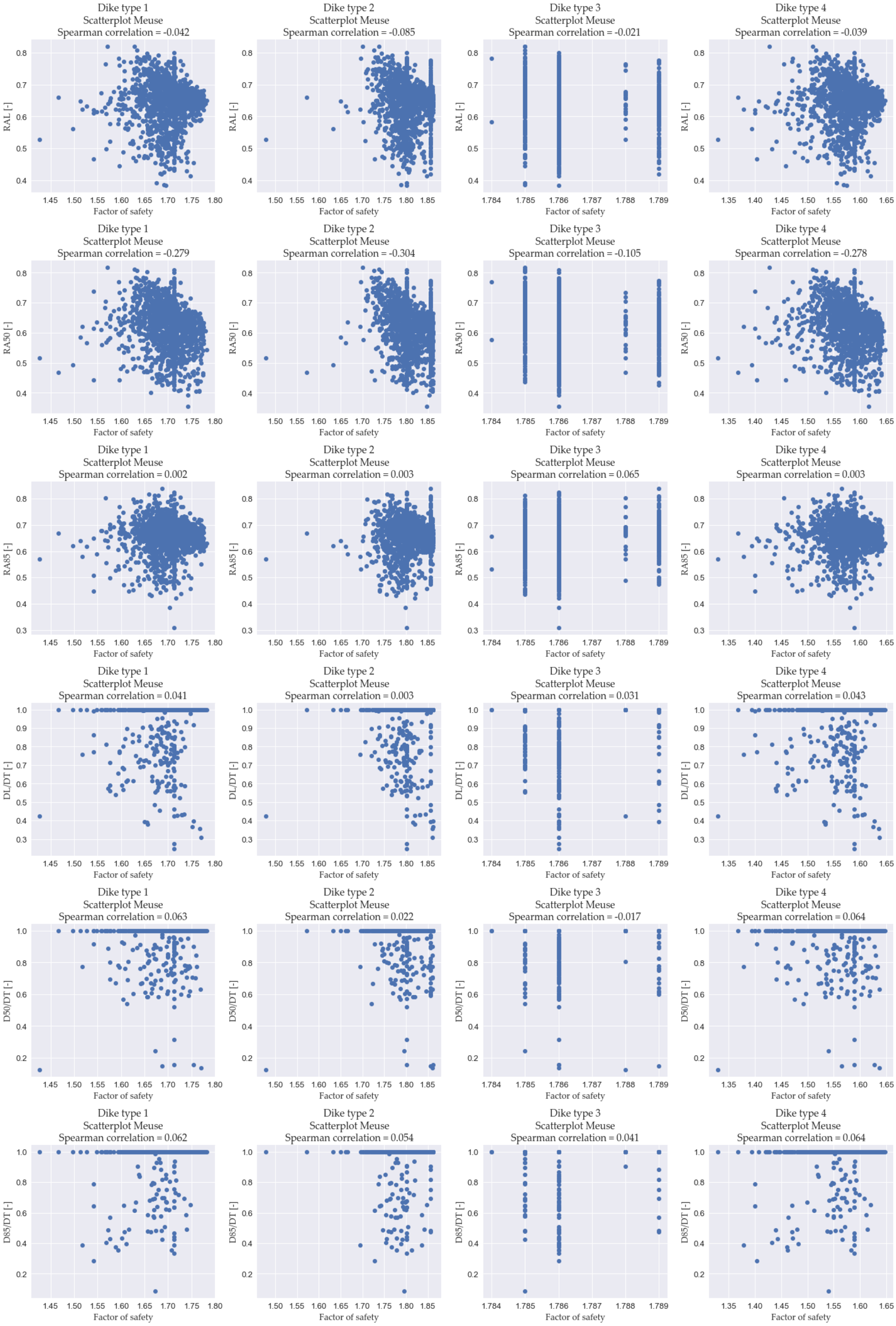
Dike type 1
Scatterplot Meuse
Spearman correlation = -0.042
RAL [-]
Factor of safety
Dike type 2
Scatterplot Meuse
Spearman correlation = -0.085
RAL [-]
Factor of safety
Dike type 3
Scatterplot Meuse
Spearman correlation = -0.021
RAL [-]
Factor of safety
Dike type 4
Scatterplot Meuse
Spearman correlation = -0.039
RAL [-]
Factor of safety
Dike type 1
Scatterplot Meuse
Spearman correlation = -0.279
RA50 [-]
Factor of safety
Dike type 2
Scatterplot Meuse
Spearman correlation = -0.304
RA50 [-]
Factor of safety
Dike type 3
Scatterplot Meuse
Spearman correlation = -0.105
RA50 [-]
Factor of safety
Dike type 4
Scatterplot Meuse
Spearman correlation = -0.278
RA50 [-]
Factor of safety
Dike type 1
Scatterplot Meuse
Spearman correlation = 0.002
RA85 [-]
Factor of safety
Dike type 2
Scatterplot Meuse
Spearman correlation = 0.003
RA85 [-]
Factor of safety
Dike type 3
Scatterplot Meuse
Spearman correlation = 0.065
RA85 [-]
Factor of safety
Dike type 4
Scatterplot Meuse
Spearman correlation = 0.003
RA85 [-]
Factor of safety
Dike type 1
Scatterplot Meuse
Spearman correlation = 0.041
DL/DT [-]
Factor of safety
Dike type 2
Scatterplot Meuse
Spearman correlation = 0.003
DL/DT [-]
Factor of safety
Dike type 3
Scatterplot Meuse
Spearman correlation = 0.031
DL/DT [-]
Factor of safety
Dike type 4
Scatterplot Meuse
Spearman correlation = 0.043
DL/DT [-]
Factor of safety
Dike type 1
Scatterplot Meuse
Spearman correlation = 0.063
D50/DT [-]
Factor of safety
Dike type 2
Scatterplot Meuse
Spearman correlation = 0.022
D50/DT [-]
Factor of safety
Dike type 3
Scatterplot Meuse
Spearman correlation = -0.017
D50/DT [-]
Factor of safety
Dike type 4
Scatterplot Meuse
Spearman correlation = 0.064
D50/DT [-]
Factor of safety
Dike type 1
Scatterplot Meuse
Spearman correlation = 0.062
D85/DT [-]
Factor of safety
Dike type 2
Scatterplot Meuse
Spearman correlation = 0.054
D85/DT [-]
Factor of safety
Dike type 3
Scatterplot Meuse
Spearman correlation = 0.041
D85/DT [-]
Factor of safety
Dike type 4
Scatterplot Meuse
Spearman correlation = 0.064
D85/DT [-]
Factor of safety

APPENDIX M. RESULTS CORRELATION ANALYSIS, VARIABLES

TABLE M.1: SPEARMAN CORRELATION BETWEEN LOCAL SHAPE VARIABLES AT LOBITH

	h_{max}	D_0	D_L	D_{50}	D_{85}	A_0	A_L	A_{50}	A_{85}	RA_0	RA_L	RA_{50}	RA_{85}	n_l	n_{50}	n_{85}
h_{max}	1.0															
D_0	-0.02	1.0														
D_L	0.66	-0.05	1.0													
D_{50}	0.25	0.26	0.57	1.0												
D_{85}	0.37	0.19	0.81	0.74	1.0											
A_0	0.12	0.62	0.22	0.63	0.54	1.0										
A_L	0.88	-0.04	0.92	0.44	0.65	0.19	1.0									
A_{50}	0.20	0.51	0.39	0.71	0.71	0.95	0.32	1.0								
A_{85}	0.15	0.50	0.4	0.52	0.69	0.87	0.3	0.93	1.0							
RA_0	0.25	-0.11	0.63	0.81	0.67	0.4	0.48	0.5	0.35	1.0						
RA_L	-0.75	0.02	-0.66	-0.35	-0.45	-0.13	-0.75	-0.22	-0.14	-0.37	1.0					
RA_{50}	0.08	-0.13	0.3	-0.26	0.32	-0.09	0.22	0.06	0.25	-0.09	-0.09	1.0				
RA_{85}	-0.55	-0.57	-0.43	-0.37	-0.36	-0.0	-0.51	-0.09	0.1	-0.42	0.75	0.07	1.0			
n_l	-0.12	-0.12	-0.23	-0.14	-0.18	-0.08	-0.19	-0.11	-0.1	-0.18	0.21	-0.09	0.13	1.0		
$n_{50\%}$	-0.01	-0.01	-0.03	-0.09	0.09	0.07	-0.02	0.12	0.15	-0.15	-0.01	0.33	0.06	0.05	1.0	
$n_{85\%}$	-0.05	-0.04	-0.18	-0.25	-0.29	-0.17	-0.13	-0.23	-0.18	-0.25	0.12	-0.09	0.18	0.11	-0.01	1.0

TABLE M.2: SPEARMAN CORRELATION BETWEEN LOCAL SHAPE VARIABLES AT BORGHAREN

	h_{max}	D_0	D_L	D_{50}	D_{85}	A_0	A_L	A_{50}	A_{85}	RA_0	RA_L	RA_{50}	RA_{85}	n_L	n_{50}	n_{85}
h_{max}	1.0															
D_0	0.06	1.0														
D_L	0.37	0.10	1.0													
D_{50}	0.18	0.58	0.58	1.0												
D_{85}	0.32	0.47	0.62	0.78	1.0											
A_0	0.11	0.73	0.13	0.76	0.63	1.0										
A_L	0.64	0.13	0.9	0.54	0.72	0.17	1.0									
A_{50}	0.18	0.66	0.32	0.84	0.79	0.95	0.36	1.0								
A_{85}	0.27	0.61	0.28	0.71	0.84	0.87	0.42	0.94	1.0							
RA_0	0.21	0.02	0.7	0.73	0.65	0.38	0.65	0.53	0.46	1.0						
RA_L	0.28	0.08	-0.05	0.03	0.44	0.13	0.26	0.21	0.46	0.07	1.0					
RA_{50}	0.27	-0.15	0.34	-0.07	0.45	-0.11	0.47	0.08	0.25	0.2	0.57	1.0				
RA_{85}	0.30	0.05	-0.07	-0.04	0.1	0.06	0.11	0.06	0.26	-0.03	0.48	0.21	1.0			
n_l	0.10	0.10	-0.05	0.07	0.19	0.11	0.07	0.14	0.19	-0.02	0.27	0.16	0.06	1.0		
$n_{50\%}$	0.03	0.03	-0.02	0.0	0.07	0.07	0.02	0.09	0.1	-0.03	0.09	0.15	0.01	0.12	1.0	
$n_{85\%}$	0.03	0.03	-0.14	-0.07	-0.06	-0.0	-0.1	-0.04	0.01	-0.13	0.07	-0.04	0.12	0.08	0.07	1.0

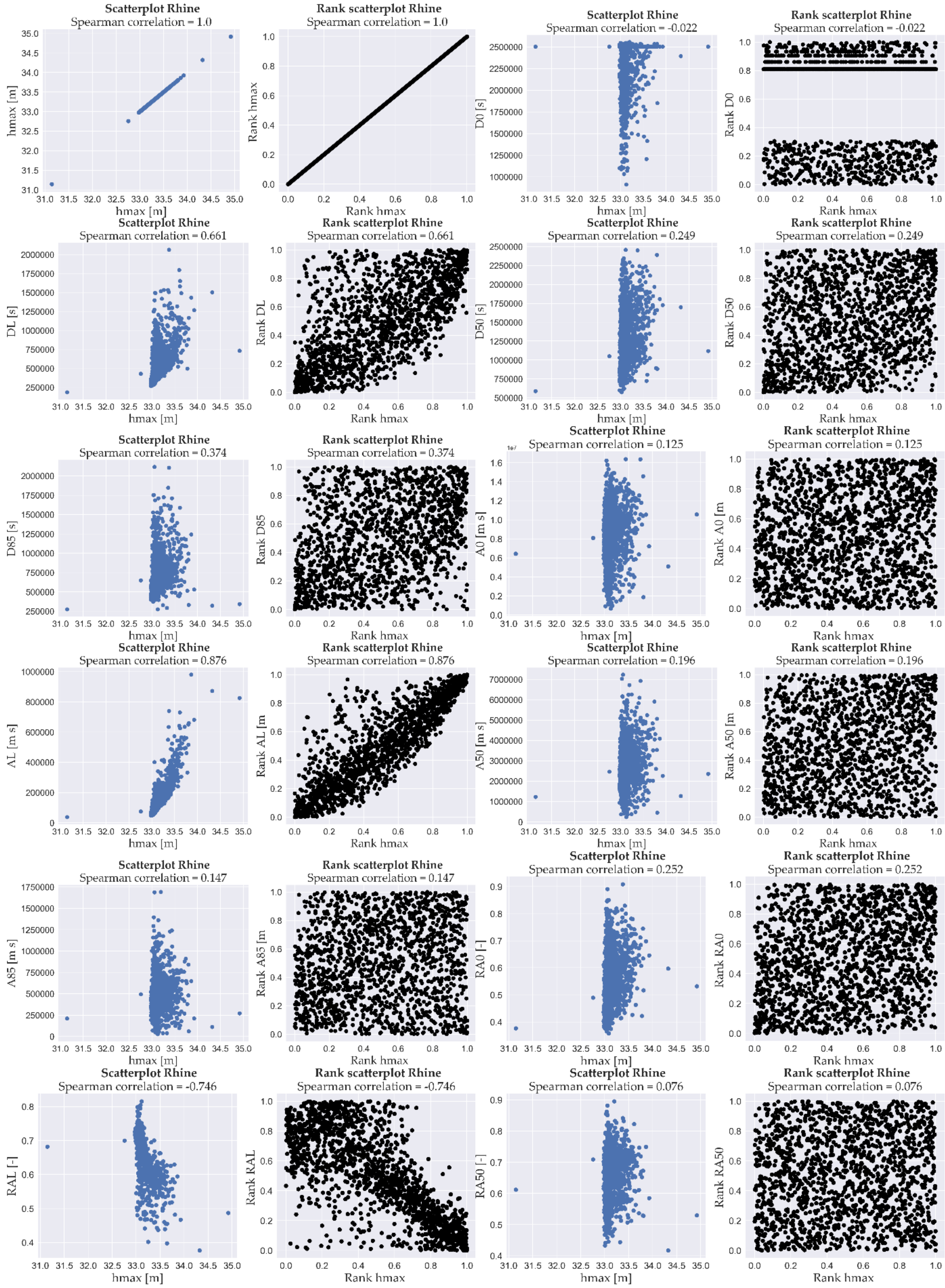
Scatterplot Rhine
Spearman correlation = 1.0
hmax [m]
hmax [m]
Rank scatterplot Rhine
Spearman correlation = 1.0
Rank hmax
Rank hmax
Scatterplot Rhine
Spearman correlation = -0.022
D0 [s]
hmax [m]
Rank scatterplot Rhine
Spearman correlation = -0.022
Rank D0
Rank hmax
Scatterplot Rhine
Spearman correlation = 0.661
DL [s]
hmax [m]
Rank scatterplot Rhine
Spearman correlation = 0.661
Rank DL
Rank hmax
Scatterplot Rhine
Spearman correlation = 0.249
D50 [s]
hmax [m]
Rank scatterplot Rhine
Spearman correlation = 0.249
Rank D50
Rank hmax
Scatterplot Rhine
Spearman correlation = 0.374
D85 [s]
hmax [m]
Rank scatterplot Rhine
Spearman correlation = 0.374
Rank D85
Rank hmax
Scatterplot Rhine
Spearman correlation = 0.125
A0 [m s]
hmax [m]
Rank scatterplot Rhine
Spearman correlation = 0.125
Rank A0 [m
Rank hmax
Scatterplot Rhine
Spearman correlation = 0.876
AL [m s]
hmax [m]
Rank scatterplot Rhine
Spearman correlation = 0.876
Rank AL [m
Rank hmax
Scatterplot Rhine
Spearman correlation = 0.196
A50 [m s]
hmax [m]
Rank scatterplot Rhine
Spearman correlation = 0.196
Rank A50 [m
Rank hmax
Scatterplot Rhine
Spearman correlation = 0.147
A85 [m s]
hmax [m]
Rank scatterplot Rhine
Spearman correlation = 0.147
Rank A85 [m
Rank hmax
Scatterplot Rhine
Spearman correlation = 0.252
RA0 [-]
hmax [m]
Rank scatterplot Rhine
Spearman correlation = 0.252
Rank RA0
Rank hmax
Scatterplot Rhine
Spearman correlation = -0.746
RAL [-]
hmax [m]
Rank scatterplot Rhine
Spearman correlation = -0.746
Rank RAL
Rank hmax
Scatterplot Rhine
Spearman correlation = 0.076
RA50 [-]
hmax [m]
Rank scatterplot Rhine
Spearman correlation = 0.076
Rank RA50
Rank hmax

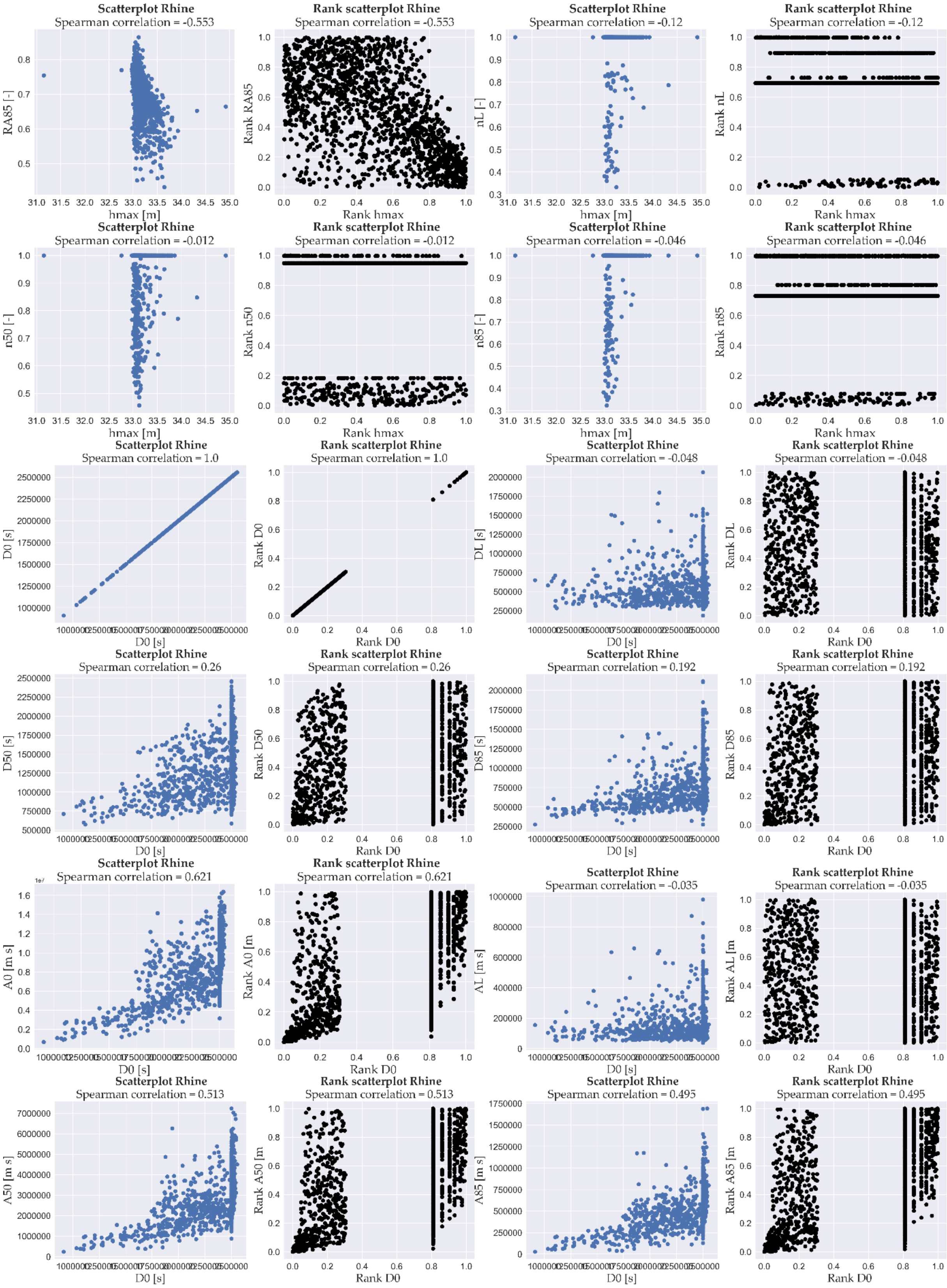
Scatterplot Rhine
Spearman correlation = -0.553
Rank scatterplot Rhine
Spearman correlation = -0.553
Scatterplot Rhine
Spearman correlation = -0.12
Rank scatterplot Rhine
Spearman correlation = -0.12
RA85 [-]
Rank RA85
nL [-]
Rank nL
hmax [m]
Rank hmax
Scatterplot Rhine
Spearman correlation = -0.012
Rank scatterplot Rhine
Spearman correlation = -0.012
Scatterplot Rhine
Spearman correlation = -0.046
Rank scatterplot Rhine
Spearman correlation = -0.046
n50 [-]
Rank n50
n85 [-]
Rank n85
Scatterplot Rhine
Spearman correlation = 1.0
Rank scatterplot Rhine
Spearman correlation = 1.0
Scatterplot Rhine
Spearman correlation = -0.048
Rank scatterplot Rhine
Spearman correlation = -0.048
D0 [s]
Rank D0
DL [s]
Rank DL
Scatterplot Rhine
Spearman correlation = 0.26
Rank scatterplot Rhine
Spearman correlation = 0.26
Scatterplot Rhine
Spearman correlation = 0.192
Rank scatterplot Rhine
Spearman correlation = 0.192
D50 [s]
Rank D50
D85 [s]
Rank D85
Scatterplot Rhine
Spearman correlation = 0.621
Rank scatterplot Rhine
Spearman correlation = 0.621
Scatterplot Rhine
Spearman correlation = -0.035
Rank scatterplot Rhine
Spearman correlation = -0.035
A0 [m s]
Rank A0 [m
AL [m s]
Rank AL [m
Scatterplot Rhine
Spearman correlation = 0.513
Rank scatterplot Rhine
Spearman correlation = 0.513
Scatterplot Rhine
Spearman correlation = 0.495
Rank scatterplot Rhine
Spearman correlation = 0.495
A50 [m s]
Rank A50 [m
A85 [m s]
Rank A85 [m

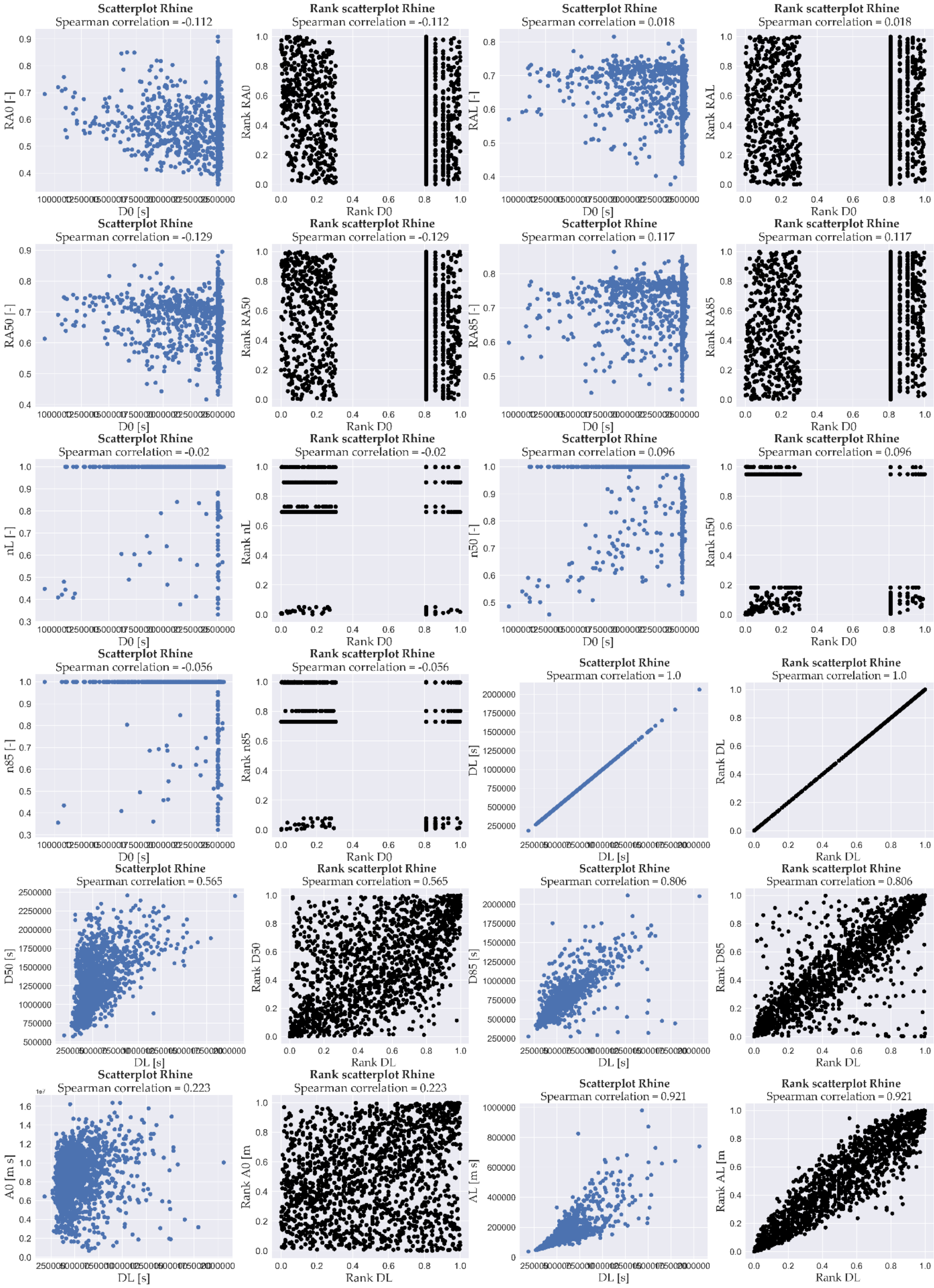
Scatterplot Rhine
Spearman correlation = -0.112
RA0 [-]
D0 [s]
Rank scatterplot Rhine
Spearman correlation = -0.112
Rank RA0
Rank D0
Scatterplot Rhine
Spearman correlation = 0.018
RAL [-]
D0 [s]
Rank scatterplot Rhine
Spearman correlation = 0.018
Rank RAL
Rank D0
Scatterplot Rhine
Spearman correlation = -0.129
RA50 [-]
D0 [s]
Rank scatterplot Rhine
Spearman correlation = -0.129
Rank RA50
Rank D0
Scatterplot Rhine
Spearman correlation = 0.117
RA85 [-]
D0 [s]
Rank scatterplot Rhine
Spearman correlation = 0.117
Rank RA85
Rank D0
Scatterplot Rhine
Spearman correlation = -0.02
nL [-]
D0 [s]
Rank scatterplot Rhine
Spearman correlation = -0.02
Rank nL
Rank D0
Scatterplot Rhine
Spearman correlation = 0.096
n50 [-]
D0 [s]
Rank scatterplot Rhine
Spearman correlation = 0.096
Rank n50
Rank D0
Scatterplot Rhine
Spearman correlation = -0.056
n85 [-]
D0 [s]
Rank scatterplot Rhine
Spearman correlation = -0.056
Rank n85
Rank D0
Scatterplot Rhine
Spearman correlation = 1.0
DL [s]
DL [s]
Rank scatterplot Rhine
Spearman correlation = 1.0
Rank DL
Rank DL
Scatterplot Rhine
Spearman correlation = 0.565
D50 [s]
DL [s]
Rank scatterplot Rhine
Spearman correlation = 0.565
Rank D50
Rank DL
Scatterplot Rhine
Spearman correlation = 0.806
D85 [s]
DL [s]
Rank scatterplot Rhine
Spearman correlation = 0.806
Rank D85
Rank DL
Scatterplot Rhine
Spearman correlation = 0.223
A0 [m s]
DL [s]
Rank scatterplot Rhine
Spearman correlation = 0.223
Rank A0 [m
Rank DL
Scatterplot Rhine
Spearman correlation = 0.921
AL [m s]
DL [s]
Rank scatterplot Rhine
Spearman correlation = 0.921
Rank AL [m
Rank DL

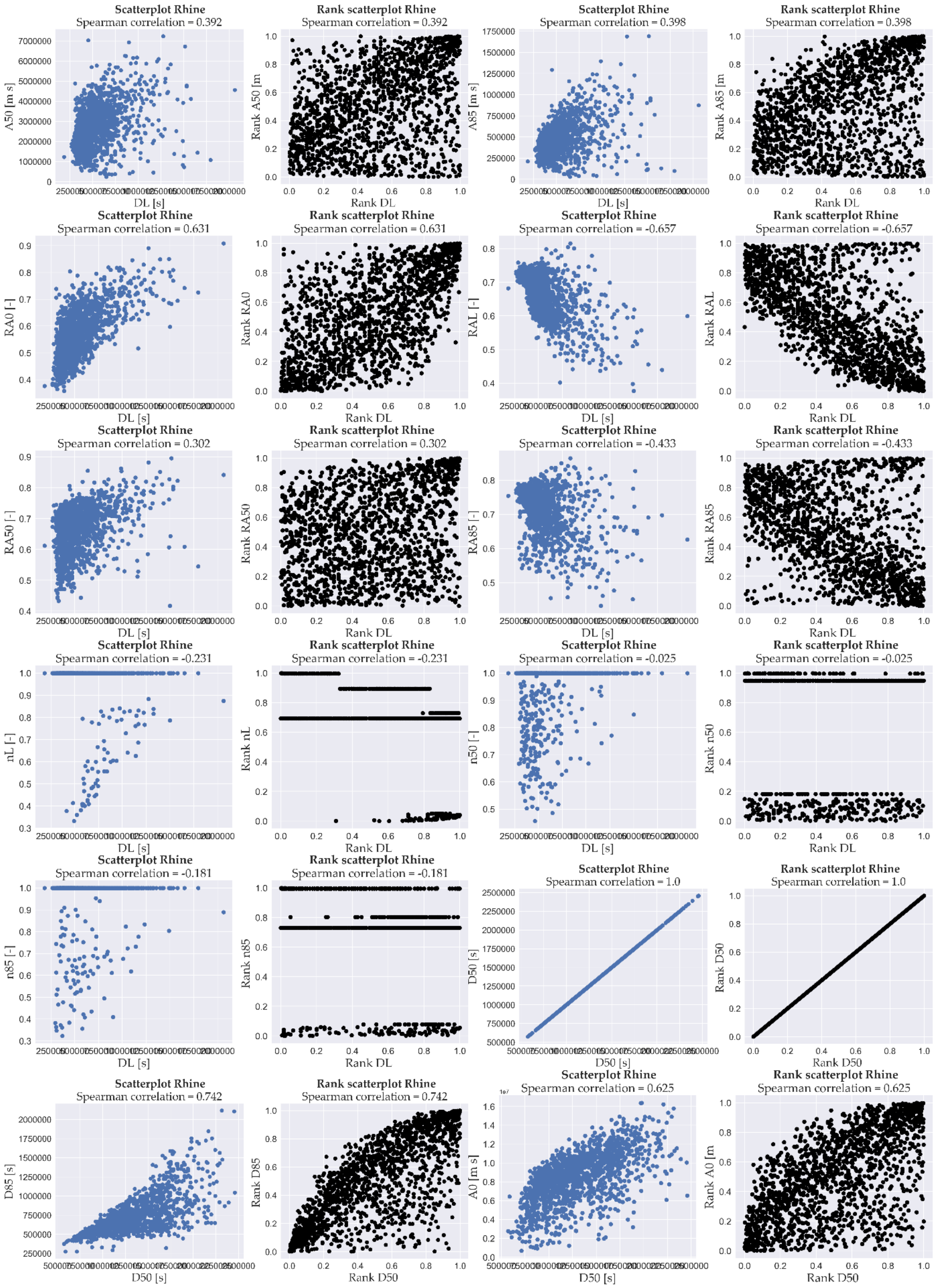
Scatterplot Rhine
Spearman correlation = 0.392
A50 [m s]
DL [s]
Rank scatterplot Rhine
Spearman correlation = 0.392
Rank A50 [m
Rank DL
Scatterplot Rhine
Spearman correlation = 0.398
A85 [m s]
DL [s]
Rank scatterplot Rhine
Spearman correlation = 0.398
Rank A85 [m
Rank DL
Scatterplot Rhine
Spearman correlation = 0.631
RA0 [-]
DL [s]
Rank scatterplot Rhine
Spearman correlation = 0.631
Rank RA0
Rank DL
Scatterplot Rhine
Spearman correlation = -0.657
RAL [-]
DL [s]
Rank scatterplot Rhine
Spearman correlation = -0.657
Rank RAL
Rank DL
Scatterplot Rhine
Spearman correlation = 0.302
RA50 [-]
DL [s]
Rank scatterplot Rhine
Spearman correlation = 0.302
Rank RA50
Rank DL
Scatterplot Rhine
Spearman correlation = -0.433
RA85 [-]
DL [s]
Rank scatterplot Rhine
Spearman correlation = -0.433
Rank RA85
Rank DL
Scatterplot Rhine
Spearman correlation = -0.231
nL [-]
DL [s]
Rank scatterplot Rhine
Spearman correlation = -0.231
Rank nL
Rank DL
Scatterplot Rhine
Spearman correlation = -0.025
n50 [-]
DL [s]
Rank scatterplot Rhine
Spearman correlation = -0.025
Rank n50
Rank DL
Scatterplot Rhine
Spearman correlation = -0.181
n85 [-]
DL [s]
Rank scatterplot Rhine
Spearman correlation = -0.181
Rank n85
Rank DL
Scatterplot Rhine
Spearman correlation = 1.0
D50 [s]
D50 [s]
Rank scatterplot Rhine
Spearman correlation = 1.0
Rank D50
Rank D50
Scatterplot Rhine
Spearman correlation = 0.742
D85 [s]
D50 [s]
Rank scatterplot Rhine
Spearman correlation = 0.742
Rank D85
Rank D50
Scatterplot Rhine
Spearman correlation = 0.625
A0 [m s]
D50 [s]
Rank scatterplot Rhine
Spearman correlation = 0.625
Rank A0 [m
Rank D50

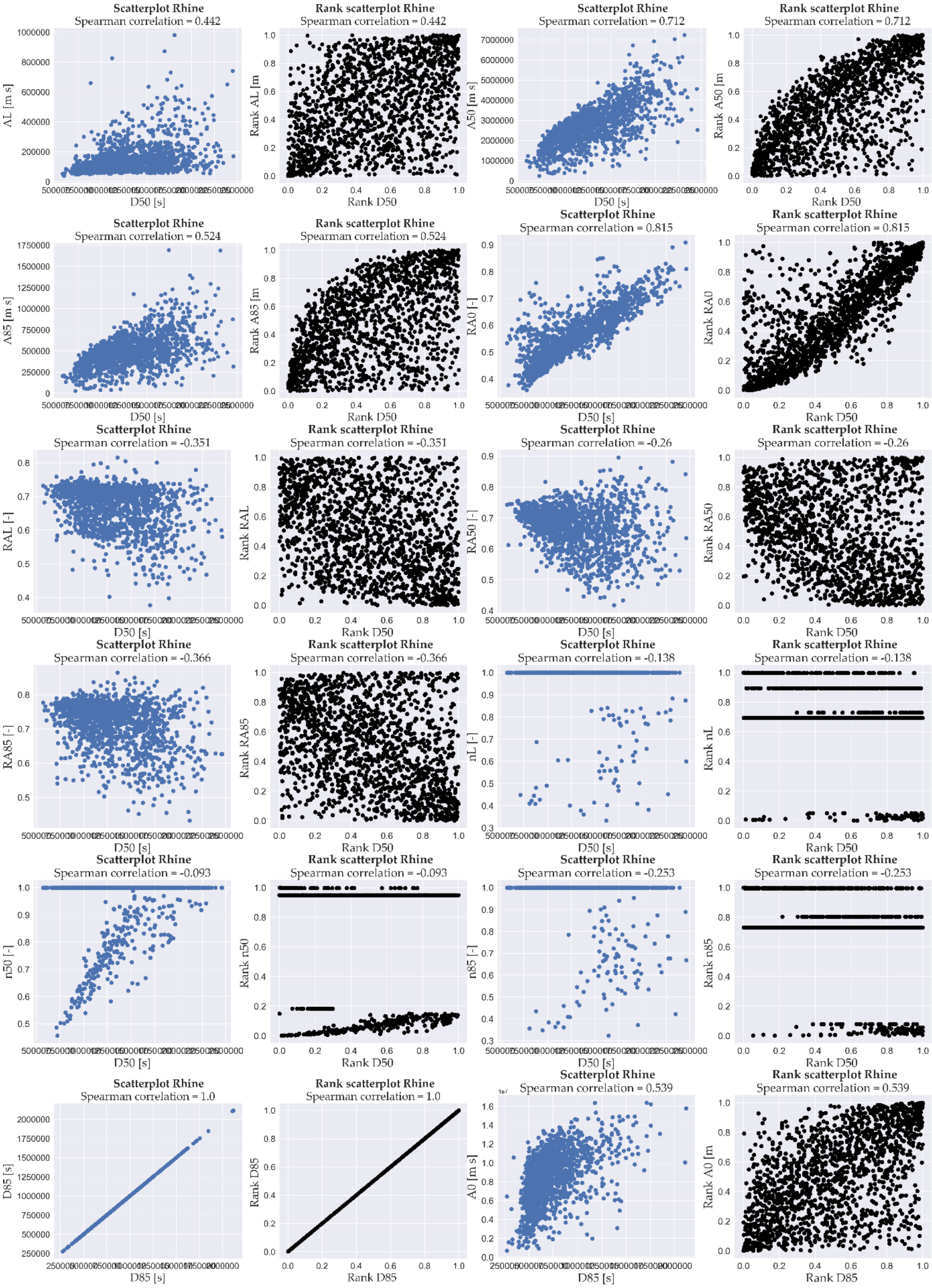
Scatterplot Rhine
Spearman correlation = 0.442
AL [m s]
D50 [s]
Rank scatterplot Rhine
Spearman correlation = 0.442
Rank AL [m
Rank D50
Scatterplot Rhine
Spearman correlation = 0.712
A50 [m s]
D50 [s]
Rank scatterplot Rhine
Spearman correlation = 0.712
Rank A50 [m
Rank D50
Scatterplot Rhine
Spearman correlation = 0.524
A85 [m s]
D50 [s]
Rank scatterplot Rhine
Spearman correlation = 0.524
Rank A85 [m
Rank D50
Scatterplot Rhine
Spearman correlation = 0.815
RA0 [-]
D50 [s]
Rank scatterplot Rhine
Spearman correlation = 0.815
Rank RA0
Rank D50
Scatterplot Rhine
Spearman correlation = -0.351
RAL [-]
D50 [s]
Rank scatterplot Rhine
Spearman correlation = -0.351
Rank RAL
Rank D50
Scatterplot Rhine
Spearman correlation = -0.26
RA50 [-]
D50 [s]
Rank scatterplot Rhine
Spearman correlation = -0.26
Rank RA50
Rank D50
Scatterplot Rhine
Spearman correlation = -0.366
RA85 [-]
D50 [s]
Rank scatterplot Rhine
Spearman correlation = -0.366
Rank RA85
Rank D50
Scatterplot Rhine
Spearman correlation = -0.138
nL [-]
D50 [s]
Rank scatterplot Rhine
Spearman correlation = -0.138
Rank nL
Rank D50
Scatterplot Rhine
Spearman correlation = -0.093
n50 [-]
D50 [s]
Rank scatterplot Rhine
Spearman correlation = -0.093
Rank n50
Rank D50
Scatterplot Rhine
Spearman correlation = -0.253
n85 [-]
D50 [s]
Rank scatterplot Rhine
Spearman correlation = -0.253
Rank n85
Rank D50
Scatterplot Rhine
Spearman correlation = 1.0
D85 [s]
D85 [s]
Rank scatterplot Rhine
Spearman correlation = 1.0
Rank D85
Rank D85
Scatterplot Rhine
Spearman correlation = 0.539
A0 [m s]
D85 [s]
Rank scatterplot Rhine
Spearman correlation = 0.539
Rank A0 [m
Rank D85

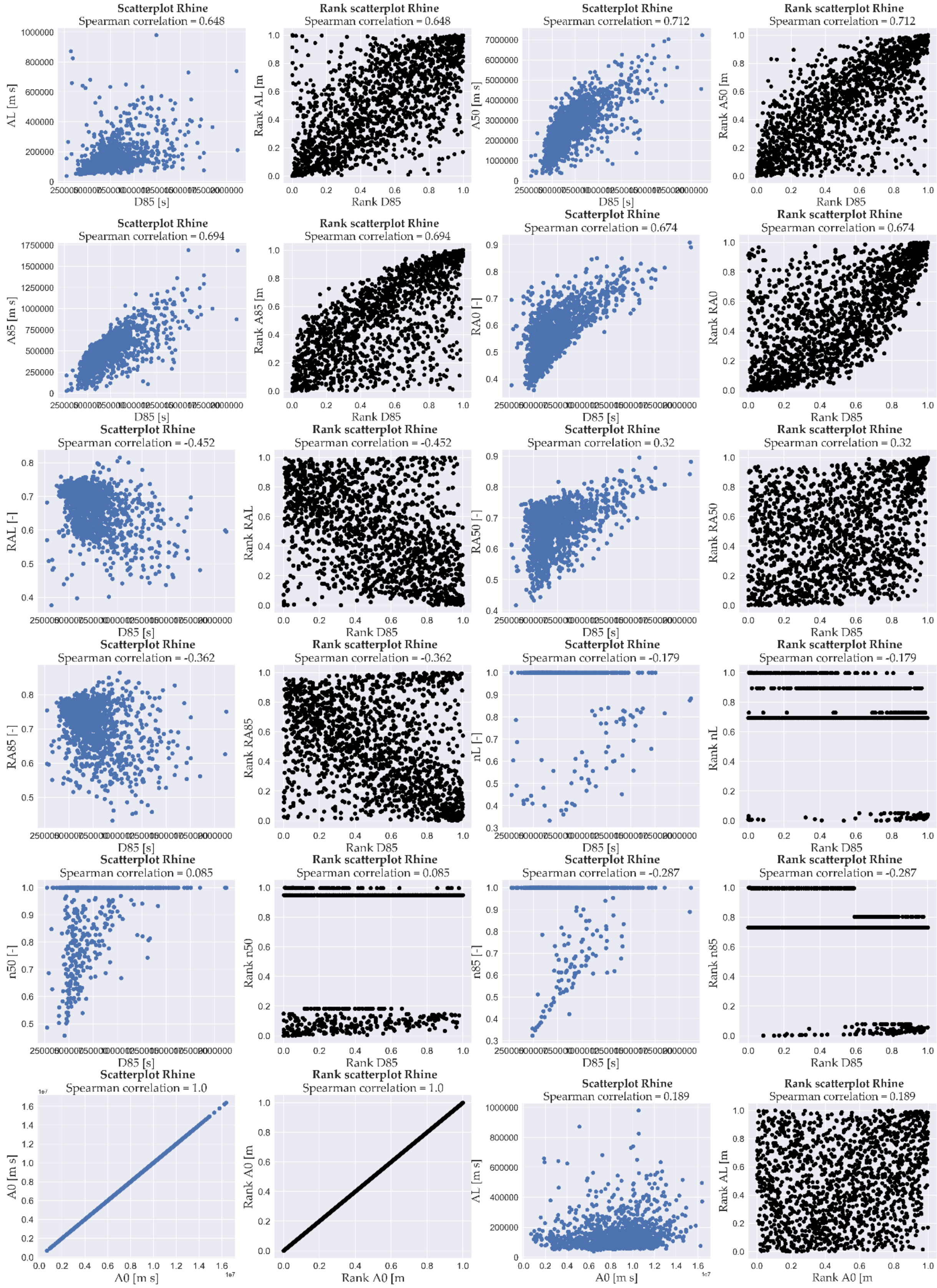
Scatterplot Rhine
Spearman correlation = 0.648
AL [m s]
D85 [s]
Rank scatterplot Rhine
Spearman correlation = 0.648
Rank AL [m
Rank D85
Scatterplot Rhine
Spearman correlation = 0.712
A50 [m s]
D85 [s]
Rank scatterplot Rhine
Spearman correlation = 0.712
Rank A50 [m
Rank D85
Scatterplot Rhine
Spearman correlation = 0.694
A85 [m s]
D85 [s]
Rank scatterplot Rhine
Spearman correlation = 0.694
Rank A85 [m
Rank D85
Scatterplot Rhine
Spearman correlation = 0.674
RA0 [-]
D85 [s]
Rank scatterplot Rhine
Spearman correlation = 0.674
Rank RA0
Rank D85
Scatterplot Rhine
Spearman correlation = -0.452
RAL [-]
D85 [s]
Rank scatterplot Rhine
Spearman correlation = -0.452
Rank RAL
Rank D85
Scatterplot Rhine
Spearman correlation = 0.32
RA50 [-]
D85 [s]
Rank scatterplot Rhine
Spearman correlation = 0.32
Rank RA50
Rank D85
Scatterplot Rhine
Spearman correlation = -0.362
RA85 [-]
D85 [s]
Rank scatterplot Rhine
Spearman correlation = -0.362
Rank RA85
Rank D85
Scatterplot Rhine
Spearman correlation = -0.179
nL [-]
D85 [s]
Rank scatterplot Rhine
Spearman correlation = -0.179
Rank nL
Rank D85
Scatterplot Rhine
Spearman correlation = 0.085
n50 [-]
D85 [s]
Rank scatterplot Rhine
Spearman correlation = 0.085
Rank n50
Rank D85
Scatterplot Rhine
Spearman correlation = -0.287
n85 [-]
D85 [s]
Rank scatterplot Rhine
Spearman correlation = -0.287
Rank n85
Rank D85
Scatterplot Rhine
Spearman correlation = 1.0
A0 [m s]
A0 [m s]
Rank scatterplot Rhine
Spearman correlation = 1.0
Rank A0 [m
Rank A0 [m
Scatterplot Rhine
Spearman correlation = 0.189
AL [m s]
A0 [m s]
Rank scatterplot Rhine
Spearman correlation = 0.189
Rank AL [m
Rank A0 [m

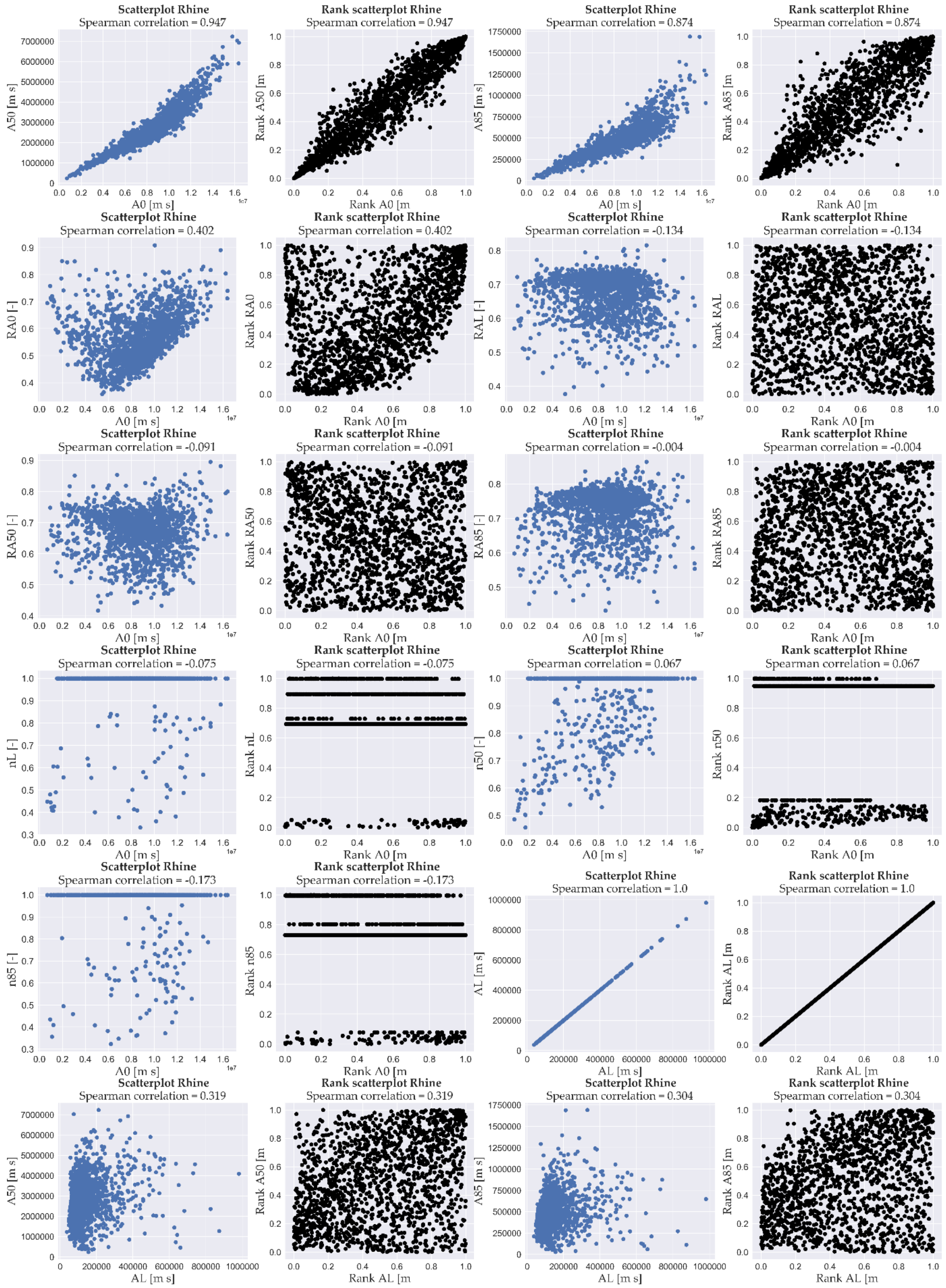
Scatterplot Rhine
Spearman correlation = 0.947
A50 [m s]
A0 [m s]
Rank scatterplot Rhine
Spearman correlation = 0.947
Rank A50 [m
Rank A0 [m
Scatterplot Rhine
Spearman correlation = 0.874
A85 [m s]
A0 [m s]
Rank scatterplot Rhine
Spearman correlation = 0.874
Rank A85 [m
Rank A0 [m
Scatterplot Rhine
Spearman correlation = 0.402
RA0 [-]
A0 [m s]
Rank scatterplot Rhine
Spearman correlation = 0.402
Rank RA0
Rank A0 [m
Scatterplot Rhine
Spearman correlation = -0.134
RAL [-]
A0 [m s]
Rank scatterplot Rhine
Spearman correlation = -0.134
Rank RAL
Rank A0 [m
Scatterplot Rhine
Spearman correlation = -0.091
RA50 [-]
A0 [m s]
Rank scatterplot Rhine
Spearman correlation = -0.091
Rank RA50
Rank A0 [m
Scatterplot Rhine
Spearman correlation = -0.004
RA85 [-]
A0 [m s]
Rank scatterplot Rhine
Spearman correlation = -0.004
Rank RA85
Rank A0 [m
Scatterplot Rhine
Spearman correlation = -0.075
nL [-]
A0 [m s]
Rank scatterplot Rhine
Spearman correlation = -0.075
Rank nL
Rank A0 [m
Scatterplot Rhine
Spearman correlation = 0.067
n50 [-]
A0 [m s]
Rank scatterplot Rhine
Spearman correlation = 0.067
Rank n50
Rank A0 [m
Scatterplot Rhine
Spearman correlation = -0.173
n85 [-]
A0 [m s]
Rank scatterplot Rhine
Spearman correlation = -0.173
Rank n85
Rank A0 [m
Scatterplot Rhine
Spearman correlation = 1.0
AL [m s]
AL [m s]
Rank scatterplot Rhine
Spearman correlation = 1.0
Rank AL [m
Rank AL [m
Scatterplot Rhine
Spearman correlation = 0.319
A50 [m s]
AL [m s]
Rank scatterplot Rhine
Spearman correlation = 0.319
Rank A50 [m
Rank AL [m
Scatterplot Rhine
Spearman correlation = 0.304
A85 [m s]
AL [m s]
Rank scatterplot Rhine
Spearman correlation = 0.304
Rank A85 [m
Rank AL [m

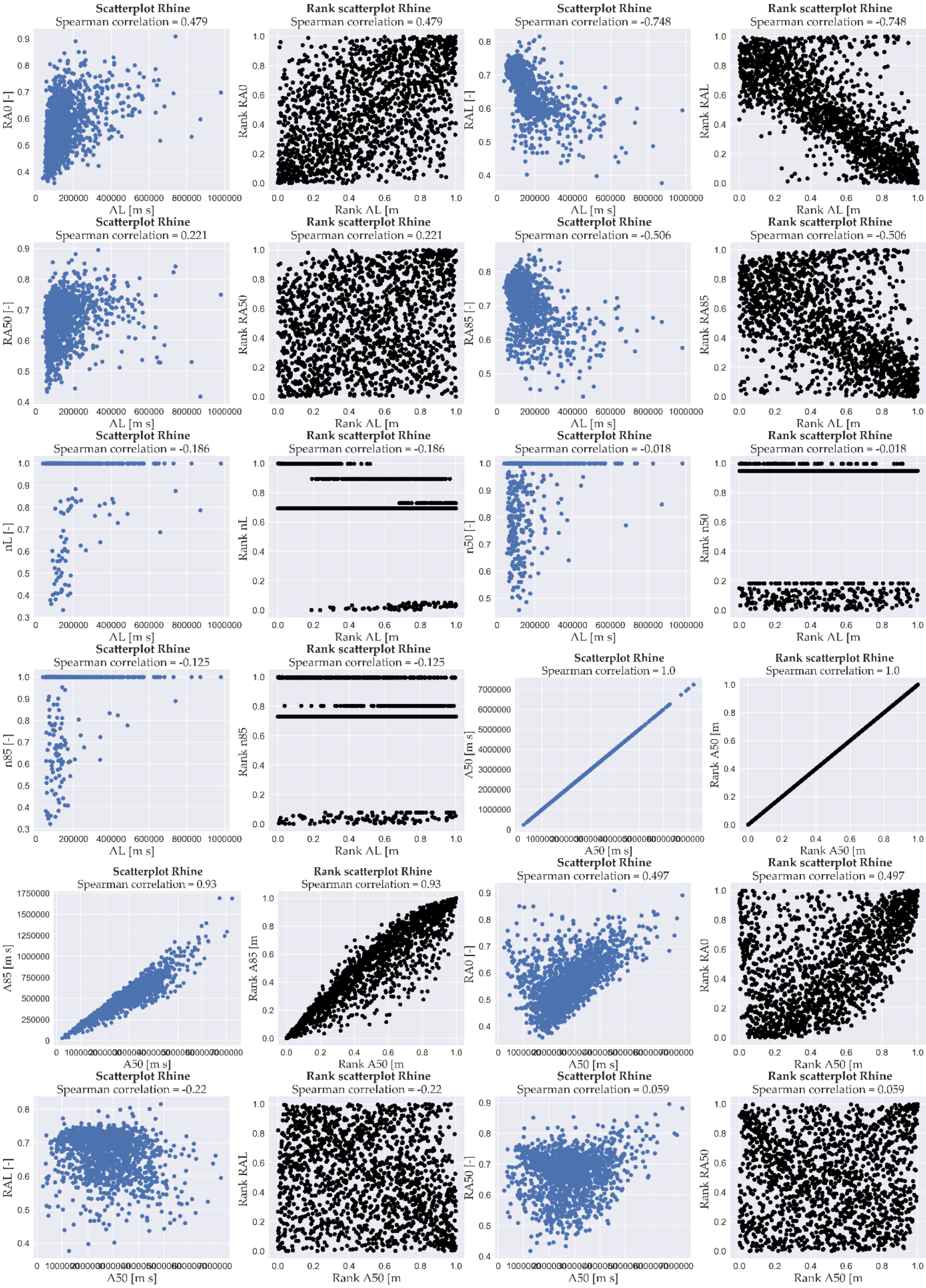
Scatterplot Rhine
Spearman correlation = 0.479
RA0 [-]
AL [m s]
Rank scatterplot Rhine
Spearman correlation = 0.479
Rank RA0
Rank AL [m
Scatterplot Rhine
Spearman correlation = -0.748
RAL [-]
AL [m s]
Rank scatterplot Rhine
Spearman correlation = -0.748
Rank RAL
Rank AL [m
Scatterplot Rhine
Spearman correlation = 0.221
RA50 [-]
AL [m s]
Rank scatterplot Rhine
Spearman correlation = 0.221
Rank RA50
Rank AL [m
Scatterplot Rhine
Spearman correlation = -0.506
RA85 [-]
AL [m s]
Rank scatterplot Rhine
Spearman correlation = -0.506
Rank RA85
Rank AL [m
Scatterplot Rhine
Spearman correlation = -0.186
nL [-]
AL [m s]
Rank scatterplot Rhine
Spearman correlation = -0.186
Rank nL
Rank AL [m
Scatterplot Rhine
Spearman correlation = -0.018
n50 [-]
AL [m s]
Rank scatterplot Rhine
Spearman correlation = -0.018
Rank n50
Rank AL [m
Scatterplot Rhine
Spearman correlation = -0.125
n85 [-]
AL [m s]
Rank scatterplot Rhine
Spearman correlation = -0.125
Rank n85
Rank AL [m
Scatterplot Rhine
Spearman correlation = 1.0
A50 [m s]
A50 [m s]
Rank scatterplot Rhine
Spearman correlation = 1.0
Rank A50 [m
Rank A50 [m
Scatterplot Rhine
Spearman correlation = 0.93
A85 [m s]
A50 [m s]
Rank scatterplot Rhine
Spearman correlation = 0.93
Rank A85 [m
Rank A50 [m
Scatterplot Rhine
Spearman correlation = 0.497
RA0 [-]
A50 [m s]
Rank scatterplot Rhine
Spearman correlation = 0.497
Rank RA0
Rank A50 [m
Scatterplot Rhine
Spearman correlation = -0.22
RAL [-]
A50 [m s]
Rank scatterplot Rhine
Spearman correlation = -0.22
Rank RAL
Rank A50 [m
Scatterplot Rhine
Spearman correlation = 0.059
RA50 [-]
A50 [m s]
Rank scatterplot Rhine
Spearman correlation = 0.059
Rank RA50
Rank A50 [m

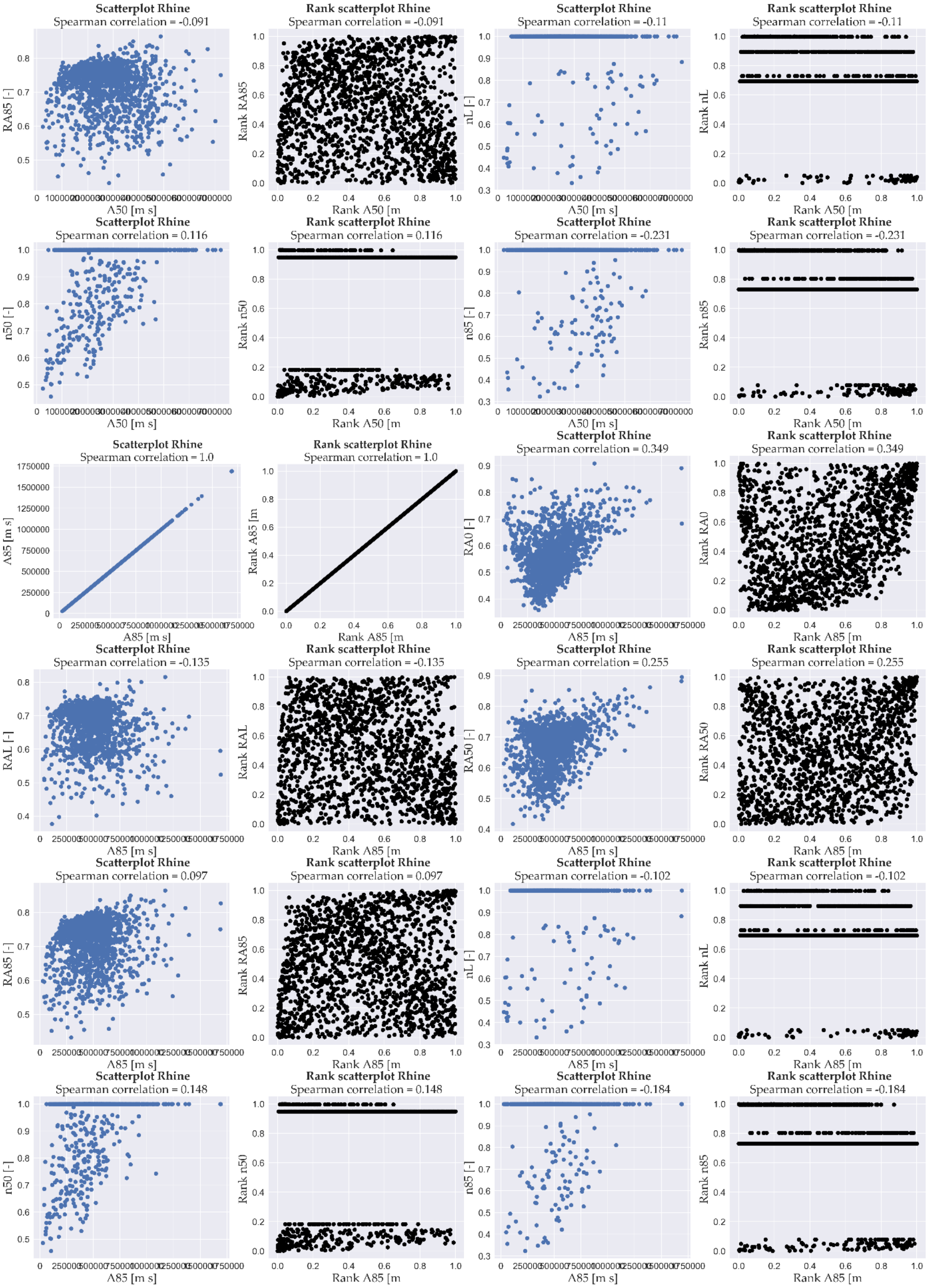
Scatterplot Rhine
Spearman correlation = -0.091
RA85 [-]
A50 [m s]
Rank scatterplot Rhine
Spearman correlation = -0.091
Rank RA85
Rank A50 [m
Scatterplot Rhine
Spearman correlation = -0.11
nL [-]
A50 [m s]
Rank scatterplot Rhine
Spearman correlation = -0.11
Rank nL
Rank A50 [m
Scatterplot Rhine
Spearman correlation = 0.116
n50 [-]
A50 [m s]
Rank scatterplot Rhine
Spearman correlation = 0.116
Rank n50
Rank A50 [m
Scatterplot Rhine
Spearman correlation = -0.231
n85 [-]
A50 [m s]
Rank scatterplot Rhine
Spearman correlation = -0.231
Rank n85
Rank A50 [m
Scatterplot Rhine
Spearman correlation = 1.0
A85 [m s]
A85 [m s]
Rank scatterplot Rhine
Spearman correlation = 1.0
Rank A85 [m
Rank A85 [m
Scatterplot Rhine
Spearman correlation = 0.349
RA0 [-]
A85 [m s]
Rank scatterplot Rhine
Spearman correlation = 0.349
Rank RA0
Rank A85 [m
Scatterplot Rhine
Spearman correlation = -0.135
RAL [-]
A85 [m s]
Rank scatterplot Rhine
Spearman correlation = -0.135
Rank RAL
Rank A85 [m
Scatterplot Rhine
Spearman correlation = 0.255
RA50 [-]
A85 [m s]
Rank scatterplot Rhine
Spearman correlation = 0.255
Rank RA50
Rank A85 [m
Scatterplot Rhine
Spearman correlation = 0.097
RA85 [-]
A85 [m s]
Rank scatterplot Rhine
Spearman correlation = 0.097
Rank RA85
Rank A85 [m
Scatterplot Rhine
Spearman correlation = -0.102
nL [-]
A85 [m s]
Rank scatterplot Rhine
Spearman correlation = -0.102
Rank nL
Rank A85 [m
Scatterplot Rhine
Spearman correlation = 0.148
n50 [-]
A85 [m s]
Rank scatterplot Rhine
Spearman correlation = 0.148
Rank n50
Rank A85 [m
Scatterplot Rhine
Spearman correlation = -0.184
n85 [-]
A85 [m s]
Rank scatterplot Rhine
Spearman correlation = -0.184
Rank n85
Rank A85 [m

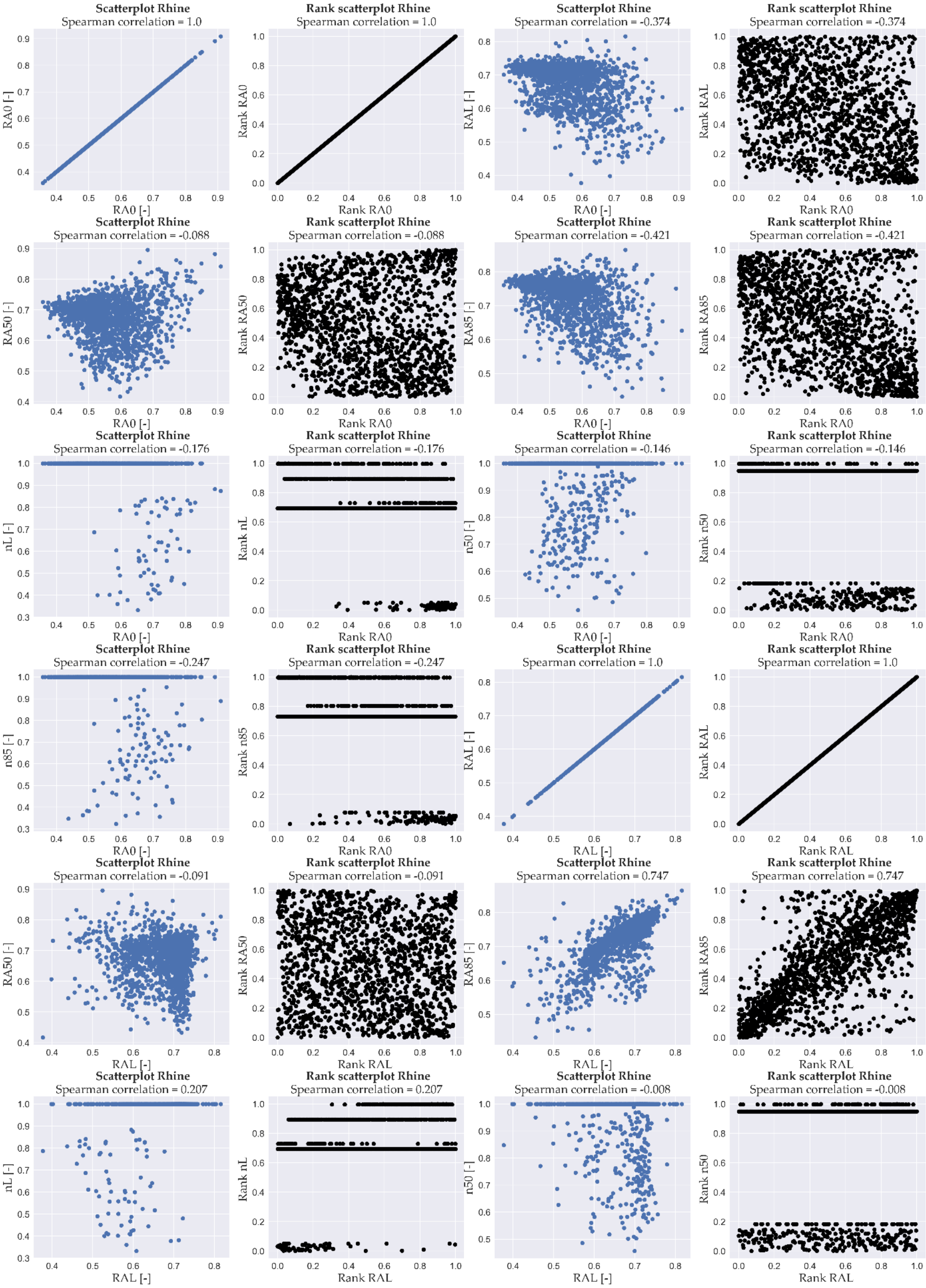

Scatterplot Rhine
Spearman correlation = 1.0
RA0 [-]
RA0 [-]
Rank scatterplot Rhine
Spearman correlation = 1.0
Rank RA0
Rank RA0
Scatterplot Rhine
Spearman correlation = -0.374
RAL [-]
RA0 [-]
Rank scatterplot Rhine
Spearman correlation = -0.374
Rank RAL
Rank RA0
Scatterplot Rhine
Spearman correlation = -0.088
RA50 [-]
RA0 [-]
Rank scatterplot Rhine
Spearman correlation = -0.088
Rank RA50
Rank RA0
Scatterplot Rhine
Spearman correlation = -0.421
RA85 [-]
RA0 [-]
Rank scatterplot Rhine
Spearman correlation = -0.421
Rank RA85
Rank RA0
Scatterplot Rhine
Spearman correlation = -0.176
nL [-]
RA0 [-]
Rank scatterplot Rhine
Spearman correlation = -0.176
Rank nL
Rank RA0
Scatterplot Rhine
Spearman correlation = -0.146
n50 [-]
RA0 [-]
Rank scatterplot Rhine
Spearman correlation = -0.146
Rank n50
Rank RA0
Scatterplot Rhine
Spearman correlation = -0.247
n85 [-]
RA0 [-]
Rank scatterplot Rhine
Spearman correlation = -0.247
Rank n85
Rank RA0
Scatterplot Rhine
Spearman correlation = 1.0
RAL [-]
RAL [-]
Rank scatterplot Rhine
Spearman correlation = 1.0
Rank RAL
Rank RAL
Scatterplot Rhine
Spearman correlation = -0.091
RA50 [-]
RAL [-]
Rank scatterplot Rhine
Spearman correlation = -0.091
Rank RA50
Rank RAL
Scatterplot Rhine
Spearman correlation = 0.747
RA85 [-]
RAL [-]
Rank scatterplot Rhine
Spearman correlation = 0.747
Rank RA85
Rank RAL
Scatterplot Rhine
Spearman correlation = 0.207
nL [-]
RAL [-]
Rank scatterplot Rhine
Spearman correlation = 0.207
Rank nL
Rank RAL
Scatterplot Rhine
Spearman correlation = -0.008
n50 [-]
RAL [-]
Rank scatterplot Rhine
Spearman correlation = -0.008
Rank n50
Rank RAL

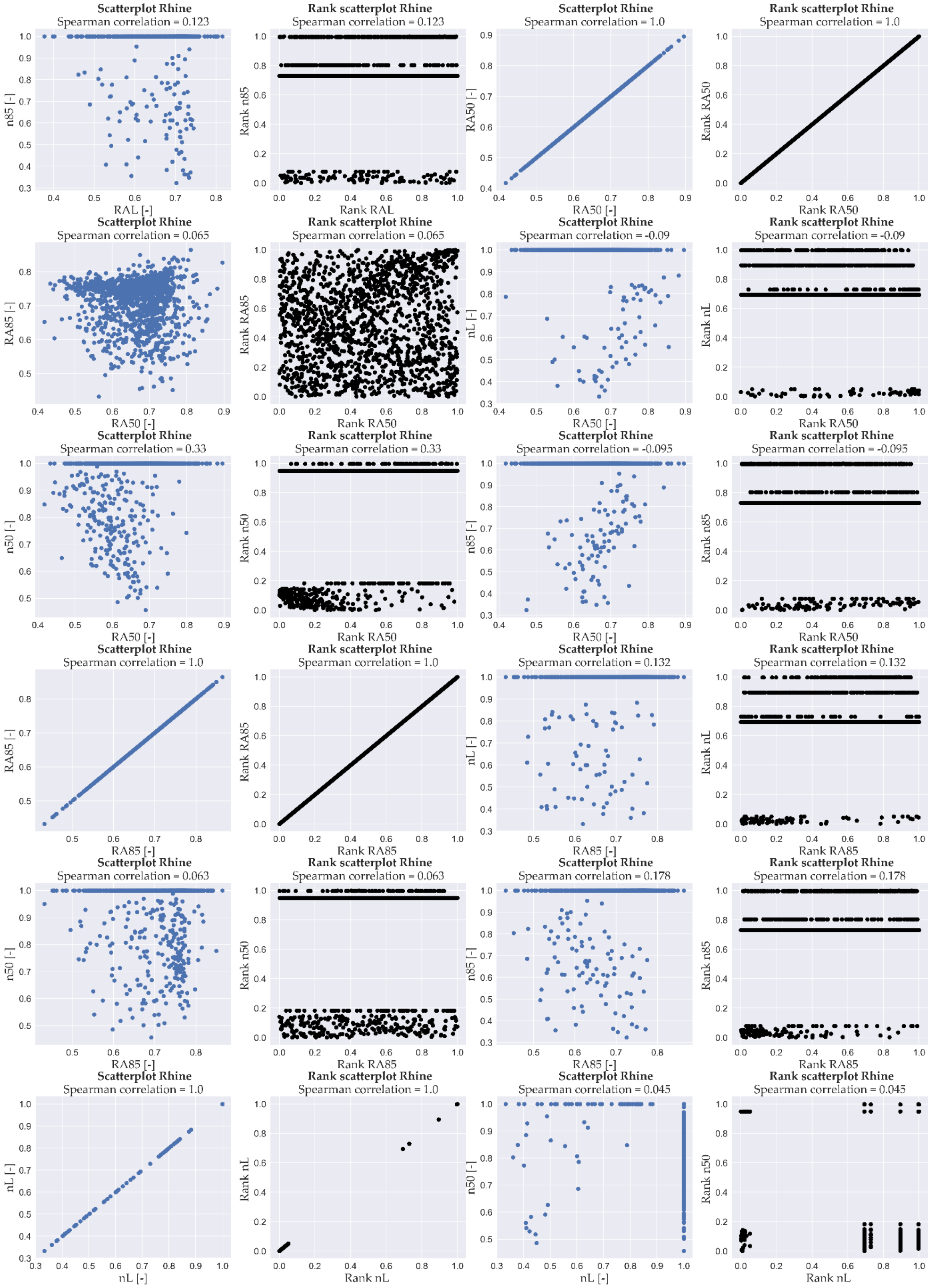
Scatterplot Rhine
Spearman correlation = 0.123
n85 [-]
RAL [-]
Rank scatterplot Rhine
Spearman correlation = 0.123
Rank n85
Rank RAL
Scatterplot Rhine
Spearman correlation = 1.0
RA50 [-]
RA50 [-]
Rank scatterplot Rhine
Spearman correlation = 1.0
Rank RA50
Rank RA50
Scatterplot Rhine
Spearman correlation = 0.065
RA85 [-]
RA50 [-]
Rank scatterplot Rhine
Spearman correlation = 0.065
Rank RA85
Rank RA50
Scatterplot Rhine
Spearman correlation = -0.09
nL [-]
RA50 [-]
Rank scatterplot Rhine
Spearman correlation = -0.09
Rank nL
Rank RA50
Scatterplot Rhine
Spearman correlation = 0.33
n50 [-]
RA50 [-]
Rank scatterplot Rhine
Spearman correlation = 0.33
Rank n50
Rank RA50
Scatterplot Rhine
Spearman correlation = -0.095
n85 [-]
RA50 [-]
Rank scatterplot Rhine
Spearman correlation = -0.095
Rank n85
Rank RA50
Scatterplot Rhine
Spearman correlation = 1.0
RA85 [-]
RA85 [-]
Rank scatterplot Rhine
Spearman correlation = 1.0
Rank RA85
Rank RA85
Scatterplot Rhine
Spearman correlation = 0.132
nL [-]
RA85 [-]
Rank scatterplot Rhine
Spearman correlation = 0.132
Rank nL
Rank RA85
Scatterplot Rhine
Spearman correlation = 0.063
n50 [-]
RA85 [-]
Rank scatterplot Rhine
Spearman correlation = 0.063
Rank n50
Rank RA85
Scatterplot Rhine
Spearman correlation = 0.178
n85 [-]
RA85 [-]
Rank scatterplot Rhine
Spearman correlation = 0.178
Rank n85
Rank RA85
Scatterplot Rhine
Spearman correlation = 1.0
nL [-]
nL [-]
Rank scatterplot Rhine
Spearman correlation = 1.0
Rank nL
Rank nL
Scatterplot Rhine
Spearman correlation = 0.045
n50 [-]
nL [-]
Rank scatterplot Rhine
Spearman correlation = 0.045
Rank n50
Rank nL

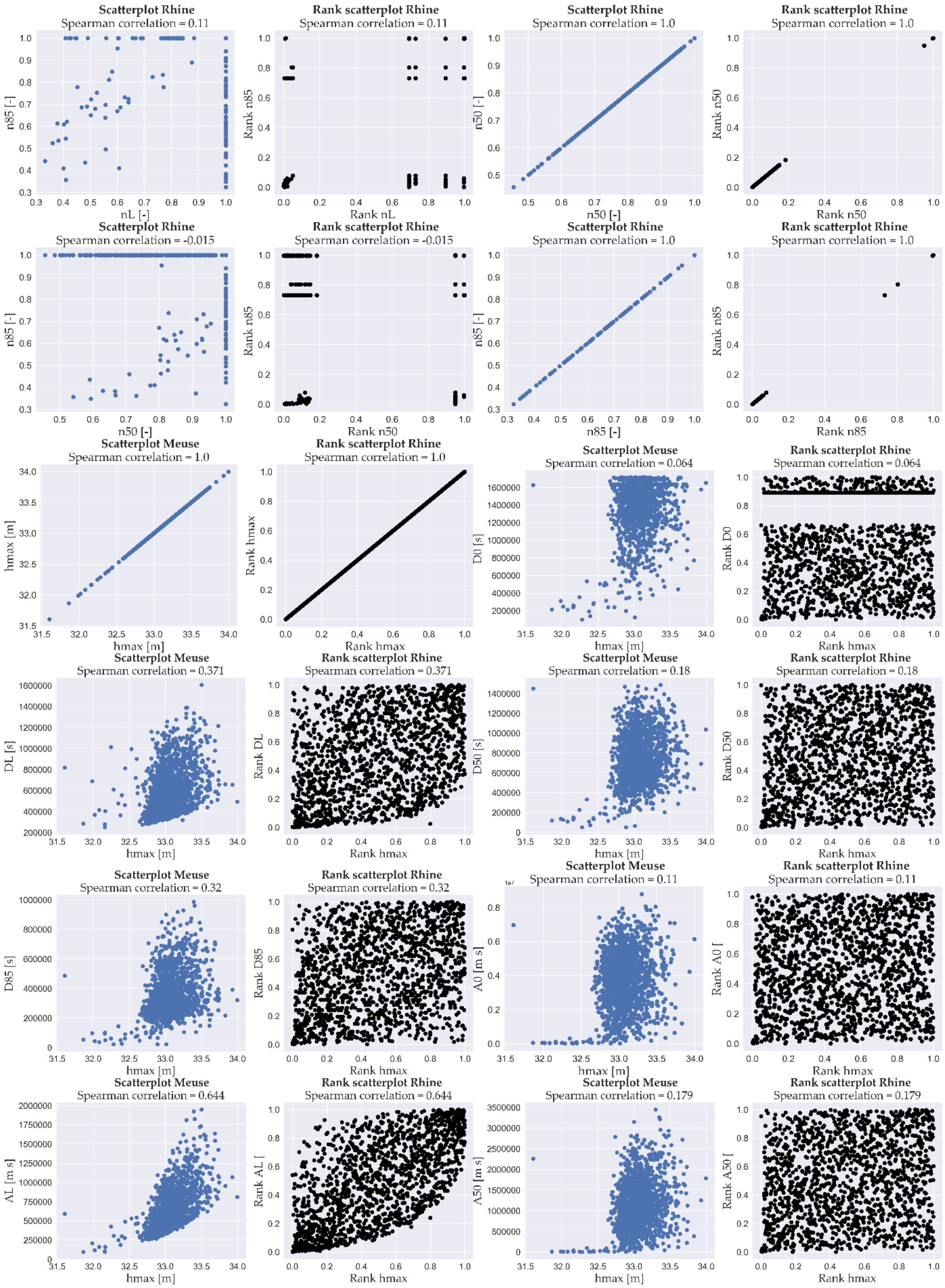
Scatterplot Rhine
Spearman correlation = 0.11
n85 [-]
nL [-]
Rank scatterplot Rhine
Spearman correlation = 0.11
Rank n85
Rank nL
Scatterplot Rhine
Spearman correlation = 1.0
n50 [-]
n50 [-]
Rank scatterplot Rhine
Spearman correlation = 1.0
Rank n50
Rank n50
Scatterplot Rhine
Spearman correlation = -0.015
n85 [-]
n50 [-]
Rank scatterplot Rhine
Spearman correlation = -0.015
Rank n85
Rank n50
Scatterplot Rhine
Spearman correlation = 1.0
n85 [-]
n85 [-]
Rank scatterplot Rhine
Spearman correlation = 1.0
Rank n85
Rank n85
Scatterplot Meuse
Spearman correlation = 1.0
hmax [m]
hmax [m]
Rank scatterplot Rhine
Spearman correlation = 1.0
Rank hmax
Rank hmax
Scatterplot Meuse
Spearman correlation = 0.064
D0 [s]
hmax [m]
Rank scatterplot Rhine
Spearman correlation = 0.064
Rank D0
Rank hmax
Scatterplot Meuse
Spearman correlation = 0.371
DL [s]
hmax [m]
Rank scatterplot Rhine
Spearman correlation = 0.371
Rank DL
Rank hmax
Scatterplot Meuse
Spearman correlation = 0.18
D50 [s]
hmax [m]
Rank scatterplot Rhine
Spearman correlation = 0.18
Rank D50
Rank hmax
Scatterplot Meuse
Spearman correlation = 0.32
D85 [s]
hmax [m]
Rank scatterplot Rhine
Spearman correlation = 0.32
Rank D85
Rank hmax
Scatterplot Meuse
Spearman correlation = 0.11
A0 [m s]
hmax [m]
Rank scatterplot Rhine
Spearman correlation = 0.11
Rank A0 [
Rank hmax
Scatterplot Meuse
Spearman correlation = 0.644
AL [m s]
hmax [m]
Rank scatterplot Rhine
Spearman correlation = 0.644
Rank AL [
Rank hmax
Scatterplot Meuse
Spearman correlation = 0.179
A50 [m s]
hmax [m]
Rank scatterplot Rhine
Spearman correlation = 0.179
Rank A50 [
Rank hmax

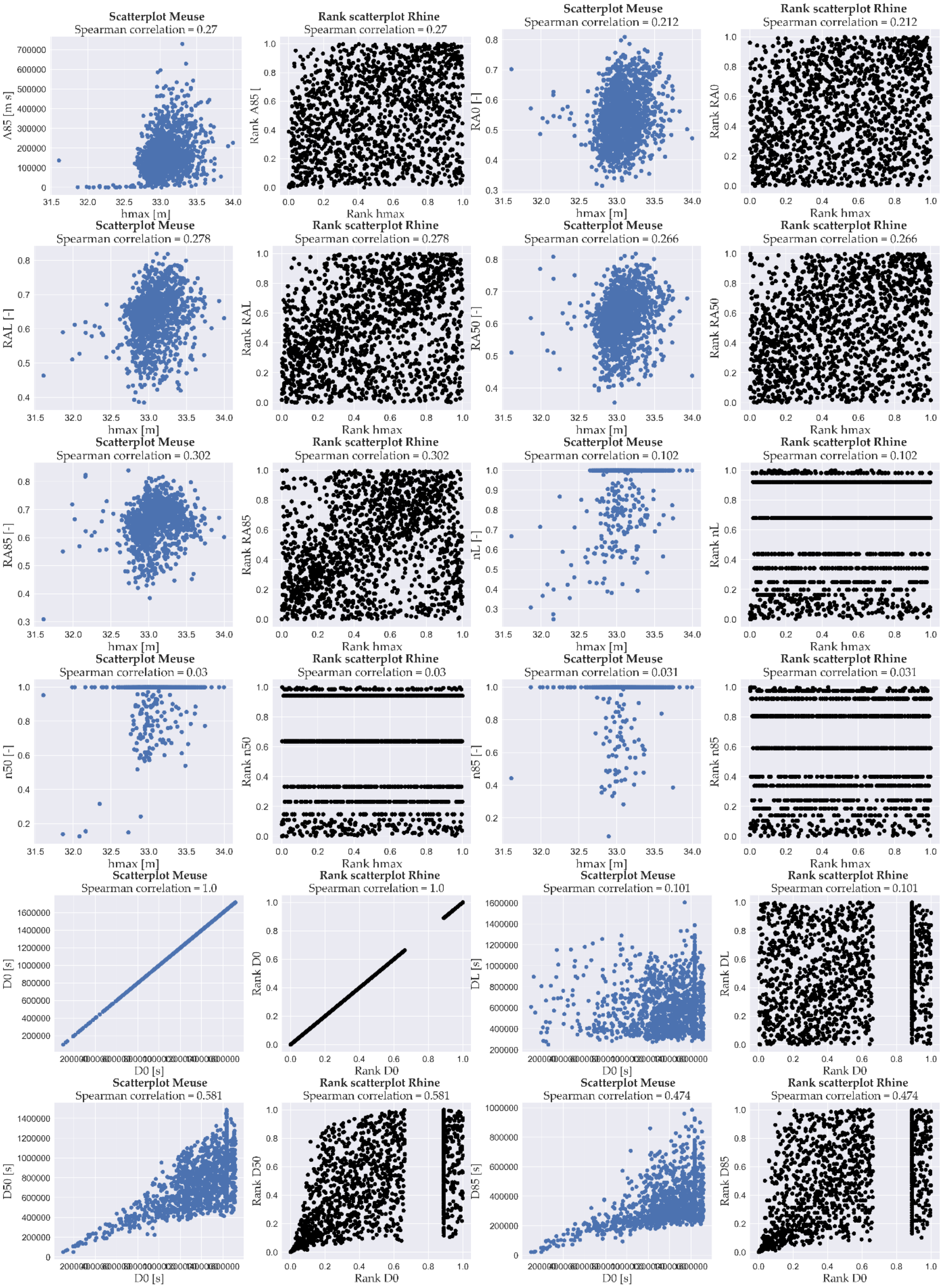
Scatterplot Meuse
Spearman correlation = 0.27
A85 [m s]
hmax [m]
Rank scatterplot Rhine
Spearman correlation = 0.27
Rank A85 [
Rank hmax
Scatterplot Meuse
Spearman correlation = 0.212
RA0 [-]
hmax [m]
Rank scatterplot Rhine
Spearman correlation = 0.212
Rank RA0
Rank hmax
Scatterplot Meuse
Spearman correlation = 0.278
RAL [-]
hmax [m]
Rank scatterplot Rhine
Spearman correlation = 0.278
Rank RAL
Rank hmax
Scatterplot Meuse
Spearman correlation = 0.266
RA50 [-]
hmax [m]
Rank scatterplot Rhine
Spearman correlation = 0.266
Rank RA50
Rank hmax
Scatterplot Meuse
Spearman correlation = 0.302
RA85 [-]
hmax [m]
Rank scatterplot Rhine
Spearman correlation = 0.302
Rank RA85
Rank hmax
Scatterplot Meuse
Spearman correlation = 0.102
nL [-]
hmax [m]
Rank scatterplot Rhine
Spearman correlation = 0.102
Rank nL
Rank hmax
Scatterplot Meuse
Spearman correlation = 0.03
n50 [-]
hmax [m]
Rank scatterplot Rhine
Spearman correlation = 0.03
Rank n50
Rank hmax
Scatterplot Meuse
Spearman correlation = 0.031
n85 [-]
hmax [m]
Rank scatterplot Rhine
Spearman correlation = 0.031
Rank n85
Rank hmax
Scatterplot Meuse
Spearman correlation = 1.0
D0 [s]
D0 [s]
Rank scatterplot Rhine
Spearman correlation = 1.0
Rank D0
Rank D0
Scatterplot Meuse
Spearman correlation = 0.101
DL [s]
D0 [s]
Rank scatterplot Rhine
Spearman correlation = 0.101
Rank DL
Rank D0
Scatterplot Meuse
Spearman correlation = 0.581
D50 [s]
D0 [s]
Rank scatterplot Rhine
Spearman correlation = 0.581
Rank D50
Rank D0
Scatterplot Meuse
Spearman correlation = 0.474
D85 [s]
D0 [s]
Rank scatterplot Rhine
Spearman correlation = 0.474
Rank D85
Rank D0

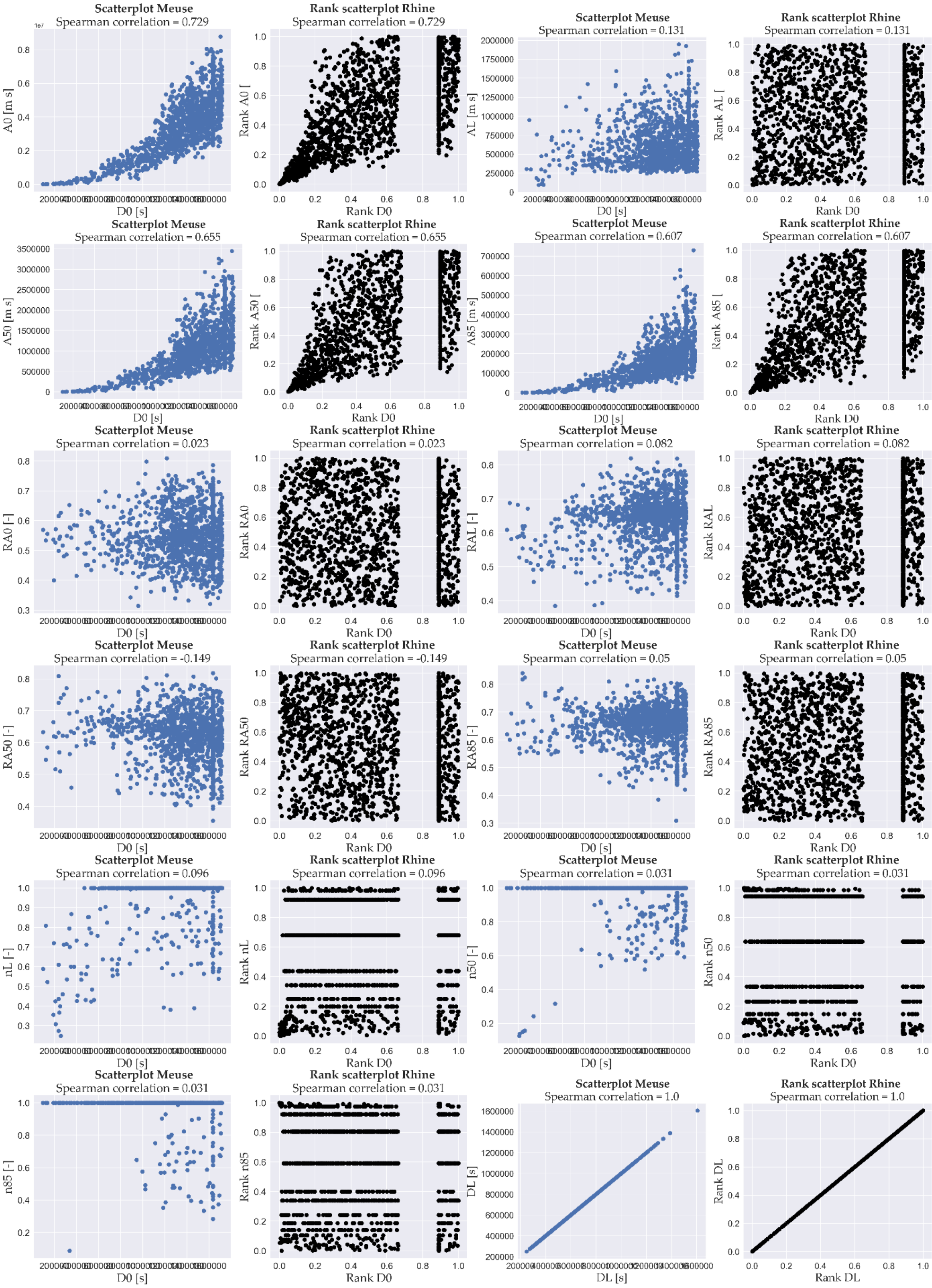
Scatterplot Meuse
Spearman correlation = 0.729
A0 [m s]
D0 [s]
Rank scatterplot Rhine
Spearman correlation = 0.729
Rank A0 [
Rank D0
Scatterplot Meuse
Spearman correlation = 0.131
AL [m s]
D0 [s]
Rank scatterplot Rhine
Spearman correlation = 0.131
Rank AL [
Rank D0
Scatterplot Meuse
Spearman correlation = 0.655
A50 [m s]
D0 [s]
Rank scatterplot Rhine
Spearman correlation = 0.655
Rank A50 [
Rank D0
Scatterplot Meuse
Spearman correlation = 0.607
A85 [m s]
D0 [s]
Rank scatterplot Rhine
Spearman correlation = 0.607
Rank A85 [
Rank D0
Scatterplot Meuse
Spearman correlation = 0.023
RA0 [-]
D0 [s]
Rank scatterplot Rhine
Spearman correlation = 0.023
Rank RA0
Rank D0
Scatterplot Meuse
Spearman correlation = 0.082
RAL [-]
D0 [s]
Rank scatterplot Rhine
Spearman correlation = 0.082
Rank RAL
Rank D0
Scatterplot Meuse
Spearman correlation = -0.149
RA50 [-]
D0 [s]
Rank scatterplot Rhine
Spearman correlation = -0.149
Rank RA50
Rank D0
Scatterplot Meuse
Spearman correlation = 0.05
RA85 [-]
D0 [s]
Rank scatterplot Rhine
Spearman correlation = 0.05
Rank RA85
Rank D0
Scatterplot Meuse
Spearman correlation = 0.096
nL [-]
D0 [s]
Rank scatterplot Rhine
Spearman correlation = 0.096
Rank nL
Rank D0
Scatterplot Meuse
Spearman correlation = 0.031
n50 [-]
D0 [s]
Rank scatterplot Rhine
Spearman correlation = 0.031
Rank n50
Rank D0
Scatterplot Meuse
Spearman correlation = 0.031
n85 [-]
D0 [s]
Rank scatterplot Rhine
Spearman correlation = 0.031
Rank n85
Rank D0
Scatterplot Meuse
Spearman correlation = 1.0
DL [s]
DL [s]
Rank scatterplot Rhine
Spearman correlation = 1.0
Rank DL
Rank DL

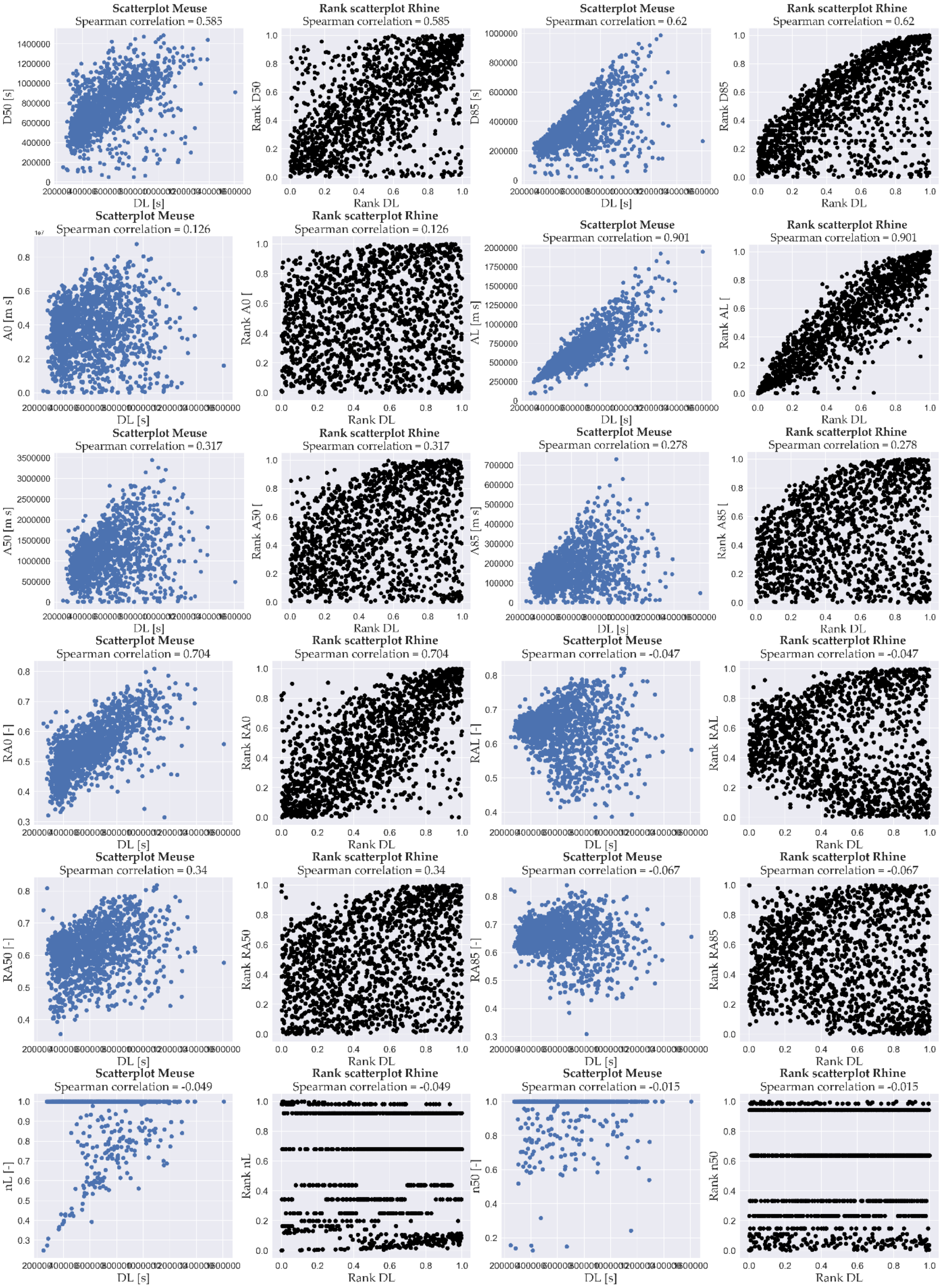
Scatterplot Meuse
Spearman correlation = 0.585
D50 [s]
DL [s]
Rank scatterplot Rhine
Spearman correlation = 0.585
Rank D50
Rank DL
Scatterplot Meuse
Spearman correlation = 0.62
D85 [s]
DL [s]
Rank scatterplot Rhine
Spearman correlation = 0.62
Rank D85
Rank DL
Scatterplot Meuse
Spearman correlation = 0.126
A0 [m s]
DL [s]
Rank scatterplot Rhine
Spearman correlation = 0.126
Rank A0 [
Rank DL
Scatterplot Meuse
Spearman correlation = 0.901
AL [m s]
DL [s]
Rank scatterplot Rhine
Spearman correlation = 0.901
Rank AL [
Rank DL
Scatterplot Meuse
Spearman correlation = 0.317
A50 [m s]
DL [s]
Rank scatterplot Rhine
Spearman correlation = 0.317
Rank A50 [
Rank DL
Scatterplot Meuse
Spearman correlation = 0.278
A85 [m s]
DL [s]
Rank scatterplot Rhine
Spearman correlation = 0.278
Rank A85 [
Rank DL
Scatterplot Meuse
Spearman correlation = 0.704
RA0 [-]
DL [s]
Rank scatterplot Rhine
Spearman correlation = 0.704
Rank RA0
Rank DL
Scatterplot Meuse
Spearman correlation = -0.047
RAL [-]
DL [s]
Rank scatterplot Rhine
Spearman correlation = -0.047
Rank RAL
Rank DL
Scatterplot Meuse
Spearman correlation = 0.34
RA50 [-]
DL [s]
Rank scatterplot Rhine
Spearman correlation = 0.34
Rank RA50
Rank DL
Scatterplot Meuse
Spearman correlation = -0.067
RA85 [-]
DL [s]
Rank scatterplot Rhine
Spearman correlation = -0.067
Rank RA85
Rank DL
Scatterplot Meuse
Spearman correlation = -0.049
nL [-]
DL [s]
Rank scatterplot Rhine
Spearman correlation = -0.049
Rank nL
Rank DL
Scatterplot Meuse
Spearman correlation = -0.015
n50 [-]
DL [s]
Rank scatterplot Rhine
Spearman correlation = -0.015
Rank n50
Rank DL

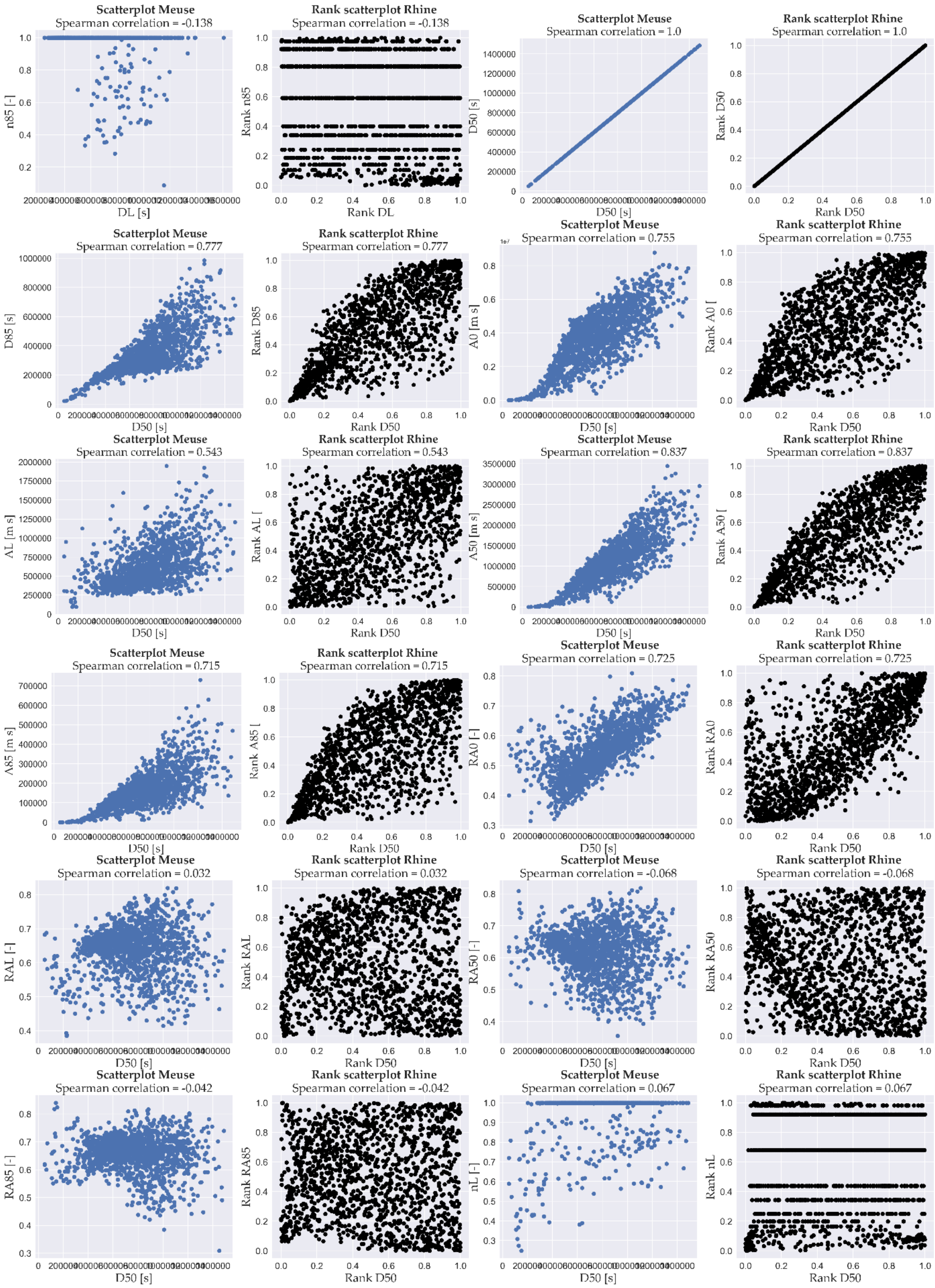
Scatterplot Meuse
Spearman correlation = -0.138
n85 [-]
DL [s]
Rank scatterplot Rhine
Spearman correlation = -0.138
Rank n85
Rank DL
Scatterplot Meuse
Spearman correlation = 1.0
D50 [s]
D50 [s]
Rank scatterplot Rhine
Spearman correlation = 1.0
Rank D50
Rank D50
Scatterplot Meuse
Spearman correlation = 0.777
D85 [s]
D50 [s]
Rank scatterplot Rhine
Spearman correlation = 0.777
Rank D85
Rank D50
Scatterplot Meuse
Spearman correlation = 0.755
A0 [m s]
D50 [s]
Rank scatterplot Rhine
Spearman correlation = 0.755
Rank A0 [
Rank D50
Scatterplot Meuse
Spearman correlation = 0.543
AL [m s]
D50 [s]
Rank scatterplot Rhine
Spearman correlation = 0.543
Rank AL [
Rank D50
Scatterplot Meuse
Spearman correlation = 0.837
A50 [m s]
D50 [s]
Rank scatterplot Rhine
Spearman correlation = 0.837
Rank A30 [
Rank D50
Scatterplot Meuse
Spearman correlation = 0.715
A85 [m s]
D50 [s]
Rank scatterplot Rhine
Spearman correlation = 0.715
Rank A85 [
Rank D50
Scatterplot Meuse
Spearman correlation = 0.725
RA0 [-]
D50 [s]
Rank scatterplot Rhine
Spearman correlation = 0.725
Rank RA0
Rank D50
Scatterplot Meuse
Spearman correlation = 0.032
RAL [-]
D50 [s]
Rank scatterplot Rhine
Spearman correlation = 0.032
Rank RAL
Rank D50
Scatterplot Meuse
Spearman correlation = -0.068
RA50 [-]
D50 [s]
Rank scatterplot Rhine
Spearman correlation = -0.068
Rank RA50
Rank D50
Scatterplot Meuse
Spearman correlation = -0.042
RA85 [-]
D50 [s]
Rank scatterplot Rhine
Spearman correlation = -0.042
Rank RA85
Rank D50
Scatterplot Meuse
Spearman correlation = 0.067
nL [-]
D50 [s]
Rank scatterplot Rhine
Spearman correlation = 0.067
Rank nL
Rank D50

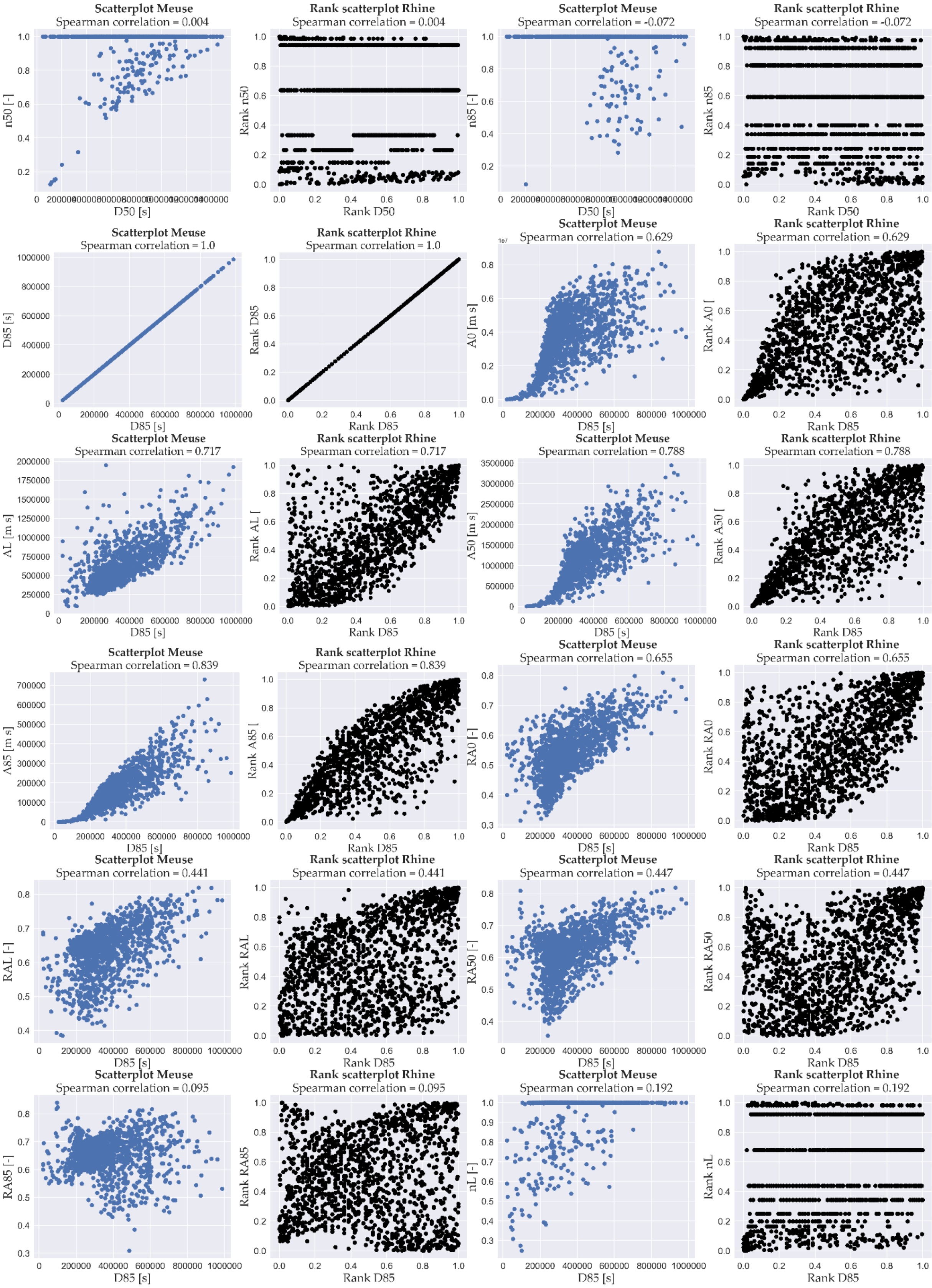
Scatterplot Meuse
Spearman correlation = 0.004
n50 [-]
D50 [s]
Rank scatterplot Rhine
Spearman correlation = 0.004
Rank n50
Rank D50
Scatterplot Meuse
Spearman correlation = -0.072
n85 [-]
D50 [s]
Rank scatterplot Rhine
Spearman correlation = -0.072
Rank n85
Rank D50
Scatterplot Meuse
Spearman correlation = 1.0
D85 [s]
D85 [s]
Rank scatterplot Rhine
Spearman correlation = 1.0
Rank D85
Rank D85
Scatterplot Meuse
Spearman correlation = 0.629
A0 [m s]
D85 [s]
Rank scatterplot Rhine
Spearman correlation = 0.629
Rank A0 [
Rank D85
Scatterplot Meuse
Spearman correlation = 0.717
AL [m s]
D85 [s]
Rank scatterplot Rhine
Spearman correlation = 0.717
Rank AL [
Rank D85
Scatterplot Meuse
Spearman correlation = 0.788
A50 [m s]
D85 [s]
Rank scatterplot Rhine
Spearman correlation = 0.788
Rank A50 [
Rank D85
Scatterplot Meuse
Spearman correlation = 0.839
A85 [m s]
D85 [s]
Rank scatterplot Rhine
Spearman correlation = 0.839
Rank A85 [
Rank D85
Scatterplot Meuse
Spearman correlation = 0.655
RA0 [-]
D85 [s]
Rank scatterplot Rhine
Spearman correlation = 0.655
Rank RA0
Rank D85
Scatterplot Meuse
Spearman correlation = 0.441
RAL [-]
D85 [s]
Rank scatterplot Rhine
Spearman correlation = 0.441
Rank RAL
Rank D85
Scatterplot Meuse
Spearman correlation = 0.447
RA50 [-]
D85 [s]
Rank scatterplot Rhine
Spearman correlation = 0.447
Rank RA50
Rank D85
Scatterplot Meuse
Spearman correlation = 0.095
RA85 [-]
D85 [s]
Rank scatterplot Rhine
Spearman correlation = 0.095
Rank RA85
Rank D85
Scatterplot Meuse
Spearman correlation = 0.192
nL [-]
D85 [s]
Rank scatterplot Rhine
Spearman correlation = 0.192
Rank nL
Rank D85

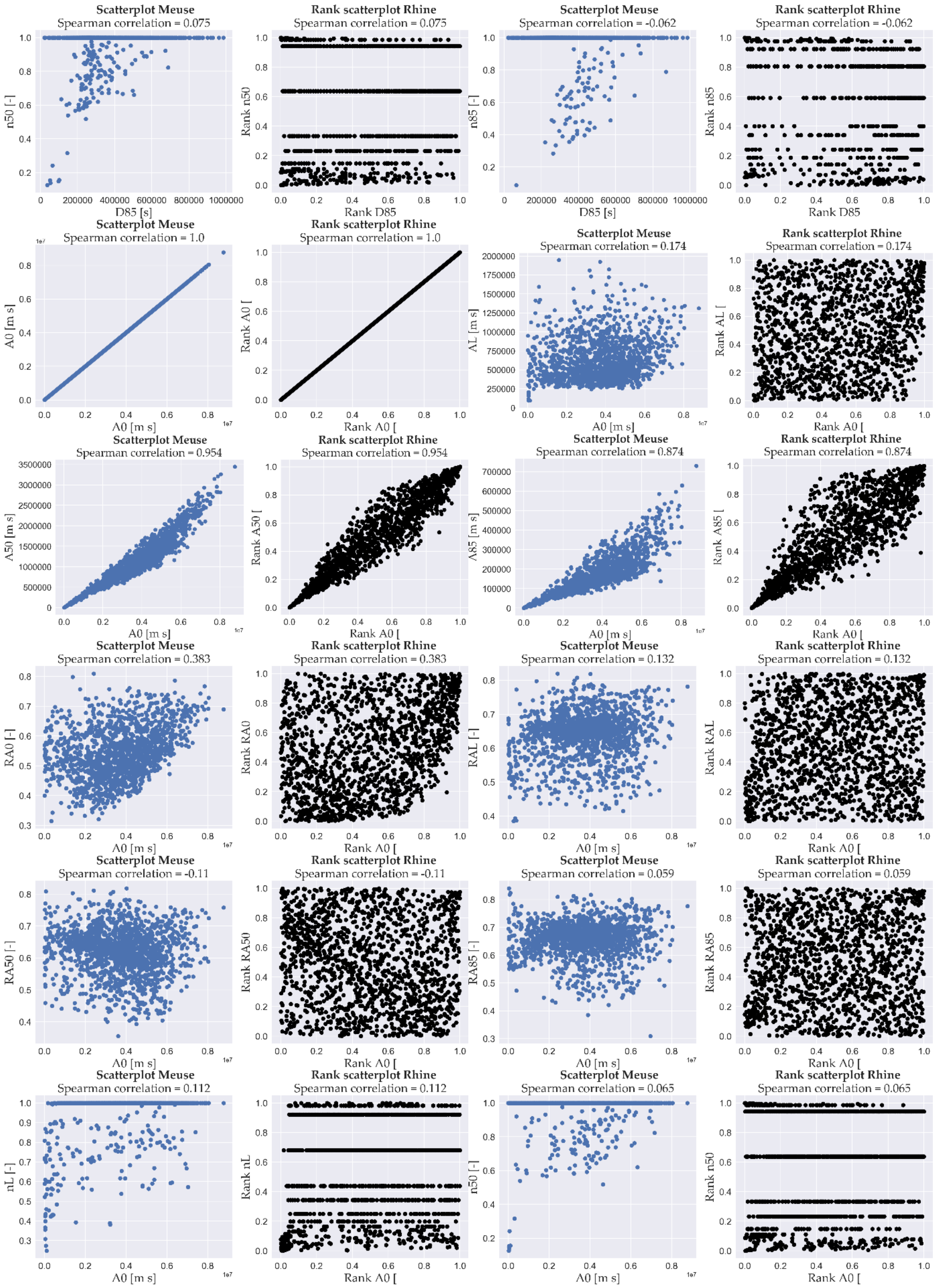
Scatterplot Meuse
Spearman correlation = 0.075
n50 [-]
D85 [s]
Rank scatterplot Rhine
Spearman correlation = 0.075
Rank n50
Rank D85
Scatterplot Meuse
Spearman correlation = -0.062
n85 [-]
D85 [s]
Rank scatterplot Rhine
Spearman correlation = -0.062
Rank n85
Rank D85
Scatterplot Meuse
Spearman correlation = 1.0
A0 [m s]
A0 [m s]
Rank scatterplot Rhine
Spearman correlation = 1.0
Rank A0 [
Rank A0 [
Scatterplot Meuse
Spearman correlation = 0.174
AL [m s]
A0 [m s]
Rank scatterplot Rhine
Spearman correlation = 0.174
Rank AL [
Rank A0 [
Scatterplot Meuse
Spearman correlation = 0.954
A50 [m s]
A0 [m s]
Rank scatterplot Rhine
Spearman correlation = 0.954
Rank A50 [
Rank A0 [
Scatterplot Meuse
Spearman correlation = 0.874
A85 [m s]
A0 [m s]
Rank scatterplot Rhine
Spearman correlation = 0.874
Rank A85 [
Rank A0 [
Scatterplot Meuse
Spearman correlation = 0.383
RA0 [-]
A0 [m s]
Rank scatterplot Rhine
Spearman correlation = 0.383
Rank RA0
Rank A0 [
Scatterplot Meuse
Spearman correlation = 0.132
RAL [-]
A0 [m s]
Rank scatterplot Rhine
Spearman correlation = 0.132
Rank RAL
Rank A0 [
Scatterplot Meuse
Spearman correlation = -0.11
RA50 [-]
A0 [m s]
Rank scatterplot Rhine
Spearman correlation = -0.11
Rank RA50
Rank A0 [
Scatterplot Meuse
Spearman correlation = 0.059
RA85 [-]
A0 [m s]
Rank scatterplot Rhine
Spearman correlation = 0.059
Rank RA85
Rank A0 [
Scatterplot Meuse
Spearman correlation = 0.112
nL [-]
A0 [m s]
Rank scatterplot Rhine
Spearman correlation = 0.112
Rank nL
Rank A0 [
Scatterplot Meuse
Spearman correlation = 0.065
n50 [-]
A0 [m s]
Rank scatterplot Rhine
Spearman correlation = 0.065
Rank n50
Rank A0 [

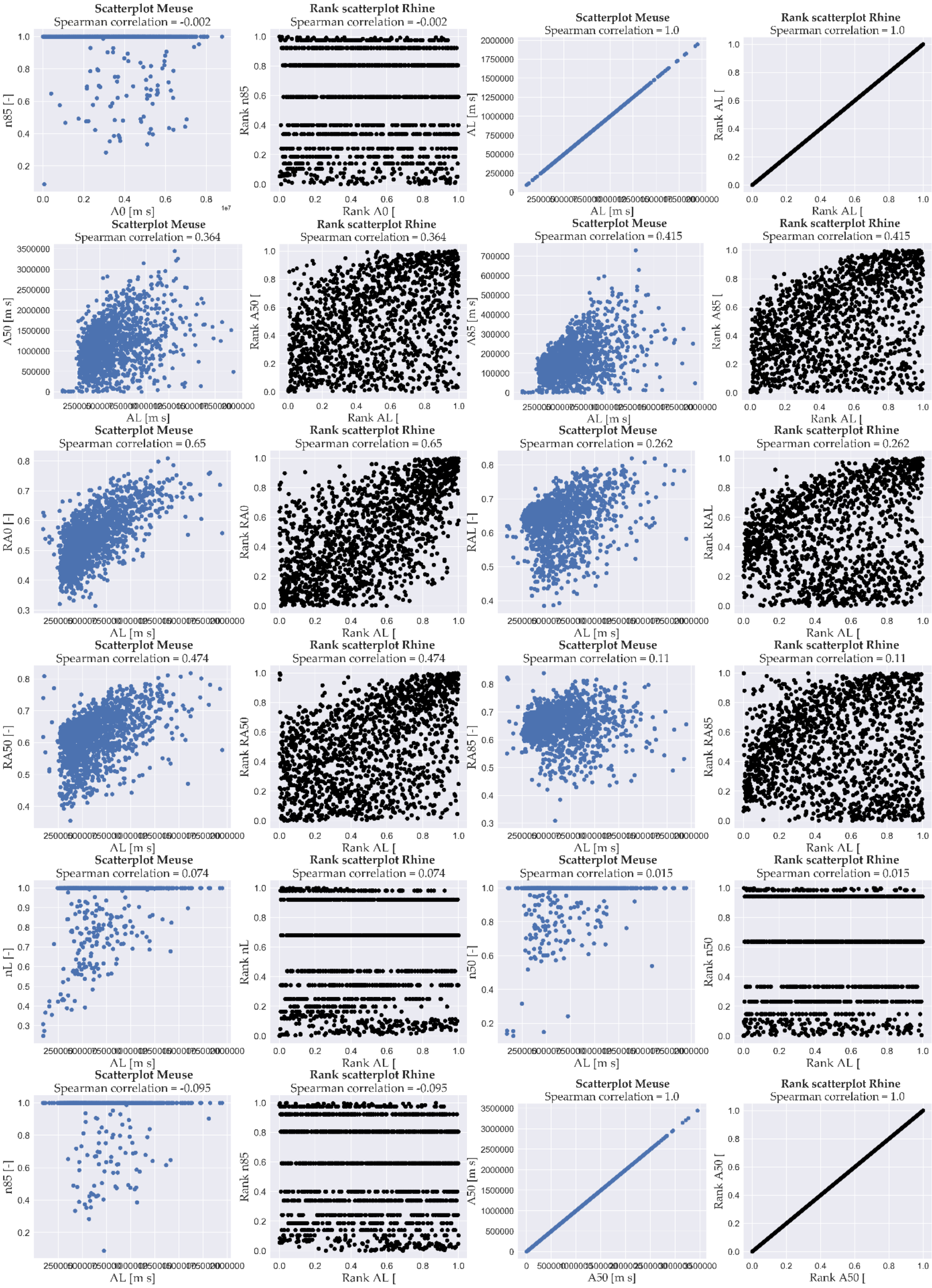
Scatterplot Meuse
Spearman correlation = -0.002
n85 [-]
A0 [m s]
Rank scatterplot Rhine
Spearman correlation = -0.002
Rank n85
Rank A0 [
Scatterplot Meuse
Spearman correlation = 1.0
AL [m s]
AL [m s]
Rank scatterplot Rhine
Spearman correlation = 1.0
Rank AL [
Rank AL [
Scatterplot Meuse
Spearman correlation = 0.364
A50 [m s]
AL [m s]
Rank scatterplot Rhine
Spearman correlation = 0.364
Rank A50 [
Rank AL [
Scatterplot Meuse
Spearman correlation = 0.415
A85 [m s]
AL [m s]
Rank scatterplot Rhine
Spearman correlation = 0.415
Rank A85 [
Rank AL [
Scatterplot Meuse
Spearman correlation = 0.65
RA0 [-]
AL [m s]
Rank scatterplot Rhine
Spearman correlation = 0.65
Rank RA0
Rank AL [
Scatterplot Meuse
Spearman correlation = 0.262
RAL [-]
AL [m s]
Rank scatterplot Rhine
Spearman correlation = 0.262
Rank RAL
Rank AL [
Scatterplot Meuse
Spearman correlation = 0.474
RA50 [-]
AL [m s]
Rank scatterplot Rhine
Spearman correlation = 0.474
Rank RA50
Rank AL [
Scatterplot Meuse
Spearman correlation = 0.11
RA85 [-]
AL [m s]
Rank scatterplot Rhine
Spearman correlation = 0.11
Rank RA85
Rank AL [
Scatterplot Meuse
Spearman correlation = 0.074
nL [-]
AL [m s]
Rank scatterplot Rhine
Spearman correlation = 0.074
Rank nL
Rank AL [
Scatterplot Meuse
Spearman correlation = 0.015
n50 [-]
AL [m s]
Rank scatterplot Rhine
Spearman correlation = 0.015
Rank n50
Rank AL [
Scatterplot Meuse
Spearman correlation = -0.095
n85 [-]
AL [m s]
Rank scatterplot Rhine
Spearman correlation = -0.095
Rank n85
Rank AL [
Scatterplot Meuse
Spearman correlation = 1.0
A50 [m s]
A50 [m s]
Rank scatterplot Rhine
Spearman correlation = 1.0
Rank A50 [
Rank A50 [

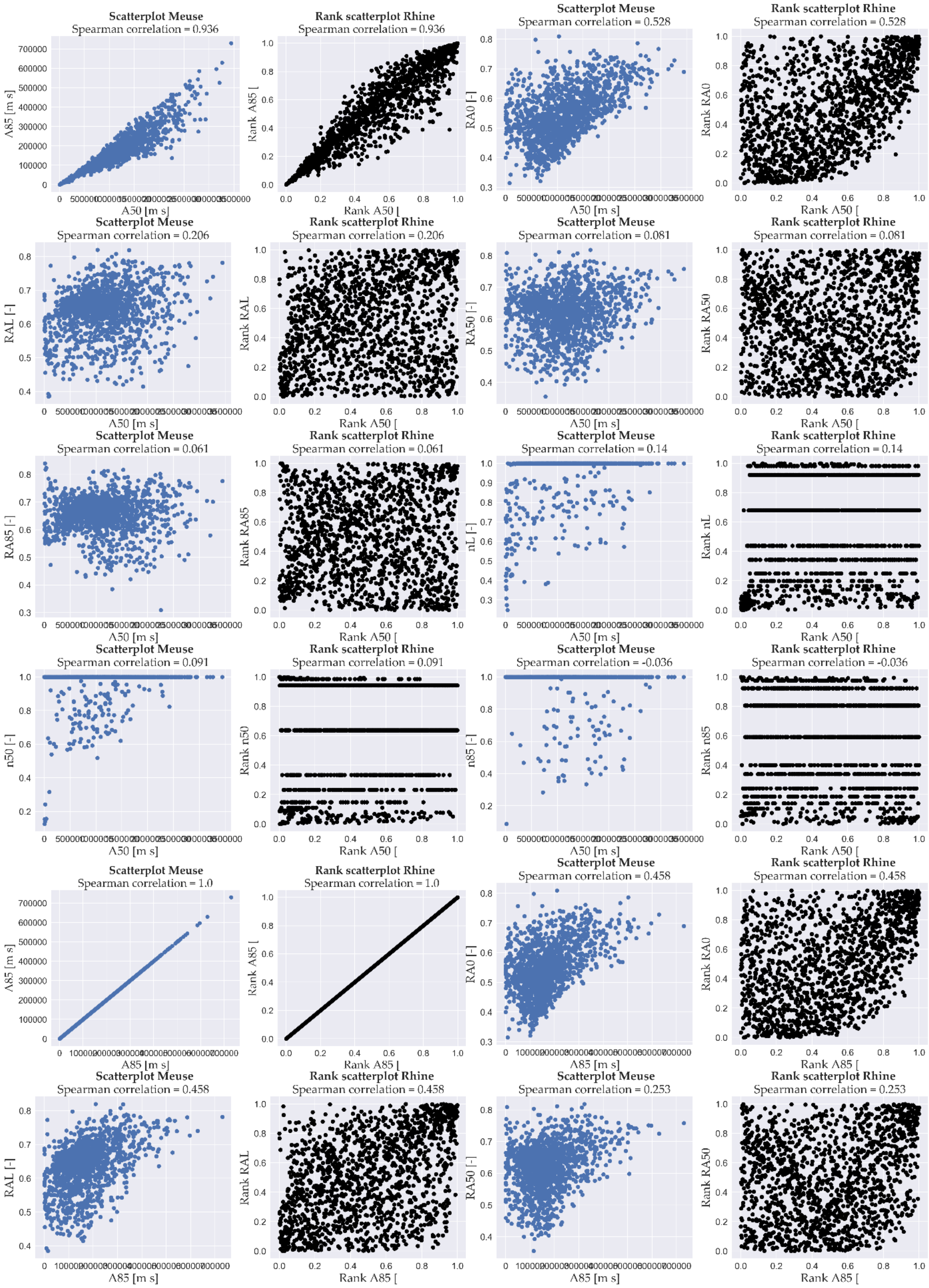
Scatterplot Meuse
Spearman correlation = 0.936
A85 [m s]
A50 [m s]
Rank scatterplot Rhine
Spearman correlation = 0.936
Rank A85 [
Rank A50 [
Scatterplot Meuse
Spearman correlation = 0.528
RA0 [-]
A50 [m s]
Rank scatterplot Rhine
Spearman correlation = 0.528
Rank RA0
Rank A50 [
Scatterplot Meuse
Spearman correlation = 0.206
RAL [-]
A50 [m s]
Rank scatterplot Rhine
Spearman correlation = 0.206
Rank RAL
Rank A50 [
Scatterplot Meuse
Spearman correlation = 0.081
RA50 [-]
A50 [m s]
Rank scatterplot Rhine
Spearman correlation = 0.081
Rank RA50
Rank A50 [
Scatterplot Meuse
Spearman correlation = 0.061
RA85 [-]
A50 [m s]
Rank scatterplot Rhine
Spearman correlation = 0.061
Rank RA85
Rank A50 [
Scatterplot Meuse
Spearman correlation = 0.14
nL [-]
A50 [m s]
Rank scatterplot Rhine
Spearman correlation = 0.14
Rank nL
Rank A50 [
Scatterplot Meuse
Spearman correlation = 0.091
n50 [-]
A50 [m s]
Rank scatterplot Rhine
Spearman correlation = 0.091
Rank n50
Rank A50 [
Scatterplot Meuse
Spearman correlation = -0.036
n85 [-]
A50 [m s]
Rank scatterplot Rhine
Spearman correlation = -0.036
Rank n85
Rank A50 [
Scatterplot Meuse
Spearman correlation = 1.0
A85 [m s]
A85 [m s]
Rank scatterplot Rhine
Spearman correlation = 1.0
Rank A85 [
Rank A85 [
Scatterplot Meuse
Spearman correlation = 0.458
RA0 [-]
A85 [m s]
Rank scatterplot Rhine
Spearman correlation = 0.458
Rank RA0
Rank A85 [
Scatterplot Meuse
Spearman correlation = 0.458
RAL [-]
A85 [m s]
Rank scatterplot Rhine
Spearman correlation = 0.458
Rank RAL
Rank A85 [
Scatterplot Meuse
Spearman correlation = 0.253
RA50 [-]
A85 [m s]
Rank scatterplot Rhine
Spearman correlation = 0.253
Rank RA50
Rank A85 [

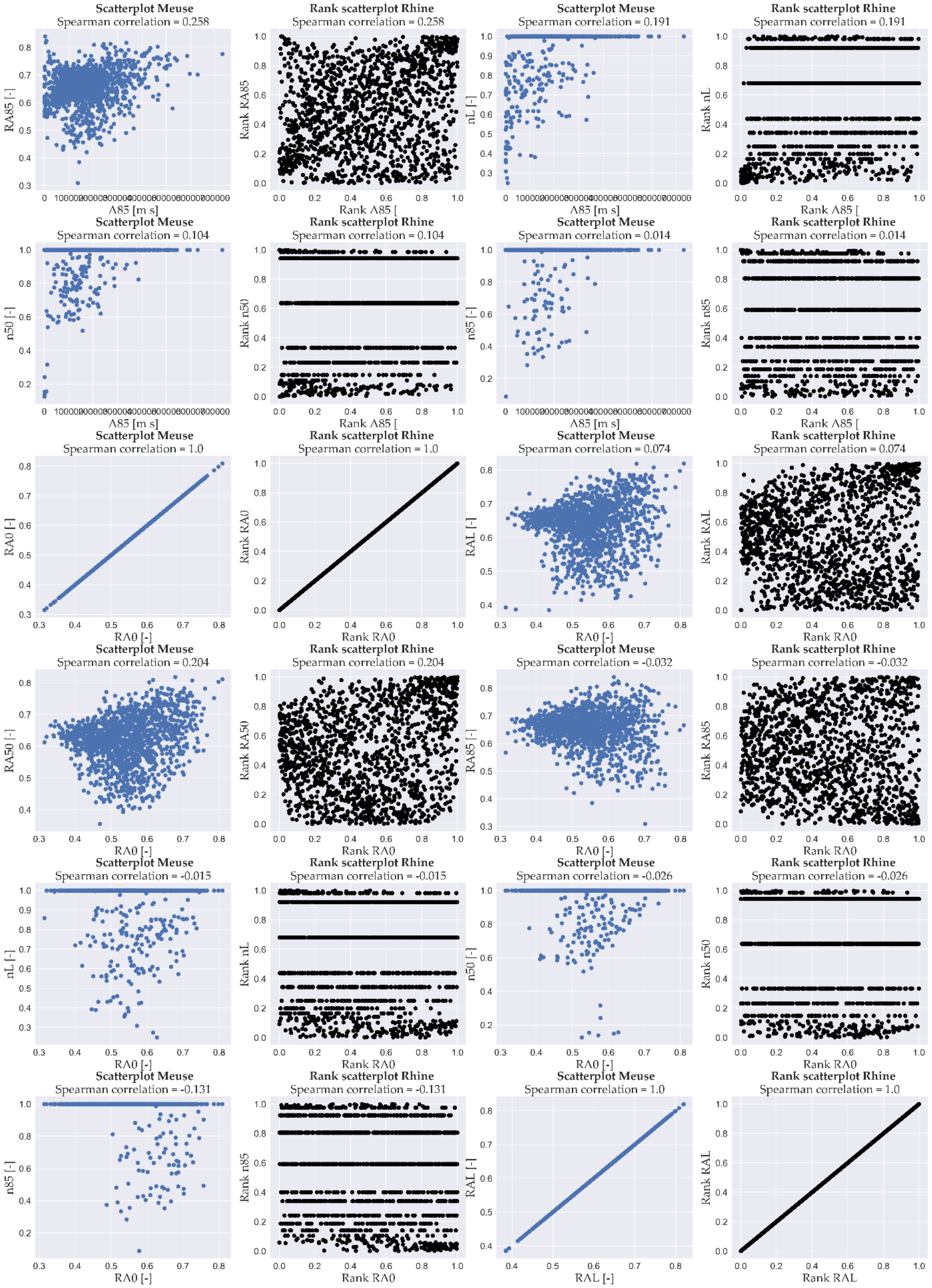
Scatterplot Meuse
Spearman correlation = 0.258
RA85 [-]
A85 [m s]
Rank scatterplot Rhine
Spearman correlation = 0.258
Rank RA85
Rank A85 [
Scatterplot Meuse
Spearman correlation = 0.191
nL [-]
A85 [m s]
Rank scatterplot Rhine
Spearman correlation = 0.191
Rank nL
Rank A85 [
Scatterplot Meuse
Spearman correlation = 0.104
n50 [-]
A85 [m s]
Rank scatterplot Rhine
Spearman correlation = 0.104
Rank n50
Rank A85 [
Scatterplot Meuse
Spearman correlation = 0.014
n85 [-]
A85 [m s]
Rank scatterplot Rhine
Spearman correlation = 0.014
Rank n85
Rank A85 [
Scatterplot Meuse
Spearman correlation = 1.0
RA0 [-]
RA0 [-]
Rank scatterplot Rhine
Spearman correlation = 1.0
Rank RA0
Rank RA0
Scatterplot Meuse
Spearman correlation = 0.074
RAL [-]
RA0 [-]
Rank scatterplot Rhine
Spearman correlation = 0.074
Rank RAL
Rank RA0
Scatterplot Meuse
Spearman correlation = 0.204
RA50 [-]
RA0 [-]
Rank scatterplot Rhine
Spearman correlation = 0.204
Rank RA50
Rank RA0
Scatterplot Meuse
Spearman correlation = -0.032
RA85 [-]
RA0 [-]
Rank scatterplot Rhine
Spearman correlation = -0.032
Rank RA85
Rank RA0
Scatterplot Meuse
Spearman correlation = -0.015
nL [-]
RA0 [-]
Rank scatterplot Rhine
Spearman correlation = -0.015
Rank nL
Rank RA0
Scatterplot Meuse
Spearman correlation = -0.026
n50 [-]
RA0 [-]
Rank scatterplot Rhine
Spearman correlation = -0.026
Rank n50
Rank RA0
Scatterplot Meuse
Spearman correlation = -0.131
n85 [-]
RA0 [-]
Rank scatterplot Rhine
Spearman correlation = -0.131
Rank n85
Rank RA0
Scatterplot Meuse
Spearman correlation = 1.0
RAL [-]
RAL [-]
Rank scatterplot Rhine
Spearman correlation = 1.0
Rank RAL
Rank RAL

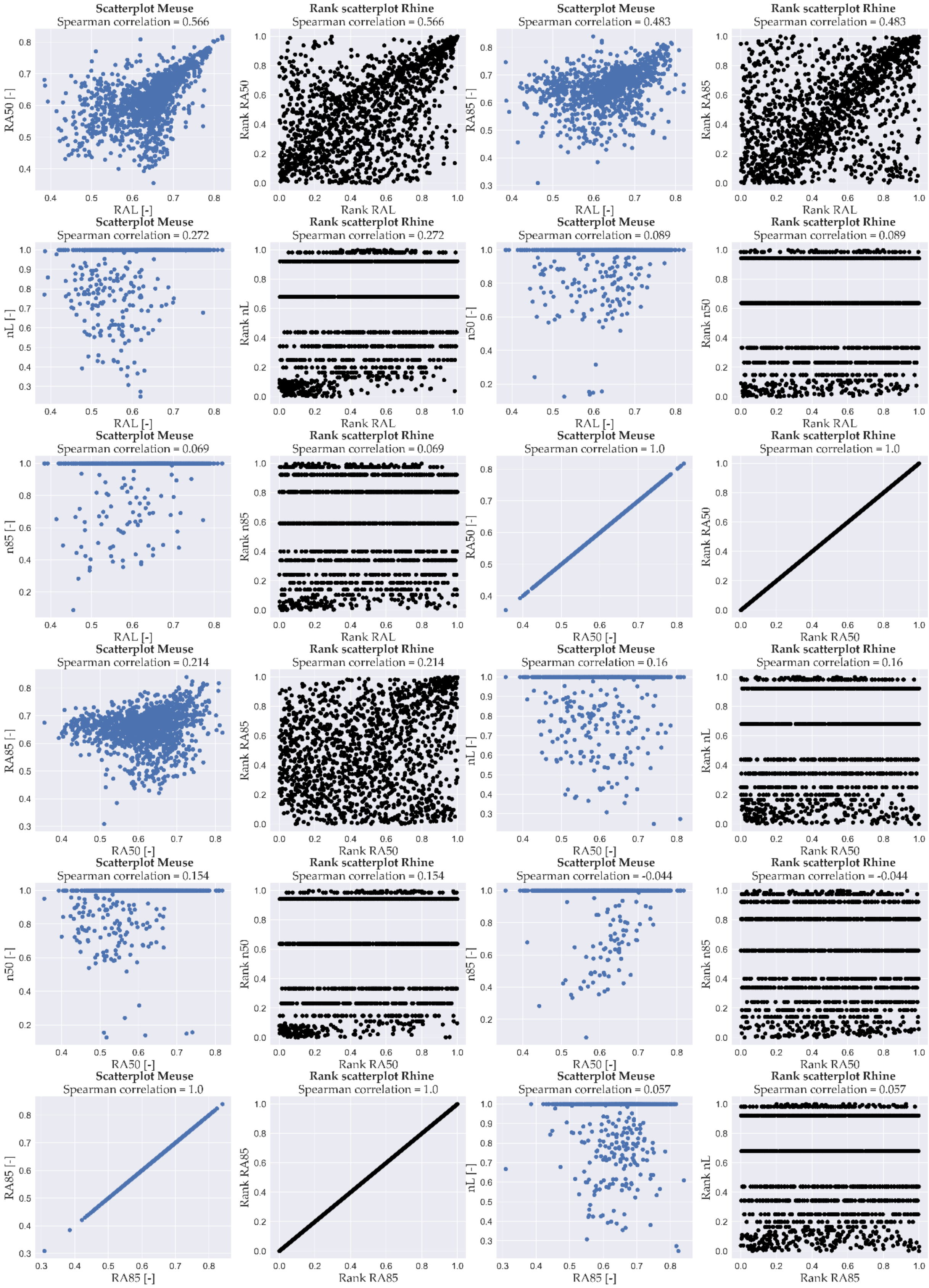
Scatterplot Meuse
Spearman correlation = 0.566
RA50 [-]
RAL [-]
Rank scatterplot Rhine
Spearman correlation = 0.566
Rank RA50
Rank RAL
Scatterplot Meuse
Spearman correlation = 0.483
RA85 [-]
RAL [-]
Rank scatterplot Rhine
Spearman correlation = 0.483
Rank RA85
Rank RAL
Scatterplot Meuse
Spearman correlation = 0.272
nL [-]
RAL [-]
Rank scatterplot Rhine
Spearman correlation = 0.272
Rank nL
Rank RAL
Scatterplot Meuse
Spearman correlation = 0.089
n50 [-]
RAL [-]
Rank scatterplot Rhine
Spearman correlation = 0.089
Rank n50
Rank RAL
Scatterplot Meuse
Spearman correlation = 0.069
n85 [-]
RAL [-]
Rank scatterplot Rhine
Spearman correlation = 0.069
Rank n85
Rank RAL
Scatterplot Meuse
Spearman correlation = 1.0
RA50 [-]
RA50 [-]
Rank scatterplot Rhine
Spearman correlation = 1.0
Rank RA50
Rank RA50
Scatterplot Meuse
Spearman correlation = 0.214
RA85 [-]
RA50 [-]
Rank scatterplot Rhine
Spearman correlation = 0.214
Rank RA85
Rank RA50
Scatterplot Meuse
Spearman correlation = 0.16
nL [-]
RA50 [-]
Rank scatterplot Rhine
Spearman correlation = 0.16
Rank nL
Rank RA50
Scatterplot Meuse
Spearman correlation = 0.154
n50 [-]
RA50 [-]
Rank scatterplot Rhine
Spearman correlation = 0.154
Rank n50
Rank RA50
Scatterplot Meuse
Spearman correlation = -0.044
n85 [-]
RA50 [-]
Rank scatterplot Rhine
Spearman correlation = -0.044
Rank n85
Rank RA50
Scatterplot Meuse
Spearman correlation = 1.0
RA85 [-]
RA85 [-]
Rank scatterplot Rhine
Spearman correlation = 1.0
Rank RA85
Rank RA85
Scatterplot Meuse
Spearman correlation = 0.057
nL [-]
RA85 [-]
Rank scatterplot Rhine
Spearman correlation = 0.057
Rank nL
Rank RA85

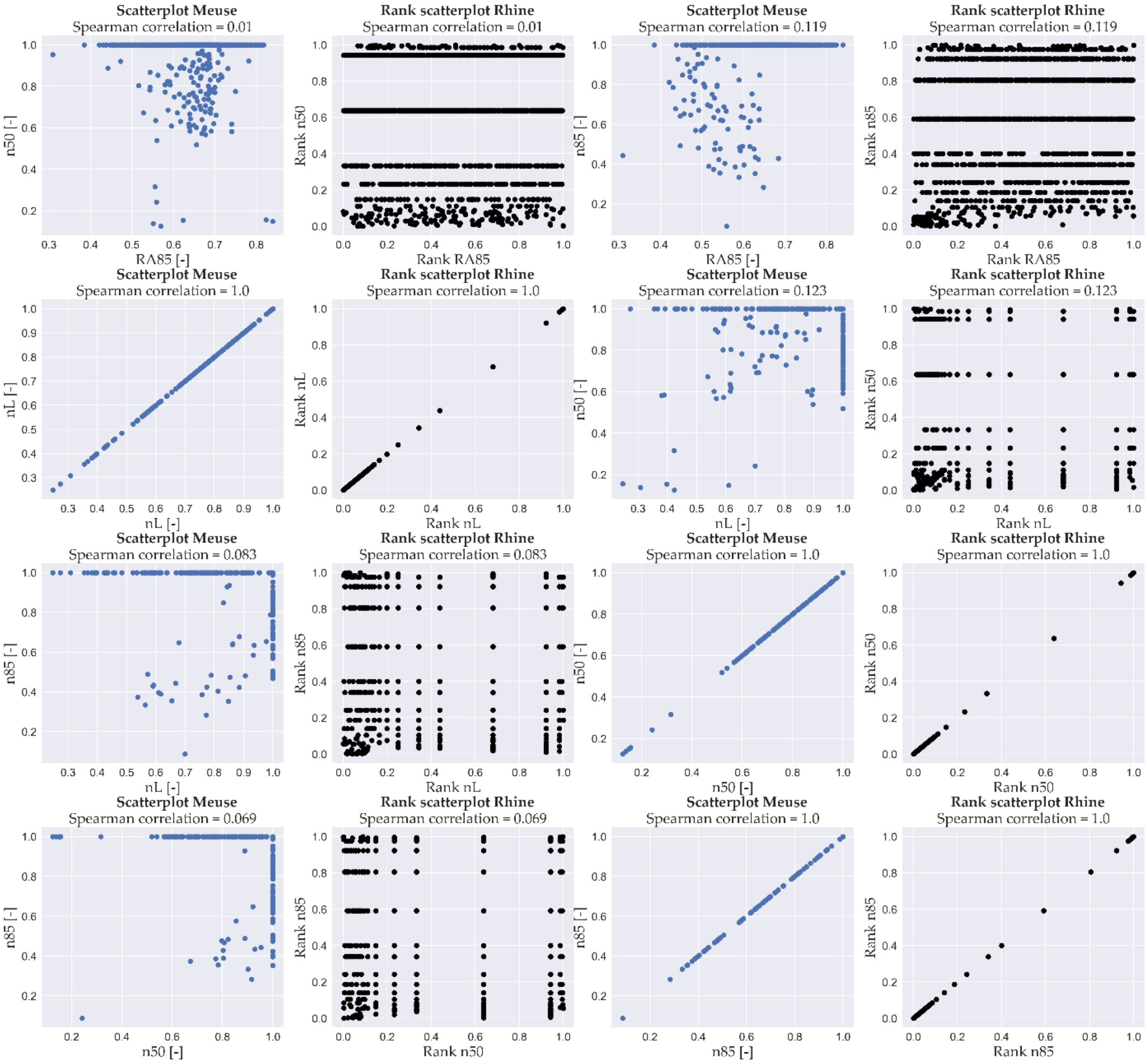
Scatterplot Meuse
Spearman correlation = 0.01
n50 [-]
RA85 [-]
Rank scatterplot Rhine
Spearman correlation = 0.01
Rank n50
Rank RA85
Scatterplot Meuse
Spearman correlation = 0.119
n85 [-]
RA85 [-]
Rank scatterplot Rhine
Spearman correlation = 0.119
Rank n85
Rank RA85
Scatterplot Meuse
Spearman correlation = 1.0
nL [-]
nL [-]
Rank scatterplot Rhine
Spearman correlation = 1.0
Rank nL
Rank nL
Scatterplot Meuse
Spearman correlation = 0.123
n50 [-]
nL [-]
Rank scatterplot Rhine
Spearman correlation = 0.123
Rank n50
Rank nL
Scatterplot Meuse
Spearman correlation = 0.083
n85 [-]
nL [-]
Rank scatterplot Rhine
Spearman correlation = 0.083
Rank n85
Rank nL
Scatterplot Meuse
Spearman correlation = 1.0
n50 [-]
n50 [-]
Rank scatterplot Rhine
Spearman correlation = 1.0
Rank n50
Rank n50
Scatterplot Meuse
Spearman correlation = 0.069
n85 [-]
n50 [-]
Rank scatterplot Rhine
Spearman correlation = 0.069
Rank n85
Rank n50
Scatterplot Meuse
Spearman correlation = 1.0
n85 [-]
n85 [-]
Rank scatterplot Rhine
Spearman correlation = 1.0
Rank n85
Rank n85

APPENDIX N. RESULTS PARTIAL CORRELATION ANALYSIS

TABLE N.1: PARTIAL CORRELATION BETWEEN THE SHAPE VARIABLES AND THE SAFETY FACTOR GIVEN D_L

	Dike type 1		**Dike type 2**		**Dike type 3**		**Dike type 4**	
	Rhine	Meuse	Rhine	Meuse	Rhine	Meuse	Rhine	Meuse
h_{max}	0.15	0.2	0.05	0.21	0.18	0	0.16	0.2
D_0	-0.12	-0.08	-0.08	-0.01	-0.13	-0.07	-0.12	-0.08
D_{50}	-0.38	-0.12	-0.31	-0.09	-0.39	-0.1	-0.39	-0.12
D_{85}	-0.09	-0.07	-0.03	-0.02	-0.05	-0.1	-0.11	-0.07
A_0	-0.15	-0.17	-0.14	-0.11	-0.12	-0.13	-0.13	-0.17
A_L	0.21	0.21	0.09	0.28	0.2	0.02	0.21	0.21
A_{50}	0.15	0.18	0.18	0.12	0.12	0.16	0.14	0.18
A_{85}	-0.35	-0.13	-0.36	-0.05	-0.32	-0.13	-0.34	-0.13
RA_0	-0.5	-0.06	-0.41	-0.08	-0.5	-0.05	-0.51	-0.06
RA_L	0.06	0.1	0.08	0.16	0.03	0.04	0.06	0.1
RA_{50}	-0.27	-0.07	-0.32	-0.1	-0.3	-0.02	-0.27	-0.07
RA_{85}	0.45	0.06	0.43	0.06	0.38	0.04	0.45	0.06
n_l	0.04	0.01	0	0.04	0.02	0.01	0.04	0.01
$n_{50\%}$	0.2	0.07	0.16	0.02	0.21	0.02	0.2	0.07
$n_{85\%}$	0.2	0.04	0.1	0.06	0.13	0.01	0.2	0.04

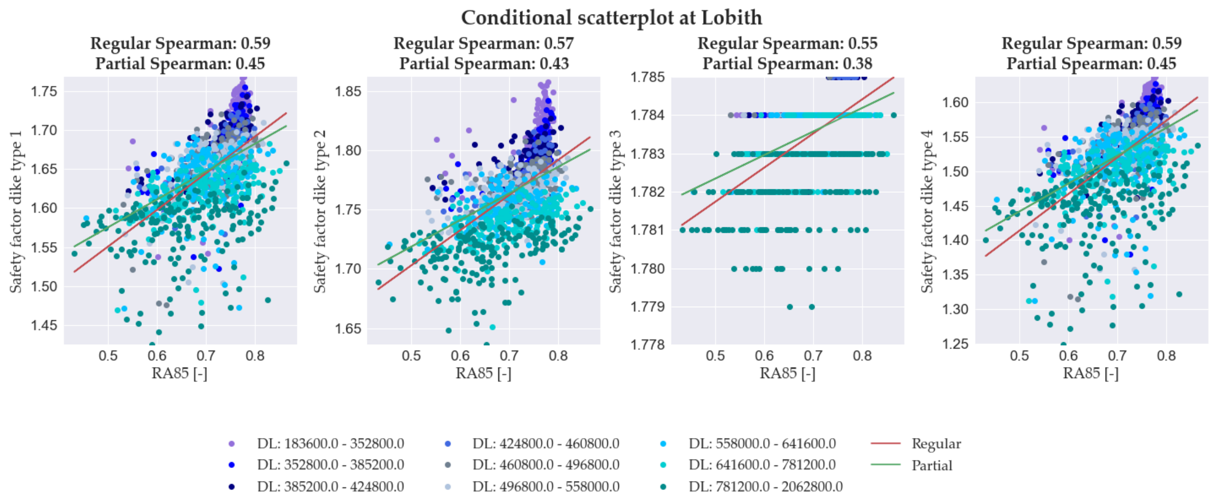

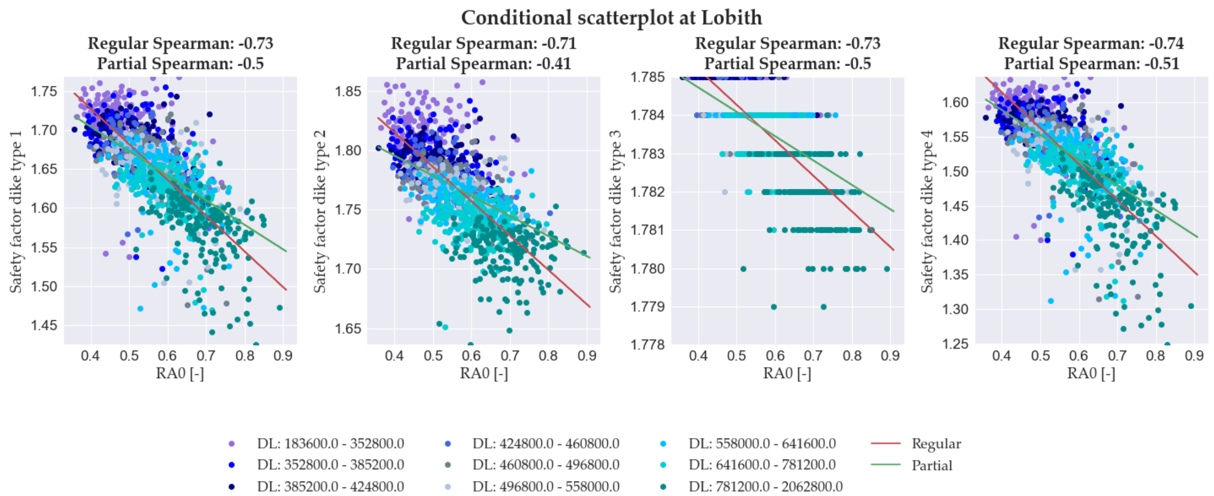

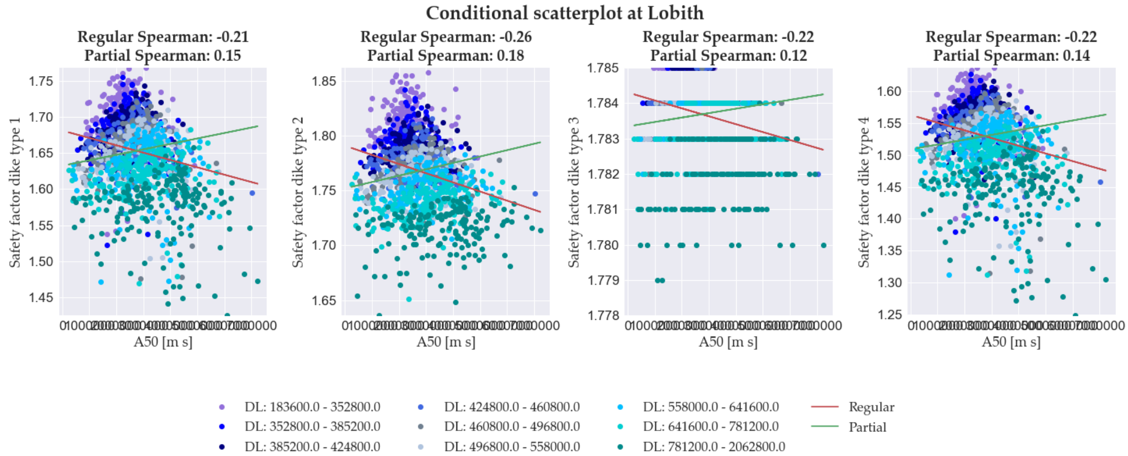
Conditional scatterplot at Lobith
Regular Spearman: -0.21
Partial Spearman: 0.15
Regular Spearman: -0.26
Partial Spearman: 0.18
Regular Spearman: -0.22
Partial Spearman: 0.12
Regular Spearman: -0.22
Partial Spearman: 0.14
Safety factor dike type 1
Safety factor dike type 2
Safety factor dike type 3
Safety factor dike type 4
A50 [m s]
DL: 183600.0 - 352800.0
DL: 352800.0 - 385200.0
DL: 385200.0 - 424800.0
DL: 424800.0 - 460800.0
DL: 460800.0 - 496800.0
DL: 496800.0 - 558000.0
DL: 558000.0 - 641600.0
DL: 641600.0 - 781200.0
DL: 781200.0 - 2062800.0
Regular
Partial

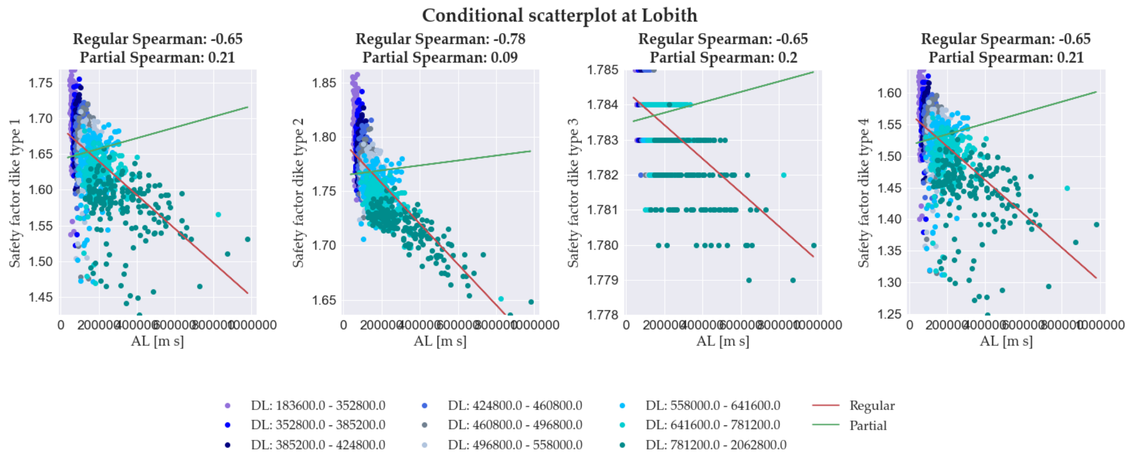
Conditional scatterplot at Lobith
Regular Spearman: -0.65
Partial Spearman: 0.21
Regular Spearman: -0.78
Partial Spearman: 0.09
Regular Spearman: -0.65
Partial Spearman: 0.2
Regular Spearman: -0.65
Partial Spearman: 0.21
Safety factor dike type 1
Safety factor dike type 2
Safety factor dike type 3
Safety factor dike type 4
AL [m s]
DL: 183600.0 - 352800.0
DL: 352800.0 - 385200.0
DL: 385200.0 - 424800.0
DL: 424800.0 - 460800.0
DL: 460800.0 - 496800.0
DL: 496800.0 - 558000.0
DL: 558000.0 - 641600.0
DL: 641600.0 - 781200.0
DL: 781200.0 - 2062800.0
Regular
Partial

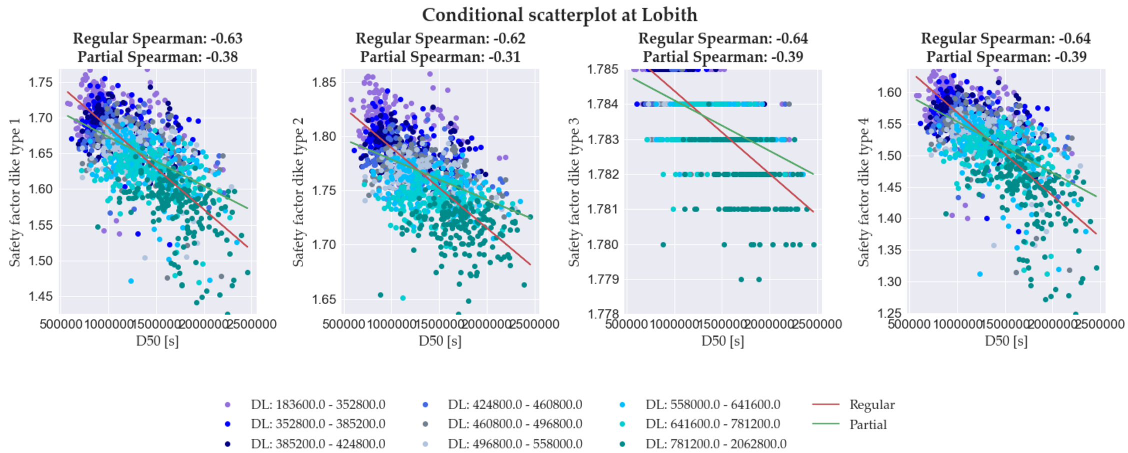
Conditional scatterplot at Lobith
Regular Spearman: -0.63
Partial Spearman: -0.38
Regular Spearman: -0.62
Partial Spearman: -0.31
Regular Spearman: -0.64
Partial Spearman: -0.39
Regular Spearman: -0.64
Partial Spearman: -0.39
Safety factor dike type 1
Safety factor dike type 2
Safety factor dike type 3
Safety factor dike type 4
D50 [s]
DL: 183600.0 - 352800.0
DL: 352800.0 - 385200.0
DL: 385200.0 - 424800.0
DL: 424800.0 - 460800.0
DL: 460800.0 - 496800.0
DL: 496800.0 - 558000.0
DL: 558000.0 - 641600.0
DL: 641600.0 - 781200.0
DL: 781200.0 - 2062800.0
Regular
Partial

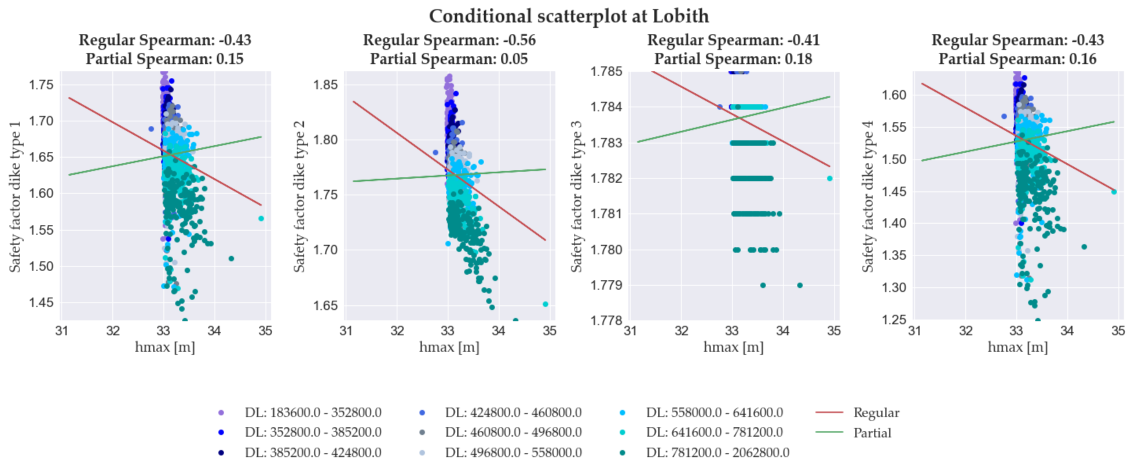
Conditional scatterplot at Lobith
Regular Spearman: -0.43
Partial Spearman: 0.15
Regular Spearman: -0.56
Partial Spearman: 0.05
Regular Spearman: -0.41
Partial Spearman: 0.18
Regular Spearman: -0.43
Partial Spearman: 0.16
Safety factor dike type 1
Safety factor dike type 2
Safety factor dike type 3
Safety factor dike type 4
hmax [m]
DL: 183600.0 - 352800.0
DL: 352800.0 - 385200.0
DL: 385200.0 - 424800.0
DL: 424800.0 - 460800.0
DL: 460800.0 - 496800.0
DL: 496800.0 - 558000.0
DL: 558000.0 - 641600.0
DL: 641600.0 - 781200.0
DL: 781200.0 - 2062800.0
Regular
Partial

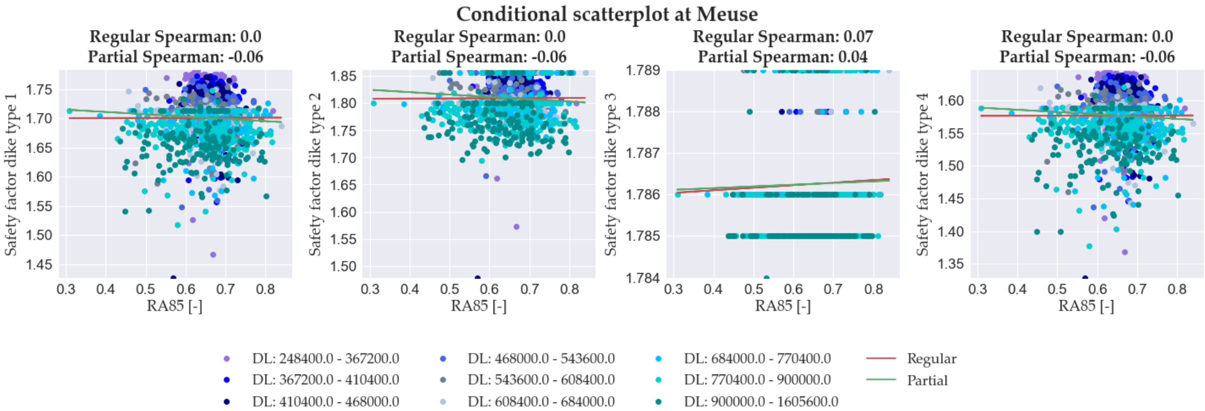
Conditional scatterplot at Meuse
Regular Spearman: 0.0
Partial Spearman: -0.06
Regular Spearman: 0.0
Partial Spearman: -0.06
Regular Spearman: 0.07
Partial Spearman: 0.04
Regular Spearman: 0.0
Partial Spearman: -0.06
Safety factor dike type 1
Safety factor dike type 2
Safety factor dike type 3
Safety factor dike type 4
RA85 [-]
DL: 248400.0 - 367200.0
DL: 367200.0 - 410400.0
DL: 410400.0 - 468000.0
DL: 468000.0 - 543600.0
DL: 543600.0 - 608400.0
DL: 608400.0 - 684000.0
DL: 684000.0 - 770400.0
DL: 770400.0 - 900000.0
DL: 900000.0 - 1605600.0
Regular
Partial

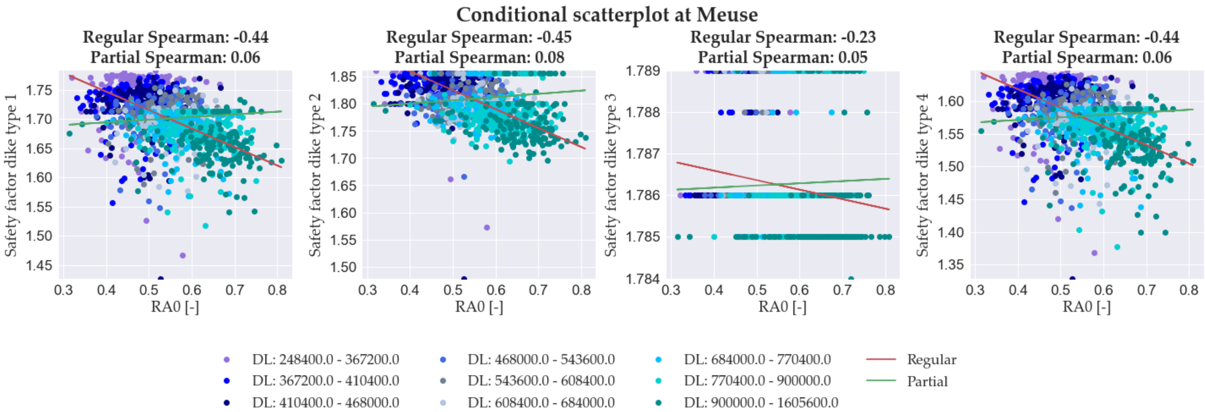
Conditional scatterplot at Meuse
Regular Spearman: -0.44
Partial Spearman: 0.06
Regular Spearman: -0.45
Partial Spearman: 0.08
Regular Spearman: -0.23
Partial Spearman: 0.05
Regular Spearman: -0.44
Partial Spearman: 0.06
Safety factor dike type 1
Safety factor dike type 2
Safety factor dike type 3
Safety factor dike type 4
RA0 [-]
DL: 248400.0 - 367200.0
DL: 367200.0 - 410400.0
DL: 410400.0 - 468000.0
DL: 468000.0 - 543600.0
DL: 543600.0 - 608400.0
DL: 608400.0 - 684000.0
DL: 684000.0 - 770400.0
DL: 770400.0 - 900000.0
DL: 900000.0 - 1605600.0
Regular
Partial

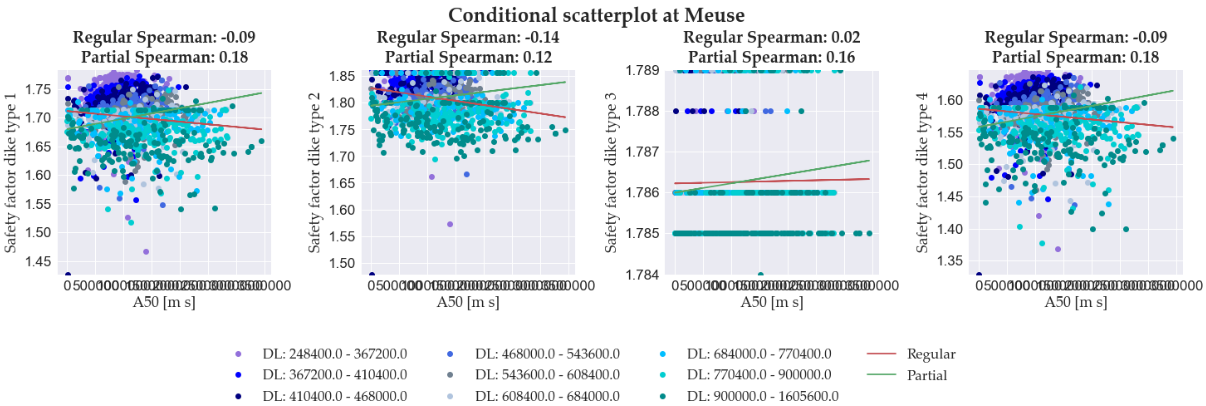
Conditional scatterplot at Meuse
Regular Spearman: -0.09
Partial Spearman: 0.18
Regular Spearman: -0.14
Partial Spearman: 0.12
Regular Spearman: 0.02
Partial Spearman: 0.16
Regular Spearman: -0.09
Partial Spearman: 0.18
Safety factor dike type 1
Safety factor dike type 2
Safety factor dike type 3
Safety factor dike type 4
A50 [m s]
DL: 248400.0 - 367200.0
DL: 367200.0 - 410400.0
DL: 410400.0 - 468000.0
DL: 468000.0 - 543600.0
DL: 543600.0 - 608400.0
DL: 608400.0 - 684000.0
DL: 684000.0 - 770400.0
DL: 770400.0 - 900000.0
DL: 900000.0 - 1605600.0
Regular
Partial

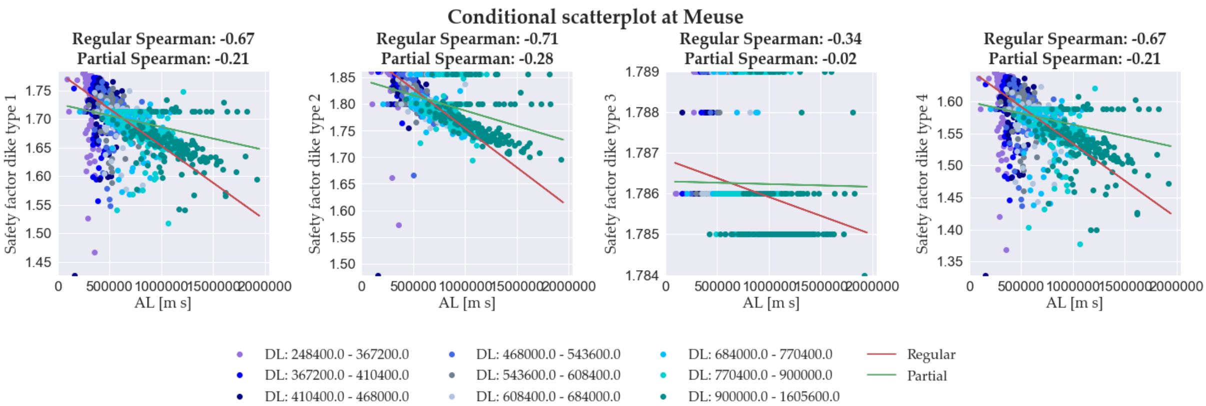
Conditional scatterplot at Meuse
Regular Spearman: -0.67
Partial Spearman: -0.21
Regular Spearman: -0.71
Partial Spearman: -0.28
Regular Spearman: -0.34
Partial Spearman: -0.02
Regular Spearman: -0.67
Partial Spearman: -0.21
Safety factor dike type 1
Safety factor dike type 2
Safety factor dike type 3
Safety factor dike type 4
AL [m s]
DL: 248400.0 - 367200.0
DL: 367200.0 - 410400.0
DL: 410400.0 - 468000.0
DL: 468000.0 - 543600.0
DL: 543600.0 - 608400.0
DL: 608400.0 - 684000.0
DL: 684000.0 - 770400.0
DL: 770400.0 - 900000.0
DL: 900000.0 - 1605600.0
Regular
Partial

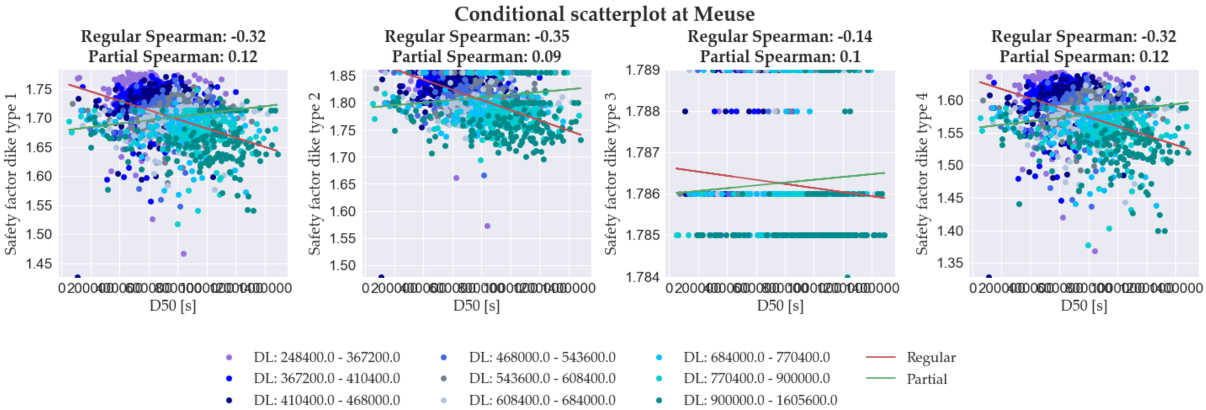

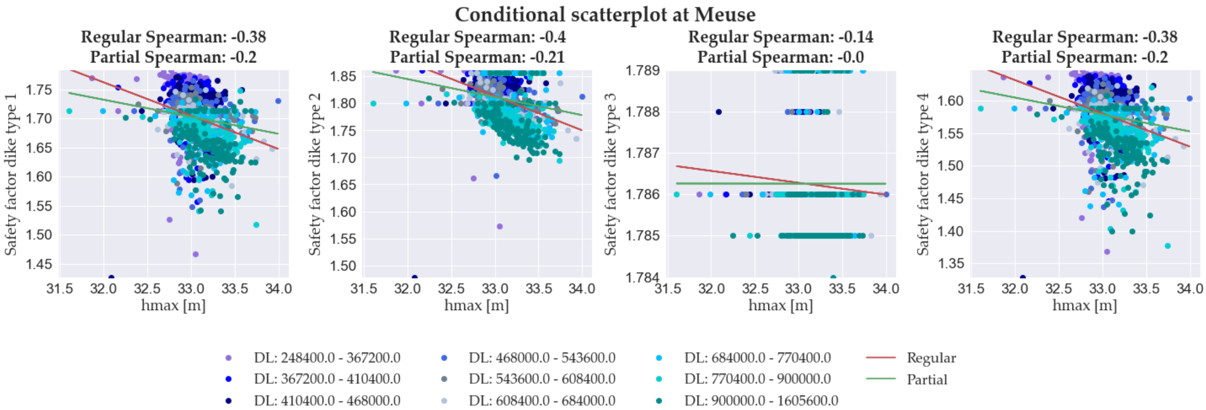

TABLE N.2: PARTIAL CORRELATION BETWEEN THE SHAPE VARIABLES AND THE SAFETY FACTOR GIVEN A_L

	Dike type 1		Dike type 2		Dike type 3		Dike type 4	
	Rhine	Meuse	Rhine	Meuse	Rhine	Meuse	Rhine	Meuse
h_{max}	-0.38	-0.09	-0.42	-0.12	-0.42	-0.12	-0.38	-0.09
D_0	-0.12	-0.11	-0.09	-0.05	-0.13	-0.08	-0.12	-0.11
D_L	-0.55	-0.2	-0.61	-0.17	-0.55	-0.15	-0.55	-0.21
D_{50}	-0.51	-0.07	-0.49	-0.06	-0.52	-0.06	-0.52	-0.07
D_{85}	-0.4	-0.2	-0.42	-0.14	-0.36	-0.14	-0.4	-0.2
A_0	-0.06	-0.21	-0.04	-0.16	-0.04	-0.15	-0.05	-0.21
A_{50}	0	-0.23	-0.02	-0.18	-0.02	-0.17	-0.01	-0.23
A_{85}	-0.14	-0.27	-0.09	-0.22	-0.12	-0.19	-0.13	-0.27
RA_0	-0.63	0	-0.61	-0.03	-0.63	0	-0.64	-0.01
RA_L	0.09	0.19	0.04	0.15	0.06	0.08	0.09	0.19
RA_{50}	-0.11	-0.06	-0.1	-0.06	-0.13	-0.07	-0.11	-0.06
RA_{85}	0.4	0.1	0.32	0.12	0.34	0.11	0.4	0.1
n_l	0.11	0.13	0.09	0.08	0.09	0.06	0.11	0.13
$n_{50\%}$	0.18	0.1	0.14	0.05	0.19	0.01	0.18	0.1
$n_{85\%}$	0.24	0	0.17	0.02	0.18	0.01	0.25	0

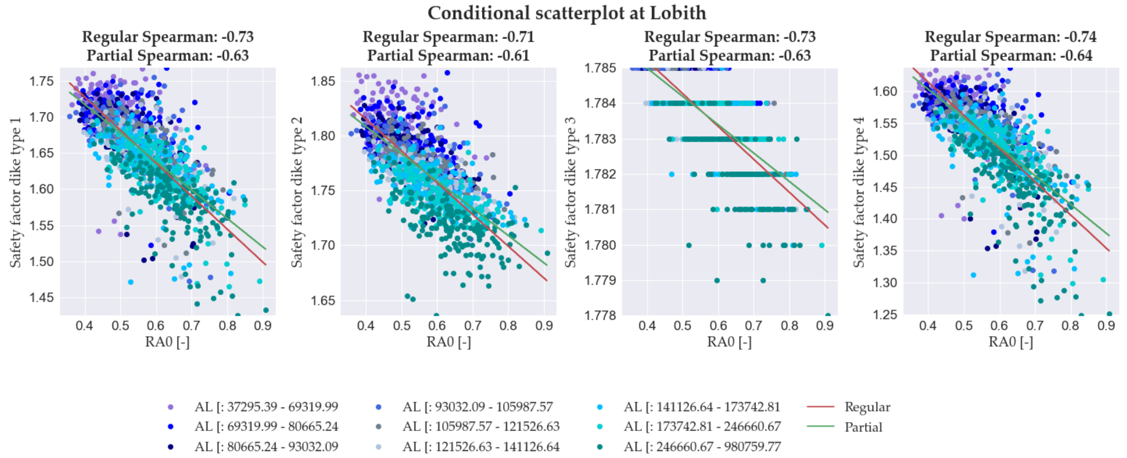
Conditional scatterplot at Lobith
Regular Spearman: -0.73
Partial Spearman: -0.63
Regular Spearman: -0.71
Partial Spearman: -0.61
Regular Spearman: -0.73
Partial Spearman: -0.63
Regular Spearman: -0.74
Partial Spearman: -0.64
Safety factor dike type 1
Safety factor dike type 2
Safety factor dike type 3
Safety factor dike type 4
RA0 [-]
AL [: 37295.39 - 69319.99
AL [: 69319.99 - 80665.24
AL [: 80665.24 - 93032.09
AL [: 93032.09 - 105987.57
AL [: 105987.57 - 121526.63
AL [: 121526.63 - 141126.64
AL [: 141126.64 - 173742.81
AL [: 173742.81 - 246660.67
AL [: 246660.67 - 980759.77
Regular
Partial

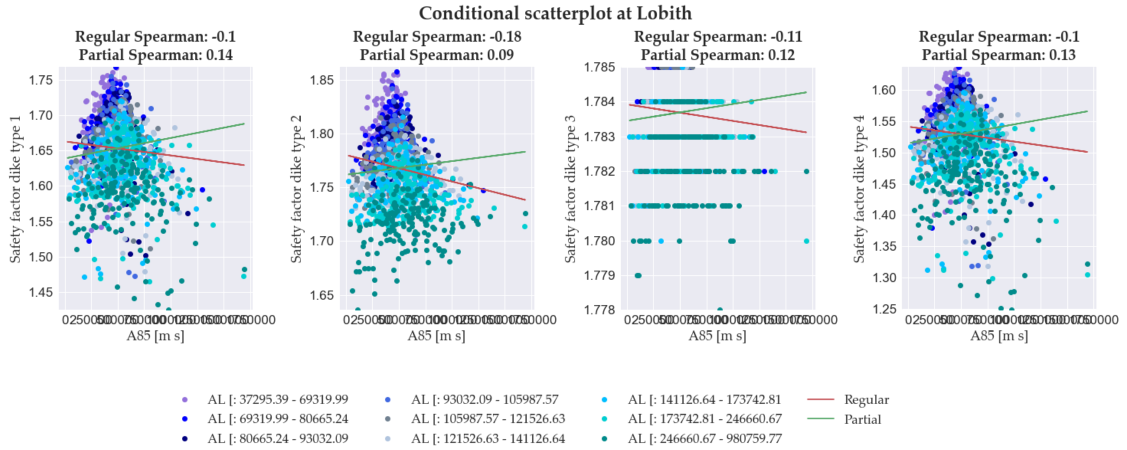
Conditional scatterplot at Lobith
Regular Spearman: -0.1
Partial Spearman: 0.14
Regular Spearman: -0.18
Partial Spearman: 0.09
Regular Spearman: -0.11
Partial Spearman: 0.12
Regular Spearman: -0.1
Partial Spearman: 0.13
Safety factor dike type 1
Safety factor dike type 2
Safety factor dike type 3
Safety factor dike type 4
A85 [m s]
AL [: 37295.39 - 69319.99
AL [: 69319.99 - 80665.24
AL [: 80665.24 - 93032.09
AL [: 93032.09 - 105987.57
AL [: 105987.57 - 121526.63
AL [: 121526.63 - 141126.64
AL [: 141126.64 - 173742.81
AL [: 173742.81 - 246660.67
AL [: 246660.67 - 980759.77
Regular
Partial

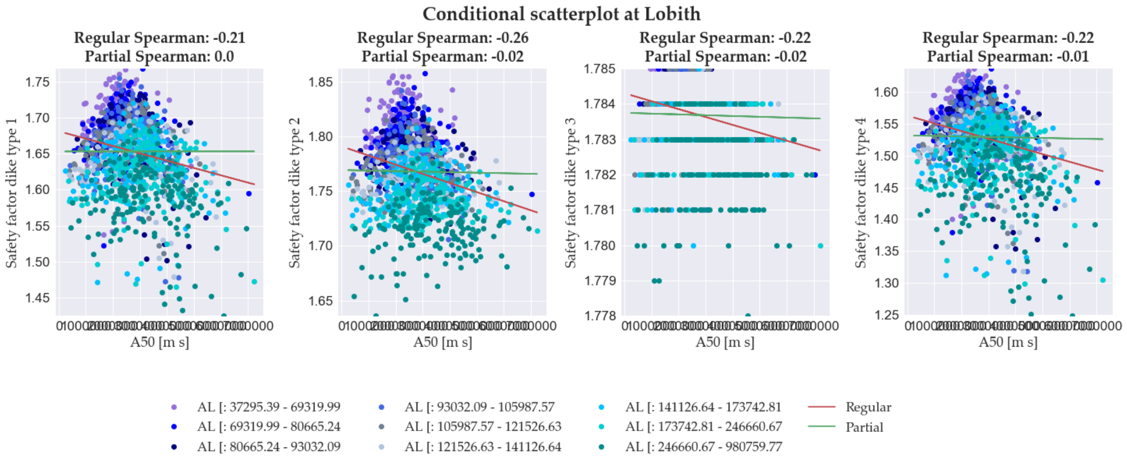
Conditional scatterplot at Lobith
Regular Spearman: -0.21
Partial Spearman: 0.0
Regular Spearman: -0.26
Partial Spearman: -0.02
Regular Spearman: -0.22
Partial Spearman: -0.02
Regular Spearman: -0.22
Partial Spearman: -0.01
Safety factor dike type 1
Safety factor dike type 2
Safety factor dike type 3
Safety factor dike type 4
A50 [m s]
AL [: 37295.39 - 69319.99
AL [: 69319.99 - 80665.24
AL [: 80665.24 - 93032.09
AL [: 93032.09 - 105987.57
AL [: 105987.57 - 121526.63
AL [: 121526.63 - 141126.64
AL [: 141126.64 - 173742.81
AL [: 173742.81 - 246660.67
AL [: 246660.67 - 980759.77
Regular
Partial

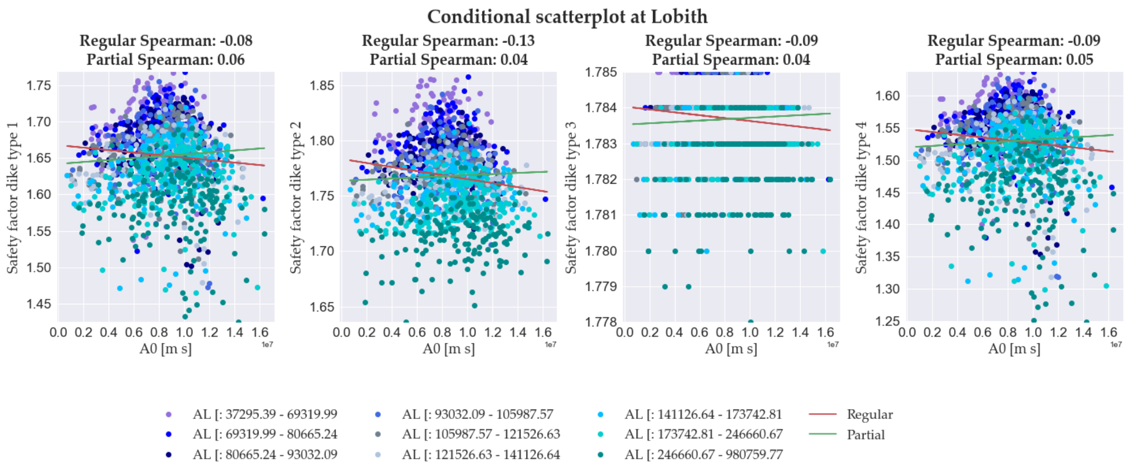
Conditional scatterplot at Lobith
Regular Spearman: -0.08
Partial Spearman: 0.06
Regular Spearman: -0.13
Partial Spearman: 0.04
Regular Spearman: -0.09
Partial Spearman: 0.04
Regular Spearman: -0.09
Partial Spearman: 0.05
Safety factor dike type 1
Safety factor dike type 2
Safety factor dike type 3
Safety factor dike type 4
A0 [m s]
1e7
AL [: 37295.39 - 69319.99
AL [: 69319.99 - 80665.24
AL [: 80665.24 - 93032.09
AL [: 93032.09 - 105987.57
AL [: 105987.57 - 121526.63
AL [: 121526.63 - 141126.64
AL [: 141126.64 - 173742.81
AL [: 173742.81 - 246660.67
AL [: 246660.67 - 980759.77
Regular
Partial

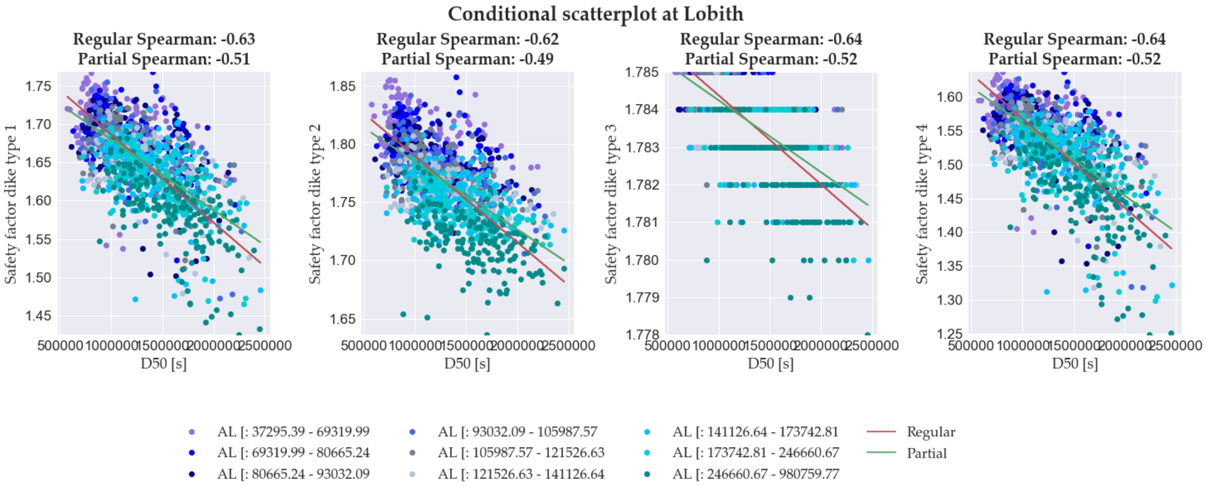
Conditional scatterplot at Lobith
Regular Spearman: -0.63
Partial Spearman: -0.51
Regular Spearman: -0.62
Partial Spearman: -0.49
Regular Spearman: -0.64
Partial Spearman: -0.52
Regular Spearman: -0.64
Partial Spearman: -0.52
Safety factor dike type 1
Safety factor dike type 2
Safety factor dike type 3
Safety factor dike type 4
D50 [s]
AL [: 37295.39 - 69319.99
AL [: 69319.99 - 80665.24
AL [: 80665.24 - 93032.09
AL [: 93032.09 - 105987.57
AL [: 105987.57 - 121526.63
AL [: 121526.63 - 141126.64
AL [: 141126.64 - 173742.81
AL [: 173742.81 - 246660.67
AL [: 246660.67 - 980759.77
Regular
Partial

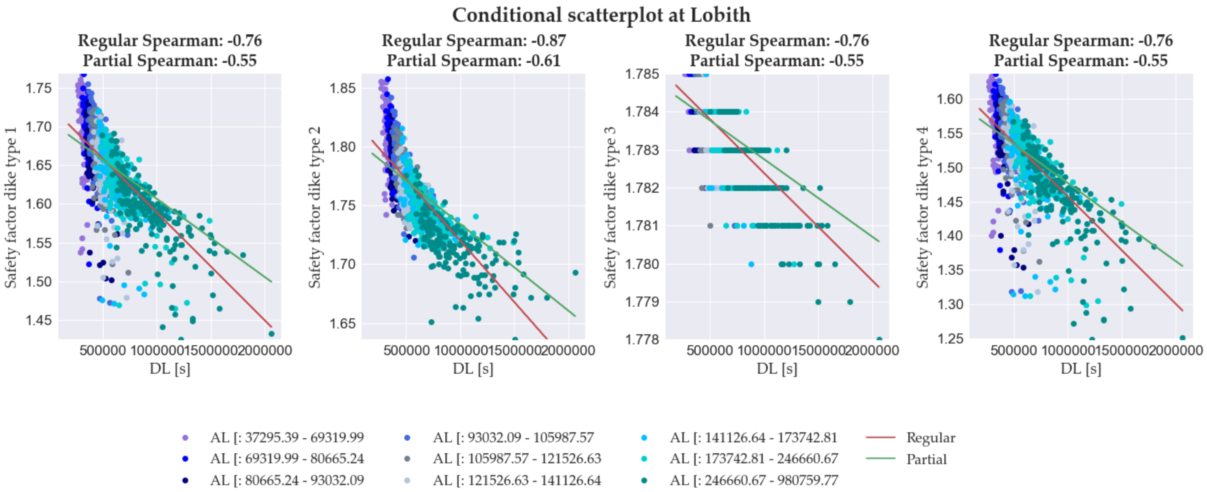
Conditional scatterplot at Lobith
Regular Spearman: -0.76
Partial Spearman: -0.55
Regular Spearman: -0.87
Partial Spearman: -0.61
Regular Spearman: -0.76
Partial Spearman: -0.55
Regular Spearman: -0.76
Partial Spearman: -0.55
Safety factor dike type 1
Safety factor dike type 2
Safety factor dike type 3
Safety factor dike type 4
DL [s]
AL [: 37295.39 - 69319.99
AL [: 69319.99 - 80665.24
AL [: 80665.24 - 93032.09
AL [: 93032.09 - 105987.57
AL [: 105987.57 - 121526.63
AL [: 121526.63 - 141126.64
AL [: 141126.64 - 173742.81
AL [: 173742.81 - 246660.67
AL [: 246660.67 - 980759.77
Regular
Partial

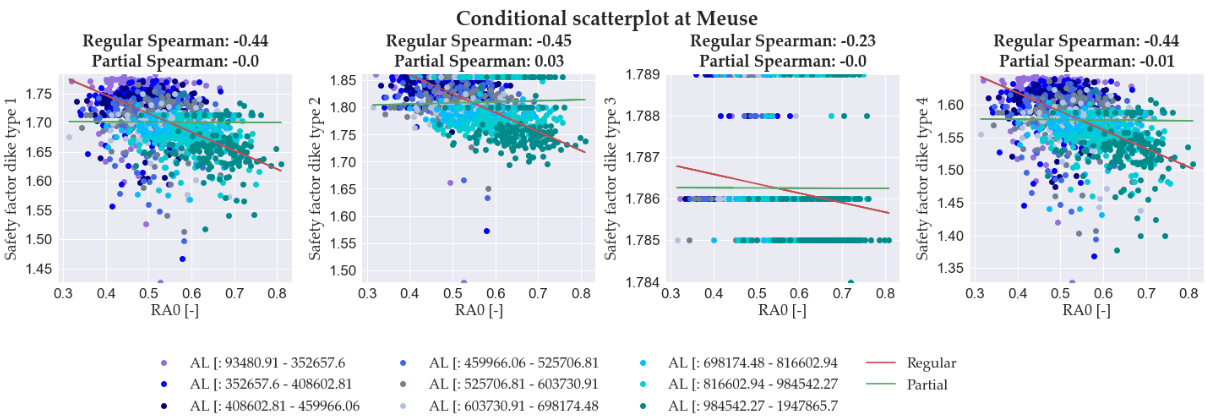
Conditional scatterplot at Meuse
Regular Spearman: -0.44
Partial Spearman: -0.0
Regular Spearman: -0.45
Partial Spearman: 0.03
Regular Spearman: -0.23
Partial Spearman: -0.0
Regular Spearman: -0.44
Partial Spearman: -0.01
Safety factor dike type 1
Safety factor dike type 2
Safety factor dike type 3
Safety factor dike type 4
RA0 [-]
AL [: 93480.91 - 352657.6
AL [: 352657.6 - 408602.81
AL [: 408602.81 - 459966.06
AL [: 459966.06 - 525706.81
AL [: 525706.81 - 603730.91
AL [: 603730.91 - 698174.48
AL [: 698174.48 - 816602.94
AL [: 816602.94 - 984542.27
AL [: 984542.27 - 1947865.7
Regular
Partial

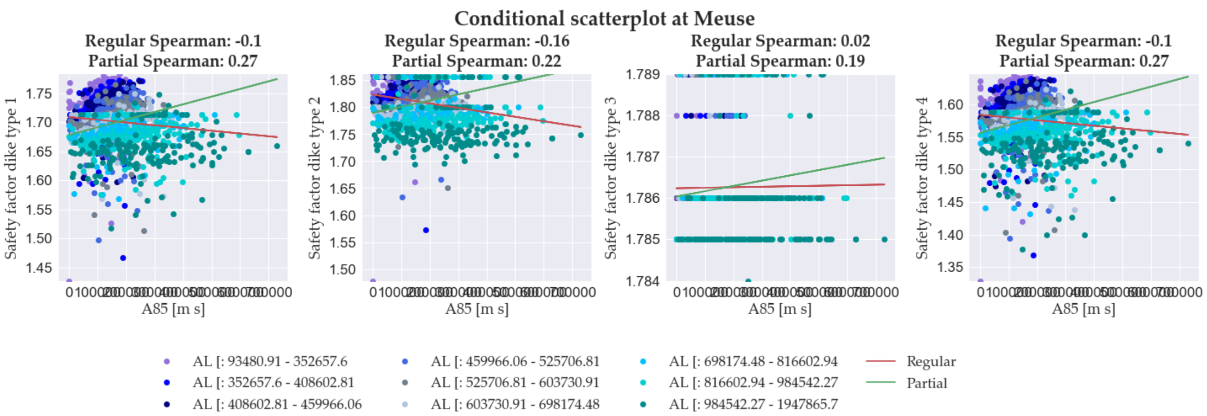
Conditional scatterplot at Meuse
Regular Spearman: -0.1
Partial Spearman: 0.27
Regular Spearman: -0.16
Partial Spearman: 0.22
Regular Spearman: 0.02
Partial Spearman: 0.19
Regular Spearman: -0.1
Partial Spearman: 0.27
Safety factor dike type 1
Safety factor dike type 2
Safety factor dike type 3
Safety factor dike type 4
A85 [m s]
AL [: 93480.91 - 352657.6
AL [: 352657.6 - 408602.81
AL [: 408602.81 - 459966.06
AL [: 459966.06 - 525706.81
AL [: 525706.81 - 603730.91
AL [: 603730.91 - 698174.48
AL [: 698174.48 - 816602.94
AL [: 816602.94 - 984542.27
AL [: 984542.27 - 1947865.7
Regular
Partial

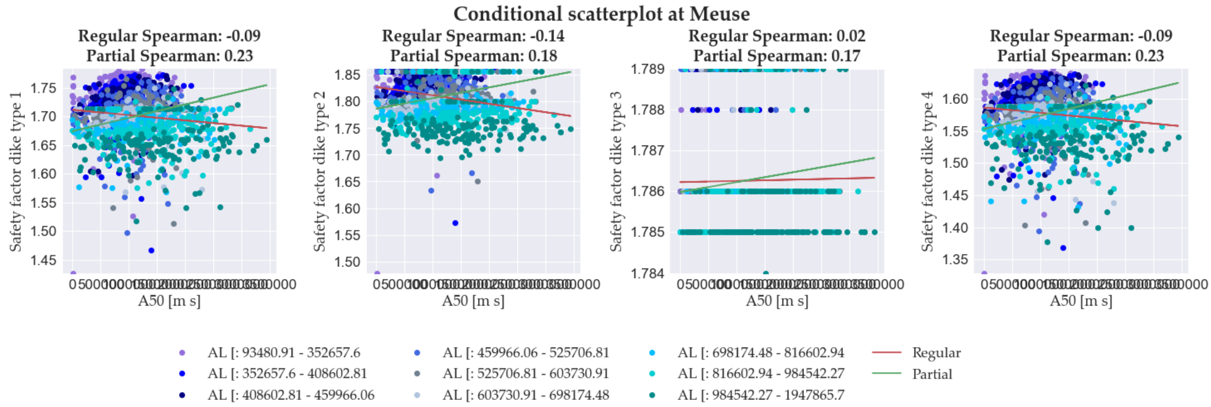
Conditional scatterplot at Meuse
Regular Spearman: -0.09
Partial Spearman: 0.23
Regular Spearman: -0.14
Partial Spearman: 0.18
Regular Spearman: 0.02
Partial Spearman: 0.17
Regular Spearman: -0.09
Partial Spearman: 0.23
Safety factor dike type 1
Safety factor dike type 2
Safety factor dike type 3
Safety factor dike type 4
A50 [m s]
AL [: 93480.91 - 352657.6
AL [: 352657.6 - 408602.81
AL [: 408602.81 - 459966.06
AL [: 459966.06 - 525706.81
AL [: 525706.81 - 603730.91
AL [: 603730.91 - 698174.48
AL [: 698174.48 - 816602.94
AL [: 816602.94 - 984542.27
AL [: 984542.27 - 1947865.7
Regular
Partial

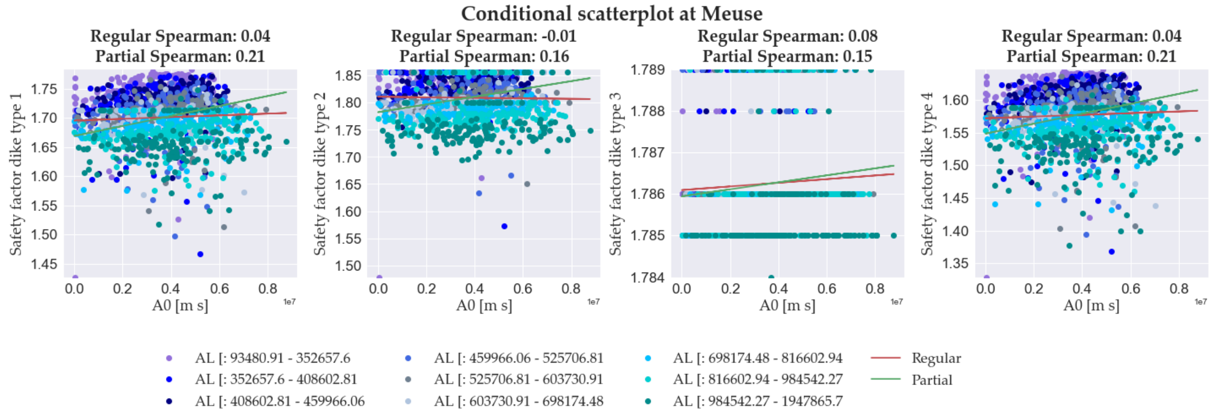
Conditional scatterplot at Meuse
Regular Spearman: 0.04
Partial Spearman: 0.21
Regular Spearman: -0.01
Partial Spearman: 0.16
Regular Spearman: 0.08
Partial Spearman: 0.15
Regular Spearman: 0.04
Partial Spearman: 0.21
Safety factor dike type 1
Safety factor dike type 2
Safety factor dike type 3
Safety factor dike type 4
A0 [m s]
1e7
AL [: 93480.91 - 352657.6
AL [: 352657.6 - 408602.81
AL [: 408602.81 - 459966.06
AL [: 459966.06 - 525706.81
AL [: 525706.81 - 603730.91
AL [: 603730.91 - 698174.48
AL [: 698174.48 - 816602.94
AL [: 816602.94 - 984542.27
AL [: 984542.27 - 1947865.7
Regular
Partial

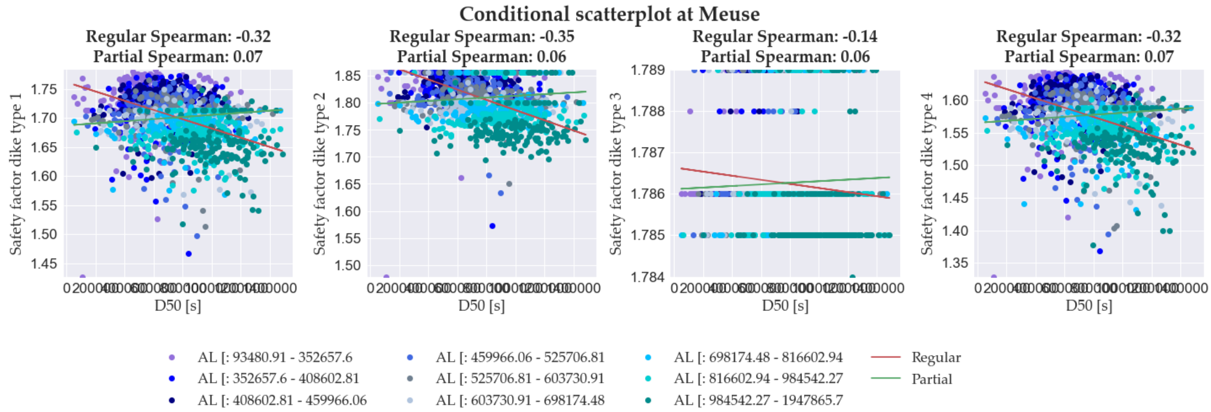
Conditional scatterplot at Meuse
Regular Spearman: -0.32
Partial Spearman: 0.07
Regular Spearman: -0.35
Partial Spearman: 0.06
Regular Spearman: -0.14
Partial Spearman: 0.06
Regular Spearman: -0.32
Partial Spearman: 0.07
Safety factor dike type 1
Safety factor dike type 2
Safety factor dike type 3
Safety factor dike type 4
D50 [s]
AL [: 93480.91 - 352657.6
AL [: 352657.6 - 408602.81
AL [: 408602.81 - 459966.06
AL [: 459966.06 - 525706.81
AL [: 525706.81 - 603730.91
AL [: 603730.91 - 698174.48
AL [: 698174.48 - 816602.94
AL [: 816602.94 - 984542.27
AL [: 984542.27 - 1947865.7
Regular
Partial

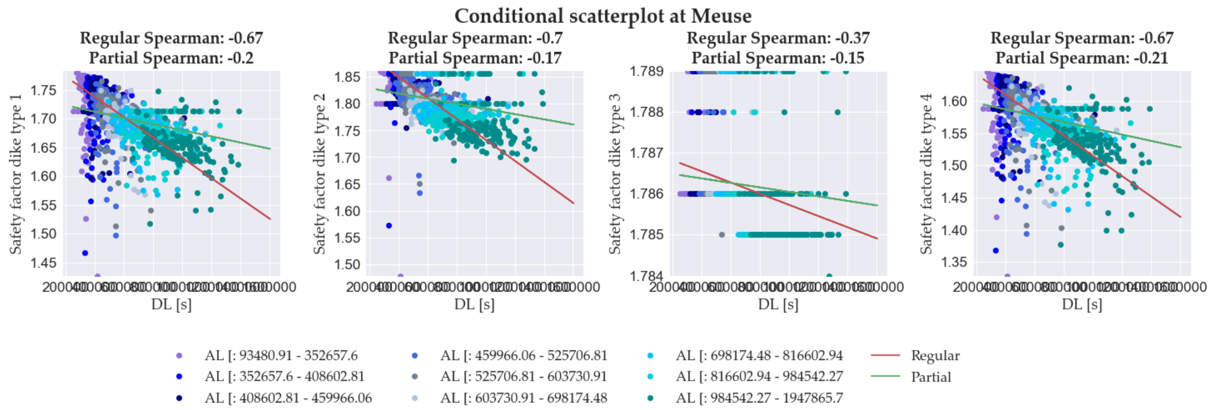
Conditional scatterplot at Meuse
Regular Spearman: -0.67
Partial Spearman: -0.2
Regular Spearman: -0.7
Partial Spearman: -0.17
Regular Spearman: -0.37
Partial Spearman: -0.15
Regular Spearman: -0.67
Partial Spearman: -0.21
Safety factor dike type 1
Safety factor dike type 2
Safety factor dike type 3
Safety factor dike type 4
DL [s]
AL [: 93480.91 - 352657.6
AL [: 352657.6 - 408602.81
AL [: 408602.81 - 459966.06
AL [: 459966.06 - 525706.81
AL [: 525706.81 - 603730.91
AL [: 603730.91 - 698174.48
AL [: 698174.48 - 816602.94
AL [: 816602.94 - 984542.27
AL [: 984542.27 - 1947865.7
Regular
Partial

TABLE N.3: PARTIAL CORRELATION BETWEEN THE SHAPE VARIABLES AND THE SAFETY FACTOR GIVEN RA_0

	Dike type 1		Dike type 2		Dike type 3		Dike type 4	
	Rhine	Meuse	Rhine	Meuse	Rhine	Meuse	Rhine	Meuse
h_{max}	-0.37	-0.33	-0.55	-0.35	-0.35	-0.09	-0.37	-0.33
D_0	-0.05	0	-0.01	-0.06	-0.06	-0.04	-0.04	0
D_L	-0.57	-0.57	-0.77	-0.6	-0.56	-0.3	-0.56	-0.57
D_{50}	-0.09	0	-0.1	-0.04	-0.11	-0.03	-0.1	0
D_{85}	-0.31	-0.13	-0.44	-0.22	-0.28	-0.01	-0.31	-0.13
A_0	-0.35	-0.25	-0.24	-0.2	-0.33	-0.18	-0.34	-0.25
A_L	-0.5	-0.57	-0.71	-0.62	-0.5	-0.26	-0.5	-0.57
A_{50}	-0.27	-0.19	-0.15	-0.13	-0.24	-0.17	-0.26	-0.19
A_{85}	-0.25	-0.13	-0.1	-0.06	-0.22	-0.14	-0.24	-0.13
RA_L	0.41	0.01	0.51	0.06	0.38	0	0.4	0.01
RA_{50}	-0.19	-0.22	-0.25	-0.24	-0.16	-0.06	-0.19	-0.21
RA_{85}	0.46	0.01	0.42	0.01	0.39	0.06	0.46	0.01
n_l	0.11	0.04	0.11	0	0.09	0.03	0.11	0.04
$n_{50\%}$	0.06	0.06	0	0.01	0.07	0.02	0.07	0.06
$n_{85\%}$	0.13	0	0.04	0.01	0.06	0.01	0.13	0.01

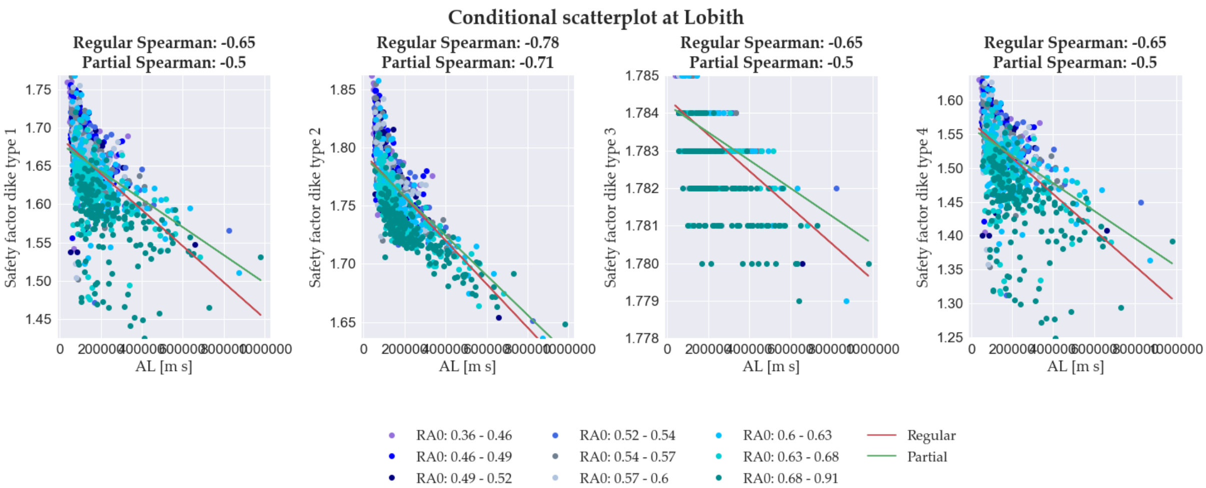

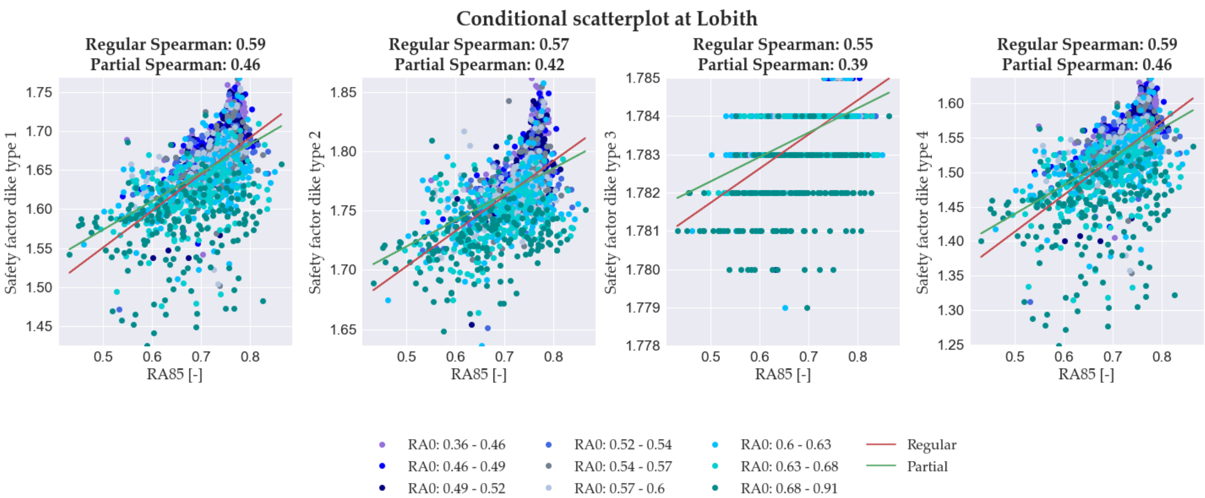

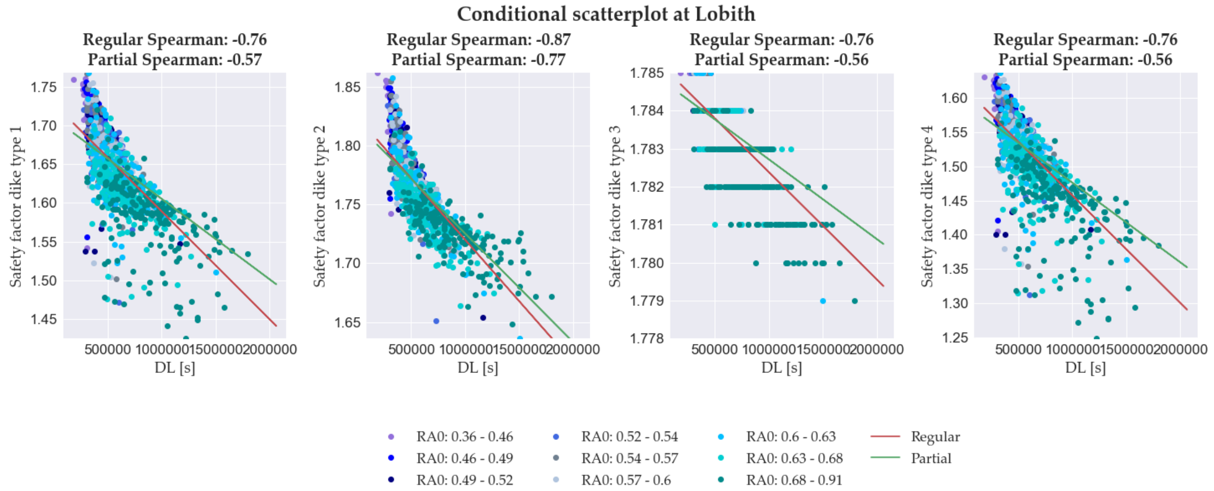
Conditional scatterplot at Lobith
Regular Spearman: -0.76
Partial Spearman: -0.57
Regular Spearman: -0.87
Partial Spearman: -0.77
Regular Spearman: -0.76
Partial Spearman: -0.56
Regular Spearman: -0.76
Partial Spearman: -0.56
Safety factor dike type 1
Safety factor dike type 2
Safety factor dike type 3
Safety factor dike type 4
DL [s]
RA0: 0.36 - 0.46
RA0: 0.46 - 0.49
RA0: 0.49 - 0.52
RA0: 0.52 - 0.54
RA0: 0.54 - 0.57
RA0: 0.57 - 0.6
RA0: 0.6 - 0.63
RA0: 0.63 - 0.68
RA0: 0.68 - 0.91
Regular
Partial

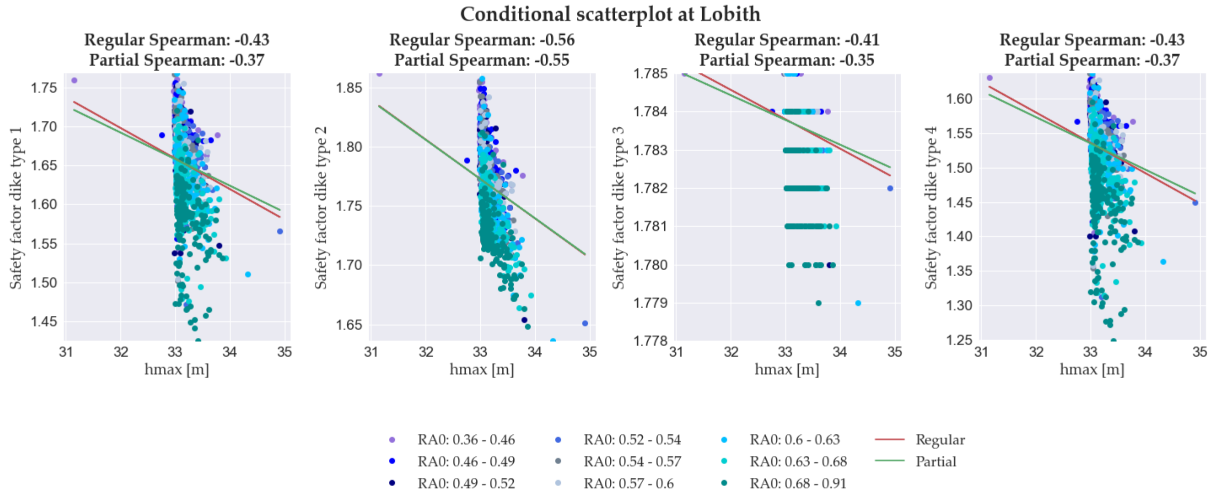
Conditional scatterplot at Lobith
Regular Spearman: -0.43
Partial Spearman: -0.37
Regular Spearman: -0.56
Partial Spearman: -0.55
Regular Spearman: -0.41
Partial Spearman: -0.35
Regular Spearman: -0.43
Partial Spearman: -0.37
Safety factor dike type 1
Safety factor dike type 2
Safety factor dike type 3
Safety factor dike type 4
hmax [m]
RA0: 0.36 - 0.46
RA0: 0.46 - 0.49
RA0: 0.49 - 0.52
RA0: 0.52 - 0.54
RA0: 0.54 - 0.57
RA0: 0.57 - 0.6
RA0: 0.6 - 0.63
RA0: 0.63 - 0.68
RA0: 0.68 - 0.91
Regular
Partial

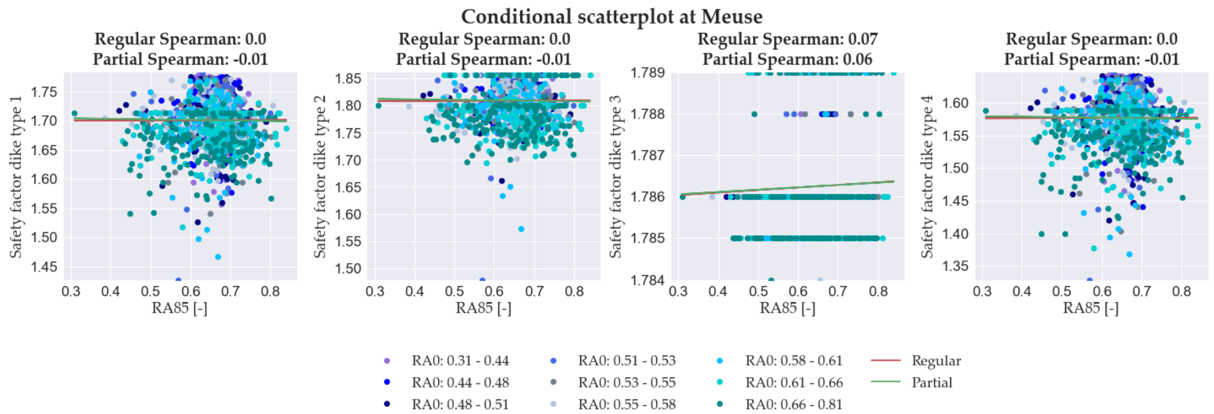
Conditional scatterplot at Meuse
Regular Spearman: 0.0
Partial Spearman: -0.01
Regular Spearman: 0.0
Partial Spearman: -0.01
Regular Spearman: 0.07
Partial Spearman: 0.06
Regular Spearman: 0.0
Partial Spearman: -0.01
Safety factor dike type 1
Safety factor dike type 2
Safety factor dike type 3
Safety factor dike type 4
RA85 [-]
RA0: 0.31 - 0.44
RA0: 0.44 - 0.48
RA0: 0.48 - 0.51
RA0: 0.51 - 0.53
RA0: 0.53 - 0.55
RA0: 0.55 - 0.58
RA0: 0.58 - 0.61
RA0: 0.61 - 0.66
RA0: 0.66 - 0.81
Regular
Partial

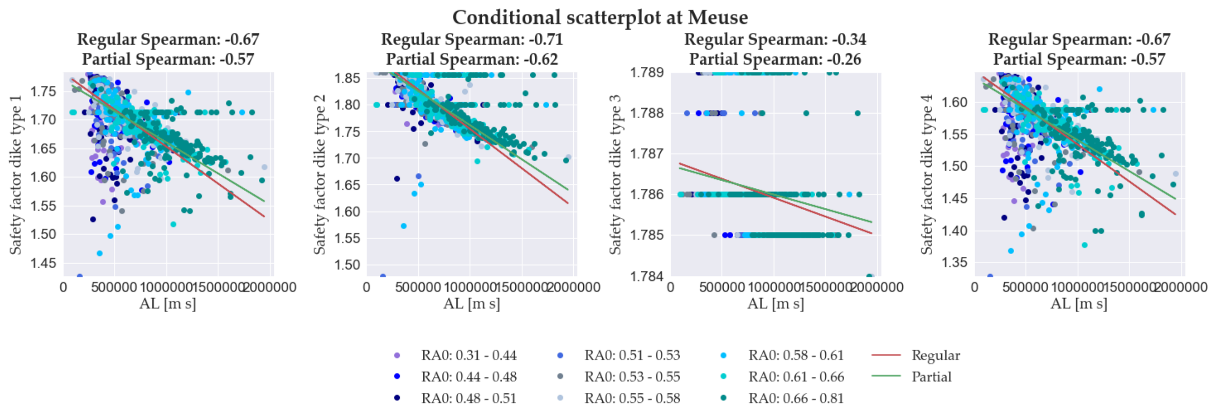
Conditional scatterplot at Meuse
Regular Spearman: -0.67
Partial Spearman: -0.57
Regular Spearman: -0.71
Partial Spearman: -0.62
Regular Spearman: -0.34
Partial Spearman: -0.26
Regular Spearman: -0.67
Partial Spearman: -0.57
Safety factor dike type 1
Safety factor dike type 2
Safety factor dike type 3
Safety factor dike type 4
AL [m s]
RA0: 0.31 - 0.44
RA0: 0.44 - 0.48
RA0: 0.48 - 0.51
RA0: 0.51 - 0.53
RA0: 0.53 - 0.55
RA0: 0.55 - 0.58
RA0: 0.58 - 0.61
RA0: 0.61 - 0.66
RA0: 0.66 - 0.81
Regular
Partial

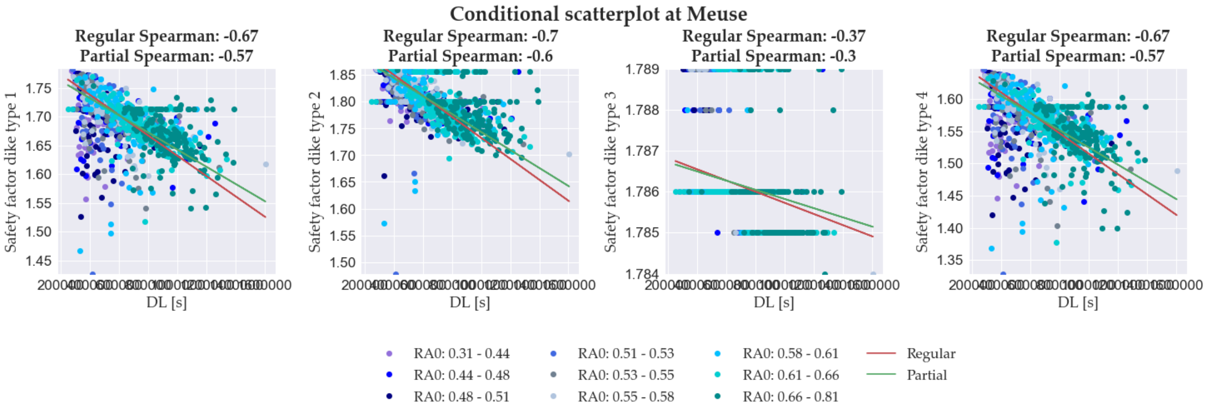

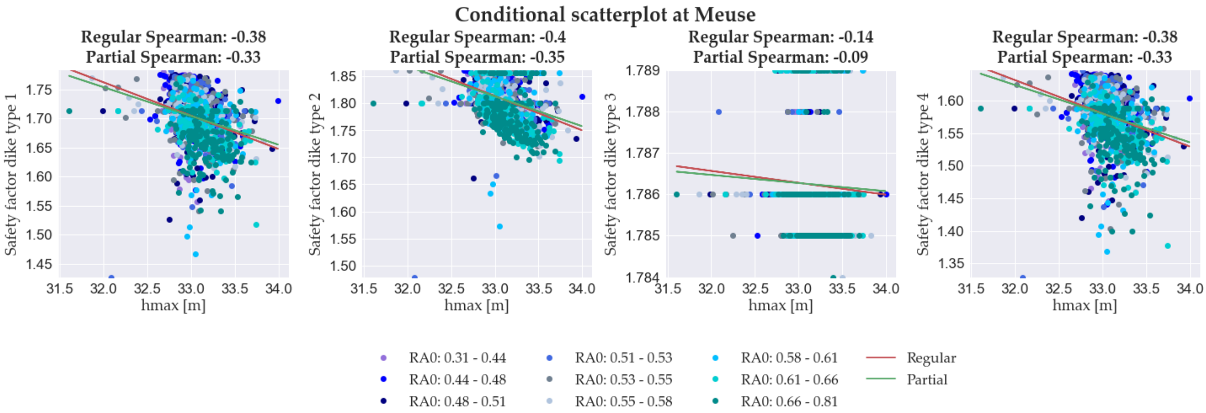

TABLE N.4: PARTIAL CORRELATION BETWEEN THE SHAPE VARIABLES AND THE SAFETY FACTOR GIVEN h_{max}

	Dike type 1		**Dike type 2**		**Dike type 3**		**Dike type 4**	
	Rhine	Meuse	Rhine	Meuse	Rhine	Meuse	Rhine	Meuse
D_0	0.12	0.02	0.09	-0.04	0.11	0.04	0.11	0.02
D_L	-0.71	-0.62	-0.80	-0.64	-0.71	-0.35	-0.71	-0.62
D_{50}	-0.60	-0.28	-0.60	-0.31	-0.61	-0.12	-0.61	-0.28
D_{85}	-0.58	-0.29	-0.65	-0.37	-0.57	-0.12	-0.59	-0.29
A_0	-0.03	0.09	-0.07	0.04	-0.04	0.09	-0.04	0.08
A_L	-0.63	-0.6	-0.73	-0.65	-0.65	-0.34	-0.63	-0.60
A_{50}	-0.14	-0.02	-0.18	-0.08	-0.16	0.05	-0.15	-0.02
A_{85}	-0.04	0.01	-0.12	-0.06	-0.06	0.06	-0.04	0.01
RA_0	-0.72	-0.4	-0.70	-0.41	-0.71	-0.2	-0.71	-0.40
RA_L	0.35	0.07	0.34	0.03	0.34	0.02	0.35	0.08
RA_{50}	-0.04	-0.2	-0.09	-0.22	-0.02	-0.07	-0.03	-0.2
RA_{85}	0.47	0.13	0.38	0.14	0.43	0.11	0.47	0.13
n_l	0.17	0.09	0.16	0.05	0.15	0.05	0.17	0.09
$n_{50\%}$	0.16	0.08	0.12	0.04	0.16	-0.01	0.16	0.08
$n_{85\%}$	0.27	0.08	0.22	0.07	0.22	0.05	0.27	0.08

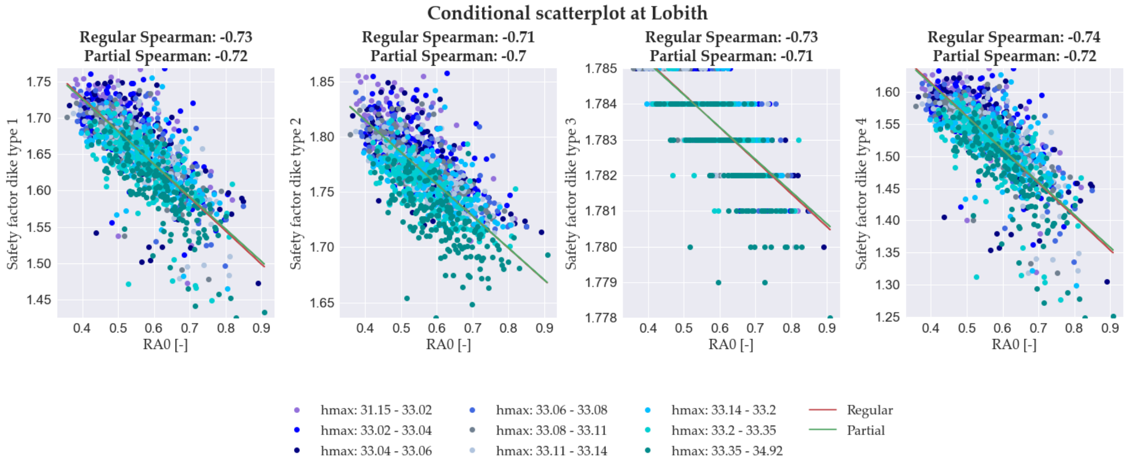
Conditional scatterplot at Lobith
Regular Spearman: -0.73
Partial Spearman: -0.72
Regular Spearman: -0.71
Partial Spearman: -0.7
Regular Spearman: -0.73
Partial Spearman: -0.71
Regular Spearman: -0.74
Partial Spearman: -0.72
Safety factor dike type 1
Safety factor dike type 2
Safety factor dike type 3
Safety factor dike type 4
RA0 [-]
hmax: 31.15 - 33.02
hmax: 33.02 - 33.04
hmax: 33.04 - 33.06
hmax: 33.06 - 33.08
hmax: 33.08 - 33.11
hmax: 33.11 - 33.14
hmax: 33.14 - 33.2
hmax: 33.2 - 33.35
hmax: 33.35 - 34.92
Regular
Partial

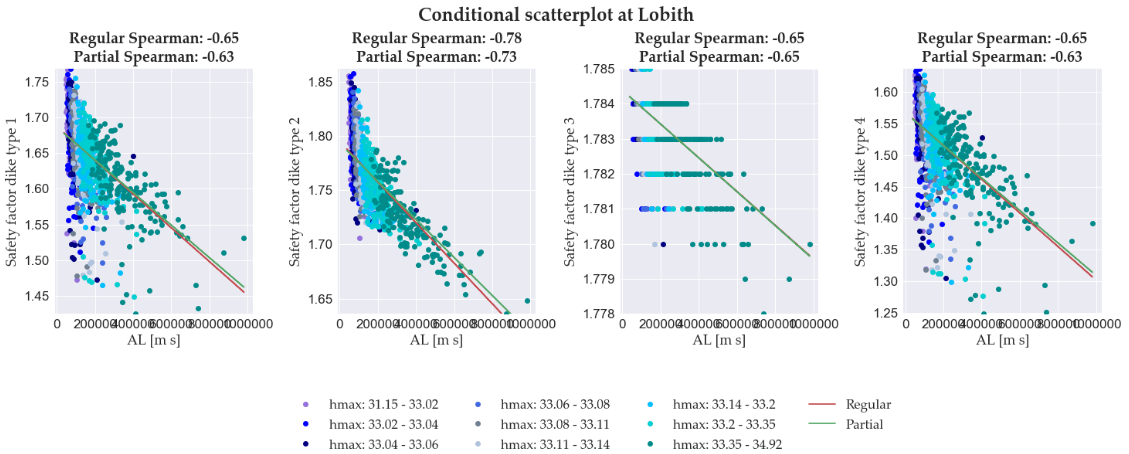
Conditional scatterplot at Lobith
Regular Spearman: -0.65
Partial Spearman: -0.63
Regular Spearman: -0.78
Partial Spearman: -0.73
Regular Spearman: -0.65
Partial Spearman: -0.65
Regular Spearman: -0.65
Partial Spearman: -0.63
Safety factor dike type 1
Safety factor dike type 2
Safety factor dike type 3
Safety factor dike type 4
AL [m s]
hmax: 31.15 - 33.02
hmax: 33.02 - 33.04
hmax: 33.04 - 33.06
hmax: 33.06 - 33.08
hmax: 33.08 - 33.11
hmax: 33.11 - 33.14
hmax: 33.14 - 33.2
hmax: 33.2 - 33.35
hmax: 33.35 - 34.92
Regular
Partial

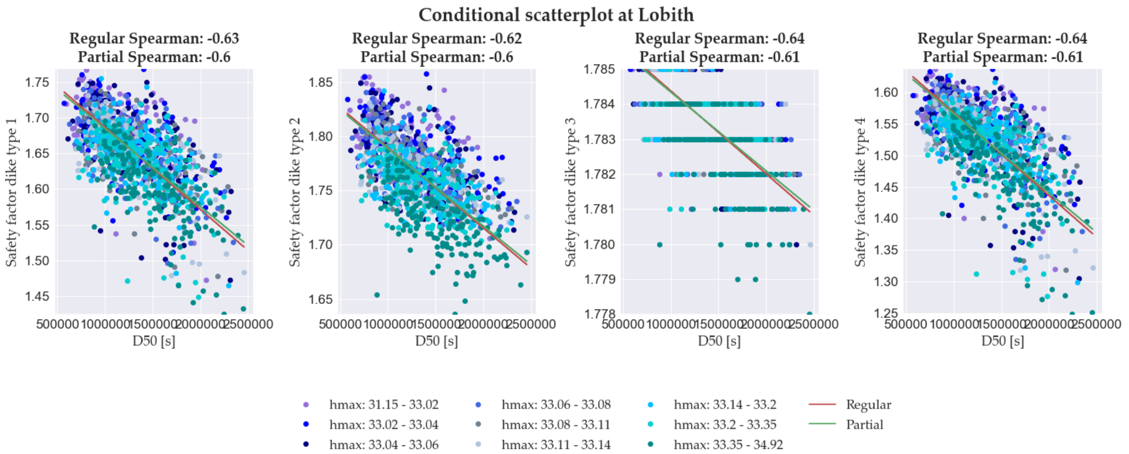
Conditional scatterplot at Lobith
Regular Spearman: -0.63
Partial Spearman: -0.6
Regular Spearman: -0.62
Partial Spearman: -0.6
Regular Spearman: -0.64
Partial Spearman: -0.61
Regular Spearman: -0.64
Partial Spearman: -0.61
Safety factor dike type 1
Safety factor dike type 2
Safety factor dike type 3
Safety factor dike type 4
D50 [s]
hmax: 31.15 - 33.02
hmax: 33.02 - 33.04
hmax: 33.04 - 33.06
hmax: 33.06 - 33.08
hmax: 33.08 - 33.11
hmax: 33.11 - 33.14
hmax: 33.14 - 33.2
hmax: 33.2 - 33.35
hmax: 33.35 - 34.92
Regular
Partial

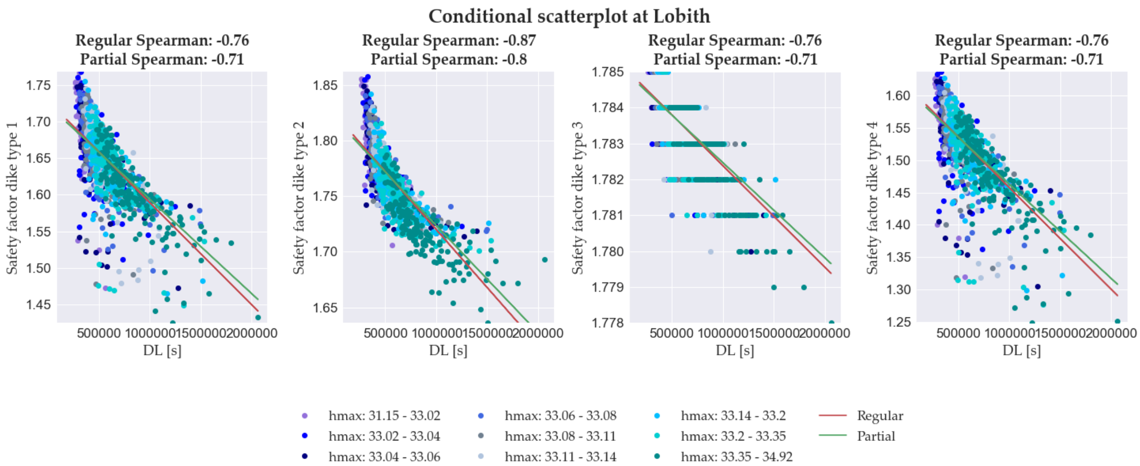
Conditional scatterplot at Lobith
Regular Spearman: -0.76
Partial Spearman: -0.71
Regular Spearman: -0.87
Partial Spearman: -0.8
Regular Spearman: -0.76
Partial Spearman: -0.71
Regular Spearman: -0.76
Partial Spearman: -0.71
Safety factor dike type 1
Safety factor dike type 2
Safety factor dike type 3
Safety factor dike type 4
DL [s]
hmax: 31.15 - 33.02
hmax: 33.02 - 33.04
hmax: 33.04 - 33.06
hmax: 33.06 - 33.08
hmax: 33.08 - 33.11
hmax: 33.11 - 33.14
hmax: 33.14 - 33.2
hmax: 33.2 - 33.35
hmax: 33.35 - 34.92
Regular
Partial

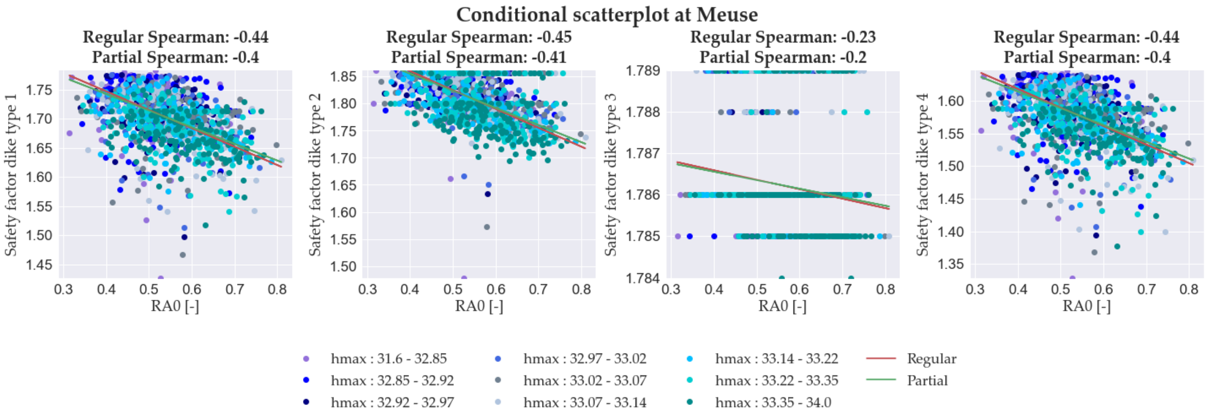
Conditional scatterplot at Meuse
Regular Spearman: -0.44
Partial Spearman: -0.4
Regular Spearman: -0.45
Partial Spearman: -0.41
Regular Spearman: -0.23
Partial Spearman: -0.2
Regular Spearman: -0.44
Partial Spearman: -0.4
Safety factor dike type 1
Safety factor dike type 2
Safety factor dike type 3
Safety factor dike type 4
RA0 [-]
hmax : 31.6 - 32.85
hmax : 32.85 - 32.92
hmax : 32.92 - 32.97
hmax : 32.97 - 33.02
hmax : 33.02 - 33.07
hmax : 33.07 - 33.14
hmax : 33.14 - 33.22
hmax : 33.22 - 33.35
hmax : 33.35 - 34.0
Regular
Partial

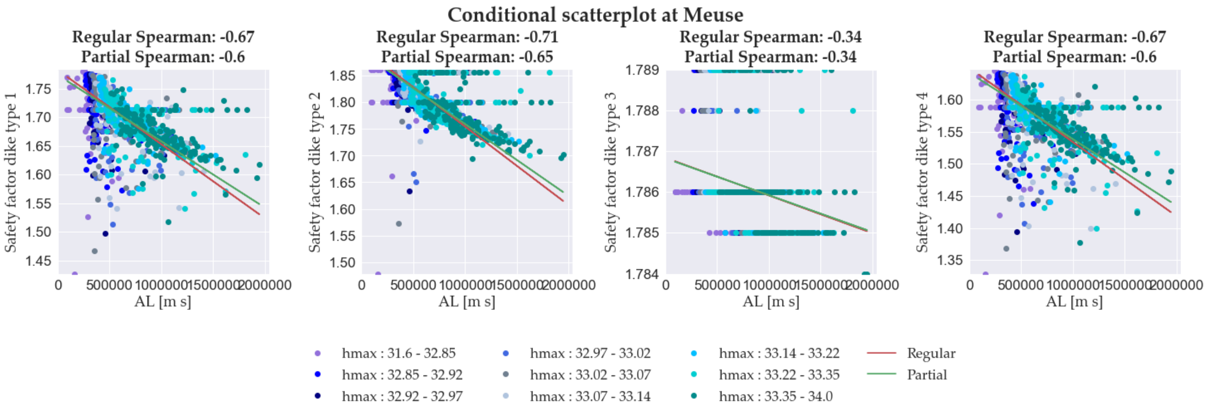
Conditional scatterplot at Meuse
Regular Spearman: -0.67
Partial Spearman: -0.6
Regular Spearman: -0.71
Partial Spearman: -0.65
Regular Spearman: -0.34
Partial Spearman: -0.34
Regular Spearman: -0.67
Partial Spearman: -0.6
Safety factor dike type 1
Safety factor dike type 2
Safety factor dike type 3
Safety factor dike type 4
AL [m s]
hmax : 31.6 - 32.85
hmax : 32.85 - 32.92
hmax : 32.92 - 32.97
hmax : 32.97 - 33.02
hmax : 33.02 - 33.07
hmax : 33.07 - 33.14
hmax : 33.14 - 33.22
hmax : 33.22 - 33.35
hmax : 33.35 - 34.0
Regular
Partial

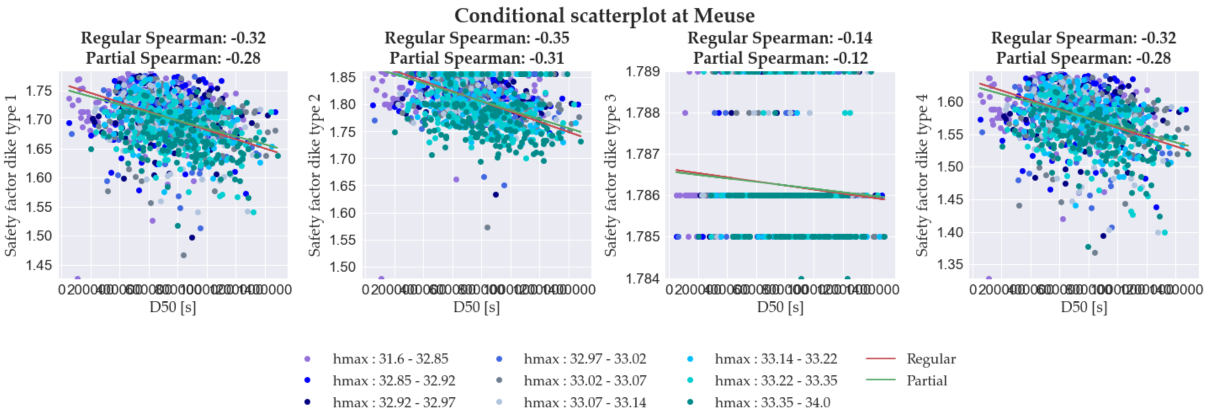
Conditional scatterplot at Meuse
Regular Spearman: -0.32
Partial Spearman: -0.28
Regular Spearman: -0.35
Partial Spearman: -0.31
Regular Spearman: -0.14
Partial Spearman: -0.12
Regular Spearman: -0.32
Partial Spearman: -0.28
Safety factor dike type 1
Safety factor dike type 2
Safety factor dike type 3
Safety factor dike type 4
D50 [s]
hmax : 31.6 - 32.85
hmax : 32.85 - 32.92
hmax : 32.92 - 32.97
hmax : 32.97 - 33.02
hmax : 33.02 - 33.07
hmax : 33.07 - 33.14
hmax : 33.14 - 33.22
hmax : 33.22 - 33.35
hmax : 33.35 - 34.0
Regular
Partial

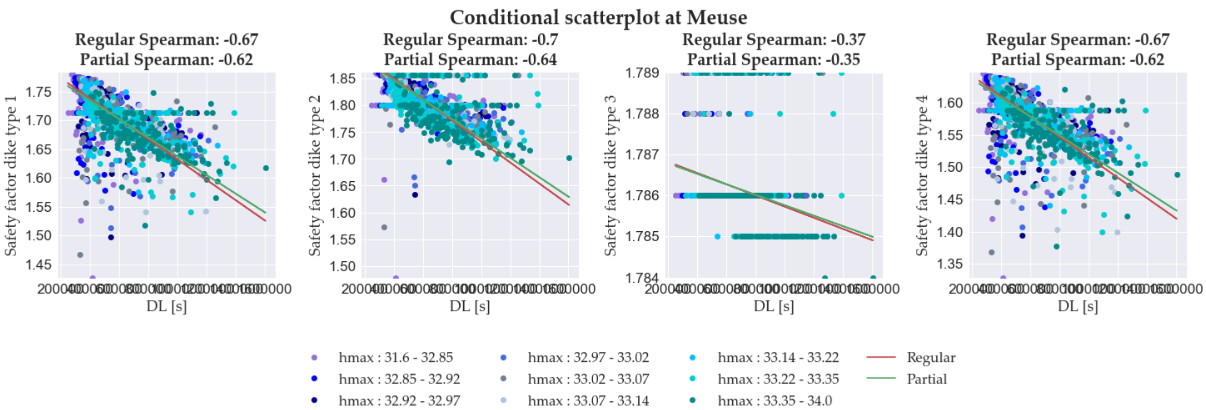
Conditional scatterplot at Meuse
Regular Spearman: -0.67
Partial Spearman: -0.62
Regular Spearman: -0.7
Partial Spearman: -0.64
Regular Spearman: -0.37
Partial Spearman: -0.35
Regular Spearman: -0.67
Partial Spearman: -0.62
Safety factor dike type 1
Safety factor dike type 2
Safety factor dike type 3
Safety factor dike type 4
DL [s]
hmax : 31.6 - 32.85
hmax : 32.85 - 32.92
hmax : 32.92 - 32.97
hmax : 32.97 - 33.02
hmax : 33.02 - 33.07
hmax : 33.07 - 33.14
hmax : 33.14 - 33.22
hmax : 33.22 - 33.35
hmax : 33.35 - 34.0
Regular
Partial

APPENDIX O. RESULTS SAFETY FACTOR FITS

$$FoS(h_{max}, D_{50}) = \rho_{00} + \rho_{10}h_{max} + \rho_{01}D_{50} + \rho_{11}h_{max}D_{50} + \rho_{20}h_{max}^2 + \rho_{02}D_{50}^2$$

TABLE O.1: COEFFICIENTS SAFETY FACTOR FIT BASED ON HMAX AND D50

		ρ_{00}	ρ_{10}	ρ_{01}	ρ_{11}	ρ_{20}	ρ_{02}
Rhine Lobith	Dike 1	-3.00	0.36	1.81e-02	-6.59e-03	-2.15e-04	-5.49e-04
	Dike 2	-5.82	0.53	5.04e-02	-8.92e-03	8.12e-05	-1.72e-03
	Dike 3	1.58	1.28e-02	2.95e-03	-2.00e-4	-4.65e-06	-8.86e-05
	Dike 4	-1.47	0.24	7.71e-02	-4.41e-03	-3.34e-04	-2.23e-03
Meuse Borgharen	Dike 1	-19.12	1.29	0.10	2.00e-02	-4.75e-04	-2.98e-03
	Dike 2	-44.52	2.82	0.15	-4.28e-02	-1.95e-04	-4.45e-03
	Dike 3	1.50	1.68e-05	2.77e-03	-2.45e-04	-1.08e-06	-8.42e-05
	Dike 4	-17.54	1.18	0.11	-1.83e-02	-4.66e-4	-3.07e-03

TABLE O.2: RMSE FIT BASED ON HMAX AND D50 & HMAX & RA0 AND DL AND AL AND RA0

	Fit Hmax & D50		**Fit Hmax & RA0**		**Fit DL**		**Fit AL**		**Fit RA0**	
	Rhine	Meuse	Rhine	Meuse	Rhine	Meuse	Rhine	Meuse	Rhine	Meuse
Dike type 1	0.0356	0.0382	0.0317	0.037	0.0325	0.0344	0.0391	0.0345	0.0345	0.0385
Dike type 2	0.0207	0.0346	0.0181	0.0333	0.0162	0.0302	0.0199	0.0297	0.0233	0.0352
Dike type 3	0.0007	0.0011	0.0006	0.0011	0.0006	0.0011	0.0007	0.0011	0.0006	0.0011
Dike type 4	0.0388	0.0362	0.0346	0.035	0.036	0.0326	0.0433	0.0328	0.0375	0.0364

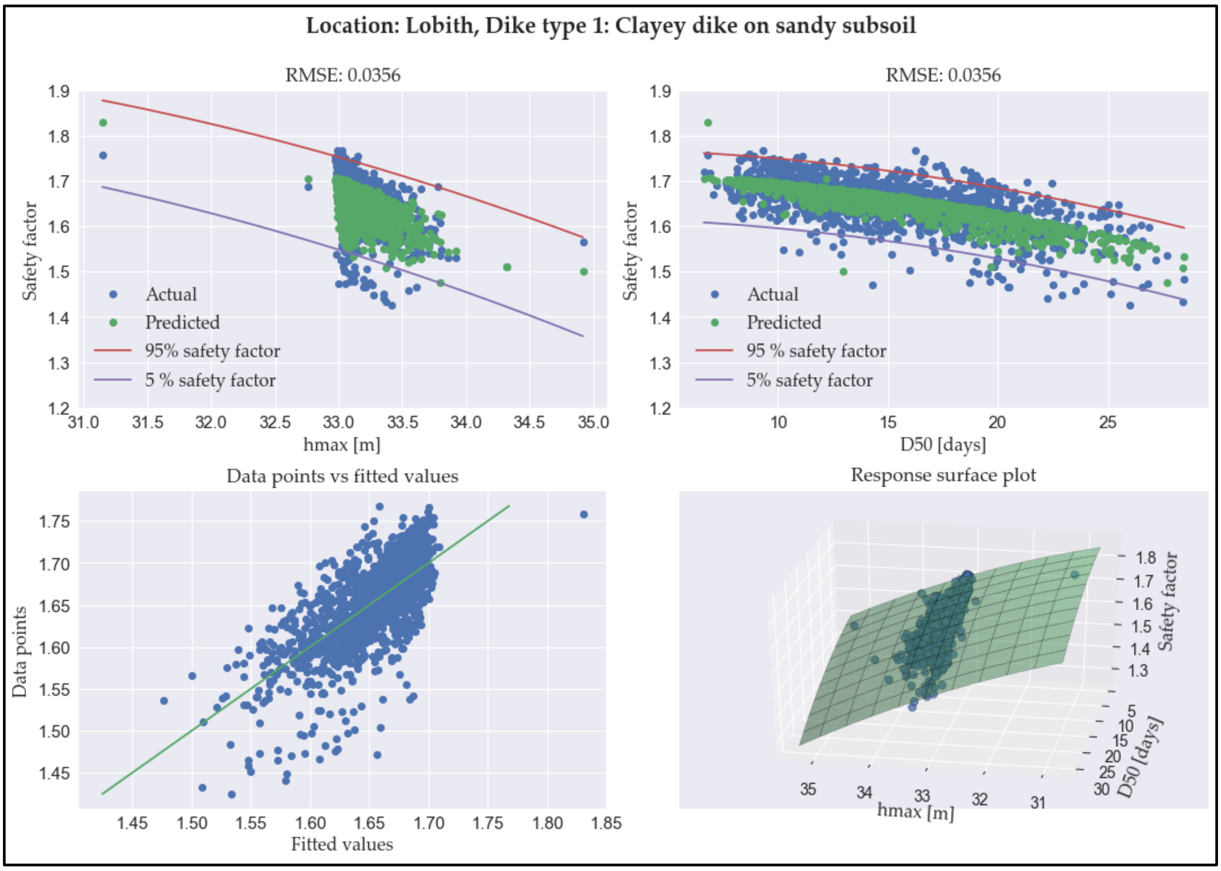

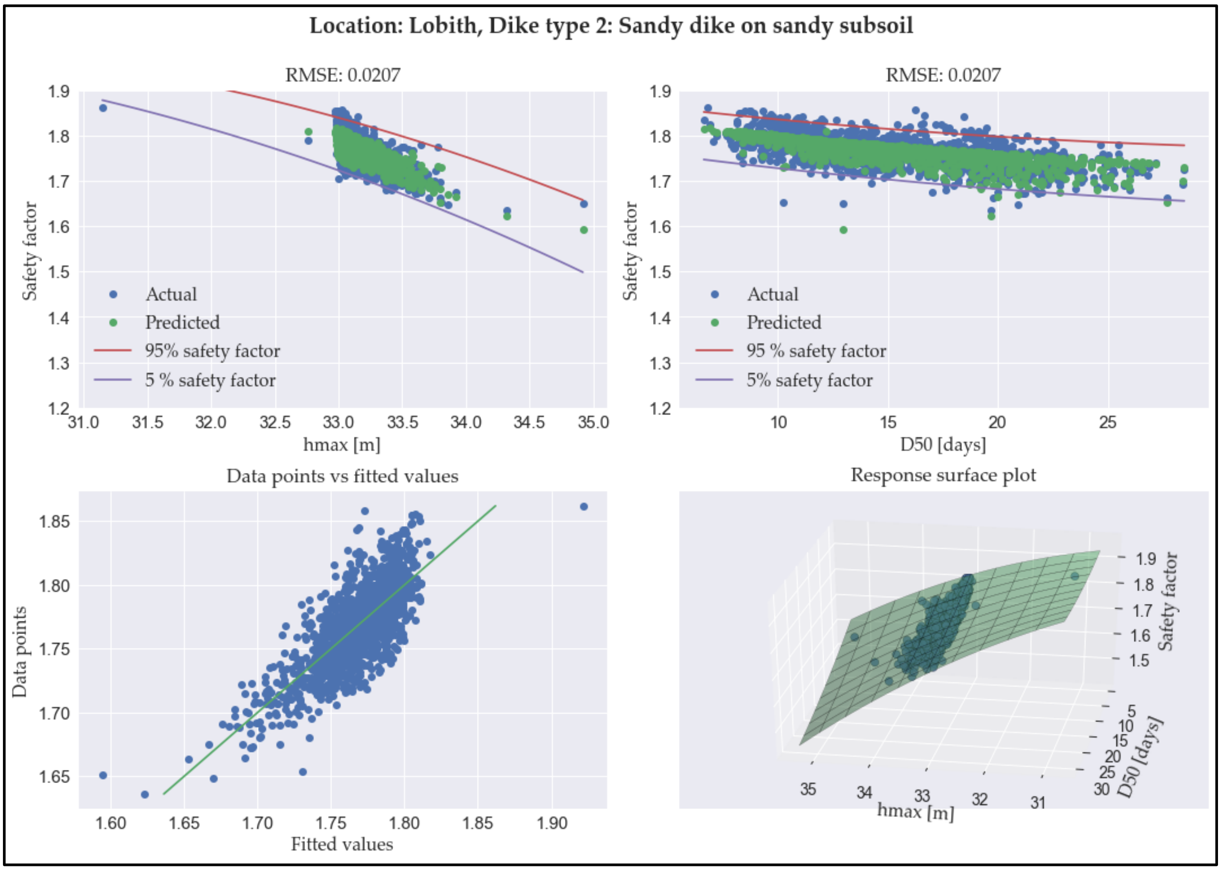

Location: Lobith, Dike type 2: Sandy dike on sandy subsoil

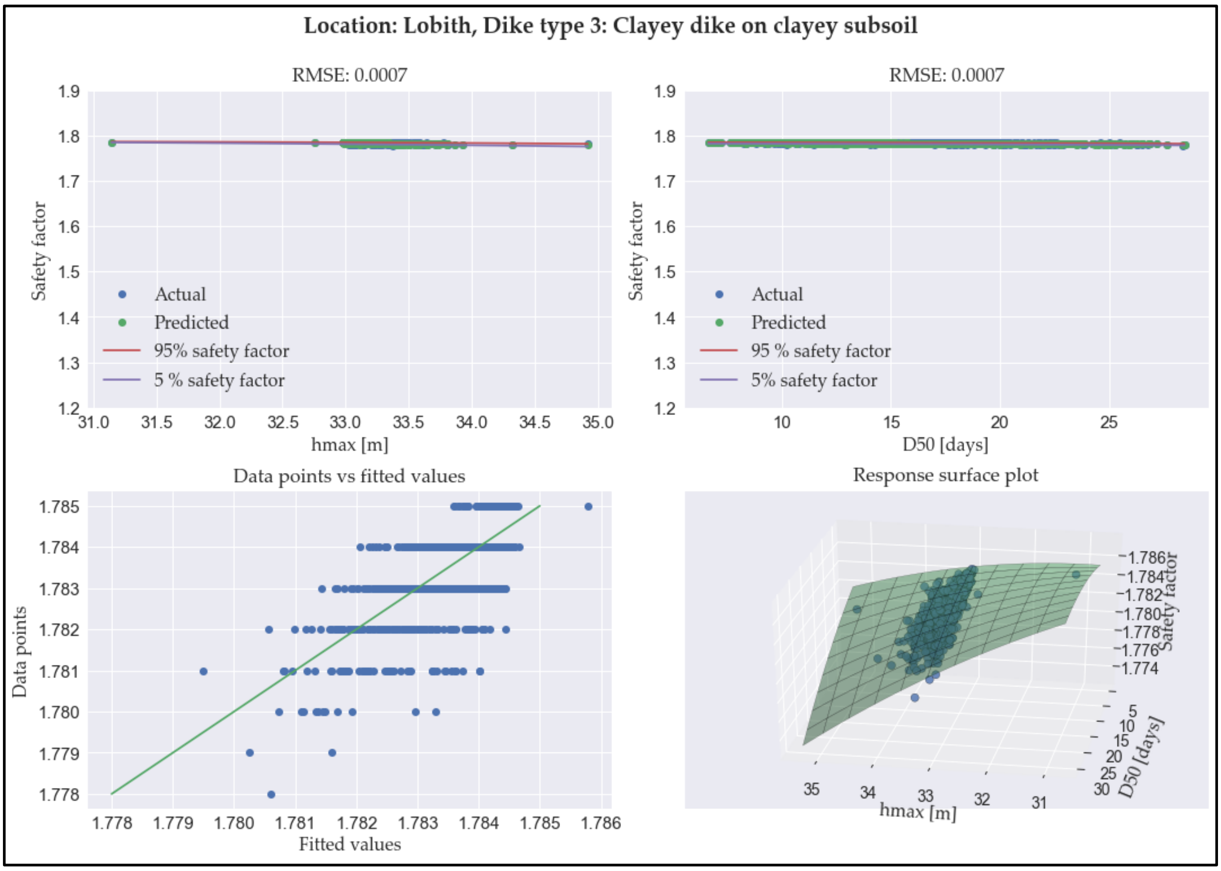

Location: Lobith, Dike type 3: Clayey dike on clayey subsoil

Location: Lobith, Dike type 4: Clayey dike with sandy core on sandy subsoil

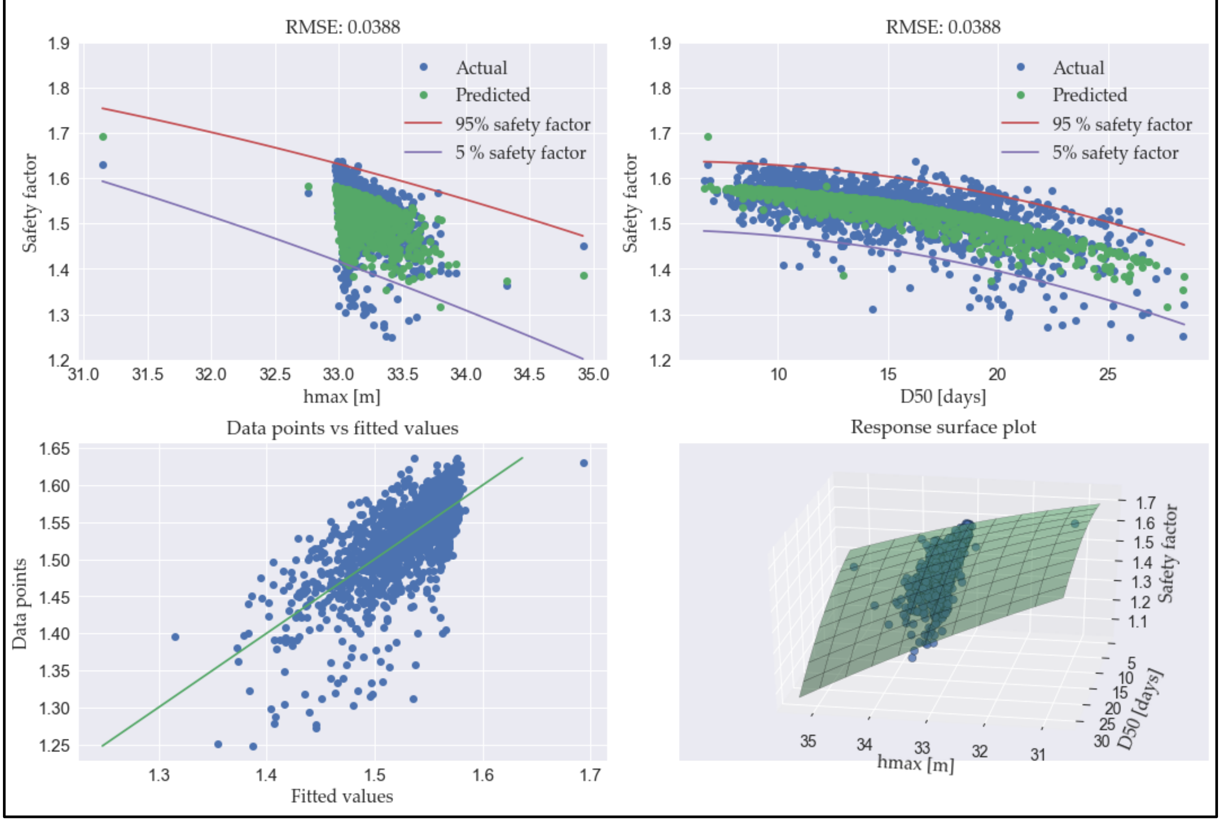

Location: Borgharen, Dike type 1: Clayey dike on sandy subsoil

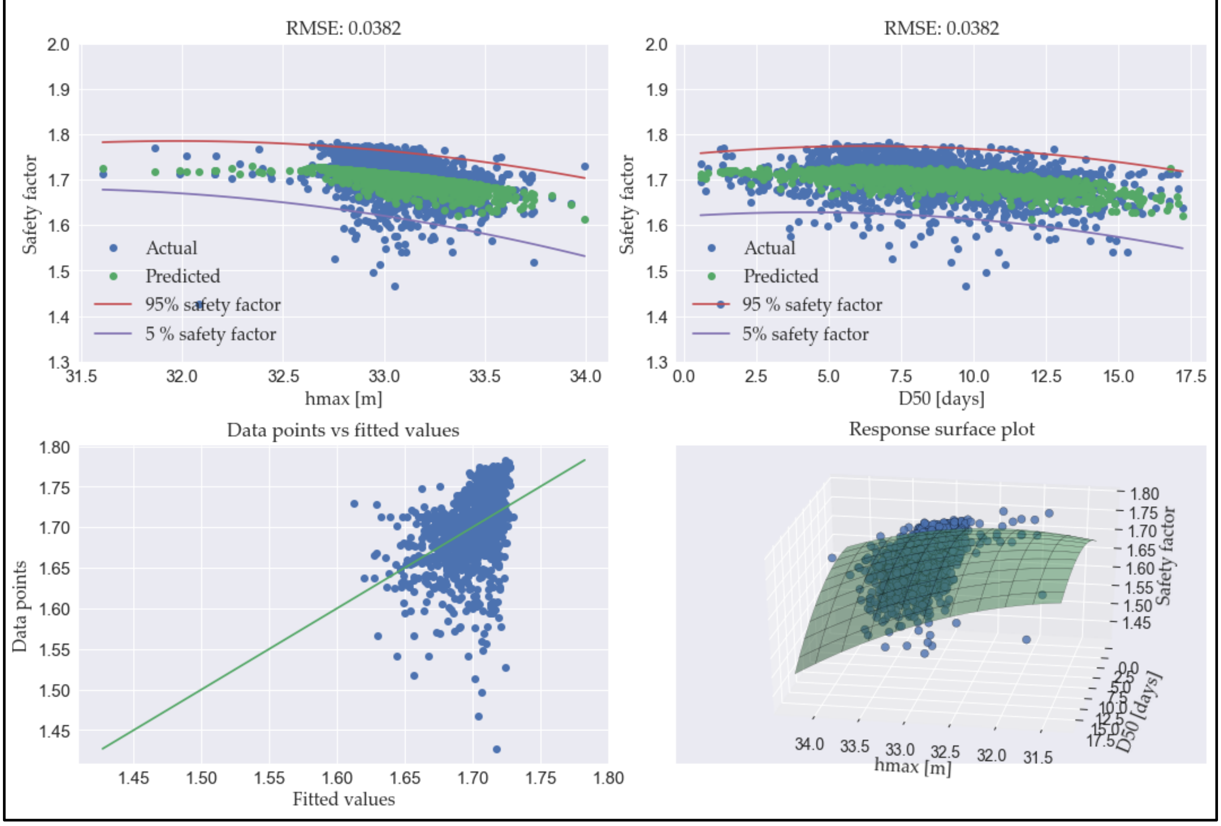

Location: Borgharen, Dike type 2: Sandy dike on sandy subsoil

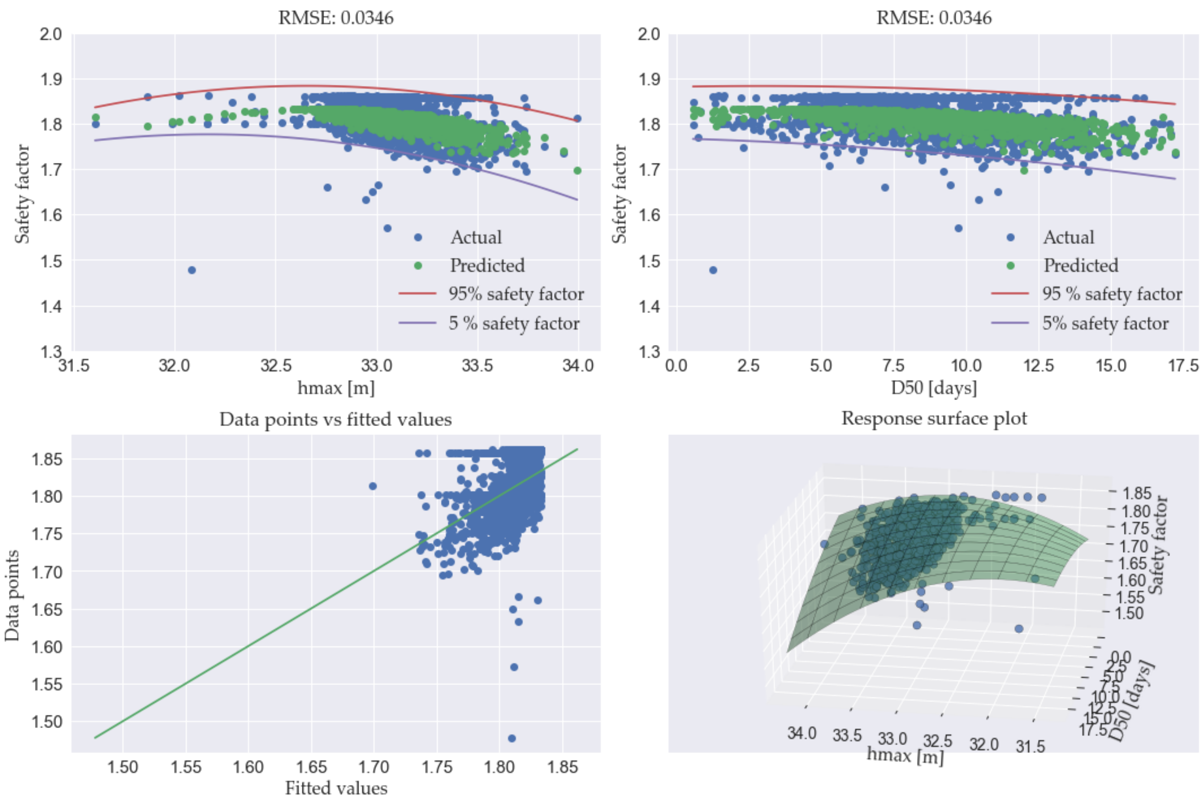

Location: Borgharen, Dike type 3: Clayey dike on clayey subsoil

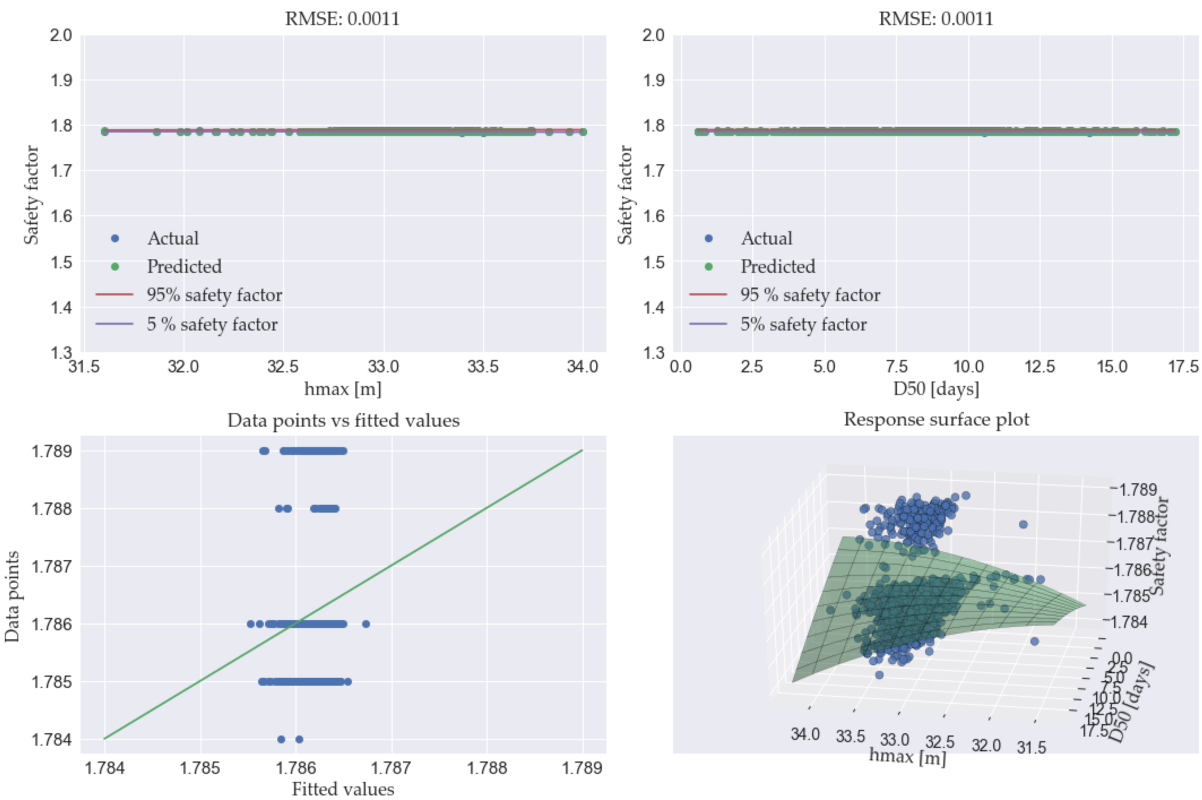

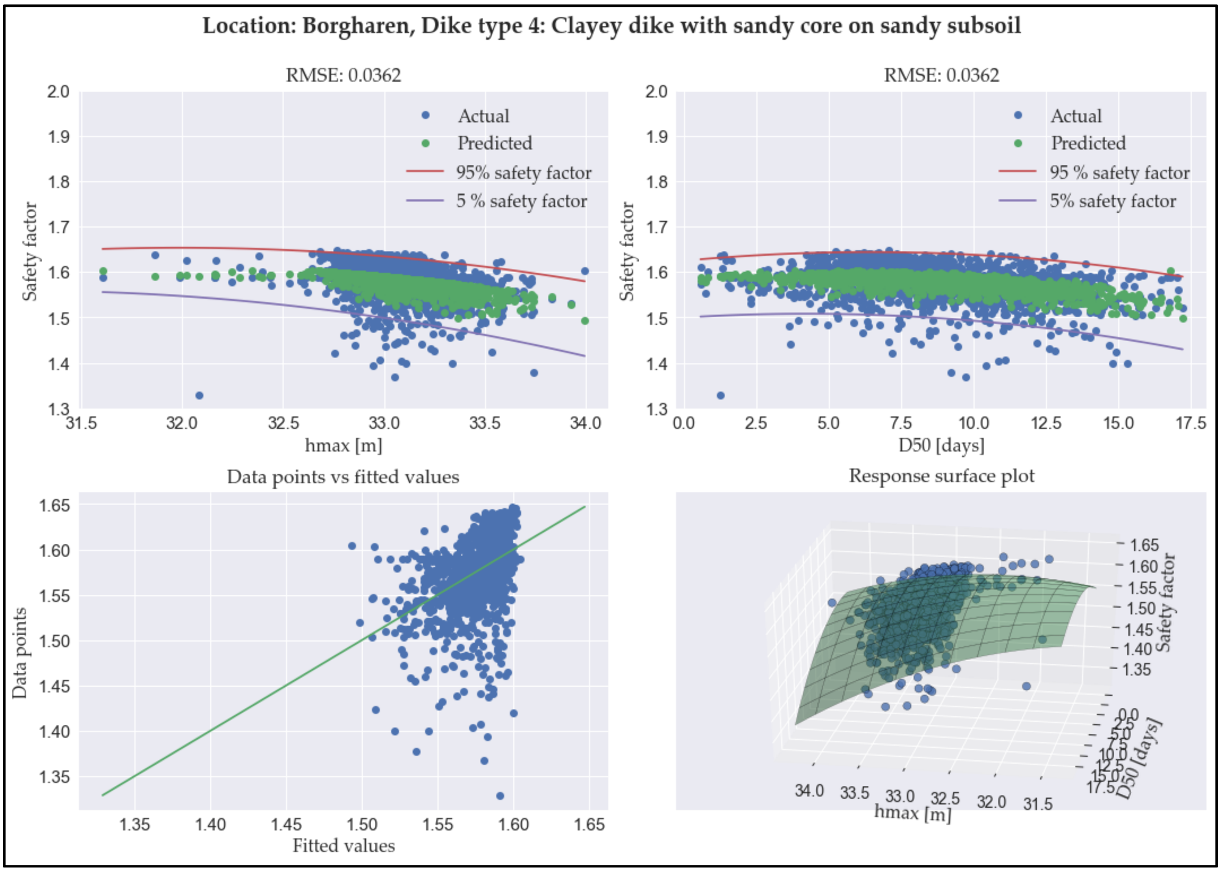

$$FoS(h_{max}, RA_0) = \rho_{00} + \rho_{10}h_{max} + \rho_{01}RA_0 + \rho_{11}h_{max}RA_0 + \rho_{20}h_{max}^2 + \rho_{02}RA_0^2$$

TABLE O.3: COEFFICIENTS SAFETY FACTOR FIT BASED ON HMAX AND RA0

		ρ_{00}	ρ_{10}	ρ_{01}	ρ_{11}	ρ_{20}	ρ_{02}
Rhine Lobith	Dike 1	-4.42	0.40	3.06	-0.01	-0.43	-0.09
	Dike 2	-7.66	0.62	2.43	-0.01	0.07	-0.08
	Dike 3	1.50	1.66e-02	0.16	-2.38e-04	-1.28e-02	-4.47e-03
	Dike 4	-2.78	0.24	6.61	-3.33e-03	-0.72	-0.19
Meuse Borgharen	Dike 1	-26.67	1.74	1.69	-2.66e-02	-0.34	-4.50e-02
	Dike 2	-46.37	2.92	2.74	-4.42e-02	-7.26e-02	-8.56e-02
	Dike 3	1.32	2.67e-02	0.11	-3.78e-04	-4.32e-03	-3.23e-03
	Dike 4	-25.99	1.68	2.17	-2.55e-02	-0.35	-5.88e-02

TABLE O.4: RMSE FIT BASED ON HMAX AND D50 & HMAX & RA0 AND DL AND AL AND RA0

	Fit Hmax & D50		Fit Hmax & RA0		Fit DL		Fit AL		Fit RA0	
	Rhine	Meuse	Rhine	Meuse	Rhine	Meuse	Rhine	Meuse	Rhine	Meuse
Dike type 1	0.0356	0.0382	0.0317	0.037	0.0325	0.0344	0.0391	0.0345	0.0345	0.0385
Dike type 2	0.0207	0.0346	0.0181	0.0333	0.0162	0.0302	0.0199	0.0297	0.0233	0.0352
Dike type 3	0.0007	0.0011	0.0006	0.0011	0.0006	0.0011	0.0007	0.0011	0.0006	0.0011
Dike type 4	0.0388	0.0362	0.0346	0.035	0.036	0.0326	0.0433	0.0328	0.0375	0.0364

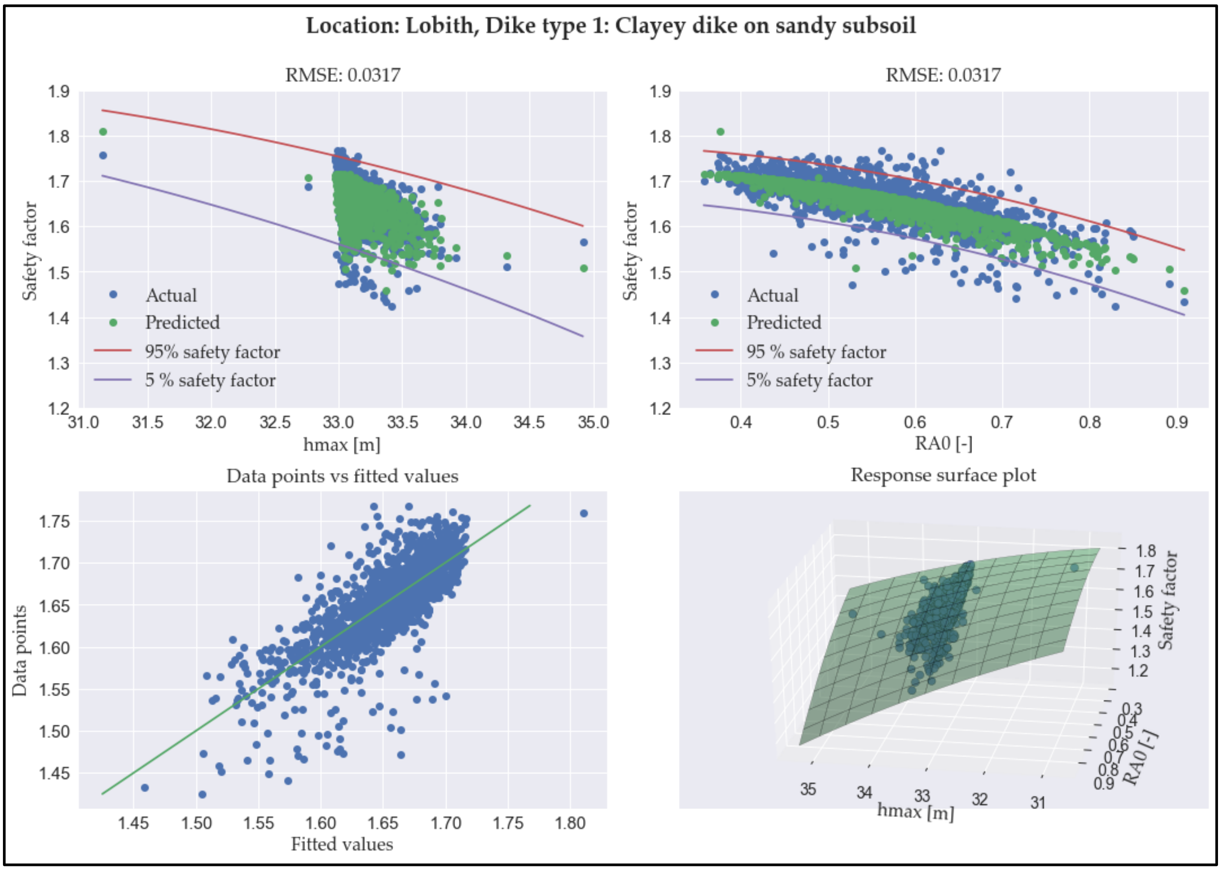
Location: Lobith, Dike type 1: Clayey dike on sandy subsoil
RMSE: 0.0317
Safety factor
hmax [m]
Actual
Predicted
95% safety factor
5 % safety factor
RMSE: 0.0317
RA0 [-]
95 % safety factor
5% safety factor
Data points vs fitted values
Data points
Fitted values
Response surface plot
Safety factor
RA0 [-]
hmax [m]

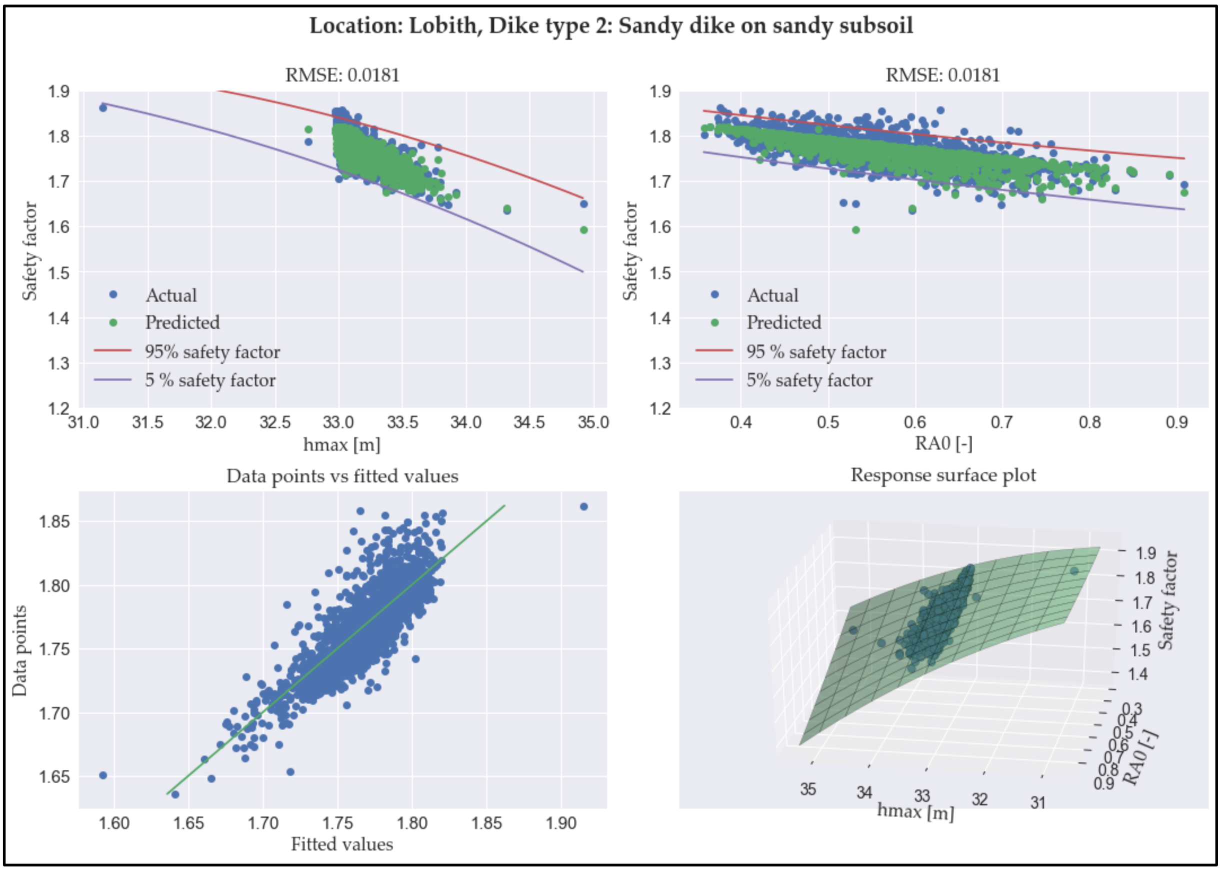
Location: Lobith, Dike type 2: Sandy dike on sandy subsoil
RMSE: 0.0181
Safety factor
hmax [m]
Actual
Predicted
95% safety factor
5 % safety factor
RMSE: 0.0181
RA0 [-]
95 % safety factor
5% safety factor
Data points vs fitted values
Data points
Fitted values
Response surface plot
Safety factor
RA0 [-]
hmax [m]

Location: Lobith, Dike type 3: Clayey dike on clayey subsoil

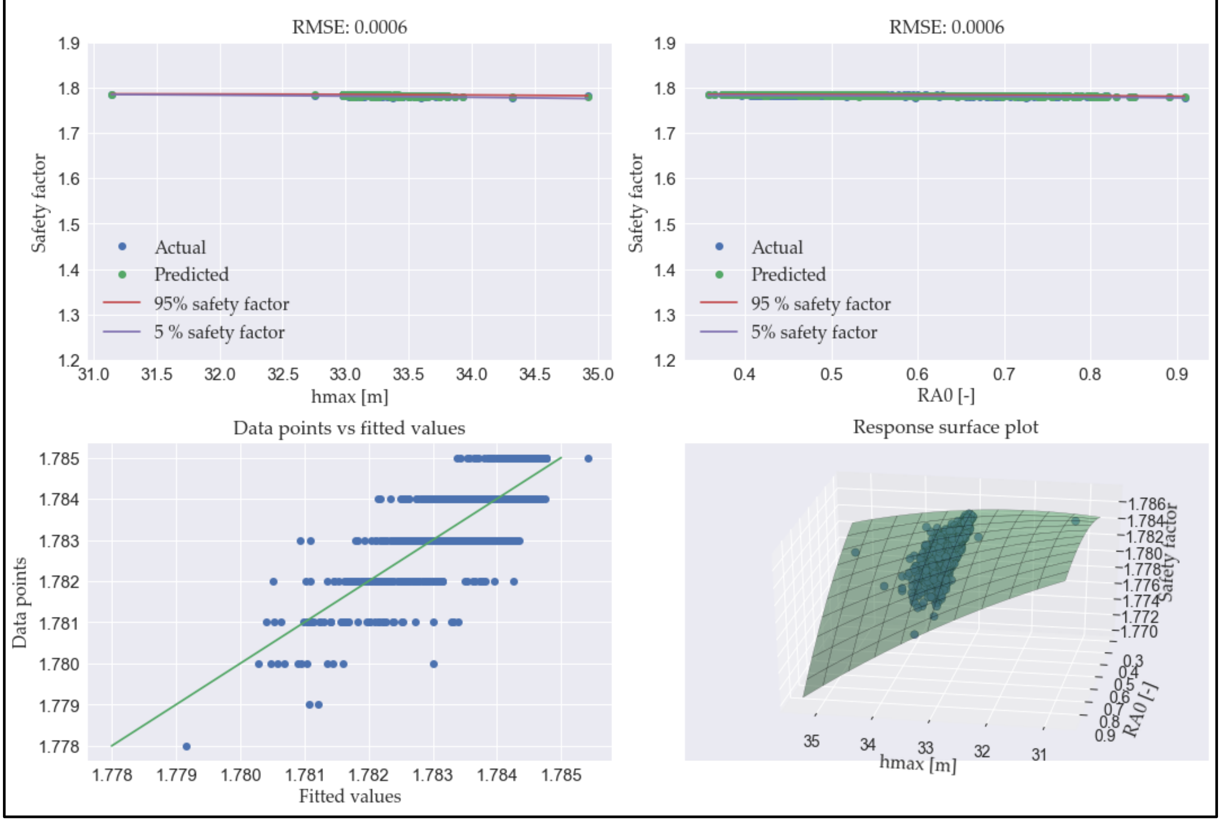

Location: Lobith, Dike type 4: Clayey dike with sandy core on sandy subsoil

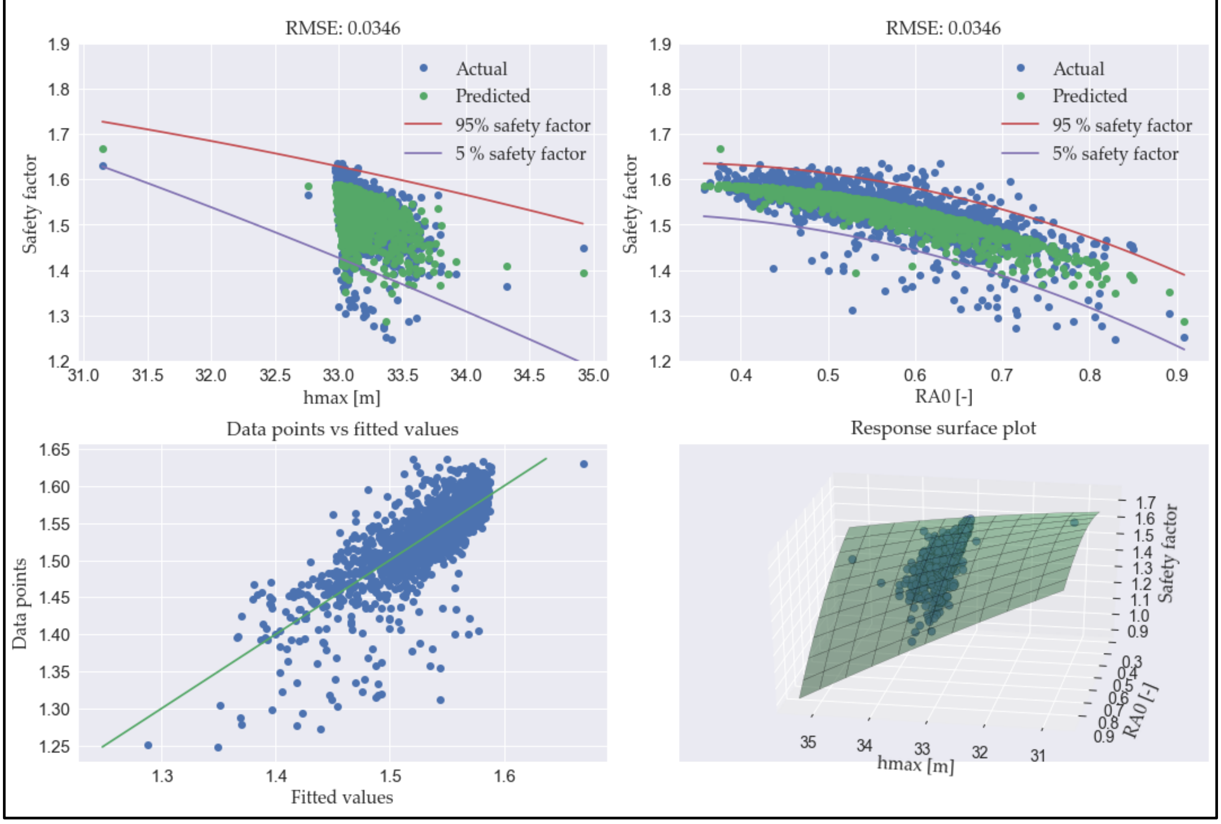

Location: Borgharen, Dike type 1: Clayey dike on sandy subsoil

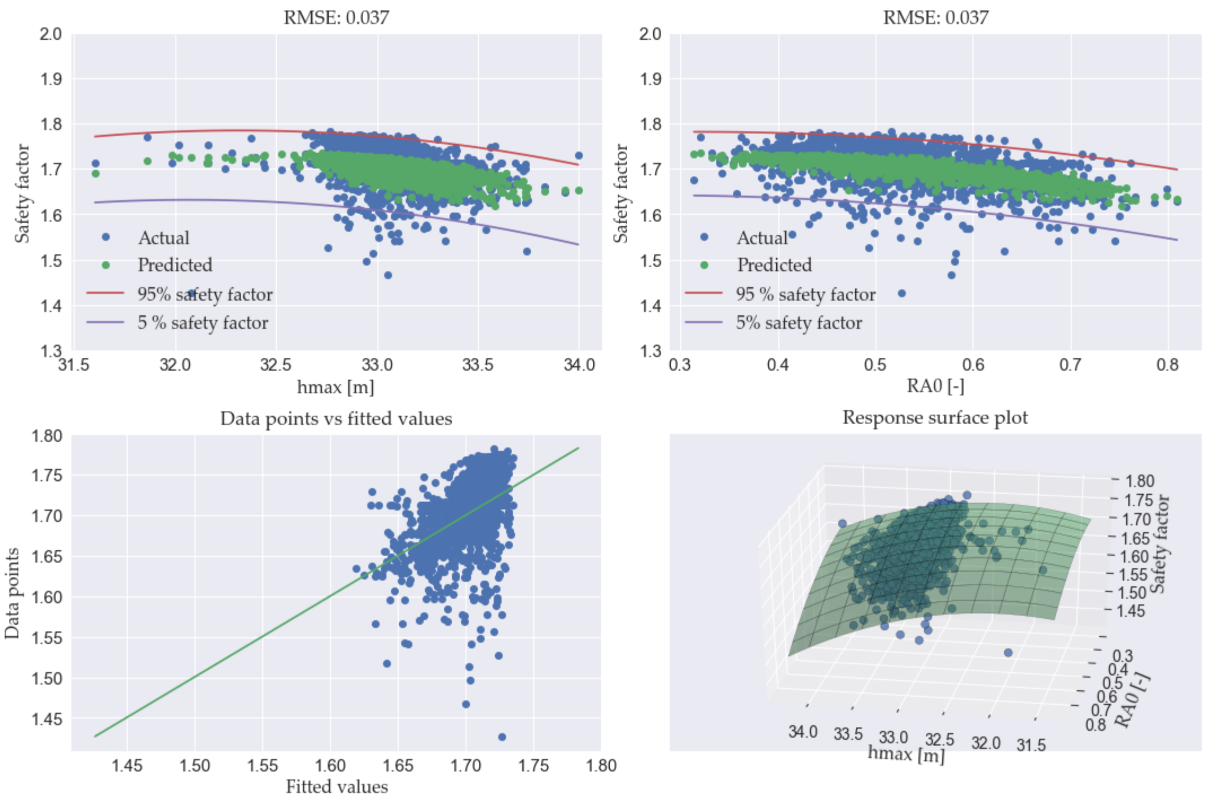

Location: Borgharen, Dike type 2: Sandy dike on sandy subsoil

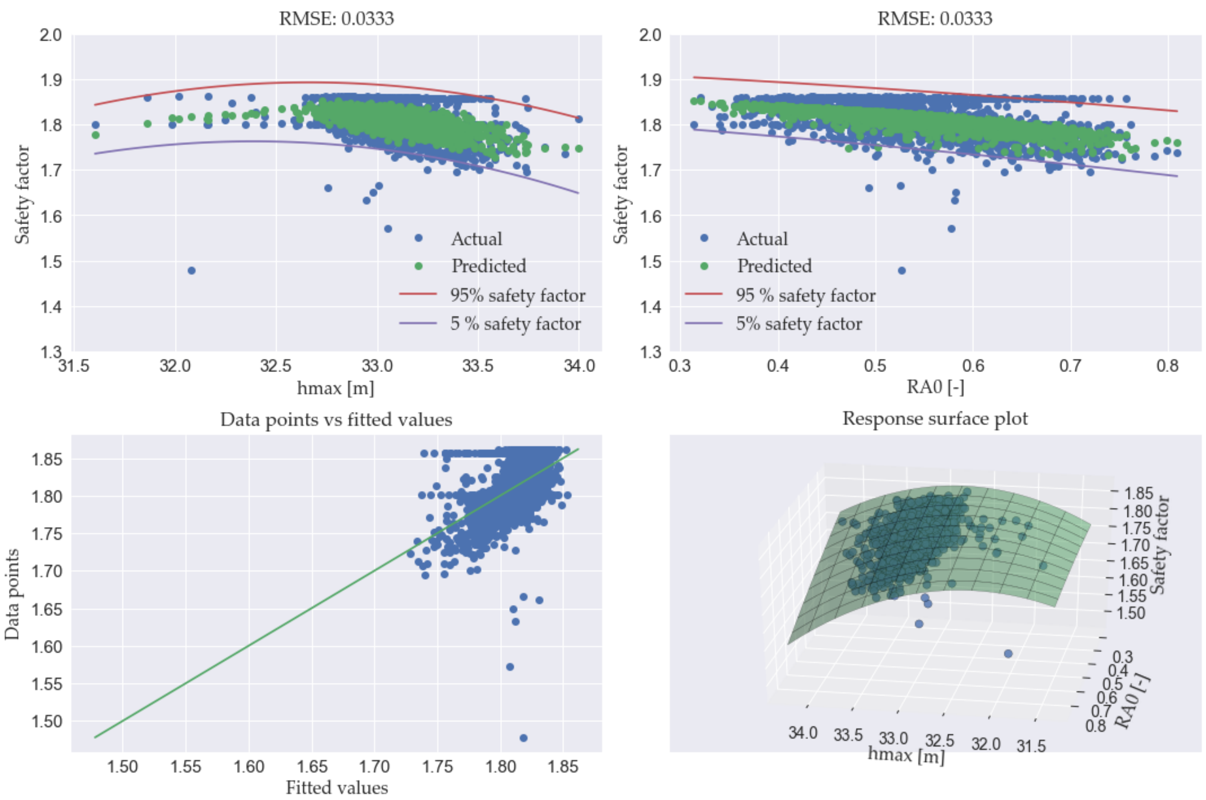

Location: Borgharen, Dike type 3: Clayey dike on clayey subsoil

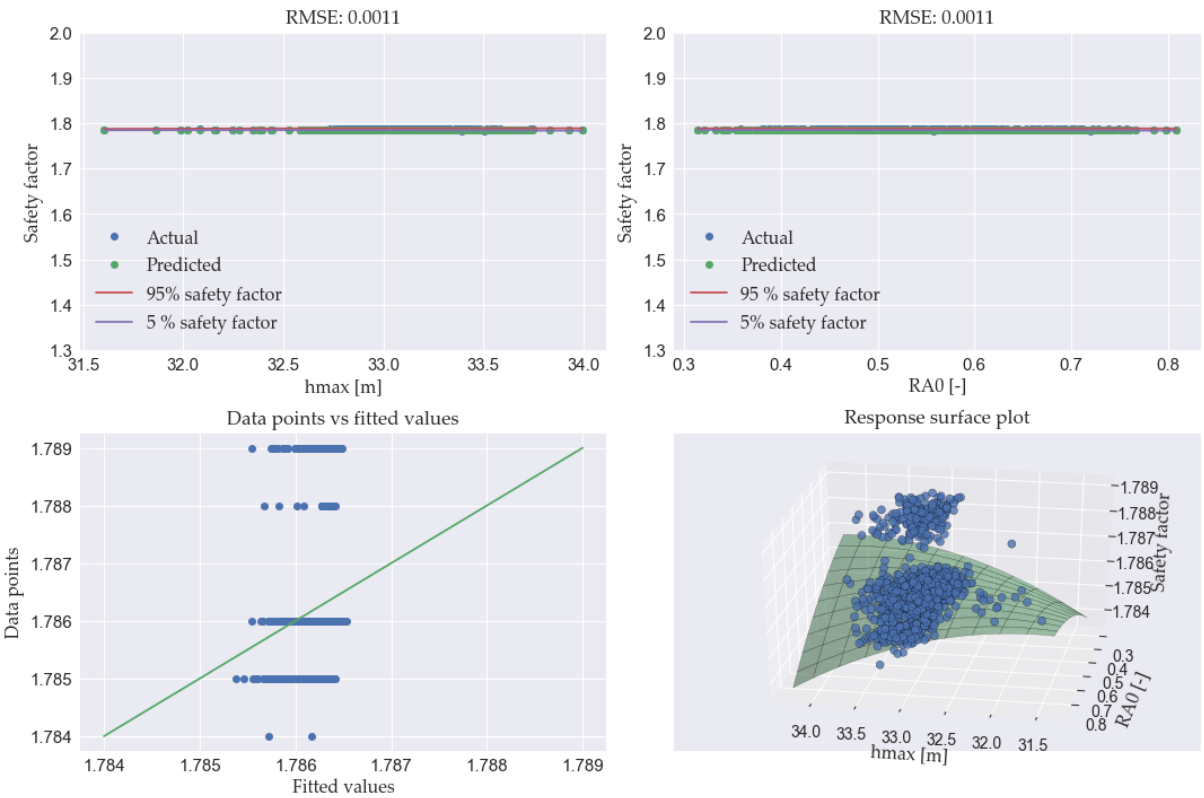

Location: Borgharen, Dike type 4: Clayey dike with sandy core on sandy subsoil

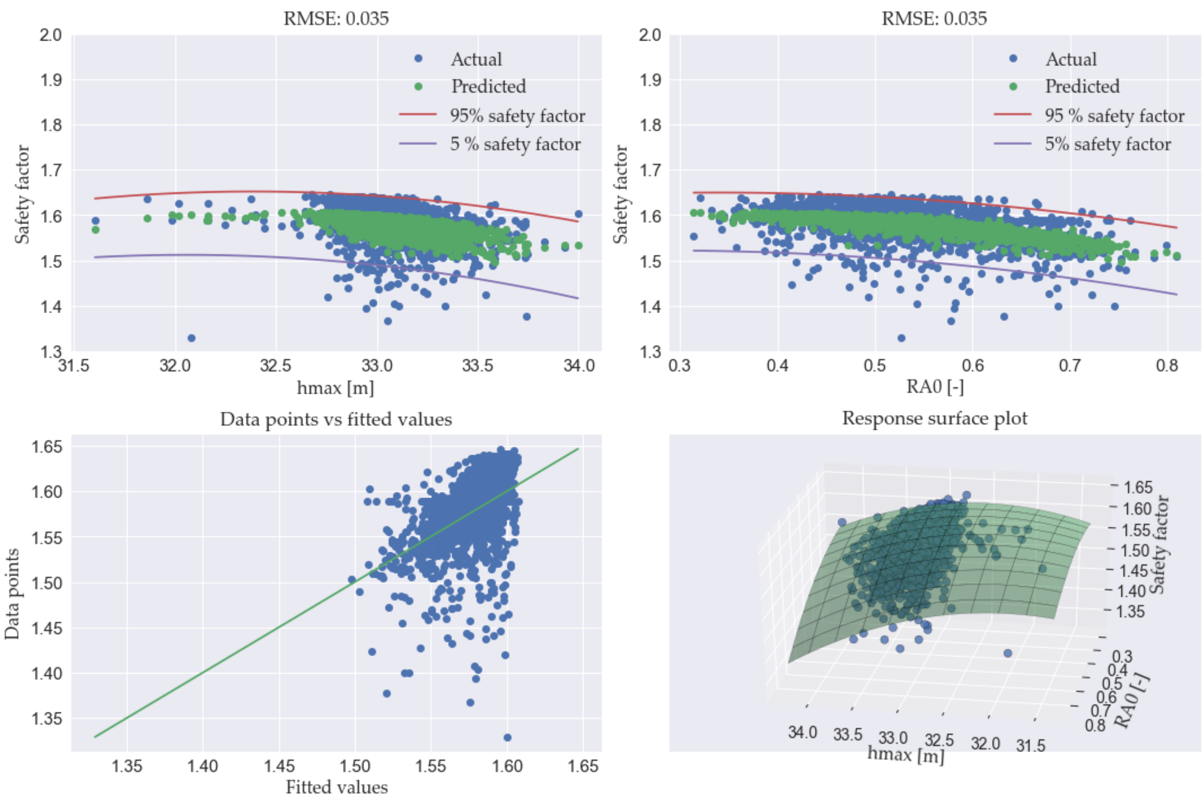

$$FoS(h_{max}, RA_0) = \rho_0 + +\rho_1 D_L + \rho_2 D_L^2$$

TABLE O.5: RMSE FIT BASED ON HMAX AND D50 & HMAX & RA0 AND DL AND AL AND RA0

	Fit Hmax & D50		Fit Hmax & RA0		Fit DL		Fit AL		Fit RA0	
	Rhine	Meuse	Rhine	Meuse	Rhine	Meuse	Rhine	Meuse	Rhine	Meuse
Dike type 1	0.0356	0.0382	0.0317	0.037	0.0325	0.0344	0.0391	0.0345	0.0345	0.0385
Dike type 2	0.0207	0.0346	0.0181	0.0333	0.0162	0.0302	0.0199	0.0297	0.0233	0.0352
Dike type 3	0.0007	0.0011	0.0006	0.0011	0.0006	0.0011	0.0007	0.0011	0.0006	0.0011
Dike type 4	0.0388	0.0362	0.0346	0.035	0.036	0.0326	0.0433	0.0328	0.0375	0.0364

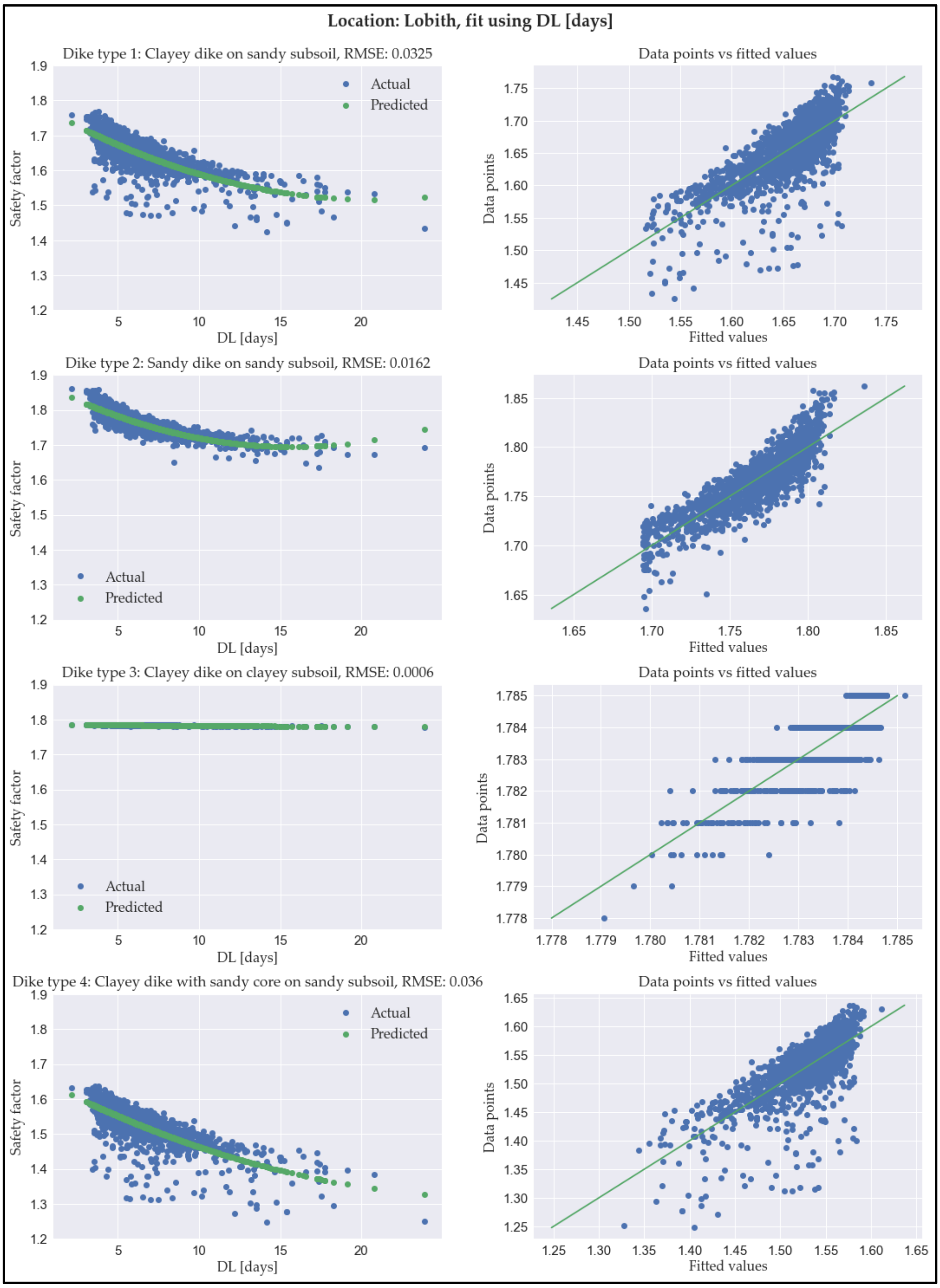

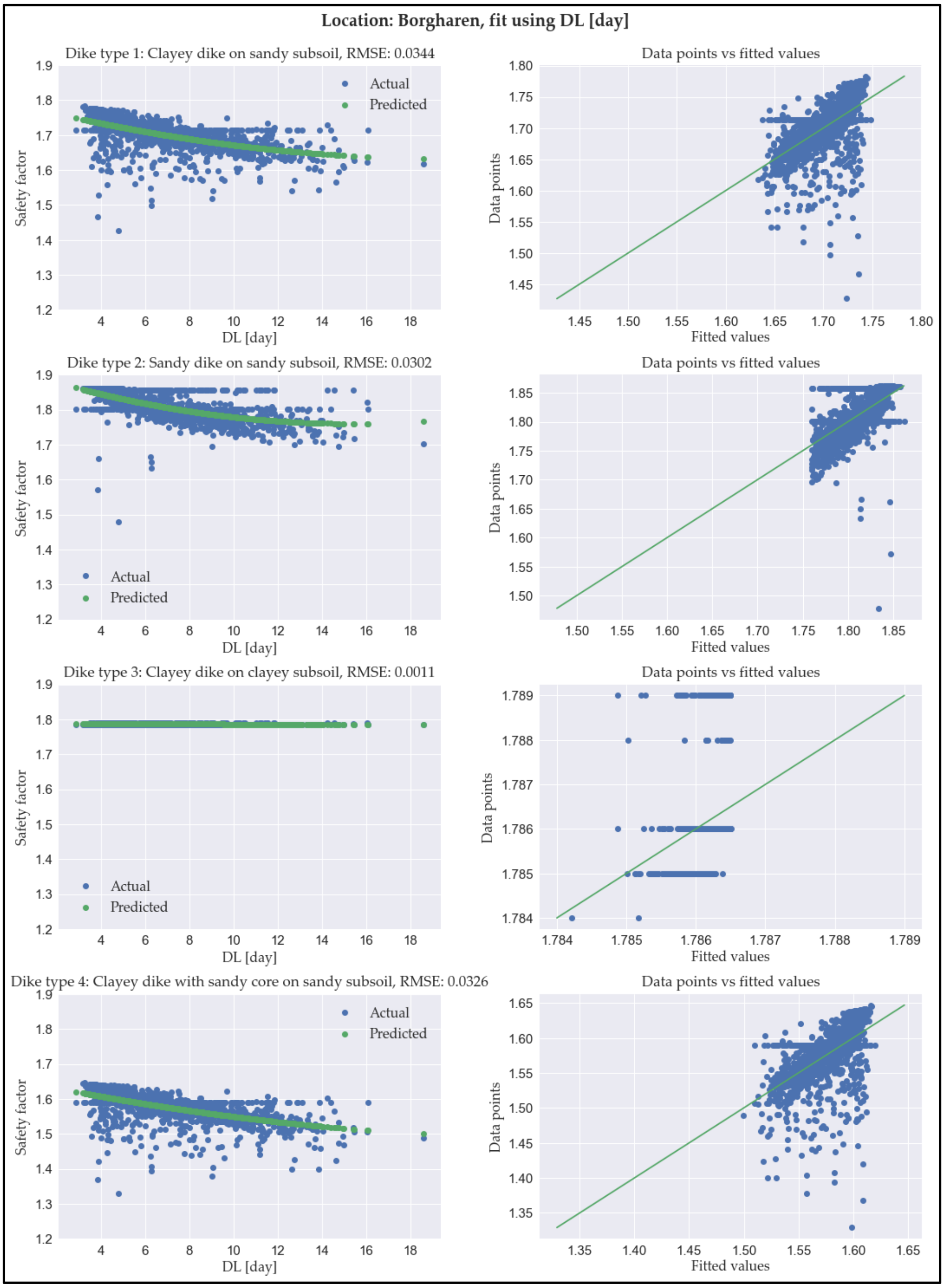

$$FoS(h_{max}, RA_0) = \rho_0 + +\rho_1 A_L + \rho_2 A_L^2$$

TABLE O.6: RMSE FIT BASED ON HMAX AND D50 & HMAX & RA0 AND DL AND AL AND RA0

	Fit Hmax & D50		Fit Hmax & RA0		Fit DL		Fit AL		Fit RA0	
	Rhine	Meuse	Rhine	Meuse	Rhine	Meuse	Rhine	Meuse	Rhine	Meuse
Dike type 1	0.0356	0.0382	0.0317	0.037	0.0325	0.0344	0.0391	0.0345	0.0345	0.0385
Dike type 2	0.0207	0.0346	0.0181	0.0333	0.0162	0.0302	0.0199	0.0297	0.0233	0.0352
Dike type 3	0.0007	0.0011	0.0006	0.0011	0.0006	0.0011	0.0007	0.0011	0.0006	0.0011
Dike type 4	0.0388	0.0362	0.0346	0.035	0.036	0.0326	0.0433	0.0328	0.0375	0.0364

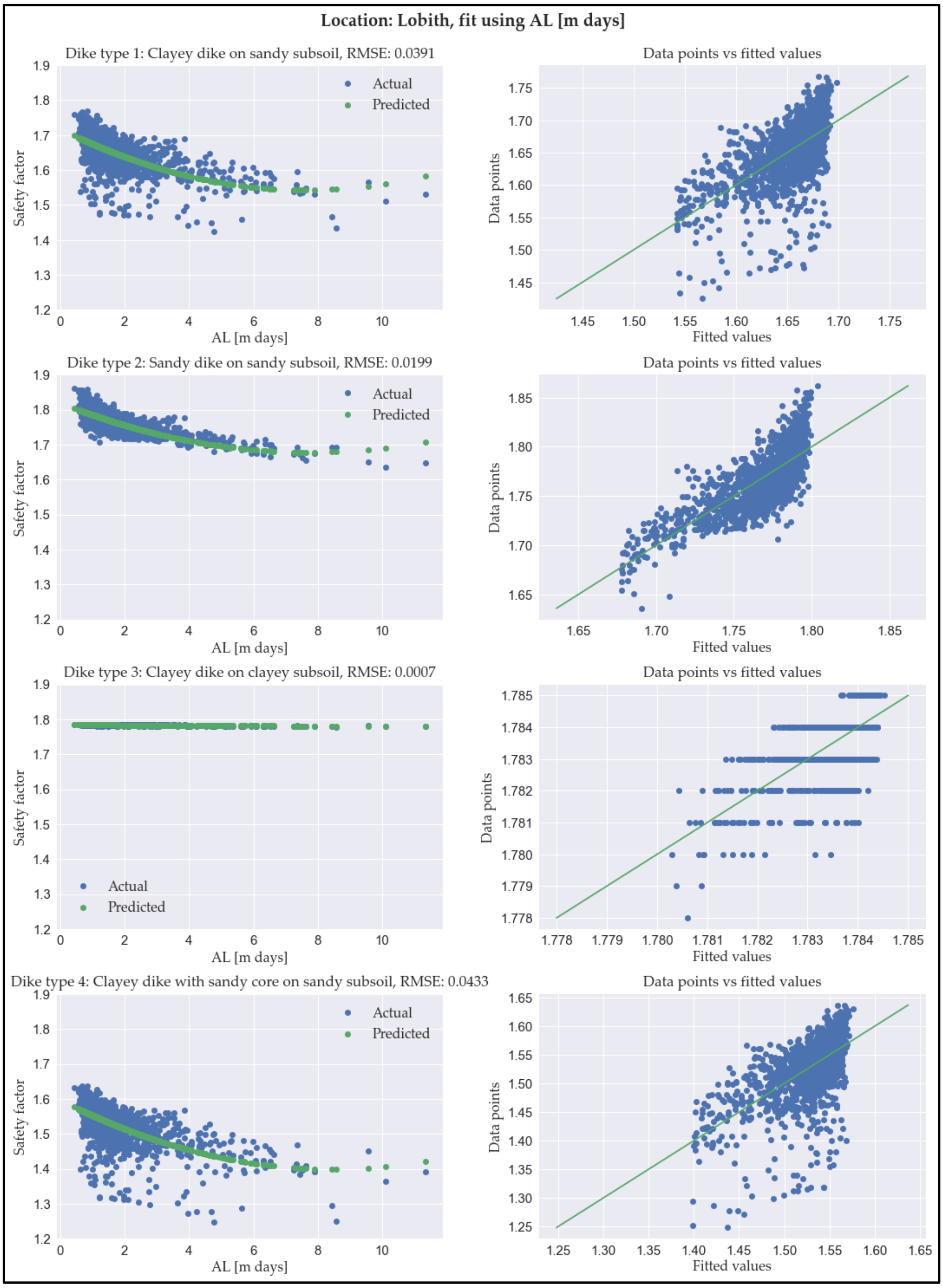
Location: Lobith, fit using AL [m days]
Dike type 1: Clayey dike on sandy subsoil, RMSE: 0.0391
Data points vs fitted values
Dike type 2: Sandy dike on sandy subsoil, RMSE: 0.0199
Data points vs fitted values
Dike type 3: Clayey dike on clayey subsoil, RMSE: 0.0007
Data points vs fitted values
Dike type 4: Clayey dike with sandy core on sandy subsoil, RMSE: 0.0433
Data points vs fitted values
Actual
Predicted
Safety factor
AL [m days]
Data points
Fitted values

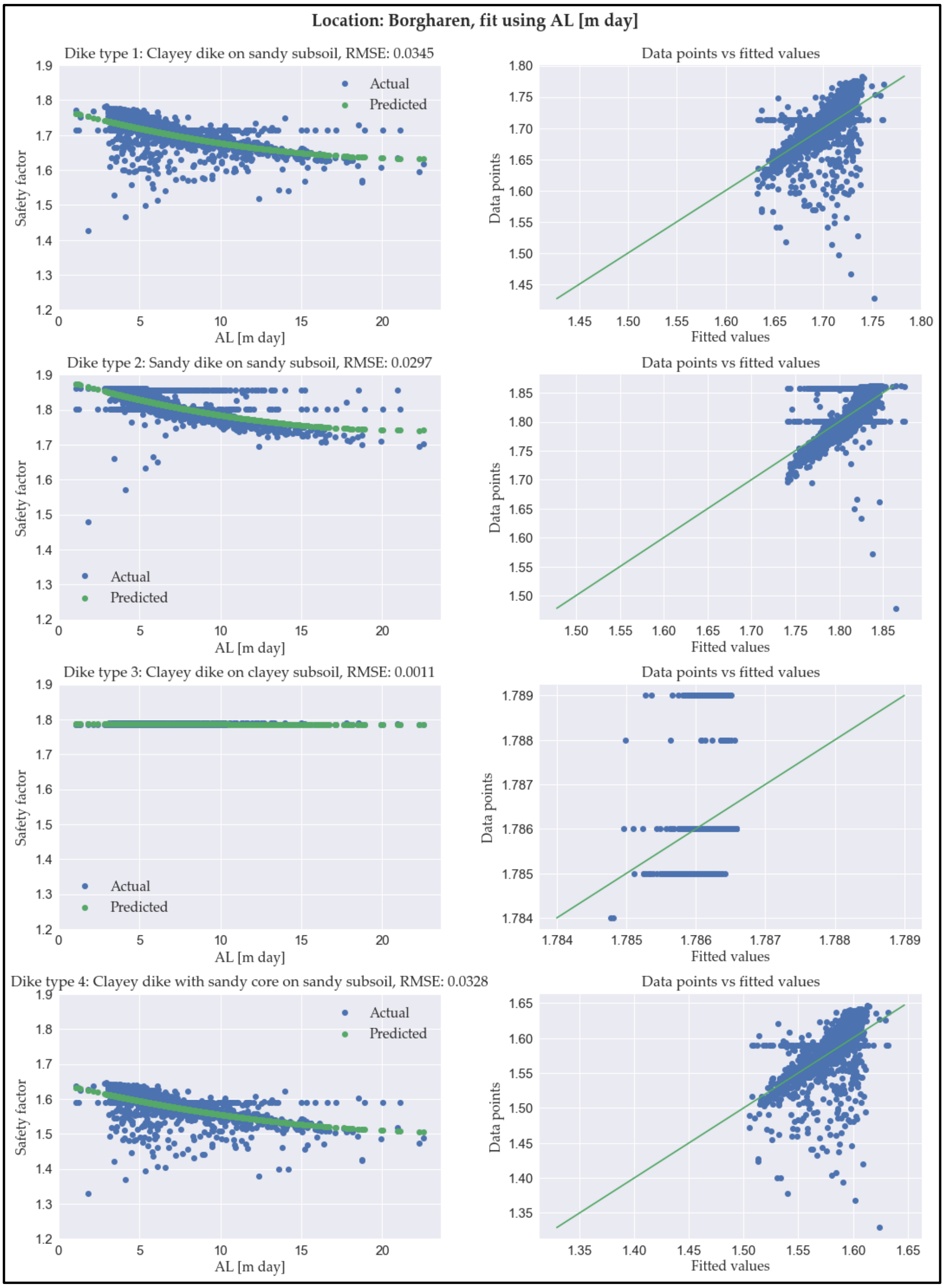
Location: Borgharen, fit using AL [m day]
Dike type 1: Clayey dike on sandy subsoil, RMSE: 0.0345
Data points vs fitted values
Dike type 2: Sandy dike on sandy subsoil, RMSE: 0.0297
Data points vs fitted values
Dike type 3: Clayey dike on clayey subsoil, RMSE: 0.0011
Data points vs fitted values
Dike type 4: Clayey dike with sandy core on sandy subsoil, RMSE: 0.0328
Data points vs fitted values
Actual
Predicted
Safety factor
AL [m day]
Data points
Fitted values

$$FoS(h_{max}, RA_0) = \rho_0 + +\rho_1 RA_0 + \rho_2 RA_0^2$$

TABLE O.7: RMSE FIT BASED ON HMAX AND D50 & HMAX & RA0 AND DL AND AL AND RA0

	Fit Hmax & D50		Fit Hmax & RA0		Fit DL		Fit AL		Fit RA0	
	Rhine	Meuse	Rhine	Meuse	Rhine	Meuse	Rhine	Meuse	Rhine	Meuse
Dike type 1	0.0356	0.0382	0.0317	0.037	0.0325	0.0344	0.0391	0.0345	0.0345	0.0385
Dike type 2	0.0207	0.0346	0.0181	0.0333	0.0162	0.0302	0.0199	0.0297	0.0233	0.0352
Dike type 3	0.0007	0.0011	0.0006	0.0011	0.0006	0.0011	0.0007	0.0011	0.0006	0.0011
Dike type 4	0.0388	0.0362	0.0346	0.035	0.036	0.0326	0.0433	0.0328	0.0375	0.0364

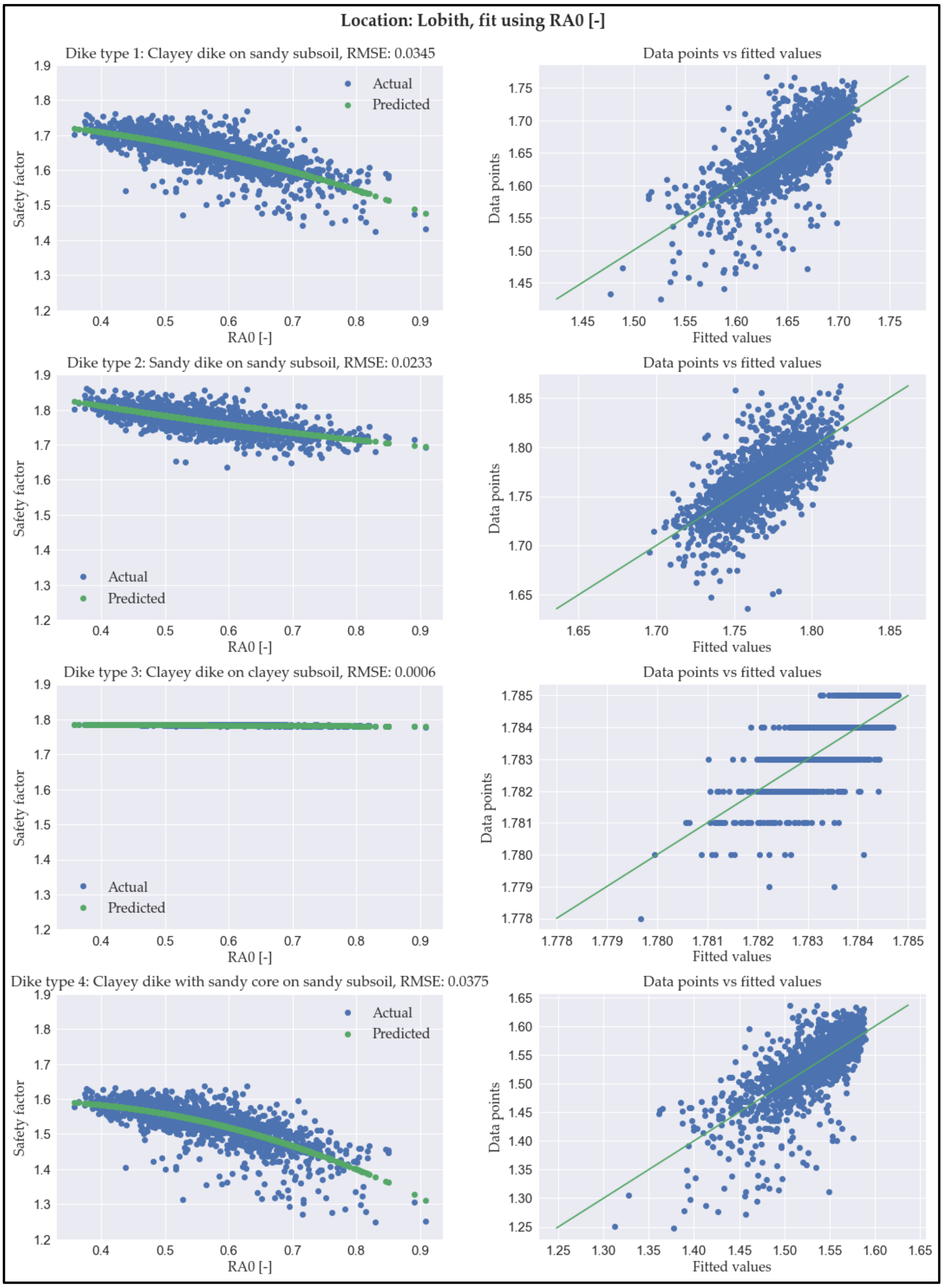

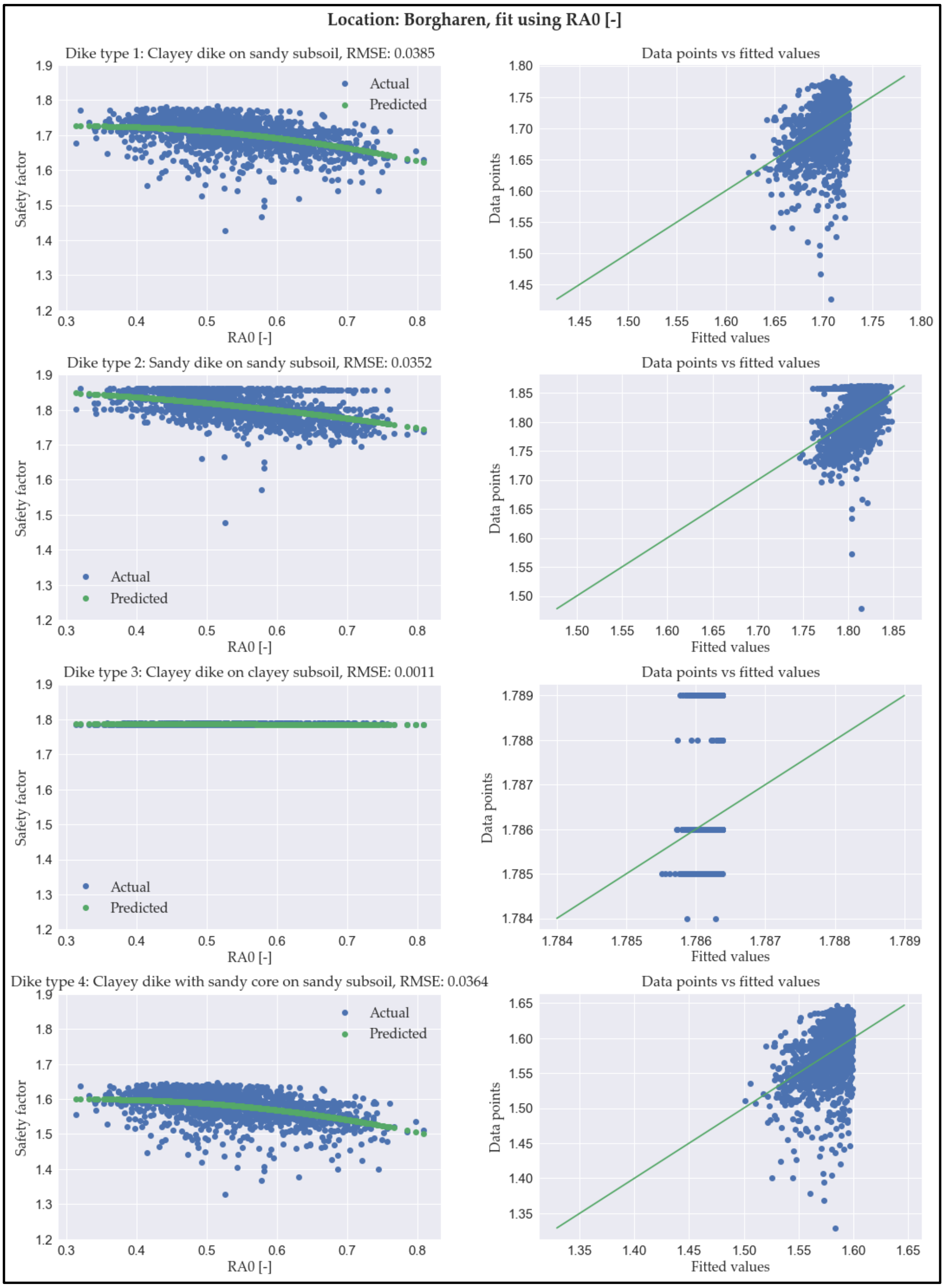

Location: Borgharen, fit using RA0 [-]
Dike type 1: Clayey dike on sandy subsoil, RMSE: 0.0385
Data points vs fitted values
Dike type 2: Sandy dike on sandy subsoil, RMSE: 0.0352
Dike type 3: Clayey dike on clayey subsoil, RMSE: 0.0011
Dike type 4: Clayey dike with sandy core on sandy subsoil, RMSE: 0.0364
Actual
Predicted
Safety factor
RA0 [-]
Data points
Fitted values

APPENDIX P. PROBABILITY DENSITY FUNCTIONS

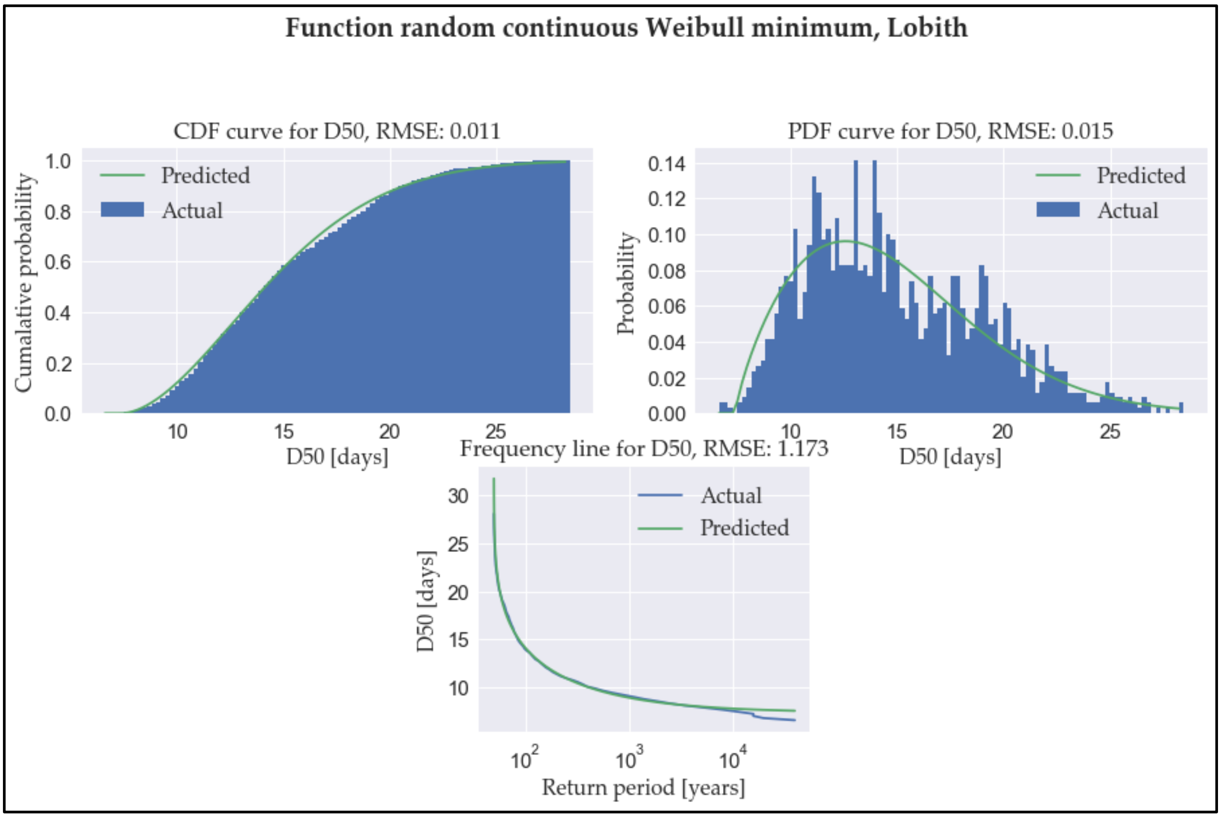
Function random continuous Weibull minimum, Lobith
CDF curve for D50, RMSE: 0.011
PDF curve for D50, RMSE: 0.015
Frequency line for D50, RMSE: 1.173
Predicted
Actual
Cumalative probability
Probability
D50 [days]
Return period [years]

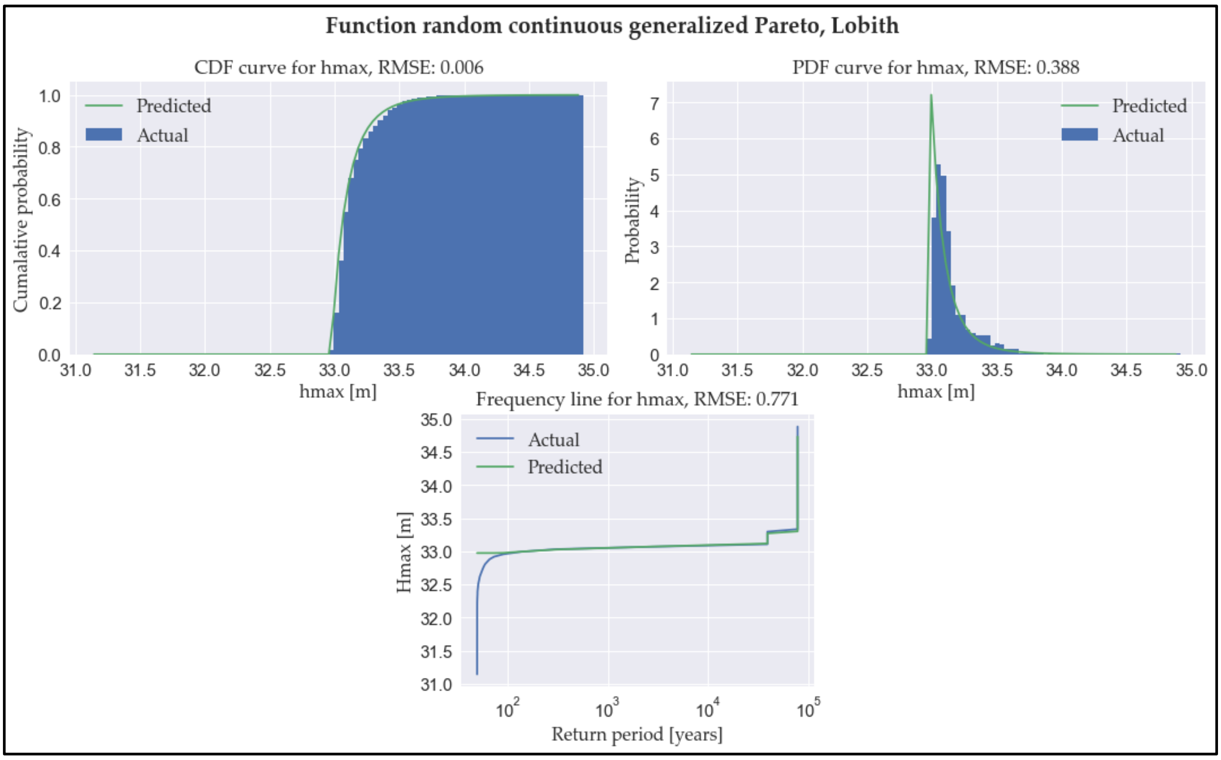
Function random continuous generalized Pareto, Lobith
CDF curve for hmax, RMSE: 0.006
PDF curve for hmax, RMSE: 0.388
Frequency line for hmax, RMSE: 0.771
Predicted
Actual
Cumalative probability
Probability
hmax [m]
Hmax [m]
Return period [years]

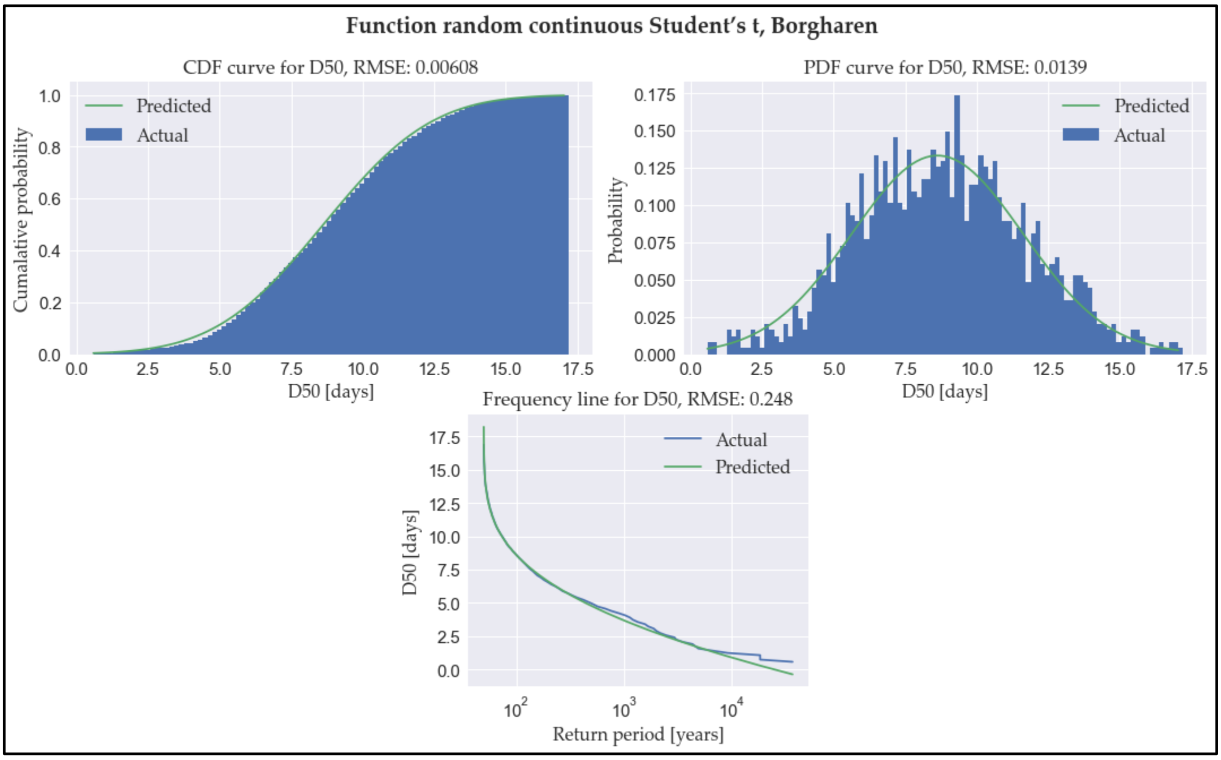
Function random continuous Student's t, Borgharen
CDF curve for D50, RMSE: 0.00608
PDF curve for D50, RMSE: 0.0139
Frequency line for D50, RMSE: 0.248
Predicted
Actual
Cumalative probability
Probability
D50 [days]
Return period [years]

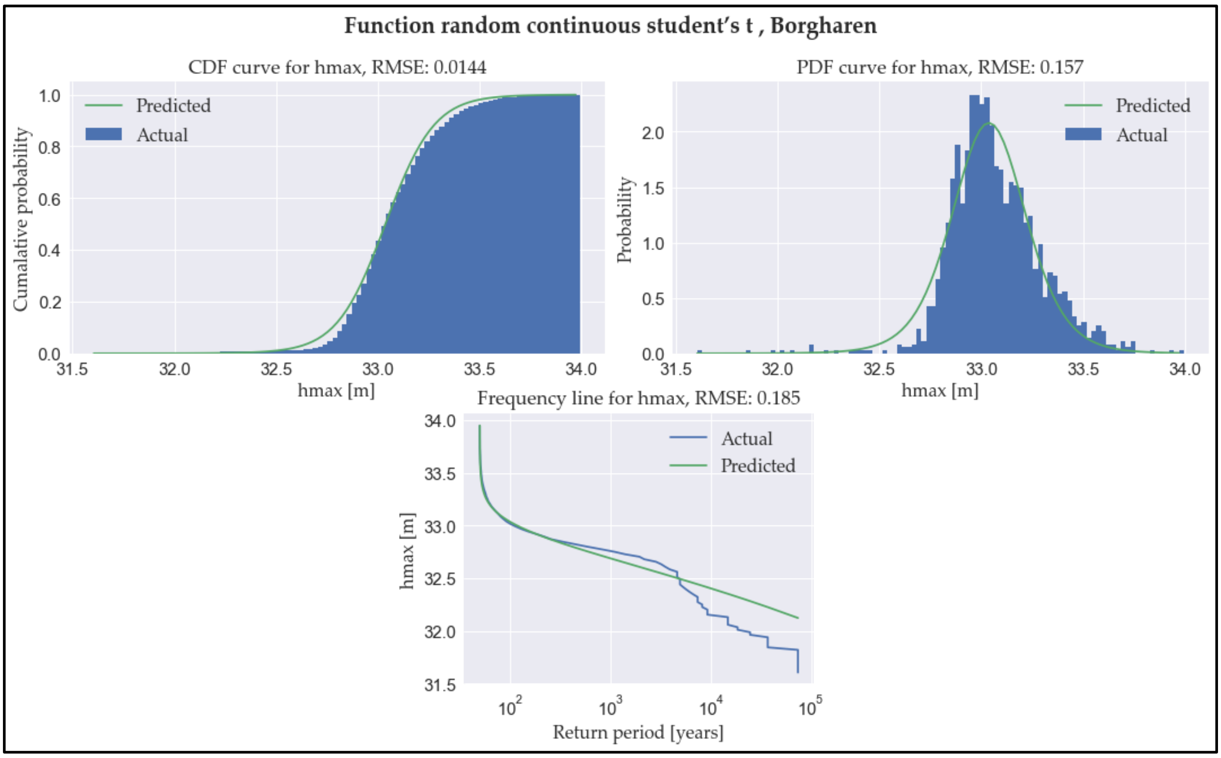
Function random continuous student's t , Borgharen
CDF curve for hmax, RMSE: 0.0144
PDF curve for hmax, RMSE: 0.157
Frequency line for hmax, RMSE: 0.185
Predicted
Actual
Cumalative probability
Probability
hmax [m]
Return period [years]

APPENDIX Q. RESULTS PROBABILISTIC ANALYSIS

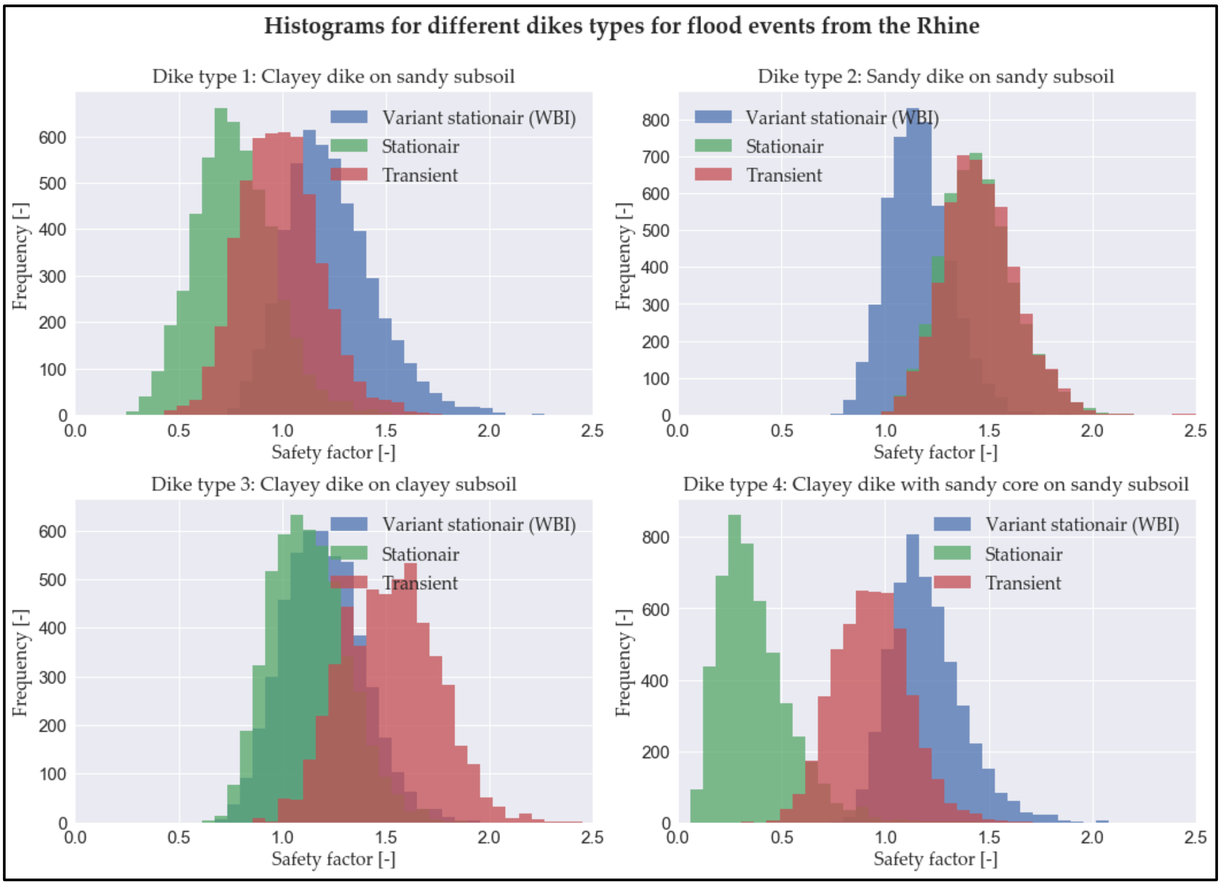
Histograms for different dikes types for flood events from the Rhine
Dike type 1: Clayey dike on sandy subsoil
Dike type 2: Sandy dike on sandy subsoil
Dike type 3: Clayey dike on clayey subsoil
Dike type 4: Clayey dike with sandy core on sandy subsoil
Variant stationair (WBI)
Stationair
Transient
Frequency [-]
Safety factor [-]

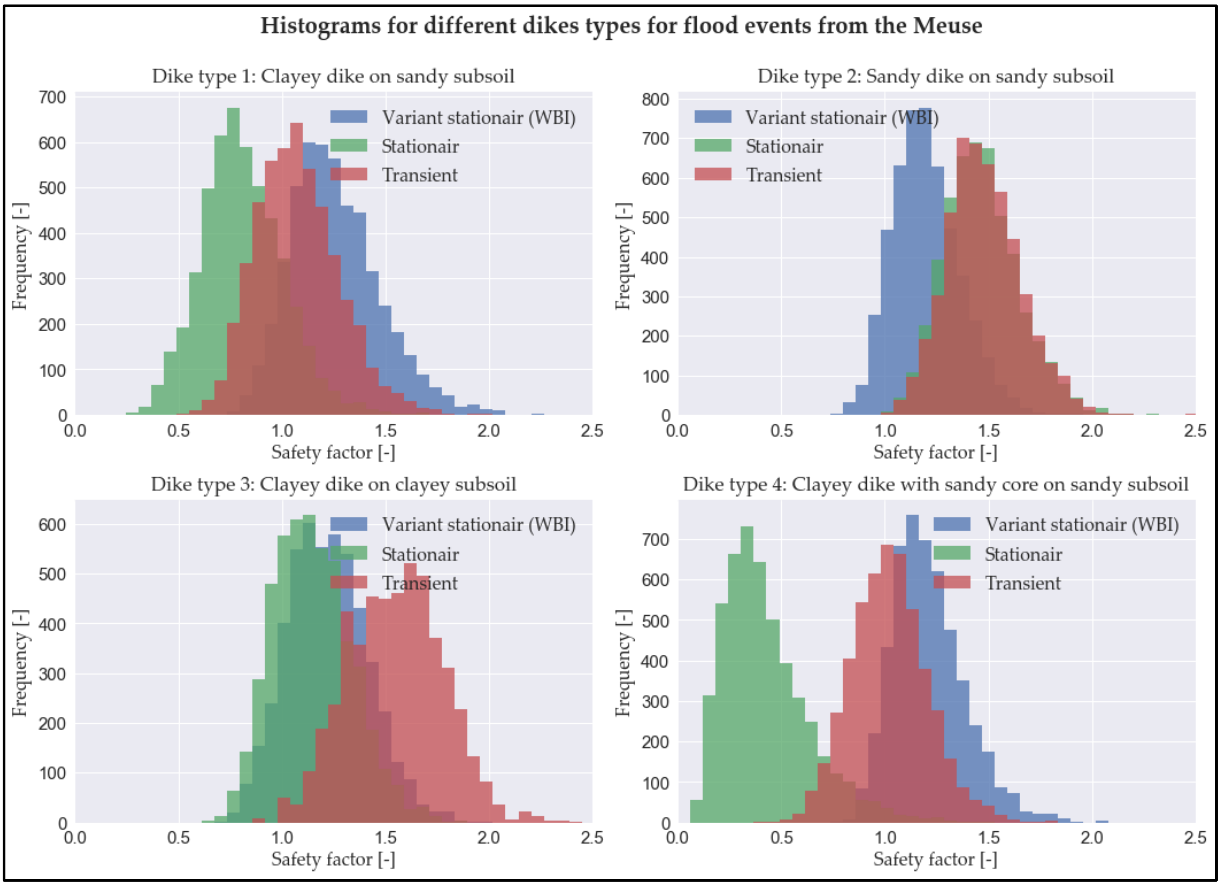
Histograms for different dikes types for flood events from the Meuse
Dike type 1: Clayey dike on sandy subsoil
Dike type 2: Sandy dike on sandy subsoil
Dike type 3: Clayey dike on clayey subsoil
Dike type 4: Clayey dike with sandy core on sandy subsoil
Variant stationair (WBI)
Stationair
Transient
Frequency [-]
Safety factor [-]

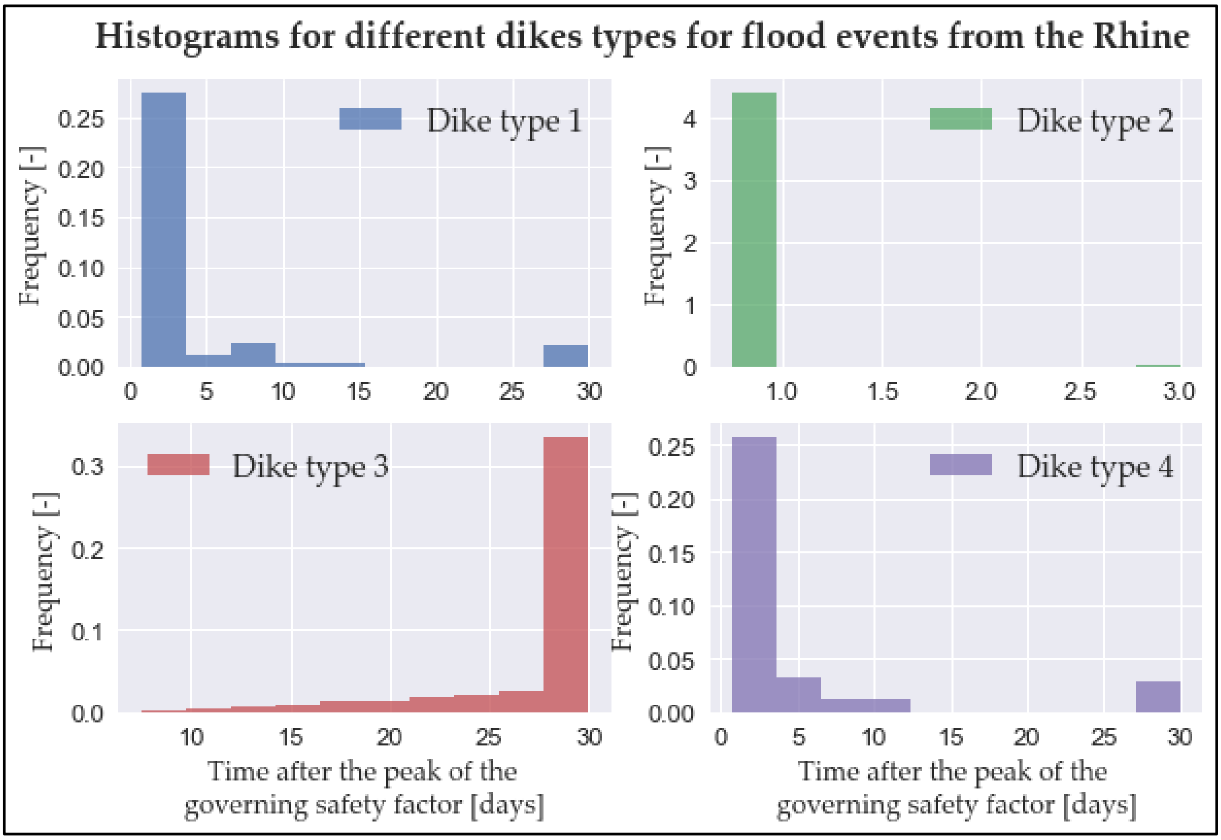
Histograms for different dikes types for flood events from the Rhine
Dike type 1
Dike type 2
Dike type 3
Dike type 4
Frequency [-]
Time after the peak of the governing safety factor [days]

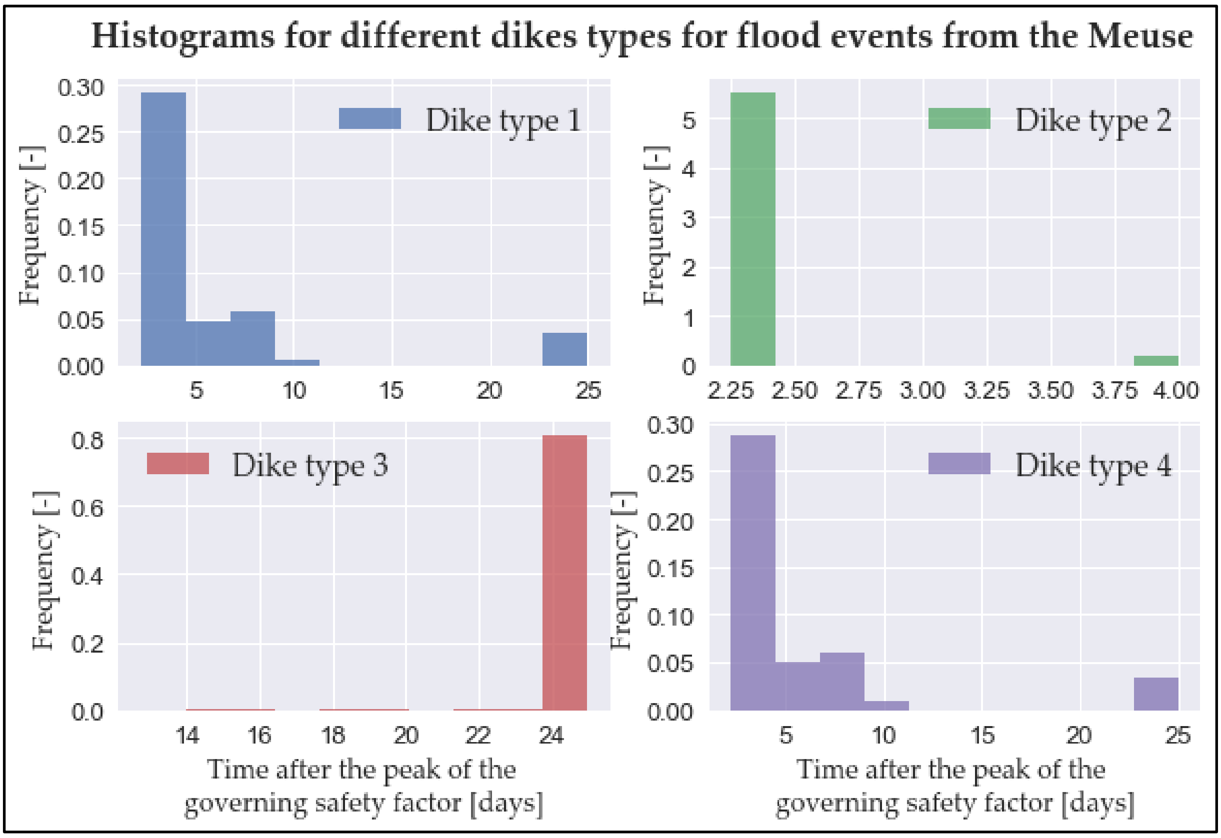
Histograms for different dikes types for flood events from the Meuse
Dike type 1
Dike type 2
Dike type 3
Dike type 4
Frequency [-]
Time after the peak of the governing safety factor [days]

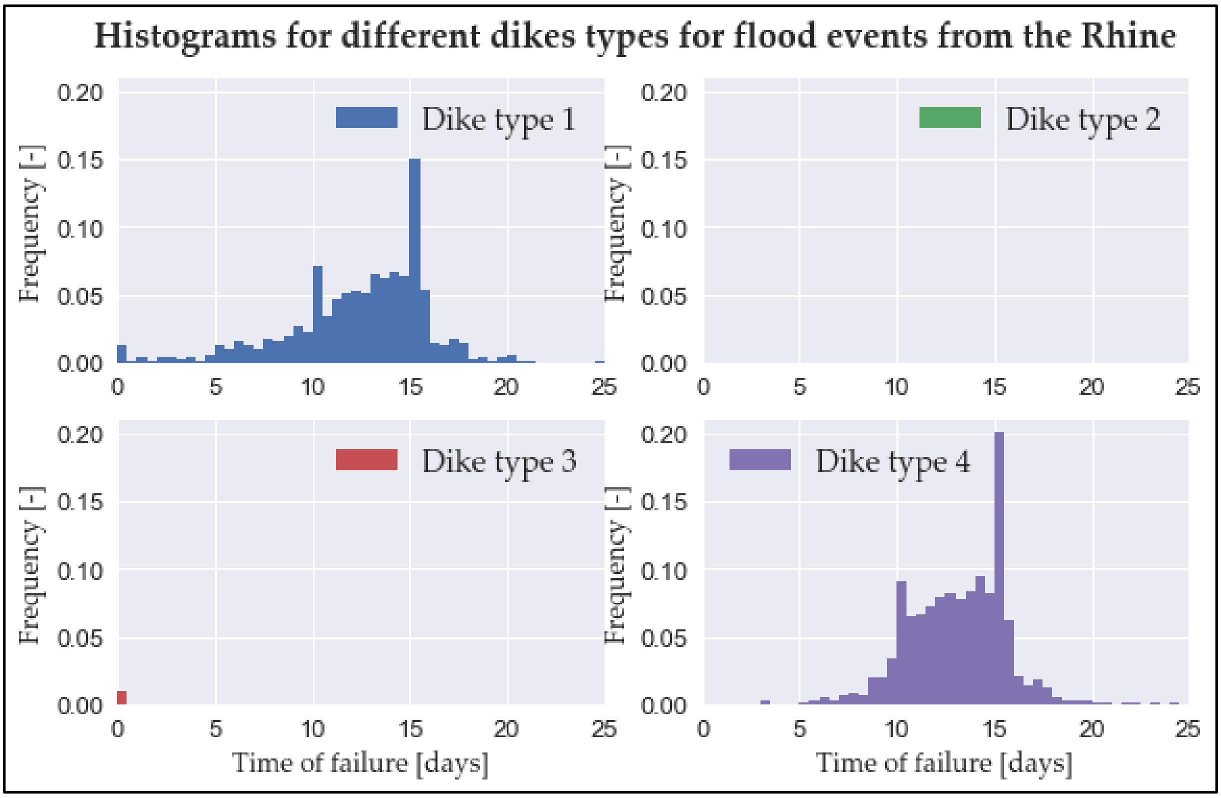
Histograms for different dikes types for flood events from the Rhine
Dike type 1
Dike type 2
Dike type 3
Dike type 4
Frequency [-]
Time of failure [days]
0.00
0.05
0.10
0.15
0.20
0
5
10
15
20
25

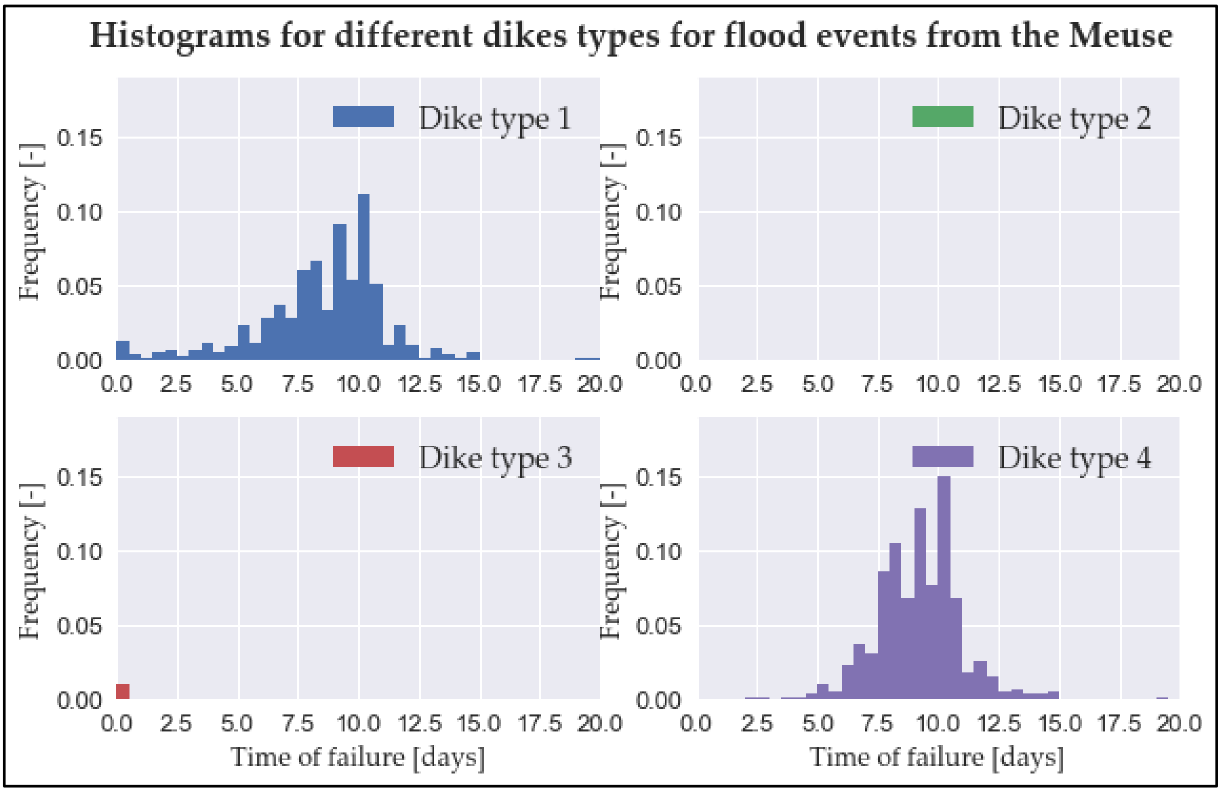
Histograms for different dikes types for flood events from the Meuse
Dike type 1
Dike type 2
Dike type 3
Dike type 4
Frequency [-]
Time of failure [days]
0.00
0.05
0.10
0.15
0.0
2.5
5.0
7.5
10.0
12.5
15.0
17.5
20.0

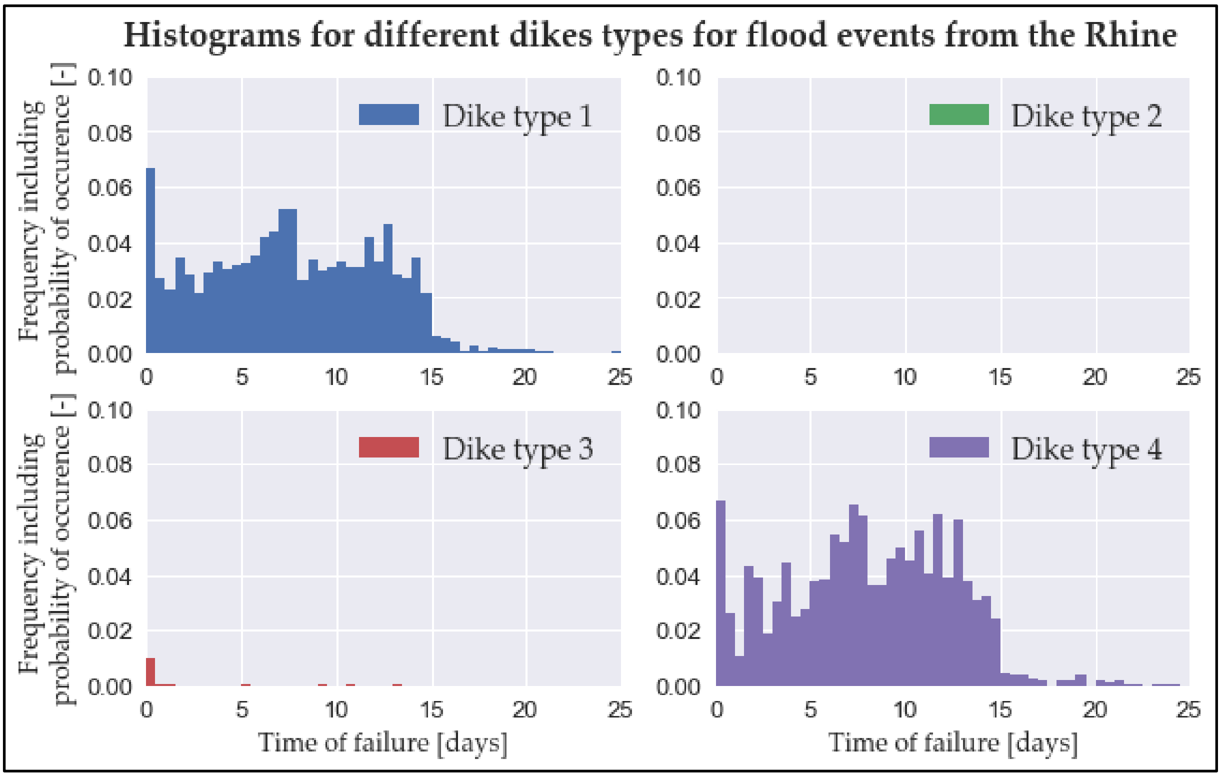
Histograms for different dikes types for flood events from the Rhine
Frequency including probability of occurence [-]
Dike type 1
Dike type 2
Dike type 3
Dike type 4
Time of failure [days]

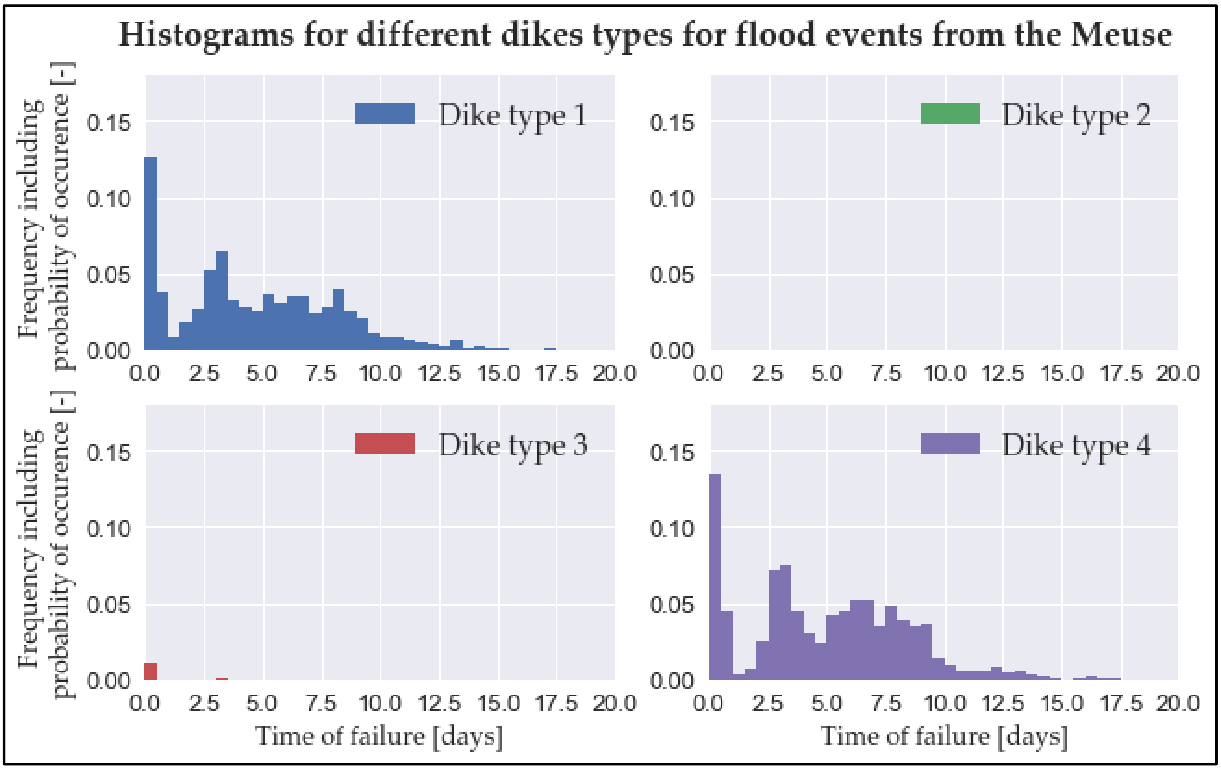
Histograms for different dikes types for flood events from the Meuse
Frequency including probability of occurence [-]
Dike type 1
Dike type 2
Dike type 3
Dike type 4
Time of failure [days]

2D-Fragility curves

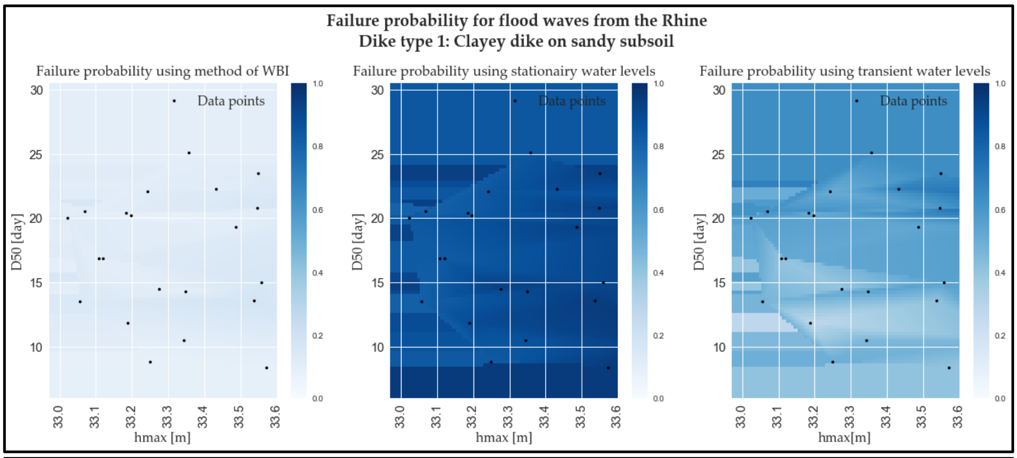

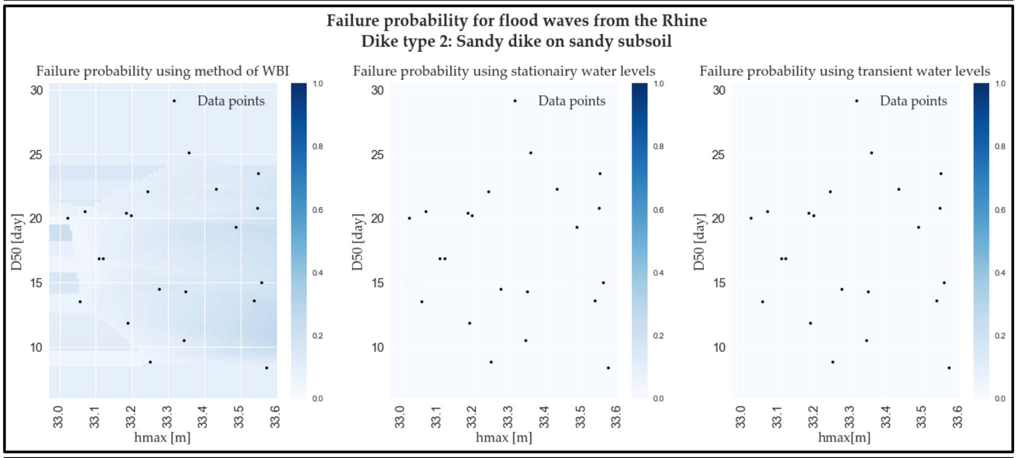

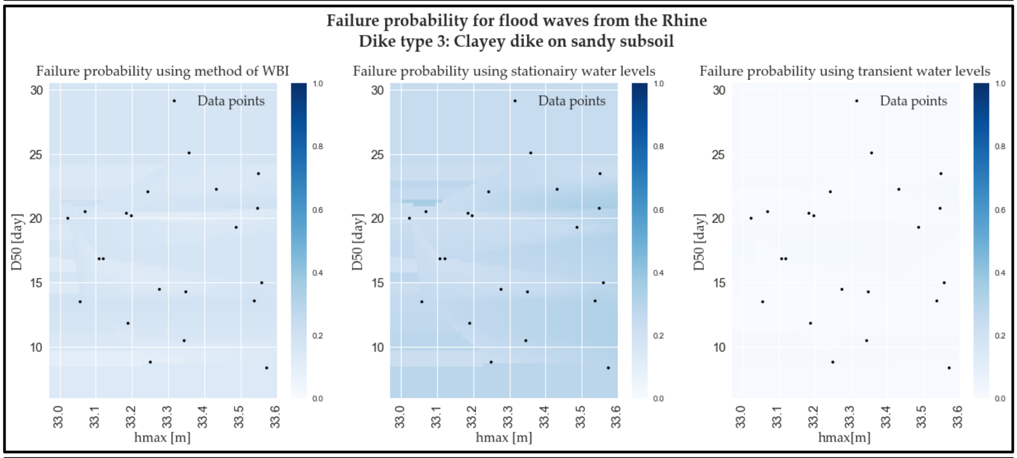

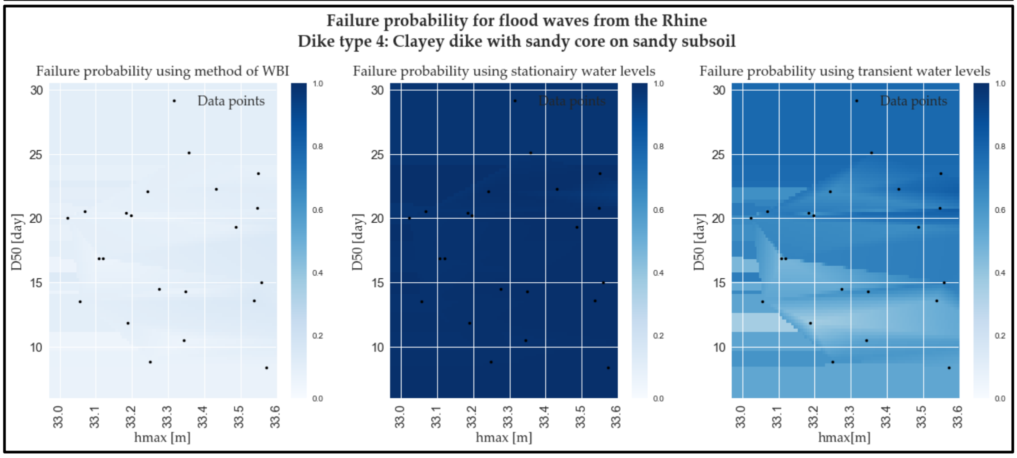

Failure probability for flood waves from the Meuse
Dike type 1: Clayey dike on sandy subsoil

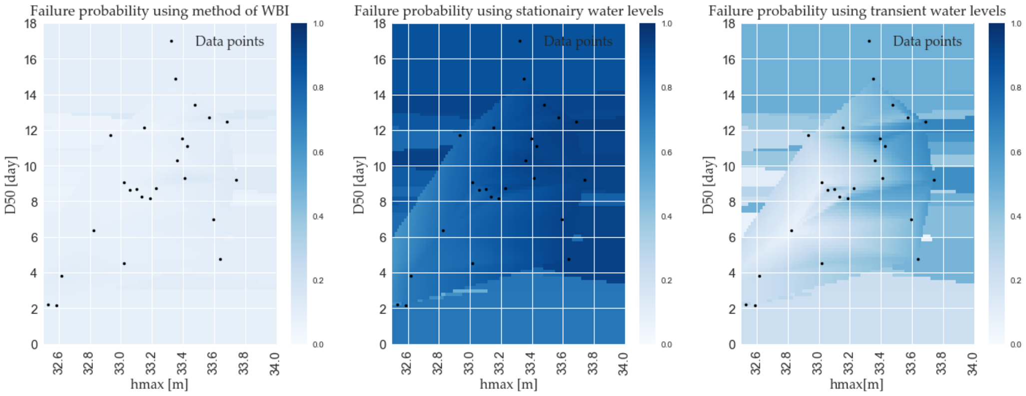

Failure probability for flood waves from the Meuse
Dike type 2: Sandy dike on sandy subsoil

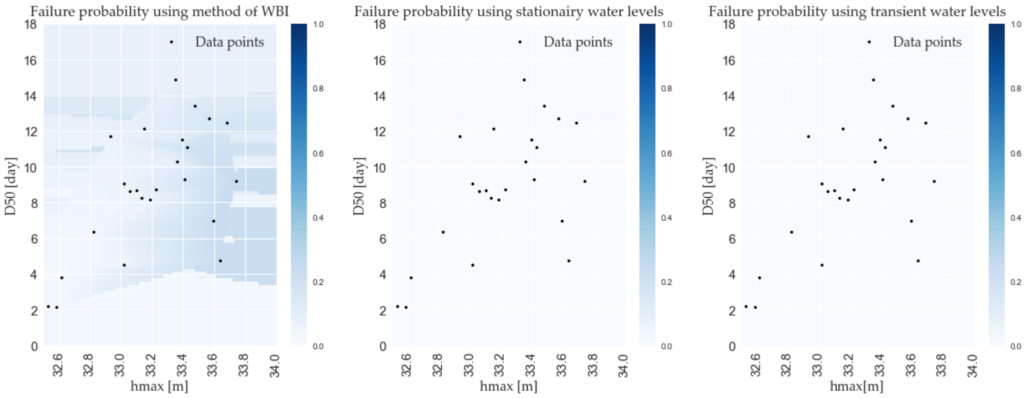

Failure probability for flood waves from the Meuse
Dike type 3: Clayey dike on sandy subsoil

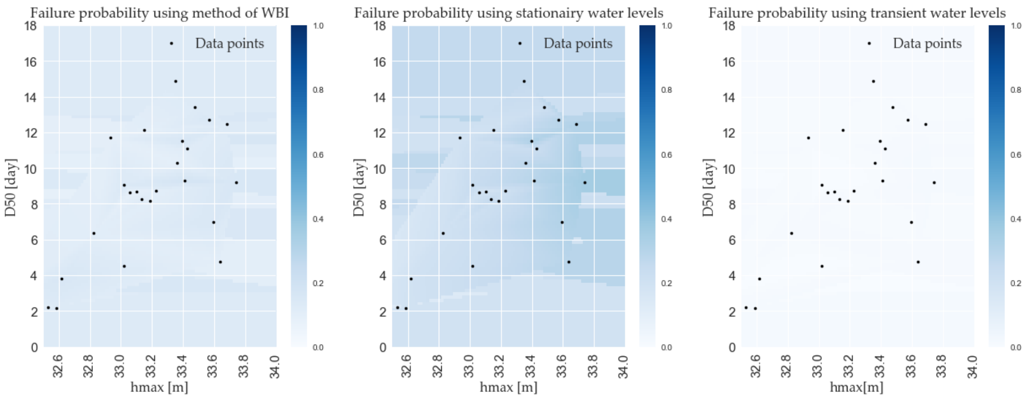

Failure probability for flood waves from the Meuse
Dike type 4: Clayey dike with sandy core on sandy subsoil

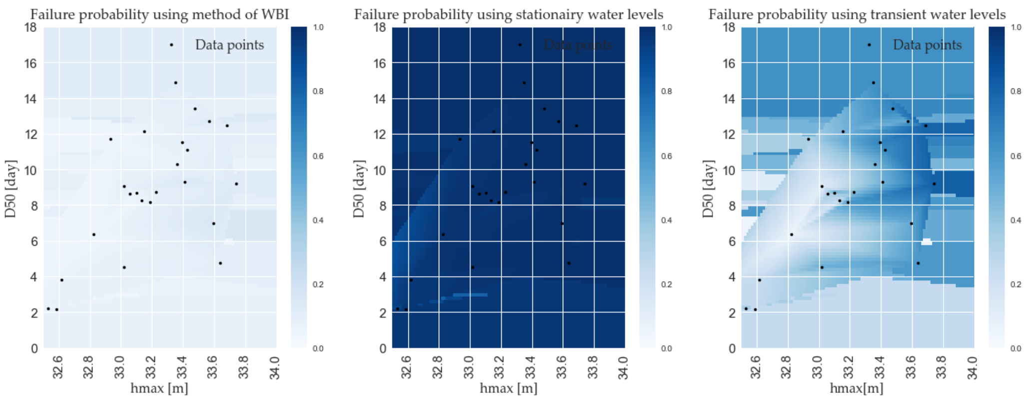

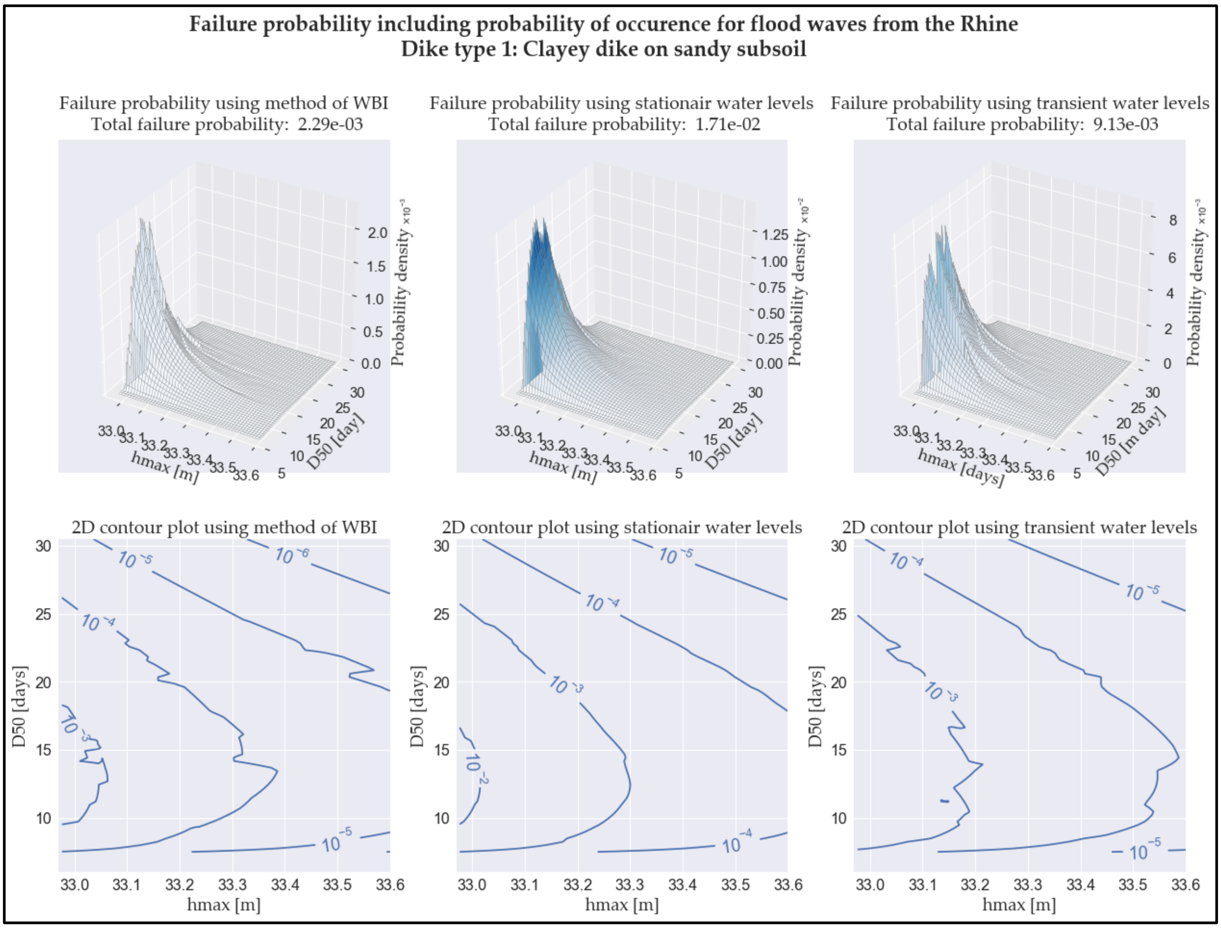
Failure probability including probability of occurence for flood waves from the Rhine
Dike type 1: Clayey dike on sandy subsoil
Failure probability using method of WBI
Total failure probability: 2.29e-03
Failure probability using stationair water levels
Total failure probability: 1.71e-02
Failure probability using transient water levels
Total failure probability: 9.13e-03
Probability density
hmax [m]
D50 [day]
hmax [days]
D50 [m day]
2D contour plot using method of WBI
2D contour plot using stationair water levels
2D contour plot using transient water levels
D50 [days]
hmax [m]

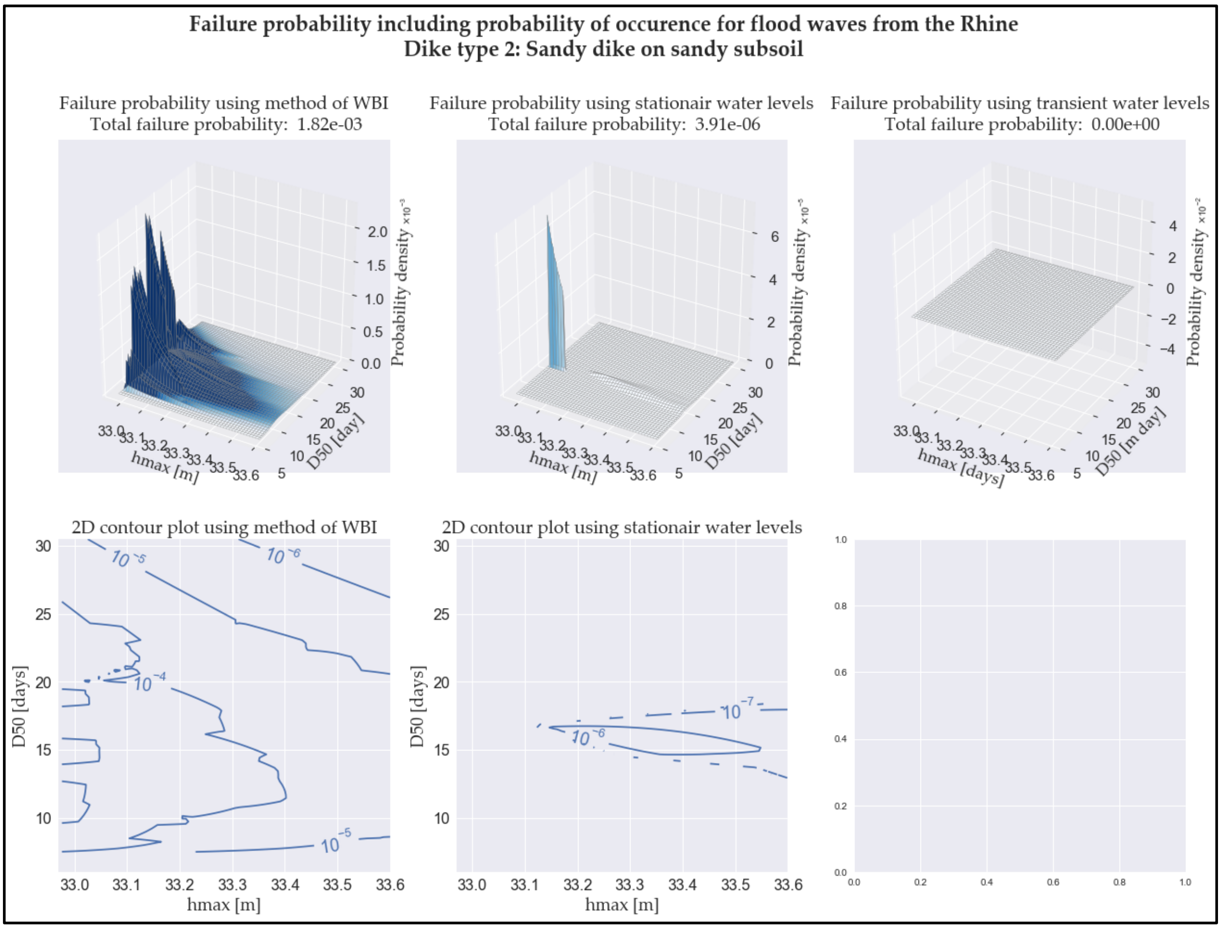
Failure probability including probability of occurence for flood waves from the Rhine
Dike type 2: Sandy dike on sandy subsoil
Failure probability using method of WBI
Total failure probability: 1.82e-03
Failure probability using stationair water levels
Total failure probability: 3.91e-06
Failure probability using transient water levels
Total failure probability: 0.00e+00
Probability density
hmax [m]
D50 [day]
hmax [days]
D50 [m day]
2D contour plot using method of WBI
2D contour plot using stationair water levels
D50 [days]
hmax [m]

Failure probability including probability of occurence for flood waves from the Rhine
Dike type 3: Clayey dike on clayey subsoil

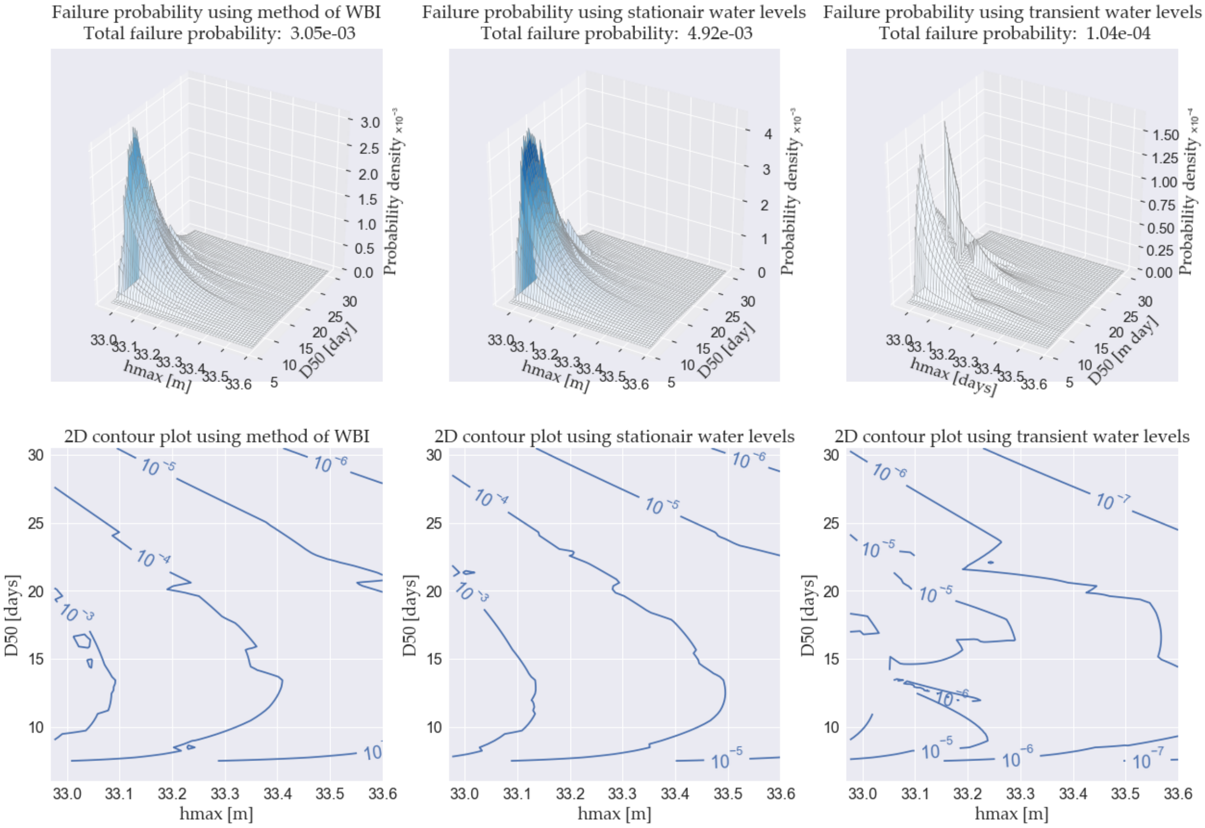

Failure probability including probability of occurence for flood waves from the Rhine
Dike type 4: Clayey dike wint sandy core on sandy subsoil

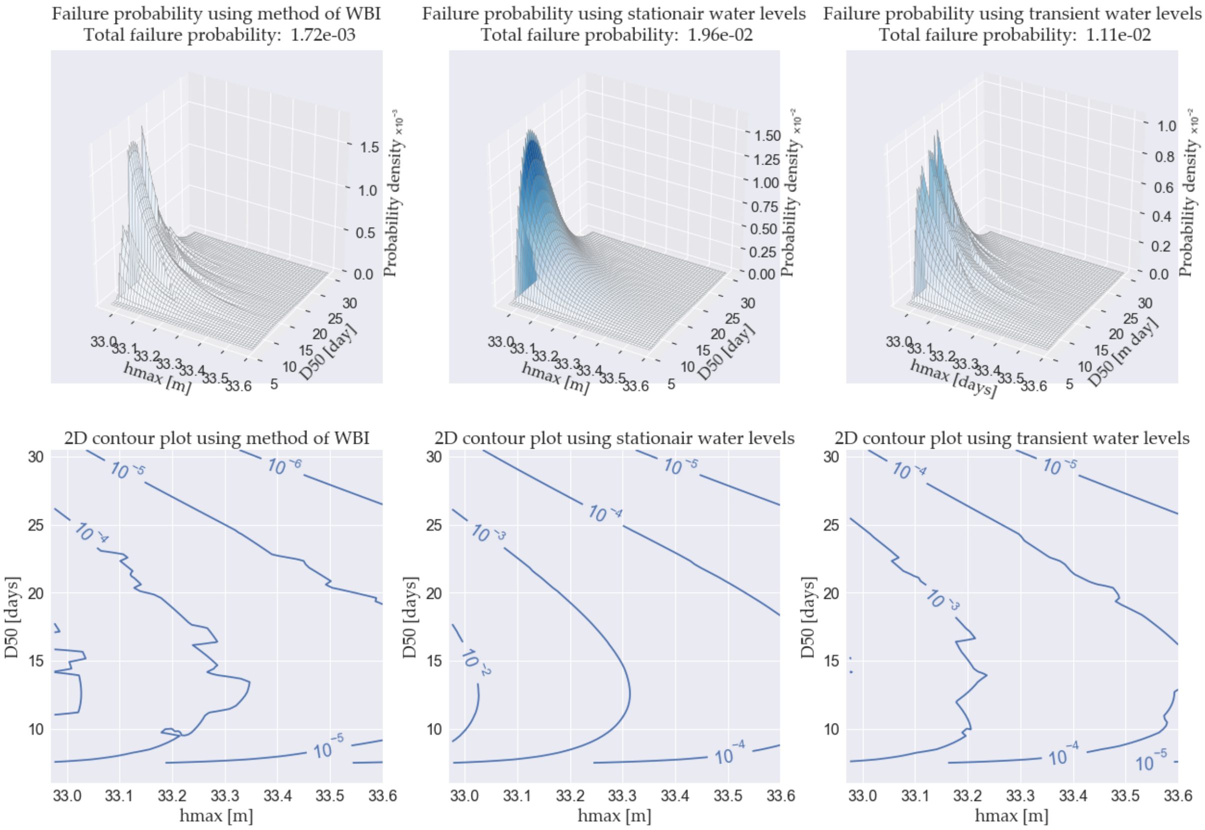

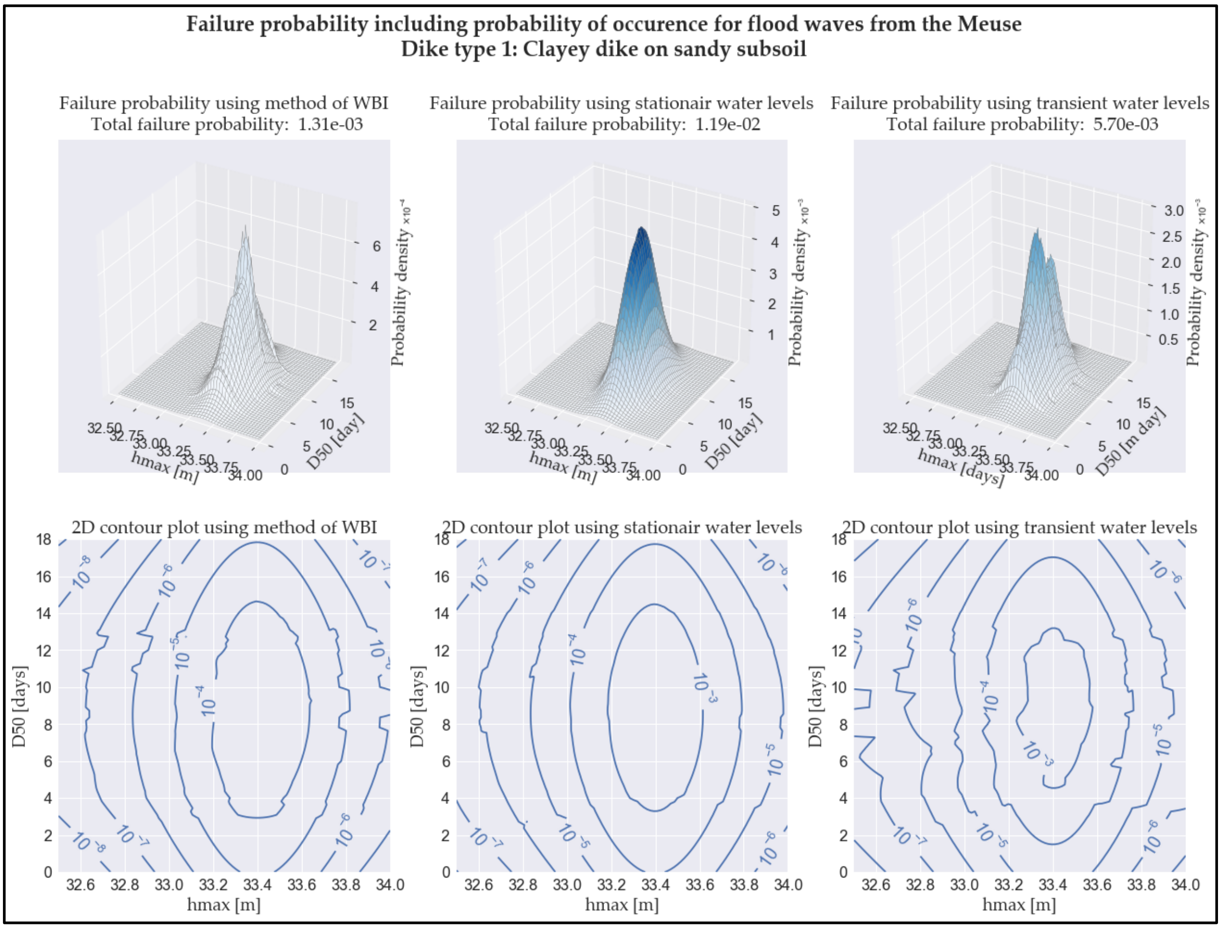
Failure probability including probability of occurence for flood waves from the Meuse
Dike type 1: Clayey dike on sandy subsoil
Failure probability using method of WBI
Total failure probability: 1.31e-03
Failure probability using stationair water levels
Total failure probability: 1.19e-02
Failure probability using transient water levels
Total failure probability: 5.70e-03
Probability density
hmax [m]
D50 [day]
hmax [days]
D50 [m day]
2D contour plot using method of WBI
2D contour plot using stationair water levels
2D contour plot using transient water levels
D50 [days]
hmax [m]

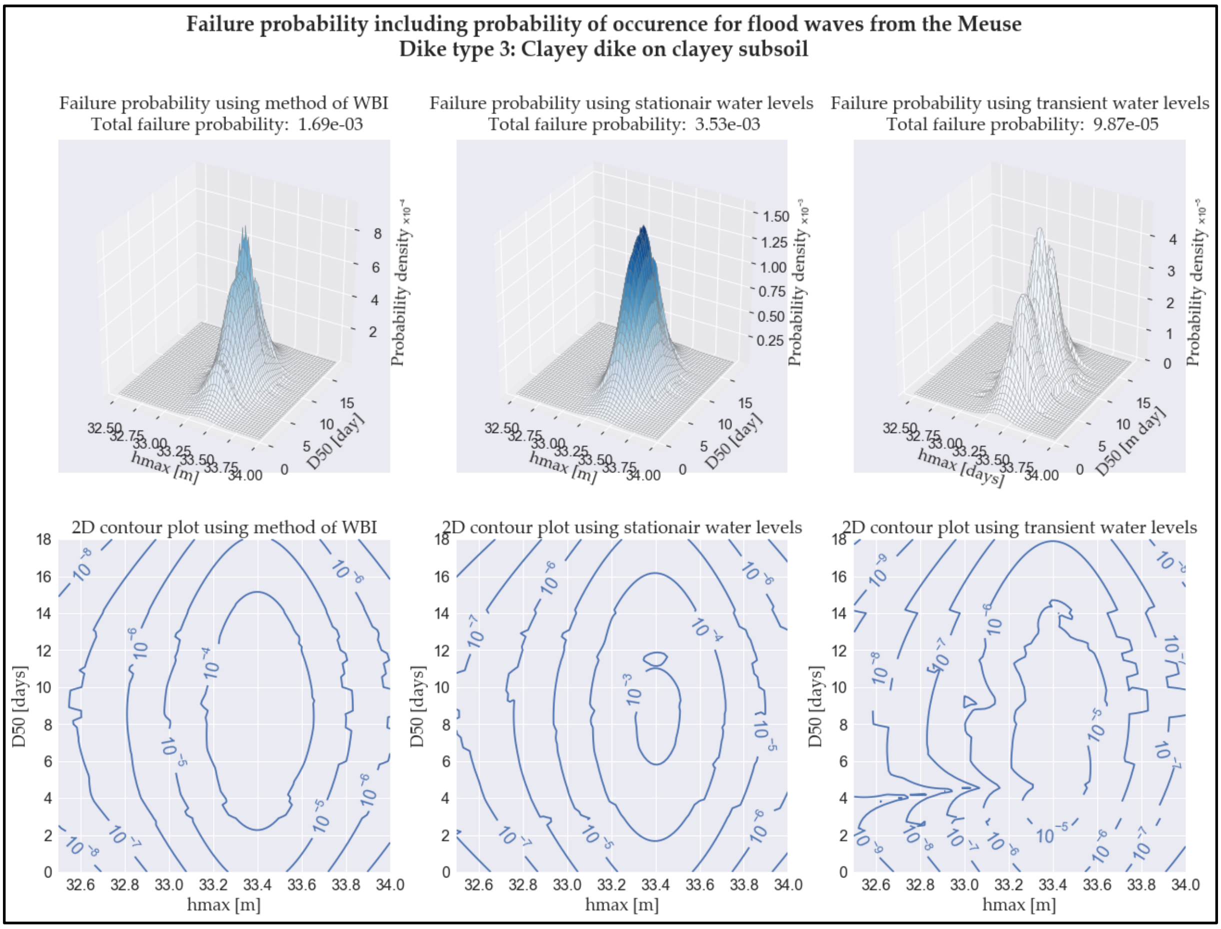
Failure probability including probability of occurence for flood waves from the Meuse
Dike type 3: Clayey dike on clayey subsoil
Failure probability using method of WBI
Total failure probability: 1.69e-03
Failure probability using stationair water levels
Total failure probability: 3.53e-03
Failure probability using transient water levels
Total failure probability: 9.87e-05
Probability density
hmax [m]
D50 [day]
hmax [days]
D50 [m day]
2D contour plot using method of WBI
2D contour plot using stationair water levels
2D contour plot using transient water levels
D50 [days]
hmax [m]

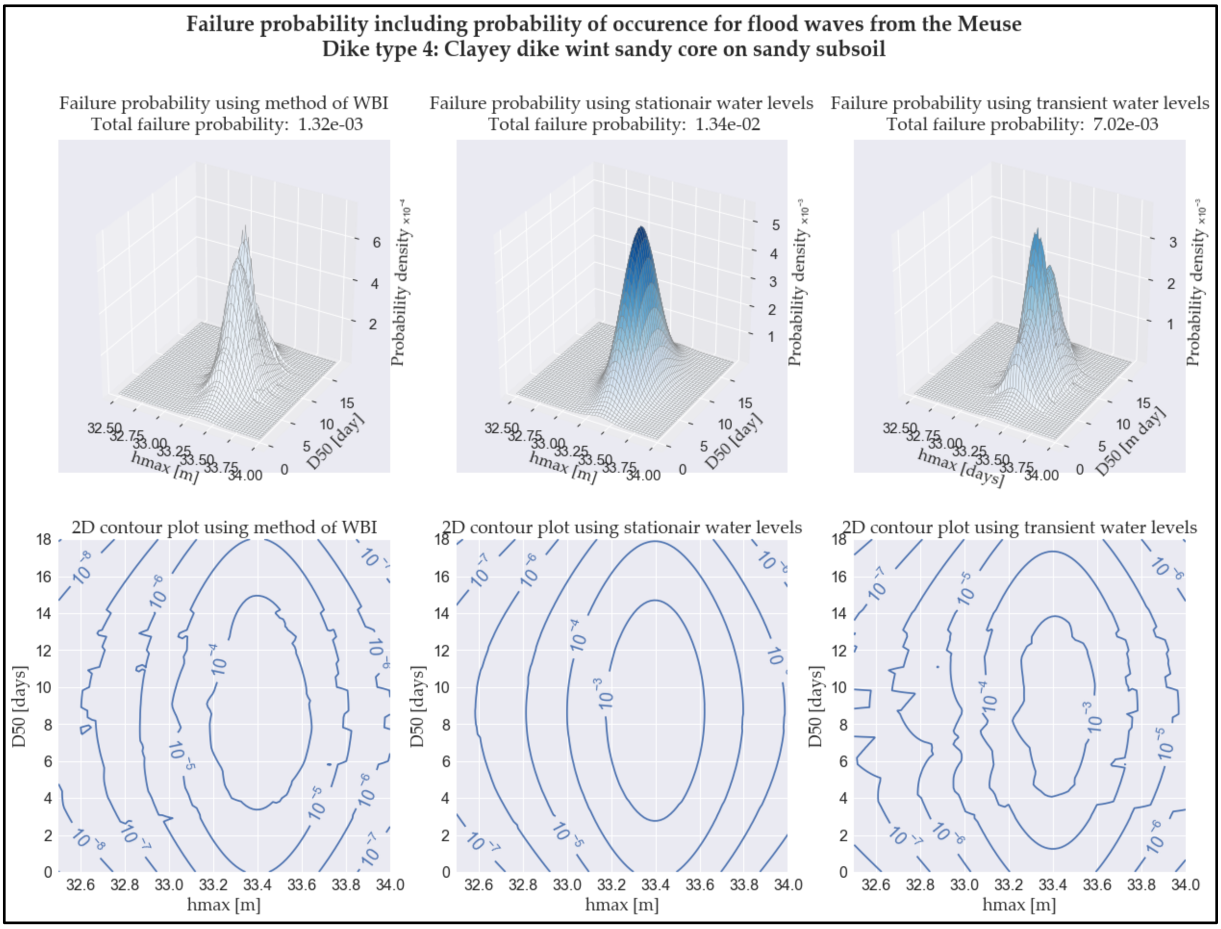
Failure probability including probability of occurence for flood waves from the Meuse
Dike type 4: Clayey dike wint sandy core on sandy subsoil
Failure probability using method of WBI
Total failure probability: 1.32e-03
Failure probability using stationair water levels
Total failure probability: 1.34e-02
Failure probability using transient water levels
Total failure probability: 7.02e-03
Probability density
hmax [m]
D50 [day]
hmax [days]
D50 [m day]
2D contour plot using method of WBI
2D contour plot using stationair water levels
2D contour plot using transient water levels
D50 [days]
hmax [m]

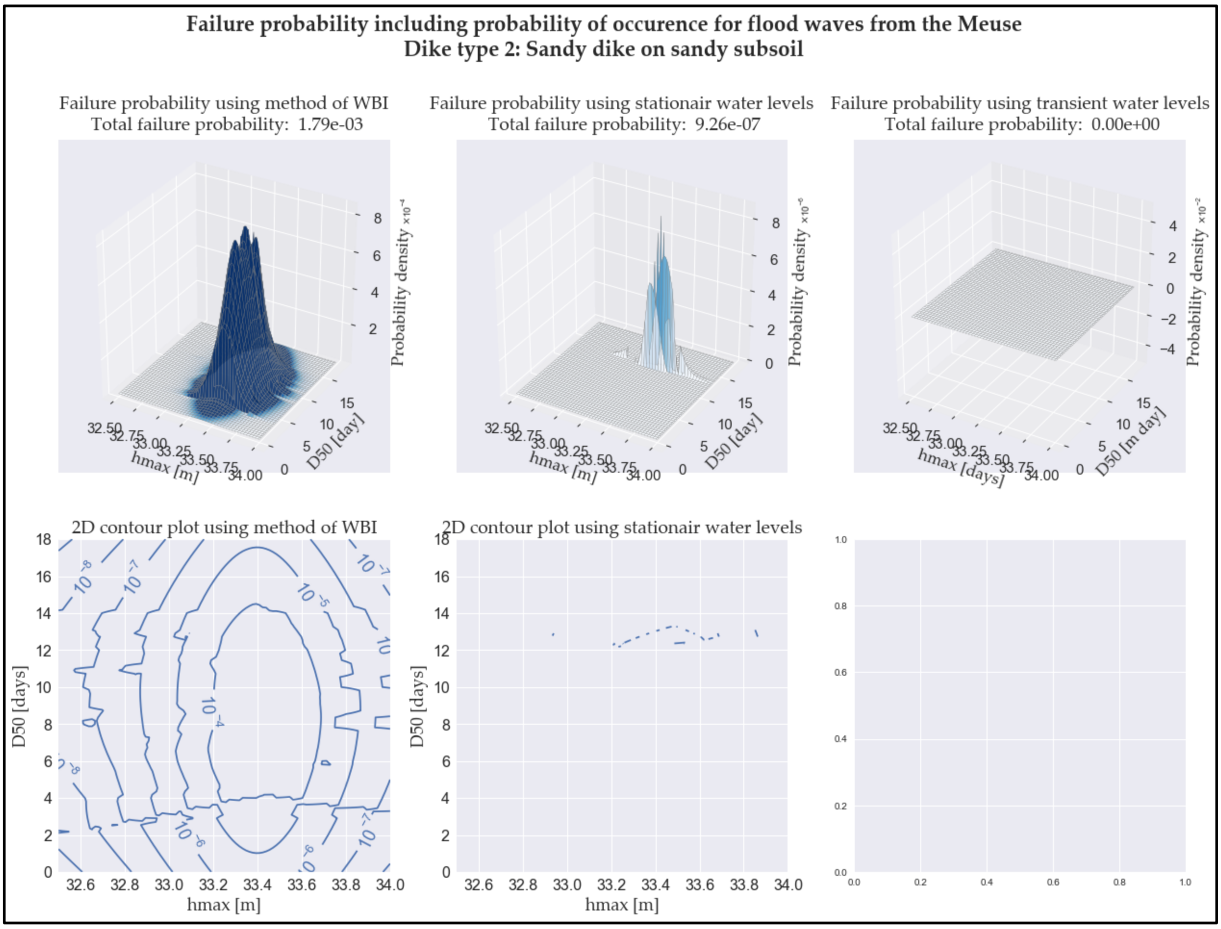
Failure probability including probability of occurence for flood waves from the Meuse
Dike type 2: Sandy dike on sandy subsoil
Failure probability using method of WBI
Total failure probability: 1.79e-03
Failure probability using stationair water levels
Total failure probability: 9.26e-07
Failure probability using transient water levels
Total failure probability: 0.00e+00
Probability density
hmax [m]
D50 [day]
hmax [days]
D50 [m day]
2D contour plot using method of WBI
2D contour plot using stationair water levels
D50 [days]
hmax [m]

Location Rhine, dike type 1

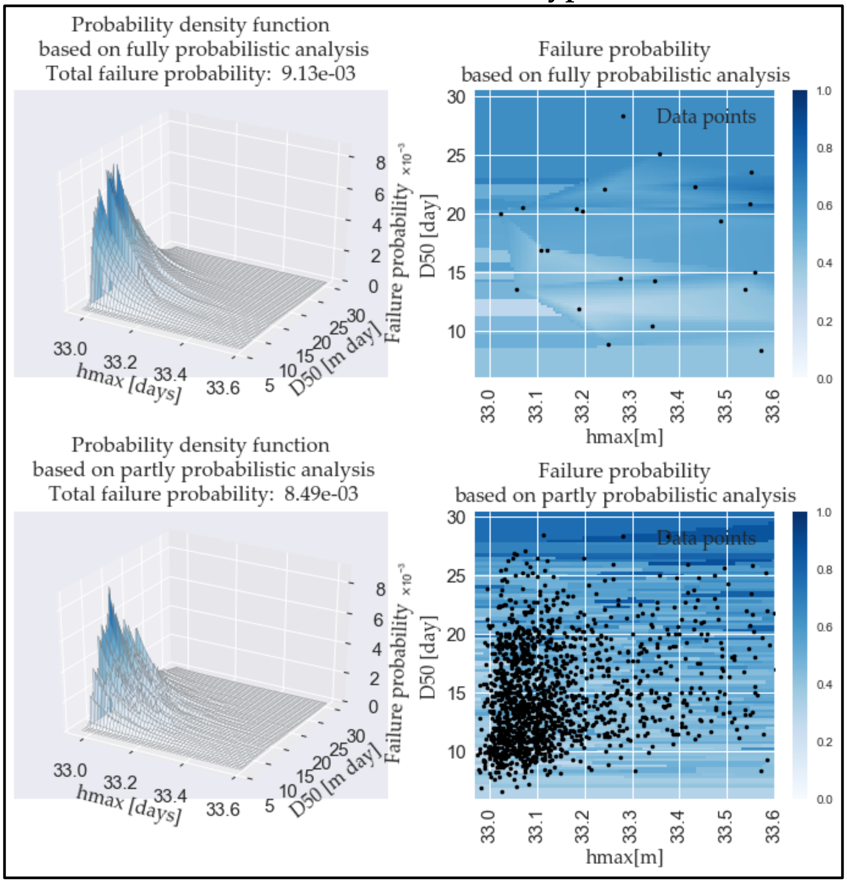

Location Rhine, dike type 2

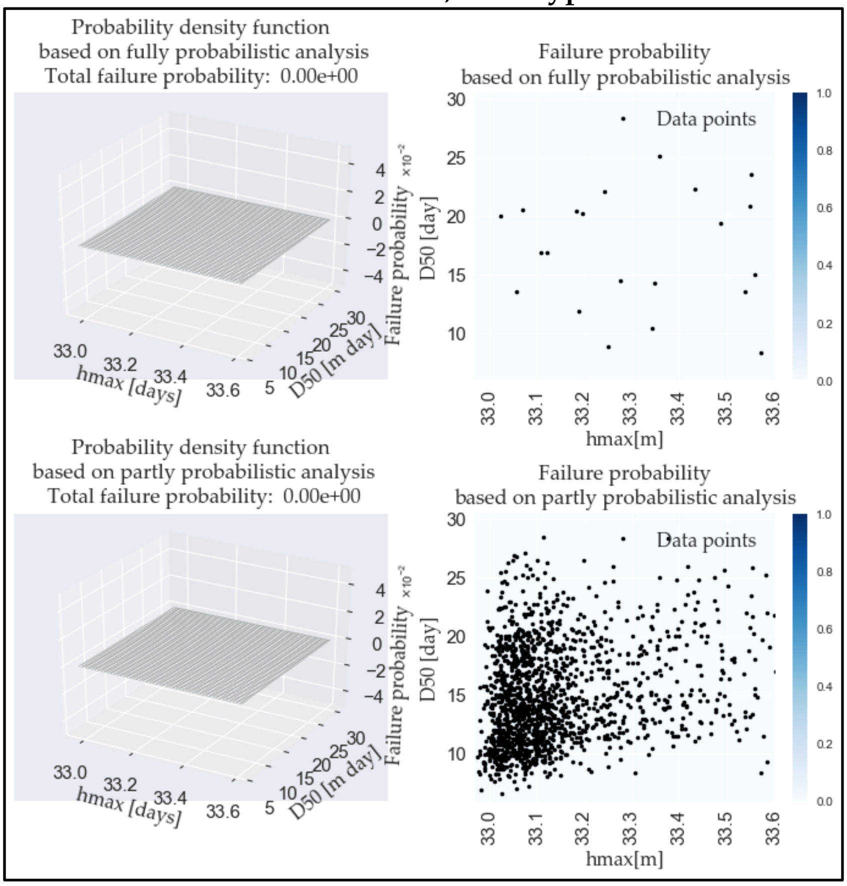

Location Rhine, dike type 3

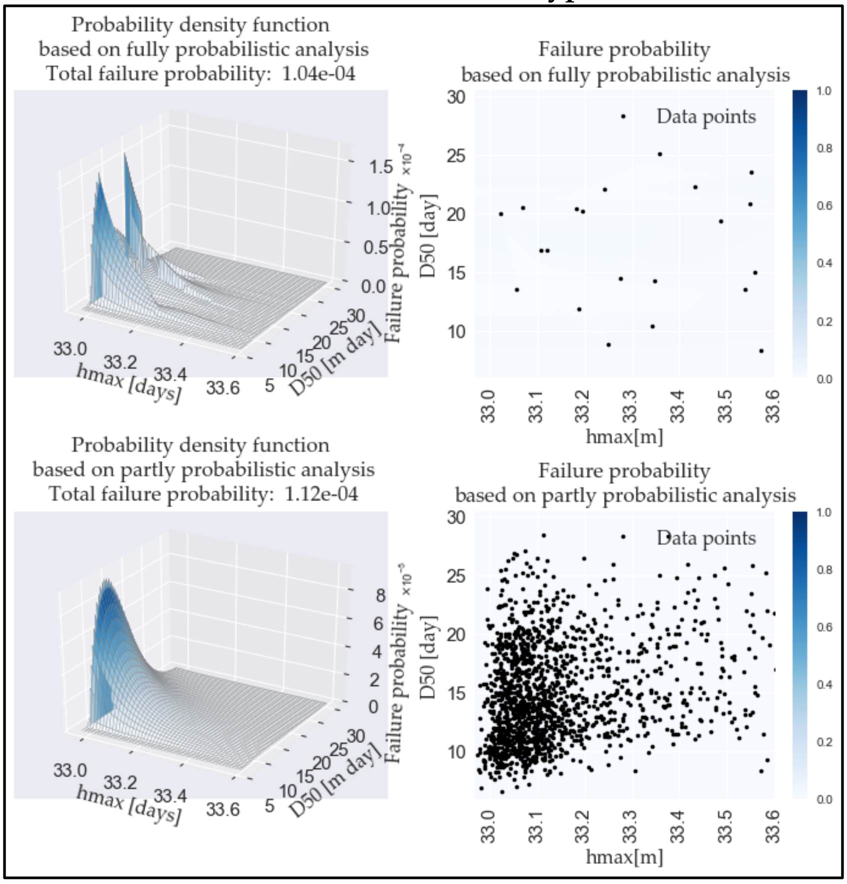

Location Rhine, dike type 4

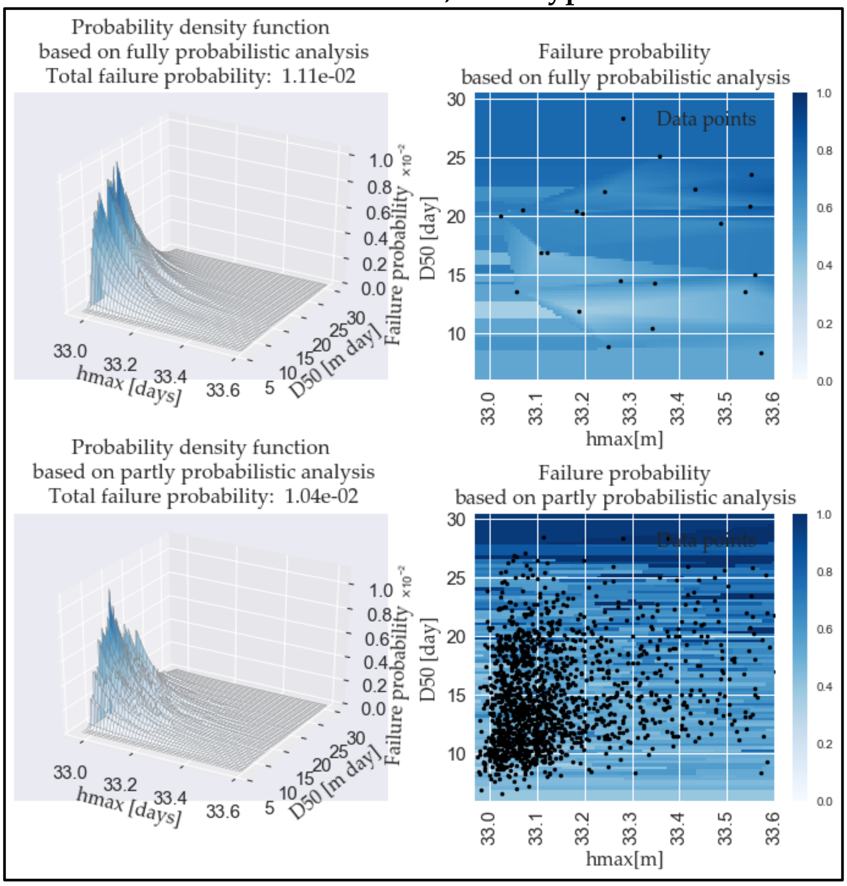

Location Meuse, dike type 1

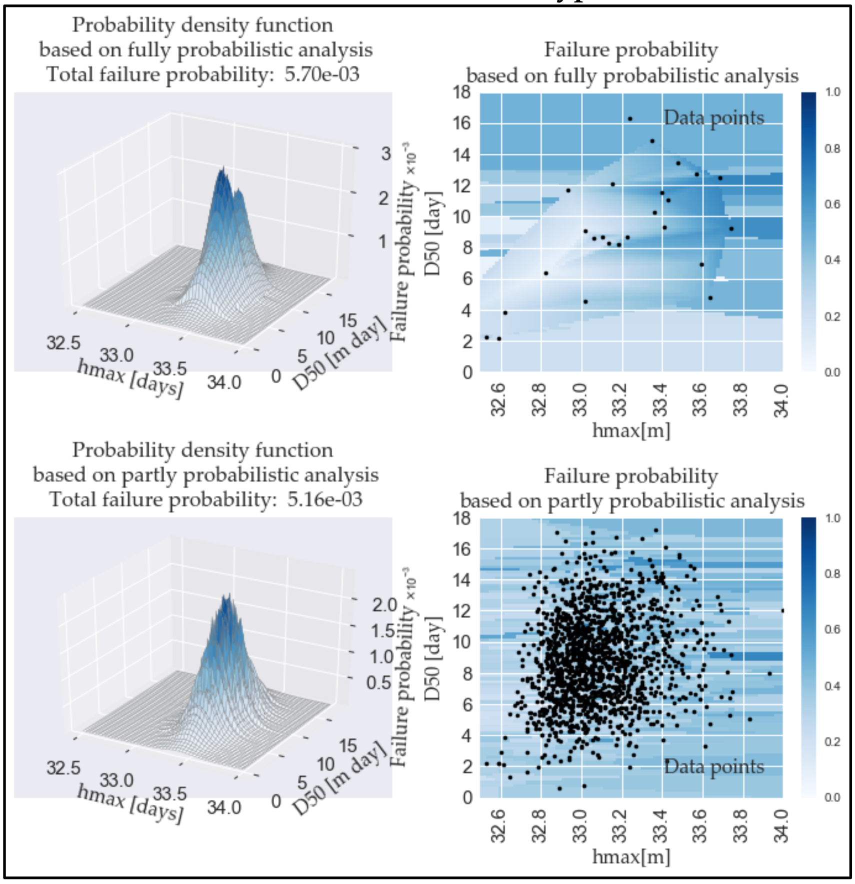

Location Meuse, dike type 2

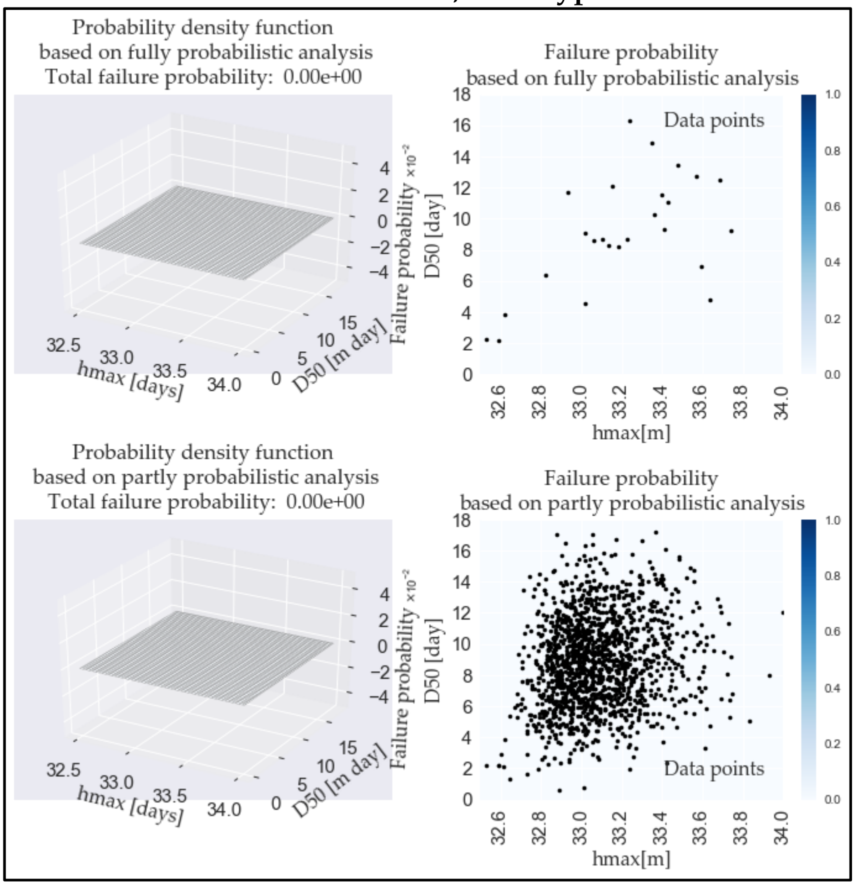

Location Meuse, dike type 3

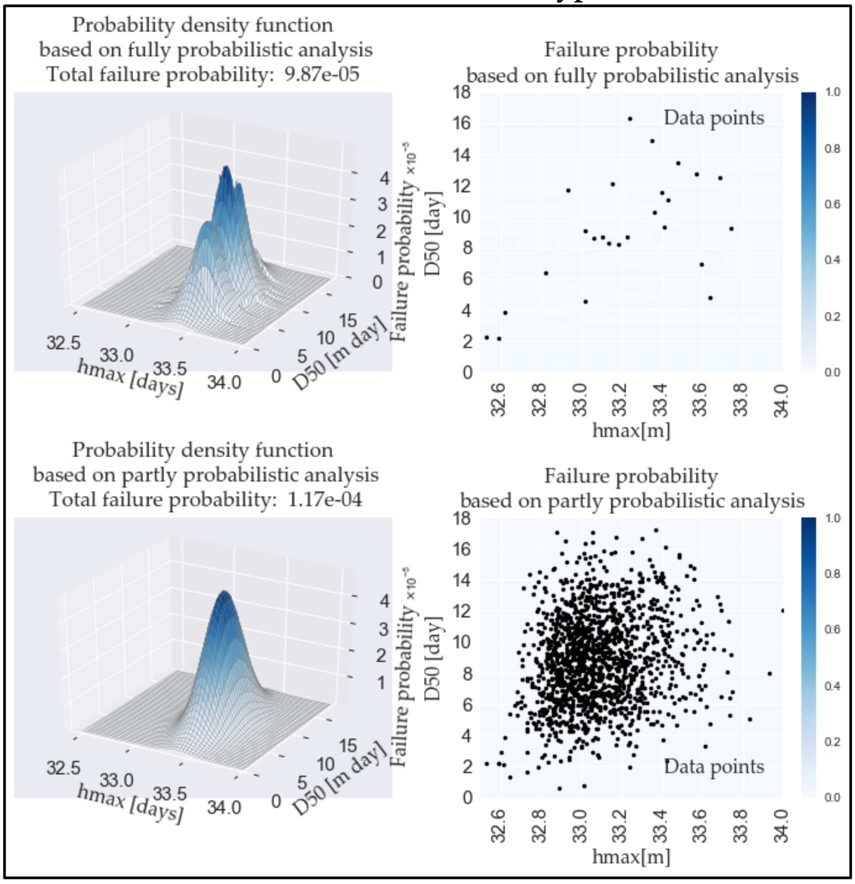

Location Meuse, dike type 4

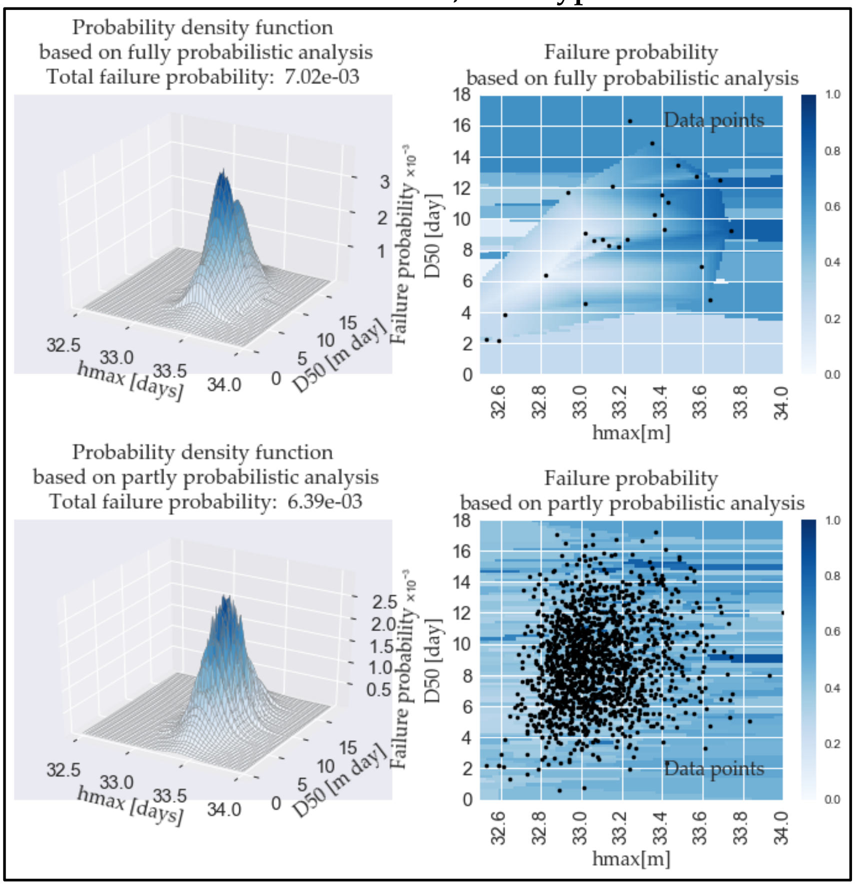

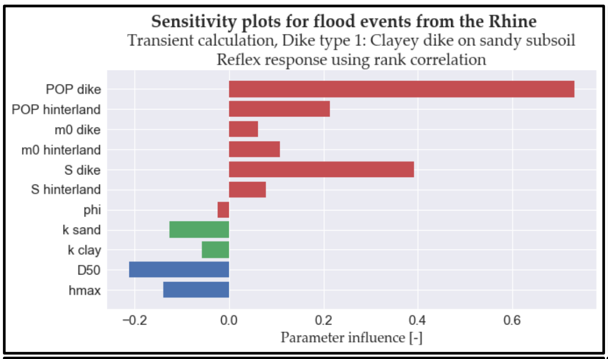
Sensitivity plots for flood events from the Rhine
Transient calculation, Dike type 1: Clayey dike on sandy subsoil
Reflex response using rank correlation
POP dike
POP hinterland
m0 dike
m0 hinterland
S dike
S hinterland
phi
k sand
k clay
D50
hmax
−0.2 0.0 0.2 0.4 0.6
Parameter influence [-]

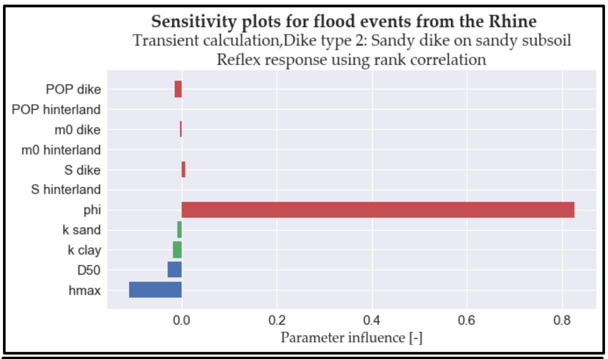
Sensitivity plots for flood events from the Rhine
Transient calculation,Dike type 2: Sandy dike on sandy subsoil
Reflex response using rank correlation
POP dike
POP hinterland
m0 dike
m0 hinterland
S dike
S hinterland
phi
k sand
k clay
D50
hmax
0.0 0.2 0.4 0.6 0.8
Parameter influence [-]

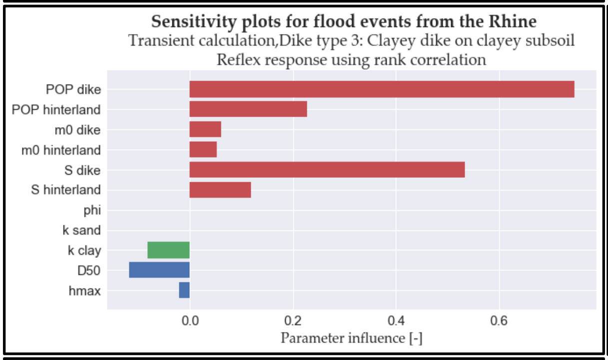
Sensitivity plots for flood events from the Rhine
Transient calculation,Dike type 3: Clayey dike on clayey subsoil
Reflex response using rank correlation
POP dike
POP hinterland
m0 dike
m0 hinterland
S dike
S hinterland
phi
k sand
k clay
D50
hmax
0.0 0.2 0.4 0.6
Parameter influence [-]

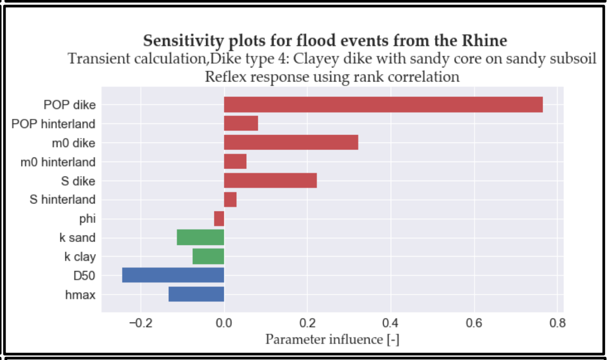
Sensitivity plots for flood events from the Rhine
Transient calculation,Dike type 4: Clayey dike with sandy core on sandy subsoil
Reflex response using rank correlation
POP dike
POP hinterland
m0 dike
m0 hinterland
S dike
S hinterland
phi
k sand
k clay
D50
hmax
−0.2 0.0 0.2 0.4 0.6 0.8
Parameter influence [-]

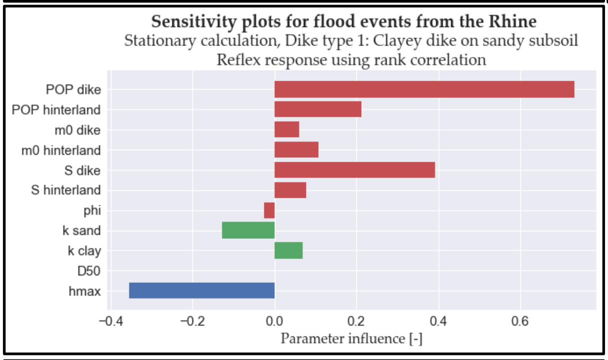
Sensitivity plots for flood events from the Rhine
Stationary calculation, Dike type 1: Clayey dike on sandy subsoil
Reflex response using rank correlation
POP dike
POP hinterland
m0 dike
m0 hinterland
S dike
S hinterland
phi
k sand
k clay
D50
hmax
−0.4 −0.2 0.0 0.2 0.4 0.6
Parameter influence [-]

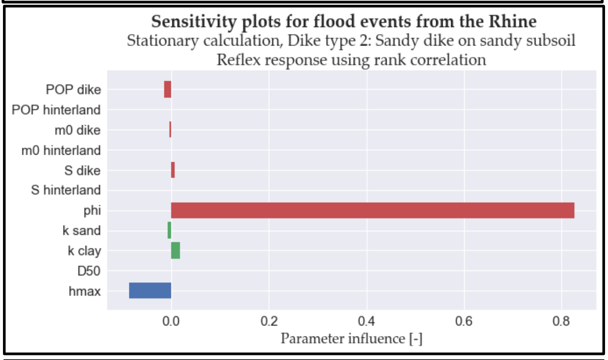
Sensitivity plots for flood events from the Rhine
Stationary calculation, Dike type 2: Sandy dike on sandy subsoil
Reflex response using rank correlation
POP dike
POP hinterland
m0 dike
m0 hinterland
S dike
S hinterland
phi
k sand
k clay
D50
hmax
0.0 0.2 0.4 0.6 0.8
Parameter influence [-]

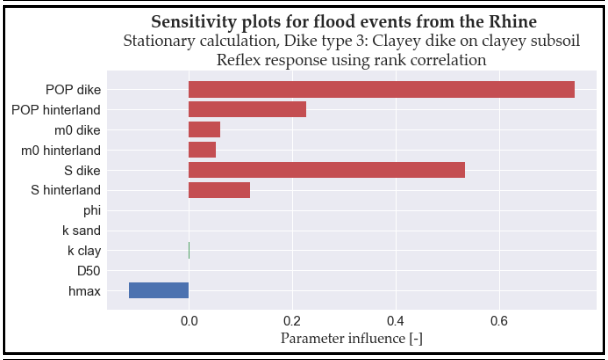
Sensitivity plots for flood events from the Rhine
Stationary calculation, Dike type 3: Clayey dike on clayey subsoil
Reflex response using rank correlation
POP dike
POP hinterland
m0 dike
m0 hinterland
S dike
S hinterland
phi
k sand
k clay
D50
hmax
0.0 0.2 0.4 0.6
Parameter influence [-]

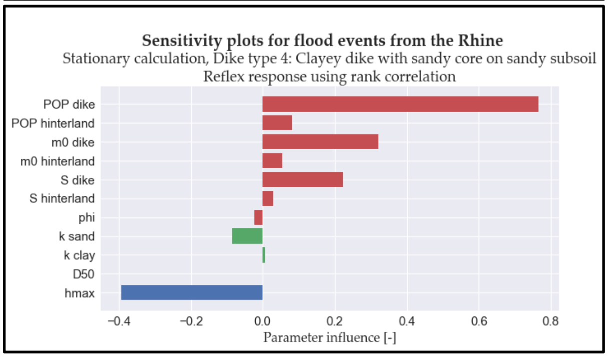
Sensitivity plots for flood events from the Rhine
Stationary calculation, Dike type 4: Clayey dike with sandy core on sandy subsoil
Reflex response using rank correlation
POP dike
POP hinterland
m0 dike
m0 hinterland
S dike
S hinterland
phi
k sand
k clay
D50
hmax
−0.4 −0.2 0.0 0.2 0.4 0.6 0.8
Parameter influence [-]

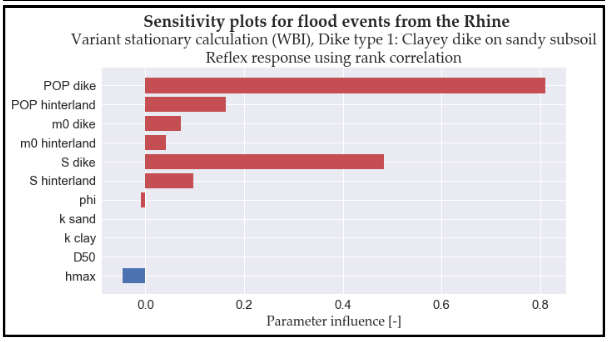
Sensitivity plots for flood events from the Rhine
Variant stationary calculation (WBI), Dike type 1: Clayey dike on sandy subsoil
Reflex response using rank correlation
POP dike
POP hinterland
m0 dike
m0 hinterland
S dike
S hinterland
phi
k sand
k clay
D50
hmax
0.0 0.2 0.4 0.6 0.8
Parameter influence [-]

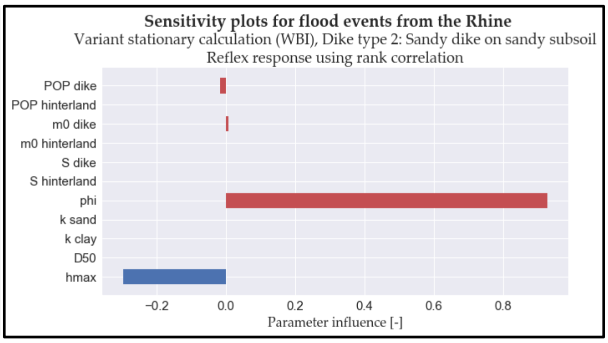
Sensitivity plots for flood events from the Rhine
Variant stationary calculation (WBI), Dike type 2: Sandy dike on sandy subsoil
Reflex response using rank correlation
POP dike
POP hinterland
m0 dike
m0 hinterland
S dike
S hinterland
phi
k sand
k clay
D50
hmax
−0.2 0.0 0.2 0.4 0.6 0.8
Parameter influence [-]

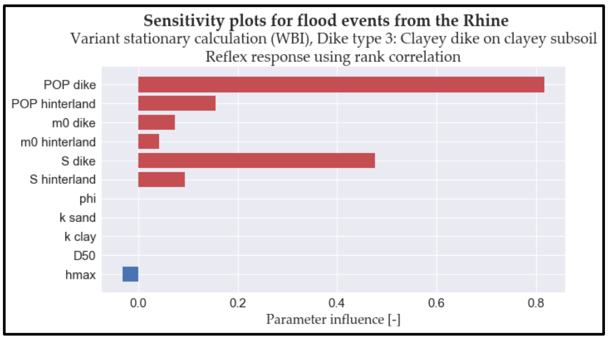
Sensitivity plots for flood events from the Rhine
Variant stationary calculation (WBI), Dike type 3: Clayey dike on clayey subsoil
Reflex response using rank correlation
POP dike
POP hinterland
m0 dike
m0 hinterland
S dike
S hinterland
phi
k sand
k clay
D50
hmax
Parameter influence [-]

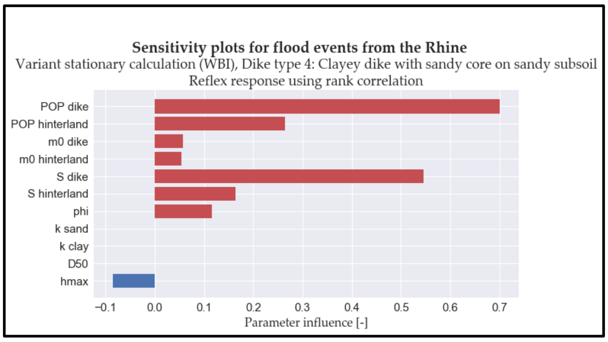
Sensitivity plots for flood events from the Rhine
Variant stationary calculation (WBI), Dike type 4: Clayey dike with sandy core on sandy subsoil
Reflex response using rank correlation
POP dike
POP hinterland
m0 dike
m0 hinterland
S dike
S hinterland
phi
k sand
k clay
D50
hmax
Parameter influence [-]

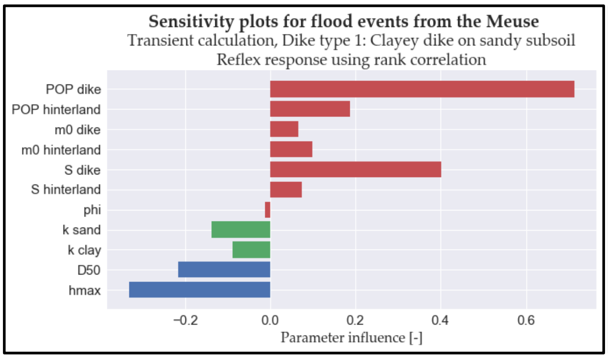
Sensitivity plots for flood events from the Meuse
Transient calculation, Dike type 1: Clayey dike on sandy subsoil
Reflex response using rank correlation
POP dike
POP hinterland
m0 dike
m0 hinterland
S dike
S hinterland
phi
k sand
k clay
D50
hmax
Parameter influence [-]

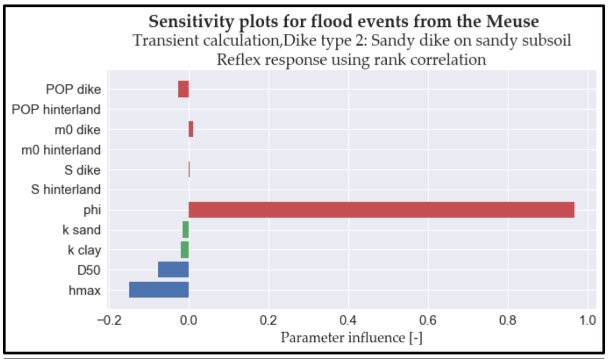
Sensitivity plots for flood events from the Meuse
Transient calculation,Dike type 2: Sandy dike on sandy subsoil
Reflex response using rank correlation
POP dike
POP hinterland
m0 dike
m0 hinterland
S dike
S hinterland
phi
k sand
k clay
D50
hmax
Parameter influence [-]

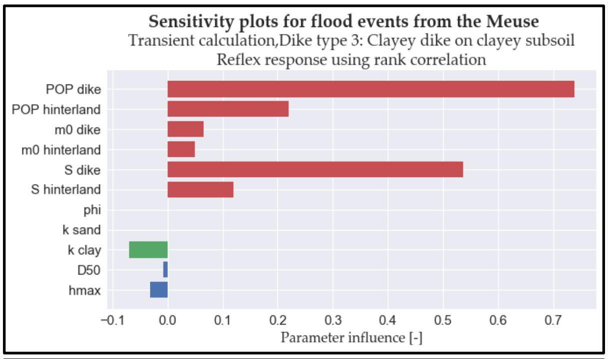
Sensitivity plots for flood events from the Meuse
Transient calculation,Dike type 3: Clayey dike on clayey subsoil
Reflex response using rank correlation
POP dike
POP hinterland
m0 dike
m0 hinterland
S dike
S hinterland
phi
k sand
k clay
D50
hmax
Parameter influence [-]

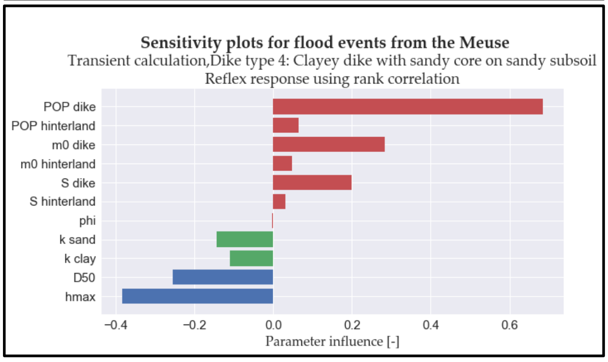
Sensitivity plots for flood events from the Meuse
Transient calculation,Dike type 4: Clayey dike with sandy core on sandy subsoil
Reflex response using rank correlation
POP dike
POP hinterland
m0 dike
m0 hinterland
S dike
S hinterland
phi
k sand
k clay
D50
hmax
Parameter influence [-]

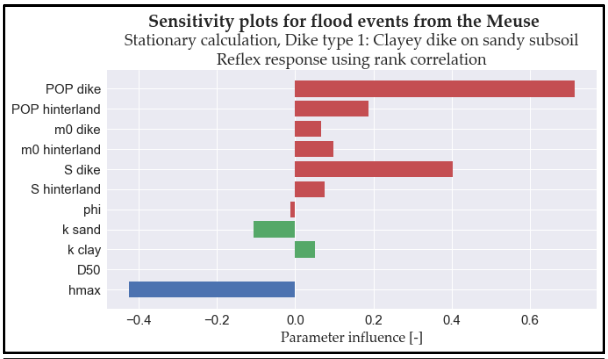
Sensitivity plots for flood events from the Meuse
Stationary calculation, Dike type 1: Clayey dike on sandy subsoil
Reflex response using rank correlation
POP dike
POP hinterland
m0 dike
m0 hinterland
S dike
S hinterland
phi
k sand
k clay
D50
hmax
Parameter influence [-]

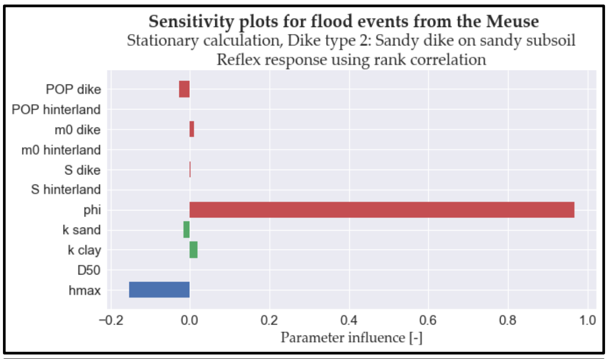
Sensitivity plots for flood events from the Meuse
Stationary calculation, Dike type 2: Sandy dike on sandy subsoil
Reflex response using rank correlation
POP dike
POP hinterland
m0 dike
m0 hinterland
S dike
S hinterland
phi
k sand
k clay
D50
hmax
Parameter influence [-]

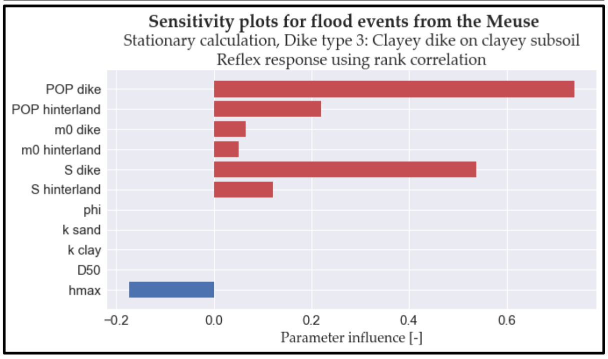
Sensitivity plots for flood events from the Meuse
Stationary calculation, Dike type 3: Clayey dike on clayey subsoil
Reflex response using rank correlation
POP dike
POP hinterland
m0 dike
m0 hinterland
S dike
S hinterland
phi
k sand
k clay
D50
hmax
Parameter influence [-]

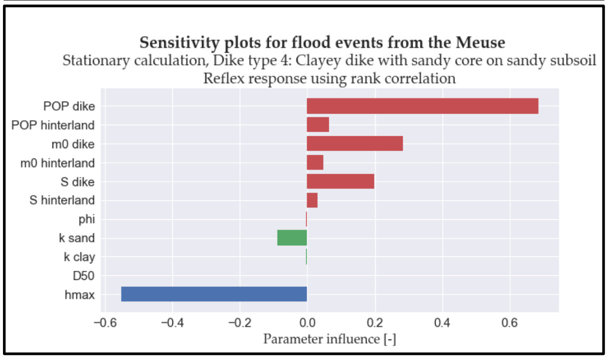
Sensitivity plots for flood events from the Meuse
Stationary calculation, Dike type 4: Clayey dike with sandy core on sandy subsoil
Reflex response using rank correlation
POP dike
POP hinterland
m0 dike
m0 hinterland
S dike
S hinterland
phi
k sand
k clay
D50
hmax
Parameter influence [-]

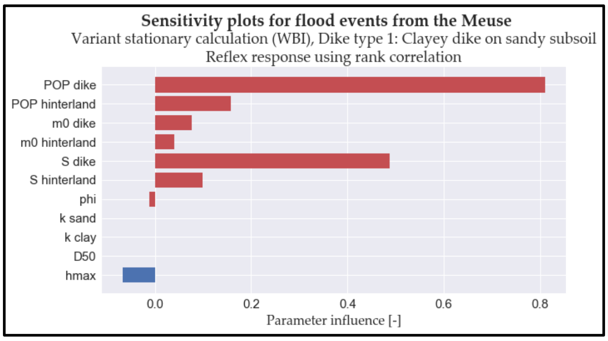
Sensitivity plots for flood events from the Meuse
Variant stationary calculation (WBI), Dike type 1: Clayey dike on sandy subsoil
Reflex response using rank correlation
POP dike
POP hinterland
m0 dike
m0 hinterland
S dike
S hinterland
phi
k sand
k clay
D50
hmax
0.0
0.2
0.4
0.6
0.8
Parameter influence [-]

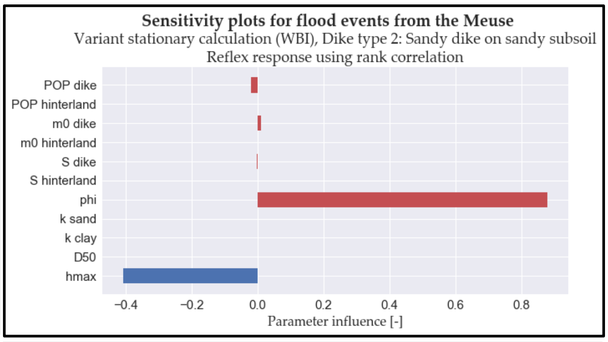
Sensitivity plots for flood events from the Meuse
Variant stationary calculation (WBI), Dike type 2: Sandy dike on sandy subsoil
Reflex response using rank correlation
POP dike
POP hinterland
m0 dike
m0 hinterland
S dike
S hinterland
phi
k sand
k clay
D50
hmax
−0.4
−0.2
0.0
0.2
0.4
0.6
0.8
Parameter influence [-]

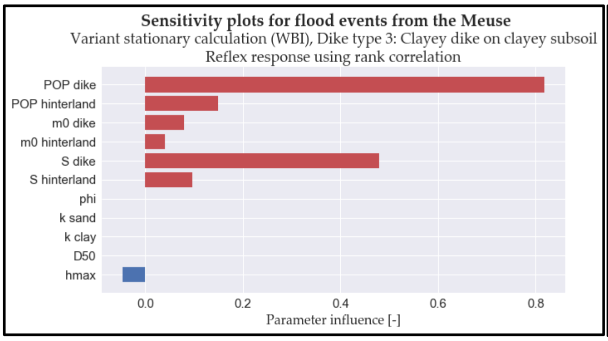
Sensitivity plots for flood events from the Meuse
Variant stationary calculation (WBI), Dike type 3: Clayey dike on clayey subsoil
Reflex response using rank correlation
POP dike
POP hinterland
m0 dike
m0 hinterland
S dike
S hinterland
phi
k sand
k clay
D50
hmax
0.0
0.2
0.4
0.6
0.8
Parameter influence [-]

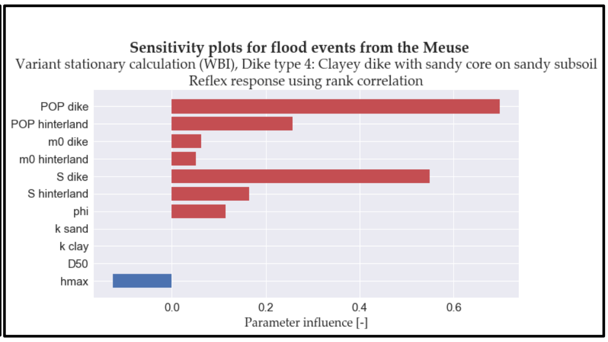
Sensitivity plots for flood events from the Meuse
Variant stationary calculation (WBI), Dike type 4: Clayey dike with sandy core on sandy subsoil
Reflex response using rank correlation
POP dike
POP hinterland
m0 dike
m0 hinterland
S dike
S hinterland
phi
k sand
k clay
D50
hmax
0.0
0.2
0.4
0.6
Parameter influence [-]